

# Polynuclear Aromatic Compounds



ADVANCES IN CHEMISTRY SERIES **217**

# Polynuclear Aromatic Compounds

**Lawrence B. Ebert, EDITOR**  
*Exxon Research and Engineering Company*

Developed from a symposium sponsored  
by the Division of Petroleum Chemistry, Inc.  
at the 192nd Meeting  
of the American Chemical Society,  
Anaheim, California  
September 7-12, 1986



American Chemical Society, Washington, DC 1988



### Library of Congress Cataloging-in-Publication Data

Polynuclear aromatic compounds

Lawrence B. Ebert, editor.

Developed from a symposium sponsored by the Division of Petroleum Chemistry at the 192nd Meeting of the American Chemical Society, Anaheim, California, September 7-12, 1986.

p. cm.—(Advances in chemistry series; no. 217).

Bibliography: p.

Includes index.

ISBN 0-8412-1014-4.

I. Polycyclic aromatic hydrocarbons—Congresses.

I. Ebert, Lawrence B. II. American Chemical Society. Division of Petroleum Chemistry.

III. American Chemical Society. Meeting (192nd:

1986; Anaheim, Calif.) IV. Series: Advances in chemistry series; 217.

QD1.A355 no. 217

[QD341.H9]

540 s—dc19

[547'.6]

87-22973

CIP

Copyright © 1988

American Chemical Society

All Rights Reserved. The appearance of the code at the bottom of the first page of each chapter in this volume indicates the copyright owner's consent that reprographic copies of the chapter may be made for personal or internal use or for the personal or internal use of specific clients. This consent is given on the condition, however, that the copier pay the stated per copy fee through the Copyright Clearance Center, Inc., 27 Congress Street, Salem, MA 01970, for copying beyond that permitted by Sections 107 or 108 of the U.S. Copyright Law. This consent does not extend to copying or transmission by any means—graphic or electronic—for any other purpose, such as for general distribution, for advertising or promotional purposes, for creating a new collective work, for resale, or for information storage and retrieval systems. The copying fee for each chapter is indicated in the code at the bottom of the first page of the chapter.

The citation of trade names and/or names of manufacturers in this publication is not to be construed as an endorsement or as approval by ACS of the commercial products or services referenced herein; nor should the mere reference herein to any drawing, specification, chemical process, or other data be regarded as a license or as a conveyance of any right or permission, to the holder, reader, or any other person or corporation, to manufacture, reproduce, use, or sell any patented invention or copyrighted work that may in any way be related thereto. Registered names, trademarks, etc., used in this publication, even without specific indication thereof, are not to be considered unprotected by law.

PRINTED IN THE UNITED STATES OF AMERICA

**American Chemical Society  
Library**

**1155 16th St., N.W.  
Washington, D.C. 20036**

# Advances in Chemistry Series

M. Joan Comstock, *Series Editor*

## 1988 ACS Books Advisory Board

Harvey W. Blanch  
University of California—Berkeley

Malcolm H. Chisholm  
Indiana University

Alan Elzerman  
Clemson University

John W. Finley  
Nabisco Brands, Inc.

Natalie Foster  
Lehigh University

Marye Anne Fox  
The University of Texas—Austin

Roland F. Hirsch  
U.S. Department of Energy

G. Wayne Ivie  
USDA, Agricultural Research Service

Michael R. Ladisch  
Purdue University

Vincent D. McGinniss  
Battelle Columbus Laboratories

Daniel M. Quinn  
University of Iowa

E. Reichmanis  
AT&T Bell Laboratories

C. M. Roland  
U.S. Naval Research Laboratory

W. D. Shults  
Oak Ridge National Laboratory

Geoffrey K. Smith  
Rohm & Haas Co.

Douglas B. Walters  
National Institute of  
Environmental Health

Wendy A. Warr  
Imperial Chemical Industries

# FOREWORD

The ADVANCES IN CHEMISTRY SERIES was founded in 1949 by the American Chemical Society as an outlet for symposia and collections of data in special areas of topical interest that could not be accommodated in the Society's journals. It provides a medium for symposia that would otherwise be fragmented because their papers would be distributed among several journals or not published at all. Papers are reviewed critically according to ACS editorial standards and receive the careful attention and processing characteristic of ACS publications. Volumes in the ADVANCES IN CHEMISTRY SERIES maintain the integrity of the symposia on which they are based; however, verbatim reproductions of previously published papers are not accepted. Papers may include reports of research as well as reviews, because symposia may embrace both types of presentation.

## ABOUT THE EDITOR



Lawrence B. Ebert is a staff chemist at Exxon's Corporate Research Laboratories in Clinton Township, New Jersey. He obtained his Ph.D. in physical chemistry from Stanford, where he was a Fannie and John Hertz Foundation Fellow, and his B. S. from the University of Chicago.

His principal research interest is in benzenoid compounds, ranging from graphite to aromatic hydrocarbons. At Exxon, he has studied a variety of messy black materials, including petroleum residua, cokes, and coals. He is the editor of the book *Chemistry of Engine*

*Combustion Deposits* (Plenum, 1985).

Ebert has intensively studied intercalation compounds of graphite, materials in which the layered graphite matrix serves as host to various guest ions and molecules. He is currently defining the frontier at which polynuclear aromatic hydrocarbon molecules begin to behave as the delocalized infinite graphite.

# PREFACE

POLYNUCLEAR AROMATIC HYDROCARBONS and heterocycles are quite abundant in fossil fuel materials such as coal and petroleum, and insights into new chemistry can potentially lead to developments in the areas of fuels, lubricants, chemicals, and carbonaceous materials. The study of large aromatic hydrocarbons is long-standing, and the symposium upon which this book is based was held on the 30th anniversary of a symposium, "Polycyclic Hydrocarbons", held in Atlantic City in September 1956 and published in Volume 1 of the Preprints of the Petroleum Division. We are fortunate to have as one of the contributors to this book, Michael Szwarc, who was an author of one of the papers of the 1956 symposium ("Reactivities of Deformed Aromatic Hydrocarbons").

The objective of this book is to present accounts of current research in polynuclear aromatic compounds, showing examples of studies both of pure compounds and of complex, fossil fuel related mixtures. This book is necessarily topical, and we do not seek an encyclopedic coverage as may be found in Clar's *Polycyclic Hydrocarbons* or Rodd's *Chemistry of Carbon Compounds*. The combination of basic and applied work is deliberate, for there is opportunity for cross-over in both directions. Such a combination could be viewed as a loss in focus; as an example, a reviewer of the book *Chemistry of Engine Combustion Deposits* termed a chapter on the chemistry of aromatic hydrocarbons "of marginal relevance" even though the engine deposits are 90% aromatic carbon. However, in the economic climate of the 1980s, investigators in both the basic and applied sciences need to be ever more closely linked to ensure their mutual success!

Coverage of aromatic chemistry in the book includes reduction, oxidation, and thermal reactions, with applications developed for both coal and petroleum materials. Other topics include quantum chemical structure-reactivity relationships, spatial configurations of large polynuclear hydrocarbons, cyclophanes, and desulfurization of heterocycles. The first and the last chapters touch on new frontiers in aromatic compounds, including the proposed  $C_{60}$  cluster ("buckminsterfullerene") and extensions to hydrogen-poor benzenoid materials, such as calcined petroleum coke and graphite. In the future, the chemistry of polynuclear aromatic compounds promises to be of relevance to exciting materials areas, including amorphous carbon and dense, "diamondlike" films (J. Robertson and E. P. O'Reilly, *Phys. Rev. B*, 1987, 35, 2946).



Much activity in aromatic hydrocarbons and carbonaceous materials is occurring outside of the United States, and we were fortunate to have the support of the Petroleum Research Fund (Grant 18537-SE) and the Exxon Education Foundation to bring foreign speakers to Anaheim for the symposium upon which this book is based. Finally, in bringing this book into existence, we thank the ACS Books Department, especially the editors who worked so hard, Robin Giroux, Karen McCeney, and Barbara Libengood.

LAWRENCE B. EBERT  
Corporate Research Laboratories  
Exxon Research and Engineering Company  
Annandale, NJ 08801

August 1987

# New Dimensions in Polynuclear Aromatic Compounds

William C. Herndon

Department of Chemistry, University of Texas at El Paso, El Paso, TX 79968-0509

*The structures of organic polynuclear aromatic compounds are not limited to planar systems of carbon and hydrogen atoms. A classification of three-dimensional aromatic compounds is proposed on the basis of the number of recognizable edges (boundaries) in the molecular structure. Aromatic structures with no edges are included in this classification; an example is the recently proposed truncated icosahedral structure for C<sub>60</sub> (Buckminsterfullerene). The current literature and activity in the subfield of nonplanar aromatic compounds is reviewed. Three-dimensional aromatic compounds are possible tools for use in studies of polynuclear aromatic chemistry, and some possible applications to the particular chemical topics presented in this book are outlined.*

**P**OLYNUCLEAR AROMATIC COMPOUNDS encompass a large and fascinating variety of structural types, even though the prototype substructure is the deceptively simple, highly symmetrical,  $\pi$  benzenoid ring composed of six  $sp^2$  hybridized carbon atoms. The possibilities of substitution of heteroatoms for one or more carbon atoms and modifications by external substituents allow the usual paradigms of structural and synthetic organic chemistry to be used to visualize new structures. An underlying polybenzenoid ring system, which can be extended in several ways, leads to unlimited numbers of structural classes. One expects and finds that the chemistry of polynuclear aromatic compounds is correspondingly diverse and complex. Besides aromatic electrophilic and nucleophilic substitution reactions, polynuclear ar-

omatic compounds undergo a variety of oxidations, reductive reactions, polymerizations, fragmentations, addition reactions, and rearrangements.

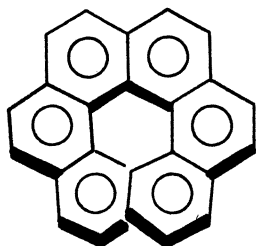
The symposium from which this book was developed (1) and the chapters of this book cover a substantial number of topics relating to polynuclear aromatic compounds. The largest group of these chapters discusses new experimental work related to the chemical reactions and physical properties of polynuclear radical anions and dianions (2–7), synthesized mainly by metal-mediated reactions. The physically oriented chapters include a detailed review of the equilibria involved in the disproportionation of radical anions (2), a study of the crystal structures and electron spin resonance properties of alkali aromatic ion pairs (3), and an NMR spectral investigation of polynuclear heterocyclic and carbocyclic dianions that discusses paratropicity and antiaromaticity (4). The other chapters in this group are primarily concerned with the subsequent chemical reactions of the radical anions. The metal–ammonia reduction process involving polynuclear aromatic hydrocarbons is reviewed (5), and the use of reductive alkylation with alkyl iodides to investigate the structures of the anionic intermediates is elaborated (6). The employment of metal-mediated reactions as a general tool for the synthesis of numerous structures containing new carbon–carbon bonds is the last chapter in this group (7).

Three studies on radical cations discuss the characterization of polynuclear aromatic radical cation salts as organic metals (8), the reactions of cation radicals with neutral radicals (9), and the magnetic–electrical properties of perfluoroaromatic radical-cation salts (10). Chapters on polynuclear aromatic compounds in nonvolatile petroleum products (11) and in coal-based materials (12) present reviews of the subject and new findings. The remaining chapters in this book discuss the thermal conversion of polynuclear aromatic compounds to carbon (13), the nitration of pyrene by mixtures of  $\text{NO}_2$  and  $\text{N}_2\text{O}_4$  (14), the spectra, structures, and chromatographic retention times of large polycyclic aromatic hydrocarbons (15), the desulfurization of polynuclear thiophenes correlated with  $\pi$  electron densities (16); and simple theoretical methods to predict and correlate polynuclear benzenoid aromatic hydrocarbon reactivities (17).

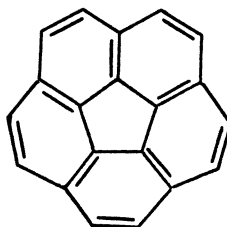
The various topics covered in this volume might seem to be more than sufficient. However, the aforementioned diversity of the general subject of polynuclear aromatic hydrocarbons has ensured that only a small fraction of the active areas of research on this topic can be discussed. I have therefore chosen as the main purpose of this introductory chapter to highlight an additional area of polynuclear aromatic hydrocarbon chemistry that is of recent personal interest, namely, nonplanar three-dimensional aromatic systems. The idiosyncrasy of this choice is mitigated by significant recent discoveries in this subfield that are apropos to other chapters of this book. Therefore, at least part of the following discussion may be not only of interest but of practical use.

### ***Single-Boundary Three-Dimensional Aromatic Hydrocarbons***

Condensed polycyclic benzenoid aromatic hydrocarbons are customarily regarded as planar molecular structures because of the geometrical constraints of carbon atoms in a state of  $sp^2$  hybridization. A well-known exception is the class of compounds called the *helicenes* (18) for which the nonbonded overlap of two terminal benzenoid rings in a cata-condensed structure, as in structure 1, forces a molecule into a nonplanar helical structure. A second exceptional class of compounds is related to corannulene (2) and other annulenes of this type (19, 20). In corannulene, strain associated with the pericondensed five- and six-membered rings requires adoption of a bowl-shaped structure (20, 21). For both structures 1 and 2 the aromatic character of the benzenoid rings is retained to an appreciable extent.

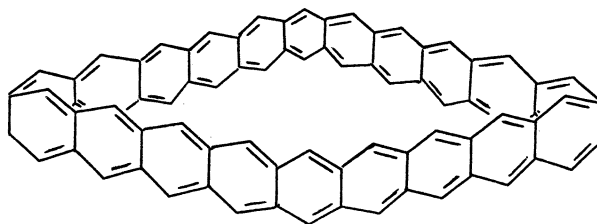


Structure 1



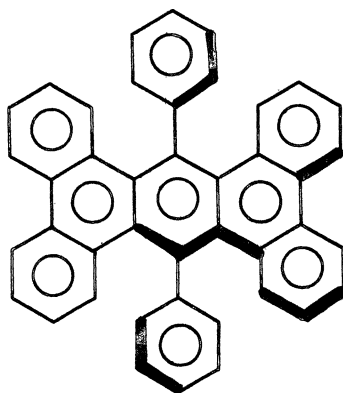
Structure 2

Structures 1 and 2 are examples of what I call single-boundary polynuclear aromatic compounds. This somewhat awkward designation distinguishes such compounds from an additional class (to be discussed later) of polynuclear aromatic compounds that have a three-dimensional Archimedean polyhedral structure with no faces larger than eight carbon atoms. Such compounds can be thought of as having a closed  $\pi$  electronic surface with no definable edges or boundaries. A third class of three-dimensional polynuclear aromatic compounds with two distinct boundaries can also be distinguished. The compounds of this class have the topology of a bracelet, as shown in structure 3. An aromatic bracelet of this type was postulated as a model for a conducting polyacene polymer by Kivelson and Chapman (23).



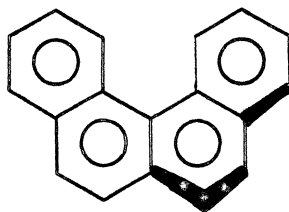
Structure 3

Pascal et al. (24) reported that highly twisted, helical, benzenoid aromatic compounds (benzenoid ribbons) can be designed in which the axis of the helix lies parallel to the aromatic ring planes rather than perpendicular, as in the helicenes. The helical geometry is achieved by introducing bulky phenyl substituents at the 9- and 18-positions of tetrabenz- $[a,c,h,j]$ anthracene, as shown in structure 4; the resulting degree of twist of the anthracene nucleus in this case is  $65.7^\circ$ , as established by X-ray crystallographic analysis. Even with this high degree of strain and nonplanarity, the molecule is highly stable because crystals of the compound do not melt or discolor when heated above  $350^\circ\text{C}$ . Pascal et al. (24) suggested that it may be possible to synthesize polycyclic benzenoid ribbons with twists of  $90^\circ$  and greater.

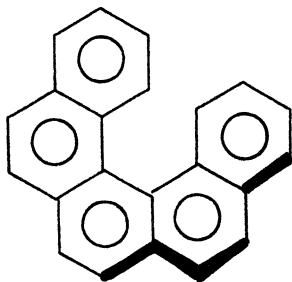


Structure 4

The realization that polycyclic aromatic compounds are not necessarily planar is not a new concept. A book published in 1964 on benzenoid hydrocarbons (24) contains a chapter on nonplanar, overcrowded, aromatic hydrocarbons; this chapter primarily describes high degrees of nonplanarity that are due to steric interactions of hydrogen atoms in benzenoid compounds that contain substructures related to benzo[ $c$ ]phenanthrene (5) (twist angle =  $31^\circ$ ) or to dibenzo[ $c,d$ ]phenanthrene (6) (twist angle = ca.  $50^\circ$ ) (26–28).



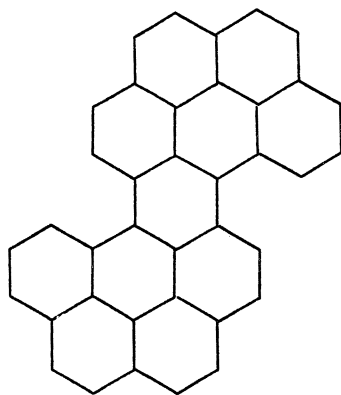
Structure 5



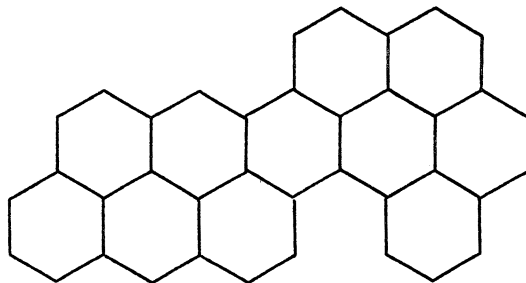
Structure 6

Newman and co-workers (29–34) synthesized many optically active compounds related to structures 5 and 6 that contained substituents in the critical sterically crowded regions and studied several of their physical properties.

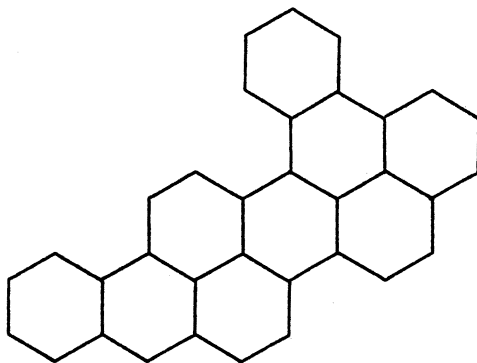
Structures determined by modern X-ray techniques show that significant nonplanarities exist in benzenoid compounds of this type. This finding infers that nonplanar polycyclic aromatic compounds are quite common. Structures 7–9, which have twist angles ranging from 30° to 42°, are examples



Structure 7

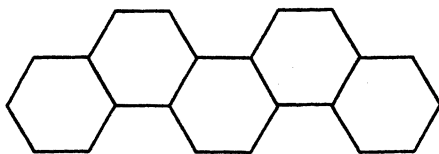


Structure 8



Structure 9

of benzenoid compounds exhibiting significant nonplanarities (35–37). Structures determined by modern X-ray techniques also show that a 1,4-CH–CH interaction, such as in phenanthrene, is not a sufficient strain-inducing factor to lead to large extents of nonplanarity. This finding is deduced from the dihedral angle between the outermost rings in picene (10), which is only  $3.7^\circ$  (38).



Structure 10

Whether the nonplanarity of single-boundary three-dimensional aromatic hydrocarbons is reflected in predictable changes in physical or chemical properties remains to be established. Good test cases could be the rates of electrophilic aromatic substitutions (39) or the relative rates of Diels–Alder reactions (40). A comparison of the predicted rates with experimental measurements, perhaps by using the procedures of Szentpály and Herndon (17) summarized in this book, might provide some new insights into the relationships among molecular structure, strain, and reactivity.

Single-boundary three-dimensional aromatic hydrocarbons do have high photoconductivities (41), but the relationship between molecular structure and photoconductivity remains unclear. In this regard, the red shift of structure 4 in comparison with the presumably planar parent compound, namely tetrabenz[*a,c,h,j*]anthracene (24) may be significant. In this book, Fetzer (15) gives UV–visible spectra for these kinds of polycyclic aromatic com-

pounds that could possibly be used to confirm whether or not spectral shifts to longer wavelengths due to nonplanarity are common. Fetzner (15) also shows that the chromatographic retention times do seem to decrease as nonplanarity (presumably) increases.

The possibility of preparing radical-cation salts of these nonplanar aromatic compounds is an interesting prospect. Many of these compounds contain pyrene and perylene substructures, both of which form well-defined salts when the procedures outlined and reviewed in the chapter by Enkelmann (8) are used. However, the morphologies of crystals of radical-cation salts derived from the nonplanar compounds are difficult to envisage. Consequently, one cannot be certain that the resulting salts will have useful conducting properties.

Dianions formed by the alkali-metal-mediated reduction of nonplanar aromatic compounds should also have a number of interesting properties. For example, one of the intriguing ideas advanced by Rabinovitz and Cohen (4) in their chapter on NMR properties and paratropicity is that the polynuclear aromatic dianion is partitioned into charged and uncharged components to reduce destabilizing paratropic effects. The preexisting nonplanarity of the  $\pi$  system of structures 4–9 might assist this partitioning and thereby lead to NMR spectra that would support this viewpoint. However, the effects observed by Rabinovitz and Cohen (4) on the NMR spectra may be a result of a geometric change from planarity in the neutral compound to nonplanarity in the dianions. Localization of negative charge, reduced conjugation, and nonplanarity are simultaneous manifestations of the desire of the molecular dianion to ameliorate destabilizing antiaromatic interactions.

### *Polyhedral Three-Dimensional Aromatic Hydrocarbons*

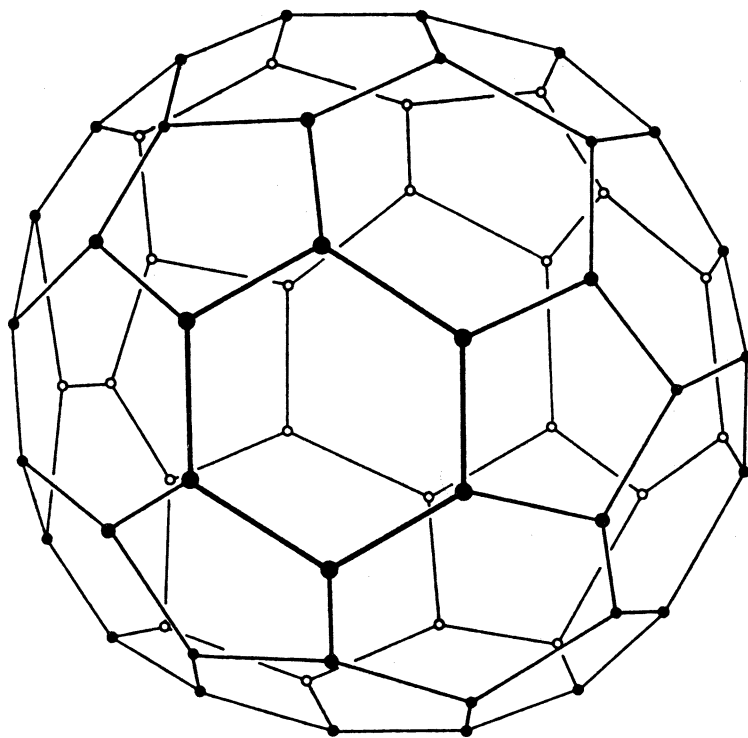
Many recent studies focus on the formation and properties of carbon-atom clusters (42–50). The initial studies were directed toward obtaining a better understanding of the formation of large polyacetylene species in interstellar space (51–55). Some of the later work suggests that small three-dimensional carbon clusters containing benzenoid rings are involved in soot formation, and some detailed mechanisms have been postulated (56). The relationship of this work to thermal reactions described in this book by Lewis and Singer (13) is not straightforward. However, these experiments with carbon clusters suggest a new subfield of polynuclear aromatic chemistry that should be interesting to many scientists.

The clusters can be formed from graphite by laser evaporation, stabilized by expansion through a supersonic nozzle, and analyzed as ions by using laser ionization and mass spectrometry (42–44). In all of these experiments, even-numbered clusters, and in particular a  $C_{60}$  species, are prevalent and presumably relatively stable. Some controversy has developed in regard to the effect of experimental conditions or charge on the cluster size distribution



(46, 49); the consensus is that the amount of any one cluster size represented in the total carbon ion signal is small. However, the "magic" number of 60 for the most intense cluster size has been observed by several researchers (42–50) under diverse experimental conditions.

In an early report of this type of research, Kroto et al. (44) suggested that the  $C_{60}$  species could be a three-dimensional, spheroidal, aromatic carbon compound with connectivity isomorphic to the seams of a soccer ball (except in the United States and Canada, a soccer ball is known as a football). This truncated icosahedral structure (11), with 20 benzene rings and 12 isolated pentagon rings was tentatively named Buckminsterfullerene (BMF-60), although a request for a more concise and sensible name was made. This particular structure was postulated because such a species can be formed with minimal strain, with no unsatisfied carbon valence, and with a great deal of stabilizing resonance energy due to the condensed benzene ring substructure.



Structure 11

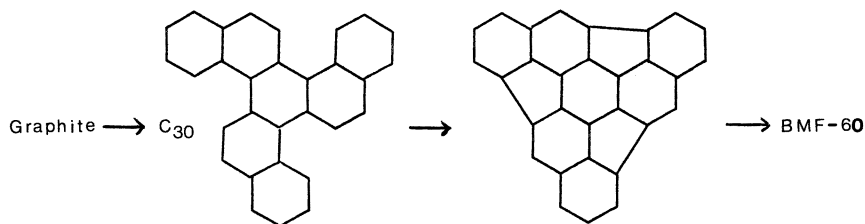
A unique feature of a polyhedral structure of this type is the absence of a discernible edge or boundary to the  $\pi$  system or to the general molecular

structure. Therefore, carbon allotropes containing a closed-surface  $\pi$  system constitute a new class of polynuclear aromatic compounds. The synthesis and study of the properties of such compounds and their heteroatom derivatives have generated much interest, and several papers on BMF-60 and related structures have been published (57-69).

The first publication of which I am aware that postulates the existence of a truncated icosahedral carbon cluster is a book by Yoshida and Osawa (70) that was published in 1971. The first Hückel calculation for BMF-60 was carried out by Bochvar and Gal'pern (71) and reported in 1973. This work is amplified by additional examples of carbon polyhedrons that were given in a review (72) published in 1984 on existing and hypothetical crystalline modifications of carbon. Hückel calculations employing a graphical theoretical approach were performed by Davidson (73) for several polyhedrons, including BMF-60, and were reported in 1981.

Various theoretical methods to calculate the electronic properties of BMF-60 and some isomers have been employed in more recent work (57-69). The methods used range from empirical valence-bond resonance theory to several types of ab initio molecular orbital calculations. All methods agree that structure 11 would be highly stabilized and presumably able to exist. Apart from these theoretical calculations, a geometrical analysis and cataloging of possible stable, closed, polyhedral structures up through  $C_{240}$  was carried out by Klein et al. (74). This work should be of particular interest to anyone contemplating additional theoretical or synthetic research in this area.

It is perhaps surprising that all of these published works are theoretical in nature and in general limited in scope to BMF-60 and closely related isomers. Since a rational synthesis to produce BMF-60 or any related compound has yet to be reported, it maybe that the lack of available experimental data has discouraged detailed studies of possible structures and mechanisms associated with large carbon clusters. In fact, the physical-chemical data on carbon clusters are not adequate to fully affirm the general theoretical prediction of a probable existence for BMF-60, and its formation from graphite has yet to be rationalized by a detailed and logical mechanism. Only an outline of a possible mechanism, shown in Scheme I, has been suggested



*Scheme I*

and tested computationally (MNDO) by McKee and Herndon (75). Given the availability of computational facilities, the limitations of reported quantum mechanical calculations are disappointing, and additional investigations should be encouraged.

### Acknowledgment

Grants from the Welch Foundation of Houston, TX, and the Texas Advanced Technology Program are gratefully acknowledged. A copy of reference 70 and a translation were kindly provided by T. Fukunaga of E. I. du Pont de Nemours and Company. I also thank the reviewers for their comments and suggestions.

### References

1. *Prepr.-Am. Chem. Soc., Div. Pet. Chem.* **1986**, 31(4), 767-862.
2. Szwarc, M., Chapter 2 in this book.
3. de Boer, E.; Gribnau, M. C. M., Chapter 3 in this book.
4. Rabinovitz, M.; Cohen, Y., Chapter 4 in this book.
5. Rabideau, P. W., Chapter 5 in this book.
6. Ebert, L. B.; Milliman, G. A.; Mills, D. M.; Scanlon, J. C., Chapter 21 in this book.
7. Eisch, J. J., Chapter 6 in this book.
8. Enkelmann, V., Chapter 11 in this book.
9. Shine, H. J.; Soroka, M., Chapter 8 in this book.
10. Richardson, J. J.; Tanzella, F. L.; Bartlett, N., Chapter 10 in this book.
11. Speight, J. G., Chapter 12 in this book.
12. Nishioka, N. and Lee, M. L., Chapter 14 in this book.
13. Lewis, I. C.; Singer, L. S., Chapter 16 in this book.
14. Rose, D. S.; Hum, G. P.; Schmitt, R. J., Chapter 9 in this book.
15. Fetzer, J. C., Chapter 18 in this book.
16. Nagai, M.; Urimoto, H.; Uetake, K.; Sakikawa, N.; Gonzalez, R. D., Chapter 20 in this book.
17. Szentpály, L. V.; Herndon, W. C., Chapter 17 in this book.
18. Meuer, K. P.; Vogtle, F. *Top. Curr. Chem.* **1985**, 127, 1; and references cited therein.
19. Barth, W. E.; Lawton, R. G. *J. Am. Chem. Soc.* **1966**, 88, 380.
20. *Ibid.* **1971**, 93, 1730.
21. Hanson, J. C.; Nordman, C. E. *Acta Crystallogr.* **1976**, B32, 1147.
22. Gleicher, G. J. *Tetrahedron* **1967**, 23, 4257.
23. Kivelson, S.; Chapman, O. L. *Phys. Rev.* **1983**, B28, 7236.
24. Pascal, R. A.; McMillan, W. D.; Van Engen, D. *J. Am. Chem. Soc.* **1986**, 108, 5652.
25. Clar, E. *Polycyclic Hydrocarbons*; Academic: New York, 1964, Vol. 1; Chapter 16.
26. Hirshfeld, A. L.; Sandler, S.; Schmidt, G. M. *J. J. Chem. Soc.* **1964**, 2108.
27. Also see Herstein, F. H.; Schmidt, G. M. *J. J. Chem. Soc.* **1954**, 3302.
28. McIntosh, A. O.; Robertson, J. M.; Vand, V. *J. Chem. Soc.* **1954**, 1661.
29. Newman, M. S.; Wheatley, W. B. *J. Am. Chem. Soc.* **1948**, 70, 1913.
30. Newman, M. S.; Wise, R. M. *Ibid.* **1956**, 78, 450.

31. Newman, M. S.; Phillips, D. K. *Ibid.* **1959**, *81*, 3667.
32. Newman, M. S.; Mentzer, R. G.; Slomp, G. *Ibid.* **1963**, *85*, 4018.
33. Karnes, H. A.; Kybett, B. D.; Wilson, M. H., Margrave, J. L.; Newman, M. S. *Ibid.* **1965**, *87*, 5554.
34. Karnes, H. A.; Rose, M. L.; Collat, J. W.; Newman, M. S. *Ibid.* **1968**, *90*, 458.
35. Oonishi, I.; Fujisawa, S.; Aoki, J.; Danno, T. *Bull. Chem. Soc. Jpn.* **1978**, *51*, 2256.
36. Fujisawa, S.; Oonishi, I.; Aoki, J.; Ohashi, Y.; Sasada, Y. *Ibid.* **1982**, *55*, 3424.
37. Oonishi, I.; Fujisawa, S.; Aoki, J.; Ohashi, Y.; Sasada, Y. *Ibid.* **1986**, *59*, 2233.
38. Ratna Ghosh, A. D.; Roychowdhury, S.; Roychowdhury, P. *Acta Crystallogr.* **1985**, *C41*, 907.
39. Shawali, A. S.; Hassane, H. M.; Parkanyi, C.; Herndon, W. C. *J. Org. Chem.* **1983**, *48*, 4800.
40. Hess, B. A., Jr.; Schaad, L. J.; Herndon, W. C.; Bierman, D.; Schmidt, W. *Tetrahedron* **1982**, *37*, 2983.
41. Kamura, Y.; Inokichi, H.; Aoki, J.; Fujisawa, S. *Chem. Phys. Lett.* **1977**, *46*, 356.
42. Rohlfing, E. A.; Cox, D. M.; Kaldor, A. *J. Chem. Phys.* **1984**, *81*, 3322.
43. Kaldor, A.; Cox, D. M.; Trevor, D. J.; Whetten, R. L. In *Catalyst Characterization Science*; Deviney, M. L.; Gland, J. L., Eds.; ACS Symposium Series 288; American Chemical Society: Washington, DC; 1985; p 111.
44. Kroto, H. W.; Heath, J. R.; O'Brien, S. C.; Curl, R. F.; Smalley, R. E. *Nature* **1985**, *318*, 162.
45. Heath, J. R.; O'Brien, S. C.; Zhang, Q.; Liu, Y.; Curl, R. F.; Kroto, H. W.; Tittle, F. K.; Smalley, R. E. *J. Am. Chem. Soc.* **1985**, *107*, 7779.
46. Cox, D. M.; Trevor, D. J.; Reichmann, K. C.; Kaldor, A. *J. Am. Chem. Soc.* **1986**, *108*, 2457.
47. Liu, Y.; O'Brien, S. C.; Zhang, Q.; Heath, J. R.; Tittel, F. K.; Curl, R. F.; Kroto, H. W.; Smalley, R. E. *Chem. Phys. Lett.* **1986**, *126*, 215.
48. Knight, R. D.; Walch, R. A.; Foster, S. C.; Miller, T. A.; Mullen, S. L.; Marshall, A. G. *Chem. Phys. Lett.* **1986**, *129*, 331.
49. Hahn, M. Y.; Honea, E. C.; Paguia, A. J.; Schriver, K. E.; Camarena, A. M.; Whetten, R. L. *Chem. Phys. Lett.* **1986**, *130*, 12.
50. O'Keefe, A.; Ross, M. M.; Baronovski, A. P. *Chem. Phys. Lett.* **1986**, *130*, 17.
51. Duley, W. W.; Williams, D. A. *Interstellar Chemistry*; Academic: New York, 1984.
52. Platt, J. R. *Astrophys. J.* **1956**, *123*, 486.
53. Donn, B. *Astrophys. J.* **1968**, *152*, L129.
54. Léger, A.; Puger, J. L. *Astron. Astrophys.* **1984**, *137*, L5.
55. Puget, J.L.; Léger, A.; Boulanger, F. *Ibid.* **1985**, *142*, L19.
56. Zhang, Q. L.; O'Brien, S. C.; Heath, J. R.; Liu, Y.; Curl, R. F.; Kroto, H. W.; Smalley, R. E. *J. Phys. Chem.* **1986**, *90*, 525.
57. Haymet, A. D. J. *Chem. Phys. Lett.* **1985**, *122*, 421.
58. Haymet, A. D. J. *J. Am. Chem. Soc.* **1986**, *108*, 319.
59. Klein, D. J.; Schmalz, T. G.; Hite, G. E.; Seitz, W. A. *J. Am. Chem. Soc.* **1986**, *108*, 1301.
60. Newton, M. D.; Stanton, R. E. *J. Am. Chem. Soc.* **1986**, *108*, 2469.
61. Haddon, R. C.; Brus, L. E.; Raghavachari, K. *Chem. Phys. Lett.* **1986**, *125*, 459.
62. Disch, R. L.; Schulman, J. M. *Chem. Phys. Lett.* **1986**, *125*, 465.
63. Hess, B. A., Jr.; Schaad, L. J. *J. Org. Chem.* **1986**, *51*, 3902.
64. Fowler, P. W.; Woolrich, J. *Chem. Phys. Lett.* **1986**, *127*, 78.
65. Ozaki, M.; Takahashi, A. *Chem. Phys. Lett.* **1986**, *127*, 242.
66. Stone, A. J.; Wales, D. J. *Chem. Phys. Lett.* **1986**, *128*, 501.

67. Schmalz, T. G.; Seitz, W. A.; Klein, D. J.; Hite, G. E. *Chem. Phys. Lett.* **1986**, *130*, 203.
68. Haddon, R. C.; Brus, L. E.; Raghavachari, K. *Chem. Phys. Lett.* **1986**, *131*, 165.
69. Hale, P. D. *J. Am. Chem. Soc.* **1986**, *108*, 6087.
70. Yoshida, Z.; Osawa, E. *Aromaticity* Chemical Monograph Series 22, Kagaku-dojin: Kyoto, Japan, 1971; pp 174-176. The authors of this monograph clearly refer to the BMF-60 species with 60  $sp^2$  hybridized carbon atoms and depict its structure in their diagram (150), although the formula is misrepresented as  $C_{60}H_{60}$ .
71. Bochvar, D. A.; Gal'pern, E. G. *Dokl. Akad. Nauk. SSSR* **1973**, *203*, 610.
72. Stankecihv, I. V.; Nikerov, M. V.; Bochvar, D. A. *Russ. Chem. Rev. (Engl. Transl.)* **1984**, *53*, 640.
73. Davidson, R. A. *Theoret. Chem. Acta* **1981**, *58*, 193.
74. Klein, D. J.; Seitz, W. A.; Schmalz, T. G. *Nature* **1986**, *323*, 703.
75. McKee, M. L.; Herndon, W. C. *J. Mol. Struct. (Theo Chem.)*, in press.

RECEIVED for review December 9, 1986. ACCEPTED March 30, 1987.

# Electron Affinities of Aromatic Hydrocarbons

## Their Radical Anions and Dianions

Michael Szwarc

Department of Chemistry, University of California at San Diego, La Jolla, CA 92093

*Various thermodynamic and kinetic problems concerning the chemistry and physics of radical anions and dianions were investigated quantitatively by electron photoejection. The approaches described allow the determination of the relative electron affinities of various aromatic hydrocarbons and the thermodynamics and kinetics of disproportionation of their radical anions into dianions. These approaches also allow the observation of unstable radical anions and their isomerization or dimerization.*

**A**ROMATIC HYDROCARBONS may be reduced to radical anions or even to dianions by appropriate reagents. Electron capture is conceptually the simplest reduction reaction:



Here, A is the hydrocarbon to be reduced,  $e^{-}$  is a free electron, and  $A^{\bullet -}$  is the radical anion of A. The exothermicity of reaction 1 is referred to as the electron affinity of A, and its absolute value is equal to the ionization potential of  $A^{\bullet -}$ . Positive values of electron affinity imply that aromatic hydrocarbons are able to capture free electrons, a phenomenon to be described later.

### *Determination of Electron Affinity*

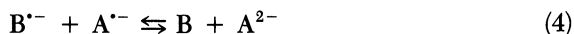
In 1956, Hoijtink et al. (1) reported relative electron affinities of some aromatic hydrocarbons. They determined these values by using a potentiometric

metric technique developed for this purpose. In the same year, Paul et al. (2) reported electron affinities for the same hydrocarbons reported in reference 1. They determined their values spectrophotometrically by investigating equilibria such as the following:



where A and B are two aromatic hydrocarbons, and  $A^{\cdot-}$  and  $B^{\cdot-}$  are their respective radical anions. The two sets of values differed appreciably and raised the question as to which technique is more reliable. Both techniques were used by Jagur-Grodzinski et al. (3) to determine the electron affinities of pyrene, anthracene, and 9,10-dimethylanthracene, and the results from both techniques were consistent with each other. This situation indicated that the discrepancies between the findings of Hoijtink et al. (1) and Paul et al. (2) were caused by factors other than the choice of experimental techniques. This chapter will show that the use of different solvents and counterions was the cause of the discrepancies just mentioned. The significance of these factors was overlooked in the past, and their importance in determining the redox equilibria will be discussed now in some detail.

The potentiometric technique of Hoijtink et al. (1) used the device shown in Figure 1. A 50/50 solution of biphenylide and biphenyl was dissolved in a rigorously dried aprotic solvent. This solution was kept in a buret, and the tip of the buret was immersed in a solution of the investigated hydrocarbon. The hydrocarbon was dissolved in the same aprotic solvent and was kept in an evacuated bulb. The hydrocarbon solution was titrated by slowly adding the biphenylide solution to the bulb. Two platinum wires were used as electrodes; one was immersed in the solution in the bulb, and the other was placed in the buret. The potential established between them was measured by a suitable high-resistance galvanometer. The results of the titration are depicted in Figure 2 as voltage versus the volume of biphenylide solution added. The two plateaus seen in the titration curve correspond to the following redox potentials:



The difference between the two plateaus gives the potential corresponding to the following disproportionation equilibrium:



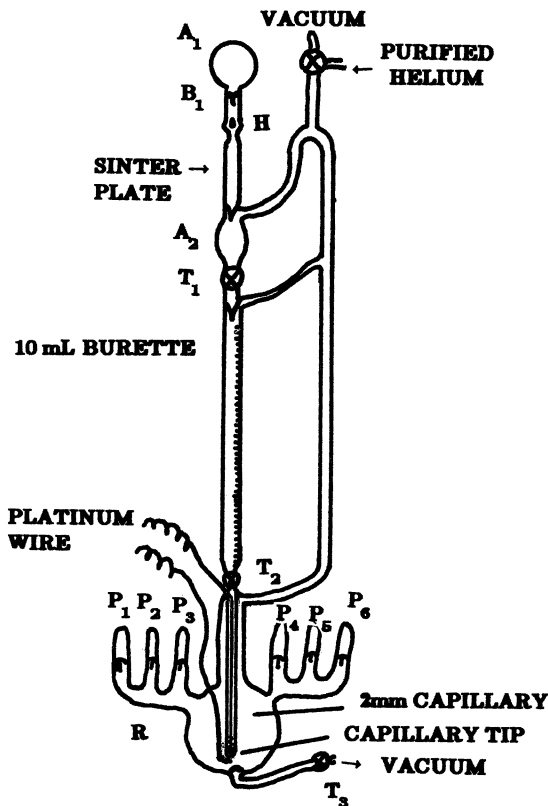


Figure 1. The device used in potentiometric titration of aromatic hydrocarbons. (Reproduced from reference 3. Copyright 1965 American Chemical Society.)

In reactions 3–5, B is biphenyl and A is the hydrocarbon investigated. Counterions are not mentioned, although the solution under study, like any matter in bulk, has to be electrically neutral. Therefore, some cations (Cat<sup>+</sup>) must be present to balance the negative charges of the anions and dianions.

The following questions arise: Are the oppositely charged ions independent of each other and able to move freely through the solution, or are they aggregated? If they are aggregated, do the aggregates have a unique structure, or do they exist in several distinct forms in equilibrium with each other? The existence of several, well-characterized aggregates formed in organic solvents by association of the oppositely charged ions has been fully documented (4). The simplest aggregates are referred to as ion pairs, and at least two kinds of ion pairs are recognized: (1) tight or contact ion pairs and (2) loose or solvent-separated ion pairs.



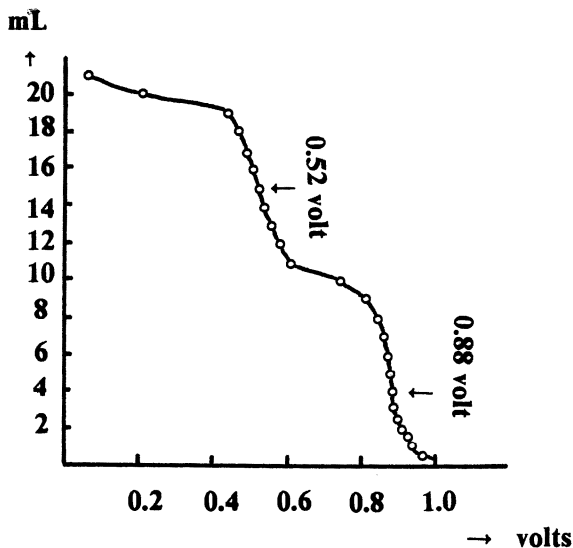


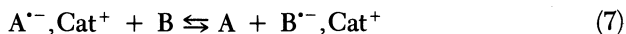
Figure 2. Titration curve: voltage versus milliliters of biphenylide solution added. (Reproduced from reference 3. Copyright 1965 American Chemical Society.)

### *Effect of Aggregation on Redox Potentials*

Aggregation affects redox potentials, that is, equilibriums such as reaction 3.  $K_-$  is the equilibrium constant for the following electron-transfer reaction:



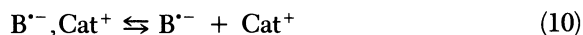
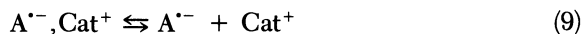
and  $K_{\pm}$  is the equilibrium constant for the reaction:



It follows that

$$K_{\pm}/K_- = K_{\text{diss},A}/K_{\text{diss},B} \quad (8)$$

where  $K_{\text{diss},A}$  and  $K_{\text{diss},B}$  are the dissociation constants of reactions 9 and 10, respectively:

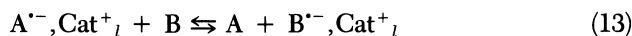
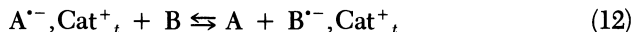


The spectrophotometric technique determines  $K_{\pm}$  whenever the fraction of free ions is very low. The concentration of the free ions may be reduced to an insignificant level by the addition of some readily dissociated salt sharing a common cation with the investigated radical anion. On the other hand, the potentiometric technique yields  $K_{\pm}$ , and its value can be used to calculate  $K_{\pm}$  if the necessary dissociation constants are known. These constants may be derived from conductometric data (5). For an anthracene and pyrene pair incorporating  $\text{Na}^+$  as the counterion and tetrahydrofuran (THF) as the solvent, the ratio of equation 8 is only 1.6, which is equivalent to 10 millivolts (mV). However, for an anthracene and naphthalene pair, the ratio is 30.3, which is equivalent to 90 mV.

As mentioned earlier, ion pairs can exist in tight (contact) or loose (solvent-separated) forms. Whenever both forms are present in a solution,  $K_{\pm}$  is directly determined as follows (subscripts  $t$  and  $l$  denote tight and loose forms, respectively):

$$K_{\pm} = \frac{[A]\{[B^{\cdot-}, \text{Cat}^+_t] + [B^{\cdot-}, \text{Cat}^+_l]\}}{[B]\{[A^{\cdot-}, \text{Cat}^+_t] + [A^{\cdot-}, \text{Cat}^+_l]\}} \quad (11)$$

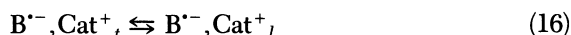
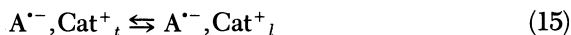
$K_{\pm}$  is a weighted average of two redox potentials, namely,  $K_{\pm,t}$  and  $K_{\pm,l}$ , which correspond to reactions 11 and 12, respectively:



The following relation is then deduced (6):

$$K_{\pm} = K_{\pm,t}(1 + K_A)/(1 + K_B) = K_{\pm,l}(1 + K_A^{-1})/(1 + K_B^{-1}) \quad (14)$$

where  $K_A$  and  $K_B$  denote the equilibrium constants of the conversion from tight to loose ion pairs shown in reactions 15 and 16, respectively:



The effect of ion-pair structure on redox potential is quite considerable (6), as revealed by Figure 3. In tetrahydropyran (THP), a relatively poor solvating agent, both ion pairs exist in tight form for the temperature range investigated. The van't Hoff plot of the equilibrium constant is given by the upper curve of Figure 3. The curve rises because the electron affinity of naphthalene is larger than that of biphenyl. In 1,2-dimethoxyethane (DME), a good solvating solvent, the pairs are loose, and the equilibrium constant is about

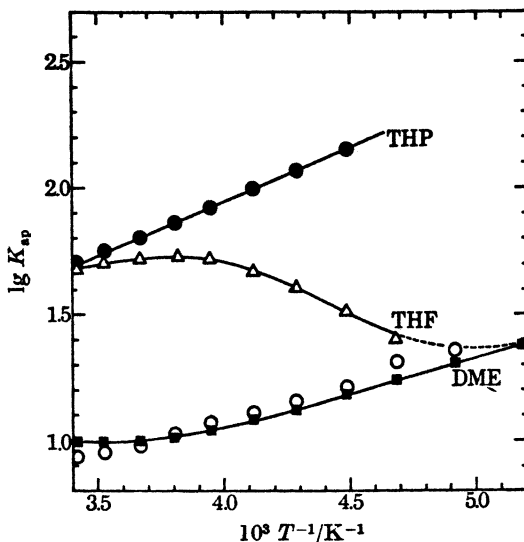
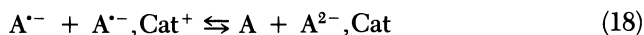


Figure 3. Plot of  $\log K_{ap}$  versus  $1/T$  for the equilibrium  $B^{\bullet-} + N \rightleftharpoons B + N^{\bullet-}$  in THP, DME, and THF containing  $Na^+$  counterions.  $B$  denotes biphenyl,  $N$  denotes naphthalene, and  $K_{ap}$  is the apparent equilibrium constant; tight pairs are in THP, and loose pairs are in DME; a change occurs from tight pairs at 25 °C to loose pairs at -70 °C in THF. (Reproduced with permission from reference 6. Copyright 1971 The Royal Society.)

50 times lower. The loose pairs are more dissociated than the tight pairs; therefore, the dissociation constants in the THP systems show less variation than the dissociation constants in the DME systems. This situation accounts for the observed difference between  $K_{\pm,t}$  and  $K_{\pm,l}$ .

The behavior of the system is most peculiar in THF, a better solvent than THP, but much poorer than DME. In THF, the pertinent pairs are mostly tight at 25 °C, but they are converted into loose pairs as the temperature decreases (the conversion of tight to loose pairs is exothermic). Consequently, as the temperature decreases from 25 to -70 °C,  $K_{\pm}$  changes from a value equal to  $K_{\pm,t}$  (observed in THP) to  $K_{\pm,l}$  (observed in DME). A curve of such shape is predicted by equation 14.

The foregoing discussion and the examples given show the important effects of solvents and counterions on redox equilibria. The most dramatic effects are seen in the disproportionation equilibria described by the following reactions:



The equilibrium constants for reactions 17, 18, and 19 are  $K_{17}$ ,  $K_{18}$ , and  $K_{19}$ , respectively, and these equilibrium constants differ greatly. For tetraphenylethene [ $(C_6H_5)_2C=C(C_6H_5)_2$ ], which will be denoted by T, all three constants are known. They were determined from the results of spectrophotometric studies (7) of the system  $T, T^{\cdot-}, Na^+$  and  $T^{2-}, 2Na^+$  in THF, in conjunction with the conductometric studies that led to the values of  $K_{diss,1}$  and  $K_{diss,2}$  for reactions 20 and 21, respectively:



The absorption spectra of  $T^{\cdot-}$  and  $T^{2-}$  were determined. From the spectra of the mixtures of T,  $T^{\cdot-}$ , and  $T^{2-}$ , the apparent equilibrium constants,  $K_{ap}$ , were calculated:

$$K_{ap} = \{[\text{total T}] [\text{total } T^{2-}]\} / [\text{total } T^{\cdot-}]^2 \quad (22)$$

The dependence of  $K_{ap}$  on the equilibriums of reactions 18 and 19 leads to the following relationship:

$$1/K_{ap}^{1/2} = 1/K_{19}^{1/2} + (K_{diss,2}^{1/2}/K_{19}^{1/4})([T][\text{total } T^{2-}])^{-1/4} \quad (23)$$

Hence, plots of  $1/K_{ap}^{1/2}$  versus  $([T][\text{total } T^{2-}])^{-1/4}$ , shown in Figure 4, provide the values of  $K_{19}$  and  $K_{diss,2}$  for the three temperatures investigated. Direct conductometric studies confirmed the value of  $K_{diss,2}$  derived from Figure 4, and they also provided the value of  $K_{diss,1}$ . Because  $K_{19}/K_{18} = K_{diss,1}/K_{diss,2}$ , the value of  $K_{18}$  was determined, too. These results are summarized in the following table:

Temperature (°C)	$K_{19}$	$K_{18}$
20	400	3.2
0	39	0.72
-20	2.6	0.10

Figure 5 shows the temperature dependence of disproportionation of the sodium salts of radical anions of tetraphenylethene. Several conclusions may be drawn from these data. Both disproportionations are endothermic, as shown by their enthalpy changes ( $\Delta H$ ):  $\Delta H_{18} = 19 \pm 2$  kcal/mol, and  $\Delta H_{19} = 13 \pm 2$  kcal/mol. These observations may not be surprising because the electron–electron repulsion in the dianion may account for the endothermicity of the disproportionation. However, the large entropy gain ( $\Delta S$ )

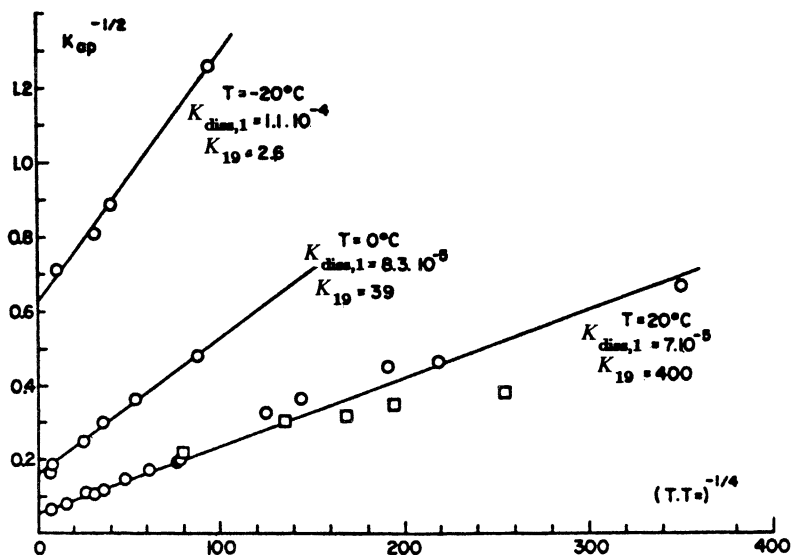
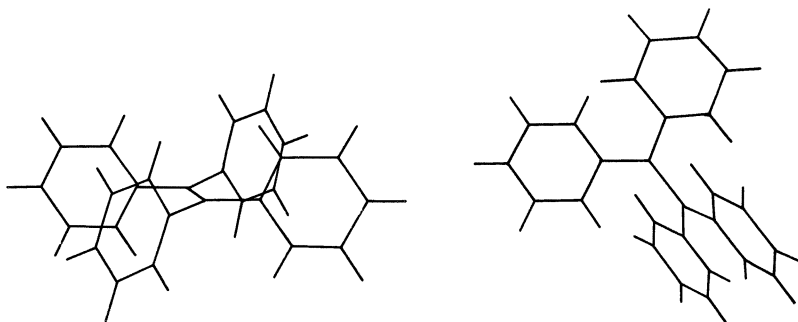


Figure 4. Plots of  $(K_{ap})^{-1/2}$  versus  $([T][T^{2-}])^{-1/4}$  for the disproportionation  $2 T^- \rightleftharpoons T + T^{2-}$  in THF containing  $Na^+$  counterions at 20, 0, and  $-20^\circ C$ . Key:  $\circ$ , data from reference 7;  $\square$ , data from reference 24. (Reproduced from reference 7. Copyright 1965 American Chemical Society.)

found for these processes, namely, 75 entropy units (eu) for  $\Delta S_{18}$  and 45 eu for  $\Delta S_{19}$ , may be surprising. The entropy gain is attributed to desolvation of the  $Na^+$  ions as the presumably loose pairs of radical anions are converted into tight associates of the dianions. The geometry of the radical-anion pair of tetraphenylethene, its C=C bond still rigid, prevents the close approach of  $Na^+$  ions to the bulky ends of the C=C bond. This situation accounts for the loose structure of the aggregate and allows for a full solvation of the cation by the molecules of THF. The doubly negative charge of the dianion and the release of rigidity of the C=C bond, which permits its twisting (see structure 1), result in a close approach of the  $Na^+$  ions to the carbanions.



Structure 1. Two views of the shape of the tetraphenylethene dianion.

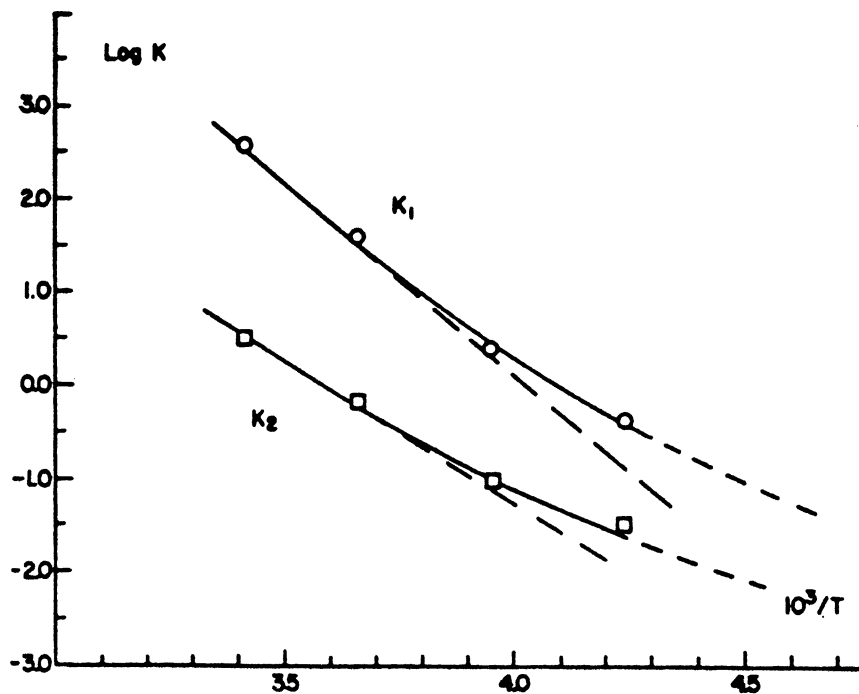


Figure 5. Temperature dependence of disproportionation of sodium salts of radical anions of tetraphenylethene. (Reproduced from reference 7. Copyright 1965 American Chemical Society.)

This condition causes desolvation of the  $\text{Na}^+$  ions and therefore a substantial gain of entropy of disproportionation. In view of this observation, the entropy changes in disproportionation of other aromatic hydrocarbons were investigated.

### *Thermodynamics of Disproportionation*

The thermodynamics of disproportionation can be readily studied with the device shown in Figure 6 (8). The device is composed of two bulbs linked by a narrow tube closed on both ends by sintered plates to prevent diffusion of solutions from one bulb to the other. One bulb contains a 50/50 solution of the hydrocarbon investigated and its radical anion in an ethereal solvent, whereas the other bulb contains a 50/50 solution of the radical anion and its dianion in the same solvent. Two platinum wires inserted in the bulbs act as electrodes, and the connecting tube, forming a liquid junction, is filled with a concentrated solution of a salt that contains the same cation as the solutions of the radical anions and dianions. The whole unit is evacuated and immersed in a Dewar flask containing a liquid kept at constant tem-

perature. A voltmeter of high resistance measures the potential established between the electrodes, which is equal to the redox potential of disproportionation, provided that the potential of the liquid junction is negligible and  $K_{\text{disp}} \ll 1$ .

The potentials are recorded for a series of alternately rising and decreasing temperatures. The results are reproducible. Plots of the measured potential ( $\Delta\epsilon$ ) versus  $t$  ( $^{\circ}\text{C}$ ) and of  $\log K_{\text{disp}}$  versus  $1/T$  (K) are shown in Figures 7 and 8. The slope of  $\Delta\epsilon$  versus  $t$  gives  $\Delta S$  of disproportionation, and the slope of  $\log K_{\text{disp}}$  versus  $1/T$  gives the corresponding  $\Delta H$ . The  $\Delta H$  and  $\Delta S$  values of disproportionation of radical anions of perylene in THF with different alkali cations are given in the following table (8):

<i>Cation</i>	<i>Temperature Range</i> ( $^{\circ}\text{C}$ )	$\Delta H$ ( <i>kcal/mol</i> )	$\Delta S$ ( <i>eu</i> )
$\text{Li}^+$	-55 to -40	13.6	0
$\text{Li}^+$	0 to +25	16.2	13.1
$\text{Na}^+$	-55 to +25	27.2	65.8
$\text{K}^+$	-55 to +25	14.2	22.2
$\text{Cs}^+$	-55 to +25	11.0	15.1

The nonmonotonic changes of  $\Delta H$  and  $\Delta S$  are the most interesting features of this table. The solvation of the small  $\text{Li}^+$  cation is very strong. This cation retains its solvation shell at low temperatures, whether it is associated with a radical anion or with a dianion; however, it loses some solvent molecules when the disproportionation takes place at ambient temperature. The larger  $\text{Na}^+$  cations keep their solvation shells when associated with radical anions but lose them when associated with dianions; this situation accounts for the large gain in entropy upon disproportionation. The big  $\text{K}^+$  and  $\text{Cs}^+$  cations are poorly solvated by THF whether they are free or associated with radical anions or dianions. Hence, not much entropy is gained by disproportionation. These conclusions about the state of solvation of alkali cations in THF were reported previously (9) and were deduced from the values of Stokes radii of these cations in THF. For example, conductometric studies (9) led to the determination of the Stokes radius of the  $\text{Na}^+$  cation in THF as  $>4 \text{ \AA}$ , but the radius of the large  $\text{Cs}^+$  cation was found to be only  $2.2 \text{ \AA}$ .

The importance of  $\Delta S$  of desolvation in disproportionation was reviewed in the foregoing discussion. However, the energetic effects resulting from the interaction of the cations with the negative species are even more important in increasing  $K_{\text{disp}}$  to values as high as a million. Table I shows the range of  $K_{\text{disp}}$  observed for naphthalene in various solvents containing different cations.

The crowding of two electrons into one orbital leads to a large increase

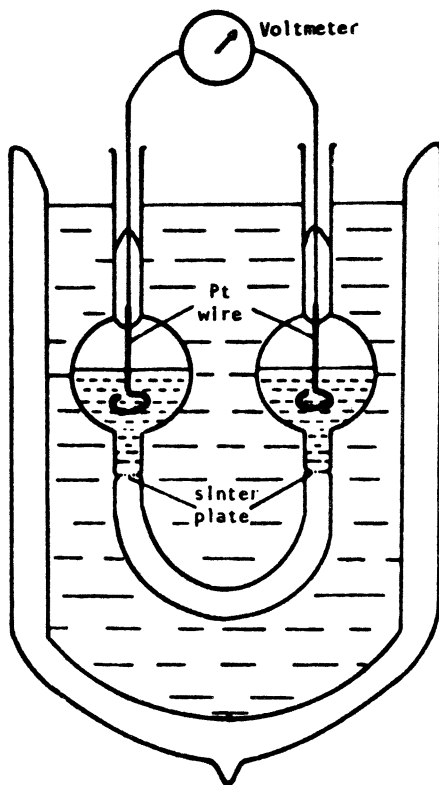
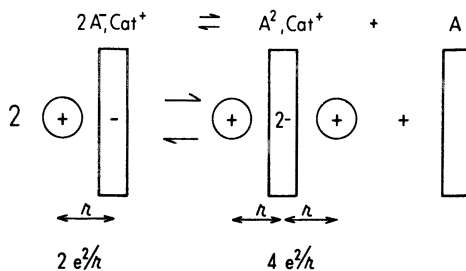


Figure 6. Device for determining the disproportionation constants of aromatic hydrocarbons as a function of temperature. (Reproduced from reference 8. Copyright 1977 American Chemical Society.)

in repulsion energy amounting to more than 100 kcal/mol; thus, the  $\Delta H$  of disproportionation is relatively low. However, the simple model depicted by Scheme I provides the basic reasons for more favorable disproportionation



Scheme I. The effect of Coulombic forces on the disproportionation of salts of radical anions.



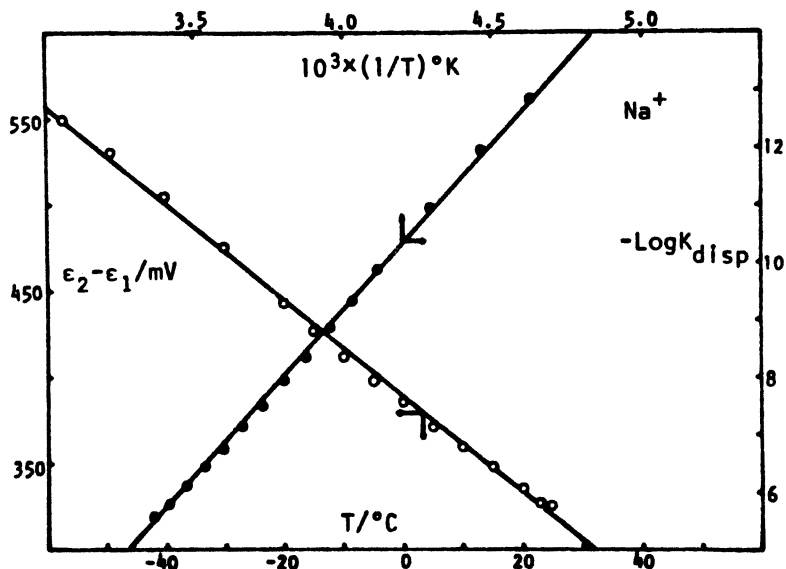


Figure 7. Plots of  $\Delta\epsilon$  versus  $t$  and of  $\log K_{disp}$  versus  $1/T$  for  $K^+$ ,  $Nap^{\bullet-}$  in THF.  $Nap^{\bullet-}$  denotes the naphthalene radical anion. (See text for description of the slopes.) (Reproduced from reference 22. Copyright 1978 American Chemical Society.)

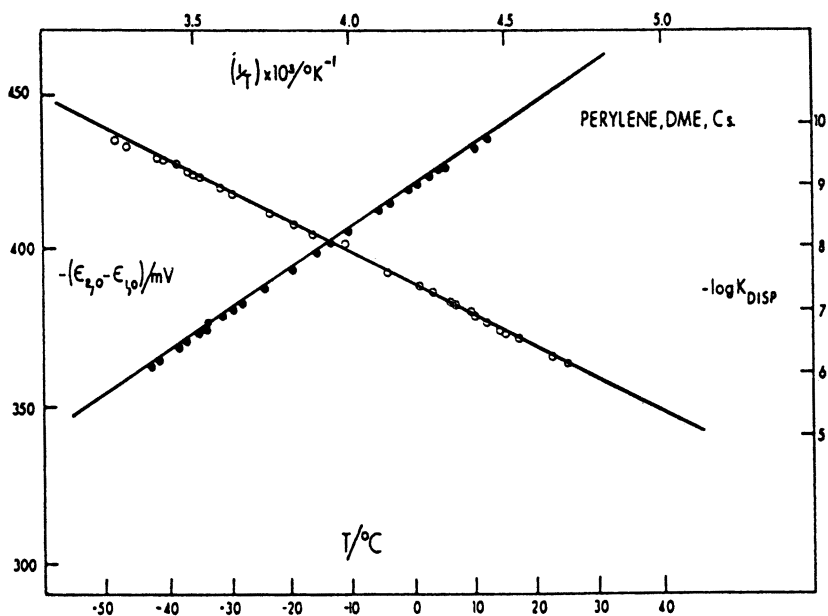


Figure 8. Plots of  $\Delta\epsilon$  versus  $t$  and of  $\log K_{disp}$  versus  $1/T$  for  $Cs^+$ ,  $Pe^{\bullet-}$  in DME.  $Pe^{\bullet-}$  denotes the perylene radical anion. (See text for description of the slopes.) (Reproduced from reference 22. Copyright 1978 American Chemical Society.)

**Table I.**  $K_{\text{disp}}$  of Naphthacene in Various Solvents Containing Different Cations at 25 °C

<i>Solvent</i> <sup>a</sup>	<i>Cation</i>	$K_{\text{disp}}$
DME	NBu <sub>4</sub> <sup>+</sup>	10 <sup>-13</sup>
THF	Li <sup>+</sup>	5.8 × 10 <sup>-9</sup>
THF	Na <sup>+</sup>	1.0 × 10 <sup>-5</sup>
THF	K <sup>+</sup>	4.6 × 10 <sup>-6</sup>
THF	Cs <sup>+</sup>	3.2 × 10 <sup>-6</sup>
DOX	Li <sup>+</sup>	6.6 × 10 <sup>-2</sup>
DOX	Na <sup>+</sup>	6.5 × 10 <sup>-2</sup>
DOX	K <sup>+</sup>	1.1 × 10 <sup>-2</sup>
DOX	Cs <sup>+</sup>	6.5 × 10 <sup>-3</sup>
EE	Li <sup>+</sup>	1.6 × 10
EE	Na <sup>+</sup>	1.2 × 10 <sup>-1</sup>
PhH	Li <sup>+</sup>	~10 <sup>6</sup>

<sup>a</sup>DOX is dioxane, EE is ethyl ether, and PhH is benzene.

in spite of the aforementioned electron–electron repulsion. Assume that the interaction between the anions and the cations in the pertinent aggregates is Coulombic and that the distance  $r$  separating the anions from the cations is the same in the radical anions as in the dianions. Then, the gain in Coulombic energy is

$$2(2e^2/r) - 2(e^2/r) - e^2/2r = (3/2)e^2/r \quad (24)$$

where  $e$  is the charge of an electron. This gain in energy amounts to more than 100 kcal/mol for  $r = 4 \text{ \AA}$ . In reality, the distance  $r$  is smaller in dianions than in radical anions, especially when the disproportionation results in the conversion of loose pairs into tight ones. Therefore, disproportionation constants as high as 10<sup>6</sup> are not surprising.

The tendency for disproportionation should be favored by localization of the negative charge in a relatively small space; hence,  $K_{\text{disp}}$  should increase as the size of the aromatic hydrocarbon decreases. This relationship is supported by the following values of  $K_{\text{disp}}$  for the indicated hydrocarbons in the system Li<sup>+</sup>, A<sup>-</sup> in ethyl ether at 25 °C (10): 1270, naphthalene; 1200, biphenylene; 42, anthracene; 16, naphthacene; 0.76, perylene; and 0.27, pyrene. These data are presented graphically in Figure 9.

Thus, three factors favor disproportionation: (1) the increase in entropy resulting from the conversion of loose pairs into tight pairs, (2) the Coulombic interaction of cations with anions, and (3) the increase in tightness of aggregates resulting from expulsion of molecules of solvents that have relatively low solvating power.

Finally, the enormous range of the values of  $K_{\text{disp}}$  requires the use of different experimental techniques to determine these values. For values of  $K_{\text{disp}}$  between 10<sup>-16</sup> and 10<sup>-2</sup>, potentiometric or polarographic techniques

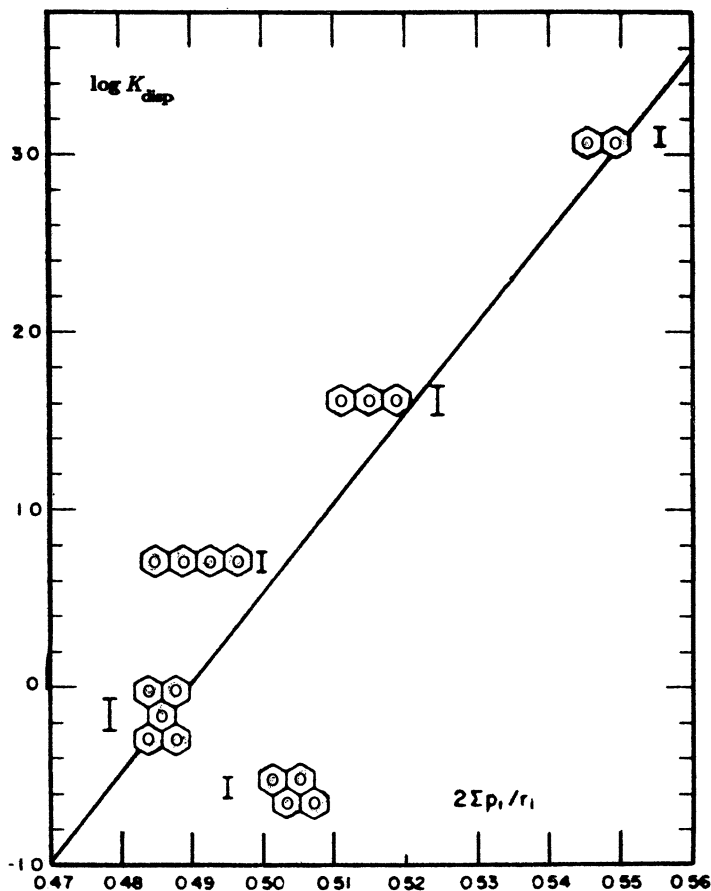


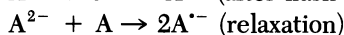
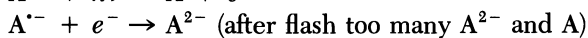
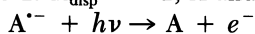
Figure 9. Plot of  $\log K_{\text{disp}}$  of  $\text{Li}^+$  salts of radical anions of aromatic hydrocarbons in ethyl ether versus the average Coulombic interaction energy of the negative charge with cations. The average energy is calculated as  $\sum e^2 \rho_i / r_i$ , where the electron charge ( $e$ ) is the charge of an electron,  $\rho_i$  is the Hückel charge density on the  $i$ th carbon, and  $r_i$  is the distance of the  $i$ th carbon from the cation located 4 Å above the center of the pertinent hydrocarbon. (Reproduced from reference 10. Copyright 1976 American Chemical Society.)

are applicable; for values between  $10^{-2}$  and  $10^2$ , spectrophotometric methods are the most convenient; and for values between  $10^2$  and  $10^6$ , electron spin resonance (ESR) techniques are used. ESR techniques take advantage of the radical anions being the only paramagnetic species in the systems studied and therefore the only species detected by ESR. Because the concentration of radical anions is low when  $K_{\text{disp}} > 10^2$ , their presence hardly affects the optical spectra of the investigated solutions; this situation allows for spectrophotometric determination of the concentration of the dianions.

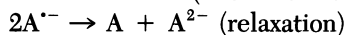
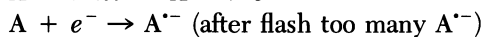
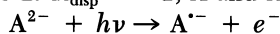
### ***Kinetics and Mechanism of Disproportionation***

The kinetics of disproportionation is conveniently studied by flash photolysis. A flash of visible light leads to the photoejection of electrons from radical anions or dianions (11). Consider an equilibrated system involving an aromatic hydrocarbon, its radical anion, and its dianion. A flash of light ejects electrons from the dianions and radical anions to convert the dianions into radical anions and the radical anions into the parent hydrocarbon. The ejected electrons are rapidly captured, mainly by the hydrocarbons; this process converts the hydrocarbons into radical anions in less than a few milliseconds. The following cases should be considered:

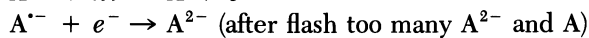
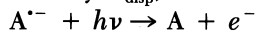
**Case 1.**  $K_{\text{disp}} \ll 1$ ; A and  $A^{\cdot-}$  present; negligible  $A^{2-}$ :



**Case 2.**  $K_{\text{disp}} \gg 1$ ; A and  $A^{2-}$  present; negligible  $A^{\cdot-}$ :



**Case 3.** Any  $K_{\text{disp}}$ ;  $A^{\cdot-}$  and  $A^{2-}$  present; negligible A:



The flash perturbs the disproportionation equilibrium regardless of the composition of the system, and the relaxation to equilibrium allows the kinetics of disproportionation to be studied. A typical difference spectrum, recorded at 25  $\mu\text{s}$  after a flash of perylene radical anions ( $\text{Pe}^{\cdot-}$ ), is shown in Figure 10. This spectrum reveals an increase in concentration of perylene and its dianions and a decrease in concentration of perylene radical anions. Kinetic data are provided by the return of the absorbance signal at any maximum wavelength ( $\lambda_{\text{max}}$ ) to the base line. The results, in conjunction with the known  $K_{\text{disp}}$ , allow calculation of  $k_1$  ( $A^{2-} + A \rightarrow 2A^{\cdot-}$ ) and  $k_2$  ( $2A^{\cdot-} \rightarrow A^{2-} + A$ ), which are the forward and backward disproportionation constants, respectively (12, 13). Some constants derived from such experiments are collected in Table II. For  $K_{\text{disp}} \ll 1$ , the rates of the exothermic electron transfer from dianions to their parent hydrocarbons are close to the diffusion limits; on the other hand, the rate constants of disproportionation are determined by the equilibrium constants. However, for larger  $K_{\text{disp}}$  that are still  $< 1$ , even the exothermic electron-transfer reaction requires activation energy, presumably because of changes in the degree of solvation. For  $K_{\text{disp}} > 1$ ,  $k_1$  is larger than  $k_2$ .

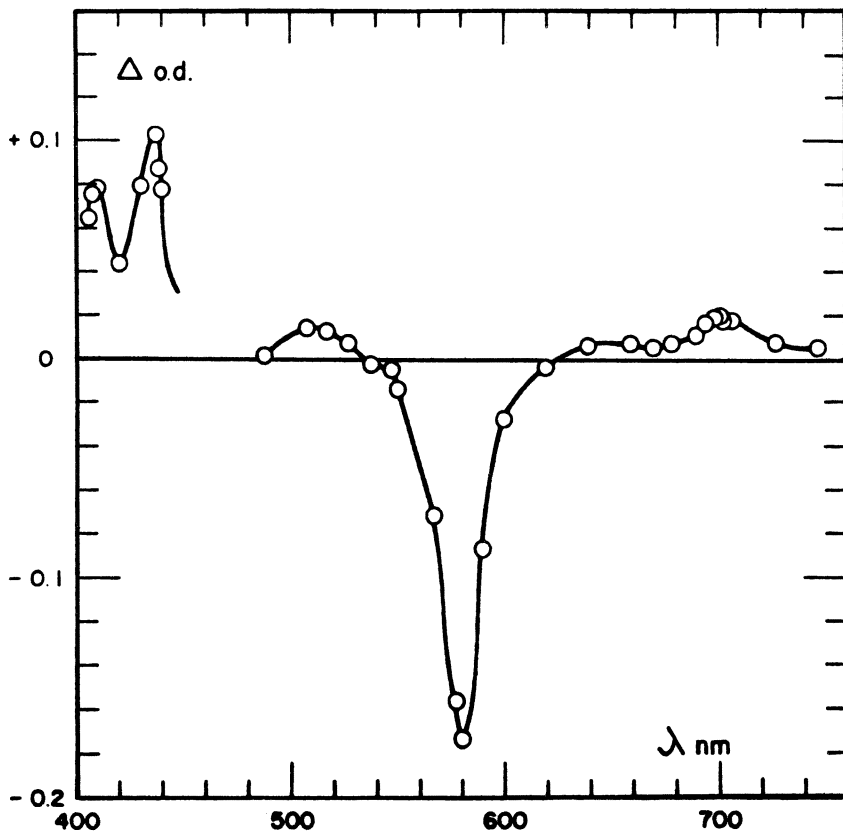
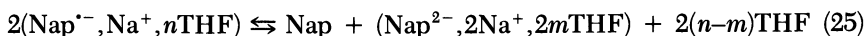


Figure 10. The difference spectrum of flashed solution of  $\text{Na}^+, \text{Pe}^{\bullet-}$  in THF 100  $\mu\text{s}$  after a flash. Note the bleaching due to photodissociation of the perylene radical anion and the absorbance resulting from the formation of an excess of perylene. (Reproduced with permission from reference 23. Copyright 1976 North-Holland.)

**Reaction of Sodium Salt of Naphthacene Dianions with Naphthacene.** An example of electron transfer that reveals the role of solvation in such a process is the reaction of the sodium salt of naphthacene dianions ( $\text{Nap}^{2-}$ ) with naphthacene ( $\text{Nap}$ ) in benzene (15). To increase the solubility of this salt in benzene, small amounts of THF are added to the solution. Apparently, more molecules of THF solvate the  $\text{Na}^+$  cations associated with naphthacene radical anions ( $\text{Nap}^{\bullet-}$ ) than the  $\text{Na}^+$  cations aggregated with  $\text{Nap}^{2-}$  dianions. Hence, the disproportionation equilibrium for this system is described by the following reaction:



**Table II. Rate Constants ( $k_1$  and  $k_2$ ) for the Disproportionation of Perylene Radical Anions in Various Solvents Containing Different Counterions at 25 °C**

<i>Solvent</i>	<i>Counterion</i>	$k_1$ ( $M \cdot s$ )	$k_2$ ( $M \cdot s$ )
THF	Li <sup>+</sup>	$3.6 \times 10$	$6.3 \times 10^9$
THF	Na <sup>+</sup>	$5.5 \times 10^4$	$5.5 \times 10^9$
THF	K <sup>+</sup>	$3.0 \times 10^4$	$6.5 \times 10^9$
THF	Cs <sup>+</sup>	$2.5 \times 10^4$	$7.8 \times 10^9$
DOX	Li <sup>+</sup>	$6.0 \times 10^6$	$1.1 \times 10^8$
DOX	Na <sup>+</sup>	$2.0 \times 10^7$	$3.1 \times 10^8$
DOX	K <sup>+</sup>	—	—
DOX	Cs <sup>+</sup>	—	—
EE	Li <sup>+</sup>	$5.9 \times 10^7$	$3.6 \times 10^6$
EE	Na <sup>+</sup>	$2.4 \times 10^8$	$2.0 \times 10^9$

NOTE: — indicates that the relaxation was too fast to be observed. SOURCE: Adapted from reference 14.

where  $n > m$ . The disproportionation equilibrium constant corresponding to reaction 25 is the following:

$$K_{\text{disp}} = [\text{Nap}][\text{Nap}^{2-}, 2\text{Na}^+]/[\text{Nap}^{\cdot-}, \text{Na}^+]^2/[\text{THF}]^{2(m-n)} \quad (26)$$

The apparent disproportionation constant corresponding to reaction 25 is the following:

$$K_{\text{dispa}} = [\text{Nap}][\text{Nap}^{2-}, 2\text{Na}^+]/[\text{Nap}^{\cdot-}, \text{Na}^+]^2 \quad (27)$$

The plot of  $\log K_{\text{dispa}}$  versus  $\log [\text{THF}]$  shown in Figure 11 is linear and has a slope of  $-2$ . This result implies that  $m - n = 1$ , that is, one additional molecule of THF solvates each  $\text{Na}^+$  cation as the dianions of naphthacene are converted into radical anions.

Two routes are available for reaction 25, as shown by Scheme II. Either the fully solvated radical anions disproportionate and yield the oversolvated dianions, which in turn rapidly desolvate (route b), or the fully solvated radical anions become desolvated and then in a rate-determining step undergo disproportionation (route a). Because the concentration of THF is relatively high ( $10^{-2}$ – $10^{-1}$  M) and the concentrations of Nap and its reduction products are on the order of  $10^{-6}$  M, the properly solvated species, namely,  $\text{Nap}^{\cdot-}, \text{Na}^+, (n+1)\text{THF}$  and  $\text{Nap}^{2-}, 2\text{Na}^+, 2n\text{THF}$ , remain in equilibrium with their under- or oversolvated counterparts. Hence, the rate of the forward reaction through route a is determined by  $k_2 K_a / [\text{THF}]^2$ ; that is, the rate is retarded by THF. However, the rate of the corresponding backward reaction that is governed by  $k_{-2}$  is independent of  $[\text{THF}]$ . For the disproportionation proceeding through route b, the rate of the forward reaction that is governed by  $k_1$  is also independent of  $[\text{THF}]$ . However, the rate of

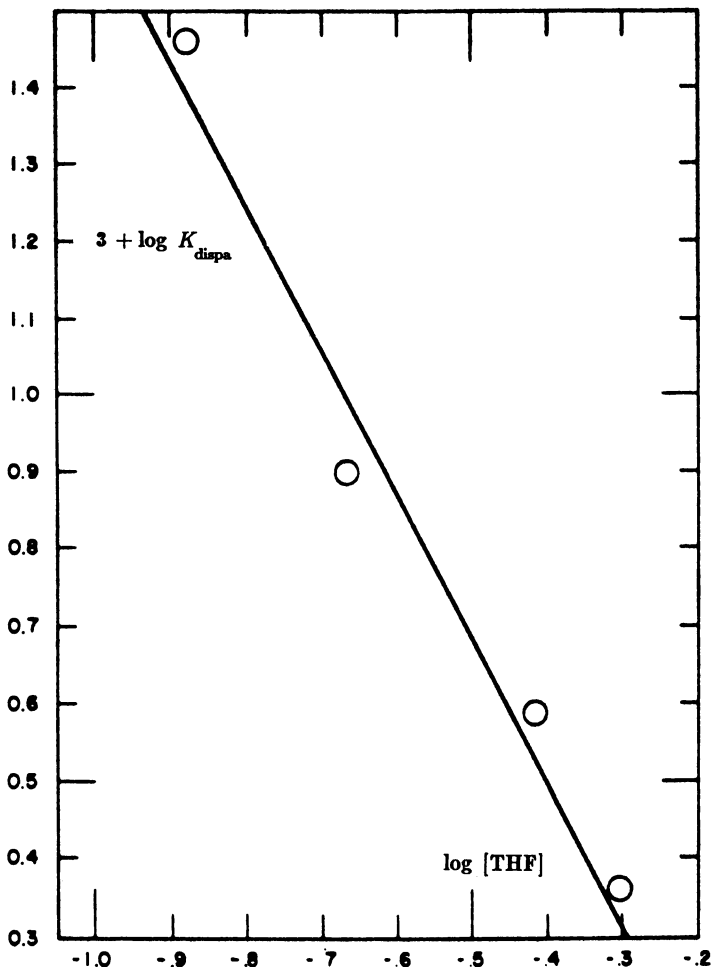
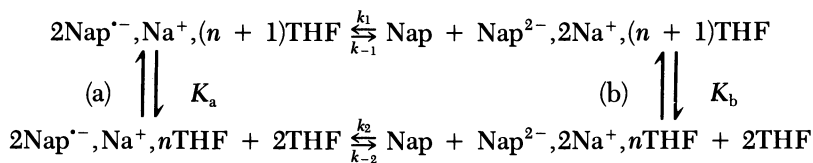


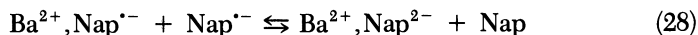
Figure 11. Plot of  $\log K_{dispa}$  versus  $\log [THF]$  for  $Na^+, Nap^-$  in benzene. The slope is  $-2$ . (Reproduced from reference 15. Copyright 1976 American Chemical Society.)

the corresponding backward reaction is proportional to  $k_{-1}[THF]^2/K_b$ ; that is, the rate is accelerated by THF. Thus, kinetic studies of this disproportionation allow these two alternatives to be distinguished, and the results demonstrate that the reaction proceeds through route b.

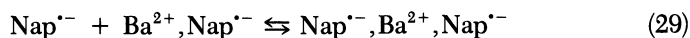


Scheme II.

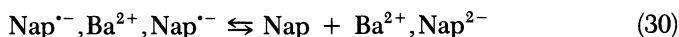
**Flash Photolysis of  $\text{Ba}^{2+}, \text{Nap}^{2-}$ .** Another example of mechanistic studies of disproportionation is furnished by flash photolysis of  $\text{Ba}^{2+}, \text{Nap}^{2-}$ . The equilibrated system of  $\text{Nap}$  and  $\text{Ba}^{2+}, \text{Nap}^{2-}$  contains an extremely low concentration of radical anions present in the form of an equimolar mixture of  $\text{Nap}^{\cdot-}$  and  $\text{Ba}^{2+}, \text{Nap}^{\cdot-}$ . A flash of light ejects electrons from  $\text{Ba}^{2+}, \text{Nap}^{2-}$ , which are then captured by  $\text{Nap}$ . Thus,  $\text{Nap}^{\cdot-}$  and  $\text{Ba}^{2+}, \text{Nap}^{\cdot-}$  are the primary products of photolysis. The return to equilibrium results either from the collision of  $\text{Nap}^{\cdot-}$  with  $\text{Ba}^{2+}, \text{Nap}^{\cdot-}$  from the right



or from the left



followed by the intramolecular transfer and the dissociation



The distinction among these alternatives is feasible if the dissociation (reaction 30) and therefore the association are slow in comparison with the rate of the electron transfer (reaction 29).

**Other Studies Using Flash Photolysis.** Flash photolysis allows the study of direct electron capture (17). A flash of light may eject an electron from  $\text{A}^{\cdot-}, \text{Cat}^+$ , for example. The primary products are a solvated electron ( $e^-$ ) and an adduct ( $\text{A}, \text{Na}^+$ ). The adduct may dissociate before electron capture and lead to the following reaction:



Or,  $e^-$  may be captured by  $\text{Cat}^+$  and yield an alkali atom (Alk), which in turn will react with the aromatic hydrocarbon:



Such reactions can be investigated by pulse radiolysis.

Studies of gaseous electron capture taking place in a plasma were reported by Wentworth et al. (18). The equilibrium established in a plasma between  $e^-$ ,  $\text{A}$ , and  $\text{A}^{\cdot-}$  allowed the determination of the absolute electron affinities of the aromatic hydrocarbons in the gas phase.

The rates of electron transfer between an aromatic radical anion, for example,  $\text{B}^{\cdot-}, \text{Cat}^+$ , and a hydrocarbon,  $\text{A}$ , of higher electron affinity than  $\text{B}$  were studied by flash photolysis (11). Flashing a mixture of  $\text{A}^{\cdot-}, \text{Cat}^+$  with



B of lower electron affinity than A yields  $B^{\cdot-}$ ,  $Cat^+$  and A, and the return to the initial state is then recorded on an oscilloscope.

### Unstable Radical Anions

**Isomerization.** Finally, some investigations of unstable radical anions will be discussed. Radical anions of *cis*-stilbene rapidly isomerize to radical anions of *trans*-stilbene; therefore, their spectra or relative electron affinities cannot be studied by conventional techniques. Flashing a solution of perylene radical anions mixed with *cis*-stilbene yields *cis*-stilbene radical anions, which persist for 200–300  $\mu s$  before the ejected electrons are recaptured by the perylene formed by the photolysis. The difference spectrum of the photolyzed solution is shown in Figure 12. The concentration of the *cis*-stilbene radical anions formed can be determined by the degree of bleaching the absorption peak of the perylene radical anions. The absorption spectrum of *cis*-stilbene radical anions can also be determined in this way (19). Similar experiments, results of which are shown in Figure 13, permit the determination of the absorption spectrum of *trans*-stilbene radical anions. Because this spectrum has been established by other methods, the reliability of the flash-photolytic method can be determined by comparing the differ-

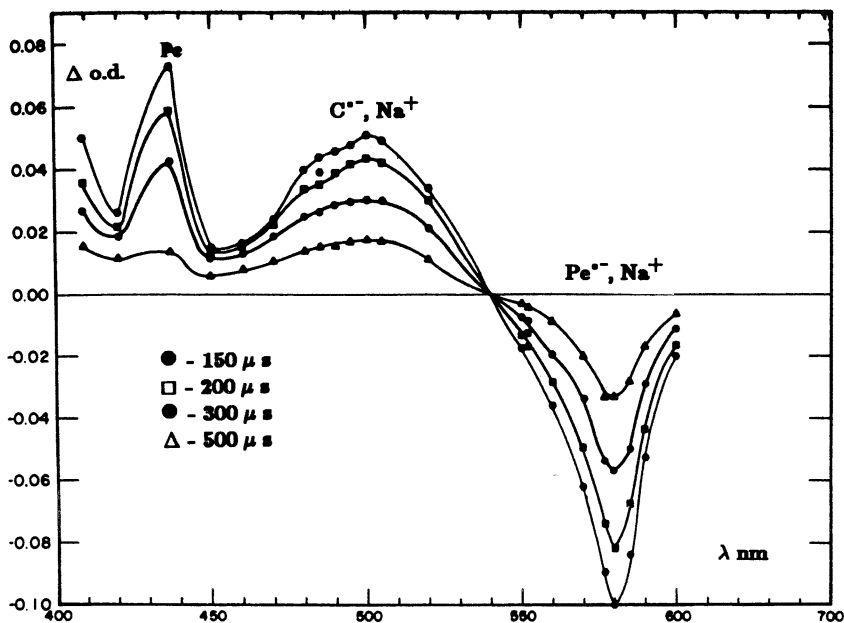


Figure 12. Difference spectra of a flashed solution of  $Na^+, Pe^{\cdot-}$  in THF containing *cis*-stilbene recorded as time progressed after the flash. (Reproduced from reference 19. Copyright 1977 American Chemical Society.)

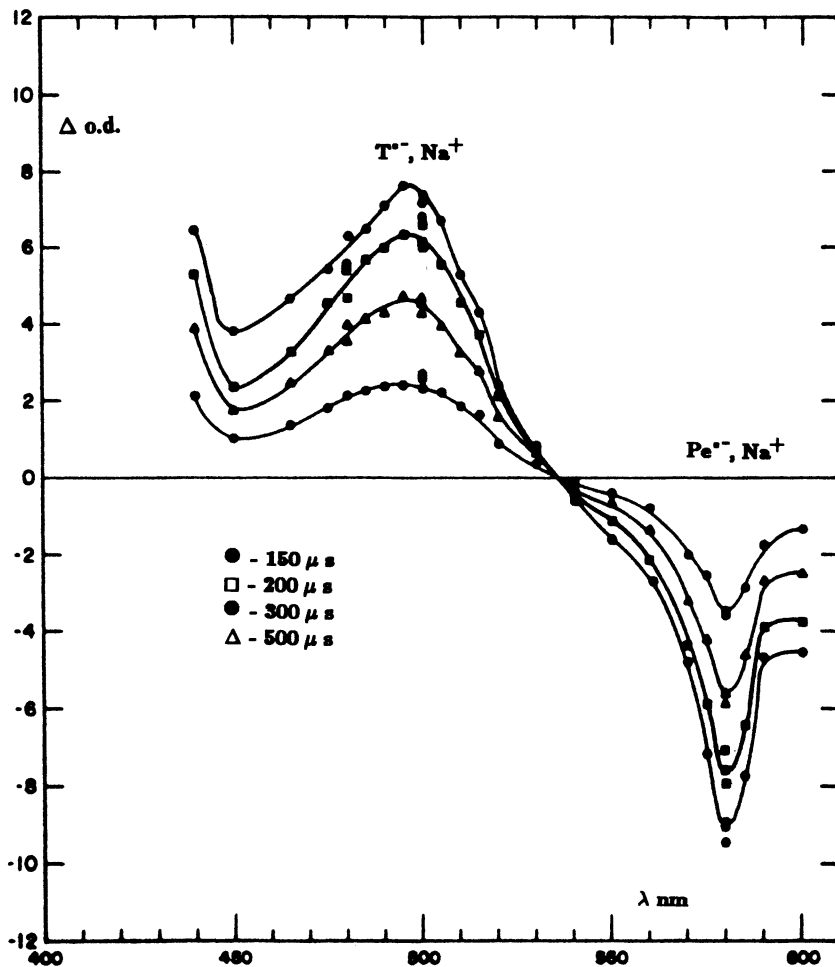


Figure 13. The same series of spectra shown in Figure 12 but for *trans*-stilbene instead of *cis*-stilbene. (Reproduced from reference 19. Copyright 1977 American Chemical Society.)

ence spectrum with the established spectrum. Both spectra are depicted in Figure 14. The spectra differ mainly in their intensity; that is, the extinction coefficient at  $\lambda_{\max}$  is much greater for *trans*-stilbene than for *cis*-stilbene (19).

The molar absorptances of both isomeric radical anions of stilbene can be used to determine the equilibrium constant of the following process:



A solution of perylene radical anions containing a 1:1 mixture of *cis*- and *trans*-stilbenes is flash photolyzed. The ejected electrons are captured by

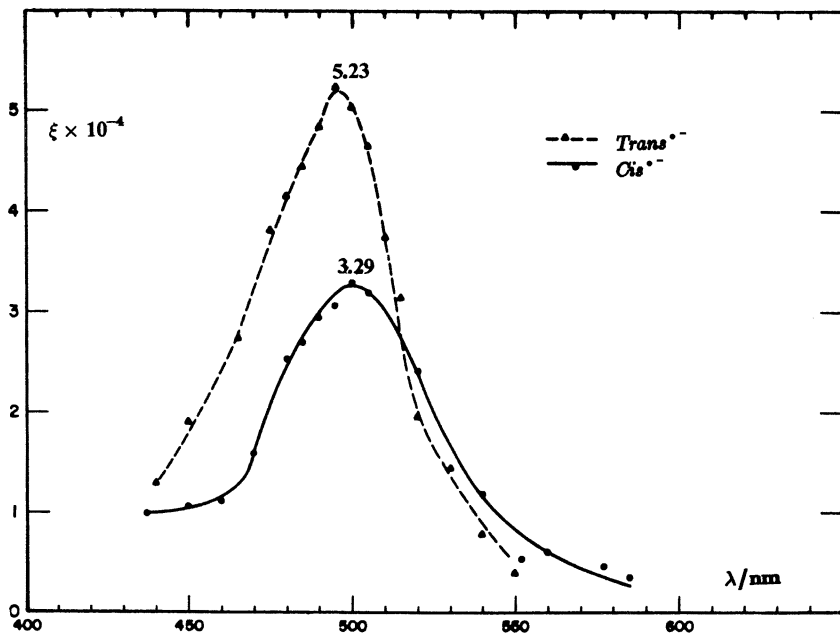
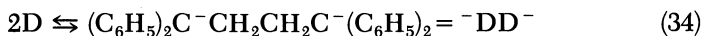


Figure 14. Absorption spectra of *cis*- and *trans*-stilbene radical anions determined by flash photolysis. (Reproduced from reference 19. Copyright 1977 American Chemical Society.)

the stilbenes to form their radical anions. Because the parent hydrocarbons are present at a relatively large concentration, the relaxation time of equilibrium (reaction 33) is extremely short and is maintained all the time. Hence, the extent of absorption at  $\lambda_{\max}$  of stilbene radical anions, compared with the bleaching of perylene radical anions, determines the ratio of the *cis*-stilbene radical anion to the *trans*-stilbene radical anion because the extinction coefficients of both isomers are known. This ratio gives the equilibrium constant of reaction 33, which is about 5.

**Dimerization.** The last problem to be discussed concerns the radical anions of 1,1-diphenylethene  $[(C_6H_5)_2C=CH_2]$ , which will be denoted by D. These radical anions, like most radical anions of ethylene derivatives, undergo rapid dimerization to yield their respective dimeric dianions:



The dimers are stable and do not add D because of excessive steric strain. A solution of the dimers containing unreduced D is flash photolyzed. The dimers decompose to form radical anions of D, as revealed by the difference spectrum shown in Figure 15. In the dark period following the flash, di-

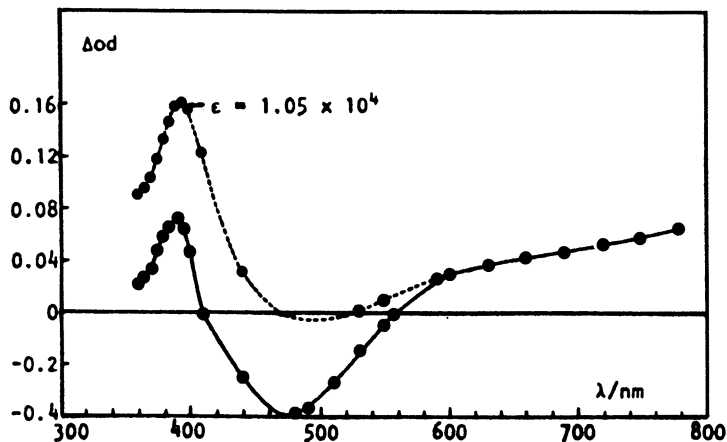
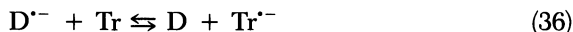


Figure 15. The difference spectrum of flashed dimeric dianions of 1,1-diphenylethene and the absorption spectrum of radical anions of 1,1-diphenylethene. (Reproduced from reference 20. Copyright 1977 American Chemical Society.)

merization of the radical anions occurs. The reaction proceeds according to second-order kinetics (20), as demonstrated by the plot of the reciprocal of optical density versus time shown in Figure 16. The rate constants of dimerization depend on the nature of the counterions. Dimerization constants  $[(\text{mol}\cdot\text{s})^{-1} \times 10^8]$  of D radical anions in THF at 25 °C are as follows for the indicated counterions: 1.2,  $\text{Li}^+$ ; 3.5,  $\text{Na}^+$ ; 10.0,  $\text{K}^+$ ; and 30.0,  $\text{Cs}^+$ .

The relative electron affinity of D was determined by a procedure similar to that used in studies of the stilbenes (20). A solution of  $\text{DD}^-$  containing a mixture of biphenyl (B) or triphenylene (Tr) and D of predetermined proportions was flashed. The ejected electrons were captured by D or by B or Tr, and the following equilibria were established:



These equilibria are established and maintained during the dimerization of  $\text{D}^{\cdot-}$ . The addition of B or Tr slows the bimolecular dimerization because the concentration of  $\text{D}^{\cdot-}$  is reduced as a result of the equilibria of reactions 35 and 36. The decrease of the slope of the curve  $1/(\text{optical density})$  versus time, compared with that seen in Figure 16, that is obtained, in the absence of the added hydrocarbons, provides the data needed to determine the equilibrium constants of the equilibria of reactions 35 and 36. Because the relative electron affinity of B or Tr is known, the electron affinity of D can be calculated. However, it depends on the cation; for example, for  $\text{Na}^+$  in THF,  $\Delta\epsilon$  for D and Tr is 24 mV. The redox potential of D is higher than that of B but lower than that of Tr.

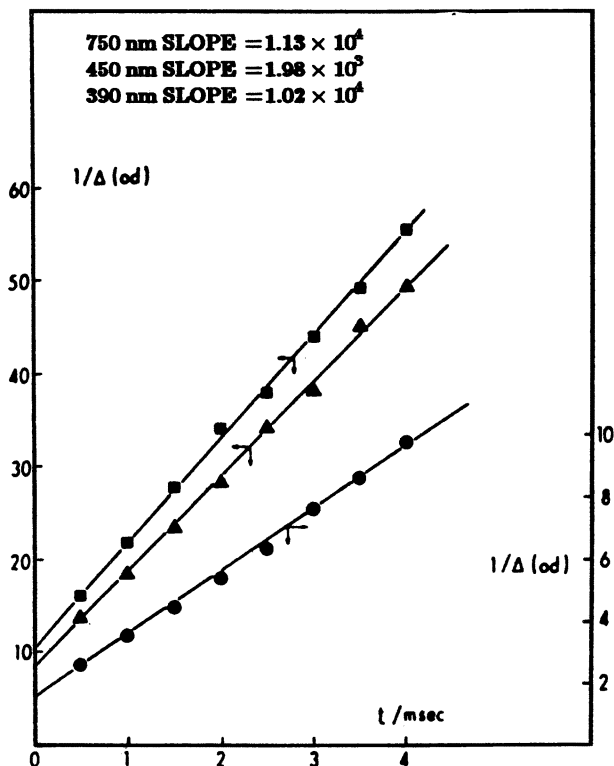


Figure 16. The plots of  $1/\text{optical density}$  of a bleached solution of the dimeric dianions of 1,1-diphenylethene as a function of time recorded at various  $\lambda_{\text{max}}$  of the difference spectrum. (Reproduced from reference 20. Copyright 1977 American Chemical Society.)

## Summary and Conclusions

This review described a range of problems, both thermodynamic and kinetic, that can be studied quantitatively by using the phenomenon of electron photoejection. It is hoped that the approaches described will be used by other researchers to solve some of the problems related to the chemistry and physics of radical anions and dianions.

## References

1. Hoijtink, G. J.; de Boer, E.; van Meij, P. H.; Weiland, W. P. *Rec. Trav. Chim.* **1956**, *75*, 487.
2. Paul, D. E.; Lipkin, D.; Weissman, S. I. *J. Am. Chem. Soc.* **1956**, *78*, 116.
3. Jagur-Grodzinski, J.; Feld, M.; Yang, S. L.; Szwarc, M. *J. Phys. Chem.* **1965**, *69*, 628.

4. Szwarc, M. *Ions and Ion-Pairs in Organic Reactions* Wiley: New York, 1972; Vol. I.
5. Slater, R. V.; Szwarc, M. *J. Phys. Chem.* **1965**, *69*, 4124.
6. Karasawa, Y.; Levin, G.; Szwarc, M. *Proc. R. Soc.* **1971**, *A 326*, 53.
7. Roberts, R. C.; Szwarc, M. *J. Am. Chem. Soc.* **1965**, *87*, 5542.
8. Wang, H. C.; Levin, G.; Szwarc, M. *J. Am. Chem. Soc.* **1977**, *99*, 5056.
9. Carvajal, C.; Tolle, K. J.; Smid, J.; Szwarc, M. *J. Am. Chem. Soc.* **1965**, *87*, 5548.
10. Levin, G.; Holloway, B. E.; Szwarc, M. *J. Am. Chem. Soc.* **1976**, *98*, 5707.
11. Rame, G.; Fisher, M.; Claesson, S.; Szwarc, M. *Proc. R. Soc.* **1972**, *A 327*, 467.
12. Levin, G.; Claesson, S.; Szwarc, M. *J. Am. Chem. Soc.* **1972**, *94*, 8672.
13. Lundgren, B. Levin, G.; Claesson, S.; Szwarc, M. *J. Am. Chem. Soc.* **1975**, *97*, 262.
14. Szwarc, M.; Levin, G. *J. Photochem.* **1976**, *5*, 119.
15. Pola, J.; Levin, G.; Szwarc, M. *J. Phys. Chem.* **1976**, *80*, 1690.
16. De Groof, B.; Levin, G.; Szwarc, M. *J. Am. Chem. Soc.* **1977**, *99*, 474.
17. Fisher, M.; Rämme, G.; Claesson, S.; Szwarc, M. *Proc. R. Soc.* **1972**, *A 327*, 481.
18. Wentworth, W. E.; Chen, E.; Lovelock, J. E. *J. Phys. Chem.* **1966**, *70*, 445.
19. Wang, H. C.; Levin, G.; Szwarc, M. *J. Am. Chem. Soc.* **1977**, *99*, 2642.
20. Wang, H. C.; Lillie, S.; Slomkowski, S.; Levin, G.; Szwarc, M. *J. Am. Chem. Soc.* **1977**, *99*, 4608.
21. Wang, H. C.; Levin, G.; Szwarc, M. *J. Am. Chem. Soc.* **1978**, *100*, 6137.
22. Jachimowicz, F.; Wang, H. C.; Levin, G.; Szwarc, M. *J. Phys. Chem.* **1978**, *82*, 1371.
23. Lillie, E. D.; van Woteghem, D.; Levin, G.; Szwarc, M. *Chem. Phys. Lett.* **1976**, *41*, 216.
24. Garst, J. F.; Zabolotny, E. R. *J. Am. Chem. Soc.* **1965**, *87*, 495.

RECEIVED for review September 29, 1986. ACCEPTED February 9, 1987.

# Single Crystals of Alkali Aromatic Ion Pairs

E. de Boer and M. C. M. Gribnau

Research Institute of Materials, University of Nijmegen, Toernooiveld, 6525 ED Nijmegen, The Netherlands

*The preparation and the crystal structures of single crystals of alkali aromatic ion pairs are discussed. A close relationship was found between the ion-pair structures in solution and in the solid state. The physical properties of the pseudo-two-dimensional magnetic alkali biphenyl crystals are reviewed. The effect of spin diffusion manifests itself clearly in the line width and line shape of the exchange-narrowed electron spin resonance (ESR) line. The monoanions of cyclooctatetraene, produced by X-ray irradiation, rotate rapidly about their eightfold axes. At 20 K this rotation is frozen, and an alternating spin density distribution is found around the ring. The equilibrium position of the monoanion is rotated by 22.5° compared with the equilibrium position of the dianion.*

**T**WO DISTINCT FORMS OF ION PAIRS IN SOLUTION were suggested by Sadek and Fuoss (1) and Winstein et al. (2) in 1954. These forms are now customarily referred to as either (a) loose or solvent-separated ion pairs or (b) tight or contact ion pairs. During the past few decades, these species have been studied in great detail with optical and magnetic resonance techniques and conductivity methods. Numerous experiments carried out by Szwarc (3) showed that ion pairs are well-defined chemical species with their own physical properties. For instance, the rate of anionic polymerization reactions can change by a factor of  $10^3$  from "free" (unassociated) solvated ionic species to completely associated ones (3).

The information obtained about ionic structures in solution is necessarily indirect. This information has been inferred from shifts in absorption bands, changes in chemical shifts, hyperfine splitting constants, changes in con-

ductance as concentration changes, and from a detailed analysis of measured line widths. To obtain direct information about ionic structures in solution, we attempted to prepare single crystals of alkali aromatic ion pairs. In 1970 Canters et al. (4) succeeded in preparing single crystals of the paramagnetic alkali biphenyl (Bp) ion pairs. Their crystal structures were successfully elucidated by X-ray diffraction. They appeared to be loose or solvent-separated ion pairs. Later, single crystals of potassium cations and cyclooctatetraene (COT) anions (5) and rubidium cations and COT anions (6) were prepared. Their crystal structures were classified as tight or contact ion pairs.

In this chapter we shall review the crystal structures and physical properties of the paramagnetic alkali biphenyl ion pairs, namely, sodium cations and Bp anions in triglyme ( $\text{NaBp}\cdot 2\text{Tg}$ ;  $\text{Tg} = \text{triglyme} = \text{CH}_3\text{O}(\text{CH}_2\text{CH}_2\text{O})_3\text{CH}_3$ ), potassium cations and Bp anions in tetraglyme ( $\text{KBp}\cdot 2\text{Ttg}$ ;  $\text{Ttg} = \text{tetraglyme} = \text{CH}_3\text{O}(\text{CH}_2\text{CH}_2\text{O})_4\text{CH}_3$ ), and rubidium cations and Bp anions in  $\text{Ttg}$  ( $\text{RbBp}\cdot \text{Ttg}$ ). Furthermore, we shall discuss the crystal structures of the diamagnetic ion pairs of potassium cations–COT anions and rubidium cations–COT anions. Irradiation of these crystals by X-rays produces the monoanion of COT. We will discuss its physical properties. Finally, we shall briefly describe the crystal structure of sodium cations and terphenyl anions in tetrahydrofuran ( $\text{Na}_2\text{Tp}\cdot 6\text{THF}$ , where  $\text{Tp} = \text{terphenyl}$  and  $\text{THF} = \text{tetrahydrofuran}$ ). The crystal structures of the ion pairs confirm the predictions made for them in solution.

### Experimental Details

All combinations of alkali metals with biphenyl were investigated in seven different solvents, namely, tetrahydropyran (THP), THF, 2-methyltetrahydrofuran, 1,2-dimethoxyethane, diglyme (Dg), Tg, and Ttg. Only four combinations produced single crystals: LiBp in THP, NaBp in Tg, KBp in Ttg, and RbBp in Ttg. All of these crystals are deep blue. The crystals of LiBp·THP form diamond-shaped plates and can grow to about  $4 \times 15 \times 15$  mm. However, these crystals are very difficult to handle because of the high volatility of the solvent molecules. In a non-solvent-saturated atmosphere, these crystals lose solvent molecules and subsequently decompose. Decomposition is no problem for the crystals containing glyme molecules because of the low vapor pressure, although the extreme sensitivity of the crystals to air and moisture must be accommodated. The NaBp·2Tg crystals form rectangular-shaped plates and can grow as large as  $2 \times 7 \times 25$  mm. The KBp·2Ttg crystals form closely packed small plates, and the RbBp·2Ttg crystals are needles about 1 mm thick and 5–7 mm long. The NaBp crystals melt at about 55 °C, but the crystals of the other three systems decompose before melting because the solvent evaporates upon heating.

To prepare the aforementioned single crystals, solutions containing 0.5–1.0 M alkali biphenyl in the appropriate solvents were cooled from 30 °C at a rate of 1 °C/h. Because the anions are sensitive to air and moisture, vacuum techniques, as described in the literature (7) were applied. For the X-ray and magnetic measurements, the crystals were mounted in thin glass capillaries with the aid of a glovebox, which contains less than 1 part per million (ppm) of oxygen and water. Because of the low melting points, the manipulations were carried out at about



-20 °C. For this purpose, a silver-plated table, cooled by an ultracryostat, was used. The thin-walled tubes were fixed onto this table. The crystals were pushed into these tubes with a thin constantan wire, and the tubes were then sealed with a hot tungsten wire.

Single crystals of COT were prepared in the following way. To a 0.8 M alkali (K or Rb) COT solution in THF, a mixture of diglyme and THF (1:2) was slowly added. After 1 day, purple single crystals separated from the solution. To get large single crystals (5 × 5 × 3 mm), the small crystals were recrystallized from THF under vacuum. The THF was evaporated very slowly from the solution by maintaining a temperature difference of 0.5 °C between the solution and the distillate. The temperature difference was kept constant by two copper blocks that could be cooled or heated. The heating current was controlled by a feedback system with thermistors as temperature probes.

The single crystal of Tp was prepared by slowly cooling a solution of Na<sub>2</sub>Tp in THF in the same fashion as the alkali biphenyl solutions were cooled.

### *Crystal Structures of NaBp·2Tg, KBp·2Ttg, and RbBp·2Ttg*

Figure 1 presents stereoscopic views of the unit-cell contents, and Table I gives a compilation of the crystallographic data. All crystals can be characterized as solvent-separated ion pairs. The alkali ions are spherically surrounded by two glyme molecules and coordinated to 8 [NaBp, (8)] or Bp (9) and RbBp (10)] oxygen atoms. NMR experiments suggested (11, 12) that solvent-separated ion pairs also exist in solution. These structures do occur in the solid state, and the X-ray diffraction experiments allow a clearer and more detailed understanding of solvent-separated ion pairs. Figure 1 illustrates that the biphenyl anions and the alkali glyme clusters are located in separate regions in the unit cell. The biphenyl anions bearing the unpaired spin are lying in a plane. The physical consequences of this arrangement will be discussed in the next paragraph.

In contrast with the neutral molecule in the solid state (13), the biphenyl anions are not planar; the dihedral angle in NaBp is 7.3°, in RbBp it is 9.4°,

**Table I. Crystallographic Data for NaBp·2Tg, KBp·2Ttg and RbBp·2Ttg**

<i>Parameter<sup>a</sup></i>	<i>NaBp·2Tg</i> (at 146 K)	<i>KBp·2Ttg</i> (at 120 K)	<i>RbBp·2Ttg</i> (at 100 K)
<i>M<sub>w</sub></i>	533.7	565.8	621.2
<i>a</i> (Å)	11.721(2)	9.654(3)	30.68(2)
<i>b</i> (Å)	13.425(2)	16.803(9)	9.79(1)
<i>c</i> (Å)	9.555(2)	21.845(7)	23.71(2)
<i>β</i>	103.08(2)	96.03(2)	103.34(6)
Volume (Å <sup>3</sup> )	1464.5	3465	6909
Space group	<i>P</i> <sub>21</sub>	<i>C</i> <sub>2/c</sub>	<i>C</i> <sub>2/c</sub>
<i>Z</i>	2	4	8
Density (g/cm <sup>3</sup> )	1.16	1.03	1.31

NOTE: Values in parentheses in column headings are the temperatures at which the parameters were measured. <sup>a</sup> Values for *a*, *b*, and *c* give the cell dimensions.

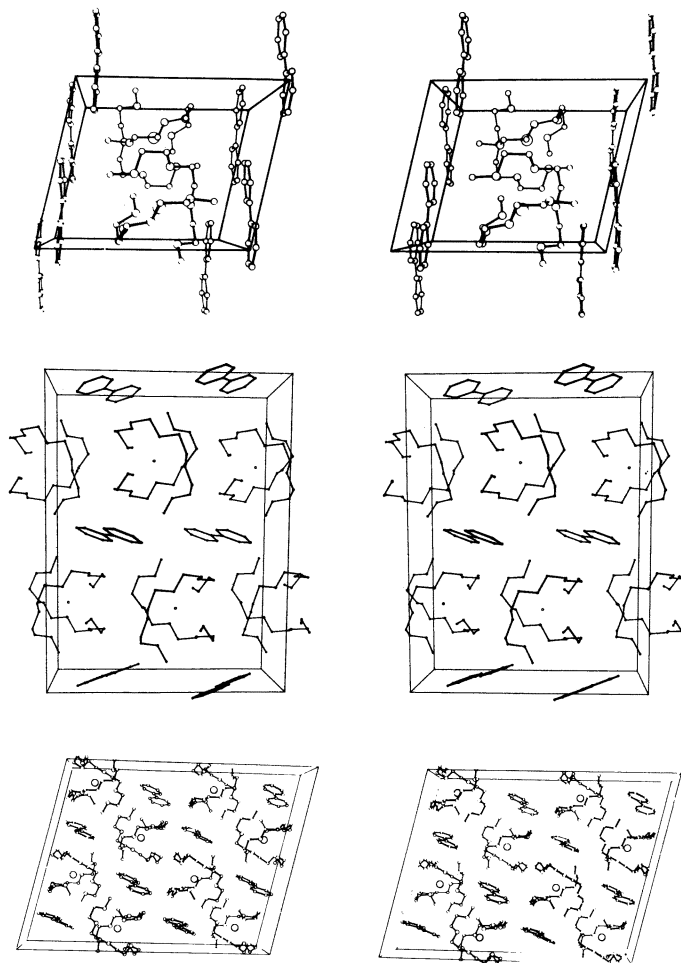


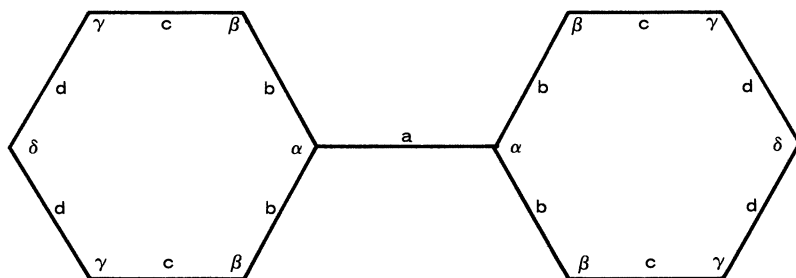
Figure 1. Stereoscopic views of the unit cell of NaBp·2Tg along the b axis (top figures), KBp·2Tg along the a axis (middle figures), and RbBp·2Tg along the b axis (bottom figures). (Reproduced with permission from reference 24. Copyright 1979.)

but in KBp it could not be determined because of disorder in the crystal (9). The bond angles and bond lengths in the biphenyl anion are given in Table II for the three types of crystals and for neutral biphenyl. (Values in Table II correspond to structure 1.) The biphenyl anion in all three crystals has a shortened central C–C bond and lengthened inner C–C bonds in comparison with neutral biphenyl. This pattern corresponds to the calculated bond-order changes in going from the neutral molecule to the anion (10). The increased ortho-hydrogen repulsion of the biphenyl anion, in comparison

**Table II. Geometry of the Biphenyl Ion and Molecule in Different Compounds**

Parameter <sup>a</sup>	<i>NaBp</i> ·2 <i>Tg</i> (150 K)	<i>RbBp</i> ·2 <i>Tg</i> (100 K)	<i>KBp</i> ·2 <i>Tg</i> ·3 <i>Bp</i> (120 K)	(110 K)
<i>a</i> (Å)	1.435	1.441	1.436	1.496
<i>b</i> (Å)	1.436	1.425	1.430	1.397
<i>c</i> (Å)	1.381	1.385	1.380	1.388
<i>d</i> (Å)	1.397	1.404	1.391	1.385
$\alpha$ (°)	114.7	115.3	115.2	117.9
$\beta$ (°)	122.2	122.1	121.9	121.0
$\delta$ (°)	117.9	117.3	118.2	118.9
$\gamma$ (°)	121.6	121.6	121.4	120.7

NOTE: Values in parentheses in column headings are the temperatures at which the parameters were measured. <sup>a</sup> Parameters correspond to structure 1. Values for *a*, *b*, *c*, and *d* are bond lengths, and values for  $\alpha$ ,  $\beta$ ,  $\delta$ , and  $\gamma$  are bond angles.

**Structure 1**

with neutral biphenyl, which is caused by the shortening of the central C–C bond, expresses itself in the values of the bond angles at the carbon atoms of the central C–C bond. These angles are significantly smaller than  $120^\circ$  (see Table II) and significantly smaller than the already reduced value of  $117.9^\circ$  in neutral biphenyl. The nonplanarity of the biphenyl anion is, of course, also related to the reduced length of the central C–C bond. The average values of the alkali–oxygen bond lengths for the three crystals and the van der Waals radius of oxygen (1.40 Å) were used to calculate the van der Waals radii of the alkali ions (column 4 of Table III). These radii agree very well with the ionic radii given by Gourary and Adrian (14), who corrected the values of Pauling (15).

If the central cations are regularly surrounded by the oxygen atoms so that the outer spherical surfaces of the atoms just touch each other, the ratios of the radii of cation and oxygen atoms are 0.73 for 8 coordination and 1.00 for 12 coordination. The relevant ratios in the biphenyl crystals are the following:  $r_{\text{Na}^+}/r_{\text{O}} = 0.83$ ,  $r_{\text{K}^+}/r_{\text{O}} = 1.06$ ,  $r_{\text{Rb}^+}/r_{\text{O}} = 1.17$ , where *r* is the radius of the indicated species. Hence 8 coordination for  $\text{Na}^+$  is feasible,

Table III. Average Alkali–Oxygen Bond Lengths and Alkali Ionic Radii

Bond	Average Bond Length	Calculated Alkali Radius	Gourary and Adrian Alkali Radius <sup>a</sup>	Pauling Alkali Radius <sup>b</sup>
Na–O	2.58	1.18	1.17	0.95
K–O	2.93	1.53	1.49	1.33
Rb–O	3.02	1.62	1.63	1.48

NOTE: All values are given in Angstroms. The van der Waals oxygen radius was 1.40 Å for all bonds. <sup>a</sup> Data are from reference 14. <sup>b</sup> Data are from reference 15.

and 10 coordination for K<sup>+</sup> and Rb<sup>+</sup> is also feasible. The fact that single crystals of NaBp in Ttg cannot be prepared may be due to the large diameter of the molecular cavity formed by the 10 oxygen atoms. In this case, the central ion has too much space, so it may move to one side and lose contact with the superfluous oxygen atoms to prevent the formation of the crystal. Single crystals could not be prepared for KBp and RbBp dissolved in Tg. Apparently, the wrapping of the cation by the Tg molecule is not complete enough to give sufficient solvation energy for stable crystals.

In summary, single crystals of biphenyl anions can only be found for very specific combinations of alkali ions and solvent molecules. When solvation is studied, the dielectric constants of the solvents and their ability to donate electrons to the cations are not the only important factors; the number of chelating sites of the solvent molecules and steric factors are also important.

### *Physical Properties of NaBp·2Tg, KBp·2Ttg, and RbBp·2Ttg*

Because of the unpaired electrons on the biphenyl ions, the alkali biphenyl systems are magnetically active. The static magnetic properties may be studied by susceptibility and magnetization measurements, but electron spin resonance (ESR) is most suitable for the characterization of the dynamical magnetic properties. The structure of these crystals—layers of biphenyl ions alternating with layers of glyme-coordinated alkali ions—strongly suggests the presence of pseudo-two-dimensional magnetic behavior. This behavior was confirmed by ESR measurements (16–18). The single exchange-narrowed ESR resonance line shows an angular dependence of the line width and a deviation of the line shape from the Lorentzian, which is typical for two-dimensional magnetic systems (16, 17). This behavior is a consequence of the presence of long-time spin correlations due to spin diffusion.

At temperatures above a few Kelvins, all three systems are in the paramagnetic phase. The magnetic structure at very low temperatures depends upon the arrangement of the biphenyl ions in the magnetic layer. In NaBp·2Tg and KBp·2Ttg, the variation in the distances between the different neighboring biphenyl ions is small. The centers of the central C–C bonds of the biphenyl ions form an almost regular hexagonal structure. Conse-

quently, the exchange constants between the different nearest neighbors may be of the same order, and long-range ordered structures are possible. Magnetization, susceptibility, and ESR measurements on NaBp·2Tg point to an antiferromagnetically ordered structure for this system at temperatures below about 1.1 K (18). However, in RbBp·2Tg, the variation in the distances between the different neighboring biphenyl ions is larger. The crystallographic structure of this compound suggests that the magnetic layer consists of dimers of biphenyl ions. Susceptibility measurements on RbBp·2Tg confirmed this picture (10). The susceptibility data may be nicely described by the singlet-triplet model, involving an antiferromagnetic ground state. Therefore, no long-range order will be present in RbBp·2Tg as opposed to NaBp·2Tg and presumably KBp·2Tg.

Different techniques showed that above 80 K the dominant exchange constant for NaBp·2Tg is ferromagnetic in nature, but below 80 K the exchange coupling shows antiferromagnetic character. This condition is ascribed to the presence of two or more exchange constants in the magnetic plane, one of which is antiferromagnetic. The high-temperature behavior is a function of the average of the different exchange constants, whereas at low temperatures an antiferromagnetic structure evolves because of the presence of the antiferromagnetic exchange constant. More details concerning the magnetic features of NaBp·2Tg may be found in a recent review (19).

### ***Crystal Structures of $K_2COT \cdot Dg$ and $Rb_2COT \cdot Dg$***

$K_2COT \cdot Dg$  and  $Rb_2COT \cdot Dg$  crystallize in the orthorhombic space group  $P_{nma}$  and are isomorphous (5, 6). In Figure 2 a projection of the structure of  $K_2COT \cdot Dg$  along the  $b$  axis is given, and in Table IV the crystallographic data are given. The cations are located above the centers of the planar COT dianions (average C-C bond length of  $1.40 \pm 0.02 \text{ \AA}$ ) and form a linear array through the crystal. One cation ( $K_2$ ) is coordinated from the outside to the oxygen atoms of the diglyme molecule, whereas the other cation ( $K_1$ ) is shielded by a zigzag chain of COT dianions. Because the distance to the center of the COT plane is about  $2.4 \text{ \AA}$ , these ion pairs are contact ion pairs.

### ***Physical Properties of Irradiated Crystals of $K_2COT \cdot Dg$ and $Rb_2COT \cdot Dg$***

If the crystals of  $K_2COT \cdot Dg$  and  $Rb_2COT \cdot Dg$  are subjected to X-rays for several hours, paramagnetic centers are created (20). At room temperature the ESR spectrum of  $K_2COT \cdot Dg$  consists of nine equally spaced lines (derivative line width is 1.9 G) with a binomial intensity distribution. This spectrum can be attributed to the monoanion of the host molecule COT. The unpaired electron of COT has a hyperfine coupling with the eight protons. The ESR spectrum of  $Rb_2COT \cdot Dg$  contained two peaks after pro-

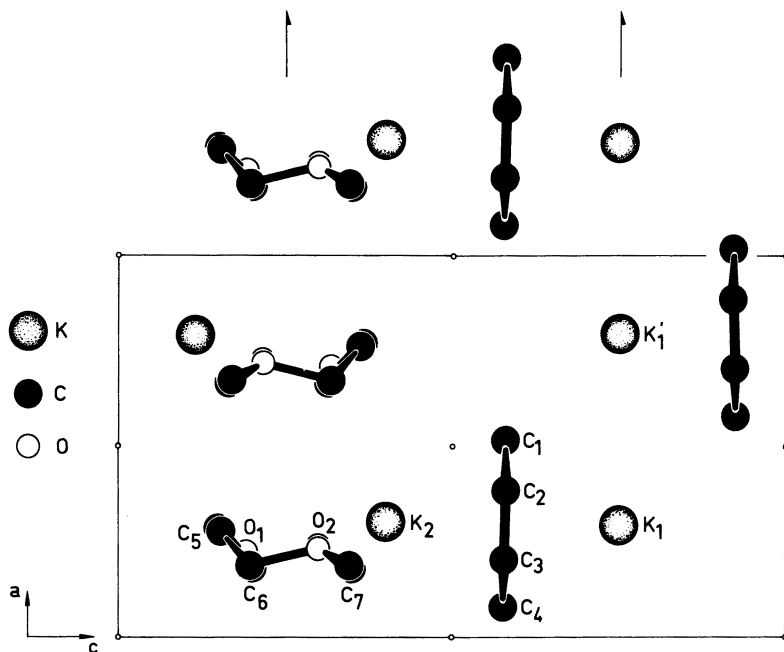


Figure 2. Projection of the structure of  $K_2COT \cdot Dg$  along the  $b$  axis on the mirror plane. (Reproduced with permission from reference 20. Copyright 1976.)

Table IV. Crystallographic Data for  $K_2COT \cdot Dg$  and  $Rb_2COT \cdot Dg$

Parameter <sup>a</sup>	$K_2COT \cdot Dg$	$Rb_2COT \cdot Dg$
$a$ (Å)	7.689(3)	7.705(8)
$b$ (Å)	15.376(5)	15.144(15)
$c$ (Å)	13.703(5)	14.300(10)
$Z$	4	4
Density (g/cm <sup>3</sup> )	1.30	1.65

<sup>a</sup> Values for  $a$ ,  $b$ , and  $c$  give the cell dimensions.

longed irradiation. One signal has an isotropic  $g$ -value and a derivative line width of 19 G. This peak is due to the monoanion of COT. The absence of hyperfine splitting is caused by the much larger magnetic moments of the rubidium isotopes compared to those of potassium. Each of the nine proton lines is split again by the rubidium hyperfine interaction, which results in an inhomogeneously broadened line. The position of the second signal in the spectrum of  $Rb_2COT \cdot Dg$  depends strongly upon the orientation of the magnetic field. When the magnetic field is in the COT plane, the  $g$ -value varies between 1.98 and 2.22. As illustrated in Figure 3, this peak contains

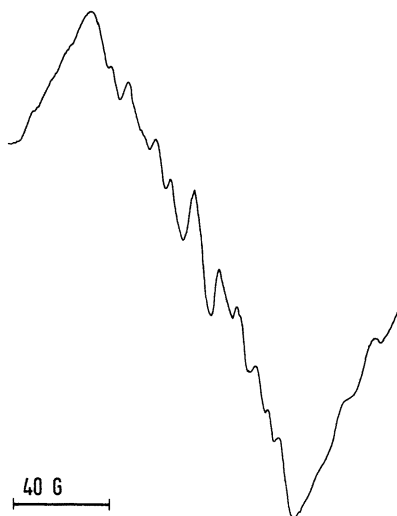


Figure 3. Hyperfine structure of the anisotropic peak in the first-derivative ESR spectrum of  $\text{Rb}_2\text{COT}\cdot\text{Dg}$ .

a rich unresolved hyperfine structure. These observations suggest that this peak is due to an electron trapped near a Rb cation. Because the line width of this peak is only 60 G, the wave function corresponding to this unpaired electron can contain only a small percentage of the Rb 5s orbital.

As expected, the spectrum of  $\text{K}_2\text{COT}\cdot\text{Dg}$  shows a variation in the  $g$ -value and the hyperfine interaction if the crystal is rotated around an axis in the COT plane. However, both experimental parameters remain constant upon rotation around an axis perpendicular to the COT plane. The constancy of the  $g$ -value is normal for axially symmetric systems. The behavior of the hyperfine interaction is unexpected. Although for aromatic systems the anisotropy of the dipolar interaction resides almost completely in the aromatic plane, the hyperfine splitting is isotropic in this plane. This condition can only be explained by assuming that the COT anion is rotating around its eightfold axis with a frequency higher than  $10^7 \text{ s}^{-1}$  at room temperature. The rapid molecular rotation of the COT monoanion in  $\text{K}_2\text{COT}\cdot\text{Dg}$  was confirmed by measuring the ESR spectrum as a function of temperature. The ESR spectra in Figure 4 clearly show that the rate of the molecular rotation changes upon cooling the crystal. Between 40 and 25 K, a transition takes place: The frequency of rotation falls below the hyperfine splitting frequencies. Below 20 K, no further change occurs.

Figure 5 shows the ESR spectra at 22 K for four orientations of the magnetic field, which is oriented in the COT plane but rotated each time by  $45^\circ$ . Interestingly, the spectra repeat not every  $45^\circ$  but every  $90^\circ$ ; this result shows the presence of only a fourfold symmetry axis. This finding

**American Chemical Society  
Library**

1155 16th St., N.W.  
Washington, D.C. 20036

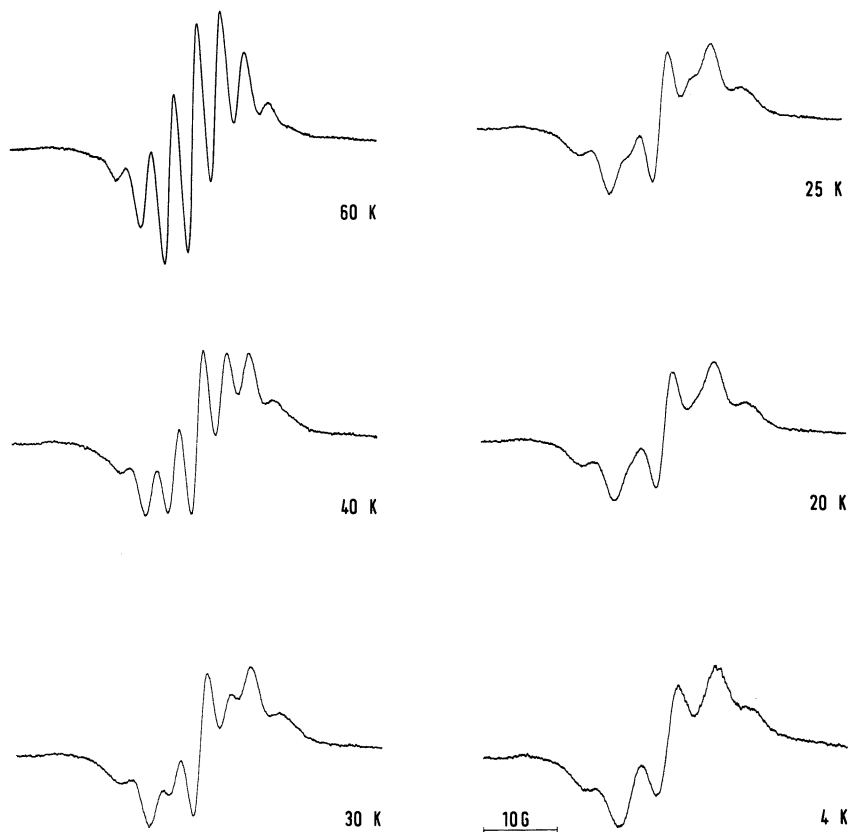


Figure 4. ESR spectrum of the monoanion of COT in  $K_2COT \cdot Dg$  as a function of temperature. (Reproduced with permission from reference 20. Copyright 1976.)

implies that the spin distribution over the carbon atoms is no longer uniform, but alternates around the COT ring. The spectra shown in Figure 5 were simulated to find the degree of spin alternation. The best agreement was found for an alternation of 20% of the average spin density equal to 0.125 (see Figure 6). In the planar free monoanion of COT, the three most energetic electrons occupy a pair of degenerate nonbonding orbitals. The degeneracy of these orbitals is lifted by the crystal field; unequal spin-densities on the distinct carbon atoms result. Calculations suggest that the amount of alternation is influenced by vibronic mixing between the two lowest molecular states.

An important consequence of the spin alternation is that the monoanion of COT must be rotated by  $22.5^\circ$  around its eightfold axis with respect to the equilibrium position of the dianion at 300 K. This rotation is dictated



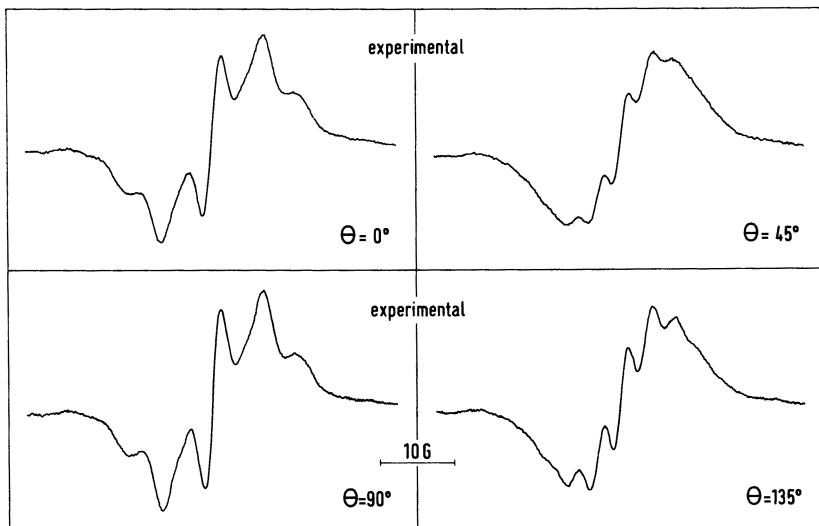


Figure 5. ESR spectrum of the COT anion in  $K_2COT \cdot Dg$  for four orientations of the magnetic field, which is oriented in the COT plane and rotated each time by  $45^\circ$ . (Reproduced with permission from reference 20. Copyright 1976.)

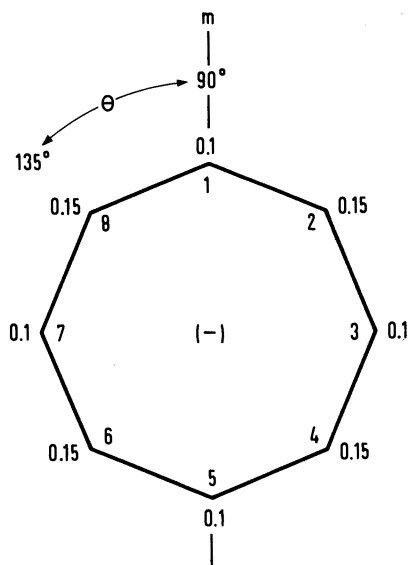


Figure 6. Spin-density distribution and molecular orientation with respect to the crystallographic mirror plane  $m$  of the COT anion in  $K_2COT \cdot Dg$  at 22 K. Numbers 1–8 on the inside of the structure represent the positions of the carbon atoms. (Reproduced with permission from reference 20. Copyright 1976.)

by the symmetry of the crystal, which has a mirror plane parallel to the *ac* plane and running through the centers of opposite C–C bonds. With this orientation of the mirror plane, no spin alternation can exist; a rotation of  $22.5^\circ$  of the COT anion is necessary to make spin alternation possible. Theoretical calculations have shown that this orientation of the monoanion is the most stable one (21).

The Jahn–Teller active vibrations for the  $E_{2u}$  electronic ground state are those with  $B_{1g}$  and  $B_{2g}$  symmetry. The  $B_{1g}$  vibration distorts the molecule in a structure with alternating bond lengths. As the mirror plane *m* runs through the carbon atoms in the 1 and 5 positions of the COT anion (Figure 6), a static distortion induced by a  $B_{1g}$  vibration is impossible. The  $B_{2g}$  vibration moves the carbon atoms alternately inward and outward. Such a distortion is in agreement with the local symmetry.

### Crystal Structure of $\text{Na}_2\text{Tp}\cdot 6\text{THF}$

The crystallographic data of the single crystal of  $\text{Na}_2\text{Tp}\cdot 6\text{THF}$  are as follows:  $M_w = 706.6$ ; monoclinic system,  $P_{2_1/c}$  space group; cell dimensions at 293 K,  $a = 11.508(6)$ ,  $b = 16.531(4)$ , and  $c = 11.200(3)$  Å;  $\beta = 95.13(3)^\circ$ ; volume =  $2122$  Å<sup>3</sup>; density =  $1.109$  g/cm<sup>3</sup>; and  $Z = 2$  (22). Figure 7 gives a stereoscopic view of the structure of the ion pair. The Na cations are situated above the center of the middle ring of the terphenyl dianion, at a distance of  $2.43$  Å. For a van der Waals radius of the Na cation of about  $1$  Å, the “half thickness” of the Bp anion is  $1.43$  Å. Each Na cation is surrounded by three tetrahydrofuran molecules in such a way that the three oxygen atoms lie at the corners of an equilateral triangle whose plane is almost parallel to the plane of the central ring. This crystal illustrates the concept of a tight or contact ion pair. Hückel calculations gave a total charge of  $0.9e$  for the central ring and a charge density of  $0.55e$  at the end rings. Hence, for energetic reasons, the position of the Na cation above the central ring is most favorable. The central C–C bond ( $1.42$  Å) connecting two phenyl rings

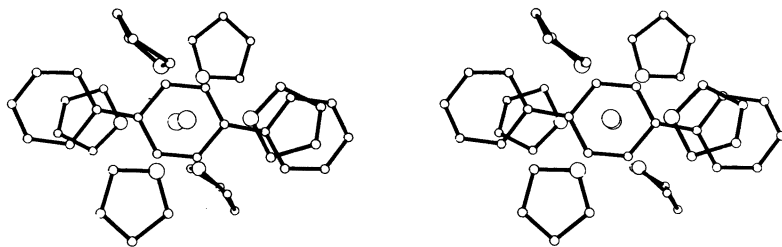


Figure 7. Stereo view of  $\text{Na}_2\text{Tp}\cdot 6\text{THF}$  projected in the plane through the three oxygen atoms. The space group is  $P_{2_1/c}$ . (Reproduced with permission from reference 25. Copyright 1980.)

is shortened with respect to the value in neutral terphenyl (23), this situation increases the ortho-hydrogen repulsion. This condition is also expressed in the values of the bond angles at the C atoms of the central C–C bond, which are significantly smaller than 120°. The change in geometry from neutral Tp to the Tp dianion corresponds to calculated (Hückel) bond-order changes and is similar to the trend observed in the biphenyl systems. Because the Tp anion is situated at an inversion center, the two end rings are parallel. The torsion angle around the central C–C bond is 4.3°.

### Acknowledgments

Part of this work was carried out under the auspices of the Netherlands Foundation of Chemical Research and with the aid of the Netherlands Organization for the Advancement of Pure Research.

Petroleum Research Fund Grant No. 18537–SE covered travel expenses to the ACS National Meeting in Anaheim, CA, where this research was presented.

### References

1. Sadek, H.; Fuoss, R. M. *J. Am. Chem. Soc.* **1954**, *76*, 5897, 5905.
2. Winstein, S.; Clippiner, E.; Fainberg, A. H.; Robinson, G. C. *J. Am. Chem. Soc.* **1954**, *76*, 2597.
3. Szwarc, M. *Ions and Ion Pairs in Organic Reactions*; Wiley– Interscience: New York, 1972; Vols. 1 and 2.
4. Canters, G. W.; Klaassen, A. A. K.; de Boer, E. *J. Phys. Chem.* **1970**, *74*, 3299.
5. Noordik, J. H.; van den Hark Th. E. M.; Mooij, J. J.; Klaassen, A. A. K. *Acta Crystallogr. Sect. B* **1974**, *30*, 833.
6. Noordik, J. H.; Degens, H. M. L.; Mooij, J. J. *Acta Crystallogr. Sect. B* **1975**, *31*, 2144.
7. Paul, D. E.; Lipkin, D.; Weissman, S. I. *J. Am. Chem. Soc.* **1956**, *78*, 116.
8. Noordik, J. H.; Beurskens, P. T.; van den Hark, Th. E. M.; Smits, J. J. M. *Acta Crystallogr. Sect. B* **1979**, *35*, 621.
9. Noordik, J. H.; Schreurs, J.; Gould, R. O.; Mooij, J. J.; de Boer, E. *J. Phys. Chem.* **1978**, *82*, 1105.
10. Mooij, J. J.; Klaassen, A. A. K.; de Boer, E.; Degens, H. M. L.; van den Hark, Th. E. M.; Noordik, J. H. *J. Am. Chem. Soc.* **1976**, *98*, 680.
11. Canters, G. W.; de Boer, E. *Mol. Phys.* **1973**, *26*, 1185.
12. Canters, G. W.; de Boer, E. *Mol. Phys.* **1974**, *27*, 665.
13. Charbonneau, G. P.; Delugeard, Y. *Acta Crystallogr. Sect. B* **1976**, *32*, 1420.
14. Gourary, B. S.; Adman, F. J. *Solid State Phys.* **1960**, *1 K*, 127.
15. Pauling, L. *The Nature of the Chemical Bond*; Cornell University Press: Ithaca, 1960; 3rd ed.
16. Takizawa, O.; Srinivasan, R.; de Boer, E. *Mol. Phys.* **1981**, *44*, 677.
17. Murugesan, R.; de Boer, E. *Chem. Phys. Lett.* **1983**, *95*, 301.
16. Gribnau, M. C. M.; Murugesan, R.; van Kempen, H.; de Boer, E. *Mol. Phys.* **1984**, *52*, 195.
19. Gribnau, M. C. M.; de Boer, E. *Electronic Magnetic Resonance of the Solid State*, Weil, J. A., Ed.; in press.

20. Mooij, J. J.; de Boer, E. *Mol. Phys.* **1976**, *32*, 113.
21. Jones, M. T.; de Boer, E. *Mol. Phys.* **1982**, *47*, 487.
22. Noordik, J. H.; Doesburg, H. M.; Prick, P. A. J. *Acta Crystallogr. Sect. B* **1981**, *37*, 1659.
23. Lisensky, G. C.; Johnson, C. K.; Levy, H. A. *Acta Crystallogr. Sect. B* **1976**, *32*, 2188.
24. de Boer, E.; Klaassen, A. A. K.; Mooij, J. J.; Noordik, J. H. *Pure Appl. Chem.* **1979**, *51*, 73.
25. de Boer, E.; Klaassen, A. A. K. *Kem.-Kemi* **1980**, *7*, 257.

RECEIVED for review September 29, 1986. ACCEPTED January 13, 1987.

# NMR Studies of $4n$ $\pi$ -Conjugated Polycyclic Anions

## Relationship of the Energy Gap Between the Highest Occupied Molecular Orbital and the Lowest Unoccupied Molecular Orbital to Paratropicity and Electronic Structure

Mordecai Rabinovitz and Yoram Cohen

Department of Organic Chemistry, The Hebrew University of Jerusalem, Jerusalem 91904, Israel

*The energy gap between the highest occupied molecular orbital (HOMO) and the lowest unoccupied molecular orbital (LUMO) determines the line shape and chemical shift of  $4n$   $\pi$  polycyclic doubly charged systems. Narrower energy gaps correspond to more significant line broadening in the  $^1\text{H}$  NMR bands. This line broadening is attributable to a singlet–triplet equilibrium that depends on the HOMO–LUMO gap. The topology of the system influences the paratropicity of these  $4n$   $\pi$  polycyclic dianions. Whereas the triphenylene dianion does not exhibit a  $^1\text{H}$  NMR spectrum, a gradual change toward a highly resolved spectrum is obtained for the tribenzo[a,c,i]phenazine dianion. A correlation between the HOMO–LUMO gap and the paratropic shift of these dianions is demonstrated.*

**T**HE NOTION OF AROMATICITY is one of the most intriguing problems in organic chemistry and has drawn the attention of chemists since Kekulé's ingenious proposal (1) in 1872 of the structure of benzene. The concept of antiaromaticity introduced by Breslow (2, 3) about a century later emphasized the perplexity of aromaticity. Nevertheless, numerous physical and chemical properties of many groups of compounds are attributed to their

aromatic characters (4–9). The concepts of aromaticity and antiaromaticity are difficult to understand because they are not physically observable (10, 11) and hence cannot be related directly to experimental data. The most comprehensive definitions of aromatic and antiaromatic molecules are based on energy content: An aromatic molecule is a species in which the  $\pi$ -electron delocalization reduces the energy content relative to a model compound lacking such cyclic conjugation; an antiaromatic molecule is a species in which the  $\pi$ -electron delocalization increases the energy content. The application of these definitions presents difficulties, especially in the case of the unstable  $4n$   $\pi$  systems. More practical definitions of aromaticity and antiaromaticity based on theoretical concepts are Hückel's rule (12), Platt's peripheral model (13), and Randić's conjugated circuits (14, 15). Hückel's rule assigns aromatic character to planar, monocyclic, conjugated systems containing  $(4n + 2)$   $\pi$  electrons in their periphery. The perimeter model suggested by Platt (13), which is an extension of Hückel's rule to polycyclic structures, endows aromatic character to a system according to the number of  $\pi$  electrons in its periphery. Molecules having a periphery of  $(4n + 2)$   $\pi$  electrons are classified as aromatic, whereas those having  $4n$   $\pi$  electrons are classified as antiaromatic. A more interesting and valuable approach is the concept of conjugated circuits proposed by Randić (14, 15). This concept considers the contributions of various skeletal components of the system where major contribution is attributed to the smallest conjugated circuits.

In terms of observable phenomena, the most useful definition of aromaticity is based on the magnetic anisotropy (10, 16–18) of a system as deduced from the  $^1\text{H}$  NMR parameters. Antiaromatic  $4n$   $\pi$  systems are expected to exhibit paratropic (high-field) shifts in their  $^1\text{H}$  NMR spectra (11, 19) in contrast to the diatropic (low-field) shifts of  $(4n + 2)$   $\pi$  systems. Although the diatropic shifts revealed by  $(4n + 2)$   $\pi$  systems are well-established, the experimental support for the relationship between paratropicity and antiaromaticity is far less satisfactory (11).

A correlation has been found between a theoretical and an experimental criterion for paratropicity, and it can be related to the antiaromatic character of  $4n$   $\pi$  carbocyclic (20) and heterocyclic dianions (21, 22). This correlation leads to a new theoretical index for antiaromaticity, namely, the magnitude of the energy gap,  $\Delta E$ , between the highest occupied molecular orbital (HOMO) and the lowest unoccupied molecular orbital (LUMO) ( $\Delta E = E_{\text{HOMO}} - E_{\text{LUMO}}$ ). An unequivocal correlation exists between the degree of paratropicity experienced by the  $4n$   $\pi$  dianions and the HOMO-LUMO energy gap as manifested by the line shapes (20–22) and chemical shifts (11) of their  $^1\text{H}$  NMR bands. The paratropcities and delocalization patterns of dianions and their relationship to the topologies of systems will be demonstrated in this chapter. Structural deviations from the symmetrical triphenylene dianion to less symmetrical systems influence paratropicity. The partitioning of the polycyclic dianions into charged and uncharged compo-

nents in a way that reduces the paratropic effect will also be demonstrated (23). This partitioning is another manifestation of the tendency of aromatic systems to remain aromatic.

Doubly charged polybenzenoid systems and their diazine analogues were selected as representatives of antiaromatic systems. As mentioned earlier, antiaromatic species are systems in which an effective delocalization of  $4n$   $\pi$  electrons occurs. Therefore, the  $4n$   $\pi$  annulenes cannot be classified as such because they exhibit bond-length alternation and severe deviation from planarity. However, in polybenzenoid systems, the rigidity due to the inner bonds reduces the bond-length alternation and the extent of deviation from planarity. The highly rigid polybenzenoid skeleton is bound to enforce planarity and reduce bond-length alternation not only in the neutral systems but also in the dianions and dications derived from these systems. The two-electron reduction or oxidation processes of the neutral compounds result in a change of the electronic structure whereas nearly no effect on other parameters (e.g., geometry) occurs. Therefore, one can attribute the changes in the system's characteristics mainly to electronic factors. However, for heterocyclic dianions, a partial deviation from planarity at the nitrogen atoms cannot be ruled out.

One of the main problems in assigning aromatic or antiaromatic character to a system is the relativity of these terms and consequently the need for proper reference compounds. Our approach overcomes this difficulty by using the neutral parent compounds as reference compounds; they are good reference compounds because they differ merely in their electronic structure. Therefore, doubly charged  $4n$   $\pi$  electron compounds are good model compounds for antiaromaticity studies. Because carbocyclic and heterocyclic dianions can be prepared from stable precursors and because they sustain moderate stability, they were selected for this study.

## Results

The relationships between the HOMO–LUMO energy gaps as deduced from HMO $\omega\beta$  calculations (24–27) and the line shapes observed for various  $4n$   $\pi$  carbocyclic (20) and heterocyclic dianions (21, 22) are given in Tables I and II. The HOMO–LUMO energy gaps of the anions are reported in  $\beta$  units, which are the energy units of molecular orbitals as obtained from  $\omega\beta$  calculations. The energy gaps of the neutral systems are much higher and are of the order of 1  $\beta$  unit, as expected for  $(4n + 2)$   $\pi$  electron aromatic systems. The  $^1\text{H}$  NMR line shapes of selected dianions, namely, the naphthacene dianion (2), 1,4-diphenylphthalazine dianion (14), 2,3-diphenylquinoxaline dianion (16), phenanthrene dianion (7) and anthracene dianion (3), are shown in Figures 1–4. For example, the electron spin resonance (ESR) spectrum of the frozen (153 K) tetrahydrofuran solution of the phenanthrene dianion

**Table I. Spectral Patterns and HOMO–LUMO Energy Gaps of Doubly Charged Carbocyclic Systems as Disodium Salts in THF-*d*<sub>6</sub>**

Structure Number	Structure	HOMO–LUMO Energy Gap <sup>a</sup>	Detectable Line Broadening <sup>b</sup>		ESR Patterns <sup>c</sup>
			303 K	213 K	
1		0.448	–	–	N
2		0.414	–	–	N
3		0.310	no spectrum	+	1590
4		0.272	no spectrum	+	1620
5		0.251	no spectrum	–	N
6		0.226	no spectrum	+++	1600
7		0.231	no spectrum	no spectrum	1595
8		0.157	no spectrum	no spectrum	1605
9		0.111	no spectrum	no spectrum	1625

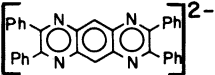
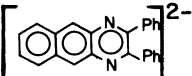
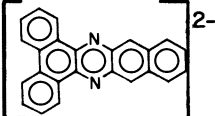
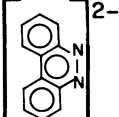
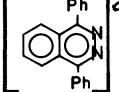
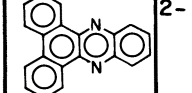
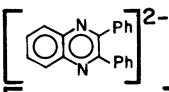
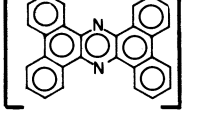
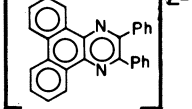
<sup>a</sup>Values ( $\Delta E = E_{\text{HOMO}} - E_{\text{LUMO}}$ ) are given in  $\beta$  units obtained from  $\omega\beta$  calculations using  $\omega = 1.4$  (24, 25). <sup>b</sup>A minus sign (–) designates no detectable line broadening in the <sup>1</sup>H NMR spectrum (300 MHz), and a plus sign (+) designates detectable line broadening. <sup>c</sup>Half-field signals are given in gauss; N indicates that no half-field signal was observed. SOURCE: Adapted from reference 20.

(7) as a disodium salt is shown in Figure 5. The ESR spectra of dianions that could not be observed by NMR or gave broad <sup>1</sup>H NMR signals consist of a broad absorption band in the range of 3200–3300 gauss (G) and sharp lines in the range of 1580–1625 G. These sharp lines at half-field correspond to a second-order forbidden transition ( $\Delta M_s = 2$  where  $M_s$  is the spin magnetic quantum number) (28) which is characteristic of triplet states.

The correlations between the HOMO–LUMO energy gap as deduced from self-consistent field molecular orbital (SCF MO) calculations (29–32) and the extent of the paratropic shifts revealed by the carbocyclic dianions are shown in Table III (11). (NOTE: For Table III, refer to Tables I and II



**Table II. Spectral Patterns and HOMO–LUMO Energy Gaps of Doubly Charged Heterocyclic Systems as Disodium Salts in THF-*d*<sub>8</sub> at Room Temperature**

Structure Number	Structure	HOMO–LUMO Energy Gap <sup>a</sup>	Detectable Line Broadening <sup>b</sup>
10		0.38	–
11		0.34	–
12		0.31	–
13		0.29	–
14		0.29	–
15		0.22	+
16		0.19	++
17		0.11 <sup>c</sup>	+++
18		0.11 <sup>c</sup>	no spectrum

<sup>a</sup>Values ( $\Delta E = E_{\text{HOMO}} - E_{\text{LUMO}}$ ) are given in  $\beta$  units obtained from  $\omega\beta$  calculations using  $\omega = 1.4$  (24–26). <sup>b</sup>A minus sign (–) designates no detectable line broadening in the <sup>1</sup>H NMR spectrum (200 or 300 MHz), and a plus sign (+) designates detectable line broadening. <sup>c</sup>Obtained from  $\omega\beta$  calculations using  $\omega = 1.0$  because energy convergence could be obtained using the habitual value for  $\omega$ , i.e.,  $\omega = 1.4$  (27). SOURCE: Adapted from references 21 and 22.

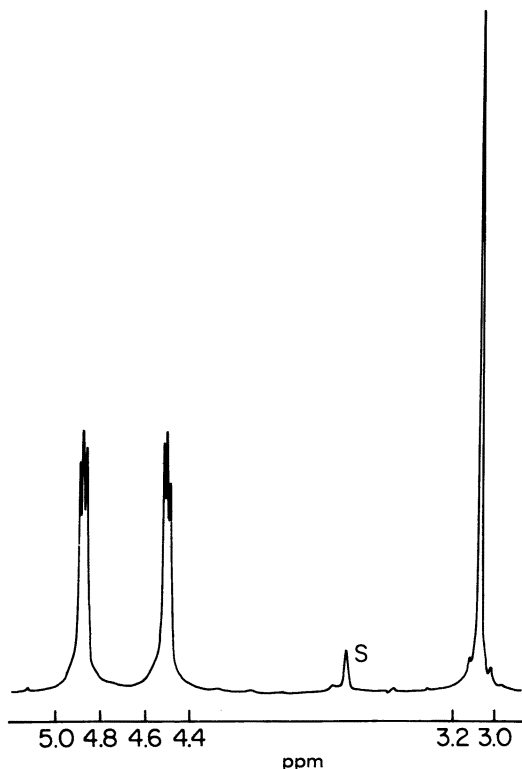


Figure 1.  $^1\text{H}$  NMR spectrum (300 MHz) of the naphthalene dianion (2) as a disodium salt in  $\text{THF-d}_6$  at room temperature (20). S indicates a solvent signal.

and Chart I for structures corresponding to the given structure numbers.) The method of calculation was the following: SCF MO calculations (29–32) were used to estimate the portion of the change in the chemical shift that is due to the charge-density factor. In each dianion, the theoretical charges on carbon atoms linked to hydrogen atoms were summed, and this sum was

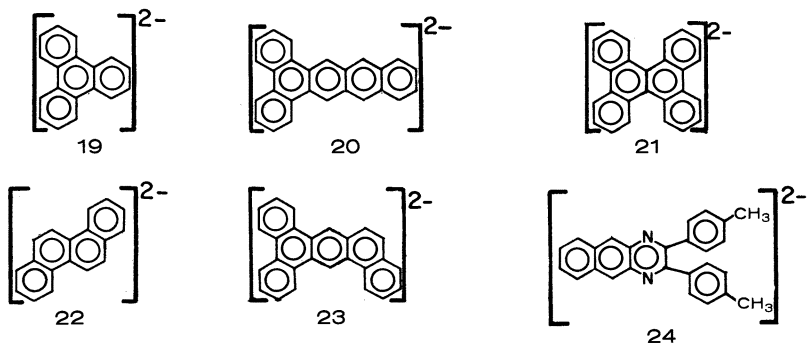
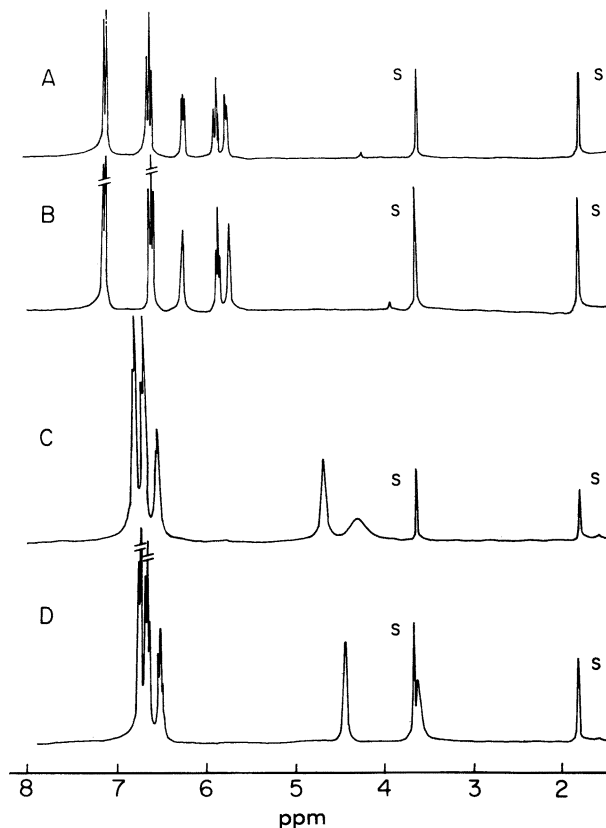


Chart I



*Figure 2.*  $^1\text{H}$  NMR spectra (300 MHz) of the 1,4-diphenylphthalazine dianion (14) and the 2,3-diphenylquinoxaline dianion (16) as disodium salts in  $\text{THF-d}_8$ . A:  $14-2\text{Na}^+$  at 300 K. B:  $14-2\text{Na}^+$  at 213 K. C:  $16-2\text{Na}^+$  at 292 K. and D:  $16-2\text{Na}^+$  at 203 K (22). S indicates a solvent signal. (Reproduced from reference 22. Copyright 1986 American Chemical Society.)

multiplied by the shift–charge correlation constant of 10.7 parts per million per unit of charge (electron charge) ( $\text{ppm}/e$ ) (33). The result was then divided by the number of protons to obtain an average value of the shielding due to charge density. This average value was subtracted from the experimental center of gravity of the  $^1\text{H}$  NMR chemical shifts of the respective neutral polycyclic hydrocarbon to derive an estimation of a theoretical center of gravity neglecting anisotropic effects. The excessive high-field shift from this calculated value, which is observed in the  $^1\text{H}$  NMR spectra of the charged systems, is taken as a measure of the paratropic shift; the paratropic shift reflects the antiaromatic nature of these species. When the HOMO–LUMO energy gap is narrow, a significant excessive high-field (paratropic) shift is observed; when the energy gap is wide, a lower-field shift is observed. A linear regression analysis of the relationship between the HOMO–LUMO

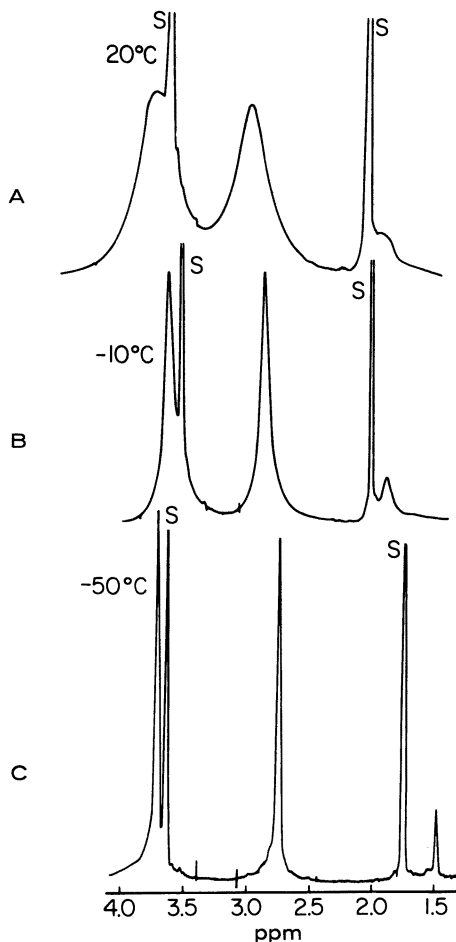


Figure 3. The effect of temperature on the line shape of the  $^1\text{H}$  NMR spectrum (300 MHz) of the anthracene dianion (**3**) as a disodium salt in  $\text{THF-d}_8$ . A: 293 K, B: 263 K, and C: 223 K. S indicates a solvent signal. (Reproduced from reference 20. Copyright 1983 American Chemical Society.)

energy gap and the high-field shift yields the following (11):

$$\Delta\delta = -2.50\Delta E + 6.40 \quad (r = 0.953)$$

where  $\Delta\delta$  is the difference in chemical shift in parts per million between the calculated and experimental center of gravity of the proton bands;  $\Delta E$  is the HOMO–LUMO energy gap expressed in electronvolts as obtained by the SCF MO calculations (Table III, Figure 6); and  $r$  is the correlation coefficient.

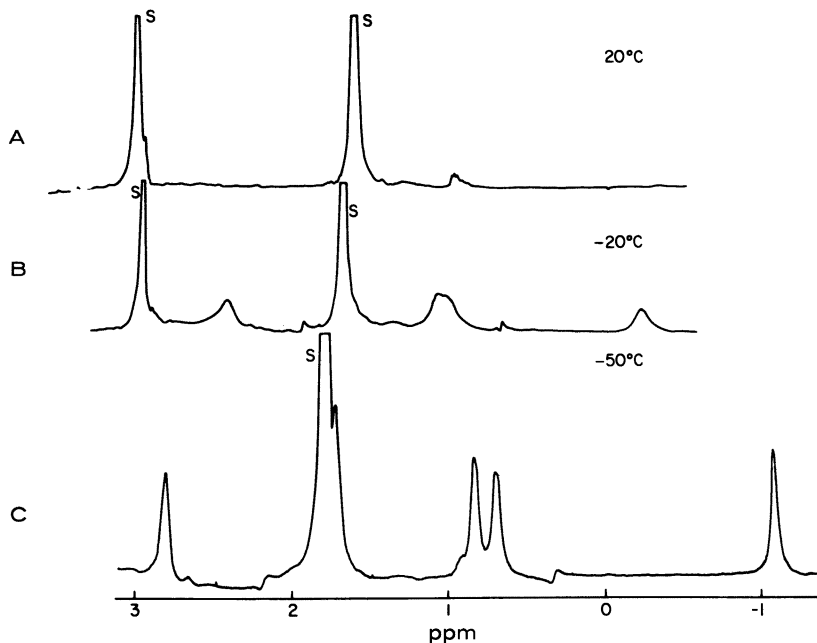


Figure 4.  $^1\text{H}$  NMR spectra (300 MHz) of the phenanthrene dianion (7) as a dilithium salt in  $\text{THF-d}_8$  at various temperatures. A: 293 K, B: 253 K, and C: 223 K. S indicates a solvent signal. (Reproduced from reference 20. Copyright 1983 American Chemical Society.)

## Discussion

### Relationship Between the HOMO–LUMO Energy Gap and the $^1\text{H}$ Line Shape of $4n$ $\pi$ Paratropic Carbocyclic and Heterocyclic Dianions.

**CARBOCYCLIC DIANIONS.** One of the characteristics of the  $^1\text{H}$  NMR spectra of  $4n$   $\pi$  electron systems is the high-field (paratropic) shift of their bands (11, 19). This paratropic shift is a result of the pronounced importance of the paramagnetic term of the proton-shielding constant in these  $4n$   $\pi$  systems, which is nearly negligible in species that are not antiaromatic. The paramagnetic term, which is a major factor governing the shielding constant of heavier atoms, is a result of a mixing between the ground state and energetically low-lying excited states (34). The antiaromatic systems are characterized by narrow HOMO–LUMO energy gaps; therefore, they should show enhanced high-field shifts in their  $^1\text{H}$  NMR spectra. If the HOMO–LUMO energy gap is sufficiently narrow, an equilibrium between the singlet ground state and a low-lying, thermally accessible triplet state may occur

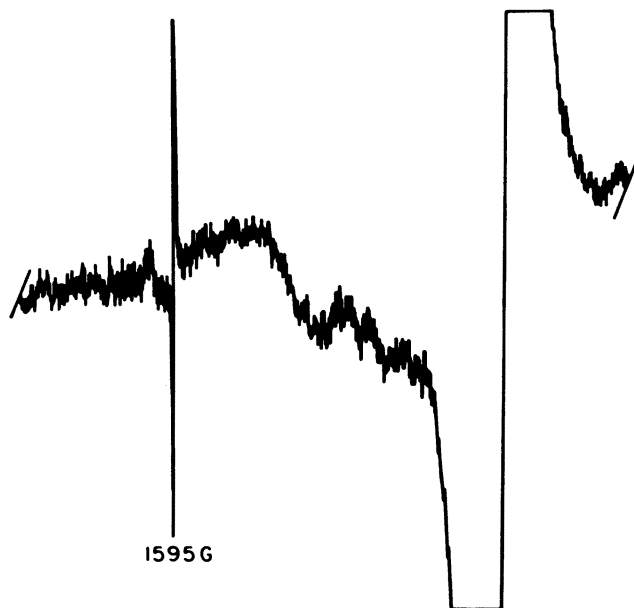


Figure 5. ESR spectrum of the phenanthrene dianion (7) in a frozen solution (153 K) of THF. (Reproduced from reference 20. Copyright 1983 American Chemical Society.)

(20) and result in detectable line broadening of the  $^1\text{H}$  NMR absorption bands.

The influence of the HOMO–LUMO energy gap on the line shape of the dianions is demonstrated in Table I. A gap of approximately  $0.4 \beta$  units, which occurs for the pentacene dianion (1) or the naphthacene dianions (2) (Figure 1), results in highly resolved spectra; however, a gap of approximately  $0.1 \beta$  units does not afford the observation of  $^1\text{H}$  and  $^{13}\text{C}$  NMR bands of the charged systems. The effect is a gradual one, and dianions having a gap of intermediary magnitude show significant line broadening. Comparison of the spectrum of the naphthacene dianion (2) in Figure 1 with the spectra of the anthracene dianion (3) and phenanthrene dianion (7) in Figures 3 and 4, respectively, shows this phenomenon (20). Only those systems that exhibit line broadening or no  $^1\text{H}$  NMR spectrum show an ESR spectrum that consists of a broad signal at 3200–3300 G along with a sharp characteristic half-field line at 1580–1620 G, as demonstrated by the disodium salt of the phenanthrene dianion (7) in Figure 5 (20).

These observations can be explained as follows: When the HOMO–LUMO energy gap is sufficiently narrow, the equilibrium between the singlet ground state and a thermally accessible triplet state prevails, and a high population of the triplet state occurs. Also, the paramagnetic dilution in-

Table III. <sup>1</sup>H NMR Paratropic Shifts and HOMO–LUMO Energy Gaps of Polybenzenoid Dianions

Structure Number	Exp. COG of Neutral Systems	Overall Paratropic Shift	Calc. COG of Charged Systems	Exp. COG of Charged Systems	Calc. $\Delta\delta$ –		Calc. HOMO–LUMO Gap
					Exp. $\Delta\delta$	Exp. $\Delta\delta$	
1	8.08	2.17	5.91	4.98	0.93		2.070
2	8.01	2.50	5.51	4.23	1.28		2.133
3	7.90	2.76	5.14	3.06	2.08		1.833
6	7.86	2.15	5.71	3.22	2.49		1.411
21	8.28	1.18	7.10	4.18	2.92		1.205
22	7.80	1.90	5.90	2.42	3.48		1.333
23	8.43	1.23	7.20 <sub>a</sub>	3.51	3.69		0.990
7	7.67	2.32	5.35 <sub>a</sub>	1.18	4.17		1.898
5	8.14	1.70	6.44	1.78	4.66		0.884

NOTE: See text for computational details. COG denotes <sup>1</sup>H NMR center of gravity, Exp. denotes experimental, and Calc. denotes calculated. All values are parts per million downfield from tetramethylsilane (SiMe<sub>4</sub>), except for the HOMO–LUMO gaps, which are given in electronvolts calculated by the SCF MO method. <sup>a</sup>Unresolved, broad NMR absorptions SOURCE: Adapted from reference 11.

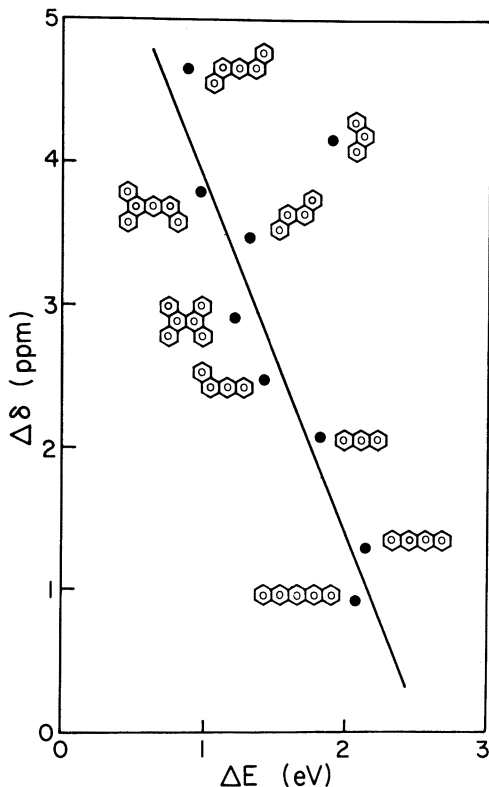


Figure 6. Correlation between the  $^1\text{H}$  NMR paratropic shifts of  $4n$   $\pi$  polycyclic aromatic dianions and the HOMO-LUMO energy gaps obtained by SCF MO calculations.

creases and results in detectable line broadening; in extreme cases, the NMR spectra totally disappear (20). The local field produced by the unpaired electron interacts with the magnetic moments of the nuclei and thus provides an efficient relaxation mechanism that leads to detectable line broadening of the proton NMR bands. Attributing the origin of these phenomena to an equilibrium between a singlet and a triplet state is supported by the appearance of the sharp half-field bands in the ESR spectra of dianions that exhibit broad  $^1\text{H}$  NMR signals or no spectra at all, for example, the benzo[*c*]phenanthrene dianion (9) and dibenz[*a,c*]anthracene dianion (8) (Table I).

An important conclusion emerges from the results in Table I: The paratropicity of the angular polycyclic  $4n$   $\pi$  electron dianions is much more pronounced than that of the linear polyacenes. For example, the naphthalene dianion (2) gave highly resolved  $^1\text{H}$  NMR lines and no half-field lines in its ESR spectrum, whereas the chrysene dianion (4) and the benz-



[*a*]anthracene dianion (6) (Table I), which are structural isomers of the naphthacene dianion, revealed only broad lines in their  $^1\text{H}$  NMR spectra. These two dianions, unlike the naphthacene dianion, gave a sharp ESR line attributed to  $\Delta M^S = 2$  in the ESR spectra (28). Another manifestation of these phenomena comes from a comparison of the anthracene dianion (3) with the phenanthrene dianion (7). Significant differences are seen by comparing the behavior of the pentacene dianion (1) with the behaviors of the dibenz[*a,h*]anthracene dianion (5) and dibenz[*a,c*]anthracene dianion (8) (Table I).

**HETEROCYCLIC DIANIONS.** Such phenomena appear also in polyheterocyclic dianions (20, 21). The data on these  $4n \pi$  dianions are summarized in Table II. The correlation between the HOMO–LUMO energy gaps and the extent of the observed line broadening of the  $^1\text{H}$  NMR spectra is well-demonstrated in Table II. Smaller calculated values for HOMO–LUMO energy gaps correspond to higher degrees of line broadening in the  $^1\text{H}$  NMR spectra. The diazine dianions exhibit less line broadening than their carbocyclic analogues. For example, the disodium salt of benzo[*c*]cinnoline (13) revealed a highly resolved  $^1\text{H}$  NMR spectrum even at room temperature, but the disodium salt of the phenanthrene dianion (7) gave no  $^1\text{H}$  NMR spectrum even at low temperatures (20). The dibenz[*a,c*]phenazine dianion (15) (Figure 7) revealed only minor line broadening, but dibenz[*a,c*]anthracene dianion (8) could not be observed by NMR regardless of the experimental conditions. The observation of two substituted diazine analogues of the naphthalene dianion, namely, the 2,3-diphenylquinoxaline dianion (16) and the 1,4-diphenylphthalazine dianion (14) is instructive. Although the naphthalene dianion has been discussed (35–37), no NMR spec-

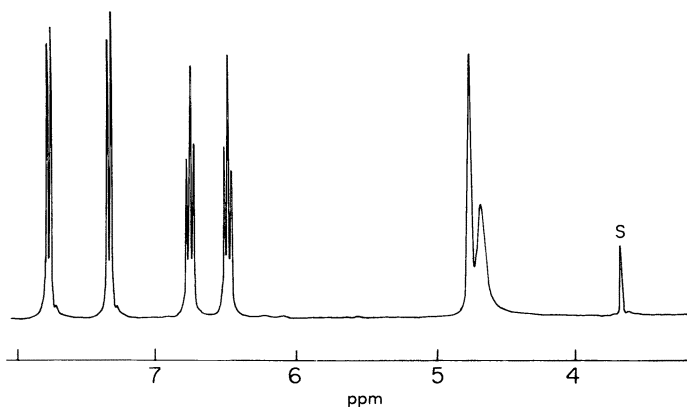


Figure 7.  $^1\text{H}$  NMR spectrum (300 MHz) of the dibenzo[*a,c*]phenazine dianion (15) as a disodium salt in  $\text{THF-d}_6$  at 293 K. S indicates a solvent signal. (Reproduced from reference 21. Copyright 1985 American Chemical Society.)

trum of this dianion has been reported. The HOMO–LUMO energy gap calculated by  $\omega\beta$  calculations for the naphthalene dianion is only 0.1  $\beta$  units. This rather low value predicts a relatively high population of the triplet state, a condition that may explain the absence of its  $^1\text{H}$  NMR spectrum.

Thus, the diazine  $4n$   $\pi$  dianions are less paratropic than their carbocyclic analogues. The decreased paratropicity can be understood by considering the introduction of an electronegative atom into the path of conjugation to result in an uneven charge delocalization. In general, the paratropicity of a system is the function of an effective delocalization of  $4n$   $\pi$  electrons. However, in the nitrogen-containing dianions, a partial charge localization occurs, and hence some quenching of their paratropicity also occurs. The lesser degree of paratropicity of the polyheterocyclic dianions in comparison with the respective carbocyclic dianions, can be attributed to a more pronounced deviation from planarity in heterocyclic  $4n$   $\pi$  dianions. This explanation cannot be ruled out because no X-ray data are currently available for such compounds.

A rather unexpected result is shown by the phenanthrazine dianion (17), which contains seven fused rings. This system shows a relatively high degree of line broadening (Figure 8) in comparison with the benzo[*c*]cinnoline dianion (13) and the 1,4-diphenylphthalazine dianion (14) (Table II), which consist of three and two fused rings, respectively. These unexpected experimental results are in accord with the low HOMO–LUMO energy gap

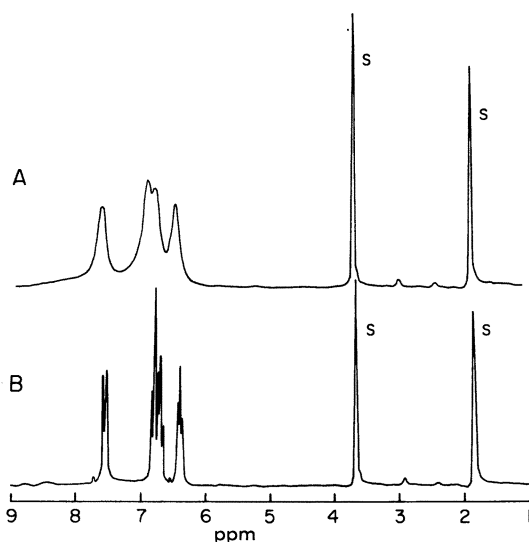


Figure 8. The effect of temperature on  $^1\text{H}$  NMR spectra (200 MHz) of the phenanthrazine dianion (17) as a disodium salt in  $\text{THF-d}_8$ . A: 293 K, B: 213 K. S indicates a solvent signal. (Reproduced from reference 22. Copyright 1986 American Chemical Society.)

(0.1  $\beta$  units) calculated for the phenanthrazine dianion (17) (Table II). This dianion supports the singlet–triplet hypothesis discussed earlier.

**Relationship of Topology and Structure to Paratropicity of  $4n$   $\pi$  Electron Dianions.** Figure 9 shows interesting relationships among  $4n$   $\pi$  electron dianions of related structures. Comparison of the heterocyclic dianions with their carbocyclic analogues shows that the heterocyclic dianions have higher HOMO–LUMO energy gaps than their respective carbocyclic analogues (21, 22). This finding is in accord with the heterocyclic dianions showing much less  $^1\text{H}$  NMR line broadening. As mentioned earlier,  $4n$   $\pi$  electron systems have the potential to exist as triplet ground states (38). Systems having higher degrees of symmetry show more pronounced tendencies toward a triplet ground state. A high degree of symmetry leads to orbital degeneracy involving singly occupied orbitals and hence to a triplet ground state. However, even systems that possess such symmetry do not need to adopt the triplet ground state because the orbital degeneracy can be split by the Jahn–Teller distortion, which will stabilize the singlet state

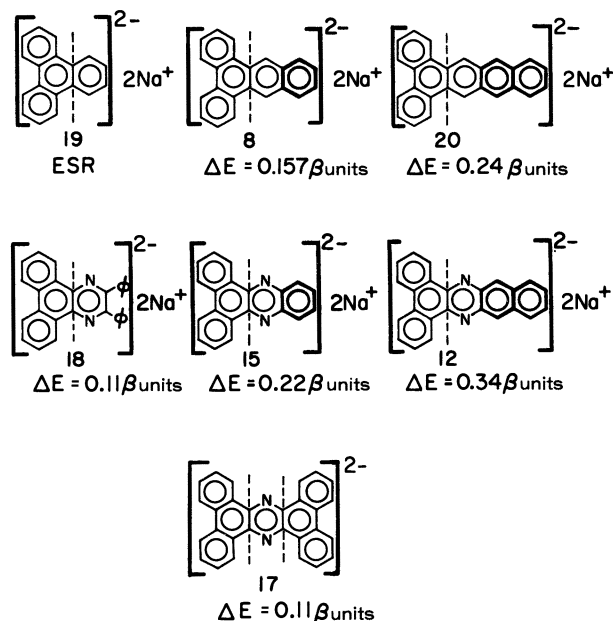


Figure 9. The relationship between topology and spectral parameters: Dianion 19 has a triplet ground state, whereas 8 shows a half-field absorption in its ESR spectrum but shows no  $^1\text{H}$  NMR spectrum. Dianion 18 does not show a  $^1\text{H}$  NMR spectrum, whereas 15, 20, and 17 show detectable line broadening of their  $^1\text{H}$  NMR spectra. Only 12 shows a  $^1\text{H}$  NMR spectrum without line broadening.

over the triplet state. This conclusion is based on a naive quantum mechanical description using a single electron configuration; a better description includes configuration interaction, which generally stabilizes the singlet state rather than the triplet state.

The triphenylene dianion (**19**), which has a high degree of symmetry and only limited possibilities of distortion, appears as a triplet ground state (39, 40) (Figure 9). The effect of removal of this symmetry on the paratropicity of the system is reflected by the calculated HOMO–LUMO energy gap and its manifestation in the line shape of the  $^1\text{H}$  NMR spectrum. This situation is shown in Figure 9. The 2,3-diphenyldibenzo[*f,h*]quinoxaline dianion (**18**), which can be described as a perturbed triphenylene dianion, shows no  $^1\text{H}$  NMR signals as a disodium salt in THF in the range of 30–70 °C. As the symmetry perturbation increases, the paratropicity is quenched, and the splitting between the two degenerate orbitals of the parent triphenylene structure increases. This removal of the orbital degeneracy is too small in the case of dibenz[*a,c*]anthracene dianion (**8**) to afford the observation of a  $^1\text{H}$  NMR spectrum. However, in the dianion of its diazine analogue (**15**), this splitting of the orbital energy is larger, and only minor line broadening is exhibited (Figure 7). The perturbation in the triphenylene structure is so pronounced in the tribenzo[*a,c,i*]phenazine dianion (**12**) that the HOMO–LUMO energy gap is considerably larger, and no line broadening is detected (Figure 10).

In principle, one can represent the dibenzo[*a,c*]naphthacene (**20**) as a combination of anthracene and phenanthrene (**23**). In the same sense, dibenzo[*a,c*]phenazine (**15**) and tribenzo[*a,c,i*]phenazine (**12**) can be considered as quinoxaline–phenanthrene and benzo[*g*]quinoxaline–phenanthrene, respectively (Figure 9). The  $^1\text{H}$  spectra of dianions **12**, **15**, and **20** are shown

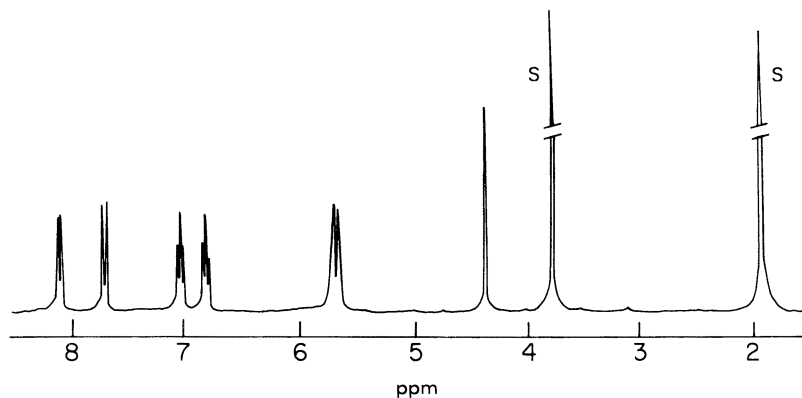


Figure 10.  $^1\text{H}$  NMR spectrum (300 MHz) of the tribenzo[*a,c,i*]phenazine dianion (**12**) as a disodium salt in  $\text{THF-d}_8$  at 203 K. S indicates a solvent signal. (Reproduced from reference 22. Copyright 1986 American Chemical Society.)

in Figures 10, 7, and 11, respectively. In these three dianions, nearly no charge is associated with their phenanthrene components, as reflected by the low-field absorptions of the protons assigned to the phenanthrene components of these charged species. The uneven delocalization is reflected also in the charge density obtained from calculations. This phenomenon associated with partitioning a system into a charged anthracene or benzo-[g]quinoxaline component and an uncharged phenanthrene component reflects the high antiaromaticity of the phenanthrene dianion (7). The phenanthrene dianion (7) is much more anti aromatic than the anthracene dianion (3) or the 2,3-diphenylbenzo[g]quinoxaline dianion (11) as reflected by the HOMO–LUMO energy gaps computed for these two dianions (0.23  $\beta$  units for 7 vs. 0.31  $\beta$  units for 3 and 0.34  $\beta$  units for 11). The calculations are supported experimentally by the  $^1\text{H}$  NMR spectra of these charged systems (chemical shifts and line shapes, cf. Figures 12 and 3 with Figure 4). Apparently, in the two-electron reduction processes to produce 15, 12, and 20, the molecules would have lost more energy if the major portion of the negative charge had been directed to the phenanthrene components of the charged molecules. Therefore, an alternative pathway of electron delocalization is preferred, namely, the one on which nearly no charge exists in the phenanthrene components, followed by a minimization of the antiaromatic contributions.

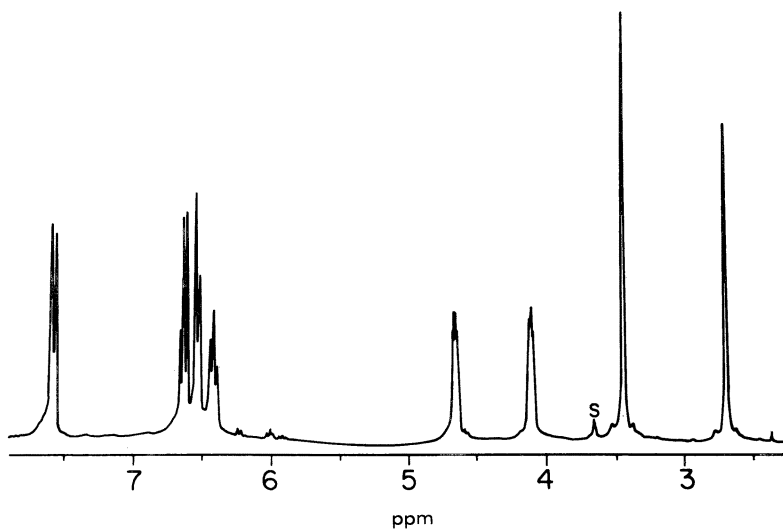


Figure 11.  $^1\text{H}$  NMR spectrum (300 MHz) of the dibenzo[a,c]naphthalene dianion (20) as a disodium salt in  $\text{THF-d}_3$  at room temperature (23). S indicates a solvent signal. (Reproduced from reference 23. Copyright 1984 American Chemical Society.)

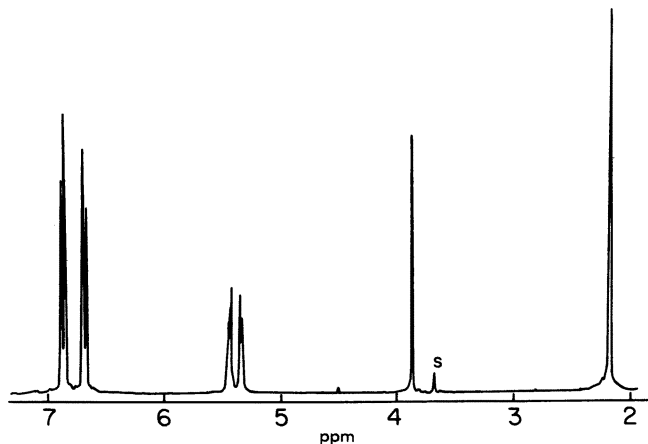


Figure 12.  $^1\text{H}$  NMR spectrum (300 MHz) of the 2,3-di-*p*-tolylbenzo-[g]quinoxaline dianion (24) as a disodium salt in  $\text{THF-d}_8$  at 294 K. S indicates a solvent signal.

**The HOMO–LUMO Energy Gap and the Paratropic Shift Experienced by  $4n \pi$  Electron Dianions.** In  $4n \pi$  electron systems in which the HOMO–LUMO gap is relatively narrow, the anisotropic term is influenced by  $\Delta E$ , thus showing a paratropic shift. If one could isolate the excessive paramagnetic shifts, their magnitude should depend upon the width of the HOMO–LUMO energy gaps. The results summarized in Table III and Figure 6 point toward an unequivocal quantitative correlation between the magnitude of the paratropic shifts and the estimated width of the HOMO–LUMO energy gaps in antiaromatic polycyclic dianions (11). The correlation coefficient is 0.953, which is rather good if one considers that the states of solvation of the various salts may not be the same. Conditions that favor contact ion-pairs shift the singlet–triplet equilibrium toward the triplet state, probably because of further decrease of the HOMO–LUMO gap. The SCF MO calculations used to compute the HOMO–LUMO energy gaps do not consider the state of solvation. Line broadening and the extra paratropic shift are two manifestations of the same characteristic of the system, namely, its paratropicity and hence its antiaromatic character. After a two-electron reduction process, linear polyacenes, which are less aromatic than nonlinear (angular) ones, produced  $4n \pi$  systems showing less pronounced paratropicity. Significant examples of this observation are the following pairs: pentacene dianion (1) versus dibenz[*a,h*]anthracene dianion (5) and naphthacene dianion (2) versus benz[*a*]anthracene dianion (6). Therefore, the aromatic nature of a system appears to depend strongly on its topology. The good correlation found between the magnitude of the paratropic shift and the extent of the HOMO–LUMO energy gap indicates that this energy gap be a useful theoretical index for antiaromaticity of the systems

under investigation. The HOMO–LUMO gap of a  $4n$   $\pi$ -electron system is manifested experimentally by the paratropicity as reflected in its  $^1\text{H}$  NMR spectrum (line shape and chemical shift).

### Acknowledgment

Financial support by the Basic Science Foundation administered by the Israel Academy of Sciences and Humanities is gratefully acknowledged.

### References

1. Kekule, A. *Liebigs Ann. Chem.* **1872**, 163, 88.
2. Breslow, R. *Chem. Eng. News* **1965**, 43, 90.
3. Breslow, R. *Acc. Chem. Res.* **1973**, 6, 393.
4. *Aromaticity, Pseudoaromaticity, Antiaromaticity*; Bergmann, E. D.; Pullman, B., Eds.; Academic: Jerusalem, 1971.
5. Garratt, P. J. *Aromaticity*, Wiley: New York, 1986.
6. Rabinovitz, M., Ed. *Isr. J. Chem.* **1980**, 20, 213–321.
7. Graovac, A.; Trinajstić, N., Eds. *Proc. Int. Sym. Arom.*, Dubrovnik, Croatia, Yugoslavia. *Pure Appl. Chem.* **1980**, 52, 1397–1667.
8. Agranat, I., Ed. Proc. ISNA-4, Jerusalem, Israel. *Pure Appl. Chem.* **1982**, 54, 927–1155.
9. Garratt, P. J., Ed. Proc. ISNA-5, St. Andrew, Scotland, UK. *Pure Appl. Chem.* **1986**, 58, 1–210.
10. Mallion, R. B. *Pure Appl. Chem.* **1980**, 52, 1541.
11. Minsky, A.; Meyer, A. Y.; Rabinovitz, M. *Tetrahedron* **1985**, 41, 785.
12. Hückel, E. *Z. Phys. Chem.* **1931**, 70, 204.
13. Platt, J. R. *J. Chem. Phys.* **1949**, 17, 484.
14. Randić, M. *Chem. Phys. Lett.* **1976**, 36, 68.
15. Randić, M. *J. Am. Chem. Soc.* **1977**, 99, 444.
16. Pople, J. A. *Mol. Phys.* **1958**, 1, 175.
17. McWeeny, R. *Mol. Phys.* **1958**, 1, 311.
18. Haigh, C. W.; Mallion, R. B. *Progr. Nucl. Magn. Reson. Spectrosc.* **1980**, 14, 303.
19. Pople, J. A.; Untch, K. G. *J. Am. Chem. Soc.* **1966**, 88, 4811.
20. Minsky, A.; Meyer, A. Y.; Poupko, R.; Rabinovitz, M. *J. Am. Chem. Soc.* **1983**, 105, 2164.
21. Minsky, A.; Cohen, Y.; Rabinovitz, M. *J. Am. Chem. Soc.* **1985**, 107, 1501.
22. Cohen, Y.; Meyer, A. Y.; Rabinovitz, M. *J. Am. Chem. Soc.* **1986**, 108, 7039.
23. Minsky, A.; Rabinovitz, M. *J. Am. Chem. Soc.* **1984**, 106, 6755.
24. Berson, J. A.; Evleth, Jr. E. M.; Manatt, S. L. *J. Am. Chem. Soc.* **1965**, 87, 2901.
25. Boyd, G. V.; Singer, N. *Tetrahedron* **1966**, 22, 3383.
26. Wohl, A. J. *Tetrahedron* **1968**, 24, 6889.
27. Looyenga, H. *Mol. Phys.* **1966**, 11, 337.
28. Gordy, W. *Theory and Applications of ESR*; Wiley: New York, 1979; pp 551–557.
29. Berthier, G.; Baudet, J.; Suard, M. *Tetrahedron* **1963**, 19, 1, Suppl. 2.
30. Meyer, A. Y.; Serre, J. *Theor. Chim. Acta* **1967**, 8, 117.
31. Meyer, A. Y.; Pasternak, R. *Theor. Chim. Acta* **1978**, 47, 27.

32. Julg, A. *J. Chim. Phys. Phys.-Chim. Biol.* **1958**, *55*, 413.
33. Schaeffer, R.; Schneider, W. G. *Can. J. Chem.* **1963**, *41*, 966.
34. Günther, H. *NMR Spectroscopy* Wiley: New York, 1980; pp 264–266.
35. Smid, J. *J. Am. Chem. Soc.* **1965**, *87*, 655.
36. Carnahan, J. C.; Closson, W. D. *J. Org. Chem.* **1972**, *34*, 4469.
37. Gia, H. B.; Jerome, R.; Teyssie, P. J. *Organomet. Chem.* **1980**, *190*, 107.
38. Breslow, R. *Pure Appl. Chem.* **1982**, *54*, 927.
39. Willigen, H.; Brackhoven, J. A. M.; De Boer, E. *Mol. Phys.* **1967**, *12*, 533.
40. Sommerdijk, J. L.; De Boer, E. *J. Chem. Phys.* **1969**, *50*, 4771.

RECEIVED for review September 29, 1986. ACCEPTED January 29, 1987.



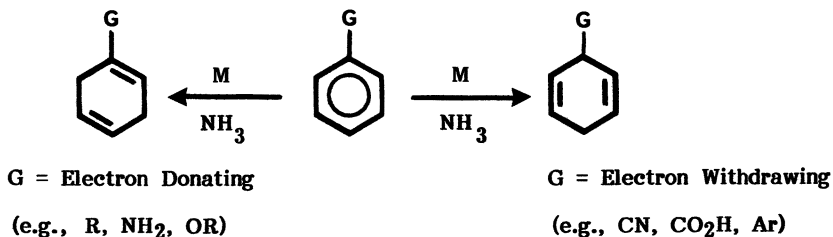
# Dissolving-Metal Reduction of Polynuclear Aromatic Compounds in Liquid Ammonia

Peter W. Rabideau

Purdue School of Science at Indianapolis, Indiana University–Purdue University  
at Indianapolis, Indianapolis, IN 46223

*This chapter deals with the conversion of aromatic compounds to dihydroaromatic compounds by the action of alkali metals in liquid ammonia; polynuclear compounds are emphasized. Various aromatic compounds are classified according to the principal intermediate that persists in ammonia solution. Possibilities include (1) radical anions, (2) dianions, and (3) monoanions; monoanions are formed by the ammonia protonation of dianions. Most two-, three-, and four-ring compounds fit into the monoanion category, including naphthalene, biphenyl, anthracene, and terphenyl. The regioselectivity of this reaction is also discussed, and computational methods such as MNDO (semi-empirical molecular orbital calculations) are used to predict products by a determination of the positions of highest electron density in the intermediate dianions. Finally, competing processes such as dimerization and bond cleavage are considered.*

**T**HE REACTION OF BENZENE or one of its derivatives with an alkali metal in liquid ammonia containing an alcohol cosolvent is known as the Birch reduction (1–6). As expected with anionic intermediates, 1-substituted-1,4-dihydro products result from electron-withdrawing groups, and 2,5-dihydro products result from electron-donating groups, as shown in Scheme I. Application of these conditions to polynuclear aromatic compounds produces complications because the products formed initially are subject to reduction under the reaction conditions (3). Although methods such as the use of iron salts minimize side reactions, more recently developed procedures avoid



Scheme I

the use of alcohol altogether and employ stronger quenching agents like water or ammonium chloride that are added after reaction with the alkali metal is complete (7–9). In the absence of alcohols, the polynuclear aromatic compound–alkali metal solutions can be reacted with alkyl halides to produce dialkylated products (e.g., anthracene) (3); this finding supports the intermediacy of dianions, which was suggested by early workers. However, later research showed that dialkylated products can arise by the initial alkylation of a monoanion (formed by monoprotection of a dianion by ammonia) followed by deprotonation via amide to produce a second monoanion (7–9). That is, the original dianion intermediate is protonated by ammonia to furnish a monoanion (and amide), which may be alkylated; but this monoalkyl dihydro product undergoes deprotonation by amide, allowing a second (or even further) alkylation to take place. This process was demonstrated for anthracene in the following manner (8).

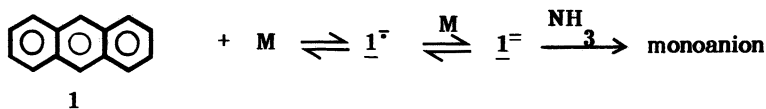
### *Equilibria of Dianions and Radical Anions with Their Neutral Precursors*

Dianions are always in equilibrium with their radical-anion counterparts (10). Moreover, the radical anions are in equilibrium with their neutral precursors. Hence, if a dianion is generated as the persistent anionic species, then in accordance with Le Chatelier's principle, the removal of metal (M) should shift the equilibrium back to the neutral aromatic hydrocarbon (ArH):

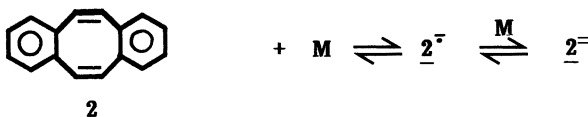


The metal can be conveniently removed because the addition of FeCl<sub>3</sub> (or other iron salts) catalyzes the reaction of the metal with ammonia to produce a metal amide plus hydrogen. When anthracene (1) was reacted with sodium and ammonia for 10 min, quenching of an aliquot with water produced 9,10-dihydroanthracene. A small amount of FeCl<sub>3</sub> was then added, and after 2 h, water quenching still produced 9,10-dihydroanthracene. These results are consistent with Scheme II, wherein the monoanion is irreversibly pro-

tonated by ammonia; thus, the previous equilibriums cannot be shifted. However, it was quickly realized that this experiment would be more convincing if reversion of the stable dianion (i.e., the dianion resistant to protonation by ammonia) back to the neutral starting material could be demonstrated (Scheme III). Dibenzocyclooctatetraene (**2**) was chosen to demonstrate this reversion because its dianion is a  $(4n + 2)$  aromatic system. The addition of  $\text{FeCl}_3$  did produce the neutral hydrocarbon **2**, even though water quenching of an aliquot before iron addition produced the dihydro compound (dibenzocyclooctatriene).



Scheme II



Scheme III

The amide back reaction during alkylation can be minimized or even eliminated by inverse-quenching procedures. When the metal–ammonia solutions of anthracene or naphthalene are added to an excess of alkyl halide, dramatic changes in the ratio of mono- to dialkylated products result (*see* Table I). The predominance of monoalkylation with inverse quenching certainly supports the presence of monoanions. Perhaps even the minor amounts of dialkylated products formed by inverse quenching are still being formed by a back reaction.

A similar mechanism was proposed by Lindow et al. (11) for the biphenyl system. However, biphenyl provides much less dialkylation (Table I) than either naphthalene or anthracene under normal quenching conditions. Perhaps the amide deprotonation is slower in this case because of the reduced acidity of the doubly allylic system (i.e., 1,4-dihydrobiphenyl) in comparison with the allylic–benzylic or doubly benzylic systems (i.e., dihydronaphthalene or dihydroanthracene, respectively).

More recently, the irreversible protonation of several dianions by ammonia was demonstrated spectroscopically by Mullen et al. (12). Upon initial contact with alkali metal, solutions of anthracene and phenanthrene in 1:5 ammonia–tetrahydrofuran (THF) gave rise to electron spin resonance (ESR) spectra characteristic of the radical anions. Further metal contact led to the

**Table I. Reductive Alkylation of Anthracene, Naphthalene, and Biphenyl in Metal-Ammonia Solutions**

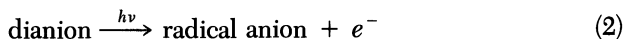
<i>Metal</i>	<i>Alkyl Halide<sup>a</sup> (RX)</i>	<i>Quench Procedure</i>	<i>Composition (%) ArH<sub>2</sub>R</i>	<i>ArHR<sub>2</sub></i>
Anthracene				
Na	MeBr	normal	15	80
Na	MeBr	inverse	88	12
Na	EtBr	normal	25	75
Na	EtBr	inverse	63	37
Li	EtBr	normal	32	68
Li	EtBr	inverse	81	9
Naphthalene				
Na	MeBr	normal	20	80
Na	MeBr	inverse	90	—
Na	EtBr	normal	25	75
Na	EtBr	inverse	90	9
Biphenyl				
Li	MeBr	normal	99	1
Na	MeBr	normal	50	41

NOTE: The anthracene and naphthalene reactions were performed at  $-78^{\circ}\text{C}$  for 15–30 min, and the biphenyl reactions were performed at  $-33^{\circ}\text{C}$  for 15–30 min.

<sup>a</sup>Me denotes methyl, and Et denotes ethyl.

SOURCE: Data for anthracene and naphthalene are from reference 8, and data for biphenyl are from reference 11.

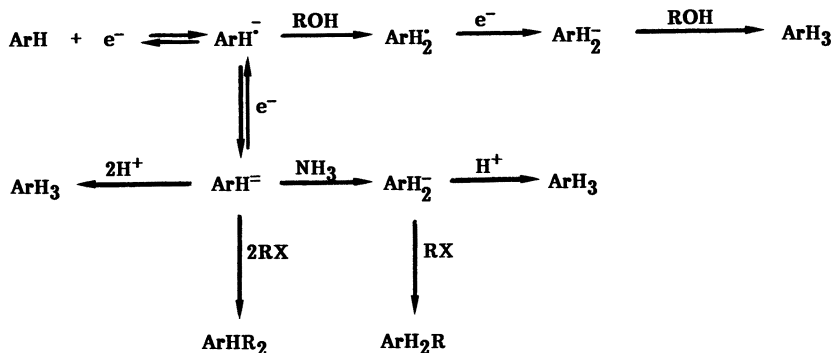
disappearance of ESR signals, and, in each case,  $^{13}\text{C}$  NMR spectra consistent with monoanions were recorded. Moreover,  $h\nu$  irradiation of the monoanion solutions did not regenerate ESR spectra, as would be expected if any dianions were present; that is, photooxidation would occur as follows:



Hence, the chemical evidence presented for anthracene was confirmed spectroscopically. Furthermore, Mullen et al. (12) categorized a number of hydrocarbons in  $\text{Li-NH}_3$  solutions into two classes: group 1 hydrocarbons that exist as monoanions in ammonia; and group 2 hydrocarbons that exist as dianions in ammonia. Group 1 includes anthracene and its 9-methyl, 9-phenyl, and 9,10-diphenyl derivatives; acenaphthylene; azulene; fluoranthene; phenanthrene; and pyrene. Group 2 includes aceheptylene, cyclooctatetraene, and perylene.

**Metal–Ammonia Reduction**

These results allow a complete description of metal–ammonia processes, as shown in Scheme IV. The upper pathway represents the classical Birch reduction (i.e., benzenes), whereas polynuclear aromatic compounds react by one of the lower routes. As indicated in Scheme IV, the protonation of dianions rather than radical anions by ammonia is favored. We previously suggested dianion protonation (8) because radical anions are not very basic (10). Recently, Mullen et al. (12) pointed out that, in some cases, dianions and radical anions of the same neutral precursor are protonated at different sites; in the cases they investigated, protonation occurred with the dianions.



Scheme IV

Thus, optimum experimental conditions will be determined by how a particular polynuclear aromatic compound fits into Scheme IV. Burkholder and I (8) suggested the following categories on the basis of the principal intermediate that persists in ammonia solution:

1. Radical anions only: Compounds with relatively low electron affinities (like benzenes) will not form dianions, and alcohols must be added to protonate the radical anion and shift the initial (often unfavorable) equilibrium. In such cases, reductive alkylation is generally not possible.

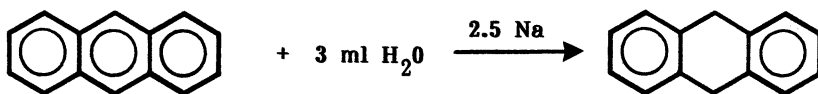
2. Stable monoanions: In these cases (e.g., anthracene, biphenyl, naphthalene) alcohols as cosolvents should be avoided, and water or ammonium chloride will serve as good quenching agents after a suitable reaction period. Inverse addition into alkyl halides will produce mainly monoalkyl products, but normal addition may furnish dialkylated or higher alkylated products because of the amide back reaction.

3. Unstable monoanions: In some cases (e.g., phenanthrene), the monoanion is protonated by ammonia, and this reaction produces a neutral compound. If the neutral compound is reactive under the reaction conditions, overreduction will result. Similarly, alkylated dihydro products cannot be obtained, although alkylation of subsequent anionic species may be possible

(e.g., 4a-methyl-2,4a,9,10-tetrahydrophenanthrene from phenanthrene) (13).

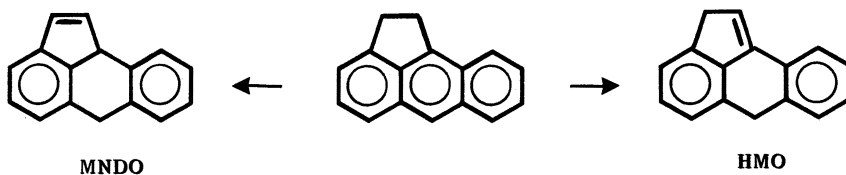
4. Stable dianions: Systems capable of forming aromatic dianions (e.g., cyclooctatetraenes) or larger polynuclear aromatic compounds (e.g., perylene) fit into this category. Again, strong quenching agents are recommended, and dialkylation is possible.

Researchers have often suggested (3, 4) that methyl-ammonia reduction must be carried out with carefully purified polynuclear aromatic compounds and scrupulously dried ammonia and ethyl ether cosolvents. Hence Burkholder and I (8) were surprised to learn that commercial anthracene could be reduced almost quantitatively without prior purification of ammonia or THF (or ethyl ether) and with a rather wide variation in the amount of metal used. More recently, my co-workers and I (14) found that 0.5 g of anthracene in ammonia-THF containing 3 mL of H<sub>2</sub>O can be reduced in excellent yield by the addition of 2.5 mol of sodium (Scheme V). These results indicate that electron addition to polynuclear aromatic compounds is a very fast process, and destruction of the metal by water is simply not competitive under these conditions.



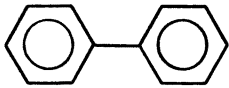
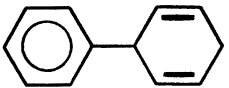
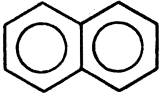
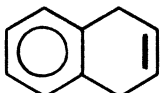
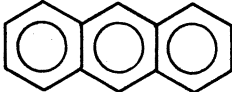
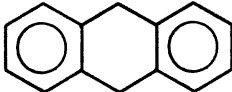
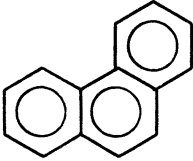
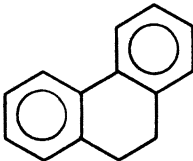
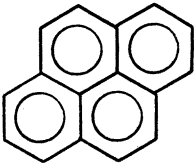
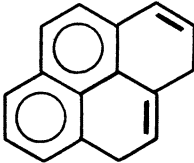
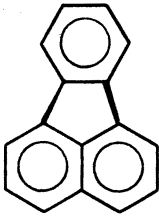
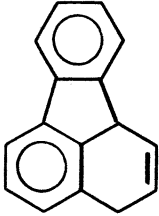
Scheme V

**Prediction of Products.** The products (i.e., regiochemistry) of metal-ammonia reduction are determined from the (initial) protonation site of the dianion as well as the (subsequent) protonation site of the monoanion. These protonations are generally considered to occur at the sites of highest electron density; thus, products can be predicted by molecular orbital calculations (12, 15–18). Several examples are shown in Table II. However, different theoretical methods may produce contrasting results, and highest occupied molecular orbital (HOMO) coefficients may be more important than overall electron densities. For example, different reduction products are predicted for aceanthrylene by MNDO (19, 20) and Hückel molecular orbital (HMO) calculations. In fact, the HMO product is the one actually formed (Scheme VI).



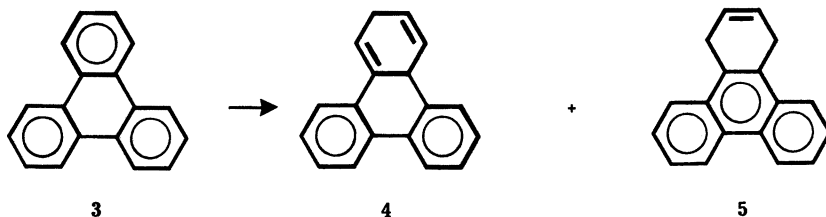
Scheme VI

Table II. Some Representative Metal–Ammonia Reduction Products

<i>Aromatic Substrate</i>	<i>Reduction Product</i>	<i>Calculated</i>
		yes
		yes
		yes
		yes
		no
		yes

SOURCE: The calculated results are from references 15 and 40, except for pyrene which is from reference 41.

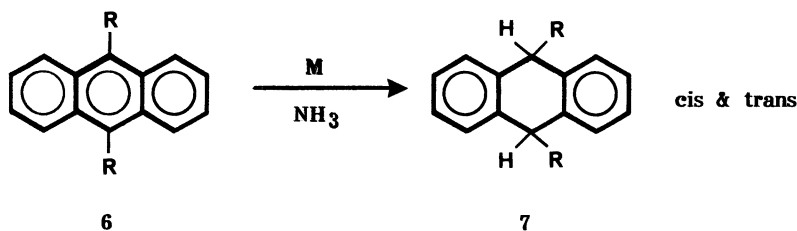
In the case of triphenylene (3), MNDO calculations predict only the 2,4a-dihydro product (4). However, sodium–ammonia reduction produces only one dihydro product (Scheme VII), assigned as 5 on the basis of carbon and proton NMR (19, 20). This result is quite remarkable because this product is unexpected from calculations as well as from comparison with the



Scheme VII

reduction of related systems like *o*-terphenyl, which gives a product similar to 4 (21).

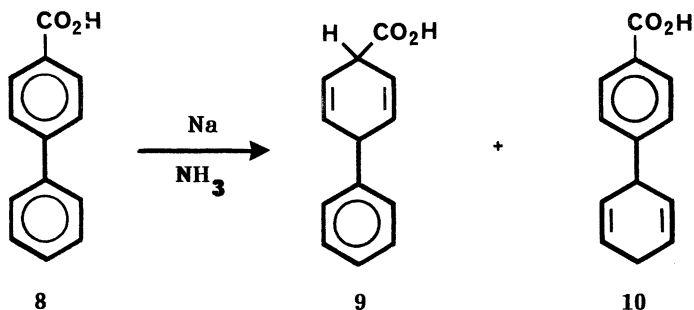
**Effect of Substituents.** Substituents are not expected to exert the same influence on polynuclear aromatic compounds as they do on benzenes because their effect may be greatly attenuated by the normal distribution of added electron density in the parent polynuclear aromatic compound. For example, even with the presence of two electron donors, 9,10-dialkylanthracenes (6) reduce in the central ring (Scheme VIII), just as the parent compound does (3). Moreover, a strong electron-withdrawing group like carboxylate does shift reduction to the substituted ring, as in 4-biphenylcarboxylic acid (8, Scheme IX), but even in this case some reduction (ca. 25%) occurs in the unsubstituted ring (22, 23). The analogous *tert*-butyl ester, however, reduces exclusively in the substituted ring (22). Electron-releasing substituents in the 1-position of naphthalene direct reduction to the adjacent ring (Scheme X), whereas electron-withdrawing groups result in 1,4-dihydro products (3, 24, 25).



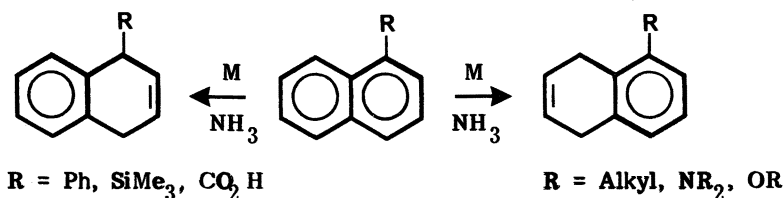
Scheme VIII

The 2-substituted naphthalenes are not as straightforward, and tend to reduce in the substituted ring regardless of the nature of the substituent. For example, 2-methylnaphthalene was claimed to reduce exclusively in the methylated ring (26). Although a reinvestigation uncovered the presence of a second isomer (12, Scheme XI), the major product is, in fact, 11 (18). This

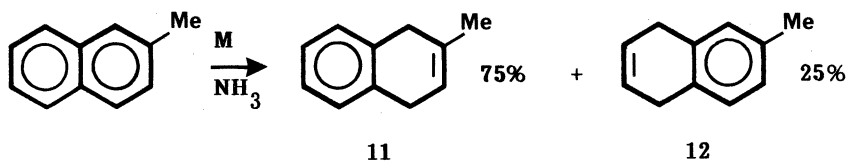




Scheme IX



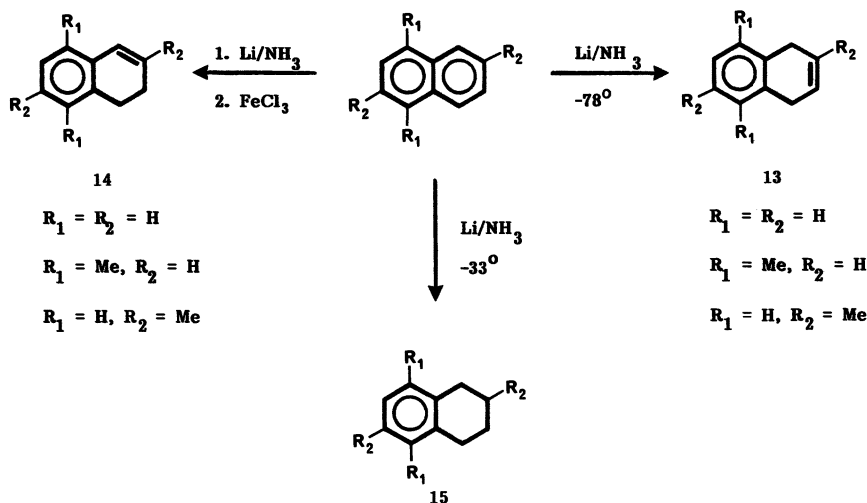
Scheme X



Scheme XI

result was explained in the following way: Methyl groups are stabilizing on  $sp^2$  carbons (e.g., olefins); therefore, lack of deactivation (or even activation) may be possible for a highly delocalized carbanion with a methyl substituent on a position that bears little of the excess charge. Another example of this situation is 3-methylbiphenyl, which bears a charge mainly at C-1(1') and C-4(4'); it reduces primarily (80%) in the substituted ring (10).

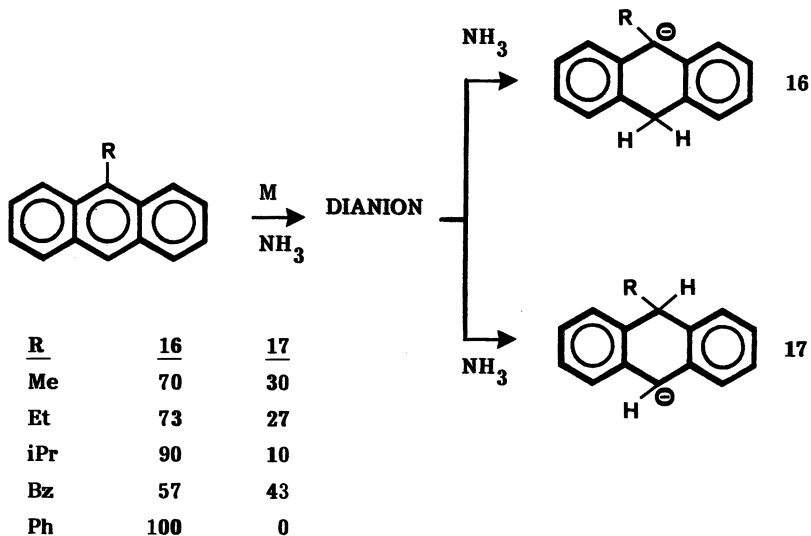
**Effect of Reaction Conditions.** The naphthalene system also provides an interesting example of how product composition may be affected by reaction conditions (27). Naphthalene, as well as its 1,4-dimethyl and 2,6-dimethyl derivatives, can be reduced smoothly (with yields greater than 90%) by lithium-NH<sub>3</sub> at -78 °C (Scheme XII) because the final monoanion (*see* the preceding discussion) is stable at this low temperature, and rapid protonation produces the 1,4-dihydro product (13). However, at reflux, the



Scheme XII

monoanion (Li salt) is also protonated, and consequently the neutral 1,4-dihydro product is formed in the reaction medium, which now contains two equivalents of lithium amide. The amide causes a rearrangement to the conjugated isomer (14). If this reaction occurs in the presence of excess metal, this isomer is further reduced; thus, simply beginning with excess lithium at  $-33^\circ\text{C}$  produces tetrahydro products (15) in 94–99% yields. By carrying out the initial reduction at  $-78^\circ\text{C}$  and then adding  $\text{FeCl}_3$  to destroy excess metal, the 1,2-dihydro isomers (14) can be produced by simply allowing the reaction mixture to warm up to reflux (82–98%).

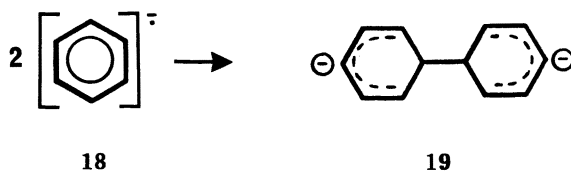
**Reduction at the Site of Substitution.** 9-Alkylanthracenes are also intriguing, because unlike the naphthalene system, reduction takes place at the site of substitution. This situation raises the question as to where the initial protonation of the dianion takes place. HOMO coefficients (MNDO) are slightly higher at C-10 for R being methyl, ethyl, and isopropyl, although total electron densities are higher at C-9 (28). In fact, methylation of the monoanions produces 9-methyl-9,10-dihydroanthracenes (i.e., from 16) as the major products (Scheme XIII). However, as suggested in 1954 by Barton (29), the stability of the monoanion may play a role in this process. Apparently, this situation is true when R is phenyl, because in this case only monoanion 16 is produced. Calculations regarding monoanion stabilities (heats of formation), however, indicate that no conflict exists between these two approaches in the present case because the 9-R anions (16) are predicted to be the most stable (28). Hence, both methods suggest that protonation should take place at C-10 in the 9-R dianions.



Scheme XIII

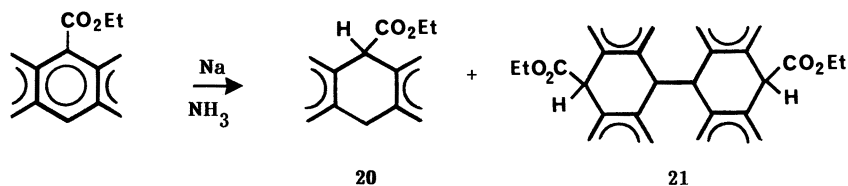
### Dimerization and Bond Cleavage

So far the conversion of aromatic rings to dihydroaromatic compounds has been discussed. Two other important processes are dimerization and bond cleavage; these processes are more important in ethers than in ammonia. Because radical anions are being generated, dimerization might be possible through a simple radical-combination reaction (Scheme XIV). However, such observations are rare (30). Dimerization is expected to be unfavorable on the basis of entropic considerations, and the presumed greater immobilization of solvent in **19** makes dimerization even more unfavorable. Moreover, as noted by Dewar and Dougherty (31), dimerization requires the conversion of two aromatic species (**18**) into a nonaromatic, albeit highly delocalized, double anion (**19**). At least two reports (32, 33) indicate that dimer (and trimer) formation can be substantial, even in ammonia-ethyl ether solvent mixtures. Neither report, however, suggests that radical dimerization is the responsible pathway.



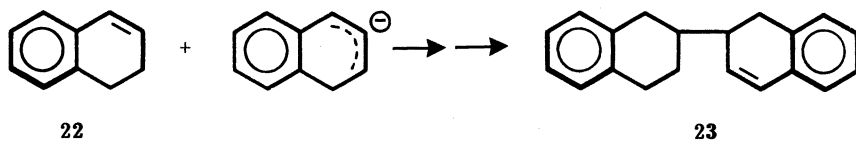
Scheme XIV

The sodium–ammonia reduction of ethyl 9-anthroate (**32**) produces both **20** and **21** (Scheme XV); the ratio of monomer to dimer varies from 40:60 to 20:80, depending on concentration (0.025–0.1 M). However, both the 9,10-dihydroanthracene monoanion and the dianion react with ethyl 9-anthroate to produce dimeric (and with the dianion, trimeric) products, and so radical intermediates are not considered responsible.



Scheme XV

Similarly, the alkali–metal reduction of naphthalene in ammonia at  $-33\text{ }^{\circ}\text{C}$  for extended reaction periods produces substantial amounts (20–70%) of oligomeric products (33–35). This result is due to a slow buildup of 1,2-dihydronaphthalene (**22**), which then adds to its monoanion to form a dimeric monoanion (Scheme XVI); the dimeric monoanion is protonated by ammonia. Hence, this process is dependent on the generation of neutral, reduced products that are formed by higher temperatures, Li over Na, and extended reaction periods. Presumably, these factors are the reasons that such products were not noted in the earlier study (32).



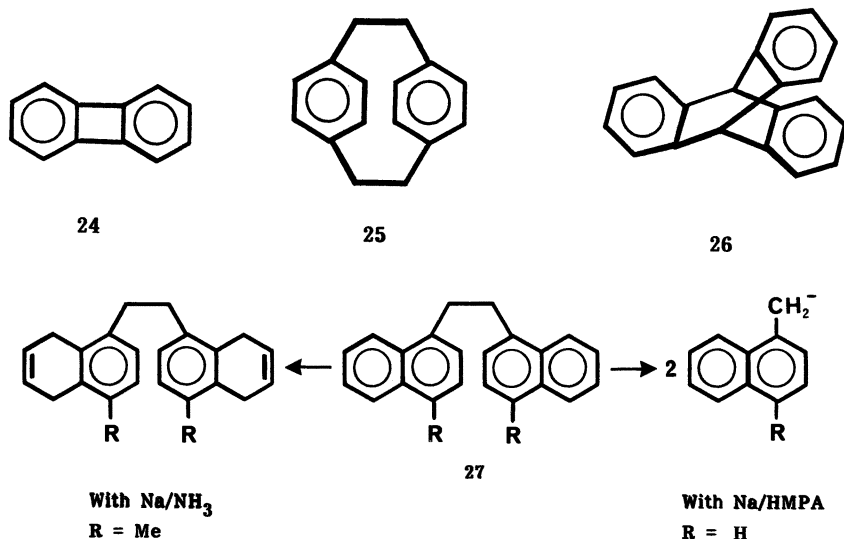
Scheme XVI

Thus, dimerization appears most likely to occur when an anion (or dianion) and a suitable acceptor molecule are both present in reasonable concentration:



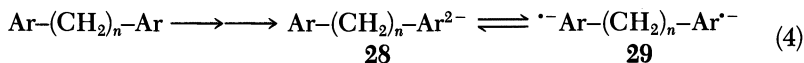
Moreover, some driving force will be provided if the  $[\text{A-acceptor}]^-$  is either especially stable (like the ethyl 9-anthroate case) or removed from equilibrium by ammonia protonation (like the naphthalene case).

The cleavage of aryl-aryl, aryl-benzyl, and benzyl-benzyl bonds can also occur during dissolving-metal reduction (34, 35). This cleavage may be due to ring strain in cases such as biphenylene (24), [2.2]-paracyclophane (25), and triptycene (26); although for triptycene, aryl-benzyl cleavage takes place in THF but not ammonia (36). Similarly, dinaphthylethanes (27) undergo cleavage (Scheme XVII) in ethyl ether and hexamethylphosphoric triamide (HMPA) (34, 35), but metal-ammonia reduction provides aromatic ring reduction (37). Interestingly, 27 appears to reduce more easily in both



*Scheme XVII*

rings (tetrahydro reduction) than in only one ring (dihydro reduction) even with a limited amount of metal. This situation may be due to an internal disproportionation:



Such processes in bridged anthracenes were recently reported by Fiedler et al. (38), and the general question of electron transfer across spacers connecting aromatic molecules has received recent attention (39).

## Conclusion

In this discussion of the metal-ammonia processes involving polynuclear aromatic compounds, some potentially important topics were omitted. One such topic is the stereochemistry of reduction, which is quite important

when the hydrogenated carbons bear substituent groups and is also important during reductive alkylation. This topic has been the subject of numerous investigations, especially those involving the anthracene system (*see* reference 14 for leading references). A second important area is ion pairing, which may play a critical role in some of these reactions. For example, protonation sites could be controlled by the cation through either prior coordination of the protonating agent or ion-pair effects on electron-density distributions. Although the systems discussed herein presumably involve solvent-separated ion pairs in ammonia, ion pairing has not been thoroughly investigated.

### Acknowledgment

I thank my many co-workers as well as the Office of Basic Energy Sciences, Division of Chemical Sciences, U.S. Department of Energy, for support of this work.

### References

1. Birch, A. J. *Q. Rev. Chem. Soc.* **1950**, *4*, 69.
2. House, H. O. *Modern Synthetic Reactions*; W. A. Benjamin: Los Angeles, CA, 1972, 2nd ed.
3. Harvey, R. G. *Synthesis* **1970**, *4*, 161.
4. Birch, A. J., Rao, G. Subba *Advances in Organic Chemistry, Methods and Results*; Taylor, E. C., Ed.; Wiley-Interscience: New York, 1972.
5. For application to fossil fuels, *see* Stock, L. M. In *Coal Science*; Gorbaty, M. L.; Laren, J. W.; Wender, I., Eds.; Academic: New York, 1982; Vol. 1
6. Ebert, L. B., In *Chemistry of Engine Combustion Deposits*; Ebert, L. B., Ed.; Plenum, 1985.
7. Lindow, D. F.; Cortez, C. N.; Harvey, R. G. *J. Am. Chem. Soc.* **1972**, *94*, 5406.
8. Rabideau, P. W.; Burkholder, E. G. *J. Org. Chem.* **1978**, *43*, 4283.
9. The properties of sodium dissolved in anhydrous liquid ammonia are quite different from the metal itself. *See* Lepoutre, G.; Sienko, M. J. *Metal-Ammonia Solutions*; Benjamin: New York, NY, 1964.
10. Szwarc, M. *Ions and Ion Pairs in Organic Reactions*; Szwarc, M., Ed.; Wiley-Interscience: New York, NY, 1972.
11. Lindow, D. F.; Cortez, C. N.; Harvey, R. G. *J. Am. Chem. Soc.* **1972**, *94*, 5406.
12. Mullen, K.; Huber, W.; Neumann, G.; Schnieders, C.; Unterberg, H. *J. Am. Chem. Soc.* **1985**, *107*, 801.
13. Rabideau, P. W.; Harvey, R. G. *J. Org. Chem.* **1970**, *35*, 25.
14. Rabideau, P. W.; Day, L. M.; Husted, C. M.; Mooney, J. L.; Wetzel, D. M. *J. Org. Chem.* **1986**, *51*, 1681.
15. Streitwieser, A., Jr.; Suzuki, S. *Tetrahedron* **1961**, *16*, 153.
16. Zimmermann, H. E. *Ibid.* **1961**, *16*, 169.
17. Birch, A. J.; Hinde, A. Li; Radom, L. *J. Am. Chem. Soc.* **1980**, *102*, 3370.
18. *See also* Rabideau, P. W.; Peters, N., K.; Huser, D. L. *J. Org. Chem.* **1981**, *46*, 1593.
19. Marcinow, Z.; Sygula, A.; Rabideau, P. W., submitted for publication.

20. MNDO is a semiempirical molecular orbital calculation method. See Dewar, M.J.S.; Thiel, W. *J. Am. Chem. Soc.* **1977**, *99*, 4899–4907.
21. Harvey, R. G.; Lindow, D. F.; Rabideau, P. W. *J. Am. Chem. Soc.* **1972**, *94*, 5412.
22. Rabideau, P. W.; Nyikos, S. J.; Huser, D. L.; Burkholder, E. G. *J. Chem. Soc. Chem. Commun.* **1980**, 210.
23. See also, Franks, D.; Grossel, M. C.; Hayward, R. C.; Knutsen, L. J. S. *J. Chem. Soc. Chem. Commun.* **1978**, 941.
24. See also Rabideau, P. W.; Burkholder, E. G.; Yates, M. J. *Syn. Comm.* **1980**, *10*, 627.
25. Rabideau, P. W.; Husted, C. A.; Young, D. M. *J. Org. Chem.* **1983**, *48*, 4149.
26. Hüchel, W.; Wartini, M. *Justus Liebigs Ann. Chem.* **1965**, *40*, 686.
27. Rabideau, P. W.; Huser, D. L. *J. Org. Chem.* **1983**, *48*, 4266.
28. Rabideau, P. W.; Maxwell, A. J.; Sygula, A. J. *J. Org. Chem.* **1986**, *51*, 3181.
29. Barton, D. H. R.; Robinson, C. H. *J. Chem. Soc., Chem. Commun.* **1954**, 3045.
30. Holy, N. L. *Chem. Rev.* **1974**, *74*, 243.
31. Dewar, M. J. S.; Dougherty, R. C. *The PMO Theory of Organic Chemistry*; Plenum: New York, 1975, p 532.
32. Rabideau, P. W.; Wetzel, D. M.; Young, D. M. *J. Org. Chem.* **1984**, *49*, 1544.
33. deVlieger, J.J.; Kieboom, P.G.; van Bekkum, H. *J. Org. Chem.* **1986**, *51*, 1389.
34. Lagendijk, A.; Szwarc, M. *J. Am. Chem. Soc.* **1971**, *93*, 5359.
35. Grovenstein, Jr., E.; Bhatti, A. M.; Quest, D. E.; Sengupta, D.; Van Derveer, D. *J. Am. Chem. Soc.* **1983**, *105*, 6290.
36. Rabideau, P. W.; Jessup, D. W.; Ponder, J. W.; Beekman, G. F. *J. Org. Chem.* **1979**, *44*, 4594.
37. Rabideau, P. W.; Marcinow, Z. *Fuel* **1985**, *64*, 871.
38. Fiedler, J.; Huber, W.; Mullen, K. *Angew. Chem. Int. Ed.* **1986**, *25*, 443.
39. See Heitele, H. and Michel-Beyerle, M.E. *J. Am. Chem. Soc.* **1985**, *107*, 8286.
40. Dewar, M. J. S.; Hashmall, J. A.; Trinajstić, N. *J. Am. Chem. Soc.* **1970**, *92*, 5555.
41. Harvey, R. G.; Rabideau, P. W. *Tetrahedron Lett.* **1970**, 3695.

RECEIVED for review September 29, 1986. ACCEPTED February 24, 1987.

# Metal-Mediated Making and Breaking of Carbon–Carbon Bonds in Aromatic Hydrocarbons

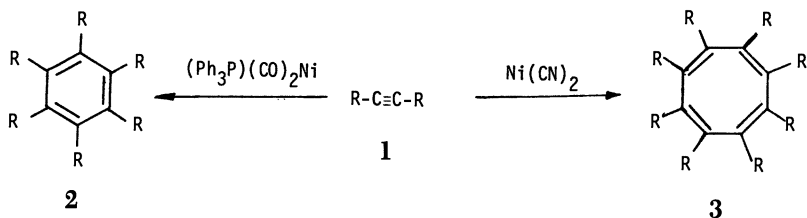
John J. Eisch

Department of Chemistry, State University of New York at Binghamton,  
Binghamton, NY 13901

*The interaction of zero- or low-valent lithium and nickel reagents with unsaturated hydrocarbons of the alkyne or arene type has been explored as a method of making carbon-carbon bonds in polynuclear aromatic hydrocarbons. Such reactions have been shown to proceed via two principal types of intermediates: (1) radical-anions, which are paramagnetic systems resulting from single-electron transfer; and (2)  $\pi$ -complexes or metallocycles, which are diamagnetic systems arising from a net oxidative addition or electron-pair transfer. The energetics of such metal-unsaturated substrate interactions is analyzed in terms of a Born–Haber cycle. Examples of useful carbon-carbon bond formations studied in this work are (1) the oligomerization of alkynes, (2) the cyclization of aromatic hydrocarbons, (3) the desulfurization of sulfur heterocycles, and (4) the dimerization of cyclobutadienoid systems.*

**T**HE INTERACTION OF ZERO- OR LOW-VALENT METALS with aromatic nuclei is a reaction of great generality encompassing the alkali-metal adducts reported by Schlenk and Bergmann (1) in 1928 as well as arene–chromium complexes elucidated by Fischer and Hafner (2) and Zeiss and Herwig (3) in 1956. Not only can arenes interact with metals, but alkynes can be cyclotrimerized to arenes by using metal catalysts. The trimerization of alkynes to benzenes (2) by  $(\text{Ph}_3\text{P})_2(\text{CO})_2\text{Ni}$  (Ph denotes phenyl) is shown in Scheme I (4). Because of the thermodynamic stability of the aromatic  $\pi$ -electron configuration, the driving force for such oligomerization of alkynes is readily

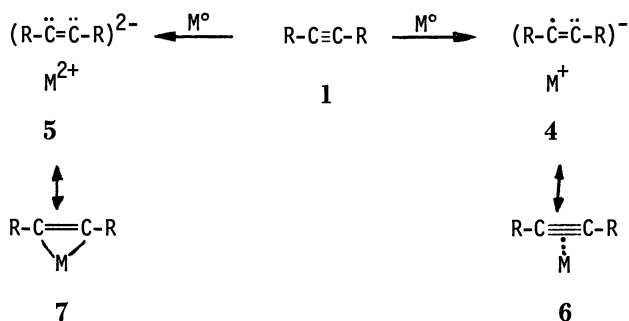




Scheme I

comprehensible. However, the similar cyclooctamerization of certain alkynes to the nonaromatic cyclooctatetraenes (3) by nickel(II) cyanide or nickel(0) complexes is, in contrast, astonishing (4).

Yet, a closer study of the behavior of low-valent transition metals, such as nickel, and of alkali metals, such as lithium, reveals that metals are able to disrupt aromatic systems almost as readily as they can induce their formation. The possibility of full (Li) or partial (Ni) electron transfer from a metal to a sufficiently low-lying antibonding  $\pi$ -molecular orbital of the reagent hydrocarbon is basic to both the formation and disruption of an aromatic nucleus by a low-valent metal reagent,  $\text{M}(0)$ . For oligomerizations of alkynes (e.g., Scheme I), two extreme types of intermediates (4 and 5 in Scheme II) can be generated by a one- or two-electron transfer: metal-radical anion pairs (4) or metal-dianion pairs (5). In a less extreme extent of electron transfer, 4 and 5 may be better represented as covalent  $\pi$ -complexes 6 and 7 (Scheme II). The ultimate products arising from intermediates 3 and 4 can be produced either catalytically from transition metals or stoichiometrically from main-group metals.



Scheme II

The extent of electron transfer between an organic substrate and a metal is a complex function of the metal's sublimation energy ( $S_1$ ) and ionization

potential ( $I$ ), as well as the organic substrate's sublimation energy ( $S_2$ ) and electron affinity ( $E$ ) (5). In terms of Gibbs free energy, one can analyze the free-energy solution potential ( $P$ ) into the foregoing energy inputs and note that energy-releasing terms, namely, ion solvation ( $H_1$  and  $H_2$ ) and ion association ( $A$ ), are necessary to yield a negative  $P$ . Such a Born–Haber treatment for the solution potential of a metal–hydrocarbon adduct is shown in Figure 1. This figure shows how crucial the role of the donor solvent is in solvating alkali-metal cations in such adducts. Such metal-cation solvation is the principal free-energy compensation ( $-G$ ) for the positive  $S_1$  and  $I$  investments. In the case of transition metals, such energy compensation can also be provided by donor ligands on the metal center, such as phosphines ( $H_1$ ), or from the association of partially charged metal and organic ligand centers ( $A$ ). This association can be considered as the back bonding invoked in transition-metal  $\pi$ -complexes.

An important extension of such electron transfer from a metal center to a hydrocarbon substrate is that the metal need not be in the zero-valent state. Rundle (6) pointed out that an electronic kinship exists between metal lattices and organometallic compounds: Both systems are electron-deficient; that is, they have too few valence electrons to fill the available low-energy

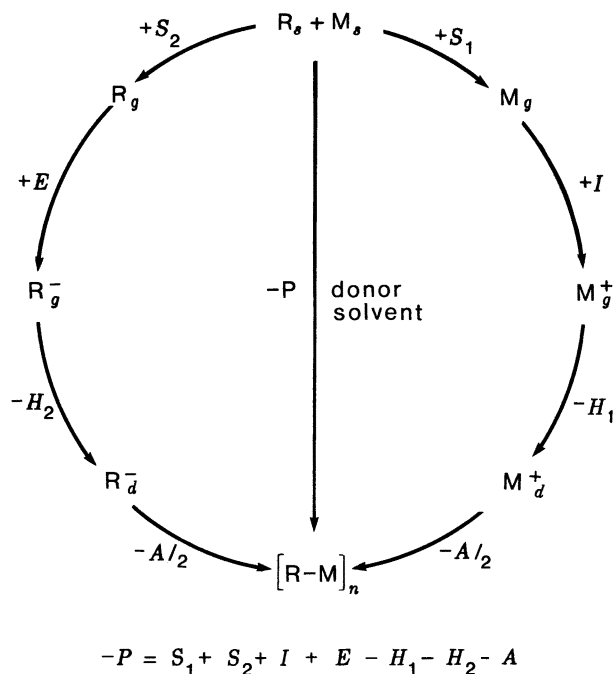
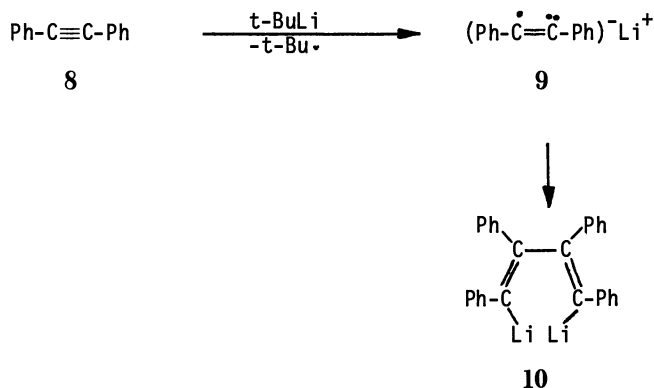


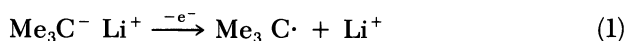
Figure 1. Born–Haber cycle for the formation of the carbon–metal bond.  
Subscripts: d, dissolved; s, solid.

bonding orbitals. The resulting electron-deficient systems are therefore expected to display greater electron delocalization, similar to their metal counterparts. Thus, the associated  $(\text{RLi})_n$ , where R is an alkyl group, should have an enhanced tendency to lose electrons, as does its corresponding cluster,  $\text{Li}_n$ . Indeed, a number of instances in which organolithium compounds have reacted by electron transfer have been observed. Especially noteworthy in this regard is *tert*-butyllithium (*t*-BuLi), which causes the reductive dimerization of diphenylacetylene (**8**) in tetrahydrofuran (THF) (**7**), as shown in Scheme III. The formation of **10** clearly shows that **9** was generated by electron transfer and then underwent dimerization. Compound **10** is also the product formed from the alkyne and lithium metal.



Scheme III

In this and other reactions, *tert*-butyllithium shows a greater tendency to undergo electron transfer than its isomer, *n*-butyllithium. *n*-Butyllithium, for example, does not form **10** from **8** but adds instead across the  $\text{C}\equiv\text{C}$  linkage (**7**). This behavior suggests that the ionization potential of the carbanionlike R group in RLi is an important determining factor in such electron transfer:



In this view, the lower ionization potential of the *tert*-butyl anion in comparison with that of the *n*-butyl anion is ascribed to the greater stability of the *tert*-butyl radical (**8**).

In 1929, Blicke and Powers (**9**) suggested such electron transfer by Grignard reagents to explain the reduction products encountered with ke-

tones. In recent years, Ashby (10) and Eisch (11) have adduced evidence for the occurrence of such single-electron transfers in a variety of organometallic processes. Accordingly, in keeping with the parallel drawn between the nature of metals and organometallic compounds (RM), one would expect that the energetics of such electron transfer from RM to substrate  $A=B$ , where A and B are unsaturated carbon, nitrogen, or oxygen centers, could be analyzed by a Born-Haber cycle that incorporates the Blicke-Powers hypothesis of single-electron transfer (SET). Such an analysis of free-energy contributions is depicted in Figure 2. This cycle allows for a stepwise carbometalation of  $A=B$  by RM or for a reductive dimerization of  $A=B$  to give  $M_2^{2+}(B-A-A-B)^{2-}$ . As in metal reactions, the solvation of metal cations ( $H_1$ ) and association factors determine a negative Gibbs energy of reaction ( $P$ ).

The study reported in this chapter examines the interactions of the alkali metal lithium and the transition metal nickel with various  $\pi$ -bonded hydrocarbons to determine the value of such metal interactions for forming new C-C  $\sigma$ -bonds in aromatic systems through preliminary disruption of C-C  $\pi$ -bonds. From the foregoing considerations, pronounced solvent or ligand effects are expected in such reactions.

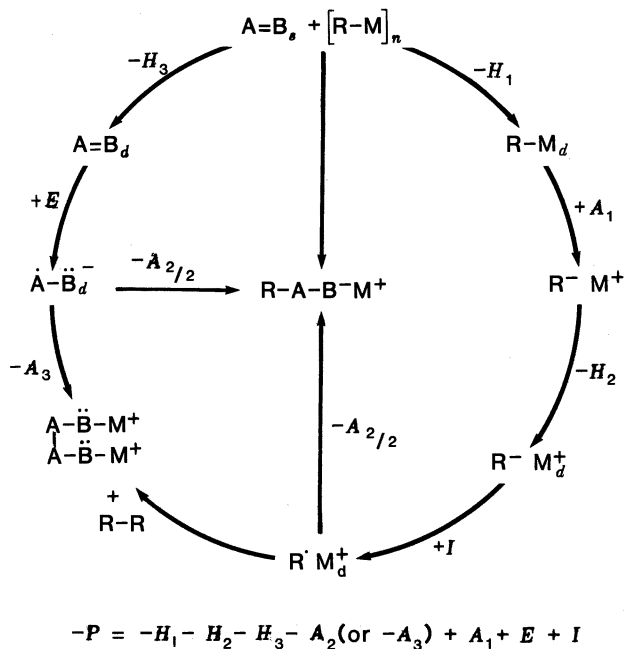


Figure 2. Born-Haber cycle for the single-electron transfer (SET) response of the carbon-metal bond, incorporating the Blicke-Powers hypothesis.

## Experimental Details

**General Operating Techniques.** All reactions involving metals or organometallic reagents were conducted under an atmosphere of a dry, oxygen-free, inert gas, which was nitrogen for lithium reactions and argon for nickel reactions. The preparation of suitably anhydrous and deoxygenated solvents, the analysis and transfer of such air- and moisture-sensitive metal reactants, and the execution of organometallic reactions have been described in detail in a recent monograph (12).

The following physical measurements and spectra were determined with the indicated instruments: (1) melting points (uncorrected) with a Thomas-Hoover Unimelt apparatus; (2) IR spectra: Perkin-Elmer spectrometer, model 137, equipped with NaCl optics; (3)  $^1\text{H}$  NMR spectra: reported on the  $\delta$  scale on which the position of the tetramethylsilane ( $\text{Me}_4\text{Si}$ ) signal is taken as 0.0 parts per million (ppm) with a Varian instrument, model A-60; (4) electron spin resonance (ESR) spectra with a Varian spectrometer, model V-4502, operating at 9.5 GHz with 100-KHz field modulation; (5) mass spectrometric (MS) data: Du Pont spectrometer model 21-491B; and (6) vapor phase chromatographic (VPC) data: chromatograph, F&M model 720, equipped with 6-ft  $\times$  0.25-in. columns of silicone gum rubber (10% SE-30) on an inorganic support (Chromosorb P).

Elemental analyses were performed by the Schwarzkopf Microanalytical Laboratory, Woodside, NY.

**Reagents.** The lithium metal, containing a maximum of 0.05% sodium, was obtained from the Lithium Corporation of America. Bis(1,5-cyclooctadiene)nickel  $[(\text{Cod})_2\text{Ni}]$  was prepared by a modification of a known procedure (13). This complex was used to prepare tetrakis(triethylphosphine)nickel  $[(\text{Et}_3\text{P})_4\text{Ni}]$ . Tetraphenylcyclobutadienenickel(II) bromide dimer was synthesized from stilbene-free diphenylacetylene (14).

Methylphenylacetylene (1-phenylpropyne), *tert*-butylphenylacetylene (1-phenyl-3,3-dimethyl-1-butyne), biphenylene, and diphenylacetylene (diphenylethyne) were prepared by reliable methods. The other hydrocarbons were purchased and then purified until they met published criteria of purity (i.e., mp, thin layer chromatography, IR, and UV). The same procedure was followed for phenoxathiin, phenothiazine, and thianthrene. Finally, silicon derivatives of alkynes, alkenes, alkadienes, and arenes were made according to published procedures.

### Illustrative Examples of Reactions with Lithium Metal.

**REDUCTIVE DIMERIZATION OF *tert*-BUTYLPHENYLACETYLENE.** Under nitrogen, a freshly cut suspension of lithium pieces (138 mg, 20 milligram-atoms (mg-at) of wire cut in 2.0-mm segments) in 3.16 g (20 mmol) of *tert*-butylphenylacetylene and 20 mL of ethyl ether was stirred vigorously as 1.2 mL of THF was added dropwise at 25 °C. During the following 3 h, the solution became red, and the amount of lithium diminished. The lithium was removed, and the red solution was treated with water (about 60 mg of Li was recovered). The mixture

was diluted with benzene, and the benzene layer was washed with water and dried over  $\text{MgSO}_4$ . Removal of volatiles in vacuo at 25 °C and  $^1\text{H}$  NMR spectral analysis of the residue showed the presence of (*E,E*)-1,4-di-*tert*-butyl-2,3-diphenyl-1,3-butadiene (55%), *tert*-butylphenylacetylene (35%), and (*Z*)- and (*E*)-1-*tert*-butyl-2-phenylethene and 3,3-dimethyl-1-phenylbutane (10%). The presence of the diene was verified by isolation (mp 162–163 °C), and that of the others was verified by VPC collection and spectral comparison with authentic samples (15).

**REDUCTIVE DIMERIZATION AND ISOMERIZATION OF METHYLPHENYLACETYLENE.** In a manner similar to the foregoing method, 5.8 g (50 mmol) of the methylphenylacetylene and 35 mL of ethyl ether were vigorously stirred with 350 mg (50 mg-at) of lithium pieces at 20 °C for 4 h. The excess lithium was removed, and the red solution was hydrolyzed. Removal of the volatiles in vacuo and crystallization of the residue from absolute ethanol gave 2.2 g (38%) of colorless leaflets of (*E,E*)-2,3-dimethyl-1,4-diphenyl-1,3-butadiene (mp 132–133 °C) (16). When the reaction was carried out on the same scale but in 30 mL of THF at –10 °C for 24 h, hydrolytic work-up (the addition of water followed by extraction with ether) gave an organic layer containing (*E,E*)-2,3-dimethyl-1,4-diphenyl-1,3-butadiene and isomers of methylphenylacetylene.

Removal of the THF under reduced pressure and distillation of the residue at 28–30 °C under 0.2 mmHg yielded a pale-yellow distillate, which was shown by gas chromatography (GC), IR, and  $^1\text{H}$  NMR to be a mixture of methylphenylacetylene ( $^1\text{H}$  NMR signal at 1.83 ppm), 3-phenylpropyne ( $\delta$  3.41, *d*;  $\delta$  2.15, *t*) and phenylallene [ $\delta$  6.13, *t*, H;  $\delta$  5.00, *d*, 2H; *J* (coupling constant) = 6.5 Hz](17).

#### MONOMOLECULAR AND BIMOLECULAR REDUCTIONS OF DIPHENYLACETYLENE.

**Cyclizing Dimerization.** A solution of 3.6 g (20 mmol) of diphenylacetylene in 8 mL of ethyl ether was stirred at 25 °C with 410 mg (60 mg-at) of lithium pieces for 2 h. The red–brown suspension was then treated dropwise with 1.6 mL (20 mmol) of dichlorophenylborane in 20 mL of ethyl ether. After the mixture was heated at reflux for 2 h, 250 mg of lithium was recovered before the mixture was treated with water. The organic products were taken up in benzene, the benzene layer was dried, and the volatiles were removed in vacuo. Column chromatography on silica gel with a petroleum ether–benzene gradient gave one principal fraction: 1.60 g, yellow solid, mp 182–184 °C (decomposition). Refluxing this sample in glacial acetic acid yielded 1,2,3-triphenyl-naphthalene, mp 148–149 °C; the melting point of a mixture with an authentic sample was un-depressed (18).

**Noncyclizing Dimerization.** A solution of 5.0 g (28 mmol) of diphenylacetylene in 200 mL of anhydrous THF was stirred vigorously by a blade-driven mechanical stirrer at 25 °C with 220 mg (32 mg-at) of lithium pieces. During the following 3 h, the solution turned dark blue. After the residual lithium was removed and the sample was weighed, a 30% consumption of lithium metal was ascertained.

Treatment of the reaction mixture, first with methanol and then with water, led to an organic solution, whose usual chromatographic separation and spectral identification showed the presence of only diphenylacetylene and (*E,E*)-1,2,3,4-tetraphenyl-1,3-butadiene (mp 181.5–183 °C) (16).

*Competitive Cyclizing and Noncyclizing Dimerizations.* When reactions such as noncyclizing dimerization were prolonged for 40–50 h, then 1,2,3-triphenylnaphthalene (mp 148–150 °C), (*Z,Z*)-1,2,3,4-tetraphenyl-1,3-butadiene (mp 146–148 °C), and (*E*)-1,2-diphenylethene (mp 124–125 °C) could be isolated from the hydrolyzed reaction mixture by column chromatography on aluminum oxide and elution with a benzene–hexane gradient. The principal product was still the (*E,E*)-1,2,3,4-tetraphenyl-1,3-butadiene.

Direct examination of the dried and evaporated organic extract (which had not been subjected to temperatures exceeding 20 °C) by <sup>1</sup>H NMR spectroscopy in CCl<sub>4</sub> revealed distinct singlets, inter alia, at 4.0 and 4.72 ppm. Thereupon, the solution was heated for 30 min at 35 °C, after which the signal at 4.72 ppm disappeared. These signals indicated the presence of the *cis* and (more thermally labile) *trans*-1,2,3,4-tetraphenylcyclobutenes in the crude reaction mixture (16).

*Long-Term Interaction with Lithium in THF.* A solution of 12.21 g (69 mmol) of diphenylacetylene in 30 mL of THF was stirred at 20–25 °C with 80 mg (11 mg-at) of lithium pieces for 140 h. Upon hydrolytic workup, 150 mg of a light-brown solid was obtained, which was insoluble in water, benzene, and acetone. This product was subjected to sublimation at 180–200 °C under 0.01 mmHg for 3 days. The colorless sublimate was identified as hexaphenylbenzene by IR and melting-point comparisons. The organic layer contained preponderantly diphenylacetylene and some (*E,E*)-1,2,3,4-tetraphenyl-1,3-butadiene (16).

**CYCLIZATION OF *o*-DIPHENYLBENZENE.** A solution of 2.30 g (10 mmol) of *o*-diphenylbenzene in 15 mL of THF was stirred with lithium pieces (350 mg, 50 mg-at) at 25 °C for 18 h. The lithium pieces were then removed, and hydrolytic workup of the mixture followed in the usual manner. The organic product was shown by MS analysis to be a mixture of *o*-diphenylbenzene, triphenylene, and a dihydro derivative of *o*-diphenylbenzene. This mixture was heated in benzene with 5.68 g (25 mmol) of 2,3-dichloro-5,6-dicyanobenzoquinone (DDQ). Column chromatography yielded 1.5 g (65%) of pure triphenylene, mp 198–199 °C (19).

**CYCLIZATION OF 1,1'-BINAPHTHYL.** A solution of 2.54 g (10 mmol) of 1,1'-binaphthyl in 20 mL of THF and 350 mg (50 mg-at) of lithium pieces, after 18 h at 25 °C and hydrolytic workup, produced a mixture of 1,1'-binaphthyl, perylene, and a dihydro derivative of 1,1'-binaphthyl. Similar treatment with DDQ provided a 55% yield of perylene, mp 272–274 °C (20).

**REDUCTIVE DIMERIZATION OF CYCLOPROPYLTRIPHENYLSILANE.** A solution of 1.10 g (3.6 mmol) of the cyclopropyltriphenylsilane in 30 mL of THF and 30 mg (4.6 mg-at) of lithium pieces, after stirring at –78 °C for 20 h and hydrolytic workup, produced an almost quantitative yield of 4,4'-bis(cyclopropyl(diphenyl)silyl)-1,1',4,4'-tetrahydrobiphenyl, which after column chromatography and recrystallization from ethyl ether melted at 145–151 °C (21).

This latter compound could also be aromatized to 4,4'-bis(cyclopropyl-(diphenyl)silyl)biphenyl with DDQ.

**CYCLIZATION OF 2-(2-BIPHENYL)-1,1-DIPHENYLETHENE.** A solution of 332 mg (1.0 mmol) of 2-(2-biphenyl)-1,1-diphenylethene in 7.5 mL of TMEDA (N,N,N',N'-tetramethyl-1,2-ethylenediamine) was treated with 2.5 mL (4.0 mmol) of *n*-butyllithium in hexane. Then the solution, which became deep red, was heated at reflux for 72 h. The black solution was hydrolyzed with 20 mL of 2 N aqueous HCl, and the organic fraction was isolated in the usual way. The <sup>1</sup>H NMR spectrum of this product showed 75% of 2-(2-biphenyl)-1,1-diphenylethene and 25% of 9-(diphenylmethyl)fluorene. After isolation, 9-(diphenylmethyl)fluorene melted at 212–214 °C; <sup>1</sup>H NMR (CDCl<sub>3</sub>) gave δ 4.1–5.02 (*d* of *d*, 2H) and δ 6.55–7.75 [*m* (multiplet), 18H] (22).

### Illustrative Reactions with Nickel(0) Complexes.

#### REACTIONS OF DIPHENYLACETYLENE.

**Trapping of the *cis*-Stilbene Precursor.** A solution of 2.34 g (8.5 mmol) of (Cod)<sub>2</sub>Ni and 2.82 g (15.8 mmol) of diphenylacetylene was formed in 25 mL of toluene to yield a burgundy–red color. Addition of 3.39 g (8.5 mmol) of 1,2-bis(diphenylphosphino)ethane led to a yellow precipitate. The suspension was stirred for 18 h at 25–30 °C and then for 1 h at 95 °C. The cooled black reaction mixture had no obvious precipitate. Addition of deoxygenated, 6 N aqueous HCl led to the deposition of the NiCl<sub>2</sub> complex with 1,2-bis(diphenylphosphino)ethane. The separated organic layer was washed with aqueous NaHCO<sub>3</sub>–NaCl and dried over anhydrous MgSO<sub>4</sub>. Concentration of this layer led to the deposition of 764 mg (27%) of hexaphenylbenzene. Column chromatography of the filtrate yielded 1.23 g of *cis*-stilbene (40%) and 82 mg of (*E,E*)-1,2,3,4-tetraphenyl-1,3-butadiene (3%) (23).

**Interception of (*E,E*)-1,2,3,4-Tetraphenyl-1,3-butadiene.** A suspension of 4.30 g (1.56 mmol) of (Cod)<sub>2</sub>Ni in 30 mL of THF was cooled to 0 °C, and then a solution of 5.55 g (31.2 mmol) of diphenylacetylene in 30 mL of THF was added dropwise over 15 min. A red solution resulted, and stirring was continued for another 15 min. Then 30 mL of 6 N DCl in D<sub>2</sub>O was added, the mixture was exposed to air as it rose to 25 °C, and then ethyl ether was added to extract the organic products. The organic extract was washed thoroughly with water, dried over anhydrous MgSO<sub>4</sub>, and evaporated in vacuo. The residue was subjected to column chromatography on neutral aluminum oxide with an eluent gradient of benzene–hexane. A 2.0-g recovery of diphenylacetylene was obtained (36%), and 276 mg of (*E,E*)-1,2,3,4-tetraphenyl-1,3-butadiene was isolated (5%). By <sup>1</sup>H NMR and MS measurements, (*E,E*)-1,2,3,4-tetraphenyl-1,3-butadiene was shown to be dideuterated at the 1,4-vinyl positions. Some hexaphenylbenzene was recovered from the top of the column (23).

**Catalytic Trimerization of Diphenylacetylene.** A mixture of 400 mg of (Cod)<sub>2</sub>Ni, 8.90 g of diphenylacetylene, and 30 mL of toluene was heated at reflux for 4 h. The precipitate formed was filtered off and washed with ethanol, acetone,



and ethyl ether to give 6.93 g of fairly pure hexaphenylbenzene (78%). A highly pure product was obtained by Soxhlet extraction with 5.96 g of  $\text{CHCl}_3$  (67%) (23).

#### RING CONTRACTION OF SULFUR HETEROCYCLES WITH 2,2'-BIPYRIDYL AND $(\text{COD})_2\text{Ni}$ .

*Phenoxathiin.* A violet solution of an equimolar mixture of  $(\text{Cod})_2\text{Ni}$  and 2,2'-bipyridyl (Bpy) in THF (10 mL per 1.5 mmol) was treated with phenoxathiin, and the resulting mixture was heated at 55 °C for 48 h (24). The cooled reaction mixture was treated with glacial acetic acid, and the organic products were isolated in the usual way. For reactions having the following sulfide: $(\text{Cod})_2\text{Ni}$  ratios, namely, 1:1, 1:2, 1:3, and 1:4, the conversions to dibenzofuran, as determined by VPC analysis, were 15%, 79%, 91%, and 78%, respectively. Thus, a sulfide: $(\text{Cod})_2\text{Ni}$  ratio of 1:2 was the most satisfactory. Also, the percentage of side production of diphenyl ether increased as the ratio changed as follows: 1:1, 1%; 1:2, 3%; and 1:3, 11%.

*Phenothiazine.* Similar to the procedure for phenoxathiin, the interaction of 3.15 mmol of  $(\text{Cod})_2\text{Ni}$  and 2,2'-bipyridyl in 20 mL of THF with 1.5 mmol of phenothiazine yielded a 75% conversion to carbazole and a 5% conversion to diphenylamine.

*Thianthrene.* Similar to the procedure for phenoxathiin, the reaction between 3.2 mmol of  $(\text{Cod})_2\text{Ni}$  and 2,2'-bipyridyl with 1.3 mmol of thianthrene gave 55% of dibenzothiophene, 15% of biphenyl, and 30% of thianthrene.

#### ISOLATION OF ORGANONICKEL INTERMEDIATES FROM BIPHENYLENE AND $(\text{Et}_3\text{P})_4\text{Ni}$ .

*Dibenzonickelole-Bis(triethylphosphine).* A solution of 7.5 g (14.1 mmol) of  $(\text{Et}_3\text{P})_4\text{Ni}$  and 1.71 g (11.2 mmol) of biphenylene in 50 mL of ethyl ether was stirred for 18 h at 0 °C (25). Temperature control was essential to retard dibenzonickelole from rearranging to the green tetrabenz-1,2-dinickelocin. Some solvent was then removed at 5 °C under reduced pressure, and the rust-brown product was crystallized from the solution at -78 °C. An 82% yield of dibenzonickelole was obtained.  $^1\text{H}$  NMR ( $\text{C}_6\text{D}_6$ ) gave  $\delta$  0.6–1.7 [broad (br) *d*, 30H],  $\delta$  6.9–7.3 (br *m*, 6H),  $\delta$  7.35–7.6 (br *m*, 2H). The calculated elemental composition for  $\text{C}_{24}\text{H}_{38}\text{NiP}_2$  is the following (values are percentages): C, 64.46; H, 8.56; and Ni, 13.12. The elemental composition found was the following: C, 64.32; H, 8.50; and Ni, 13.01. (The sample had to be kept cold until it was analyzed to prevent the loss of  $\text{Et}_3\text{P}$  and rearrangement to the green tetrabenz-1,2-dinickelocin).

*Tetrabenz-1,2-dinickelocin-1,2-Bis(triethylphosphine).* A solution of 7.5 g (14.1 mmol) of  $(\text{Et}_3\text{P})_4\text{Ni}$  and 1.71 g (11.2 mmol) of biphenylene in 100 mL of THF was stirred for 5 h at 18 °C and for 15 h at 0 °C. Then the solvent was removed at 10 °C under reduced pressure, and the residual solid was washed with three 20-mL portions of cold pentane (~0 °C). The product was suspended in a mixture of 60 mL of pentane and 30 mL of ethyl ether for 15 h at 20 °C. Then about half of the solvent was evaporated. Some  $\text{Et}_3\text{P}$  was added to the residual solution, and the solution was stored at -78 °C overnight. Dark-green

crystals of tetrabenz-1,2-dinickelcin were deposited (88% yield).  $^1\text{H}$  NMR ( $\text{C}_6\text{D}_6$ ) gave  $\delta$  0.5–1.5 (br *m*, 30H),  $\delta$  6.2 (*d*, 2H, 7.0 Hz),  $\delta$  6.7 (*t*, 2H, 7.0 Hz),  $\delta$  6.82 (*d* of *d*, 2H, 7.0 and 2.0 Hz), and  $\delta$  7.1 (*m*, 10H). The calculated elemental composition for  $\text{C}_{36}\text{H}_{46}\text{Ni}_2\text{P}_2$  is the following (values are percentages): C, 65.70; H, 7.04; Ni, 17.84; and P, 9.41. The elemental composition found was the following: C, 65.49; H, 7.13; Ni, 17.83; and P, 9.55.

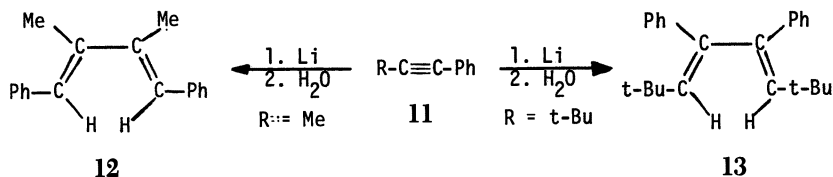
In a sealed capillary tube under an argon atmosphere, tetrabenz-1,2-dinickelcin had an apparent melting point of 146 °C. Heating of the green crystals between 150 and 200 °C led to the deposition of a nickel mirror on the glass vessel and the formation of tetraphenylene.

**REDUCTIVE RING OPENING OF TETRAPHENYLCYCLOBUTADIENENICKEL(II) BROMIDE DIMER.** A suspension of 710 mg (1.2 mmol) of tetraphenylcyclobutadienenickel(II) bromide dimer and 710 mg (2.4 mmol) of triphenylphosphine in 80 mL of toluene was stirred at –78 °C while being treated with 1.2 mL of 2 M *tert*-butyllithium in pentane. The red–brown mixture was stirred for 6 h at –78 °C and then brought to 25–30 °C. The solution was concentrated under reduced pressure, pentane was added, and the resulting mixture was cooled at –78 °C to give the brown nickelole (40%). Recrystallization twice from pentane–toluene at –78 °C gave a diamagnetic product ( $^1\text{H}$  NMR:  $\delta$  6.5–7.5, *m*) that was allowed to react with different compounds to produce various products: (1) CO provided tetraphenylcyclopentadienone (45%); (2) glacial acetic acid gave (*E,E*)-1,2,3,4-tetraphenyl-1,3-butadiene (70%), (3) diphenylacetylene (20-fold excess) refluxed with toluene gave hexaphenylbenzene (58%), and (4) thermolysis at 50 °C followed by hydrolysis with 12 N HCl yielded principally (*E,E*)-octaphenyl-1,3,5,7-octatetraene and a small amount of (*E,E*)-1,2,3,4-tetraphenyl-1,3-butadiene (26).

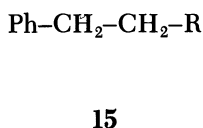
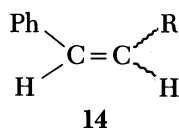
## Results and Discussion

### Reaction and Oligomerization of Alkynes.

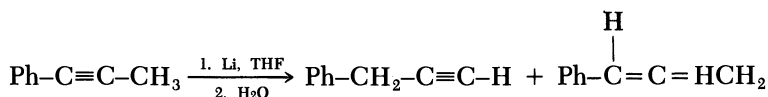
**REACTION PRODUCTS AND ORGANOMETALLIC INTERMEDIATES WITH LITHIUM.** All three of the alkynes examined, namely, methylphenylacetylene, *tert*-butylphenylacetylene, and diphenylacetylene, gave as the principal reaction product in either ethyl ether or THF the (*E,E*)-tetrasubstituted 1,3-butadiene (Scheme IV). Methylphenyl- and *tert*-butylphenylacetylene (**11**) gave reduced dimers of opposite regiochemistry (**12** and **13**, respectively). In addition, a minor amount of the starting alkyne was reduced to its *E*- and *Z*-alkenes (**14**) and alkane (**15**). As workup of such reaction mixtures with  $\text{D}_2\text{O}$  showed, products **14** and **15** arose largely from proton-abstraction reactions of radical-anion intermediates during exposure to the lithium, because they were mostly undeuterated.



Scheme IV



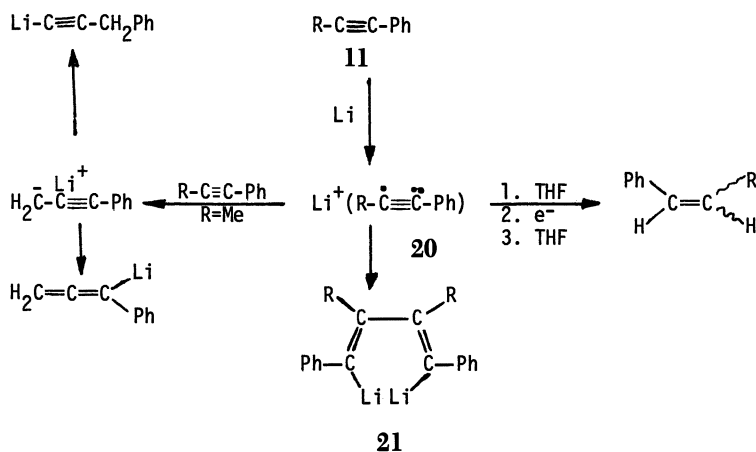
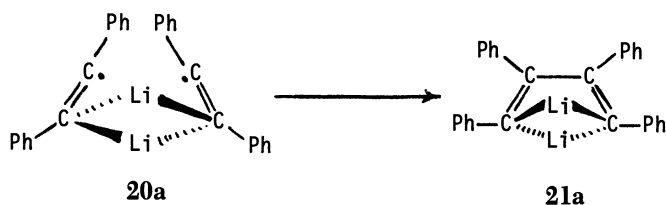
Especially in THF, methylphenylacetylene was found to undergo a base-catalyzed rearrangement to its isomeric alkyne and allene:



Whereas the foregoing products were formed in relatively short contact times with lithium, the longer reaction times studied with diphenylacetylene and lithium in THF led to other dimers and trimers such as the (*Z,Z*)-1,3-butadiene (**16**), 1,2,3-triphenyl-naphthalene (**17**), *cis* and *trans*-tetraphenylcyclobutenes (**18**) and hexaphenylbenzene (**19**); **18** and **19** can be viewed as arising from intermediate **21**. All of these products can be explained the initial formation of an ion pair containing a lithium cation and an alkyne radical anion (**20**) (27–30). Such an adduct can dimerize to **21**, undergo reduction by proton abstractions from THF and electron transfer, or act as a strong base in isomerizing methylphenylacetylene (Scheme V). If radical **20** dimerizes as governed by the steric properties of R, the different regiochemistry of dimerization for methylphenylacetylene or *tert*-butylphenylacetylene becomes understandable (Scheme IV).

However, the reason for the favored stereoselectivity with which **20** dimerizes to **21** requires some thought. The crystal structure of the bis-TMEDA complex of **21** shows that the lithium centers bridge across the C-1 and C-4 centers of the diene and thus hold it in an *s*- and *cis*-configuration (**21a**) (31). A similar bridging in the associated, dimeric, radical ion **20a** allows for the observed stereoselective coupling (Scheme VI).

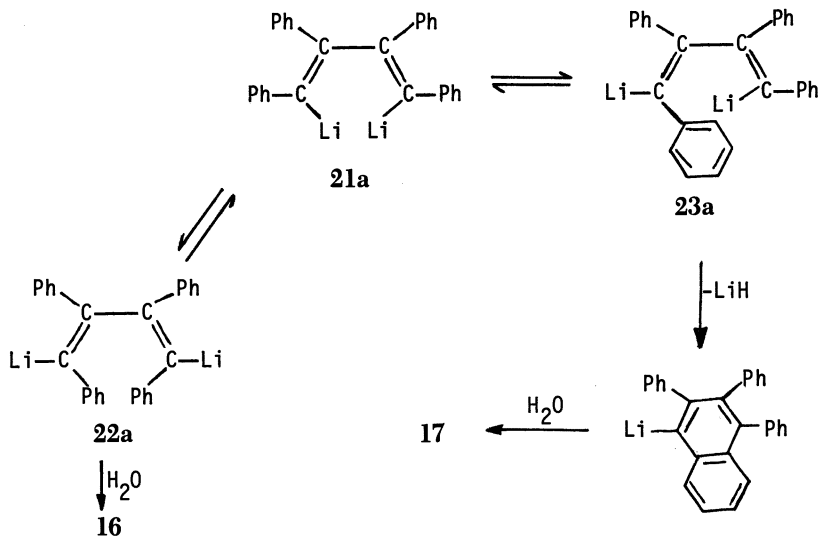
The products obtained by long-term reaction with lithium, namely, **16**–**19**, readily arise from **21**. Phenyl-substituted vinylolithiums readily undergo *cis-trans* isomerization in THF (32), and thus **21** could isomerize to forms

*Scheme V**Scheme VI*

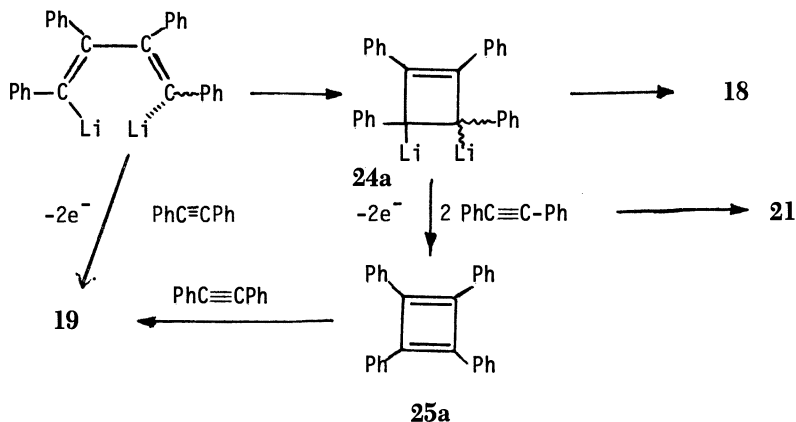
that could yield either **16** upon hydrolysis or **17** upon cyclization (**33**) (Scheme VII). Likewise, isomeric **18** could arise from an electrocyclic ring closure of **21a**, **22a**, or **23a** and protonation by THF (**34**). Intermediate **24a** might form **25a** by electron transfer, and **25a** would immediately react with diphenylacetylene to yield **19** (Scheme VIII).<sup>1</sup>

These alkynes do not undergo such smooth dimerizations to alkadiene derivatives such as **21** or **22** when sodium or potassium is employed or when the reaction is conducted in other solvents (**27–30**). The potassium adduct of *tert*-butylphenylacetylene (cf. **13**) dimerizes through the *para*-position of the phenyl group (**35**). These observations indicate that the special reactivity of lithium may reside in the greater autoassociation tendency of its radical-anion adducts (**20a**).

<sup>1</sup>The conversion of **24a** into intermediate **25a** is given as a double single-electron transfer (SET) reaction. Alternatively, a Diels–Alder reaction of **21a** could produce **19a**.



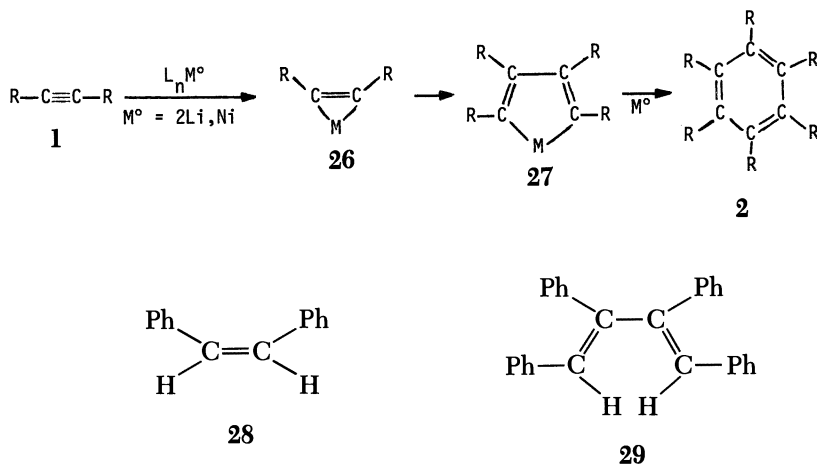
Scheme VII



Scheme VIII

**REACTION PRODUCTS AND ORGANOMETALLIC INTERMEDIATES WITH NICKEL(0) COMPLEXES.** Nickel(0) complexes such as  $(Cod)_2Ni$ , show a striking parallel with lithium(0) complexes in their reactions with diphenylacetylene: a sequence of monomolecular reduction; bimolecular, stereospecific reduction; and cyclotrimerization (Scheme IX). Consonant with the suggestion that nickel(0) forms nickelirene (**26**) and nickelole (**27**) intermediates in the course of cyclotrimerization of diphenylacetylene is the isolation of (*Z*)-1,2-diphenylethene (**28**) and (*E,E*)-1,2,3,4-tetraphenyl-1,3-butadiene (**29**) upon hydrolysis. Furthermore, when DCl was used in the workup, both **28** and **29**

were dideuterated at their vinylic positions. This finding suggests that there are C–Ni bonds at these vinylic positions in the organonickel precursors of **28** and **29**. Recent studies have firmly established **26** and **27** as the catalytic carriers in nickel-catalyzed alkyne oligomerizations (23, 26).

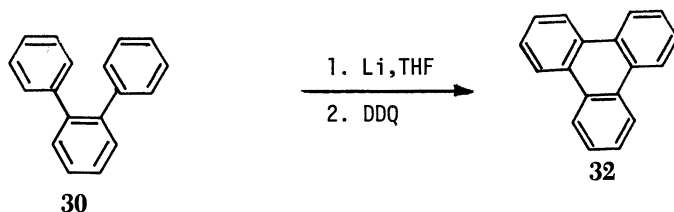


*Scheme IX*

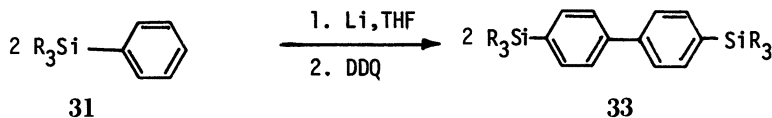
### Coupling of Aromatic Rings with Lithium Reagents.

**CARBON–CARBON BOND FORMATION MEDIATED BY LITHIUM METAL.** A second, most general method of coupling aromatic rings involves the use of lithium metal in THF. The reaction can be fostered if the electron affinity of the aryl rings is enhanced (i.e., if  $E$  is made less positive in Figure 1) by placing electron-withdrawing substituents on the rings to be coupled. Such substituents can be other aryl groups or an  $\text{R}_3\text{Si}$  group, as the following examples show.

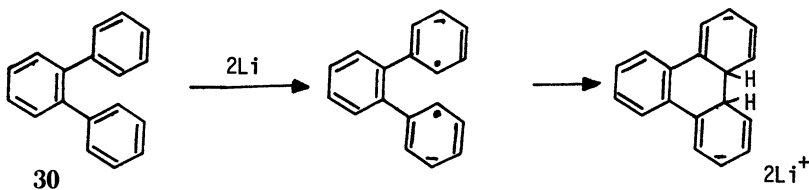
This reaction can be achieved either intramolecularly (Scheme X) or intermolecularly (Scheme XI). In both reactions the crucial step is the transfer of electrons to the rings to be coupled and the dimerization of the resulting radical anions (Scheme XII).



*Scheme X*



Scheme XI



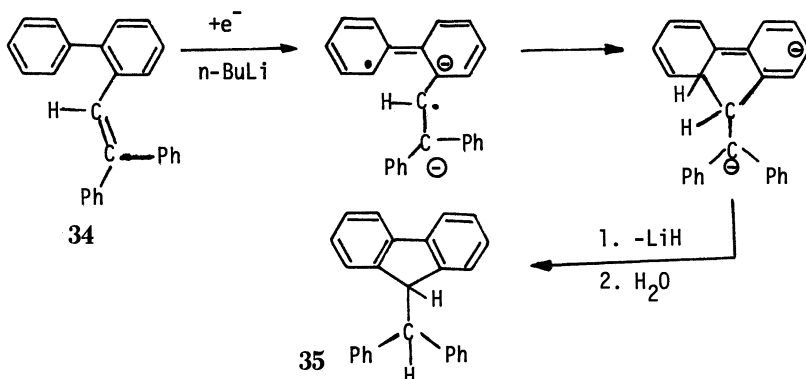
Scheme XII

The attachment of a  $\text{R}_3\text{Si}$  (31) or an biphenyl (30) group enhances the electron affinity of a benzene ring. Such substitution permits biphenyl rings (33) or the triphenylene system (32) to be generated readily. Collateral evidence in support of radical-anionic intermediates in these reactions has been obtained (5). Another example of the intramolecular cyclization is the formation of perylene from 1,1'-binaphthyl.

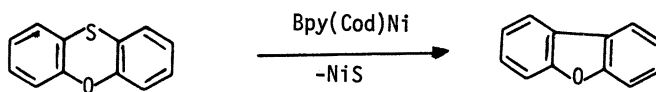
**ORGANOLITHIUM COMPOUNDS AS ELECTRON-TRANSFER AGENTS IN CARBON-CARBON BOND FORMATION.** An instructive example of how  $\text{RLi}$ , rather than lithium metal, can act as an electron source (cf. Figure 2) is the cyclization of 2-(2-biphenyl)-1,1-diphenylethene (34) by *n*-butyllithium. To enhance electron transfer, the chelating strong-donor TMEDA was employed. The observed cyclization to 9-(diphenylmethyl)fluorene (35) can best be explained by electron transfer (Scheme XIII).<sup>2</sup>

**Coupling of Aromatic Rings with Nickel(0) Reagents.** Nickel(0) complexes are able to couple aromatic groups to each other through the preliminary disruption of relatively weak  $\sigma$  bonds. Again, examples of such coupling are known for both intramolecular (Scheme XIV) and for intermolecular (Scheme XV) situations. The type of cyclizing desulfurization depicted in Scheme XIV has also been observed with phenothiazine and thianthrene (24), and evidence has shown the importance of electron-transfer processes in such ring couplings (24,36). The process given in Scheme XV,

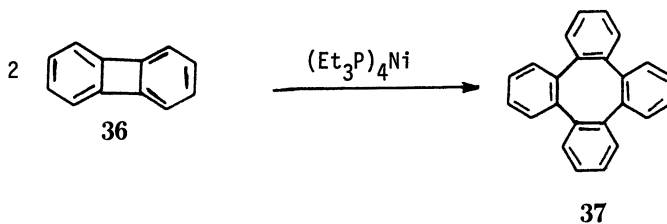
<sup>2</sup>For the ring-coupling reactions shown in Schemes XII and XIII, bis-radical anions are suggested as the reactive intermediates. One might demur that in such conjugated systems the dianions exist as electron-paired diamagnetic intermediates. In this case, the unpairing of such electrons requires only a modest promotional energy.



Scheme XIII



Scheme XIV



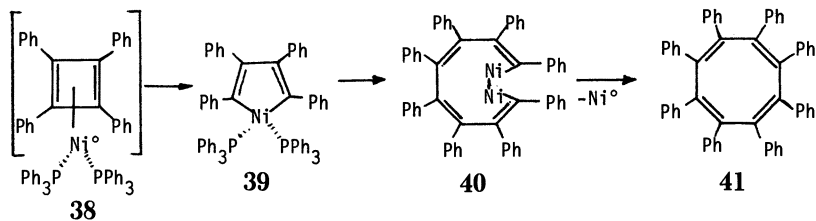
Scheme XV

on the other hand, has been demonstrated to proceed by way of dibenzonickelole and tetrabenzonickelole intermediates (25).

Closely related to the dimerization of biphenylene (36) to tetraphenylene (37, Scheme XV) is the dimerization of an aryl-substituted cyclobutadiene to octadienes or cyclooctadienes by way of nickel complexes. A useful source of the cyclobutadiene group is its air-stable complex with  $\text{NiBr}_2$ . Reduction of this complex with *tert*-butyllithium (electron-transfer agent) gives the tetraphenylcyclobutadiene–nickel(0)–triphenylphosphine complex (38), which isomerizes to the nickelole (39). The dimerization of 39 leads to 40, whose protonation yields the octadiene. Alternatively, at higher temperatures, 40 can extrude  $\text{Ni}(0)$  to produce 41 (26, Scheme XVI).

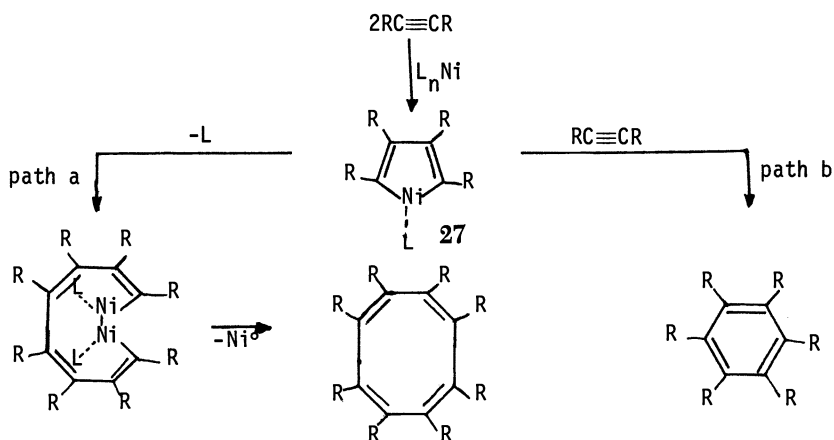
These observations, in addition to those made in the stepwise oligomerization of alkynes by nickel(0) complexes (Scheme IX), help to clarify





Scheme XVI

the mechanistic pathways involved in the Reppe and Schweckendiek (4) oligomerization of alkynes. Nickeloles (27) are intermediates common to both cyclotrimerizations and cyclotetramerizations. Depending upon conditions and the structure of the alkyne, either process can ensue from 27 (Scheme XVII). The mechanistic pathways from the nickelole to the final oligomer diverge, depending upon whether the nickelole dimerizes (path a to tetramer) or reacts preferentially with alkyne (path b to trimer). Preference for path a or path b is highly dependent upon the substituents (R) and ligands (L) on nickelole 27. A recent study showed that the ease of dimerization of the dibenzonickelole to the dibenzodinicolecin increased as L changed from Et<sub>3</sub>P to Ph<sub>3</sub>P (25).



Scheme XVII

## Summary

This study showed that the lithium- and nickel-mediated formation of carbon-carbon bonds has considerable promise for the rational construction of polycyclic aromatic nuclei. Not only can such aromatic systems be elaborated

from simple derivatives of alkynes and benzene in an intermolecular fashion, but intramolecular ring couplings and ring closures can also be achieved by employing sulfur heterocycles or *o*-diaryl aromatic compounds. In all of these processes, electron transfer from the metal to the unsaturated substrate was shown to play a decisive role.

### Acknowledgments

I am grateful to the National Science Foundation and the U.S. Department of Energy for support of this research under Grant No. CHE-8308251 and Grant No. FG22-84PC70786. Furthermore, I am indebted to my co-workers for their skillful and dedicated experimentation. Their individual contributions are specified in the references because much of this research is being published here for the first time.

### References

1. Schlenk, W.; Bergmann, E. *Justus Liebigs Ann. Chem.* **1928**, *463*, 1.
2. Fischer, E. O.; Hafner, W. *Z. Naturforsch.* **1955**, *10b*, 665.
3. Zeiss, H. H.; Herwig, W. *J. Am. Chem. Soc.* **1956**, *78*, 5959.
4. Reppe, W.; Schweckendiek, W. *Justus Liebigs Ann. Chem.* **1948**, *560*, 104.
5. Eisch, J. J. *Pure Appl. Chem.* **1984**, *56*, 35.
6. Rundle, R. E. *J. Phys. Chem.* **1957**, *61*, 45.
7. Mulvaney, J. E.; Gardlund, Z. G.; Gardlund, S. L. *J. Am. Chem. Soc.* **1963**, *85*, 3897.
8. Eisch, J. J.; Behrooz, M.; Galle, J. E. *Tetrahedron Lett.* **1984**, *25*, 4851.
9. Blicke, F. F.; Powers, L. D. *J. Am. Chem. Soc.* **1929**, *51*, 3378.
10. Ashby, E. C. *Pure Appl. Chem.* **1980**, *52*, 545.
11. Eisch, J. J. *The Chemistry of Organometallic Compounds*; Macmillan: New York, 1967; pp 13–33.
12. Eisch, J. J. *Organometallic Syntheses*; Vol. 2, Academic: New York, 1981, pp 3–60.
13. Bogdanovic, B.; Kröner, M.; Wilke, G. *Justus Liebigs Ann. Chem.* **1966**, *699*, 1.
14. Piotrowski, A. M.; Eisch, J. J. In *Organometallic Syntheses*; King, R. B.; Eisch, J. J. Eds.; Elsevier: Amsterdam, 1986; p 116.
15. Eisch, J. J.; Galle, J. E.; Brown, J. H., unpublished studies.
16. Eisch, J. J.; Brown, J. H., Masters Thesis of J. H. Brown, Catholic University of America, 1971.
17. Levin, G.; Szwarc, M. *Chem. Commun.* **1971**, 1029.
18. Eisch, J. J.; Kozima, S., unpublished results.
19. Eisch, J. J.; Kovacs, C. A., unpublished results.
20. Eisch, J. J., unpublished results.
21. Eisch, J. J.; Gupta, G. J. *Organomet. Chem.* **1979**, *168*, 139.
22. Eisch, J. J.; Chobe, P., unpublished results. (1985).
23. Eisch, J. J.; Galle, J. E.; Aradi, A. A.; Boleslawski, M. P. *J. Organomet. Chem.* **1986**, *312*, 399.
24. Eisch, J. J.; Han, K. I.; Hallenbeck, L. E. *J. Am. Chem. Soc.* **1986**, *108*, 1763.
25. Eisch, J. J.; Piotrowski, A. M.; Han, K. I.; Krüger, C.; Tsai, Y. H. *Organometallics* **1985**, *3*, 224.

26. Eisch, J. J.; Piotrowski, A. M.; Aradi, A. A.; Krüger, C.; Romao, M. J. Z. *Naturforsch.* **1985**, *40b*, 624.
27. Holy, N. L. *Chem. Rev.* **1974**, *74*, 243.
28. Sioda, R. E.; Cowan, D. O.; Koski, W. S. *J. Am. Chem. Soc.* **1967**, *89*, 230.
29. Dodley, D. A.; Evans, A. G. *J. Chem. Soc. Chem. Commun.* **1968**, 107.
30. Levin, G.; Jagur-Grodzinski, J.; Szwarc, M. *J. Am. Chem. Soc.* **1970**, *92*, 2268.
31. von Rague Schleyer, P., personal communication, 1986.
32. Curtin, D. Y.; Koehl, W. J. Jr. *J. Am. Chem. Soc.* **1962**, *84*, 1967.
33. Leavitt, F. C.; Manuel, T. A.; Johnson, F.; Matternas, L. U.; Lehman, D. S. *J. Am. Chem. Soc.* **1960**, *82*, 5099.
34. Freedman, H. H.; Doorakian, G. A.; Sandel, V. R. *J. Am. Chem. Soc.* **1965**, *87*, 3019.
35. Csürös, Z.; Caluwe, P.; Szwarc, M. *J. Am. Chem. Soc.* **1973**, *95*, 6171.
36. Eisch, J. J.; Hallenbeck, L. E.; Han, K. I. *J. Org. Chem.* **1983**, *48*, 2963.

RECEIVED for review September 29, 1986. ACCEPTED February 24, 1987.

# Reductive Alkylation of Aromatic Compounds Perylene, Decacyclene, and Dibenzothiophene

Lawrence B. Ebert, George E. Milliman, Daniel R. Mills, and Joseph C. Scanlon

Corporate Research Laboratories, Exxon Research and Engineering Company, Annandale, NJ 08801

*The reduction of three polynuclear aromatic compounds, namely, perylene, decacyclene, and dibenzothiophene, with potassium metal in tetrahydrofuran at 25 °C, followed by quenching with alkyl iodides, was investigated. With perylene, a dianion was obtained, which on reaction with methyl iodide added two methyl groups; the main regioisomer had one methyl group on C-1 and one methyl group on the adjacent nonprotonated carbon, C-14. The reductive alkylation of decacyclene also led to alkyl groups on quaternary carbon atoms. The reduction of dibenzothiophene led to a loss of sulfur and proton uptake from solvent to yield biphenyl as the product after 24 h of reduction.*

**R**EDUCTIVE ALKYLATION is a useful means of investigating a variety of fossil-fuel materials, as proposed by Sternberg and co-workers (1, 2). A refractory carbonaceous substance, such as coal, is reduced with the radical anion of naphthalene in the presence of excess alkali metal in tetrahydrofuran (THF) at room temperature. The resultant ensemble of reduced species (e.g., "coal anion") is quenched with any of a variety of alkylating agents, most frequently alkyl iodides. The resultant alkylated product typically has enhanced solubility in common organic solvents. This result allows investigation by liquid-state techniques, which cannot be used on the initial refractory material. Lewis and Singer (3) show the use of this approach in their chapter in this book on the determination of molecular weight distributions of petroleum cokes that have been solubilized by reductive alkylation. The initial chemistry of Sternberg and co-workers (1, 2), and related

approaches have been applied to a number of fossil-fuel systems, and the results are discussed in recent reviews (4–7).

Curiously, the chemistry of model aromatic hydrocarbons under the conditions of Sternberg and co-workers (1, 2) has been studied incompletely (8, 9) and sometimes in contexts far removed from fossil fuels (10). In this chapter, we discuss the chemistry of three model compounds, namely perylene, decacycene, and dibenzothiophene. Our studies used reduction by  $K^0$  in THF followed by alkylation, and our new findings are the following: (1) In the reductive methylation of both perylene and decacycene, methyl groups were found on nonprotonated carbon atoms in the products. This situation can be shown either by  $^1H$  NMR in which the proton resonance of the methyl group is a singlet rather than a doublet, as would be the case for a methyl group bound to a carbon bearing one proton or by  $^{13}C$  NMR by comparing proton coupled to proton decoupled spectra. (2) In the case of the reductive methylation of perylene, the dominant isomeric product contained a methyl group on the C-1 carbon and the adjacent nonprotonated carbon, C-14. The stereochemistry of the addition was *trans*. This regiochemistry is consistent with molecular orbital calculations of Minsky et al. (10), which showed maximum electron density in perylene anions to be on C-1. (3) In the reductive alkylation of dibenzothiophene, both a 2-biphenyl, alkyl sulfide and biphenyl were recovered after reaction times of a few hours, and only biphenyl was recovered after longer reaction times. The use of  $[^2H_8]$ THF showed that the two additional protons in biphenyl came from the solvent.

## Background

Herein, we focus on NMR characterization of the products of reductive alkylation; however, reductive alkylation has other interesting and sometimes controversial aspects. We briefly mention a few of these controversial points: (1) In the reductive alkylation of perylene, we found products of molecular weight corresponding to the addition of two alkyl groups to a perylene molecule (MW = 252); in previous literature, these molecules have been called by some people dialkyldihydroperylenes (9). For example, mass spectrometry (MS) of our product of methylation showed a molecular ion that has a mass-to-charge ratio ( $m/z$ ) of 282, which is consistent with the addition of two  $CH_3$  groups to perylene. Such a product is consistent with a perylene dianion precursor. Abbott et al. (9) claimed reductive alkylation products to be monoalkyldihydroperylenes (indicative of hydridoperylene carbanion precursors). Minsky et al. (10) claimed the product of reductive protonation to be tetrahydroperylene (indicative of a tetraanion precursor). One of us (L. B. E.) addressed both of these claims elsewhere (11, 12); the evidence presented herein further strengthens the case for the dianion of perylene under these reaction conditions. In this chapter, we shall refer to

our products as dialkyldihydroperylene to keep with past terminology, although our NMR results demonstrate this usage to be incorrect. (2) In the reductive alkylation of decacyclene, we found potential evidence for trianions and tetraanions, although dianions did seem to predominate. This result is consistent with past work (13) and is not further explored herein. (3) In the reductive alkylation of dibenzothiophene, we found the nonalkylated product biphenyl, as others have reported (8). We also found the 2-biphenyl alkyl sulfide and evidence for proton donation from solvent. Our work, done at room temperature, did not suggest the recently proposed dibenzothiophene dianion to have appreciable stability at room temperature (14).

### **Experimental Details**

Perylene, decacyclene, dibenzothiophene, and methyl iodide were obtained from Aldrich, potassium metal was obtained from Alfa, and THF was obtained from Fisher (THF was distilled from benzophenone ketyl prior to use). Aromatic anions were generated under a helium atmosphere within a glovebox (VAC Atmospheres) by the addition of potassium metal to a solution of the aromatic hydrocarbon in THF at room temperature. The highly colored anion of the aromatic hydrocarbon was observed within seconds of the addition of potassium; the color persisted until quenching. During reduction, excess metal was present at all times. For quenching, excess metal was removed, and the anion solution was placed in a glass vessel, fitted with a rubber septum, and equilibrated in an ice bath (0 °C). The quenching agent, either neat or diluted with THF, was slowly added to the anion solution with a syringe; typically, the quenching agent was equilibrated at 0 °C. As one example, 2.848 g (10.5 mmol) of perylene in 34.314 g of THF was reacted with 1.708 g (43.7 mmol) of potassium metal for 13 days. A total of 2.01 K atoms were consumed per perylene molecule, and the anion solution was quenched with 3 g of <sup>13</sup>C-enriched methyl iodide. Further details of our work with the perylene dianion were published previously (12).

The nuclear Overhauser effect (NOE) was measured with a Varian XL-300 spectrometer. A difference technique was used in which two different free-induction decays (FID) were obtained: one with the decoupler set on-resonance and the other with it set far off-resonance. The off-resonance FID was then subtracted from the on-resonance FID, and the result was Fourier transformed to give a spectrum revealing NOE enhancements. Peaks in such a difference spectrum reflect increases in the integrated intensity of the NMR absorption as a result of the concurrent saturation of the given resonance. This enhancement arises from cross relaxation between nuclei of the saturated resonance (denoted by S) and the enhanced ensemble (denoted by I). In the case of our alkylated perylene molecule, the mechanism of cross relaxation between I and S is presumably dipolar. The magnitude of the cross relaxation depends upon the distance between the I spins and the S spins and specifically varies as the 10<sup>-6</sup> of that distance (15). Enhancements are expected only for those nuclei near the nucleus that is saturated. The magnitude of NOE enhancements of the I ensemble created by saturating S can depend on the cross relaxation between the I ensemble and the spins that are not enhanced (denoted by N). Thus, it is not true that the "closer the spins, the larger the NOE enhancement." The enhancement magnitudes depend on the relative proximity of the I spins to the S and N spins (15).

The connectivity in our alkylated perylene was also studied by heteronuclear-correlated two-dimensional NMR, the details of which will be published elsewhere.

In addition to spectra obtained with a Varian XL-300 spectrometer, proton spectra were acquired with a JEOL FX-400 spectrometer (400 MHz), and carbon spectra were acquired with a Varian FT-80 spectrometer (20 MHz). Spectra of solids were obtained with a Varian WL-112 spectrometer, which is a wide-line instrument that uses sinusoidal field modulation with detection via a lock-in amplifier ( $^{13}\text{C}$  at 15 MHz and  $^2\text{H}$  at 12 MHz). (The symbol  $\delta$  denotes parts-per-million downfield from tetramethylsilane.)

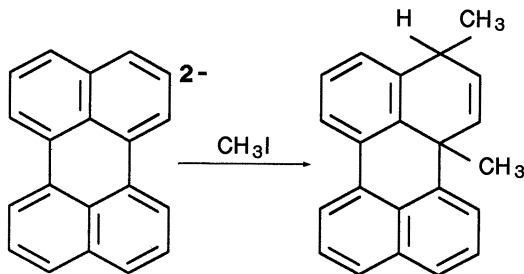
X-ray diffraction was performed with a Siemens D-500 unit employing copper radiation and a graphite monochromator.

Gas chromatography-mass spectrometry (GC-MS) was performed with a Hewlett-Packard 5595 spectrometer equipped with two parallel GC columns; the effluent from one column went to a flame-ionization detector, and the effluent from the other column went to a quadrupole mass filter (18).

## Results

**Perylene Chemistry.** Capillary GC analysis of the crude reductive methylation product indicated that one dimethyldihydro isomer was 6.6 times more abundant than the next most abundant isomer (12). The  $^1\text{H}$  spectrum of the crude product, shown in Figure 1, is consistent with this finding because it shows only two dominant methyl resonances:  $\delta$  0.79 (doublet) and  $\delta$  1.42 (singlet). The presence of a singlet and a doublet immediately provides some information about the regiochemistry of the product, which can be seen by considering the molecular structure. The conventional numbering scheme for the protons of perylene is shown in Figure 2. Protonated carbons are assigned the numbers of the adjacent protons. We will designate the nonprotonated carbon bonded to C-1 as C-14. Within this chapter, we will refer to C-14 as C-q to emphasize that a quaternary carbon is involved in the chemistry. Specifically, the presence of a singlet and a doublet for the  $\text{CH}_3$  resonances immediately rules out an isomer in which methyl groups are attached to C-2 and C-3 because this isomer would show two doublets (each methyl group split by the methine proton).

Two regioisomers are possible. In one isomer, methyl groups are attached to C-3 and C-q, and H-1 and H-2 are olefinic (Scheme I); in the



Scheme I. Formation of C-3/C-q isomer of dimethyldihydroperylene.

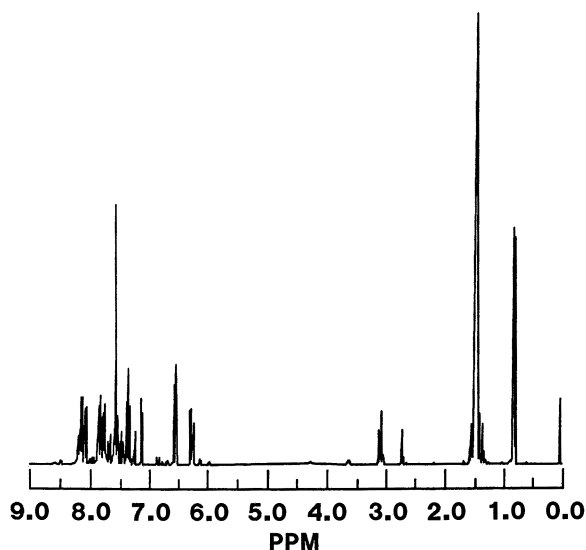
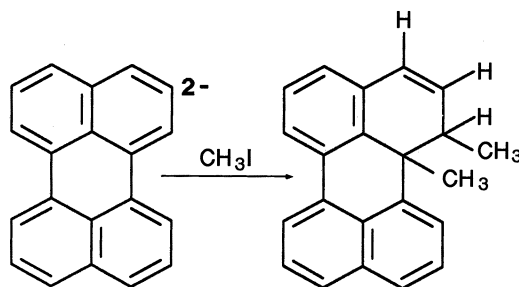


Figure 1.  $^1\text{H}$  NMR spectrum (400 MHz,  $25^\circ$ ) of the product of reductive methylation of the dianion of perylene (dimethyldihydroperylene).

other isomer, methyl groups are attached to C-1 and C-q, and H-2 and H-3 are olefinic (Scheme II). The large difference in observed chemical shifts of the olefinic protons ( $\delta$  6.25 and  $\delta$  6.52, in Figure 1) argues for, but does not prove, the C-1/C-q isomer.



Scheme II. Formation of C-1/C-q isomer of dimethyldihydroperylene.

**NOE APPROACH.** To make an unambiguous assignment of regiochemistry, several NOE experiments were performed to establish the connectivity of the protons. Proton-NOE enhancements are observed between nuclei separated by less than about  $5 \text{ \AA}$ . NOE difference spectra exhibit peaks only for those protons that are close to the proton being irradiated.



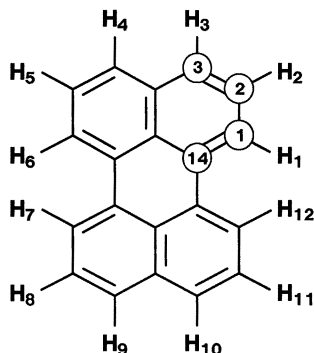


Figure 2. Proton-numbering scheme for perylene.

**IRRADIATION OF METHINE C-H.** Figure 3 shows a difference spectrum obtained by irradiation of the methine resonance at  $\delta$  3.07. In the C-1/C-q isomer (Scheme II), this resonance is for H-1; in the C-3/C-q isomer (Scheme I) this resonance is for H-3. An NOE was observed for four different resonances: those for both methyl groups, that for the  $\delta$  6.25 olefinic proton, and that for an aromatic proton at  $\delta$  7.53. Because the methine proton interacts with both methyl groups, the C-1/C-q isomer is suggested in which the methine C-H is close to both methyl groups rather than the C-3/C-q isomer, in which the methine C-H of C-3 is quite distant from the methyl group on C-q. In the C-1/C-q isomer, the aromatic proton at  $\delta$  7.53 is H-12; in the C-3/C-q isomer, the aromatic proton at  $\delta$  7.53 is H-4.

**IRRADIATION OF THE  $\delta$  6.52 OLEFINIC RESONANCE.** In a second NOE experiment, the olefinic resonance at  $\delta$  6.52 was irradiated, and an NOE was seen for two resonances: that for the other olefinic proton at  $\delta$  6.25 and that for the one aromatic proton at  $\delta$  7.12. In the C-1/C-q isomer (Scheme II), the single aromatic proton is H-4; in the C-3/C-q isomer (Scheme I), the aromatic proton is H-12. This observation is further evidence for the C-1/C-q isomer because the  $\delta$  6.52 resonance corresponds to H-3, which should not show an NOE on either methyl group. In the C-3/C-q isomer, either olefinic proton (H-1 or H-2) should show an NOE on a methyl group.

**IRRADIATION OF METHYL SINGLET AT  $\delta$  1.42.** In a third NOE experiment, the singlet methyl resonance at  $\delta$  1.42 was irradiated, and an NOE was seen for four resonances: the methine at  $\delta$  3.07, an aromatic proton at  $\delta$  7.53, the olefin at  $\delta$  6.52 and the olefin at  $\delta$  6.25. The NOE on an aromatic proton at  $\delta$  7.53 was proof of the presence of the C-1/C-q isomer in which both the methine C-H (H-1) and the methyl group on C-q are near the same aromatic proton (H-12). The first and third NOE experiments demonstrated that this situation is the case.

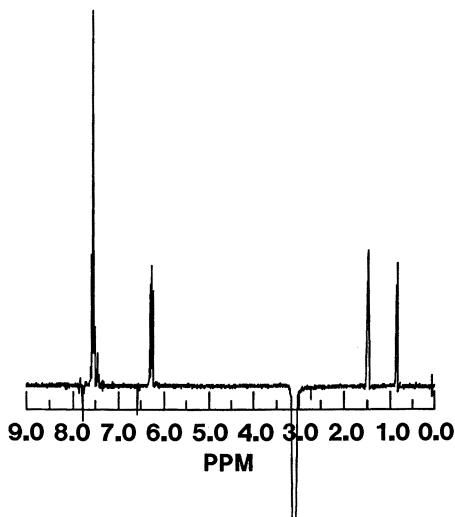


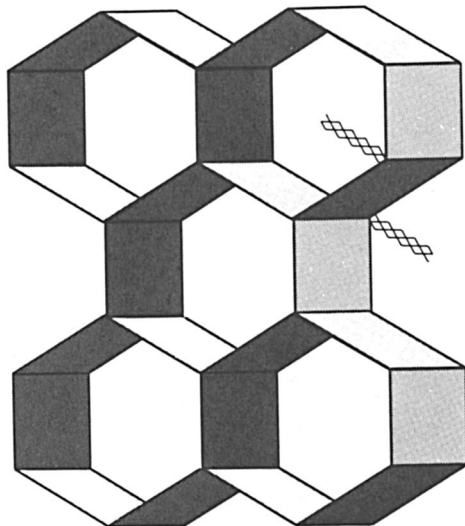
Figure 3. NOE difference spectrum arising from saturation of the methine resonance at  $\delta$  3.07.

In contrast, in the C-3/C-q isomer, the methine C-H (H-3) is the closest to the aromatic H-4 and the methyl group on C-q is closest to the aromatic H-12. The second NOE experiment showed that in the C-3/C-q model, H-12 must be at  $\delta$  7.12; however, the third NOE experiment showed that in the C-3/C-q model, H-12 must be at  $\delta$  7.55.

Thus, the C-1/C-q model self-consistently accounts for the three NOE experiments, and the C-3/C-q model does not. The dominant regioisomer of the reductive methylation of perylene has methyl groups at C-1 and the adjacent nonprotonated carbon (*see* Scheme II).

A remaining question concerns the stereochemistry of the C-1/C-q isomer: Are the methyl groups on the same side of the perylene plane (*cis*) or on opposite sides (*trans*)?

**IRRADIATION OF THE METHYL DOUBLET AT  $\delta$  0.79.** To address the question just proposed, a fourth NOE experiment was performed in which the methyl doublet at  $\delta$  0.79 was irradiated. An NOE was seen for the two olefinic peaks (H-2 and H-3), for the aromatic H-12 at  $\delta$  7.55 and the methine C-H on H-1; however, an NOE was not seen for the singlet methyl at  $\delta$  1.4. The third and fourth NOE experiments demonstrated that no intermethyl NOE occurs. This observation is suggestive of the *trans*-isomer, for which the distance between methyl carbon atoms is 3.9 Å and the interproton distances are too long for NOE, rather than of the *cis*-isomer, for which the distance between methyl carbon atoms is 2.9 Å. The *trans*-isomer is depicted as structure 1.



Structure 1. *The trans-isomer of C-1/C-q dimethyldihydroperylene.*

**SECOND MOMENT NMR ANALYSIS.** We have also approached the stereochemistry question by second-moment analysis of the  $^{13}\text{C}$  resonance of di[ $^{13}\text{C}$ ]methylidihydroperylene in the solid state. We formed this compound with  $^{13}\text{C}$ -enriched methyl iodide (99.7%  $^{13}\text{C}$ , Merck) and observed a line width  $\leq 0.05$  millitesla (mT), or 0.5 gauss (G). Because the intramolecular carbon-carbon dipolar interaction of the methyl groups of the *cis*-isomer corresponds to a Gaussian line width of 0.36 G (second moment =  $0.0352 \text{ G}^2 = 22.642/2.938^6$ ), most likely the total predicted second moment of the *cis*-isomer is larger than the observed moment. This situation is still being investigated.

**LIQUID-STATE  $^{13}\text{C}$  NMR OF ENRICHED MATERIALS.** High-resolution  $^{13}\text{C}$  NMR spectra of solutions of the  $^{13}\text{C}$ -enriched product allowed investigation of methyl shifts of the most abundant dimethyldihydroperylene isomer and of the other products previously determined by GC-MS (12). In the most abundant isomer, namely, the C-1/C-q isomer, the methyl group attached to C-1 was at  $\delta$  15.8 and the methyl group attached to C-q was at  $\delta$  33.9. Methyl resonances in the minor products of reductive methylation occurred at  $\delta$  19.7, 24.5, 25.5, 33.1, 33.2, and 40.6. Consistent with our previous GC-MS work, the integrated intensity of any of these minor methyl peaks was about 10 times smaller than either of the methyl peaks of the main C-1/C-q isomer. We also proposed the presence of a trimethyldihydroperylene on the basis of GC-MS fragmentation patterns; significantly, two-dimensional NMR demonstrated a carbon methyl bound directly to an aromatic carbon, and the shift of this methyl group was  $\delta$  19.7 ( $^{13}\text{C}$  NMR at an observation frequency of 75.43 MHz).

**LIQUID-STATE  $^{13}\text{C}$  NMR OF OTHER MATERIALS.** We report results of  $^{13}\text{C}$  NMR of a di[ $^2\text{H}_3$ ]methylidihydroperylene product for comparison with work on reductively alkylated decacyclene reported later. The two rehybridized carbons, namely, C-1 and C-q, appeared at  $\delta$  38.6 and 41.7 respectively. The two methyl carbons, which are split by C-D coupling of 19.5 Hz, appeared at  $\delta$  14.6 and 33.0. Several aromatic resonances spanned the range from  $\delta$  119.0 to 141.6 ( $^{13}\text{C}$  NMR data at an observation frequency of 100.4 MHz).

To unambiguously confirm the assignment of the rehybridized carbons C-1 and C-q,  $^{13}\text{C}$  NMR spectra of a dimethylidihydroperylene were obtained both with and without proton decoupling. The resonance at  $\delta$  41.7 was unchanged (proving it to be C-q), and the resonance at  $\delta$  38.6 became a doublet without decoupling (proving it to be C-1). The H-C coupling constant for the doublet was 127 Hz, which is consistent with its identity as an  $sp^3$ -hybridized carbon (17).

**PERYLENE REDUCTION IN THE PRESENCE OF NAPHTHALENE.** The chemistry that we have discussed is similar to that of Sternberg and co-workers (1, 2) in using an excess of potassium metal in THF at room temperature. In the Sternberg and co-workers approach, however, naphthalene was used to transfer electrons from potassium metal to the substrate under investigation whether it was a fossil fuel, such as coal (2), or a model compound, such as dibenzothiophene (8). Thus, the results of our work on the direct reduction of perylene by  $\text{K}^0$  might differ from results of a reaction in which naphthalene is present.

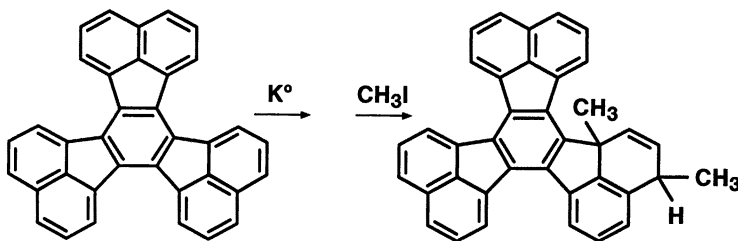
To address this possibility, we combined naphthalene (0.924 g, 7.2 mmol), pyrene (0.503 g, 2.5 mmol), and perylene (0.399 g, 1.6 mmol) with  $\text{K}^0$  (2.504 g, 64 mmol) in THF (32.467 g). Quenching an aliquot with methyl iodide after 29 h of reaction showed the C-1/C-q dimethylidihydroperylene isomer to be the single most abundant perylene-derived product; it was approximately 7 times more abundant than recovered perylene. Significantly, we recovered tetramethyltetrahydroperylene [MS: molecular ion at  $m/z = 312$ , intensity ( $I$ ) = 13; base ion reflecting methyl loss at  $m/z = 297$ ,  $I = 100$ ; second methyl-loss ion at  $m/z = 282$ ,  $I = 13$ ; third methyl-loss ion at  $m/z = 267$ ,  $I = 26$ ; and fourth methyl-loss ion at  $m/z = 252$ ,  $I = 53$ ). The GC-FID intensity was 7.2 times less than that of the C-1/C-q dimethylidihydroperylene isomer. In contrast with perylene, pure naphthalene was 28.9 times more abundant than the dominant dimethylidihydro-naphthalene product. In fact, the reduction of methyl iodide by the naphthalene radical anion to yield methyl radicals may be the origin of the methyl groups in the tetramethyltetrahydroperylene.

At the same time, a second aliquot was quenched with pentyl iodide. A dipentylidihydroperylene (MS: molecular ion at  $m/z = 394$ ,  $I = 1.4$ ; pentyl-loss ion at  $m/z = 323$ ,  $I = 54$ ; and second pentyl-loss ion at  $m/z = 252$ ,  $I = 100$ ) was the predominant perylene-containing species; it was 32 times more abundant than the recovered perylene.

With the naphthalene ensemble, recovered naphthalene was only 1.8 times more abundant than the most prevalent dipentylidihydronaphthalene isomer; it was only 1.2 times more abundant than the two most prevalent dipentylidihydronaphthalene isomers. In the stoichiometric alkylation of an aromatic radical anion, 1 mol of the aromatic compound is recovered for every mole of the dialkyl dihydroaromatic compound recovered.

Thus, the radical anion of naphthalene reacted differently with methyl iodide (to form methyl radicals) than with pentyl iodide (to undergo substitution). Perylene, on the other hand, underwent substitution with methyl iodide whether or not naphthalene was present; perylene also underwent substitution with pentyl iodide when naphthalene was present.

**DECACYCLENE CHEMISTRY.** Unlike perylene, which consumes 2 mol of K per mole of perylene, decacycene consumes between 2.2 and 3.0 mol of K per mole of decacycene. As with perylene, we wanted to determine if reductive methylation could yield a product with a methyl group on a quaternary carbon, as in the C-3/C-q dimethyldihydrodecacycene isomer depicted in Scheme III.



*Scheme III. The reductive methylation of decacycene illustrated for hypothetical C-3/C-q dimethyldihydrodecacycene product.*

Reductive methylation with  $\text{CD}_3\text{I}$  led to a product containing six  $^{13}\text{C}$  NMR resonances in the aliphatic region and a cluster in the aromatic region from  $\delta$  121 to 148 ( $^{13}\text{C}$  NMR observation frequency was 20 MHz, and protons were decoupled). The  $\text{CD}_3$  groups, appearing broadened by unresolved C–D coupling, were at  $\delta$  12 and 20, and the rehybridized carbons appeared at  $\delta$  36 and 50. Two sharp peaks of lower intensity occurred at  $\delta$  29 and 32. Additionally, deuterium NMR of the solid compound (12 MHz, 1.83 T, dispersive mode, 23 °C) showed only a quadrupole split resonance with derivative maximum separation of 5.66 mT (56.6 G), which is indicative of methyl groups rotating about their threefold axes.

To determine if alkylation had occurred on nonprotonated carbons, another high-resolution spectrum was obtained with the proton decoupler turned off. The two  $\text{CD}_3$  resonances remained broad; the peak at  $\delta$  36 and

the minor peaks at  $\delta$  29 and 32 broadened, but the major peak at  $\delta$  50 had the same line width as that in the proton-decoupled spectrum. This result suggests that the  $\delta$  50 peak represents a rehybridized quaternary carbon, analogous to C-q in the dimethyldihydroperylene compound discussed earlier.

This assignment is consistent with  $^{13}\text{C}$  NMR spectra of reductively ethylated, pentylated, and decylated decacyclenes, all of which have such a low-field resonance at  $\delta$  55.

An additional reductive alkylation experiment was performed with  $\text{CH}_3\text{I}$ . With an uptake of 3 mol of K per mole of decacyclene, the product showed a proton NMR spectrum including a doublet at  $\delta$  0.53, a singlet at  $\delta$  1.43, and distinct olefinic clusters near  $\delta$  6.22 and 6.65. However, other peaks in the range between  $\delta$  1.5 and 2.0 suggested additional complexity, possibly from impurities in the initial decacyclene, from decomposition of the solvent, or from the presence of tetramethyltetrahydrodecacyclenes (probe MS shows ions of  $m/z = 480, 495, \text{ and } 510$ ). Furthermore, the aromatic region of the proton NMR of the product was complex; although pure decacyclene showed three peaks —  $\delta$  7.69 (*t*),  $\delta$  8.61 (*d*), and  $\delta$  7.81 (*d*) (18)— the reductively methylated material had roughly nine “packets” in the aromatic region, including ones at  $\delta$  7.78, 7.91, 8.78, and 7.45.

**Structures of Perylene and Decacyclene Products.** After obtaining intramolecular structural information from NMR experiments, intermolecular ordering was investigated by means of X-ray diffraction. This study extended work that we already published on the diffraction of liquidlike organic compounds (19–21). Noting that the diffraction pattern of  $\text{di}[^2\text{H}_3]\text{methylidihydroperylene}$  published in reference 21 showed both sharp Bragg peaks and broad Debye peaks, we melted the compound at 110 °C and allowed it to recrystallize at 25 °C. The diffraction pattern of the product showed two sharp peaks at 10.2 and 5.13 Å (which were present before melting) and two intense broad peaks at 6.6 and 4.4 Å, in addition to the broad “(100)” intramolecular peak at 2.2 Å. The pattern, which is similar to that of a discotic liquid crystal, is shown in Figure 4.

Inspection of the reductively methylated, hexylated, and octylated decacyclenes shows evidence only for the broad Debye peaks; no hydrocarbon material in the product gave Bragg peaks (e.g., as found in the initial decacyclene). The reductively methylated decacyclene showed a peak at 5.9 Å of full width at half maximum of  $3.3^\circ 2\theta$  on top of a much broader peak. The reductively hexylated material showed peaks at 4.0 Å (major) and 5.3 Å (minor).

Previously, we showed (19–21) that single-phase organic liquids of a given functionality (e.g., *n*-paraffins, aromatic compounds, or naphthenes) can give rise to peaks of characteristic *d* values. Our reductively alkylated mol-

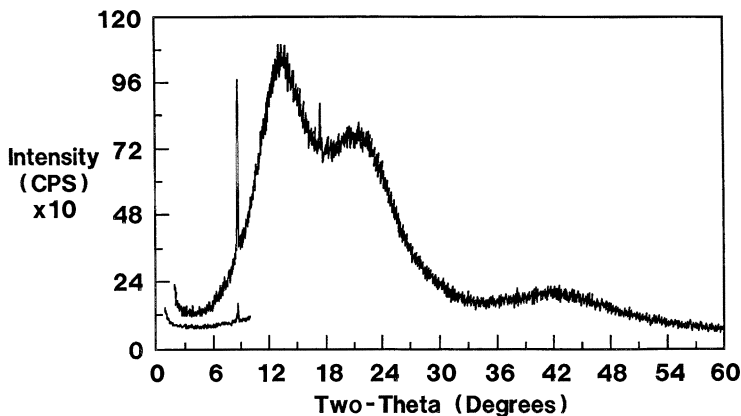


Figure 4. X-ray diffraction pattern (Cu) of reductively methylated perylene following melting and resolidification. Sharp peaks are at 10.15 and 5.13 Å, and broad peaks are at 6.55, 4.36, and 2.15 Å.

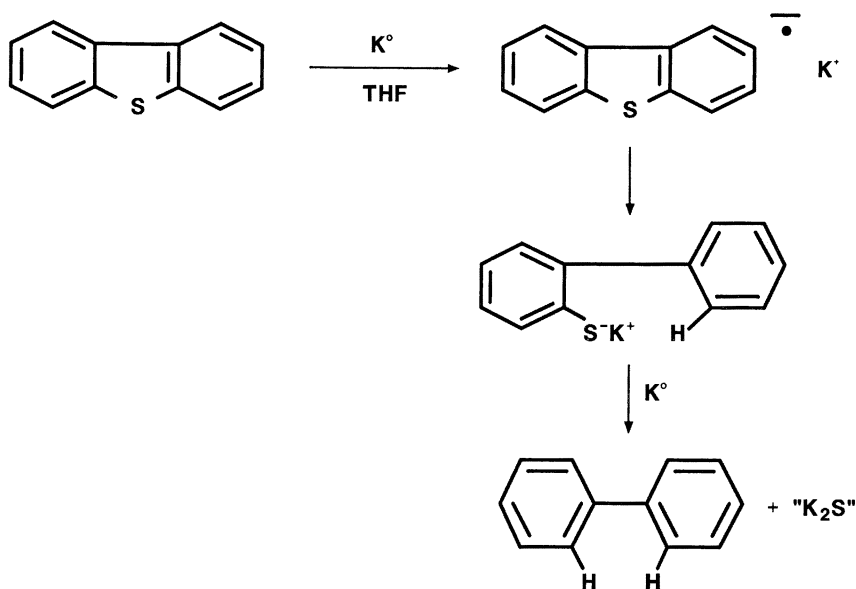
ecules, which do not fit neatly into any of these categories, showed diffraction patterns distinct from those of *n*-paraffins, aromatic compounds, and naphthenes.

**Dibenzothiophene Chemistry.** Unlike with perylene and decacylene, for which reductive alkylation leads simply to the addition of alkyl groups to aromatic compounds, the reductive alkylation of dibenzothiophene can lead to biphenyl (8). This product occurs by the loss of sulfur from dibenzothiophene, followed by the uptake of two protons. Using reaction times of 1–4 h at room temperature, one can isolate a 2-biphenyl, alkyl sulfide; this finding indicates that the anion on sulfur can have some stability. We investigated this situation by performing  $^2\text{H}$  NMR on a product of the reaction of  $\text{CD}_3\text{I}$  with a dibenzothiophene anion solution formed by adding 2 mol of K per mole of dibenzothiophene.

Deuterium NMR of the quenched, unevaporated product solution showed three peaks:  $\delta$  2.07 (dimethyl sulfide, also seen in MS analysis with  $m/z = 68$ ),  $\delta$  2.18 (methyl iodide), and  $\delta$  2.33 (presumably 2-biphenyl methyl sulfide which is also called 2-phenylthioanisole). Only the last peak remained in the product following rotary evaporation.

The presence of only one deuterium resonance in the evaporated product suggests that a monomethylated derivative is present; MS confirms this condition. This finding implies that the intermediate picks up protons from the solvent or other source. To investigate this matter, we performed the reduction in  $[^2\text{H}_8]\text{THF}$  (with 4.3 K/dibenzothiophene) and found only biphenyl as a  $\text{CH}_3\text{I}$  quench product after 24 h. MS analysis of the 42-h quench product showed appreciable deuterium incorporation ( $m/z = 154$ , intensity

= 100; 155, 96; 156, 44; 157, 13; 158, 3). Thus, deuterium incorporation from solvent was confirmed. Our mechanism is summarized in Scheme IV.



*Scheme IV. Reduction of dibenzothiophene with  $K^0$  in THF at room temperature.*

## Discussion

The results just discussed demonstrate the complexity of the reductive alkylation reaction, even with relatively simple model compounds such as perylene, decacyclene, and dibenzothiophene.

With perylene, one might have expected either the C-3/C-q dimethyl dihydro isomer, in analogy to the known chemistry of naphthalene, or the C-2/C-3 dimethyl dihydro isomer because of steric constraints at C-q. Yet, the C-1/C-q dimethyl dihydro isomer was obtained overwhelmingly. This result is in accord with the prediction of Minsky et al. (10) that C-1 bears the highest electron density (and once C-1 picks up an alkyl group in the quench, only one regioisomer can be made).

Curiously, in reacting with methyl iodide so readily to make dimethyl dihydro products, the perylene dianion is distinct from the radical anion of naphthalene, which primarily reduces methyl iodide to the methyl radical and the iodide anion.

With both perylene and decacyclene, alkylation occurs at quaternary carbons. Because the  $^{13}\text{C}$  chemical shifts of these alkylated quaternary compounds are so far downfield ( $\delta$  42 in the perylene compound and  $\delta$  50–55



in decacyclene), these results must be considered in seeking the correct interpretation of NMR spectra of reductively alkylated fossil fuels.

For example, although the presence of quaternary  $sp^3$ -hybridized carbon has been recognized in the product of reductive butylation of Illinois No. 6 coal, this carbon has been postulated to arise from multiple butylation reactions (22, 23). A simple model for this carbon would be the quaternary C-9 in 9,9,10-tri(*n*-butyl)-10-hydroanthracene. More recently, Stock and Willis (22–25) have suggested that reductive alkylation can lead to quaternary  $sp^3$ -hybridized carbon via the following:

1. Attachment of the alkyl group to an aromatic carbon bearing an intrinsic alkyl group to generate a quaternary carbon bearing one added alkyl group and one intrinsic alkyl group (as compared with two added alkyl groups in the initial postulate embodied by the anthracene example given in the preceding paragraph). Recent work by Rabideau (26) presented in this book is relevant to this proposal in suggesting that electron-releasing alkyl groups will direct attack away from the aromatic carbon bearing the alkyl group.
2. Attachment of an alkyl group to a carbanion formed by metalation of a tertiary (acidic) C–H to generate a quaternary  $sp^3$ -hybridized carbon from a tertiary  $sp^3$ -hybridized carbon.

Our work demonstrates that a quaternary  $sp^3$ -hybridized carbon can arise in a manner entirely unanticipated in the work by Stock and Willis (24, 25) via the addition of an alkyl group to a nonprotonated (initially) aromatic carbon.

The details of the chemical shifts that we have presented are also relevant to past work relating to fossil fuels. Analysis of the product of the reductive butylation of Illinois No. 6 coal revealed seven sharp peaks in  $^{13}\text{C}$  NMR. Whereas a peak at  $\delta$  67.8 was assigned to the  $\alpha$ -methylene group in a butyl aryl ether, no signal corresponding to  $\alpha$ -methylene group in a carbon-alkylated product was discernible (23). A later study with  $^{13}\text{C}$ -enriched methyl groups did not show any narrow, well-defined peaks assignable to methyl groups on carbon (25). Our work, using  $^{13}\text{C}$ -enriched methyl groups, is interesting in showing the rather large range of chemical shifts observable for the methyl resonances in what are demonstrably dimethyldihydroperylene:  $\delta$  15.6–40.6. Furthermore, relevant to work performed with natural isotopic abundances we have shown that the resultant quaternary  $sp^3$ -hybridized carbons can come quite far downfield:  $\delta$  41.7 for C-q in C-1/C-q dimethyldihydroperylene and  $\delta$  50–55 for C-q in reductively alkylated decacyclenes. In the past, resonances in this region have been associated more strongly with alkyl groups on nitrogen or on oxygen (27, 28).

With respect to the use of analysis of NOE enhancements to infer stereochemistry of the C-1/C-q dimethyldihydroperylene isomer, our work is an extension of many studies of the related naphthalene and anthracene systems (29–33). Perylene is somewhat interesting in being one of the smallest polynuclear aromatic hydrocarbons to contain formally single bonds (34). Furthermore, although perylene has significant crowding of hydrogens (H-1 and H-12, as well as H-6 and H-7, are only 1.81 Å apart), the slight deviations from planarity of perylene are considered to arise from intermolecular packing effects (34). Picene, which has the same type of hydrogen crowding as perylene (interhydrogen distances are 1.88 Å), deviates from planarity by 3.72° between the first and fifth ring (35). The regiochemistry of reductive alkylation may be driven, in part, to relieve strain in such molecules.

With dibenzothiophene, potassium reaction leads to sulfur removal from dibenzothiophene and proton removal from the solvent, which introduces another level of complexity into the analysis. Ito et al. (14) claimed the existence of a dianion of dibenzothiophene with potassium cations in THF; this dianion is sufficiently stable at 20 °C so that its formation can be monitored with traditional UV–visible techniques. Furthermore, this dianion is the product of cleavage of one C–S bond; one charge is on sulfur, and the other is presumably on carbon. Our GC–MS data, in showing deuterium incorporation from [<sup>2</sup>H<sub>8</sub>]THF, do not suggest that the negative charge on the carbon system has stability in the solvent at room temperature. Furthermore, at no time during the reduction did we find that a quench with alkyl iodide yielded a product with two alkyl groups, which would be expected from the stable dianion of dibenzothiophene discussed by Ito et al. (14). Significantly, the data supporting a recent claim of a dianion of benzo[*b*]thiophene with sodium were obtained at –78 °C; raising the temperature to –20 °C changed the reaction pathway to a metalation (36).

Nevertheless, in terms of analysis of sulfur functionality, the observed chemistry of sulfur loss and protonation from solvent could serve as a useful complement to existing physical probes (37, 38).

For the three compounds we studied, namely, perylene, decacyclene, and dibenzothiophene, we have discussed issues in the identity of the intermediate reduction products [tetranions of perylene and decacyclene and dianions of dibenzothiophene and even naphthalene (5)], which are relevant not only to the study of aromatic hydrocarbons but also to the study of graphite. In aromatic molecules, added charge tends to segregate to the periphery of the compound (39) in a predictable way (40–43); this situation allows a prediction of regiochemistry, as we have done here for perylene. In graphite, added charge in part goes to internal carbons (39) and thereby generates graphitic chemistry possibly different from aromatic hydrocarbon chemistry.

One example of this divergence may be seen in reductive protonation.

For the dianion of perylene, the addition of ammonium chloride in water yields two distinct products: tetrahydroperylene (ca. 15% of initial perylene) and dihydroperylene (ca. 15% of the initial perylene); the rest of the recovered product is perylene. A small amount of hydrogen gas is also produced. With deuterated water and deuterated ammonium chloride, the following products are obtained: tetradeuteroperylene (molecular ion at  $m/z = 260$  and base ion at  $m/z = 230$ , which arises from the loss of deuterated ethylene,  $C_2H_2D_2$ ), dideuteroperylene (molecular ion at  $m/z = 256$ ), and perylene containing significant amounts of deuterium (ion at  $m/z = 253$  shows 53% of the intensity of the ion at 252). Significantly, the most abundant isomer of hydrogen gas is HD (65% of all hydrogen). The  $D^+$  adds to the periphery of the perylene, and slight amounts of the hydroaromatic compound decompose to the aromatic compound and hydrogen gas. (A detailed account of this reaction appears in reference 44.) In the past, researchers studying fossil fuels believed that reductive protonation could also rehybridize graphitic  $sp^2$  carbon to  $sp^3$  carbon (45). However, such reactions are now known to lead to intercalation compounds or residual compounds, which do contain the molecule used for protonation but do not contain  $sp^3$ -hybridized carbon (44, 46, 47).

The diffraction work on reductively methylated perylene is relevant to the understanding of fossil-fuel structures. Coals and petroleum-derived solids are poorly crystalline in comparison with graphite; typical crystallites are less than 20 Å. In fact, coals containing 89% carbon are considered to approach an ideal liquidlike arrangement (48) in which only short-range stacking interactions of aromatic moieties over distances of 7–10 Å occur. Studies of reductively alkylated aromatic compounds allow us to focus on the relative importance of aromatic–aromatic and aliphatic–aliphatic interactions over such short distances. Furthermore, changing the length of the alkyl group changes the relative abundances of aromatic and aliphatic atoms so that the effects of these interactions on the structure of such poorly crystalline materials can be determined. Thus, in the future, the model-compound chemistry of both polynuclear aromatic hydrocarbons and graphite will be useful in elucidating the chemistry of fossil fuels.

### **Acknowledgments**

We thank J. Bradley and E. Hill for furnishing us with the high-quality THF; R. Kastrop for early NMR work on the perylene and decacyclene and current work on two-dimensional heteronuclear-correlated NMR; K. Rose for the deuterium NMR and R. Pancirov for the MS on dimethyl sulfide; and V. Brodtkin for figure design. M. Melchior suggested the use of the NOE experiment, and R. Pancirov provided helpful data and insights concerning

MS of the compounds. M. Maturro performed molecular mechanics MMPI calculations on *cis* and *trans* (1,q)dimethyl dihydroperylene isomers to give us atomic coordinates.

## References

1. Sternberg, H. W.; Delle Donne, C. L. *Prepr. Pap.-Am. Chem. Soc., Fuel Chem.* **1968**, *12*(4), 13.
2. Sternberg, H. W.; Delle Donne, C. L.; Pantages, P.; Moroni, E. C.; Markby, R. E. *Fuel* **1971**, *50*, 432.
3. Lewis, I. C.; Singer, L. S., Chapter 16 in this book.
4. Wender, I.; Heredy, L. A.; Neuworth, M. B.; Dryden, I. G. C. In *Chemistry of Coal Utilization*; Elliot, M. A., Ed.; Wiley: New York, 1981; 2nd Suppl. Vol.; pp 425-479.
5. Stock, L. M. In *Coal Science*; Gorbaty, M. L.; Larsen, J. W.; Wender, I., Eds.; Academic: New York, 1982; Vol. 1, pp 161-281.
6. Ebert, L. B. In *Chemistry of Engine Combustion Deposits*; Ebert, L. B., Ed.; Plenum: New York, 1985; pp 303-376.
7. Hessley, R. K.; Reasoner, J. W.; Riley, J. T. *Coal Science: An Introduction, Technology, and Utilization*; Wiley: New York, 1985; pp 106-109.
8. Ignasiak, T.; Kemp-Jones, A. V.; Strausz, O. P. *J. Org. Chem.* **1977**, *43*, 312.
9. Abbott, J. M.; Erbatur, O.; Gaines, A. F. *Fuel* **1984**, *63*, 1441.
10. Minsky, A.; Meyer, A. Y.; Rabinovitz, M. *J. Am. Chem. Soc.* **1982**, *104*, 2475.
11. Ebert, L. B. *Fuel* **1986**, *65*, 144.
12. Ebert, L. B. *Tetrahedron* **1986**, *42*, 497.
13. Saji, T.; Aoyagui, S. *J. Electroanal. Chem. Interfacial Electrochem.* **1979**, *102*, 139.
14. Ito, O.; Aruga, T.; Matsuda, M. *J. Chem. Soc., Perkin Trans. 2* **1982**, 1113.
15. Noggle, J. H.; Schirmer, R. E. *The Nuclear Overhauser Effect: Chemical Applications*; Academic: New York, 1971; pp 45-48.
16. Miller, P. E.; Denton, M. B. *J. Chem. Ed.* **1986**, *63*, 617.
17. Muller, N.; Pritchard, D. E. *J. Chem. Phys.* **1959**, *31*, 1471.
18. Drake, J. A. G.; Jones, D. W. *Org. Mag. Reson.* **1980**, *14*, 272.
19. Ebert, L. B.; Scanlon, J. C.; Mills D. R. *Prepr. Pap.-Am. Chem. Soc., Div. Petrol. Chem.* **1983**, *28*(5), 1353.
20. Ebert, L. B.; Scanlon, J. C.; and Mills, D. R. *Liq. Fuels Technol.* **1984**, *2*, 257.
21. Ebert, L. B.; Scanlon, J. C.; Mills, D. R. *Prepr. Pap.-Am. Chem. Soc., Div. Petrol. Chem.* **1985**, *30*(4), 636.
22. Wender, I.; Heredy, L. A.; Neuworth, M. B.; Dryden, I. G. C. In *Chemistry of Coal Utilization*; Elliot, M. A., Ed.; Wiley: New York, 1981; 2nd Suppl. Vol.; pp 442-443.
23. Stock, L. M. In *Coal Science*; Gorbaty, M. L.; Larsen, J. W.; Wender, I., Eds.; Academic: New York, 1982; Vol. 1, pp 268-272.
24. Stock, L. M.; Willis, R. S. *Prepr. Pap.-Am. Chem. Soc., Div. Fuel Chem.* **1985**, *30*, 21.
25. Stock, L. M.; Willis, R. S. *J. Org. Chem.* **1985**, *50*, 3566.
26. Rabideau, P. W., Chapter 5 in this book.
27. Stock, L. M., In *Coal Science*; Gorbaty, M. L.; Larsen, J. W.; Wender, I., Eds.; Academic: New York, 1982; Vol. 1, p 275.
28. Rose, K. D.; Francisco, M. A. *Prepr. Pap.-Am. Chem. Soc., Div. Petrol. Chem.*, **1985**, *30*, 262.

29. Harvey, R. G.; Davis, C. C. *J. Org. Chem.* **1969**, *34*, 3607.
30. Panek, E. J.; Rodgers, T. J. *J. Am. Chem. Soc.* **1974**, *96*, 6921.
31. Rabideau, P. W.; Burkholder, E. G. *J. Org. Chem.* **1979**, *44*, 2354.
32. Rabideau, P. W.; Lipkowitz, K. B.; Nachbar, R. B. *J. Am. Chem. Soc.* **1984**, *106*, 3119.
33. Rabideau, P. W.; Mooney, J. L.; Hardin, J. N. *J. Org. Chem.* **1985**, *50*, 5737.
34. Camerman, A.; Trotter, J. *Proc. Roy. Soc. London A* **1963**, *220*, 311.
35. De, A.; Ghosh, R.; Roychowdhury, S.; Roychowdhury, P. *Acta Crystallogr., Sect. C* **1985**, *41*, 907.
36. Cohen, Y.; Klein, J.; Rabinovitz, M. *J. Chem. Soc., Chem. Commun.* **1985**, 1033.
37. Ruiz, J.-M.; Carden, B. M.; Lena, L. J.; Vincent, E. J.; Escalier, J. C. *Anal. Chem.* **1982**, *54*, 688.
38. Spiro, C. L.; Wong, J.; Lytle, F. W.; Greeger, R. B.; Maylotte, D. H.; Lamson, S. H. *Science* **1984**, *226*, 48.
39. Calkin, M. G.; Kiang, D.; Tindall, D. A. *Nature* **1986**, *319*(6053), 454.
40. Herndon, W. C. *Tetrahedron* **1982**, *38*, 1389.
41. Showali, A. S.; Herndon, W. C.; Parkanyi, C. *Electrochim. Acta* **1982**, *27*, 817.
42. Stein, S. E.; Brown, R. L. *Carbon* **1985**, *23*, 105.
43. Komenda, J.; Hess, U. *Z. Phys. Chem. (Leipzig)* **1984**, *265*, 17.
44. Ebert, L. B.; Mills, D. R.; Scanlon, J. C. *Solid State Ionics* **1986**, *22*, 143.
45. Wender, I.; Heredy, L. A.; Neuworth, M. B.; Dryden, I. G. C. In *Chemistry of Coal Utilization*; Elliot, M. A., Ed.; Wiley: New York, 1981; 2nd Suppl. Vol.; pp 433, 446.
48. Schlogl, R.; Boehm, H. P. *Carbon* **1984**, *22*, 351.
47. Ebert, L. B.; Mills, D. R.; Garcia, A. R.; Scanlon, J. C. *Mater. Res. Bull.* **1985**, *20*, 1453.
48. Hirsch, P. B. *Proc. Roy. Soc. London A* **1954**, *226*, 143.

RECEIVED for review September 29, 1986. ACCEPTED January 27, 1987.

# Coupling of Aromatic and Heterocyclic Cation Radicals with Neutral Radicals

Henry J. Shine<sup>1</sup> and Miroslaw Soroka<sup>2</sup>

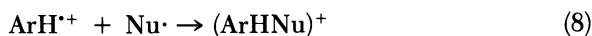
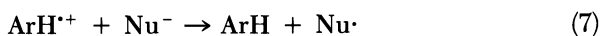
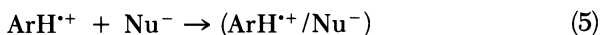
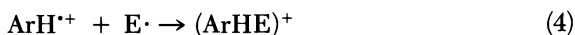
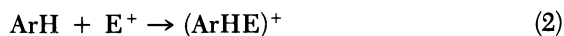
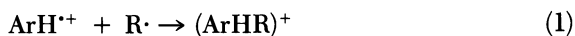
<sup>1</sup> Department of Chemistry and Biochemistry, Texas Tech University, Lubbock, TX 79409

<sup>2</sup> Institute of Organic and Physical Chemistry, Technical University, Wroclaw, Poland

*Evidence is presented that aromatic and heteroaromatic cation radicals can couple with the free radical NO<sub>2</sub> and that the thianthrene cation radical (Th<sup>•+</sup>) can couple with alkyl radicals. Evidence for reactions with NO<sub>2</sub> was taken from the literature wherein controversy is found as to whether or not the coupling reaction is a step in conventional nitration reactions. Evidence for alkyl-radical coupling was obtained from reactions of Grignard reagents with Th<sup>•+</sup>. In particular, reaction with 5-hexenylmagnesium chloride was found to lead to a mixture of sulfonium ion perchlorates, ThR<sup>+</sup>ClO<sub>4</sub><sup>-</sup>, containing a large amount of R as the cyclopentylmethyl group. Attempts to find similar evidence for the formation and coupling of radicals in analogous reactions of Th<sup>•+</sup> with dialkylmercurial compounds, including bis(5-hexenyl)mercury, were not conclusive. Few reactions of neutral radicals with aromatic and heteroaromatic cation radicals, other than those noted, have been reported.*

**T**HIS CHAPTER IS CONCERNED WITH A REACTION of aromatic and heterocyclic cation radicals about which only little is so far known: their ability to react with neutral radicals. The reaction is expressed simply for the coupling of an aromatic cation radical (ArH<sup>•+</sup>) with a radical (R<sup>•</sup>) in equation 1. This simple equation, presently only poorly documented, is nevertheless part of current thinking in two reactions of wide scope: electrophilic aromatic substitution and reactions of cation radicals with nucleophiles. The product of equation 1 is a  $\sigma$  complex, (ArHR)<sup>+</sup>, which is structurally the same as that

obtained in electrophilic aromatic substitution and is shown in equation 2 with the electrophile  $E^+$ . The two reactions are intimately connected, and researchers are currently showing considerable interest in finding whether the reaction of  $ArH$  with  $E^+$  involves electron transfer (equation 3) and radical coupling (equation 4). The product  $(ArHR)^+$  is also structurally like the  $\sigma$  complex,  $(ArH\nu)^+$ , which would be obtained from the overall reaction of a cation radical  $(ArH^{+\cdot})$  with a negatively charged nucleophile ( $Nu^-$ ). This reaction is written in two steps, equations 5 and 6, in the manner of Hamerich and Parker's formulation of reactions of cation radicals with nucleophiles (1). In these steps,  $(ArH^{+\cdot}/Nu^-)$  is a  $\pi$ -complex, not well defined, which becomes a covalently bound complex in the redox step of equation 6. The connection of equation 1 with equations 5 and 6 is mechanistically important because, as with electrophilic aromatic substitution, a second electron-transfer sequence of steps can be written for the nucleophilic reaction, that is, equations 7 and 8. In equation 8, the equivalent of equation 1 can be seen.



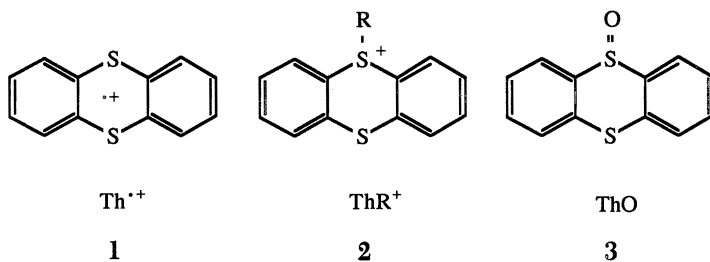
The main emphasis of this chapter will be on our attempts to find evidence for radical coupling in reactions of the thianthrene cation radical ( $Th^{+\cdot}$ ) with nucleophiles, that is, for the occurrence of steps such as equations 7 and 8. However, because discussions of reactions of cation radicals with radicals are relatively sparse, we will refer first to other works that principally deal with aromatic nitration.

The structure of the thianthrene cation radical is shown in structure 1 as  $Th^{+\cdot}$ . Its electron spin and charge are fully delocalized (2), yet reactions with nucleophiles occur principally at one of the sulfur atoms (3). Therefore,

in the context of equations 1–8, we should replace equation 1 with equation 9,



in which the symbol  $\text{S}^{++}$  represents the thianthrene cation radical. The symbols  $\text{ThR}^+$  and  $\text{ThO}$  (thianthrene 5-oxide) will be used frequently in this chapter; they correspond to structures 2 and 3, respectively.



### Experimental Details

Acetonitrile (Eastman Kodak) and methylene chloride (Merck) were distilled over  $\text{P}_2\text{O}_5$  in an argon atmosphere and stored under dry argon. Butane, 1-butene, butyl chloride, 1-hexene, methylcyclopentane (MCP), 5-hexen-1-ol, and octane were obtained from commercial sources. Dibutylmercury ( $\text{Bu}_2\text{Hg}$ ) was prepared by reaction of butylmagnesium chloride ( $\text{BuMgCl}$ ) with mercuric chloride ( $\text{HgCl}_2$ ) in a standard way. Butyl-, cyclopentylmethyl-, and 5-hexenylmercuric chloride ( $\text{BuHgCl}$ ,  $\text{CPMHgCl}$ , and 5-hexenyl $\text{HgCl}$ , respectively) were prepared by reaction of the Grignard reagent with  $\text{HgCl}_2$  (4). Two 1/8-in. stainless steel columns were used in gas-liquid chromatographic (GLC) analyses: (1) a 6-ft, 10% OV-101 (methylsilicone) on Chrom WHP (calcined diatomaceous earth, white, high performance), 80/100 mesh for analyses of hydrocarbons and some of the higher molecular weight products, and (2) an 18-in, 5% OV-101 on Chrom WHP 100/120 mesh for higher molecular weight products, especially thianthrene (Th) and derivatives. Gas chromatographic–mass spectrometric (GC–MS) data were obtained with a quadrupole instrument (Hewlett-Packard 5995).

#### Reaction of $\text{Th}^{++}\text{ClO}_4^-$ with $\text{Bu}_2\text{Hg}$ .

**RUN 1.** A stirrer bar and 632 mg (2.0 mmol) of  $\text{Th}^{++}\text{ClO}_4^-$  were kept under vacuum in a septum-capped vial for 3 h, after which dry argon and 5 mL of  $\text{CH}_3\text{CN}$  was added with a syringe. To the stirred mixture, a 0.56 M solution of  $\text{Bu}_2\text{Hg}$  in  $\text{CH}_3\text{CN}/\text{CH}_2\text{Cl}_2$  (1:1) was added dropwise with a syringe until the color of  $\text{Th}^{++}$  disappeared. This step required 1.04 mmol of  $\text{Bu}_2\text{Hg}$ . Thereafter, 200 mg of  $\text{LiCl}$



was added, and the mixture was stirred for 2 h at 0 °C and stored overnight at room temperature. Then, 7 mL of  $\text{CH}_2\text{Cl}_2$  was added to dissolve solid Th, and the solution was analyzed by GLC. Standard samples were used to determine concentration factors (CFs) of known compounds. For unknown compounds, namely, butylthianthrene and dibutylthianthrene (BuTh and  $\text{Bu}_2\text{Th}$ , respectively), CFs were considered to be the CFs of the groups present. The last known peak in the GLC on 5% OV-101 was for ThO. Thereafter, two peaks followed and were found by GC-MS to correspond with BuTh ( $\text{M}^+$ ,  $m/z = 272$ ). The larger of these peaks was assigned to 2-BuTh, and the smaller peak was assigned to 1-BuTh. In addition to the BuTh peaks, a group of peaks was identified collectively by GC-MS as corresponding to  $\text{Bu}_2\text{Th}$  ( $\text{M}^+$ ,  $m/z = 328$ ).

**RUNS 2 AND 3.** Two other similar runs in the reaction of  $\text{Th}^{++}\text{ClO}_4^-$  with  $\text{Bu}_2\text{Hg}$  were performed, each with 790 mg (2.5 mmol) of  $\text{Th}^{++}\text{ClO}_4^-$  and 1.00 mmol of  $\text{Bu}_2\text{Hg}$  in solution. In these reactions, and when addition of  $\text{Bu}_2\text{Hg}$  was finished, 0.5 mL of a 2.5 M  $\text{K}_2\text{CO}_3$  solution was added to quench unused  $\text{Th}^{++}$ . Addition of  $\text{K}_2\text{CO}_3$  took place immediately after adding the  $\text{Bu}_2\text{Hg}$  in run 2, but 8 h after adding the  $\text{Bu}_2\text{Hg}$  in run 3. The reason for this difference was to find if BuTh and  $\text{Bu}_2\text{Th}$  were being formed by the transfer of  $\text{Bu}^+$  from  $\text{ThBu}^+$  to Th.

**RUN 4.** GLC analysis was carried out only after solid products were separated on preparative-scale thin-layer chromatographic (TLC) plates (Merck, 2-mm silica gel, No. 5766). Thus, after addition of  $\text{K}_2\text{CO}_3$  solution, and omitting addition of LiCl, 20 mL of  $\text{CH}_2\text{Cl}_2$  was added. The separated aqueous phase was extracted with  $4 \times 10$  mL of  $\text{CH}_2\text{Cl}_2$ , and the combined  $\text{CH}_2\text{Cl}_2$  solution was dried over  $\text{MgSO}_4$  and evaporated to dryness. The white solid (920 mg) obtained was dissolved in a small amount of  $\text{CH}_2\text{Cl}_2$  and separated into four broad bands, which were extracted and assayed by GLC and GC-MS. The uppermost band, extracted with  $\text{CH}_2\text{Cl}_2$ , gave 354 mg of solid consisting of Th (1.53 mmol), 1-BuTh (0.011 mmol), 2-BuTh (0.021 mmol), and  $\text{Bu}_2\text{Th}$  (0.0065 mmol). The second band ( $\text{CH}_2\text{Cl}_2$ ) gave Th (0.016 mmol) and ThO (0.242 mmol). The third band contained  $\text{ThBu}^+\text{ClO}_4^-$ , and was removed first with 250 mL of  $\text{CH}_2\text{Cl}_2$  and next with 175 mL of a mixture of acetone and  $\text{CH}_2\text{Cl}_2$ . The solvent was evaporated under high vacuum to give 297 mg of an oily residue. This residue was dissolved in 5 mL of  $\text{CH}_3\text{CN}$  and treated with 200 mg of LiCl for 24 h, after which 5 mL of  $\text{CH}_2\text{Cl}_2$  was added to dissolve Th. GLC analysis gave butyl chloride (BuCl, 0.695 mmol), butylmercuric chloride ( $\text{BuHgCl}$ , 0.046 mmol), Th (0.536 mmol), 1-BuTh (0.013 mmol), 2-BuTh (0.090 mmol), and  $\text{Bu}_2\text{Th}$  (0.018 mmol). Thus, the total amount of Th-containing products in this band was 0.657 mmol, close to the amount of BuCl. The last band at the origin was removed with 75 mL of acetone. The solution was stirred for 30 min with 1 g of LiCl, followed by workup (addition of water and extraction with ethyl ether), to give 254 mg of white solid. GLC analysis in 10 mL of  $\text{CH}_2\text{Cl}_2$  gave  $\text{BuHgCl}$  (0.830 mmol), Th (0.025 mmol), and ThO (0.003 mmol).

**Preparation of Bis(5-hexenyl)mercury.** A solution of 5-hexenylmagnesium chloride (5-hexenylMgCl) in ether was prepared from 1-chloro-5-hexene and was found to contain cyclopentylmethylmagnesium chloride (CPMMgCl) such that the ratio of 5-hexenylMgCl to CPMMgCl was 10.4:1. Thus, when 5-hexenylMgCl is discussed in this chapter, we are actually referring to the 10.4:1 mixture of 5-hexenylMgCl and CPMMgCl. To 25 mmol of Grignard reagent was added 2.7 g (10 mmol) of  $\text{HgCl}_2$  dissolved in 50 mL of dry ether. After being stirred for several days, the mixture was poured into an ice-water slurry. The ether layer was removed, dried over  $\text{MgSO}_4$  and evaporated to give 3.4 g (93%) of product. Attempts to distill

a portion of the product under vacuum caused its decomposition (5). The product was purified by chromatography on a column of silica gel (Woelm). Elution with petroleum ether gave bis(5-hexenyl)mercury [(5-hexenyl)<sub>2</sub>Hg] as a colorless oil; overall yield was 82% (6).

The composition of the product was determined in three ways. (1) A sample of 250  $\mu\text{L}$  of the mercurial compound was stirred overnight with 0.5 mL of 12 N HCl. To this was added 10 mL of methylene chloride, and the solution was analyzed by GLC for 1-hexene, MCP, 5-hexenylMgCl (HxHgCl in Table VII), and CPMHgCl. The results are given under run 5 in Table VII. The data gave an average linear/cyclic (*L/C*) ratio of 8.1. (2) The <sup>1</sup>H NMR spectrum was recorded for a solution of 250  $\mu\text{L}$  of the mixture of mercurial compounds in 0.25 mL of deuteriochloroform containing 20  $\mu\text{L}$  of hexamethyldisiloxane (HMDSO) as an internal standard (7). Integration of the vinylic H and the aliphatic H gave an *L/C* ratio of 8.1 (3). A solution of 250  $\mu\text{L}$  of the mercurial compound in 10 mL of methylene chloride was analyzed by GLC (6-ft column). Three peaks with retention times of 37.15, 38.06 and 39.1 min were obtained, and were assumed from their relative sizes to be (5-hexenyl)<sub>2</sub>Hg, 5-hexenyl(cyclopentylmethyl)mercury (5-hexenylHgCPM), and bis(cyclopentylmethyl)mercury [(CPM)<sub>2</sub>Hg]. Because not all of the appropriate authentic compounds were available for determining real CFs, the CF for cyclopentylmethylmercuric chloride (CPMHgCl) was used as the integrating-computer standard. Integration gave the amounts of (5-hexenyl)<sub>2</sub>Hg, 5-hexenylHgCPM, and (CPM)<sub>2</sub>Hg as 0.91, 0.13, and 0.03 mmol, respectively. These data give an *L/C* ratio of 10.3.

#### Reaction of Bis(5-hexenyl)mercury with Th<sup>++</sup>ClO<sub>4</sub><sup>-</sup>.

**RUN 1.** Solid Th<sup>++</sup>ClO<sub>4</sub><sup>-</sup> (790 mg, 2.5 mmol) and a magnetic stirrer were placed in a septum-capped vial which was evacuated and filled with argon. Next, 5 mL of dry CH<sub>3</sub>CN was injected. To the solution, stirred at 0 °C, 2.5 mL of a 0.4 M solution of (C<sub>6</sub>H<sub>11</sub>)<sub>2</sub>Hg in a mixture of CH<sub>3</sub>CN and CH<sub>2</sub>Cl<sub>2</sub> (1:1) was added dropwise with a syringe. After 2 min of further stirring, 1 mL of 2.5 M aqueous K<sub>2</sub>CO<sub>3</sub> was injected, followed by 20 mL of CH<sub>2</sub>Cl<sub>2</sub>. The phases were separated, and the aqueous phase was extracted with 6 × 10 mL of CH<sub>2</sub>Cl<sub>2</sub>. The collected CH<sub>2</sub>Cl<sub>2</sub> solution was evaporated almost to dryness at <20 °C. The residue was dissolved in a minimum amount of CH<sub>2</sub>Cl<sub>2</sub> and separated on a 2-mm preparative TLC plate (Merck 60F254) by using CH<sub>2</sub>Cl<sub>2</sub> development. Three broad bands were obtained. The uppermost band was removed and extracted with a total of 250 mL of CH<sub>2</sub>Cl<sub>2</sub>. The solvent was evaporated to give 397 mg of a white solid, which was dissolved in CH<sub>2</sub>Cl<sub>2</sub> and analyzed by GLC, by using both of the OV-101 columns. Analysis gave small amounts of 1-hexene (0.016 mmol), as well as MCP (0.0054 mmol), Th (1.51 mmol), and ThO (0.023 mmol). Three minor peaks analyzed by GC-MS corresponded with formula C<sub>6</sub>H<sub>11</sub>Th (0.015 mmol) and traces of compounds with formula (C<sub>6</sub>H<sub>11</sub>)<sub>2</sub>Th. The CFs for known compounds were determined with standard solutions. For RTh and R<sub>2</sub>Th, CFs were taken as the sum of the CFs for Th and RH.

The second TLC band was extracted with 400 mL of acetone/CH<sub>2</sub>Cl<sub>2</sub> (1:1) and gave, after evaporation of the solution, 352 mg of a viscous oil. The <sup>1</sup>H NMR spectrum (CDCl<sub>3</sub>, HMDSO) was essentially that of 5-(5-hexenyl)thianthrenium perchlorate. Immediately after recording the <sup>1</sup>H NMR spectrum, the product was dissolved in 5 mL of CH<sub>3</sub>CN, and the solution was stirred for 24 h after adding 200 mg of LiCl. This solution was then analyzed by GLC on the OV-101 columns and gave 1-chloro-5-hexene (0.693 mmol), cyclopentylmethyl chloride (CPMCl, 0.039 mmol), Th (0.647 mmol), and ThO (0.038 mmol). Three peaks analyzed by GC-MS corresponded with

$C_6H_{11}Th$  ( $M^+$ ,  $m/z = 298$ ) and amounted to 0.114 mmol, and some small peaks analyzed by GC-MS corresponded with  $(C_6H_{11})_2Th$  ( $M^+$ , 380) and amounted to 0.017 mmol.

The third TLC band, at the origin, was removed with 150 mL of acetone. The solution was stirred for 30 min with 1 g of LiCl and then evaporated. The residue was extracted with  $6 \times 5$  mL of  $CH_2Cl_2$  and gave 309 mg of a white solid that was analyzed by both  $^1H$  NMR and GLC.  $^1H$  NMR gave  $L/C = 1.8$  while the more reliable GLC analysis gave 0.639 mmol of 5-hexenylHgCl and 0.222 mmol of CPMHgCl, that is, an  $L/C$  ratio of 2.9. The CF of CPMHgCl was used for both of the RHgCl compounds.

**RUNS 2-4.** The same reaction procedure was used in run 2, but workup differed. After unused  $Th^{+}ClO_4^{-}$  was quenched with a  $K_2CO_3$  solution, 500 mg of LiCl was added to the reaction mixture. The mixture was stirred for 24 h, and 6.5 mL of  $CH_2Cl_2$  was added (to dissolve Th). GLC analysis was then carried out directly. In run 3, the same procedure was used, except that the reactants were stirred for an additional 2 h before quenching with  $K_2CO_3$ . Run 4 was the same as run 2, except that neat  $(C_6H_{11})_2Hg$  was added dropwise with a syringe.

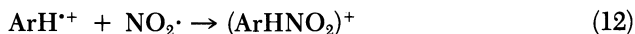
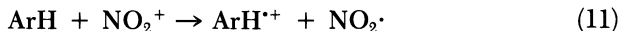
### Aromatic Nitration

**In Solution.** During the 1940s and 1950s, proposals were made by separate groups of workers that charge-transfer complexes had a role in electrophilic aromatic substitution (8-12). The idea was that in a reaction of an aromatic compound (ArH) with an electrophile (E), covalent bonding was preceded by transfer of charge from ArH to E:



where CT indicates a charge-transfer complex.

This important idea concerning the mechanism of one of organic chemistry's major reactions has not elicited much interest. More recently, the idea was again brought to our attention, and the participation of charge-transfer complexes in a number of aromatic substitution reactions was characterized incontrovertably by Fukuzumi and Kochi (13-17). The relationship of Kochi's elegant work to cation-radical reactions has been discussed by Hammerich and Parker (1). Curiously, once again, the fact that charge transfer plays a role in aromatic substitution does not appear to have elicited general interest among organic chemists. A more pointed interest in these ideas arose, however, from the analogous, specific claim by Perrin (18) that the nitration of certain reactive aromatic compounds with  $NO_2^+$  was preceded by complete charge transfer (equation 11); that is, the bond-forming reaction was, in fact, between the aromatic cation radical and the neutral radical,  $NO_2$  (equation 12).



In equation 12 can be seen the type of reaction with which this chapter is concerned.

Eberson and Radner (19–23) have explored some of the scope of the reaction of  $\text{NO}_2$  with  $\text{ArH}^{\bullet+}$ . They prepared the solid hexafluorophosphates of the naphthalene cation radical and some methylnaphthalene cation radicals, for example,  $\text{C}_{10}\text{H}_8^{\bullet+} \text{PF}_6^-$ , and carried out reactions of the solid salts with  $\text{NO}_2$  in dichloromethane at temperatures near  $-25^\circ\text{C}$  (19–23). Reaction was found to occur according to equation 12. The results of their reactions are summarized in Table I (19). This table also lists the results of nitrating the parent hydrocarbons by the conventional route ( $\text{NO}_2^+$ ) and with  $\text{N}_2\text{O}_4$ . The results prompted Eberson and Radner to dismiss the possibility that conventional nitration of these compounds was preceded by electron transfer (equations 11 and 12), because the proportions of isomers from the reaction of  $\text{ArH}^{\bullet+}$  with  $\text{NO}_2$  were quite different from those from the reactions of  $\text{ArH}$  with  $\text{NO}_2^+$  and with  $\text{N}_2\text{O}_4$ . Eberson and Radner set out to determine whether or not the conventional nitration of naphthalene and methylnaphthalenes involved the electron-transfer step. In so doing they became, to our knowledge, the first to show that a neutral radical ( $\text{NO}_2$ ) will react with an aromatic cation radical.

The data in Table I show that the coupling pathway to nitration gives a different ratio of nitro isomers than given by the other, electrophilic pathways. Eberson and Radner (19) have pointed out also that the coupling results can be correlated, but only partly with expectations based on the distribu-

**Table I. Ratio of the Most Abundant  $\alpha$ -Nitro Isomer to the Sum of All Other Nitro Isomers Formed in the Nitration of Naphthalene and Some Methylnaphthalenes**

<i>Substituent on Naphthalene<sup>a</sup></i>	$E^0(V)^b$	$\text{NO}_2^+{}^c$	$\text{N}_2\text{O}_4^c$	$\text{ArH}^{\bullet+} + \text{NO}_2^c$
H	2.08	11	24	>40
1-Me	1.99	1.3	1.9	7.3
2-Me	2.02	1.3	1.9	7.0
1,4-Me <sub>2</sub>	1.81	5.8	1.7	0.05
1,8-Me <sub>2</sub>		2.3	7.3	>12
2,3-Me <sub>2</sub>	1.90	3.3	3.3	9
2,6-Me <sub>2</sub>		3.5	5.3	9

<sup>a</sup>Me denotes the methyl group.

<sup>b</sup>Values are versus a normal hydrogen electrode and are taken from references 19 and 23.

<sup>c</sup>Values are the ratios corresponding to the indicated mode of nitration.

SOURCE: Adapted from reference 19.

tions of spin densities in the relevant cation radicals. The distribution of isomers obtained experimentally and the corresponding spin densities are listed in Table II.

The predominant isomer is in all cases the one expected from coupling at the position of highest spin density, except for the 1,4-dimethylnaphthalene cation radical. The reason for the exception is not known. The data show some instances in which concordance between positional reactivity and spin density fails for other positions, but whether or not these differences are significant is again not known. The predominant isomer, in all cases except that of 1,4-dimethylnaphthalene, corresponds to the most stable  $\sigma$  complex, as judged by resonance structure contributions. Perrin (18) had suggested, in connection with his proposal for the electron-transfer route to nitration, that bond formation in a cation radical-radical pair would occur at the position of highest spin density and where the most stable  $\sigma$  complex will be formed (18). The coupling data of Table II are for the most part in accord with this suggestion, although the isomer-ratio data (Table I) do not support the concept of participation of electron transfer in the pathway of the conventional nitrations of these substrates.

One of the important features of the coupling reaction that was brought out by Ebersson and Radner (19, 20) is that it does not work for all  $\text{ArH}^{+\cdot}$ . In particular, the perylene and pyrene cation radicals did not couple with  $\text{NO}_2$ . Reaction of the pyrene-dimer cation radical,  $(\text{pyrene})_2^{+\cdot} \text{PF}_6^-$ , with  $\text{NO}_2$ , for example, gave mainly tarry materials and less than 1% of 1-nitropyrene (19, 20). Ebersson and Radner (19, 20) concluded that only cation

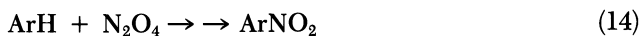
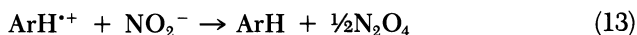
**Table II. Orders of Positional Reactivities Toward  $\text{NO}_2$  and Hyperfine Spin Densities of Naphthalene and Some Methylnaphthalene Cation Radicals**

<i>Substituent on Naphthalene</i>	<i>Positional Reactivity</i>	<i>Spin Density<sup>a</sup></i>
H	1 > 2	1 > 2
1-Me	4 > 2 > 8 > 5	4 > 8 > 2 > 5
2-Me	1 > 4 > 8 = 5	1 > 8 > 4 > 5
1,4-Me <sub>2</sub>	2 > 5	5 > 2 > 6
1,8-Me <sub>2</sub>	4 > 2 > 3	4 > 2 > 3
2,3-Me <sub>2</sub>	1 > 5 > 6	1 > 5 > 6
2,6-Me <sub>2</sub>	1 > 4 > 3	1 > 4 > 3

<sup>a</sup>Values taken from reference 61.

SOURCE: Adapted from reference 19.

radicals of ArH having  $E^0$  greater than about 1.7 V (vs. normal hydrogen electrode) will couple with  $\text{NO}_2$ . Pyrene ( $E^0$ , 1.6 V) and perylene ( $E^0$ , 1.3 V) are not among these; the coupling reactions for their cation radicals are estimated, in fact, to be endergonic (19, 23). This finding has a bearing on earlier proposals from our own laboratory that the nitrite ion reacts readily as a nucleophile with the perylene and pyrene cation radicals. Pyrene was found to be nitrated easily by shaking a solution of it with a mixture of iodine and silver nitrite (24). Ebersson and Radner (19, 20) concluded that the nitrations in these cases were of the parent ArH by  $\text{N}_2\text{O}_4$  (equations 13 and 14), instead of by direct reaction of  $\text{ArH}^{+\cdot}$  as we proposed earlier.



Ridd and co-workers have also proposed that aromatic cation radicals couple with  $\text{NO}_2$ ; their proposal was based on chemically induced dynamic nuclear polarization (CIDNP) data obtained in some nitrations. The results support the views of Ebersson and Radner (19, 23) about the role of the coupling reaction in aromatic nitration. For example, the nitration of mesitylene with  $\text{NO}_2^+$ , under conditions suppressing coincidental nitrous acid catalyzed nitration, was found to be unaccompanied by CIDNP-signal phenomena; this finding indicated that a radical-coupling route was not occurring. On the other hand, in the nitrous acid catalyzed nitration of mesitylene, CIDNP signals were obtained; these signals were consistent with the formation of nitromesitylene by the coupling of mesitylene $^{+\cdot}$  with  $\text{NO}_2$ . In this case, it was proposed that mesitylene $^{+\cdot}$  was formed by oxidation of mesitylene by  $\text{NO}^+$ , and it coupled with  $\text{NO}_2$  that was formed in solution by other redox reactions (25).

Analogous results were obtained for the nitrous acid catalyzed nitration of durene (26). Here, however, CIDNP signals were obtained also in the nitration of durene by  $\text{NO}_2^+$ , and their character suggested that durene $^{+\cdot}$  and  $\text{NO}_2$  were being formed not by the direct transfer of an electron from durene to  $\text{NO}_2^+$ , but by the homolysis of an ipso intermediate. Recombination of durene $^{+\cdot}$  and  $\text{NO}_2$  then led to nitrodurene.

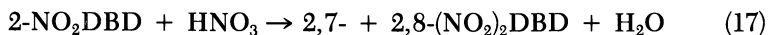
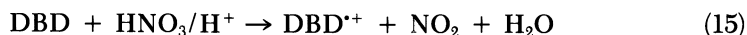
The results of these reactions support the views of Ebersson and Radner (19, 23), but with a proviso. On the basis of the relative oxidation potentials in acetonitrile solution, the oxidation of mesitylene by  $\text{NO}^+$  and the dissociative formation of durene $^{+\cdot}$  and  $\text{NO}_2$  in the reaction of durene with  $\text{NO}_2^+$  are thought to be too endothermic to be probable (27). The proviso, then, is that the endothermicity of these reactions should be moderated in the solvent, aqueous trifluoroacetic acid, which had been used.

The purpose of this chapter is not to argue for or against the role of electron transfer in aromatic nitration; the major concern of this chapter is

whether or not coupling reactions occur. We have to point out, however, that evidence of the formation of  $\text{ArH}^{+\cdot}$  in some conventional nitrations has been claimed in a qualitative way as evidence for the participation of the coupling reaction in those nitrations. For example, Morkovnik et al. noted that nitration of phenothiazine with  $\text{HNO}_3$  gave 2,7-dinitrophenothiazine 5-oxide and that the same product was formed in 90% yield from the reaction of phenothiazine cation radical perchlorate ( $\text{phen}^{+\cdot}\text{ClO}_4^-$ ) with  $\text{NO}_2$  in  $\text{CH}_3\text{CN}$  (28). Their conclusion was that the result is consistent with single-electron transfer (SET) as an intermediate stage in the electrophilic nitration; that is, in the electrophilic nitration of phenothiazine, the cation radical  $\text{phen}^{+\cdot}$  is formed, and in a sequence of steps, is converted ultimately to 2,7-dinitrophenothiazine 5-oxide.

Along the same lines, Morkovnik (29) found that phenothiazine was oxidized in  $\text{HNO}_3/\text{HClO}_4$  solution to  $\text{phen}^{+\cdot}\text{ClO}_4^-$  in 81% yield. Nitric oxide (72%) was also formed; therefore,  $\text{NO}^+$  was designated as the oxidant. Analogously, phenoxazine gave phenoxazine $^{+\cdot}\text{ClO}_4^-$  (79%) and  $\text{NO}$  (75%). The point is that Morkovnik (29) associates such results with an SET pathway in nitration, and says: "...reactions like this are probably widespread, but that fast follow-up reactions of  $\text{ArH}^{+\cdot}$  may mask the radical-ion nature of such reactions and create an illusion of their nonradical nature." Similar reasoning was applied to reactions of naphthalene with nitrating agents ( $\text{NO}_2^+\text{BF}_4^-$ ,  $\text{HNO}_3$ , and  $\text{NO}_2$ ) in trifluoroacetic acid. When the molar ratio of nitrating agent to naphthalene was low (0.2) the product was the naphthalene dimer cation radical,  $(\text{naphthalene})^{+\cdot}$  this result was regarded as direct evidence for the formation and involvement of  $\text{naphthalene}^{+\cdot}$  in the conventional nitration of naphthalene (30).

The coupling of the dibenzodioxin (DBD) cation radical with  $\text{NO}_2$  was also proposed as part of the pathway of the conventional nitration of DBD. The character of the nitration of DBD with  $\text{HNO}_3/\text{HClO}_4$  depended on the molar ratio of the reactants. When this ratio was in the range of 0.3–0.5, the only product was  $\text{DBD}^{+\cdot}$ . If the ratio was  $\geq 2$ , the product was a mixture of 2,7- and 2,8-dinitrodibenzodioxin (2,7- and 2,8- $(\text{NO}_2)_2\text{DBD}$ ), whereas if the ratio was  $>0.6$  but  $<2$ , a mixture of  $\text{DBD}^{+\cdot}$  and 2,7- and 2,8- $(\text{NO}_2)_2\text{DBD}$  was obtained. A list of reactions and products is given in Table III from which it was concluded that the nitration of DBD occurs as in equations 15–17 (31).



Entries 1 and 2 in Table III seem not to be in concordance, however.

**Table III. Products of Reaction of DBD and DBD<sup>•+</sup>SbCl<sub>6</sub><sup>-</sup> with Nitrating Agents**

Reactant	Nitrating Agent		2-NO <sub>2</sub> DBD	2,7-(NO <sub>2</sub> ) <sub>2</sub> DBD	2,8-(NO <sub>2</sub> ) <sub>2</sub> DBD
	Solvent				
DBD	N <sub>2</sub> O <sub>4</sub>	CH <sub>3</sub> CN	71		
DBD <sup>•+</sup> SbCl <sub>6</sub> <sup>-</sup>	N <sub>2</sub> O <sub>4</sub>	CH <sub>3</sub> CN		44	37
DBD	HNO <sub>3</sub>	TFA <sup>a</sup>		49	38
DBD	N <sub>2</sub> O <sub>4</sub>	TFA <sup>a</sup>		50	44

NOTE: Values are the percentages obtained of the indicated products.

<sup>a</sup>TFA is trifluoroacetic acid.

SOURCE: Adapted from reference 31.

The conclusions from Morkovnik's laboratory, drawn from comparisons of product formations, contradict in two ways the conclusions of Ebersson and Radner, who sought isomer distributions, rather than products only. The first contradiction is that the cation radicals that Morkovnik feels do couple with NO<sub>2</sub> are, for the most part, those coming from easily oxidizable heteroaromatic compounds for which  $E^0 < 1.7$  V. Ebersson and Radner regard such reactions as endergonic and improbable. The second contradiction is that Morkovnik concludes that the coupling reaction is involved in electrophilic nitration of these easily oxidizable heteroaromatic compounds, whereas Ebersson and Radner (19) believe that nitro compounds obtained from the reaction of NO<sub>2</sub> with the cation radicals of heteroaromatic compounds with low oxidation potentials are likely to have been formed via direct electrophilic nitration by N<sub>2</sub>O<sub>4</sub>. Ebersson and Radner (19) further believe that cation radicals detected in such nitrations are formed by the dissociation of the  $\sigma$  complex (ArHNO<sub>2</sub>)<sup>+</sup> and not by direct electron transfer from ArH to NO<sub>2</sub><sup>+</sup>. These different views show the apparent anomaly of the nitration of naphthalene, in which Morkovnik has found the cation radical dimer, (naphthalene)<sub>2</sub><sup>•+</sup>. This cation radical should fit well into the coupling reaction with NO<sub>2</sub>. How this finding is to be reconciled with the views of Ebersson and Radner remains to be seen.

**In the Gas Phase.** Schmitt et al. (32, 33) found that ArH<sup>•+</sup> and NO<sub>2</sub> couple in the gas phase to give the  $\sigma$  complex (ArHNO<sub>2</sub>)<sup>+</sup>. The ArH<sup>•+</sup> was produced by ionization of ArH with photons emitted from pulse-radiation excited argon atoms. Reactions were carried out in a flow system within the source of a quadrupole mass spectrometer. In contrast, reactions of the corresponding ArH with NO<sub>2</sub><sup>+</sup> were found not to go directly to (ArHNO<sub>2</sub>)<sup>+</sup> but to lead either to ArH<sup>•+</sup> and NO<sub>2</sub> by fast electron transfer or to (ArHO)<sup>+</sup> and NO by oxygen-atom transfer. From these results, Schmitt et al. (32, 33) concluded that "aromatic radical cations are a plausible intermediate in the mechanism for aromatic nitration."

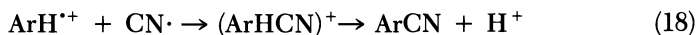


Among  $\text{ArH}^{+\cdot}$  which coupled readily with  $\text{NO}_2$  in the gas-phase, were cation radicals of benzene, toluene, *p*-xylene, mesitylene, and fluorobenzene, all of which couple at about the same rate ( $1.2\text{--}3.7 \text{ cm}^3 \text{ molecule}^{-1} \text{ s}^{-1}$ ). The cation radicals of *m*- and *p*-difluorobenzene coupled with  $\text{NO}_2$  about 10 times more slowly. Naphthalene $^{+\cdot}$ , which was anticipated to couple easily, did so only very slowly. These results may be related to the relative stabilities of the cation radicals and their corresponding  $\sigma$ -complexes in the gas phase.

More recently gas-phase nitration was treated theoretically with MNDO (modified neglect of diatomic differential overlap) and INDO (intermediate neglect of differential overlap) self-consistent field calculations (34). Electron transfer and radical-pair recombination were favored for the nitration of toluene and the xylenes but not for nitrobenzene, for which a classical nitration route via a  $\pi$  complex was favored. The calculations could not make a distinction between the two routes in the nitration of benzene. More information is needed about these coupling reactions and how they differ in the gas and heterogeneous-solution phases.

### Other Reactions

In his dissertation, Radner (23) wrote the following: "...during the course of this work, a literature search revealed almost complete lack of knowledge of the coupling reaction of radical cations with radicals other than  $\text{NO}_2$ ." In this regard, we experienced the same finding as Radner. Radicals cannot easily be generated in the presence of a cation radical, and few stable radicals with structures of interest are available to explore these reactions. Consequently, nothing other than reactions with  $\text{NO}_2$  had been explored. Ebersson (35) pointed out that the reaction of cyanide ion with cation radicals may involve the coupling of the cation radical with the cyano radical. The reason for this belief lies in the relatively low oxidation potential of the cyanide ion. Anodic oxidation of an aromatic compound, for example, should occur at a potential at which the cyanide ion is also oxidized. The next result would be, then, the following coupling reaction (equation 18):



However, to our knowledge, this reaction has not been clearly validated. Reaction of a pre-prepared cation radical with the cyanide ion may also take place by the electron-transfer route of reactions 7 and 8.

"Scavenging" of alkoxy radicals by the paraquat cation radical ( $\text{PQ}^{+\cdot}$ ) received much attention at one time. Scavenging of these radicals took place by electron transfer and gave the alkoxide ion and  $\text{PQ}^{2+}$ . Reaction of  $\text{PQ}^{+\cdot}$  with  $(\text{CH}_3)_2\text{C}(\text{CN})$  may have involved coupling, but the polymeric products could not be characterized adequately (3).

Some olefinic cation radicals have been found to add triplet oxygen with ease (1, 36); The final products are dioxetanes. In contrast, the aromatic and heterocyclic cation radicals with which we are currently concerned appear to be quite unreactive with triplet oxygen.

In regard to the reactions of cation radicals with stable radicals, such as 1,1-diphenyl-2-picrylhydrazyl, and with well-known spin traps, virtually nothing can be found in the literature. The pyridine cation radical has been reported to add to the spin trap phenyl-*N-tert*-butyl nitron (37).

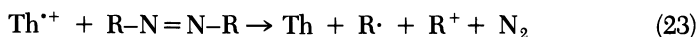
Our own interest in the coupling of radicals with cation radicals grew out of our work with reactions of  $\text{Th}^{++}\text{ClO}_4^-$  with diaryl- and dialkylmercurials. These reactions gave 5-thianthrenium perchlorates in good yields according to equation 19, in which R was  $\text{CH}_3$ ,  $\text{C}_6\text{H}_5$ , and *o*-, *m*-, and *p*-substituted  $\text{C}_6\text{H}_4$  (38).



We sought evidence for the possibility that these reactions involved the formation and trapping of radicals (equations 20–22):



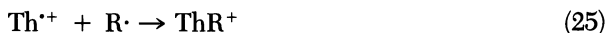
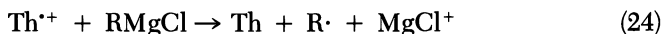
We carried out the reaction with diethylmercury ( $\text{Et}_2\text{Hg}$ ) in the presence of labeled oxygen. The idea was to scavenge ethyl radicals, if they were formed, with oxygen (a scavenging reaction known to occur at diffusion-controlled rates) and to identify the products of scavenging. We found evidence for oxygen scavenging but were still unable to prevent the formation of  $\text{ThEt}^+$  (39). The result suggested that if ethyl radicals were being formed (equation 21), they must react with  $\text{Th}^{++}$  (equation 22) very rapidly, in competition with  $\text{O}_2$ . The possibility that alkyl radicals react rapidly with  $\text{Th}^{++}$  persuaded us to find ways of generating radicals in the presence of  $\text{Th}^{++}$  by using known, established methods. We turned to the photolysis of azoalkanes in solutions of  $\text{Th}^{++}$ . Here, the reactions did not go according to plan and were not in that sense successful. We discovered that the chosen azoalkanes were readily decomposed, oxidatively, by  $\text{Th}^{++}$  (equation 23),



so that our plan for using the photolysis of these compounds for generating radicals was subverted. Instead, a chemistry evolved of the oxidative decomposition and oxidative cycloaddition of hydrazones, which are tautomeric with azoalkanes, to solvent nitriles (40–42).

Circumstantial evidence for the trapping of  $R\cdot$  by  $Th^{++}$  was found, however, in one of these reactions. When (phenylazo)triphenylmethane was used, one of the products obtained was  $ThPh^+ClO_4^-$ , and its formation was attributed to the trapping of phenyl radicals by  $Th^{++}$ .

Thus, the literature taught us that particular aromatic cation radicals would couple with  $NO_2$ , whereas our own work gave evidence, but only circumstantial, for the coupling of phenyl and possibly ethyl radicals with  $Th^{++}$ . We turned then to a twofold plan. First to trap radicals with  $Th^{++}$  after generating them in situ by reaction of  $Th^{++}$  with Grignard agents (equations 24 and 25):



Among the Grignard agents was the well-known probe for radical reactions, namely, 5-hexenylMgCl. This part of our plan was carried out successfully. The results are summarized here but given in detail elsewhere (43). The second part of the plan was to use the 5-hexenyl probe again in the form of (5-hexenyl)<sub>2</sub>Hg. This part of the plan is described here also. The results, however, still leave unsettled the question of whether radicals are formed and trapped in the oxidative decomposition of  $R_2Hg$  by  $Th^{++}$ .

### *Reaction of $Th^{++}ClO_4^-$ with $RMgCl$*

In 1978, Ebersson et al. (44) commented on the reaction of  $ArH^{++}$  with a carbanion as follows:

In view of the ease of oxidation of carbanions (in the form of organometallics, say  $RLi$  or  $RMgX$ ), one would predict that the reaction between a carbanion and a radical cation of even low oxidizing power would lead to very rapid initial electron transfer and hence that products would be derived from attack of  $R\cdot$  on  $ArH$ . Somewhat surprisingly, such studies have to our knowledge not been performed before but should be of considerable interest....

We began such a study in 1983 with  $Th^{++}ClO_4^-$  and Grignard reagents. Reactions were carried out in ether and in tetrahydrofuran (THF), but heterogeneously, because  $Th^{++}ClO_4^-$  is insoluble in these Grignard solvents. For the most part, an excess of  $Th^{++}ClO_4^-$  was used to enhance the chance of trapping  $R\cdot$  by  $Th^{++}$  according to equations 24 and 25. Tables IV and V summarize only the results of reactions in ether. The details of all reactions are given elsewhere (43).

Table IV lists the products of reaction of "5-hexenylMgCl" and

Table IV. Products of Reaction of 5-HexenylMgCl and CPMMgCl with  $\text{Th}^+\text{ClO}_4^-$  in Ether

RMgCl	Reactants			Products (mmol)						Account (%) <sup>a</sup>		
	R	$\text{mmol}$	$\text{Th}^+\text{ClO}_4^-$ (mmol)	$\text{H}_2\text{O}$ (mL)	RH	1-Hexene	MCP	5-Hx <sup>b</sup>	CPM	Th	ThO	Th <sup>+</sup>
5-Hx <sup>c</sup>	1.0	3.0	3.0		0.24	0.039	0.36 <sup>d</sup>	0.20 <sup>d</sup>	1.88	0.58	101	84
5-Hx <sup>c</sup>	1.0		0.25	0.98	0.094							107
CPM	1.2	3.0		0.0	0.31			0.56 <sup>e</sup>	1.97	0.50	101	73
CPM	1.2		0.25	0.0	1.24							103

<sup>a</sup>Values are sums of product yields based on each reactant.<sup>b</sup>5-Hx refers only to 5-hexenyl in this case.<sup>c</sup>5-Hx refers to a mixture of 5-HxMgCl and CPMMgCl (10.4:1) assayed by reaction with water.<sup>d</sup>Assay was by <sup>1</sup>H NMR. A second assay by GLC after conversion to 5-hexenylCl and CPMCl gave 0.27 mmol and 0.12 mmol, respectively; Th (0.51 mmol) was also obtained.<sup>e</sup>Value is the isolated yield. A second assay by GLC after conversion to CPMCl gave 0.52 mmol; Th (0.50 mmol) was also obtained. SOURCE: Adapted from reference 43.

Table V. Products of Reaction of Grignard Reagents with  $\text{Th}^+\text{ClO}_4^-$  in Ether

RMgCl	Reactants		Products (mmol)							Account (%) <sup>a</sup>	
	mmol	$\text{Th}^+\text{ClO}_4^-$ (mmol)	$\text{H}_2\text{O}$ (mL)	RH	R(-H)	RR	Th	ThO	ThR + $\text{ClO}_4^-$	Th <sup>+</sup>	RMgCl
Bu	1.2	3.00		0.29	0.032	0.048	1.88	0.54	0.58	100	82
Bu	1.2		0.25	1.24	0.000	0.008					104
sec-Bu	1.6	2.0		0.73	0.290	0.050	1.77	0.084		93	76 <sup>b</sup>
sec-Bu	1.6		0.25	1.58	0.008	0.007					100
tert-Bu	1.0	3.0		0.63	0.240	0.015	2.04	0.970		100	104 <sup>c</sup>
tert-Bu	1.0		0.50	1.10	0.024	0.007					114

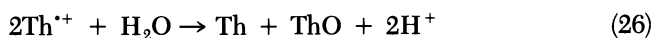
<sup>a</sup>Values are sums of product yields based on each reactant and adjusted for the amount of RR, R(-H), and a presumed equivalent amount of RH already in the RMgX solution (see reaction with water).

<sup>b</sup>sec-BuCl (0.13 mmol) was also obtained and is included.

<sup>c</sup>tert-BuCl (0.20 mmol) was also obtained and is included.

SOURCE: Adapted from reference 43.

CPMgCl with  $\text{Th}^{++}\text{ClO}_4^-$ . Again, as mentioned in the Experimental Details, the 5-hexenylMgCl is really a 10.4:1 mixture of 5-hexenylMgCl and CPMgCl as determined from the amounts of 1-hexene and MCP obtained by decomposing aliquots of the Grignard reagent with water. The entries in Table IV show that sulfonium perchlorates,  $\text{ThR}^+\text{ClO}_4^-$  (i.e., products that correspond with radical trapping, equation 25), were obtained. Other products were Th, ThO, and the hydrocarbons RH corresponding to RMgCl. The ThO was formed by hydrolysis during workup of the unused excess of  $\text{Th}^{++}\text{ClO}_4^-$ :



The key to our understanding of the reaction of  $\text{Th}^{++}\text{ClO}_4^-$  with RMgCl lies in the composition of  $\text{ThR}^+\text{ClO}_4^-$  and in the formation of RH. First, the cyclopentylmethylsulfonium salt prepared separately was used (entry 3, Table IV). It was characterized by  $^1\text{H}$  NMR and was used as the model to show that reaction with LiCl in acetone gave the corresponding chloride in good yield (cyclopentylmethyl chloride, 93%). Reaction of 5-hexenylMgCl with  $\text{Th}^{++}$  gave a mixture of 1-hexene and MCP in a linear/cyclic *L/C* ratio of 6.2, as well as a mixture of sulfonium salts in a *L/C* ratio of approximately 2. The mixture of sulfonium salts was assayed in two ways. First, by  $^1\text{H}$  NMR (with the cyclopentylmethylsulfonium salt as the control), which gave an *L/C* ratio of 1.8. Second, the mixture of sulfonium salts was converted into a mixture of the corresponding alkyl chlorides by reaction with LiCl in acetone. Assay of the alkyl chlorides gave an *L/C* ratio of 2.3. These ratios, when compared with the *L/C* ratio of 10.4 in the Grignard reagent, show that the 5-hexenyl radical was liberated from the Grignard reagent by SET to  $\text{Th}^{++}$  and cyclized to the CPM radical before being trapped by a second unit of  $\text{Th}^{++}$ .

The formation of hydrocarbon products, 1-hexene, and MCP can be attributed to abstraction of hydrogen atoms from the ethyl ether solvent. In this case, the *L/C* ratio of 6.2 is also indicative that cyclization of some 5-hexenyl radicals occurred before reaction with the solvent. The ratio of 6.2 appears to be too high, however, because the rate of abstraction of hydrogen atom from the solvent is thought to be smaller (at least by an order of magnitude) than the rate of cyclization of 5-hexenyl radical (45). The seeming discrepancy in our result may lie in our having lost hydrocarbon product, because 16% of the Grignard reagent's alkyl groups were lost from our accounting. If all of this loss (0.16 mmol) were considered (unreasonably, however) to be entirely MCP, the *L/C* ratio of 6.2 would be lowered to 1.2. This value may still be too high for reactions of alkyl radicals that react with solvent only after diffusing from their point of origin and therefore give 5-hexenyl radicals time to cyclize. The ratio of 6.2 may then be more real than we expect. It may be that alkyl radicals, formed by SET, are formed close

to solvent molecules complexed with the Grignard reagent; in that way, 5-hexenyl radicals would have the opportunity to react with such solvent molecules before cyclizing, as if in a solvent cage.

We would have thought that the  $L/C$  ratio of the sulfonium salts should be even lower than 2.0. The ratio in the sulfonium salts may not be lower than that which was found because 5-hexenyl radicals from the Grignard reagent are formed on or near the surface of insoluble  $\text{Th}^{++}\text{ClO}_4^-$  and, to some extent, are scavenged before they can diffuse away and cyclize. The situation may be somewhat like that in the formation of 5-hexenylMgCl itself; this involves reaction of the 5-hexenyl radical with magnesium, but the rate of formation of the Grignard reagent at the magnesium surface is faster than that of cyclization and leads, therefore, to the high  $L/C$  ratio (approximately 10) in the Grignard reagent (45).

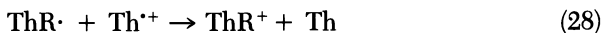
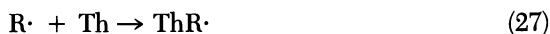
The reaction with 5-hexenylMgCl helps us to understand the reactions of the other Grignard reagents (Table V). We can illustrate with *tert*-butylmagnesium chloride (*tert*-BuMgCl). Because 0.97 mmol of ThO was obtained (entry 5, Table V), 0.97 mmol of Th must also have been formed by the hydrolysis of unused  $\text{Th}^{++}$  (equation 26) in the workup. This condition requires, then, that after reaction with *tert*-BuMgCl, 1.94 mmol of  $\text{Th}^{++}$  remained for hydrolysis. Consequently, in the initial reaction, the Grignard reagent (1.0 mmol) reduced its equivalent of  $\text{Th}^{++}$  completely (experimentally, 1.07 mmol). The data are in good agreement for complete SET between  $\text{Th}^{++}$  and *tert*-BuMgCl. Analogously, reaction with *sec*-BuMgCl and BuMgCl led to SET, but only in the case of BuMgCl were radicals trapped as  $\text{ThR}^+$  (entry 1). Apparently, *tert*-Bu and *sec*-Bu radicals may be too bulky to be trapped, or, if they are trapped, the corresponding sulfonium ions are too unstable to be isolated (as perchlorates).

If we accept that all of the BuMgCl (1.2 mmol, Table V) was used in reducing  $\text{Th}^{++}$  and that 0.58 mmol of Bu· was successfully trapped, the two reactions accounted for 1.78 mmol of  $\text{Th}^{++}$ . Thus, 1.22 mmol of  $\text{Th}^{++}$  was unused and available for hydrolysis during this workup. The amount of ThO obtained (0.54 mmol) requires that 1.08 mmol of  $\text{Th}^{++}$  remained for hydrolysis after the Grignard reaction was finished; this value is in reasonable agreement with the preceding value (1.22 mmol).

Alkyl radicals that were not trapped as  $\text{ThR}^+$  engaged in H-atom abstraction from the solvent, disproportionation, and recombination. The extents of these reactions can be calculated after compensating for the amounts of alkane, alkene, and hydrocarbon dimer (RH, R(-H), and RR, respectively) already present in the Grignard solution. The amounts are given in parentheses for the indicated radicals as follows: Bu· (64%, 16%, and 20%), *sec*-Bu· (40%, 52%, and 8%), and *tert*-Bu· (46%, 52%, and 2%). These analyses may be in error because we were unable to account for all of the alkyl groups in the RMgCl that was used. However, the analyses signify that alkyl radical reactions resulted from reactions of RMgCl with  $\text{Th}^{++}$  in ether.

We believe, then, that the reactions with 5-hexenylMgCl, CPMMgCl, and BuMgCl are the first coupling reactions of alkyl radicals with a cation radical to have been reported (43).

Could the sulfonium ions ( $\text{ThR}^+$ ) have been formed by reaction of  $\text{R}\cdot$  with Th (equations 27 and 28)?



This route corresponds with Ebersson's proposal (44) for the SET reaction of  $\text{ArH}^{++}$  with  $\text{R}^-$ ; that is, the reaction of  $\text{ArH}$  with  $\text{R}\cdot$  would follow. We think that this is not likely to have occurred in our reactions. Saeva and Morgan (46) showed that phenyl and (1-naphthyl)dialkylsulfuranyl radicals are highly unstable. When formed by anodic reduction of sulfonium ions,  $(\text{ArRR}')\text{S}^+$ , the sulfuranyl radicals appear to lose an alkyl radical at the time of electron transfer (46). This observation suggests that sulfuranyl radicals of the type  $\text{ThR}\cdot$  may also have a short life. This condition does not rule them out as intermediates in the alkylation reaction (equations 27 and 28); however, it does not encourage belief in that route.

### *Reactions of $\text{Th}^+\text{ClO}_4^-$ with $\text{Bu}_2\text{Hg}$*

Data from four runs in the reaction of  $\text{Bu}_2\text{Hg}$  with  $\text{Th}^+\text{ClO}_4^-$  are given in Table VI. They show that a sulfonium salt ( $\text{ThBu}^+\text{ClO}_4^-$ ) was formed in good yield (55–65% of theory, equation 19), and  $\text{BuHg}^+$ , isolated as  $\text{BuHgCl}$ , was formed in excellent yield (90–100%, as determined by GLC). The results give no indication as to whether a radical-trapping reaction (e.g., equations 20–22) occurred. The reactions differ from those of  $\text{Th}^+$  with  $\text{RMgCl}$  in two ways. First, very little of the hydrocarbons (i.e., butane, 1-butene, and octane) was obtained. This result might suggest that radicals were not formed in the  $\text{Bu}_2\text{Hg}$  reaction. However, H-atom abstraction from  $\text{CH}_3\text{CN}$  is not necessarily a facile reaction (42); therefore, the absence of much butane in the  $\text{Bu}_2\text{Hg}$  reaction may not be diagnostic of a nonradical reaction. Second, ring-alkylated products of the type  $\text{BuTh}$  and  $\text{Bu}_2\text{Th}$  were obtained. These designations were made on the basis of GC–MS data; GC–MS data also indicated the presence of two isomers of  $\text{BuTh}$  and several isomers of  $\text{Bu}_2\text{Th}$ . The new products were found to be in both the Th and  $\text{ThBu}^+\text{ClO}_4^-$  TLC fractions; this finding suggested that the products were formed not only as  $\text{BuTh}$  and  $\text{Bu}_2\text{Th}$  but also as  $\text{BuThBu}^+\text{ClO}_4^-$  and  $\text{Bu}_2\text{ThBu}^+\text{ClO}_4^-$ . We do not know yet how these products were formed. An experiment was carried out by delaying the quenching of the reaction (run 3) to find indirectly if butyl-group transfer from  $\text{ThBu}^+$  to Th was occurring. No substantial change in the product distribution was found (cf. run 2).



**Table VI. Yields of Products of Reaction of Bu<sub>2</sub>Hg with Th<sup>+</sup>ClO<sub>4</sub><sup>-</sup> in Acetonitrile**

<i>Product</i>	<i>1</i>	<i>2</i>	<i>3</i>	<i>4</i>
BuH	0.056	0.018	0.005	
Bu(-H)	0	0.001	0	
Bu <sub>2</sub>	0.016	0.008	0.006	
BuCl	0.748	0.811	0.778	0.695
BuHgCl	1.00	0.982	1.019	0.901
Th	1.83	2.107	2.138	2.103
ThO	0.014	0.244	0.225	0.245
1-BuTh	0.025	0.020	0.023	0.024
2-BuTh	0.130	0.106	0.111	0.111
Bu <sub>2</sub> Th	0.042	0.029	0.027	0.027
BuTh <sup>+</sup> (%) <sup>a</sup>	27.6 <sup>b</sup>	32.7 <sup>b</sup>	30.9 <sup>b</sup>	28.7 <sup>c</sup>
BuHgCl (%) <sup>d</sup>	48.2	49.1	51.0	45.0
Total Bu (%) <sup>e</sup>	100	101	100	
Total Th (%) <sup>f</sup>	102	100	103	100

NOTE: Values are the yields of products given in millimoles for the corresponding run number, unless indicated otherwise. In run 1, 2.00 mmol of Th<sup>+</sup>ClO<sub>4</sub><sup>-</sup> reacted with 1.04 mmol. of Bu<sub>2</sub>Hg; in runs 2-4, 2.50 mmol of Th<sup>+</sup>ClO<sub>4</sub><sup>-</sup> reacted with 1.00 mmol of Bu<sub>2</sub>Hg.

<sup>a</sup>Percent of Bu<sub>2</sub>Hg converted to ThBu<sup>+</sup>.

<sup>b</sup>Minimum value, which was obtained by deducting the sum of all 1-BuTh, 2-BuTh, and Bu<sub>2</sub>Th (mmol), as listed in the table from the yield of BuCl (mmol).

<sup>c</sup>Real value, which was obtained by deducting the sum of 1-BuTh, 2-BuTh, and Bu<sub>2</sub>Th (mmol) as assayed by GLC in the workup of the isolated sulfonium perchlorate mixture with LiCl, from the yield of BuCl (mmol).

<sup>d</sup>Percent of Bu<sub>2</sub>Hg converted to BuHg<sup>+</sup>.

<sup>e</sup>Sum of all Bu groups.

<sup>f</sup>Sum of all Th groups.

### **Reactions of Th<sup>+</sup>ClO<sub>4</sub><sup>-</sup> with (5-Hexenyl)<sub>2</sub>Hg**

The designation (5-hexenyl)<sub>2</sub>Hg refers to the mixture of dialkylmercurial compounds obtained from the reaction of 5-hexenylMgCl with HgCl<sub>2</sub>. The composition of the mixture is described in the Experimental Details. The results of reactions of Th<sup>+</sup> with (5-hexenyl)<sub>2</sub>Hg are given in Tables VII and VIII. Unlike the reactions with 5-hexenylMgCl, these reactions were ho-

**Table VII. Yields and *L/C* Ratios of Products of Reaction of (5-Hexenyl)<sub>2</sub>Hg with Th<sup>•+</sup>ClO<sub>4</sub><sup>-</sup>**

Products	1	2	3	4	5
1-Hexene	0.016	0.006	0.010	0.001	0.90
MCP	0.0054	0.004	0.023	0.006	0.082
1-Chloro-5-hexene	0.69	0.75	0.65	0.71	
CPMCl	0.039	0.024	0.039	0.036	
HxHgCl	0.65	0.69	0.60	0.67	0.81
CPMHgCl	0.024	0.22	0.23	0.21	0.13
Th	2.17	2.21	2.15	2.02	
ThO	0.16	0.13	0.16	0.19	
C <sub>6</sub> H <sub>11</sub> Th <sup>a</sup>	0.13	0.13	0.13	0.11	
(C <sub>6</sub> H <sub>11</sub> ) <sub>2</sub> Th <sup>b</sup>	0.018	0.013	0.016	0.010	
<i>L/C</i> (1) <sup>c</sup>	17.7	31.3	16.7	19.7	
<i>L/C</i> (2) <sup>d</sup>	2.9	3.1	2.6	3.2	

NOTE: All values, except for the *L/C* ratios, are the yields of products given in millimoles. In runs 1–4, 2.50 mmol of Th<sup>•+</sup>ClO<sub>4</sub><sup>-</sup> reacted with 1.00 mmol of (5-hexenyl)<sub>2</sub>Hg; in run 5, 0.5 mL of 12 N HCl reacted with 1.0 mmol of (5-hexenyl)<sub>2</sub>Hg. The mixture of isomers of (5-hexenyl)<sub>2</sub>Hg is described in the Experimental Details. After reaction with the mercurial compound was finished in runs 1–4, the products were treated with LiCl (*see* Experimental Details). This reaction converted ions such as ThR<sup>+</sup> into Th and RCl, and RHg<sup>+</sup> into RHgCl. This situation accounts for such halides being listed in column 1.

<sup>a</sup>Sum of isomeric compounds having M<sup>+</sup> (GC-MS) of 298.

<sup>b</sup>Sum of isomeric compounds having M<sup>+</sup> (GC-MS) of 380.

<sup>c</sup>*L/C* ratio for RCl obtained from ThR<sup>•+</sup>ClO<sub>4</sub><sup>-</sup>.

<sup>d</sup>*L/C* ratio for RHgCl.

**Table VIII. Material Balance in Reactions of (C<sub>6</sub>H<sub>11</sub>)<sub>2</sub>Hg with Th<sup>•+</sup>ClO<sub>4</sub><sup>-</sup> and with HCl**

Product Type	1	2	3	4	5
RH	1.1	0.5	1.7	0.35	49.1
RCl	36.5	38.7	34.5		
RHgCl	44.5	45.5	41.5	44.0	47.0
Th	86.8	88.4	86.0	80.8	
ThO	6.4	5.2	8.0	7.6	
RTh <sup>a</sup>	5.2	5.2	5.2	4.4	
RTh <sup>b</sup>	6.5	6.5	6.5	5.5	
R <sub>2</sub> Th <sup>a</sup>	0.72	0.52	0.6	0.4	
R <sub>2</sub> Th <sup>b</sup>	1.8	1.3	1.6	1.0	
Total R	90.3	92.5	85.8	88.2	96.1
Total Th	99.1	100.6	100	93.2	

NOTE: Details of products and yields in millimoles are in Table VII. Values are the percent C<sub>6</sub>H<sub>11</sub> group or Th group in each type of product on the basis of 1 mmol of (C<sub>6</sub>H<sub>11</sub>)<sub>2</sub>Hg and 2.5 mmol of Th<sup>•+</sup>ClO<sub>4</sub><sup>-</sup>. R means any C<sub>6</sub>H<sub>11</sub> group.

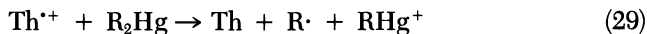
<sup>a</sup>This entry is for percent Th.

<sup>b</sup>This entry is for percent R.

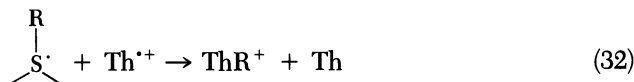
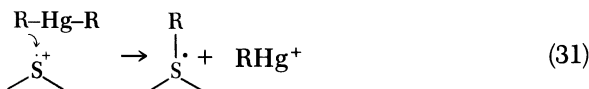
American Chemical Society  
Library

1155 16th St., N.W.  
Washington, D.C. 20036

mogeneous in acetonitrile solution. We anticipated that a clear answer would be obtained as to whether or not the reaction took place via initial SET (equations 29 and 30):

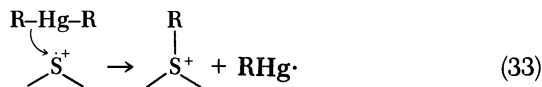


That is, we anticipated that if the  $L/C$  ratio in the product  $\text{ThR}^+$  turned out to be small, as in the reactions with 5-hexenylMgCl, we would have a clear indication of the electron-transfer route. To our surprise, we found that the  $L/C$  ratios for  $\text{ThR}^+$ , as expressed by conversions into 1-chloro-5-hexene and CPMCl, were very high (Table VI); they averaged approximately 21 for the four runs. In contrast, the  $L/C$  ratios for 5-hexenylHgCl and CPMHgCl, representing R in  $\text{RHg}^+$ , were very low; they averaged 2.9 for the four runs. The results suggest that the 5-hexenyl group is placed selectively in  $\text{ThR}^+$ , and the CPM group is placed selectively in  $\text{RHg}^+$ . If electron transfer does occur in these reactions, the 5-hexenyl radical must not only have been obtained selectively, but must have been trapped without the occurrence of cyclization at all. Trapping without cyclization contradicts the results from using the Grignard reagent; however, that reaction was heterogeneous in comparison with the homogeneous reaction of the mercurial compound in  $\text{CH}_3\text{CN}$ . If reaction with the mercurial compound does not involve electron transfer, we are confronted with the alternative reaction: selective displacement of the 5-hexenyl group from the mercurial compound. Displacement may be looked upon in two ways, each of which has a point of contention. Electrophilic displacement (equations 31 and 32), acceptable on the basis of known electrophilic displacements on mercurial compounds (47, 48), has the disadvantage of forming the anticipated labile sulfuranyl radical (equation 31). Unless this radical is rapidly oxidized (equation 32) it should dissociate into Th and the 5-hexenyl radical, which can be cyclized.



Another point may be relevant here, too. Electrophilic displacement by the cation radical implies a two-electron bond-forming process, that is, one in which a pair of electrons from  $\text{R}_2\text{Hg}$  is used in forming the new bond at sulfur. This process would constitute, in effect, the direct bonding between a nucleophile, say  $\text{Nu}^-$ , with a cation radical, a process recently described

as energetically improbable by Pross (49). Radical displacement (equations 33 and 34) removes the problem of the sulfuranyl radical but gives the problem of the equally (or more?) labile RHg radical (equation 35). Such radicals (RHg·) have been found to be very unstable (50–53). If R in RHg· is 5-hexenyl we should expect the formation of (cyclizable) 5-hexenyl radical.



If the 5-hexenyl group were selectively placed in  $\text{ThR}^+$ , by any route, the composition of our (5-hexenyl)<sub>2</sub>Hg (*see* Experimental Details) would lead to maximum *L/C* ratios of 34.7 in  $\text{ThR}^+$  and 5.7 in  $\text{RHgCl}$ . The only component of the mixture of (C<sub>6</sub>H<sub>11</sub>)<sub>2</sub>Hg mercurial compounds in our (5-hexenyl)<sub>2</sub>Hg that allowed the selection between 5-hexenyl and CPM was the mixed mercurial compound, 5-hexenylHgCPM. If 85% of the 5-hexenyl groups (0.11 mmol out of 0.13 mmol) in this compound became 5-hexenyl in  $\text{ThR}^+$ , the *L/C* ratio for  $\text{ThR}^+$  would be 20, whereas the *L/C* ratio for  $\text{RHgCl}$  would be 6.6. Thus, the selectivity has to be so good as to be questionable as a concept. Consequently, we feel that the results from using (5-hexenyl)<sub>2</sub>Hg cannot at this time answer the question originally posed: concerning whether or not electron transfer and radical trapping occur.

Reactions of (5-hexenyl)<sub>2</sub>Hg were similar to reactions of Bu<sub>2</sub>Hg with  $\text{Th}^{++}$  insofar as the formation of  $\text{RTh}$  and  $\text{R}_2\text{Th}$  is concerned. These products, like those from reaction with Bu<sub>2</sub>Hg, were obtained mainly from treating the mixture of sulfonium salts with LiCl. Again, this result suggested that the products existed initially as  $\text{RThR}^+\text{ClO}_4^-$  and  $\text{R}_2\text{ThR}^+\text{ClO}_4^-$  (in which R is C<sub>6</sub>H<sub>11</sub>). The results indicate that a fundamental difference exists in the way the two organometallic compounds (RMgCl and R<sub>2</sub>Hg) react with  $\text{Th}^{++}\text{ClO}_4^-$ .

### *Reaction of Perylene<sup>•+</sup>ClO<sub>4</sub><sup>-</sup> with Me<sub>2</sub>Hg*

Some years ago, following the discovery that  $\text{Th}^{++}$  can be alkylated at sulfur by reaction with R<sub>2</sub>Hg, numbers of unsuccessful attempts were made to methylate the perylene cation radical with dimethylmercury (Me<sub>2</sub>Hg). The cation radical was reduced completely to perylene, but no evidence of methylperylene could be found (54). In particular, no trace of a perylene carboxylic acid was found when the aromatic hydrocarbon product was subjected to oxidation procedures that had been shown independently to convert meth-

ylperylene into perylene carboxylic acids. This result (the formation of perylene) may be indicative of an initial electron transfer, analogous to reaction 29, and the failure of subsequent coupling is then in line with the observation of Ebersson and Radner (20) about the inertness of the perylene cation radical to coupling with  $\text{NO}_2$ ; that is, after electron transfer and formation of  $\text{Me}\cdot$ , coupling between  $\text{Me}\cdot$  and perylene cation radical may not have been able to occur.

### *Reflections on the Electron-Transfer and Coupling Steps in Reactions of $\text{RMgCl}$ and $\text{R}_2\text{Hg}$ with $\text{Th}^{++}\text{ClO}_4^-$*

Electron transfer occurs in the reaction between  $\text{Th}^{++}\text{ClO}_4^-$  and  $\text{RMgCl}$  and is followed by coupling between  $\text{Th}^{++}$  and some types of  $\text{R}\cdot$ . Thus, the net result in some cases is the finding of a new route (equations 24 and 25) to reaction between  $\text{Th}^{++}$  and a nucleophile. The finding that electron transfer occurs from readily oxidizable carbanions should not be surprising. The likelihood that electron transfer will occur between a cation radical and a nucleophile can be assessed, in fact, by Ebersson's method (55–57), on the basis of the Marcus theory and a knowledge or assessment of the oxidation potentials of the reactants and the reorganization energies ( $\lambda$ ) of the respective redox pairs. Thus, in connection with the reaction between  $\text{Th}^{++}$  and  $\text{RMgCl}$  (equation 36), we know that  $E^0$  ( $\text{Th}^{++}/\text{Th}$ ) is 1.54 V (vs. NHE), and we can assume that  $E^0$  values for the couple  $\text{RMgBr}^{++}/\text{RMgBr}$  (58) will suffice for the corresponding couple,  $\text{RMgCl}^{++}/\text{RMgCl}$ .



The respective reorganization energies are as follows  $\text{Th}^{++}/\text{Th} = 10$  kcal/mol and  $\text{RMgCl}^{++}/\text{RMgCl} = 70$  kcal/mol (55, 56). With these data,  $\Delta G^\ddagger$  can be calculated for electron transfer (equation 36) and, thereby, an assessment of the electron-transfer process can be obtained. Data are given in Table IX, and they indicate that electron transfer should be very fast ( $\Delta G^\ddagger$  values  $< 3$  kcal/mol). An analogous calculation can be made for electron transfer between  $\text{Th}^{++}$  and  $\text{Bu}_2\text{Hg}$ . We have done this calculation by using both the value (41 kcal/mol) for  $\lambda$  in the electron transfer from a variety of organometallic compounds to tris(1,10-phenanthroline)iron(III), and the expression (equation 37) analogous to that for  $(\Delta G^\ddagger)^{1/2}$  developed by Kochi (59).

$$(\Delta G^\ddagger)^{1/2} = \left[ \frac{\lambda^{1/2}}{2} + \frac{F}{2\lambda^{1/2}} \left( E_{\text{RM}}^0 + \frac{W_p}{F} \right) \right] - \left( \frac{F}{2\lambda^{1/2}} E_{\text{Th}}^0 \right) \quad (37)$$

We have assumed also that the term for the oxidation potential [ $E_{\text{RM}}^0 + (W_p/F)$ ] (in which  $W_p$  is the work term for separation of products, and  $F$  is

**Table IX. Calculations of  $\Delta G^\ddagger$  for Electron Transfer between  $\text{Th}^{+\cdot}$  and  $\text{RMgCl}$** 

<i>R in RMgCl</i>	$E^0$ (V) <sup>a</sup> ( $\text{RMgCl}^{\cdot+}/\text{RMgCl}$ )	$\Delta G^0$ (kcal/mol)	$\lambda$ (kcal/mol)	$\Delta G^\ddagger$ (kcal/mol)
Me	-0.25	-39.0	40	0
Et	-0.66	-50.7	40	0.72
Bu	-0.53	-47.7	40	0.40
<i>sec</i> -Bu	-0.87	-55.6	40	1.52
<i>tert</i> -Bu	-1.07	-60.2	40	2.50
Cyclopentyl	-0.88	-55.8	40	1.56

<sup>a</sup>Values are for  $\text{RMgBr}^{\cdot+}/\text{RMgBr}$  and taken from reference 58.

the Faraday consistent) for  $\text{Bu}_2\text{Hg}$  is the same as that given for diethylmercury ( $\text{Et}_2\text{Hg}$ ), namely, 1.21 eV (59). In this way,  $\Delta G^\ddagger$  for electron transfer between  $\text{Th}^{+\cdot}$  and  $\text{Bu}_2\text{Hg}$  is calculated to be 6.8 kcal/mol, which is lower than  $\Delta G^\ddagger$  for electron transfer to the  $\text{FeL}_3^{3+}$  oxidants (where L denotes a ligand) used by Kochi (59). This calculation indicates that electron transfer from  $\text{Bu}_2\text{Hg}$  to  $\text{Th}^{+\cdot}$  should not be difficult. Furthermore, Rollick and Kochi (60) showed that electron transfer occurs readily from  $\text{Me}_2\text{Hg}$  to an oxidant, tris(1,10-phenanthroline)iron(III), whose reduction potential versus a saturated calomel electrode (0.99V) is smaller than that of  $\text{Th}^{+\cdot}$  (1.30 V). Thus, in comparison, electron transfer from  $\text{R}_2\text{Hg}$  to  $\text{Th}^{+\cdot}$  should be facile.

Our experimental results for reactions with  $\text{RMgCl}$  agree, as has been shown, with what one would anticipate from the calculations of  $\Delta G^\ddagger$ , but the results for reactions with  $\text{R}_2\text{Hg}$  are ambiguous, and we still need to find where the problem lies.

The overall result, then, is that we have found that coupling between  $\text{Th}^{+\cdot}$  and alkyl radicals is a viable reaction. It takes its place, along with the reaction of  $\text{NO}_2$  with  $\text{ArH}^{+\cdot}$ , as a new mode in the repertoire of cation radical reactions. No doubt, further examples of such coupling reactions lie hidden among organic reactions and await uncovering.

### *Note Added in Proof*

Kochi and co-workers (62) reported that conventional electrophilic nitration of some aromatic ethers gave the same products and had the same characteristics as nitration of the ethers with tetranitromethane via charge-transfer activation. An arene cation radical- $\text{NO}_2$  pair was shown to be the source of products in the latter method. Insofar as the aromatic ethers are concerned, therefore, there seems to be little doubt that the products of conventional

nitration also originate from the formation and recombination of a cation radical- $\text{NO}_2$  pair.

### Acknowledgments

We thank the National Science Foundation for support of this work under Grant No. 8314947. This chapter was written during the tenure of a Humboldt Foundation Senior U.S. Scientist Award. Henry J. Shine thanks the Foundation and the Institut für Organische Chemie, Universität Hamburg, for gracious hospitality.

### References

1. Hammerich, O.; Parker, V. D. *Adv. Phys. Org. Chem.* **1984**, *20*, 55.
2. Shine, H. J.; Sullivan, P. D. *J. Phys. Chem.* **1968**, *72*, 1390.
3. Bard, A. J.; Ledwith, A.; Shine, H. J. *Adv. Phys. Org. Chem.* **1976**, *13*, 155.
4. Costa, L. C.; Young, G. B.; Whitesides, G. M. *J. Organomet. Chem.* **1977**, *134*, 151.
5. Dolzine, T. W.; Oliver, J. P. *J. Organomet. Chem.* **1974**, *78*, 165. These workers were able to distill the product at 10-6 torr and characterized it by NMR and mass spectrometry. The method of preparation was the reduction of 5-hexenylHgCl (made from 5-hexenylMgCl) by sodium stannite. Although the origin of the Grignard was 1-chloro-5-hexene, from which some CPMMgCl is usually obtained too, no indication was given of the presence of 5-hexenylcyclopentylmethylmercury or of bis(cyclopentylmethyl)mercury.
6. Quirk, R. P.; Lea, R. E. *J. Am. Chem. Soc.* **1976**, *98*, 5973. These workers purified bis(5-hexenyl)mercury by column chromatography on silica. In this case the necessary 5-hexenylMgBr was prepared from 1,2,6-tribromohexane. The final product may not then have contained isomeric mercurials.
7. Our  $^1\text{H}$  NMR spectrum was qualitatively like that reported by Denis, J.; Oliver, J. P.; Dolzine T. W.; Smart, J. B. *J. Organomet. Chem.* **1974**, *71*, 314.
8. Weiss, J. *Trans. Far. Soc.* **1946**, *42*, 101.
9. Nagakura, S.; Tanaka, J. *J. Chem. Phys.* **1954**, *22*, 563.
10. Nagakura, S.; Tanaka, J. *Bull. Chem. Soc. Jpn.* **1959**, *32*, 734.
11. Nagakura, S. *Tetrahedron Suppl.* **2** **1963**, *19*, 361.
12. Brown, R. D. *J. Chem. Soc.* **1959**, 2224, 2232.
13. Fukuzumi, S.; Kochi, J. K. *J. Am. Chem. Soc.* **1980**, *102*, 2141.
14. Fukuzumi, S.; Kochi, J. K. *Ibid.* **1981**, *103*, 2783, 7240.
15. Fukuzumi, S.; Kochi, J. K. *J. Phys. Chem.* **1980**, *84*, 2246.
16. Fukuzumi, S.; Kochi, J. K. *Tetrahedron* **1982**, *38*, 1035.
17. Fukuzumi, S.; Kochi, J. K. *Int. J. Kinetics* **1983**, *15*, 249.
18. Perrin, C. L. *J. Am. Chem. Soc.* **1977**, *99*, 5516.
19. Ebersson, L.; Radner, F. *Acta Chem. Scand.* **1986**, *B40*, 71.
20. Ebersson, L.; Radner, F. *Ibid.* **1985**, *B39*, 357.
21. Ebersson, L.; Radner, F. *Ibid.* **1984**, *B38*, 861.
22. Ebersson, L.; Radner, F. *Ibid.* **1980**, *B34*, 739.
23. Radner, F. Dissertation, Lund University, Lund, Sweden, 1985. We thank Dr. Radner for a copy of his dissertation and for permission to reproduce the table of results.
24. Ristagno, C. B.; Shine, H. J. *J. Am. Chem. Soc.* **1971**, *93*, 1811.
25. Clemens, A. H.; Ridd, J. H.; Sandall, J. P. B. *J. Chem. Soc., Perkin Trans. 2* **1984**, 1659.

26. Clemens, A. H.; Ridd, J. H.; Sandall, J. P. B. *Ibid.* **1984**, 1227.
27. Ebersson, L.; Radner, F. *Acc. Chem. Res.* **1987**, *20*, 53. We thank Prof. Ebersson for a pre-print and for helpful discussions.
28. Morkovnik, A. S.; Okhlobystin, O. Yu.; Belinskii, E. Yu. *J. Org. Chem. USSR* **1979**, *15*, 328.
29. Morkovnik, A. S. *J. Gen. Chem. USSR* **1982**, *52*, 1664.
30. Morkovnik, A. S.; Dobaeva, N. M.; Okhlobystin, O. Yu.; Bessonov, V. V. *J. Org. Chem. USSR* **1981**, *17*, 2337.
31. Morkovnik, A. S.; Belinskii, E. Yu.; Dobaeva, N.M.; Okhlobystin, O. Yu. *J. Org. Chem. USSR* **1982**, *18*, 328.
32. Schmitt, R. J.; Buttrill, S. E. Jr.; Ross, D. S. *J. Am. Chem. Soc.* **1984**, *106*, 926.
33. Schmitt, R. J.; Buttrill, S. E., Jr.; Ross, D. S. *Ibid.* **1981**, *103*, 5265.
34. Feng, J.; Zheng, X.; Zerner, M. C. *J. Org. Chem.* **1986**, *51*, 4531.
35. Ebersson, L. *Acta Chem. Scand.* **1980**, *B34*, 747.
36. For a recent discussion, see Chanon, M. *Bull. Soc. Chim. France* **1985**, 209.
37. Ledwith, A.; Russell, P. J. *J. Chem. Soc., Perkin Trans. 2*, **1974**, 582.
38. Bandlish, B. K.; Porter, W. R., Jr.; Shine, H. J. *J. Phys. Chem.* **1978**, *82*, 1168.
39. Sugiyama, K.; Shine, H. J. *J. Org. Chem.* **1982**, *48*, 143.
40. Shine, H. J.; Bae, D. H.; Hoque, A. K. M. M.; Kajstura, A.; Lee, W.-K.; Shaw, R. W.; Soroka, M.; Engel, P. S.; Keys, D. E. *Phosph. and Sulf.* **1985**, *23*, 111.
41. Hoque, A. K. M. M.; Kovelesky, A. C.; Lee, W.-K.; Shine, H. J. *Tetrahedron Lett.* **1985**, 5655.
42. Bae, D. H.; Engel, P. S.; Hoque, A. K. M. M.; Keys, D. E.; Lee, W.-K.; Shaw, R. W.; Shine, H. J. *J. Am. Chem. Soc.* **1985**, *107*, 2561.
43. Soroka, M.; Shine, H. J. *Tetrahedron* **1986**, *42*, 6111.
44. Ebersson, L.; Jonsson, L.; Wistrand, L.-G. *Acta Chem. Scand.* **1978**, *B32*, 520.
45. Garst, J. F.; Deutsch, J. E.; Whitesides, G. M. *J. Am. Chem. Soc.* **1986**, *108*, 2490.
46. Saeva, D. D.; Morgan, B. P. *J. Am. Chem. Soc.* **1984**, *106*, 4121.
47. Jensen, F. R.; Rickborn, B. *Electrophilic Substitution of Organomercurials*; McGraw-Hill: New York, 1968.
48. Nugent, W. A.; Kochi, J. K. *J. Am. Chem. Soc.* **1976**, *98*, 5979.
49. Pross, A. *J. Am. Chem. Soc.* **1986**, *108*, 3537.
50. Giese, B. *Angew. Chem. Int. Ed. Engl.* **1985**, *24*, 553.
51. Singh, R.; Khanna, R. K. *Tetrahedron Lett.* **1983**, *973*, 1411.
52. Russell, G. A.; Hershberger, J.; Owens, K. *J. Organomet. Chem.* **1982**, *225*, 43.
53. Nugent, W. A.; Kochi, J. K. *Ibid.* **1977**, *124*, 327, 349.
54. J. Y. Chung., unpublished results.
55. Ebersson, L. *Adv. Phys. Org. Chem.* **1982**, *18*, 79.
56. Ebersson, L. *Acta Chem. Scand.* **1984**, *B38*, 439.
57. Ebersson, L. *Electron Transfer Reactions in Organic Chemistry*; Springer Verlag: New York, 1987. We thank Prof. Ebersson for helpful discussions and guidance with the calculations.
58. Holm, T. *Acta Chem. Scand.* **1983**, *B37*, 567.
59. Fukuzumi, S.; Wong, C. L.; Kochi, J. K. *J. Am. Chem. Soc.* **1980**, *102*, 2928.
60. Rollick, K. L.; Kochi, J. K. *J. Am. Chem. Soc.* **1982**, *104*, 1319.
61. Sharma, K. K.; Boyd, R. J. *Theor. Chim. Acta* **1979**, *53*, 309.
62. Sankararaman, S.; Haney, W. A.; Kochi, J. K. *J. Am. Chem. Soc.* **1987**, *109*, 5235.

RECEIVED for review September 29, 1986. ACCEPTED February 6, 1987.



# Nitration of Pyrene by $\text{NO}_2$ and $\text{N}_2\text{O}_4$

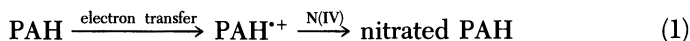
David S. Ross, Georgina P. Hum, and Robert J. Schmitt

SRI International, Menlo Park, CA 94025

*The nitration of pyrene by N(IV) ( $\text{NO}_2$ ,  $\text{N}_2\text{O}_4$ ) in methylene chloride at 25 °C under conditions in which the N(IV) is primarily the tetroxide demonstrates first-order product formation both in pyrene and N(IV). The order in N(IV) shifts to second order when the starting N(IV) concentration is increased. N(IV) nitrates pyrene directly; nitric acid, that is, N(V), does not. Under first-order conditions, the addition of  $\text{NO}$  [ $\text{NO}$ ]  $\gg$  [ $\text{N(IV)}$ ] shifts the product formation to second order and substantially accelerates the reaction. The reaction scheme involves the initial formation of a pyrene- $\text{N}_2\text{O}_4$  complex, followed by (1) the unimolecular collapse of the complex to product and (2) the addition of a second  $\text{N}_2\text{O}_4$  to the pyrene in the complex. The second path leads directly to polynitropyrenes when the concentration of N(IV) is sufficiently high.*

**T**HE NITRATION OF AROMATIC COMPOUNDS has been studied for decades, and benzene and its derivatives have been used almost exclusively as the substrates (1, 2). Nitric acid, usually in sulfuric acid, has generally been the nitrating reagent; the nitronium ion,  $\text{NO}_2^+$ , has presumably been the specific nitrating agent. Nitric acid and the nitronium are both N(V) species.

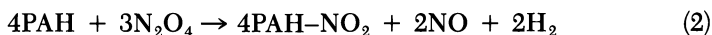
Interest in the study of the nitration of polynuclear aromatic hydrocarbons (PAHs) has developed recently, partly because of the significance of combustion-derived nitrated PAHs in the environment (3–6). The nitration of PAHs in innocuous media such as methylene chloride by N(IV) ( $\text{NO}_2$  and  $\text{N}_2\text{O}_4$ ) has been of particular interest, because the textbook view of aromatic nitration has been the acid-catalyzed route. PAH nitration by N(IV) is surprisingly rapid at ambient temperatures, and Ebersson and Radner (7, 8) and Pryor et al. (9) focused on electron transfer as the key to the reaction:



The study reported here was prompted by the still unsettled question of just how the reaction takes place. This chapter includes studies of the reaction kinetics and stoichiometry and covers the effects of oxygen and NO.

## Background

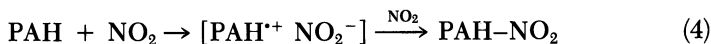
Eberson and Radner (7, 8) presented a series of papers describing the nitration of PAHs with N(IV). Their work dealt with the synthetic and mechanistic aspects (7) and included a study of the reaction of electrochemically generated PAH radical cations with N(IV) (reference 8 and citations therein). They also covered the effects of acidic and basic additives; the overall stoichiometry of the reaction was considered to be as follows:



The electron-transfer aspect of the reaction was studied by using Marcus theory and various thermodynamic cycles. Thus, the thermochemistries of a number of electron-transfer schemes were considered. Through a series of logical arguments, the scheme settled upon was not electron transfer per se but rather electrophilic attack of PAH by nitrosated nitrogen tetroxide:



A somewhat different picture was presented by Pryor et al. (9), who concluded that electron transfer to charge-separated species did occur for some PAHs, and NO<sub>2</sub> was the electron acceptor:



This reaction was supported by a correlation found between rate data and results from molecular orbital calculations.

## Experimental Details

**Materials.** Methylene chloride (Mallinckrodt) was distilled from calcium hydride before use. Pyrene (Aldrich) was used without further purification. Nitrogen tetroxide (Matheson) was purified with oxygen before use. Nitric acid (100%) was prepared by distilling fuming nitric acid from oleum.

**Kinetic Measurements.** Kinetic runs were conducted under pseudo-first-order conditions. The limiting reagent was at a concentration of  $\sim 10^{-5}$  M, and the excess reagent was at a concentration of  $10^{-4}$  to  $10^{-1}$  M. Fresh stock solutions of the reagents were used. An aliquot of solvent was added to the reaction cell, and aliquots of the pyrene and N<sub>2</sub>O<sub>4</sub> stock solutions were added at the desired concentrations. The formation of 1-nitropyrene was monitored at 430 nm on a UV-visible spectrophoto-

tometer (Hewlett–Packard 8450A) with a thermostated cell holder at 25 °C. Reactions performed under an atmosphere of argon or oxygen were conducted in a special vacuum cell designed to allow for degassing of the reactants by freeze–thaw cycles with liquid nitrogen.

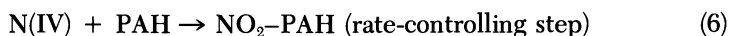
**Product Analyses.** The reaction was scaled up to  $10^{-3}$  M to allow for product analyses. The reaction mixtures were analyzed by using a silicone capillary column (SE–54) on a gas chromatograph (Varian 3700) at 250 °C. Gas chromatographic–mass spectrometric (GC–MS) data were obtained on a gas chromatograph (Hewlett–Packard 5890) with a mass-selective detector (model 5970). A bonded-phase silicone capillary column (DP–1701) was used at 250 °C.

## Results

A number of aspects of the reaction require clarification, including the roles of nitric acid, oxygen, and NO. Also, although the reaction has been presumed to be first order in both PAH and N(IV) (7), preliminary evidence suggests that the process may be far more complicated (9). In this regard, the position of the  $\text{NO}_2$ – $\text{N}_2\text{O}_4$  equilibrium under reaction conditions must be considered as well as whether  $\text{NO}_2$  or  $\text{N}_2\text{O}_4$  is the reacting species.

Included in this chapter are kinetic studies of the nitration of pyrene by N(IV) in methylene chloride in which first the PAH and then the N(IV) was the limiting reagent. The study was conducted spectrophotometrically; in all cases, 1-nitropyrene was the sole product, as determined by both UV spectrometry and GC analysis of the product mixture. (Dinitropyrenes were sought but were not found.) The effects of oxygen and NO were determined by using a cell designed so that the reaction could be run under argon and known quantities of oxygen and NO could be added at will.

The degrees of N(IV) dissociation are important to the interpretation of the observed order of the reaction in N(IV). For example, for the sequence



the observation of a reaction that is first order in N(IV) can be interpreted differently, depending on the major N(IV) species. If the equilibrium step is far to the left, then the N(IV) species in the rate controlling step must be  $\text{NO}_2$ . Alternatively, if the equilibrium is far to the right, then the N(IV) in the slow step must be  $\text{N}_2\text{O}_4$  (or  $2\text{NO}_2$ ). The problem can become more complicated for observations of reaction orders other than 1.0.

The dissociation constant for N(IV) in methylene chloride has not been reported. However, the constant in carbon tetrachloride was reported to be  $1.8 \times 10^{-4}$  M (10). For the range of N(IV) concentrations used here ( $5 \times 10^{-5}$  to  $1 \times 10^{-3}$  M), in the equilibrium  $\text{CCl}_4$  would favor the tetroxide,

except at the lowest levels. However, because the dissociation decreases as the polarity of the medium increases (10), we presume that  $[N_2O_4] \gg [NO_2]$  for all of our work.

**Initial Work: Nitric Acid as Nitrating Agent.** Because of the generally large role of nitric acid in nitration, its specific action during nitration in media such as methylene chloride was important to establish initially. The acid exists virtually entirely in its molecular form in such solvents, and past accounts of nitrations in such media included complicated kinetics with orders in N(V) up to values of 5 or 6 (11).

We conducted several nitrations of pyrene in methylene chloride in which we compared N(IV) and N(V). The results are shown in Figure 1, which presents product profiles (arbitrary ordinate scale) for periods of 1000–2000 s. Figure 1a, with pyrene as the limiting reactant and the two N species at the same concentration, shows that on the time scale for N(IV) nitration, nitric acid is unreactive with pyrene. The situation does not change much when the conditions are reversed and the N species are limiting, as Figure 1b shows. In this case, an induction period is apparent; this observation suggests that the nitric acid decomposes to N(IV), which is then responsible for the nitration in some manner. In Figure 1c, in which the pyrene levels have been increased by a factor of about 20 over those of Figure 1b, the induction period appears to have been overcome, although the reaction in the N(V) case is still considerably slower than the N(IV) reaction. Seemingly, the PAH triggers the N(V) decomposition in the initial stages.

No further work was done with N(V) nitration; however, on the basis of these observations, we assert that nitric acid itself does not nitrate pyrene in methylene chloride. This finding can be contrasted with the results of Grosjean et al. (3), who concluded in atmospheric pollutant studies that the opposite view is correct. Specifically, their results from vapor-phase experiments suggested that  $NO_2$  was not active in nitration of filter-deposited PAHs, whereas nitric acid was necessary for nitration. The differences in conditions must be considered when comparing these data with those from this work. Nonetheless, it is difficult to refute the absence of nitration activity by N(V) under our conditions, and the important questions concerning the nitrating species in the environmental work remain.

**N(IV) Nitration of Pyrene.** Kinetic runs were conducted with both N(IV) and pyrene as limiting reactants; in each case, the runs were conducted in both a standard 10-mm UV cell with a small headspace ( $\sim 3.2$  mL of liquid volume and  $\sim 0.5$  mL of headspace) and in our vacuum UV cell with a headspace of about 50 mL. In the vacuum UV cell, the head gas was 1 atm of argon. As discussed in the following paragraphs, the order of addition was important, and in the work described here, aliquots of pyrene stock solutions were added to prepared N(IV) solutions. The results from the two different

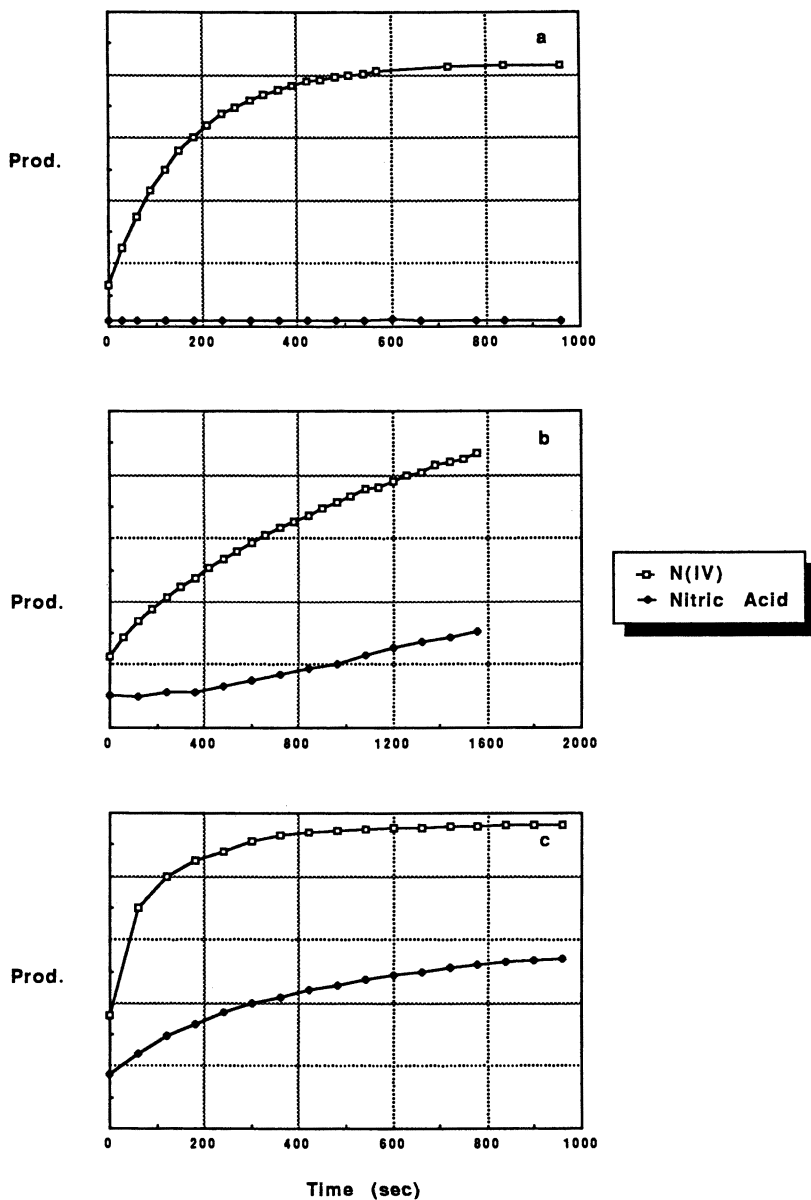


Figure 1. Comparison of  $\text{N}_2\text{O}_4$  and  $\text{HNO}_3$  for the nitration of pyrene (Py) in methylene chloride. (a)  $[\text{HNO}_3]/[\text{Py}] = 7.5 \times 10^{-4} \text{ M}/4.9 \times 10^{-5} \text{ M}$ ;  $[\text{N}_2\text{O}_4]/[\text{Py}] = 8.4 \times 10^{-4} \text{ M}/5.7 \times 10^{-5} \text{ M}$ . (b)  $[\text{HNO}_3]/[\text{Py}] = 2.9 \times 10^{-5} \text{ M}/1.5 \times 10^{-2} \text{ M}$ ;  $[\text{N}_2\text{O}_4]/[\text{Py}] = 5.1 \times 10^{-5} \text{ M}/1.5 \times 10^{-2} \text{ M}$ . (c)  $[\text{HNO}_3]/[\text{Py}] = 5.3 \times 10^{-5} \text{ M}/2.8 \times 10^{-1} \text{ M}$ ;  $[\text{N}_2\text{O}_4]/[\text{Py}] = 7.3 \times 10^{-5} \text{ M}/2.6 \times 10^{-1} \text{ M}$ .

sets of limiting conditions were surprising. The orders for pyrene and N(IV), which changed as shown in Figure 2 for the nitration of pyrene in methylene chloride at 25 °C, are summarized as follows: For excess pyrene (Py) ( $[\text{Py}] = 7 \times 10^{-3}$  to  $2 \times 10^{-1}$  M), the nitration was first-order in both pyrene and N(IV); for excess N(IV) ( $[\text{N(IV)}] = 3 \times 10^{-4}$  to  $2 \times 10^{-3}$  M;  $[\text{Py}] \simeq 4 \times 10^{-5}$  M), the nitration was first order in pyrene and second-order in N(IV).

Pryor et al. (9) also noted a second-order dependence on N(IV) in an account of their preliminary results. This change in order with change in N(IV) concentration demonstrates aspects of the reaction central to the details of the reaction mechanism. One feature of the high order in N(IV) is the need to conduct the kinetic experiments by adding the N(IV) to the pyrene rather than vice versa. We found invariably that the opposite order of addition brought about unpredictable and decidedly unreproducible results.

A cell effect was evident for the  $[\text{N(IV)}] \gg [\text{Py}]$  case. The rate constants for runs in the cell with the significant headspace were below the linear extrapolation of the line in the plot. Additionally, the ultimate yields of 1-nitropyrene in the gas cell as estimated by the final absorbances were considerably lower than those in the conventional cell. Evidently, the rate of

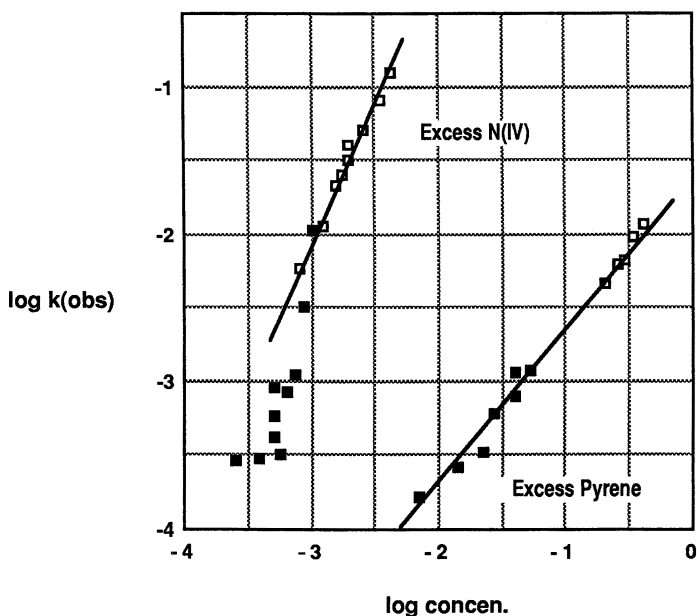


Figure 2. Determination of reaction order. Abscissa values correspond in each case to the concentration of the reactant in excess. Key: □, conventional cell; ■, vacuum cell.

loss of N(IV) out of the medium and into the vapor phase is rapid relative to the nitration rate.

**Effects of Oxygen and NO.** The potential importance of this chemistry to environmental issues suggested that the effects of  $\text{O}_2$  and NO should be investigated. The results are summarized in Table I.

The results of runs with added  $\text{O}_2$  under conditions of limiting pyrene show that  $\text{O}_2$  increases the rate of nitration under these conditions. In these cases, the product production was first order. However, when the condition was switched to limiting N(IV), the effect of added oxygen also switched, as shown in Figure 3. Here, the  $\text{O}_2$  severely slows the nitration, and the product profile reflects no simple rate law. The profile can be reasonably well-matched with a process that is sixth order in N(IV); this result is reminiscent of the high order in nitric acid mentioned earlier (11). However, a more likely explanation is a reaction or reactions operating parallel to and competitive with nitration in which the pyrene or the N(IV) is consumed in a process not yielding nitropyrene. Product profiles from parallel first-order reactions can mimic higher order reactions. Consistent with this surmise is the observation that yields of 1-nitropyrene from the  $\text{O}_2$  runs, were consid-

**Table I. Effects of Oxygen and NO on the Nitration of Pyrene in Methylene Chloride at 25 °C**

Starting Concentration ( $M \times 10^4$ )		Head Gas (1 atm)	$k_{\text{obs}}$ ( $s^{-1} \times 10^4$ )
N(IV)	Pyrene		
Limiting Pyrene <sup>a</sup>			
5.0	0.34	argon	9.1
	0.34	oxygen	23.2
6.3	0.34	argon	8.5
	0.34	oxygen	52.9
7.5	0.34	argon	11.0
	0.34	oxygen	45.1
Limiting N(IV)			
0.68	141	oxygen	1/ $m^b$
0.67	280	argon and NO (22 torr)	2.2 <sup>c</sup>

<sup>a</sup>First-order production of 1-nitropyrene in all cases.

<sup>b</sup>The rate law was not easily defined.

<sup>c</sup>This value is the observed second-order rate constant ( $M^{-1}s^{-1} \times 10^4$ ).

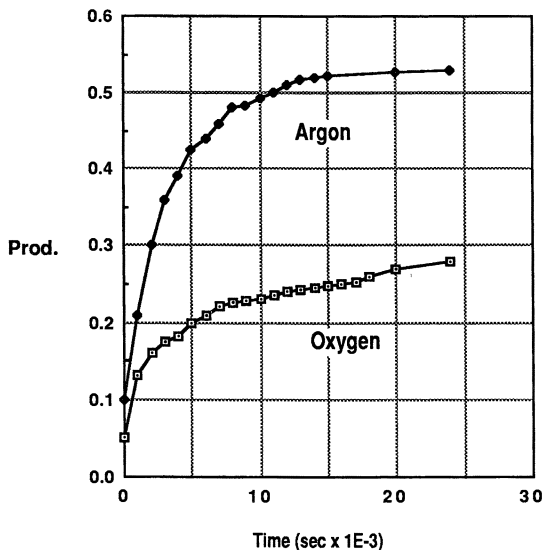
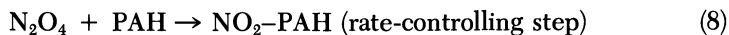


Figure 3. Effects of oxygen in Py nitration.  $[Py] = 1.4 \times 10^{-2} M$ ;  $N_2O_4 = 6.8 \times 10^{-5} M$ . Argon and oxygen are both at 1 atm.

erably below quantitative levels, as demonstrated by the product profiles such as the one shown in Figure 3.

The effect of added NO is more straightforward. In a single run under argon, 22 torr of NO was added to the gas cell. The cell contained 5 mL of a methylene chloride solution of pyrene ( $2.8 \times 10^{-2} M$  and N(IV) ( $6.7 \times 10^{-5} M$ ); on a molar basis,  $[NO] \gg [N(IV)]$ . In this case, the development of product smoothly followed second-order behavior, in contrast with the first-order production of 1-nitropyrene under the same conditions but in the absence of NO.

This result is the major clue to understanding the process; the order shift reveals the specific N-reactant, and the reaction rate demonstrates that the arene radical cation is a key intermediate. The rationale goes as follows: First, the addition of NO drives the N(IV) virtually fully to  $N_2O_3$  and the  $N_2O_4$ -NO<sub>2</sub> balance shifts to favor the dioxide.  $N_2O_3$  is not expected to be a reactant. As discussed earlier, the shift from first order to second order dictates that the tetroxide or 2NO<sub>2</sub> accompanies pyrene in the transition state. Because the NO<sub>2</sub> case would be the result of a trimolecular reaction, we conclude that the tetroxide is the specific species reacting with pyrene. Thus, we rewrite reactions 5 and 6 as follows:





In regard to the reaction rate, if the equilibrium levels of the tetroxide are responsible for the nitration, then we would anticipate that the NO addition would slow the reaction. However, because the rate of product production with NO addition is comparable to that without NO addition, NO must be part of the reaction scheme. The role of NO in organic reactions is limited, but NO readily forms stable  $\pi$  complexes with aromatic radical cations (12). We conclude, therefore, that such ions, or in the very least ion pairs tending toward radical-cation character, are part of the nitration of PAHs by  $\text{N}_2\text{O}_4$ .

**Headspace Effects and Stoichiometry.** In the earlier accounts of pyrene nitration by N(IV), NO was a prominent reaction product, and each  $\text{N}_2\text{O}_4$  ultimately yielded 1/3 nitropyrenes (7, 9). Our work found substantial effects of NO on reaction rate, as just discussed, and also effects of headspace on nitropyrene yields, as estimated spectrophotometrically. Specifically, we found in the runs with  $[\text{Py}] \gg [\text{N(IV)}]$  that with a large headspace the 1-nitropyrene/ $\text{N}_2\text{O}_4$  ratio ranged from 0.9 to 1.3; however, with a small headspace, this ratio approached and in some cases exceeded 2.0.

Accordingly, a study of the stoichiometry of pyrene nitration by N(IV) in methylene chloride was conducted by using gas chromatography for analysis. The results are summarized as follows: Starting with 79.1  $\mu\text{mol}$  of pyrene and 7.6  $\mu\text{mol}$  of N(IV) led to a mass balance of 97.5% and a 1-nitropyrene/ $\text{N}_2\text{O}_4$  ratio of 2.4; starting with 109.8  $\mu\text{mol}$  of pyrene and 15.1  $\mu\text{mol}$  of N(IV) led to a mass balance of 94.3% and a 1-nitropyrene/ $\text{N}_2\text{O}_4$  ratio of 1.8.

The two factors to consider are the mass balances, which were satisfactory, and the yield ratios, which were less than satisfactory. In other words, we can account for the carbon-containing components of the mixture, but the range in the ratios reflects some difficulty in introducing N(IV) to the system with adequate precision. These results show, however, that in our hands the 1-nitropyrene/ $\text{N}_2\text{O}_4$  ratio must be closer to 2.0 than it is to 1.3.

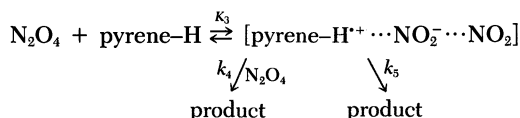
Thus, for  $\text{N}_2\text{O}_4$  being limiting, both  $\text{NO}_2$  reactants were accounted for in the nitropyrene product. This result indicates that some component in the system can act as a sink for hydrogen. We considered that pyrene might act as an oxidant; however, although our starting pyrene contained some dihydropyrene, no significant increase in dihydropyrene was found after a run. We also considered that the methylene chloride medium might be the ultimate H sink, but a careful search for HCl after nitration was negative. Currently, we suspect small quantities of oxygen to be responsible, even though we made every effort to eliminate  $\text{O}_2$  from the system. This aspect of the work remains to be clarified.

## Discussion

The accumulated evidence for the nitration of pyrene includes the fact that in methylene chloride, nitric acid does not directly nitrate pyrene, whereas N(IV) readily does. With limited pyrene and under the condition  $[\text{N}_2\text{O}_4] >$

[NO<sub>2</sub>], the reaction is second order in the tetroxide. The order shifts to first order with declining N(IV) concentration or increasing pyrene concentration at levels at which the tetroxide is still maintained as the major N(IV) species. The view that the tetroxide rather than the dioxide is the specific reactant is supported by the observation that with added NO, which shifts the condition to [NO<sub>2</sub>] > [N<sub>2</sub>O<sub>4</sub>], the production of product shifts from a first-order to a second-order process. Less directly explainable are the effects of the purposeful addition of oxygen, which either accelerates or slows the nitration for limiting amounts of pyrene or N(IV), respectively.

**Reaction Scheme and Rate Algebra.** Scheme I can account for the observations just discussed. It includes the initial, rapid, and reversible formation of a pyrene–N<sub>2</sub>O<sub>4</sub> donor–acceptor complex; such complexes have been reported (13, 14).  $K_3$  is the equilibrium constant for the formation of the complex, and  $k_4$ , and  $k_5$  are the rate constants for the subsequent parallel routes to product. The pyrene in the complex then reacts with a second N<sub>2</sub>O<sub>4</sub> to yield the product in corresponding to  $k_4$ . In a parallel step corresponding to  $k_5$ , the complex breaks down to yield the same product.



*Scheme I*

An expression for the observed rate constant,  $k_{\text{obs}}$ , can be derived for Scheme I for the case of limiting pyrene:

$$k_{\text{obs}}/c_{\text{N}_2\text{O}_4} = K_3 k_4 c_{\text{N}_2\text{O}_4} + K_3 k_5 \quad (9)$$

where  $c_{\text{N}_2\text{O}_4}$  is the concentration of nitrogen tetroxide. A plot of  $k_{\text{obs}}/c_{\text{N}_2\text{O}_4}$  versus  $c_{\text{N}_2\text{O}_4}$  provides a test of the proposed mechanism. The plot should yield a line passing through the origin if the step corresponding to  $k_5$  is unimportant and a nonzero intercept if this step is significant. As shown in Figure 4, such a plot does provide a reasonably sound line ( $r^2 = 0.96$ ), and the nonzero intercept shows that the second route is operative. The slope and intercept give the following values, respectively:  $K_3 k_4 = 5585 \text{ M}^{-2} \text{ s}^{-1}$ ;  $K_3 k_5 = 3.2 \text{ M}^{-1} \text{ s}^{-1}$ .

**Reaction Mechanism.** The pyrene in the charge-separated complex has radical-cation character, whereas the N<sub>2</sub>O<sub>4</sub> can dissociate to accommodate its radical-anion character. Direct electron transfer from PAH to both

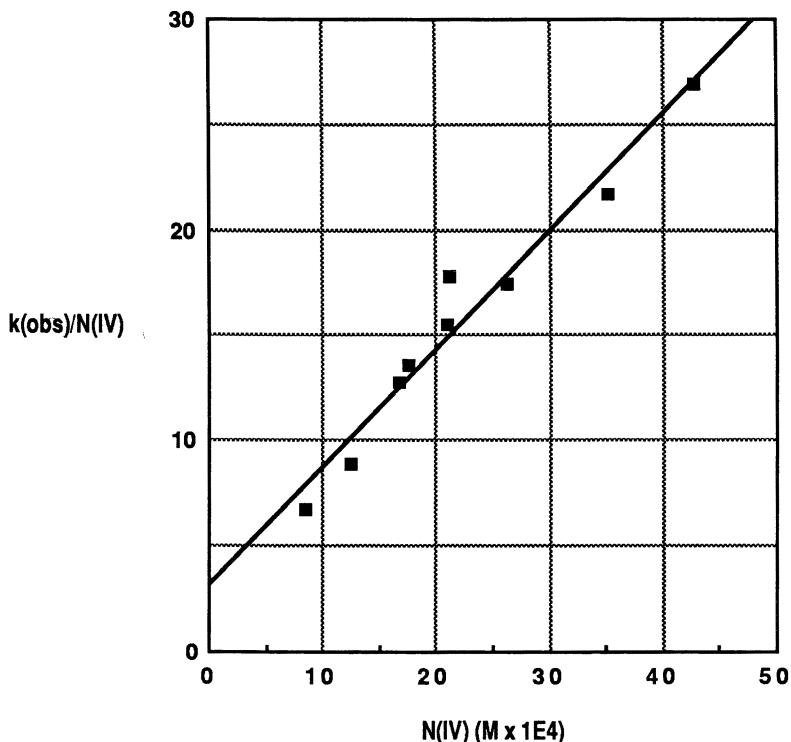
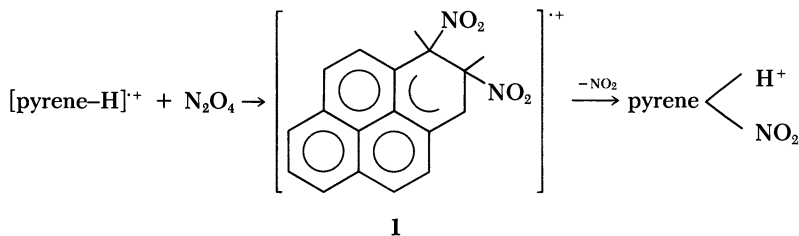


Figure 4. Plot of  $k_{\text{obs}}/[N(\text{IV})]$  versus  $[N(\text{IV})]$ .

$\text{NO}_2$  and  $\text{N}_2\text{O}_4$  was considered by Ebersson and Radner (7) but was rejected on the basis of their Marcus theory calculation. However, rather than complete charge separation, we would expect ion-pair formation in a medium with only modest polarity, such as methylene chloride. This factor could overcome the objections posed by the calculations, although currently the matter is not settled. This dissociative attachmentlike process is the non-photochemical analogue to that proposed by Masnovi and Kochi (15) for the photochemically promoted reaction between anthracene and tetranitromethane. In that case (15), electron acceptance by tetranitromethane was accompanied by the simultaneous split to  $\text{NO}_2$  and the trinitromethanide anion.

Following the formation of the complex, the charge-separated pyrene reacts along two competitive routes. As discussed earlier, collapse within the complex in the step corresponding to  $k_5$  leads to the  $\sigma$  intermediate commonly considered in electrophilic nitration (16).

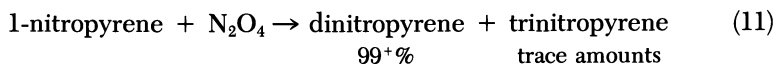
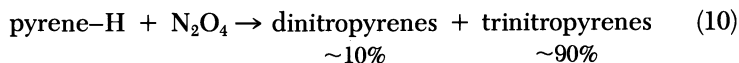
Alternatively, the pyrene could react in the step corresponding to  $k_4$  with a second, external  $\text{N}_2\text{O}_4$ . We viewed this reaction as an addition of the tetroxide across the unsaturated arene system, which leads to adducts such as structure I, which could then lose  $\text{NO}_2$  to form the same  $\sigma$  intermediate (Scheme II). To test this possibility, we allowed small quantities of solid



Scheme II

pyrene to react with liquid  $\text{N}_2\text{O}_4$  at ambient temperatures in a small-scale experiment. The same thing was done with 1-nitropyrene. If the addition of the tetroxide to the pyrene radical cation were an active route, then in neat  $\text{N}_2\text{O}_4$ , the addition of yet another tetroxide following the first could be competitive with the loss of  $\text{NO}_2$  and polynitropyrenes would be formed.

This view was readily confirmed. The reactions with both substrates were virtually instantaneous and essentially quantitative. In the pyrene case, a mixture of trinitropyrenes, which contained some dinitropyrenes, was isolated. (WARNING: Dinitropyrenes are highly mutagenic.) In the 1-nitropyrene case, a mixture of 1,3-, 1,6-, and 1,8-dinitropyrene was identified, and small quantities of trinitropyrenes were present.



Thus, in agreement with Scheme II, pyrene directly forms polynitropyrenes without first forming nitropyrene. Indeed, pyrene yields the more substituted products. This observation is a new one and is to be investigated further.

To our knowledge, this procedure is the most simple route to these materials. The reported methods (reference 17 for dinitropyrenes, and reference 18 for trinitropyrenes) involve high temperatures and concentrated nitric acid and sometimes provide only modest yields. The reaction of 1-nitropyrene is surprisingly rapid and most likely follows a similar route.

The conventional acid-promoted nitration of pyrene to dinitropyrene yields the 1,6- and 1,8-isomers (18, 19). However, on the basis of the rules of electrophilic nitration, these isomers should be formed in the minority, if at all, because they would result from  $\sigma$  cationic intermediates with contributing structures containing positive charges adjacent to a nitro group (16). Thus, the chemistry discussed here must be operative in acidic nitration media as well, at least for PAHs and other relatively easily oxidized aromatic

compounds. This point goes to the heart of the mechanism of conventional aromatic nitration and deserves further study.

This situation also raises an interesting contrast with the position of Ebersson and Radner (7). Their thesis is that the nitrous acid catalyzed (NAC) nitration observed for electron-rich substrates in acidic media is what is operative for N(IV) in methylene chloride. We agree that the two processes are the same but view that what is termed NAC in acidic media is rather the N(IV) nitration described here. In this regard, the role of acid in N(IV) PAH nitration, including both the added acids and the nitrous acid (HONO) generated in the nitration, has to be clarified.

Finally, the effects of oxygen we observed cannot be fully explained. However, expecting the chemistry related to the charge separation to be affected by oxygen is reasonable because donor-acceptor complexes between aromatic hydrocarbons and  $\text{O}_2$  are known (20). The formation of HONO in the nitration ultimately leads to the  $1\frac{1}{3}$  stoichiometry reported by other workers. As described by Ebersson and Radner (7), HONO decomposes to water, NO, and  $\text{NO}_2$ . However, in our case, NO must be oxidized by oxygen or other oxidants present in the system back to  $\text{NO}_2$ . Alternatively, HONO could be oxidized; its reaction with oxygen in solution very rapid (21).

### Acknowledgment

We acknowledge the support of this work by the U.S. Army Research Office. We also acknowledge useful comments from Lennart Ebersson.

### References

1. Hoggett J. G.; Moodie R. B.; Penton, J. R.; Schofield, K. *Nitration and Aromatic Reactivity*, Cambridge University Press: Cambridge, 1971.
2. Schofield, K. *Aromatic Nitration*, Cambridge University Press: Cambridge, 1980.
3. Grosjean, D.; Fung K.; Harrison, J. *Environ. Sci. Technol.* **1983**, *17*, 673-679.
4. Butler, J.; Crossley, P. *Atmos. Environ.* **1981**, *15*, 91-94.
5. Pitts, J., Jr.; Sweetman, J.; Zeilinska, B.; Atkinson, R; Winer, A.; Harger, W. *Environ. Sci. Technol.* **1985**, *19*, 1115-1121.
6. Zielinska, B.; Arey, J.; Atkinson, R.; Ramdahl, T.; Winer, A.; Pitts, J., Jr. *J. Am. Chem. Soc.* **1986**, *108*, 4126-4132.
7. Ebersson, L.; Radner, F. *Acta Chem. Scand.* **1985**, *B39*, 343-356.
8. Ebersson, L.; Radner, F. *Acta Chem. Scand.* **1986**, *B40*, 71-78.
9. Pryor, W. A.; Gleicher, G.; Cosgrove, J. P.; Church, D. F. *J. Org. Chem.* **1984**, *49*, 5189-5194.
10. Redmond T. P.; Wayland, B. B. *J. Phys. Chem.* **1968**, *72*, 1626-1629.
11. Ref. 1, pp 35-36.
12. Reents, W. D., Jr.; Frieser, B. S. *J. Am. Chem. Soc.* **1980**, *102*, 271-275.
13. Addison, C. C.; Sheldon, J. C. *J. Chem. Soc. Chem. Commun.* **1957**, 1937-1945.
14. Niciecki, E.; Vosper, A. J. *J. Chem. Soc. Dalton Trans.* **1978**, 1721-1723.
15. Masnovi, J. M.; Kochi, J. K. *J. Am. Chem. Soc.* **1985**, *105*, 7880-7893.

16. Gould, E. S. *Mechanism and Structure in Organic Chemistry*; Henry Holt: New York, 1959; pp 428–440.
17. *Beilsteins Handbuch der Organischen Chemie, Vierte Auflage, Drittes Ergänzungswerk, Funfter Band, Vierter Teil*; Boit, H-G., Ed.; Springer-Verlag: Berlin, 1965; p 2287.
18. Ruehl, P. H.; Bosch, L. C.; Duncan, W. P. In *Nitrated Polycyclic Aromatic Hydrocarbons*; White, C. M., Ed.; Dr. Alfred Huethig Verlag: Heidelberg, 1985; p 228.
19. Albrechtiniski, T. M.; Michalovic, J. G.; Gibson, T. L. In *Polynuclear Aromatic Hydrocarbons*; Cooke M.; Dennis, A. J. Eds.; Battelle: Columbus, OH, 1985; pp 69–86.
20. Evans, D. F. J. *Chem. Soc. Chem. Commun.* **1953**, 345–347.
21. Pogrebnaya, V. L.; Usov, A. P.; Baranov, A. V.; *Zh. Prikl. Khim. (Leningrad)* **1976**, 49, 720–724; *Chem. Abstr.* **1976**, 85, 25821m.

RECEIVED for review September 29, 1986. ACCEPTED March 10, 1987.

# Comparison of Polynuclear Aromatic Hydrocarbon Cation Salts with Salts of Simple Fluoroaromatic Cations

Thomas J. Richardson, Francis L. Tanzella, and Neil Bartlett

Department of Chemistry, University of California at Berkeley, and the Materials and Molecular Research Division, Lawrence Berkeley Laboratory, Berkeley, CA 94720

*Electron oxidation of the fluoroaromatic compounds  $C_6F_6$  and  $C_{10}F_8$  by  $O_2^+$  salts yields salts of the radical cations  $C_6F_6^+$  and  $C_{10}F_8^+$  which are Curie law paramagnets. The fluoroanalogues of the metallic  $(C_{10}H_8)_2^+$  salts do not exist. Repulsive interactions involving the electron-rich fluorine ligands of the fluoroaromatic compounds are probably responsible for the failure of these species to make metallic stacks. Attempts to prepare  $C_6H_6^+$  salts have produced the poly(p-phenylene) cation salts  $(C_6H_4)_n^+AsF_6^-$ , which are good electronic conductors. Electron oxidation of polynuclear aromatic hydrocarbons by  $C_6F_6^+$  salts or by  $AsF_5$ , (e.g.,  $3AsF_5 + 2C_{24}H_{12} \rightarrow 2C_{24}H_{12}^+AsF_6^- + AsF_3$ ) yields what appear to be salts of the polynuclear aromatic cations. The magnetic and electrical properties of such salts are described.*

**R**ADICAL-CATION SALTS derived from hexafluorobenzene (1), octafluorotoluene (2), pentafluoropyridine (3), and octafluoronaphthalene (4) have been known for some time, and some of their reaction chemistry has been discussed in a recent publication (5). Hexafluorobenzenehexafluoroarsenate,  $C_6F_6^+AsF_6^-$ , has oxidizing power sufficient to electron oxidize most other mono- and polycyclic aromatic compounds.

Fritz et al. (6) prepared bis(naphthalene) salts,  $(C_{10}H_8)_2^+MF_6^-$  ( $M =$

P, As) in which the aromatic molecules occur in stacks; this situation results in metal-like electrical conductivity ( $\sigma$ ) ( $\sigma = 0.12 \pm 0.046 \Omega^{-1} \text{ cm}^{-1}$  for a polycrystalline pellet). This finding suggested the possibility of analogous behavior in the fluoroaromatic series. Materials containing dimeric cations, however, have not been isolated from reaction mixtures containing excess amounts of the neutral monomers or from controlled reduction of monocation salts. In each case, the cations are monomeric and magnetically independent of one another.

Attempts to prepare salts containing  $\text{C}_6\text{H}_6^+$  have led to polymerization with HF elimination, and the resulting solid contains electron oxidized poly(*p*-phenylene) (7).

Thermally stable blue–green powders have been obtained by the oxidation of coronene with  $\text{O}_2\text{AsF}_6$ ,  $\text{C}_6\text{F}_6\text{AsF}_6$ , or  $\text{AsF}_5$ . IR spectra of these materials show the presence of the  $\text{AsF}_6^-$  ion in addition to the coronene-like cation. Gravimetry and elemental analyses indicate compositions ranging from  $(\text{C}_{24}\text{H}_{12})_{4.0}\text{AsF}_6$  to  $(\text{C}_{24}\text{H}_{12})_{0.25}\text{AsF}_6$ ; at least three crystallographically distinct phases are indicated. In the X-ray powder diffraction patterns of these solids very strong reflections with *d* spacings of about 3.3 Å suggest that the coronene species may be interplanar stacked in a platelike fashion. Crude resistance measurements on pellets of the polycrystalline powders indicate ambient-temperature conductivity for these salts in excess of  $1.0 \times 10^{-3} \Omega^{-1} \text{ cm}^{-1}$ .

### Experimental Details

The syntheses of cation salts of the monocyclic fluoroaromatic compounds and of octafluoronaphthalene have been described elsewhere (1–5). Manipulations of air- or moisture-sensitive materials were carried out in a Vacuum Atmospheres Dri-Lab or in a stainless steel vacuum line fitted with a Teflon FEP[poly(tetrafluoroethylene)] reaction vessel (Chemplast) or a fused silica reaction vessel.

**Reaction of Benzene with  $\text{O}_2\text{AsF}_6$ .** In a typical reaction, benzene (0.403 g, 5.16 mmol) was co-condensed at 77 K with sulfuryl chloride fluoride (8 mL) into a Teflon FEP reaction vessel containing  $\text{O}_2\text{AsF}_6$  (0.912 g, 4.13 mmol, prepared as in reference 8). On warming to 195 K, a green solution was obtained from which oxygen evolved steadily for a period of 15 min as the color faded. When the solvent and volatile products were removed at room temperature, a dark-brown solid (0.893 g) remained. The product was washed with liquid anhydrous hydrogen fluoride to remove  $(\text{C}_6\text{H}_5)_2\text{AsF}_2\text{AsF}_6$ , which was formed by the reaction of benzene with  $\text{AsF}_5$  present in the reaction mixture as a result of the thermal decomposition of  $\text{O}_2\text{AsF}_6$ . The resulting brown powder (0.182 g) was diamagnetic and had a room-temperature conductivity (pressed pellet) in excess of  $1.0 \times 10^{-2} \Omega^{-1} \text{ cm}^{-1}$ . The analysis was the following:  $[(\text{C}_6\text{H}_4)_n\text{AsF}_6]$ ,  $n = 4.05$ , based on the C/As ratio] C, H, As, F: calculated, 21.05; found, 22.07. The IR spectrum (Figure 1) of the powder contains absorptions due to oxidized poly(*p*-phenylene) (9) and the hexafluoroarsenate(V) ion.

**Reaction of Benzene with  $\text{C}_6\text{F}_6\text{AsF}_6$ .**  $\text{C}_6\text{F}_6\text{AsF}_6$  was prepared in situ by reacting  $\text{O}_2\text{AsF}_6$  (0.473 g, 2.14 mmol) with an excess of  $\text{C}_6\text{F}_6$  in  $\text{SO}_2\text{ClF}$  prior to the



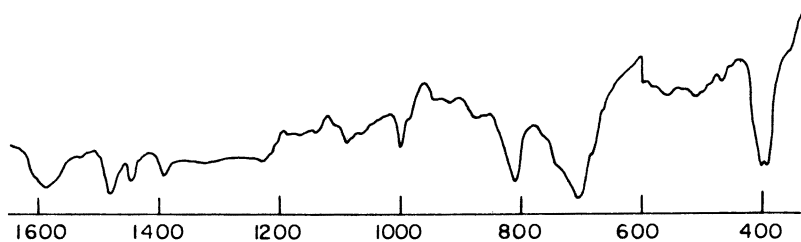


Figure 1. IR spectrum of oxidized poly(*p*-phenylene).

addition of benzene (0.323 g, 4.14 mmol). The reaction was complete in 1 h at 195 K. The product (0.546 g, 0.134 g after washing with HF) was identical to that produced from  $O_2AsF_6$ . Elemental analyses of samples from four preparations gave values for  $n$  ranging from 1.8 to 4.4. The C/H ratio varied from 3.6 to 4.4 in eight analyzed samples.

**The Reaction of Naphthalene with Excess  $AsF_5$ .** Naphthalene (0.20 g, 1.6 mmol) was dissolved in hexafluorobenzene (5 mL) in an evacuated Teflon reactor.  $AsF_5$  was admitted to the vessel at room temperature until a total pressure of 1 atm was attained. Copious amounts of a fluffy purple solid precipitated. The analysis was the following: C, 59.78; H, 2.81; and C/H ratio, 1.77. The solid was amorphous to X-rays.

In another experiment, a small amount of  $AsF_5$  was added slowly to a solution of naphthalene in  $CH_2Cl_2$  (mol ratio of  $AsF_5$  to  $C_{10}H_8$  was ca. 1:6). Above the surface of the solution, where an excess of  $AsF_5$  was present, the purple solid just described was formed. In the solution, however, a much darker, nearly black solid precipitated. Over a period of 1–2 h following removal of the solvent, both products became gray. No X-ray pattern could be obtained from these solids.

**Oxidation of Coronene with  $O_2AsF_6$ .**  $O_2AsF_6$  (0.342 g, 1.55 mmol) was placed in a Teflon FEP reaction vessel. A disk of Teflon filter paper was inserted above the solid, and coronene (0.464 g, 1.55 mmol) was placed on the filter. Sufficient  $SO_2ClF$  was condensed into the vessel to cover the coronene. At 195 K, the reaction proceeded slowly; it reached completion in 1 h. The vessel was allowed to warm to room temperature, and volatile products were removed under vacuum after 1 h. The product was a green, free-flowing powder. The analysis was the following:  $[(C_{24}H_{12})_{0.97}AsF_6]$  C, H. The IR spectrum of this solid (Figure 2) contains, in addition to bands similar to those in neutral coronene, characteristic absorptions at approximately 700 and 400  $cm^{-1}$  due to hexafluoroarsenate(V). The magnetic susceptibility was found to follow the Curie–Weiss law down to 12 K; the effective Weiss constant ( $\mu_{B,eff}$ ) = 0.36 and magnetic moment  $\theta = -1.8^\circ$ .

**Oxidation of Coronene with Excess  $C_6F_6AsF_6$ .**  $C_6F_6AsF_6$  was prepared in situ from  $O_2AsF_6$  (1.0 g, 4.5 mmol) in  $SO_2ClF$ . The reaction vessel was held at 77 K in a dry nitrogen-filled glovebag while coronene (0.15 g, 0.50 mmol) was added. The mixture was warmed to 195 K, and the reaction was allowed to proceed for 90 min. The product, obtained after removal of volatile compounds at room-temperature, was a dark-green friable powder. The analysis was the following:  $[(C_{24}H_{12})_{0.51}AsF_6]$  C, H. The IR spectrum of this solid (Figure 2c) is similar to the more coronene-rich

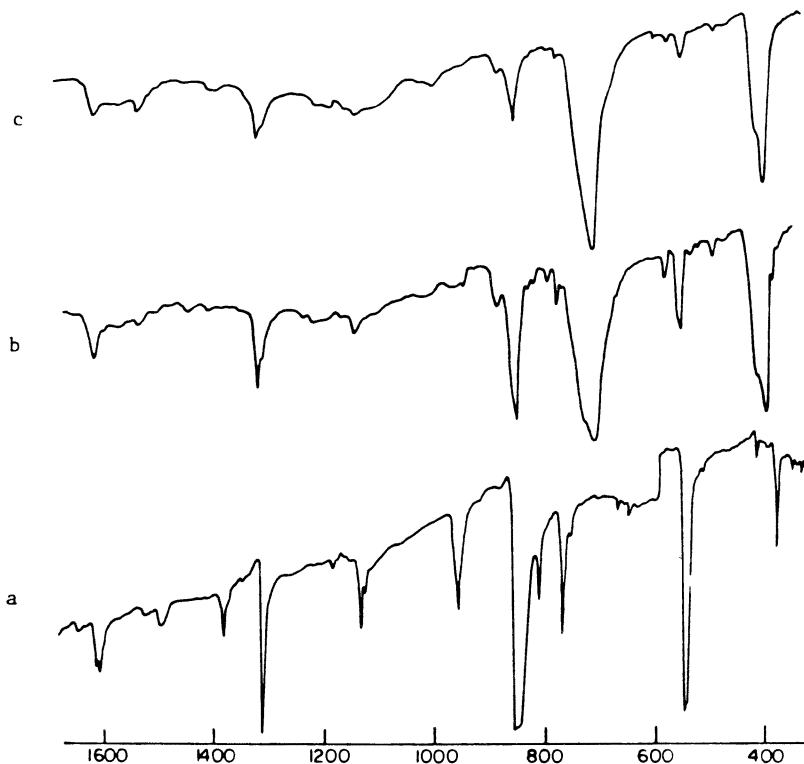


Figure 2. IR spectra of coronene and coronene salts. a: coronene; b:  $(C_{24}H_{12})_nAsF_6$ ,  $n = 0.97$ ; and c:  $(C_{24}H_{12})_nAsF_6$ ,  $n = 0.51$

material described earlier, but the absorptions due to  $AsF_6^-$  are relatively more intense. The magnetic susceptibility exhibits Curie-Weiss behavior down to 6 K;  $\mu_{B,ef} = 0.83$  and  $\theta = -5.9^\circ$ .

**Oxidation of Coronene with  $AsF_5$ .** Coronene reacted rapidly to give green and blue-green free-flowing powders upon exposure to gaseous  $AsF_5$  in a variety of solvents and at varying  $AsF_5$  partial pressures. Solvents used included sulfuric chloride fluoride, hexafluorobenzene, dichloromethane, trichlorofluoromethane, and 1,1,1-trichloro-2,2,2-trifluoroethane. Arsenic trifluoride was detected as a reaction product by IR spectroscopy. The color of the solid thus produced seems to be a qualitative measure of the extent of oxidation; the more highly oxidized materials were bluer than the coronene-rich solids. Product compositions were determined by gravimetry on the basis of the assumption that arsenic is present only as  $AsF_6^-$  and that coronene is present as neutral molecules or electron-oxidized cations. Observed mole ratios of coronene to hexafluoroarsenate varied widely (4.0–0.25); the smaller values were associated with the higher concentrations of  $AsF_5$ . Debye-Scherrer photographs of the polycrystalline powders (*see* box) show that the products

**X-ray Powder Diffraction Data (d-spacings) for Coronene Salts:  
(C<sub>24</sub>H<sub>12</sub>)<sub>n</sub> AsF<sub>6</sub>**

$$n = 0.51$$

10.92w, 9.52m, 8.63vw, 7.57ms, 6.96s, 6.53s, 6.10w, 5.64w, 5.28s,  
4.93m, 4.70m, 4.51vs, 4.44m, 3.98s, 3.52m, 3.33vs, 3.19w, 3.07vw,  
2.78m

$$n = 0.89$$

12.42mw, 10.89w, 8.54m, 7.09vs, 6.49m, 6.08m, 5.43s, 5.14m, 4.79w,  
4.58vvs, 4.36m, 4.17vw, 4.03m, 3.71vw, 3.54mw, 3.45mw, 3.35vs,  
3.21s, 3.01w, 2.87w, 2.15w, 1.65w

$$n = 1.88$$

14.37w, 10.86ms, 7.54vs, 7.04m, 6.54vs, 5.31vs, 4.94vs, 4.67w, 4.35s,  
4.19s, 4.02s, 3.72w, 3.61w, 3.50w, 3.32vvs, 3.16w, 2.33w, 1.66vw

$$n = 4.00$$

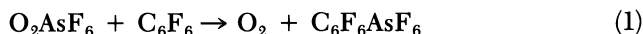
10.78w, 9.49s, 7.58vs, 6.47vs, 5.97vw, 5.25s, 5.11mw, 4.91w, 4.72w,  
4.35s, 3.95s, 3.51s, 3.43m, 3.31vs, 3.20w, 3.16w, 3.06m, 2.77w,  
2.66vw, 2.33m, 2.05vw, 1.96vw, 1.90w, 1.65vw, 1.47w

NOTE: w denotes weak, s denote strong, m denotes medium, v denotes very.

differ significantly over the composition range and that neutral coronene, if present, is incorporated into the structures and is not coexisting as a separate phase.

**Results and Discussion**

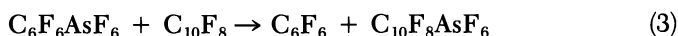
Chemical syntheses of radical-cation salts by electron oxidation of neutral aromatic precursors require powerful oxidizing agents and stabilizing anions with high ionization energies (*I*) (e.g., AsF<sub>6</sub><sup>-</sup>, ReF<sub>6</sub><sup>-</sup>, SbF<sub>6</sub><sup>-</sup>, and Sb<sub>2</sub>F<sub>11</sub><sup>-</sup>) (5). The stable salt of an aromatic cation of sufficient oxidizing strength can be employed as a synthetic reagent in the electron oxidation of other aromatic compounds with lower ionization energies. Thus, hexafluorobenzenehexafluoroarsenate(V), C<sub>6</sub>F<sub>6</sub>AsF<sub>6</sub>, provides a convenient one-electron oxidizing agent somewhat less energetic than the dioxygenyl salt from which it is most easily prepared (10) [*I*(O<sub>2</sub>) = 281 kcal/mol, and *I*(C<sub>6</sub>F<sub>6</sub>) = 230 kcal/mol]:



The reduction product is the relatively inert and volatile hexafluorobenzene molecule. Moreover,  $C_6F_6AsF_6$  decomposes at room temperature to volatile products (5):



This occurrence means that an oxidation can be carried out with an excess of  $C_6F_6AsF_6$ . The remaining oxidant is then allowed to decompose in situ at room temperature, and the volatile side products are removed under vacuum. This technique has been applied in the quantitative preparation of octafluoronaphthalenehexafluoroarsenate [ $I(C_{10}F_8) = 204$  kcal/mol]:



In the two fluoroaromatic cation salts, the cations appear to be well-separated from one another by the anions. In  $C_6F_6AsF_6$ , each ion is surrounded by eight nearest neighbors of opposite charge in a distorted CsCl-type lattice. In the case of  $C_{10}F_8AsF_6$ , although details of the structure are not yet known, the symmetry and unit-cell dimensions seem to preclude an arrangement involving coplanar stacks of cations.

Octafluoronaphthalenehexafluoroarsenate is exceptionally stable (decomposition occurs at 395 K), and in light of the report (6) of conductivity in  $(C_{10}H_8)_2PF_6$ , we sought to prepare the fluoro analogue of this "synthetic metal". However, despite repeated attempts using a variety of approaches, we did not obtain such a material. Metallic behavior in partially charged organic stacks derives from bonding interactions that occur as a consequence of overlapping of the highest occupied molecular orbitals (HOMOs) and singly occupied molecular orbitals (SOMOs) of the stacked ring systems. This overlapping requires that the planar aromatic species be closer together than their van der Waals thickness of about 3.3 Å, as has been observed in  $(C_{10}H_8)_2PF_6$ . Such a close juxtaposition of octafluoronaphthalene molecules, however, would also bring the electron-rich F ligands close together. This interaction is probably sufficiently strongly repulsive to offset the weak bonding interaction between the electron-oxidized and neutral aromatic rings. Attempts to prepare a bis(hexafluorobenzene)<sup>+</sup> salt were also unsuccessful.

$AsF_5$  is able to electron oxidize:



However, its oxidizing power is weaker than that of  $C_6F_6^+$ . In the case of benzene,  $AsF_5$  and  $C_6H_6$  react quantitatively in HF or  $SO_2ClF$  (10) to give the colorless crystalline solid  $(C_6H_5)_2AsF_2^+AsF_6^-$ :



With  $O_2^+$  or  $C_6F_6^+$ , however, benzene reacts to give poly(*p*-phenylene) derivatives. Although polymerization is never observed in the  $AsF_5$  reaction, some of the diphenylarsonium salt is always formed in the  $O_2^+$  and  $C_6F_6^+$  reactions because of the presence in the reaction mixture of  $AsF_5$  formed in the decomposition of the oxidizing agents. This finding suggests that the first step toward polymerization is electron oxidation of  $C_6H_6$  [ $I(C_6H_6) = 212$  kcal/mol] to  $C_6H_6^+$ , and that  $AsF_5$  is not able to achieve this oxidation:



Subsequent abstraction of  $H^+$  by the anion may also occur:

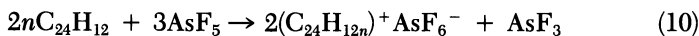
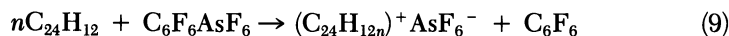
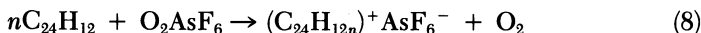


Such interpretations are consistent with the conclusions of other investigators as to the cationic nature of intermediates in the preparation of poly(*p*-phenylene) (11–12). As the number of fused or linked rings in a series of polynuclear aromatic molecules increases, the ionization energies of the neutral molecules decrease [ $I(\text{biphenyl}) = 183$  kcal/mol,  $I(\text{terphenyl}) = 181$  kcal/mol,  $I(\text{naphthalene}) = 187$  kcal/mol,  $I(\text{anthracene}) = 171$  kcal/mol,  $I(\text{naphthacene}) = 161$  kcal/mol].

The polymer that results when benzene is reacted with the powerful oxidizers  $O_2^+$  and  $C_6F_6^+$  is readily oxidized by  $AsF_5$  (13, 14). ( $AsF_5$ , although not capable of initiating the polymerization of benzene, can polymerize the more easily oxidized phenylene oligomers, including biphenyl).

Although the aromatic compounds undergo hydrogen elimination readily upon oxidation [benzene (15) and naphthalene (16) can be polymerized electrochemically; binaphthyl is formed in the thermal decomposition of bis(naphthalene)hexafluorophosphate], the analogous elimination of  $F^+$  in the fluoroaromatic compounds is not energetically feasible.

For large, planar, fused-ring systems, the tendency toward coplanar stacking gives rise to behavior similar to that observed for graphite intercalation compounds. Coronene is rapidly oxidized by  $O_2AsF_6$ ,  $C_6F_6AsF_6$ , or  $AsF_5$ :



The extent of oxidation and thus the observed stoichiometry vary widely in the materials prepared by the oxidation of coronene. The X-ray diffraction patterns of these solids are characteristic of the particular stoichiometries;

however, they have common features. The most striking common feature is the presence in each pattern of a strong reflection with a  $d$  spacing of about 3.3 Å, which is the thickness of a coronene molecule. This condition suggests the possibility that these materials are layered and that the anions occupy positions within and not between the layers.

H<sup>+</sup> elimination cannot be ruled out in the syntheses of the coronene derivatives just described, or for any other aromatic system. Although the materials reported here appear to be homogeneous and nonpolymeric, containing arsenic only as AsF<sub>6</sub><sup>-</sup>, the magnetic susceptibility data are not easily explained in terms of purely ionic formulations. The observed electrical conductivity may, therefore, be due either to stacking of the cations or to linking through HF elimination at the edges of the planar ring systems, or to a combination of the two. Thus, the structures adopted by these materials are strongly influenced by the extent of oxidation and the sizes and number of anionic species present.

### Acknowledgments

This work was supported by the Director, Office of Energy Research, Office of Basic Energy Sciences, Division of Chemical Sciences, U.S. Department of Energy, under Contract No. DEAC03-76SF00098.

### References

1. Richardson, T. J.; Bartlett, N. J. *Chem. Soc. Chem. Commun.* **1974**, 427-428.
2. Tanzella, F. L. Ph.D. Thesis, University of California at Berkeley, 1980.
3. Zuchner, K.; Richardson, T. J.; Glemser, O.; Bartlett, N. *Angew. Chem. Int. Ed. Engl.* **1980**, *19*, 944-945.
4. Richardson, T. J. Ph.D. Thesis, University of California at Berkeley, 1974.
5. Richardson, T. J.; Tanzella, F. L.; Bartlett, N. *J. Am. Chem. Soc.* **1986**, *108*, 4937-4943.
6. Fritz, H. P.; Gebauer, H.; Friedrich, P.; Schubert, U. *Angew. Chem. Int. Ed. Engl.* **1978**, *17*, 275-276.
7. Bartlett, N.; Biagioni, R. N.; McCarron, G.; McQuillan, B.; Tanzella, F., In *Molecular Metals*; Hatfield, W. E., Ed.; Plenum: New York, 1979; pp 293-299.
8. McKee, D. E.; Bartlett, N. *Inorg. Chem.* **1973**, *12*, 2738.
9. Tanzella, F. L.; Bartlett, N. *Z. Naturforscher* **1981**, *36b*, 1461-1464.
10. *Ionization Potential and Appearance Potential Measurements 1971-1981*; U. S. Govt. Printing Office: Washington, DC, 1982; (NSRDS-NBS 71).
11. Hsing, C.-F.; Kovacic, P.; Khoury, I. A. *J. Polymer Sci., Polymer Chem. Ed.* **1983**, *21*, 457-466.
12. Milosevich, S. A.; Saichek, K.; Hinchey, L.; England, W. B.; Kovacic, P. *J. Am. Chem. Soc.* **1983**, *105*, 1088-1090.
13. Shacklette, L. W.; Eckhardt, H.; Chance, R. R.; Miller, G. G.; Ivory, D. M.; Baughman, R. H. *J. Chem. Phys.* **1980**, *73*, 4098-4102.
14. Eckhardt, H.; Miller, G. G.; Baughman, R. H. *Synth. Met.* **1984**, *9*, 441-450.
15. Rubinstein, I. *J. Electrochem. Soc.* **1983**, *130*, 1506-1509.
16. Satoh, M.; Uesugi, F.; Tabata, M.; Kaneto, K.; Yoshino, K. *J. Chem. Soc., Chem. Commun.* **1986**, 550-551.

RECEIVED for review September 29, 1986. ACCEPTED February 12, 1987.

# Radical-Cation Salts of Arenes

## A New Family of Organic Metals

V. Enkelmann

Max-Planck-Institut für Polymerforschung, Welder-Weg 11, D-6500 Mainz,  
Federal Republic of Germany

*Stable radical-cation salts of a variety of simple arenes can be prepared by anodic oxidation in the presence of suitable counterions, for example,  $\text{ClO}_4^-$ ,  $\text{BF}_4^-$ ,  $\text{PF}_6^-$ ,  $\text{AsF}_6^-$ , and  $\text{SbF}_6^-$ . These highly conducting crystals of the composition  $\text{Ar}_{2-y}^{+\cdot}\text{X}^-$  (where  $\text{Ar}_{2-y}^{+\cdot}$  is a radical cation of 2-Y aromatic hydrocarbons and  $\text{X}^-$  is an anion), which are deposited on the anode during the electrocrystallization as shiny black needles, can be considered as a new family of organic metals built up from simple, easily obtainable building blocks. The packing found between the aromatic rings in the radical-cation salts can be regarded as a model for interchain interactions in conducting polymers, for example, doped polyacetylene and poly(p-phenylene).*

### Electrocrystallization

Stable radical-cation salts of many aromatic hydrocarbons (Ar) can be prepared by anodic oxidation of a solution in  $\text{CH}_2\text{Cl}_2$ , tetrahydrofuran (THF), chlorobenzene, or  $\text{CH}_2\text{ClCHCl}_2$  in the presence of a suitable supporting electrolyte, for example,  $(\text{NBu}_4)^+\text{X}^-$ , where  $\text{NBu}_4$  is tetra-*n*-butylammonium and  $\text{X}^-$  is  $\text{ClO}_4^-$ ,  $\text{BF}_4^-$ ,  $\text{PF}_6^-$ ,  $\text{AsF}_6^-$ , or  $\text{SbF}_6^-$  (1-5). As shown in Figure 1, crystals form directly on the anode, which can be various shapes, sizes, and materials (e.g., Pt, Au, Ni, Cu, Ge, or graphite). The electrochemical processes that lead to crystal growth can be split into three independent main reactions (3, 6):





The key reaction of these three is the dimerization (reaction 2) in which the short-lived intermediate monomer radical cation is stabilized. The equilibrium constant ( $K_1$ ) of this reaction determines not only the stability of the reactive intermediates but also the kinetics of crystal growth and the composition of the crystals.

Fluoranthene (FA) is one example in which  $K_1$  is very high. In this case, under all experimental conditions tested so far, crystals of the ideal composition  $\text{Ar}_2\text{X}$  are always obtained. This situation is not the case with pyrene (Py), perylene, and many other arenes. Depending on the solvent, temperature, counterion, applied voltage, and current density, a variety of different complexes are formed. A number of well-characterized radical-cation salts are listed in Table I as well as some details of the experimental conditions. Inspection of this table shows that if the composition deviates from  $\text{Ar}_2\text{X}$ , the arene-to-counterion ratio is always  $<2:1$ . In some cases, for example,  $\text{Py}_7\text{Py}_4\text{X}_4(\text{CH}_2\text{Cl}_2)_4$ , additional rings that are not part of the con-

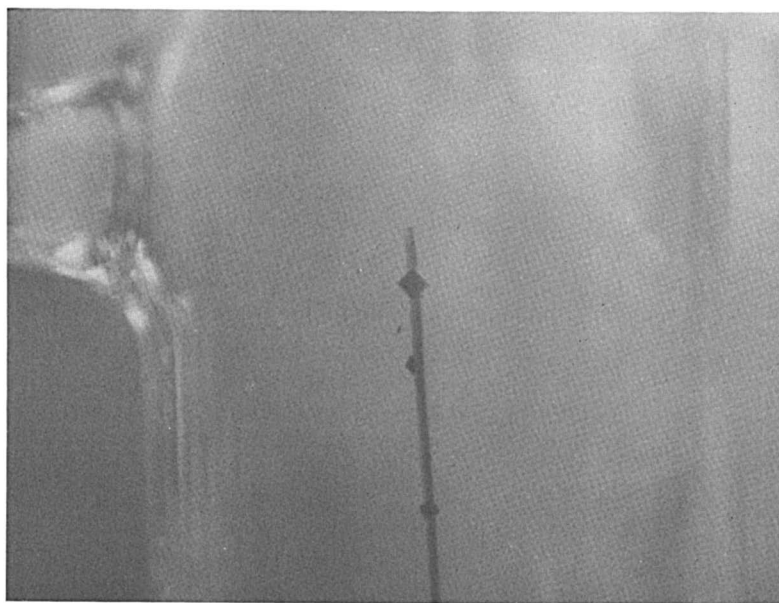


Figure 1. Crystals of the radical-cation salt of 2,6-dimethylnaphthalene (DMN),  $\text{DMN}_3(\text{SbF}_6)_2(\text{CH}_2\text{Cl}_2)$ , on the anode during electrocrystallization.



ductive stack but fill empty space between the counterions are incorporated into the structure. In the example just given, four pyrene rings that carry no charge are oriented approximately perpendicularly to the stack (c.f. Figure 7). The assumption can be made that these additional rings do not take part in the complex formation; thus, in terms of the discussion regarding the equilibrium (reaction 2), the arene-to-counterion ratio is 7:4. This condition implies that in these systems, a certain fraction of monomer radical cations was incorporated into the structure before the radical cations were able to dimerize. Studies (7, 8) have shown that perylene and pyrene, for which this effect is most pronounced, are cases in which  $K_1$  is small. In some other cases, the solvent or neutral arenes are found in the structure and thus lead to very complex stoichiometries and crystal structures.

The stability of radical-cation salts varies from rapid decomposition in air (e.g., naphthalene salts) to stability for several months under ambient conditions (e.g., perylene and decacyclene salts). The stability correlates with the oxidation potential: As a rule of thumb, salts of extended aromatic systems are more stable than those of smaller ones, and salts of the ideal 2:1 composition are more stable than those of other compositions.

### *Structural Principles of Radical-Cation Salts*

**Structure and Phase Transitions of Fluoranthene Salts.** As mentioned earlier, the electrocrystallization of fluoranthene is characterized by a rapid and complete dimerization to the dimer radical cation  $FA_2^{*+}$ ; thus, under all experimental conditions tested so far, only crystals of the ideal composition  $FA_2X$  are formed (3, 4). By using these relatively simple structures, common structural principles and phase transitions that are typical for all radical-cation salts can be investigated.

All radical-cation salts crystallize in columnar structures. The aromatic rings are packed in stacks that are arranged in a pseudo-hexagonal or pseudotetragonal fashion, which allows for channels in which the counterions are located. In more complex cases, other molecules, such as solvent molecules, are also located in the channels. Anions of different sizes can be incorporated in these channels without causing much change in the packing; thus, in many cases, salts containing different anions are isostructural.

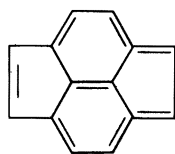
The crystal structure of  $FA_2AsF_6$  is shown in two projections in Figure 2. The planes of the rings are oriented perpendicularly to the stacking axis, and the rings are packed with very short interplanar spacings of 3.2–3.3 Å. Among the most fascinating features of the radical-cation salts are the unusual overlap patterns that result from this packing. In  $FA_2X$ , the rings are alternately rotated by 180°. Because the rings are oriented perpendicularly to the stacking direction, some interatomic distances range between 3.2 and 3.3 Å; these distances are substantially smaller than the van der Waals radius

Table I. Conditions of the Electrocrystallization and Composition of Radical-Cation Salts of Arenes

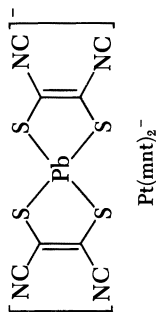
Arene	X <sup>-</sup>	Solvent	Temperature (°C)	Composition	Reference
Naphthalene	PF <sub>6</sub> <sup>-</sup>	CH <sub>2</sub> Cl <sub>2</sub>	-60	naphth <sub>2</sub> X	2
	AsF <sub>6</sub> <sup>-</sup>				
Fluoranthene	PF <sub>6</sub> <sup>-</sup>	CH <sub>2</sub> Cl <sub>2</sub>	-30	FA <sub>2</sub> X	3, 4
	AsF <sub>6</sub> <sup>-</sup>	CHCl <sub>2</sub> CH <sub>2</sub> Cl			
	SbF <sub>6</sub> <sup>-</sup>	THF			
	ClO <sub>4</sub> <sup>-</sup>	CH <sub>3</sub> COOCH <sub>3</sub>			
Pyrene	PF <sub>6</sub> <sup>-</sup>	CH <sub>2</sub> Cl <sub>2</sub>	0	Py <sub>7</sub> Py <sub>4</sub> X <sub>4</sub> (CH <sub>2</sub> Cl <sub>2</sub> ) <sub>4</sub>	7
	AsF <sub>6</sub> <sup>-</sup>				
Isopyrene 2,6-Dimethyl- naphthalene Terphenyl Quaterphenyl Decacycene	SbF <sub>6</sub> <sup>-</sup>	CH <sub>2</sub> Cl <sub>2</sub>	0	Py <sub>12</sub> (SbF <sub>6</sub> ) <sub>7</sub>	7
	AsF <sub>6</sub> <sup>-</sup>	CHCl <sub>2</sub> CH <sub>2</sub> Cl	0	Py <sub>2</sub> AsF <sub>6</sub>	7
	ClO <sub>4</sub> <sup>-</sup>	CH <sub>2</sub> Cl <sub>2</sub> , THF	20	Py <sub>2</sub> ClO <sub>4</sub> (?)	1
	AsF <sub>6</sub> <sup>-</sup>	CH <sub>2</sub> Cl <sub>2</sub> /CHCl <sub>2</sub> CH <sub>2</sub> Cl	20	Py <sub>12</sub> (AsF <sub>6</sub> ) <sub>10</sub>	8
	SbF <sub>6</sub> <sup>-</sup>	CH <sub>2</sub> Cl <sub>2</sub>	0	Py <sub>7</sub> Py <sub>4</sub> (SbF <sub>6</sub> ) <sub>4</sub> (CH <sub>2</sub> Cl <sub>2</sub> ) <sub>4</sub>	8
	SbF <sub>6</sub> <sup>-</sup>	CH <sub>2</sub> Cl <sub>2</sub>	20	<i>i</i> -Py <sub>2</sub> SbF <sub>6</sub>	8
	AsF <sub>6</sub> <sup>-</sup>	CH <sub>2</sub> Cl <sub>2</sub>	-50	DMN <sub>3</sub> X <sub>2</sub> (CH <sub>2</sub> Cl <sub>2</sub> )	9
	SbF <sub>6</sub> <sup>-</sup>	CH <sub>2</sub> Cl <sub>2</sub>	-10	TP <sub>3</sub> TP(SbF <sub>6</sub> ) <sub>3</sub>	10, 11
	SbF <sub>6</sub> <sup>-</sup>	CH <sub>2</sub> Cl <sub>2</sub>	-10	QP <sub>3</sub> QP(SbF <sub>6</sub> ) <sub>3</sub>	10, 11
	AsF <sub>6</sub> <sup>-</sup>	CH <sub>2</sub> Cl <sub>2</sub> /TCB	20	DZ <sub>3</sub> (AsF <sub>6</sub> ) <sub>2</sub>	7

Triphenylene	AsF <sub>6</sub> <sup>-</sup> PF <sub>6</sub> <sup>-</sup> PF <sub>6</sub> <sup>-</sup>	CH <sub>2</sub> Cl <sub>2</sub>	0	TPh <sub>2</sub> X	7
Perylene	AsF <sub>6</sub> <sup>-</sup> SbF <sub>6</sub> <sup>-</sup>	CH <sub>2</sub> Cl <sub>2</sub>	20	Pe <sub>2</sub> (PF <sub>6</sub> ) <sub>1.11</sub> (CH <sub>2</sub> Cl <sub>2</sub> ) <sub>0.8</sub> Pe <sub>2</sub> (AsF <sub>6</sub> ) <sub>1.11</sub> (CH <sub>2</sub> Cl <sub>2</sub> ) <sub>0.7</sub>	5
	PF <sub>6</sub> <sup>-</sup> AsF <sub>6</sub> <sup>-</sup> SbF <sub>6</sub> <sup>-</sup>	THF	20	Pe <sub>2</sub> (SbF <sub>6</sub> ) <sub>2</sub> (CH <sub>2</sub> Cl <sub>2</sub> ) <sub>0.75</sub> Pe <sub>2</sub> (PF <sub>6</sub> ) <sub>1.4</sub> (THF) <sub>0.6</sub> Pe <sub>2</sub> (AsF <sub>6</sub> ) <sub>1.5</sub> (THF) <sub>0.5</sub>	5
	AsF <sub>6</sub> <sup>-</sup> AsF <sub>6</sub> <sup>-</sup>	CHCl <sub>2</sub> CH <sub>2</sub> Cl-TCB	20	Pe <sub>2</sub> (AsF <sub>6</sub> ) <sub>1.43</sub>	7
	Pt(mnt) <sub>2</sub>	CH <sub>2</sub> Cl <sub>2</sub>	20	Pe <sub>2</sub> [Pt(mnt) <sub>2</sub> ]	12, 13
	ClO <sub>4</sub> <sup>-</sup> ClO <sub>4</sub> <sup>-</sup>	THF	20	Pe <sub>2</sub> Fe <sub>4</sub> ClO <sub>4</sub>	14
	PF <sub>6</sub> <sup>-</sup>	THF	20	Pe <sub>2</sub> FeClO <sub>4</sub>	14
		THF	20	Pe <sub>4</sub> Pe <sub>3</sub> (ClO <sub>4</sub> ) <sub>3</sub> (THF) <sub>2</sub>	

NOTE: Naphth is naphthalene, *i*-Py is isopyrene, DMN is 2,6-dimethylnaphthalene, TP is terphenyl, QP is quaterphenyl, DZ is decaacylene, TPh is triphenylene, Pe is perylene, TCB is 1,2,4-trichlorobenzene. Also,



isopyrene



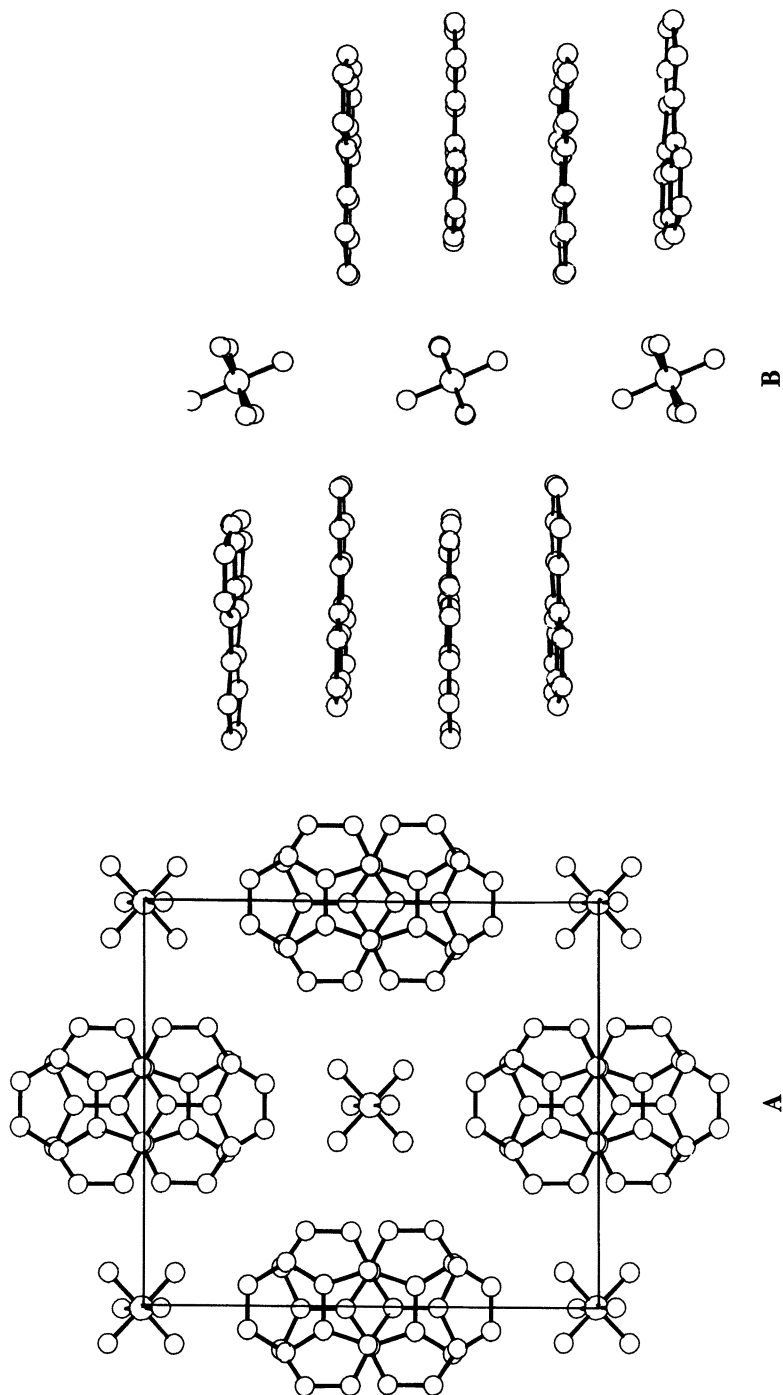


Figure 2. Crystal structure of  $FA_2AsF_6$  at 300 K. A: Projection in the stacking direction, and B: projection perpendicular to the stacks.

of 3.6 Å. The angle of rotation ( $\psi$ ) between neighboring rings is typical for each arene. For example, naphthalene forms columns with  $\psi = 90^\circ$ ; in pyrene radical-cation salts,  $\psi = 0, 60, \text{ and } 90^\circ$ . The number of short interplanar atom contacts is optimized by the choice of  $\psi$ .

Because of crystal symmetry in  $\text{FA}_2\text{X}$ , all rings are identical; that is, the radical-cation charge is delocalized along the stack. In this direction, the highest conductivity is observed.

In most radical-cation salts, structural phase transitions near 200 K are observed. Investigation of these transitions demonstrates the large effect of the geometry of the molecular overlap on the electrical and magnetic properties. The structural changes during the phase transition in  $\text{FA}_2\text{X}$  have been worked out in detail (4). Projections of the crystal structures of  $\text{FA}_2\text{AsF}_6$  at 300 and 120 K are shown in Figure 3. In the high-temperature phase (space group  $A2/m$ ), the fluoranthene rings are located on mirror planes. At the phase transition, the space group changes to  $P2_1/c$ ; thus, the constraint on the molecular orientation vanishes, and both stacks and counterions are free to rotate from the high-temperature orientation. The phase transition can be monitored in X-ray diffraction experiments by the appearance of reflections that are symmetry forbidden in the high-temperature phase. The appearance of these reflections is well-correlated with a change from metallic to semiconducting behavior and anomalies in the magnetic properties. However, at the phase transition temperature, a distortion perpendicular to the stack is observed; this dimerization is not in the stacking direction, as is the case for phase transitions of many other organic metals (Peierls transition). Even at room temperature, a small dimerization in the stacking direction is observed and is virtually retained in the whole temperature range without any anomaly (Figure 4). Hence, this small dimerization cannot be the reason for the metal-insulator transition.

In addition to the rotation of stacks and anions, a small distortion of the molecular overlap occurs during the transition. As seen in Figure 5, the mirror plane causes the overlap in the high-temperature phase to be strictly symmetrical. At the transition, this constraint vanishes, and a small distortion ( $\sim 0.05 \text{ \AA}$ ) perpendicular to the stacking axis is observed. Apparently, this distortion is responsible for the metal-insulator transition.

**Polymorphism in Pyrene Radical-Cation Salts.** In contrast with fluoranthene, a variety of different pyrene salts can be grown by only minor changes in the conditions of the electrocrystallization (cf. Table I). This situation offers the possibility to study the influence of the interstack interactions without changing the building elements. If pyrene is electrocrystallized in  $\text{CH}_2\text{Cl}_2$  in the presence of  $\text{PF}_6^- \text{ AsF}_6^-$ , isostructural shiny black needles of the composition  $\text{Py}_7\text{Py}_4\text{X}_4(\text{CH}_2\text{Cl}_2)_4$  are obtained. When  $\text{SbF}_6^-$  anions are used, salts of different compositions and structures can be isolated.  $\text{Py}_7\text{Py}_4(\text{SbF}_6)_4(\text{CH}_2\text{Cl}_2)_4$  is not isostructural with the  $\text{AsF}_6^-$  and  $\text{PF}_6^-$  salts

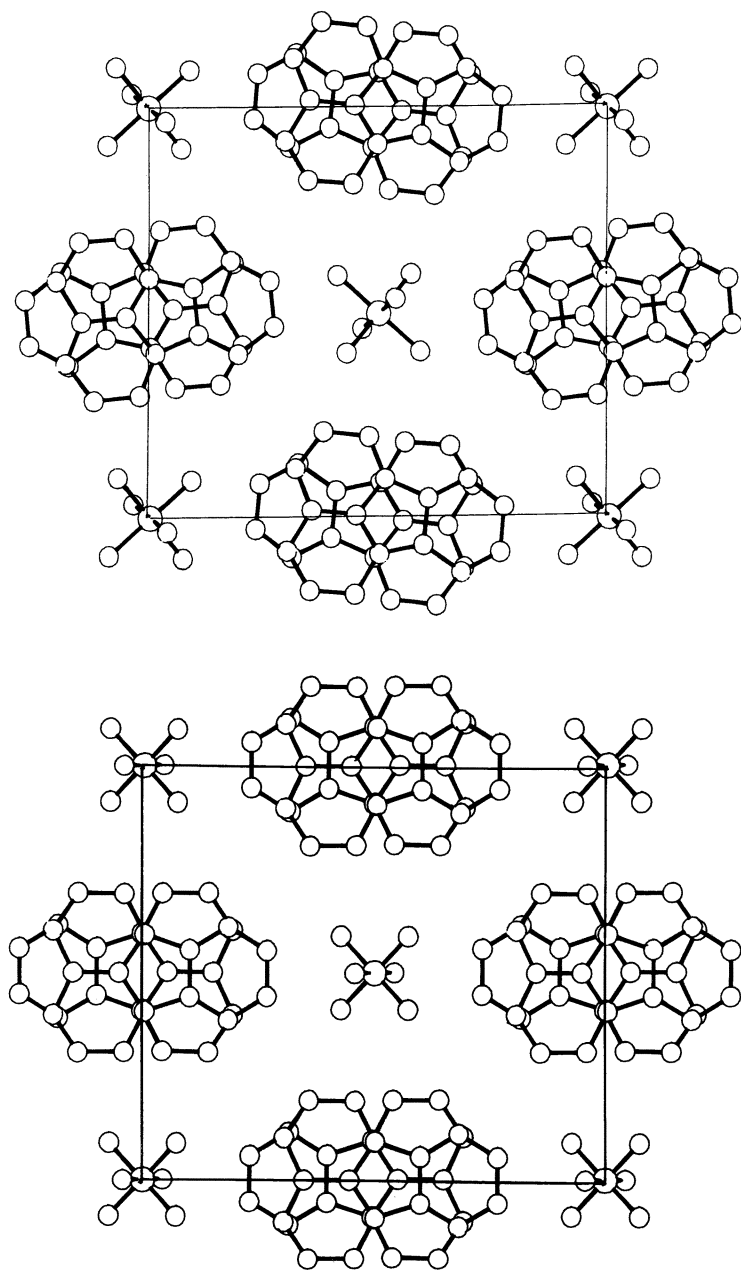


Figure 3. Projection of the crystal structure of  $F_2AsF_6$  on the  $bc$  plane above (left) and below (right) at 120 K the phase transition.

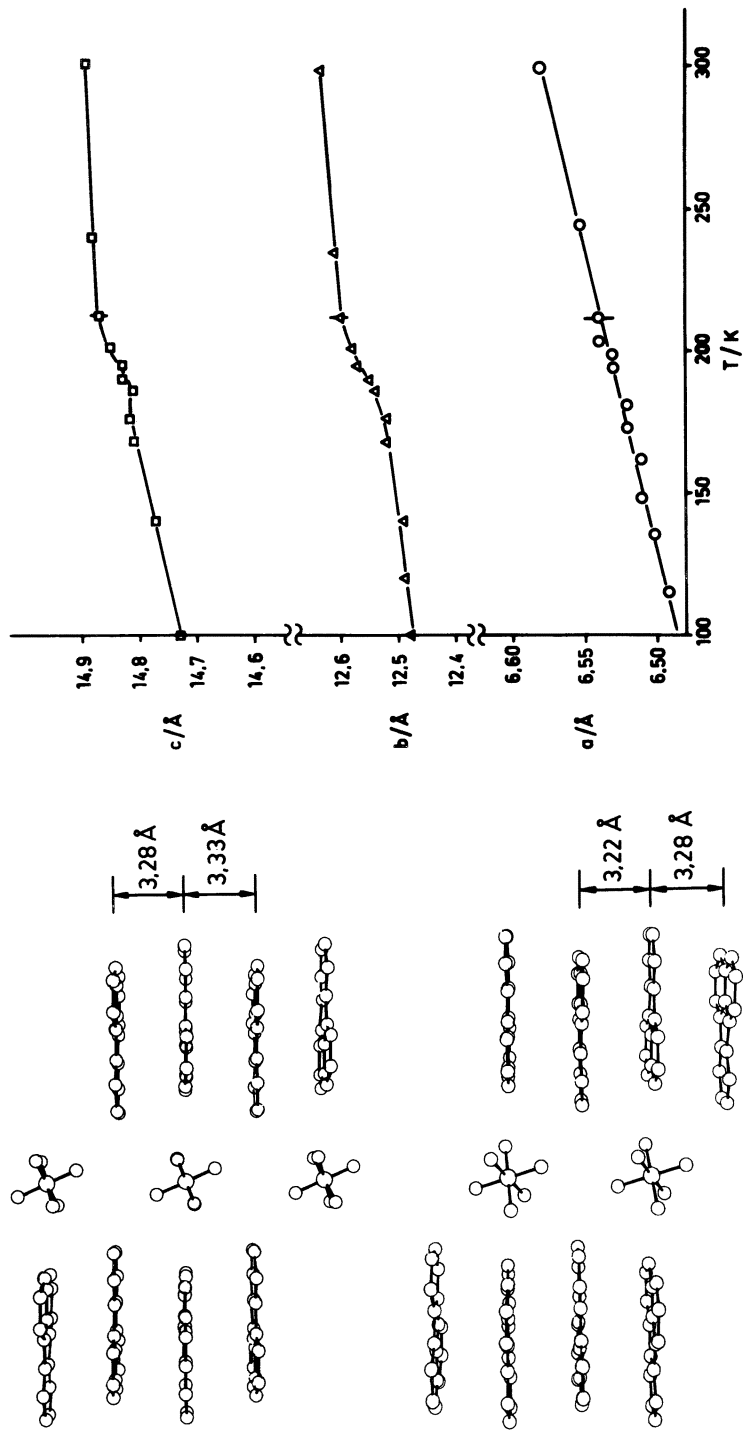


Figure 4. left: Projection of the crystal structure of  $FA_3AsF_6$  perpendicular to the stacks at 300 K (top) and 120 K (bottom), and right: temperature dependence of the lattice parameters of  $FA_3AsF_6$ .

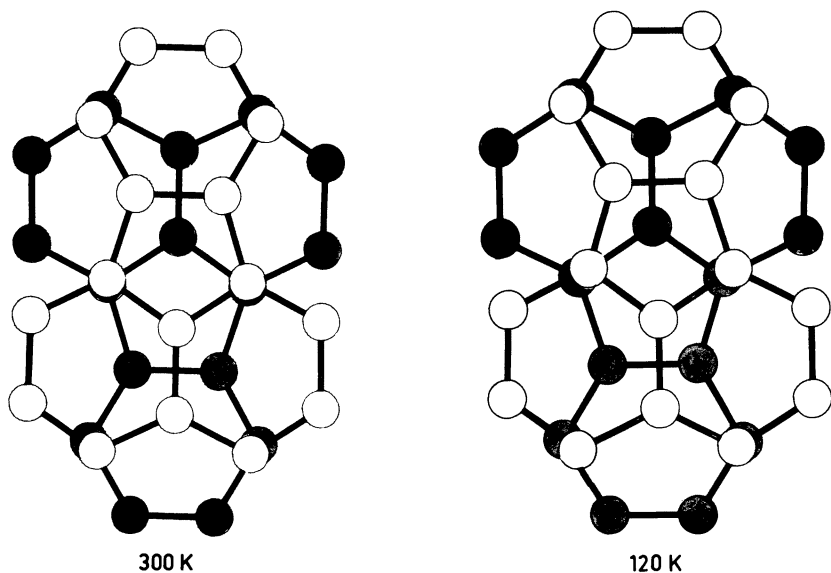


Figure 5. Molecular overlap in  $FA_2AsF_6$ .

and  $Py_{12}(SbF_6)_7$ . If a solvent such as  $CHCl_2CH_2Cl$  is used, which is too large to be incorporated into the structure, crystals of the ideal composition  $Py_2AsF_6$  and tetragonal  $Py_{19}(AsF_6)_{10}$  can be obtained. I have not been able to reproduce the work of Chiang et al. (1), who reported the preparation of  $Py_2ClO_4$ . In addition, the density given does not correspond to the density calculated from the lattice parameters; thus, the composition is probably  $Py_2ClO_4 \cdot \frac{1}{2}THF$ . Pertinent crystallographic data for the pyrene salts are given in Table II.

Rotation photographs taken along the stacking axes of three pyrene radical-cation salts are shown in Figure 6. Apart from the different lengths of the stacking axes, these photographs show as a common feature intense layer lines with a spacing of  $3.35 \text{ \AA}$ . This value corresponds to the average interplanar spacings. In  $Py_{12}(SbF_6)_7$ , two sets of intense layer lines are found for which the indexes are multiples of 6 and 7. Apart from small satellites, the other reflections are almost completely missing. This crystal structure can be described as being built up by two sublattices of the cations and anions, which are commensurate only after 12 periods of the cations and seven periods of the anions.  $Py_{19}(AsF_6)_{10}$  gives similar, even more complex scattering diagrams, which are not shown in Figure 6. These, to a first approximation, look like a modulated structure of  $Py_2AsF_6$  with weak satellite reflections on the 1st, 9th, 11th, 19th, and 21st layer lines near the intense ones.

The crystal structure of  $Py_7Py_4(AsF_6)_4(CH_2Cl_2)_4$  has been solved. Pro-



Table II. Crystallographic Data of Pyrene Radical-Cation Salts

Compound	a (Å)	b (Å)	c (Å)	$\alpha$ (°)	$\beta$ (°)	$\gamma$ (°)	Space Group	$D_x$ (g/cm <sup>3</sup> )
Py <sub>7</sub> Py <sub>4</sub> (PF <sub>6</sub> ) <sub>4</sub> (CH <sub>2</sub> Cl) <sub>2/4</sub>	23.66 (4)	21.01 (4)	14.73 (2)	92.9 (3)	85.9 (3)	90.9 (3)	I1	1.44
Py <sub>7</sub> <sup>a</sup>	16.993 (4)	17.140 (4)	14.680 (3)	113.67 (2)	110.98 (2)	75.97 (2)	P1	1.51
Py <sub>4</sub> (AsF <sub>6</sub> ) <sub>4</sub> (CH <sub>2</sub> Cl) <sub>4</sub>	40.34 (4)	14.36 (3)	13.70 (3)		103.0 (3)		A2/m	1.75
Py <sub>12</sub> (SbF <sub>6</sub> ) <sub>7</sub>	19.58 (3)	18.59 (2)	6.73 (1)				P2 <sub>1</sub> 2 <sub>1</sub> 2	1.61
Py <sub>2</sub> AsF <sub>6</sub>	17.78	12.92	11.42		98.4		P2/n	1.29 <sup>c</sup>
Py <sub>2</sub> ClO <sub>4</sub>	13.46 (1)		64.18 (4)				tetragonal	1.64
Py <sub>19</sub> (AsF <sub>6</sub> ) <sub>10</sub>	25.989 (7)	23.750 (18)	12.768 (2)	89.51 (3)	109.31 (2)	91.08 (4)	C1	1.57
Py <sub>4</sub> (SbF <sub>6</sub> ) <sub>4</sub> (CH <sub>2</sub> Cl) <sub>4</sub>								

NOTE: The values in parentheses are the estimated standard deviation.

<sup>a</sup>The experimental density given by Chiang et al. (1) (1.37 g/cm<sup>3</sup>) does not correspond to the density calculated for Py<sub>2</sub>ClO<sub>4</sub>. For Py<sub>2</sub>ClO<sub>4</sub>·½THF, a density of 1.38 g/cm<sup>3</sup> was calculated.

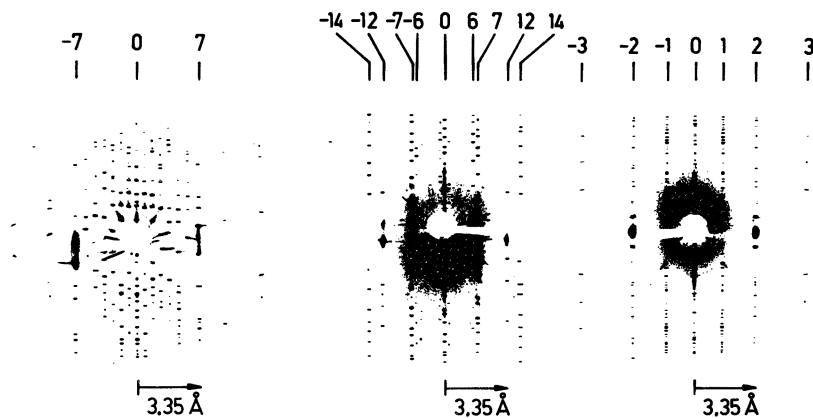


Figure 6. Rotation photographs for  $\text{Py}_7\text{Py}_4(\text{AsF}_6)_4(\text{CH}_2\text{Cl}_2)_4$  (left),  $\text{Py}_{12}(\text{SbF}_6)_7$  (middle), and  $\text{Py}_2\text{AsF}_6$  (right).

jections along and perpendicular to the stacking direction are shown in Figure 7. They reveal a variation of the structural principle just discussed. Here, the stack consists of seven rings that are oriented along the (111) body diagonal of the triclinic unit cell given in Table II. The stacking direction corresponds to the needle axis (the  $a$  axis of the body-centered isostructural cell is given for the  $\text{PF}_6^-$  salt). As in  $\text{FA}_2\text{X}$ , the stacks are packed parallel to each other in a pseudo-hexagonal way. However, as a variation to the structural principle, they are separated not only by the anions but also by additional pyrene rings that are not part of the stack and by solvent molecules. One of the pyrene rings (Py1) is located on a symmetry center and is disordered; that is, two orientations are statistically occupied.

Again, the molecular overlap pattern is one of the most interesting features of the pyrene salts. In  $\text{Py}_7\text{Py}_4\text{X}_4(\text{CH}_2\text{Cl}_2)_4$ , two different relative orientations with  $\psi = 60^\circ$  (type 1) and  $\psi = 0^\circ$  (type 2) are observed (Figure 8). The stacking distances, which range from 3.26 to 3.51 Å, are well-correlated with the overlap type. Type 1 (e.g., Py2–Py3 and Py3–Py4) is connected with small distances. The distance for molecules with type-2 overlap (e.g., Py4–Py4'; 3.51 Å) compares well with the distance found for the dimers in the pyrene crystal structure (3.53 Å); these dimers are packed in a similar way. Finally, the contact between disordered Py1, Py1', and Py2 can be considered a mixture of both types and consequently has almost exactly the average spacing of the two extremes.

Because of the large unit cells and the limited stabilities of some pyrene salts, analyses of more complex phases and phase transitions are time-consuming and complicated tasks and are still in progress. However, knowledge of the space groups allows the conclusion of at least one more overlap with  $\psi = 90^\circ$ .  $\text{Py}_{12}(\text{SbF}_6)_7$  crystallizes in the same space group ( $A2/m$ ) as  $\text{FA}_2\text{X}$

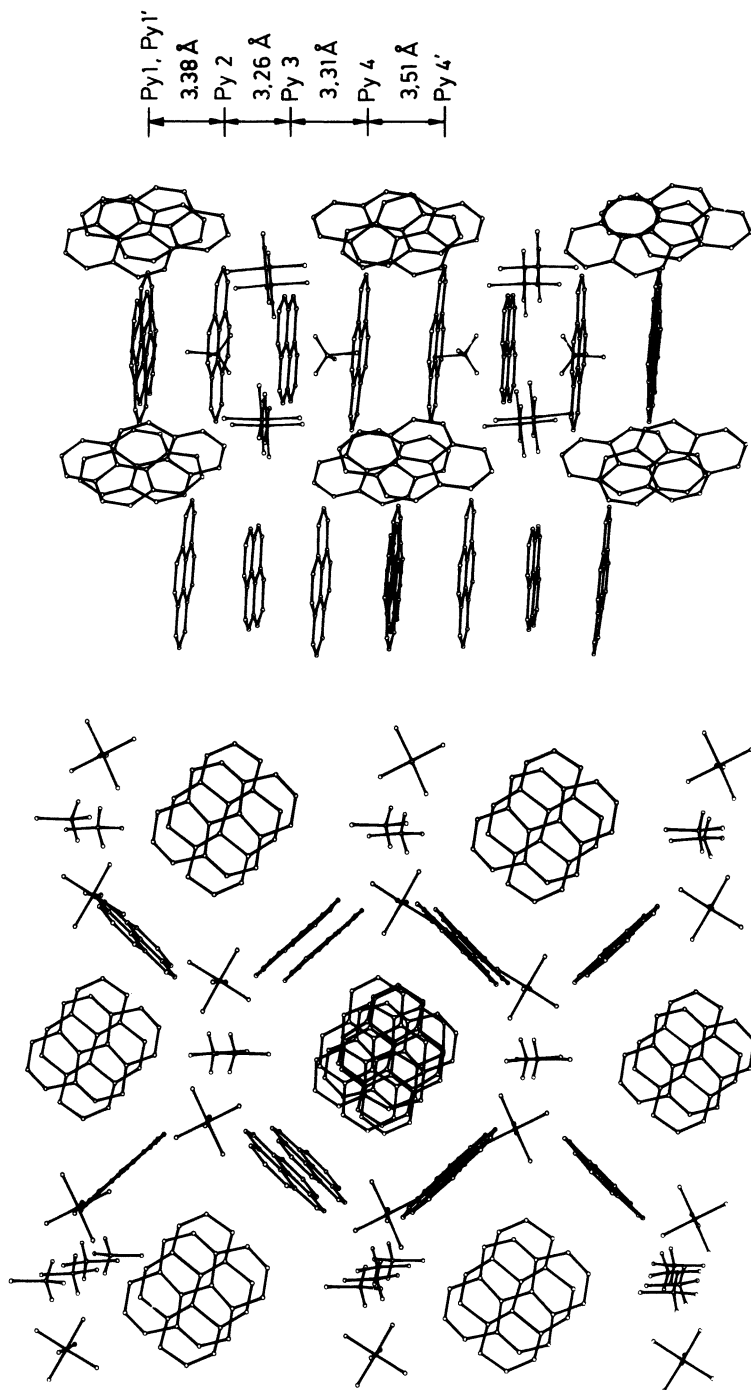
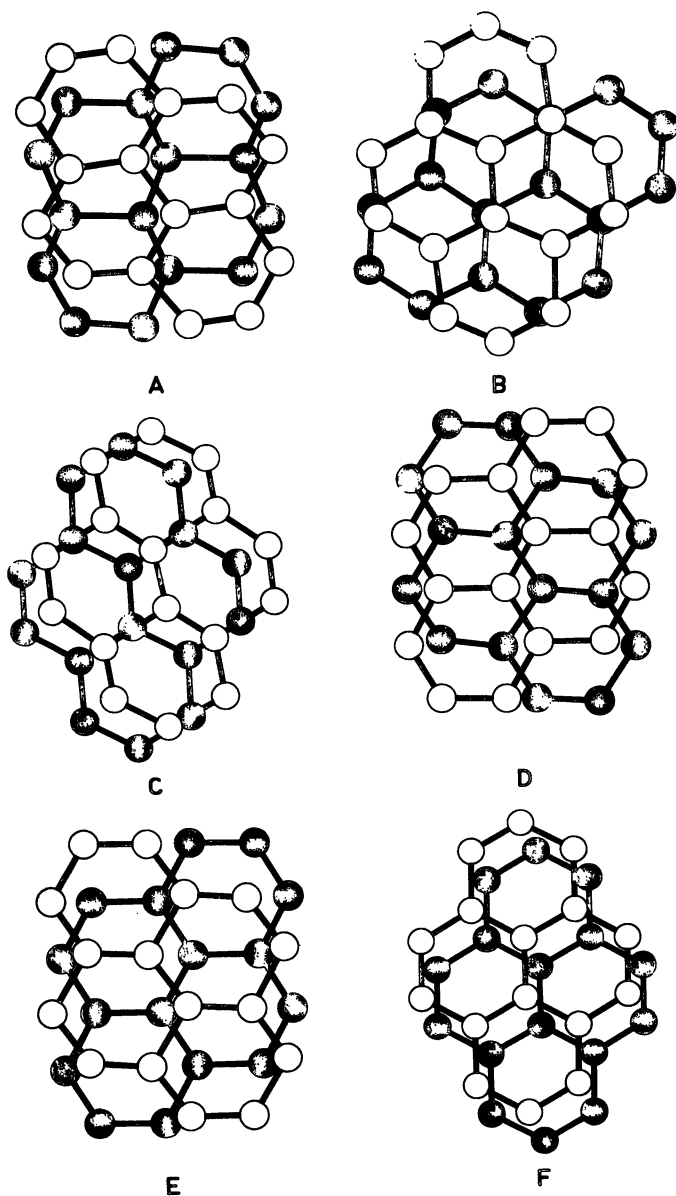


Figure 7. Crystal structure of  $\text{Py}_7\text{-Py}_4(\text{AsF}_6)_4(\text{CH}_2\text{Cl}_2)_4$ . Left: Projection in the stacking direction, and right: projection perpendicular to the stacks.



**Figure 8.** Molecular overlaps in  $\text{Py}_7\text{Py}_4(\text{AsF}_6)_4(\text{CH}_2\text{Cl}_2)_4$ . A: disordered  $\text{Py}_1\text{-Py}_1'$ , B:  $\text{Py}_1\text{-Py}_2$ , C:  $\text{Py}_1'\text{-Py}_2$ , D:  $\text{Py}_2\text{-Py}_3$ , E:  $\text{Py}_3\text{-Py}_4$ , and F:  $\text{Py}_4\text{-Py}_4'$ .

with similar  $b$  and  $c$  lattice parameters. For pyrene rings located on mirror planes, only overlaps with  $\psi = 0^\circ$  and  $\psi = 90^\circ$  are possible. However, the translation between the rings and the order in which contacts of type 2 and 3 will occur in the stack cannot be predicted.

A projection of  $\text{Py}_2\text{AsF}_6$  is shown in Figure 9. It consists of two independent stacks with different setting angles but identical overlap (type 1). Because the crystal exhibits polysynthetic twinning, a full crystal structural analysis has not been undertaken. Preliminary data indicate that in a phase transition, both stacks become identical; that is, the structure is face-centered in the low-temperature phase. This conclusion is supported by electron spin resonance (ESR) data.

**Radical-Cation Salt of 2,6-Dimethylnaphthalene.** Because of their columnar structures, the radical-cation salts discussed so far can be described as one-dimensional systems. The rapid spin exchange and high carrier mobility are oriented in the stacking direction. Anisotropies larger than 100 have been reported for  $\text{FA}_2\text{X}$  (15). The salt of 2,6-dimethylnaphthalene (DMN),  $\text{DMN}_3(\text{SbF}_6)_2(\text{CH}_2\text{Cl}_2)$ , is the first example in which the structural principle presented earlier is modified in such a way that a two-

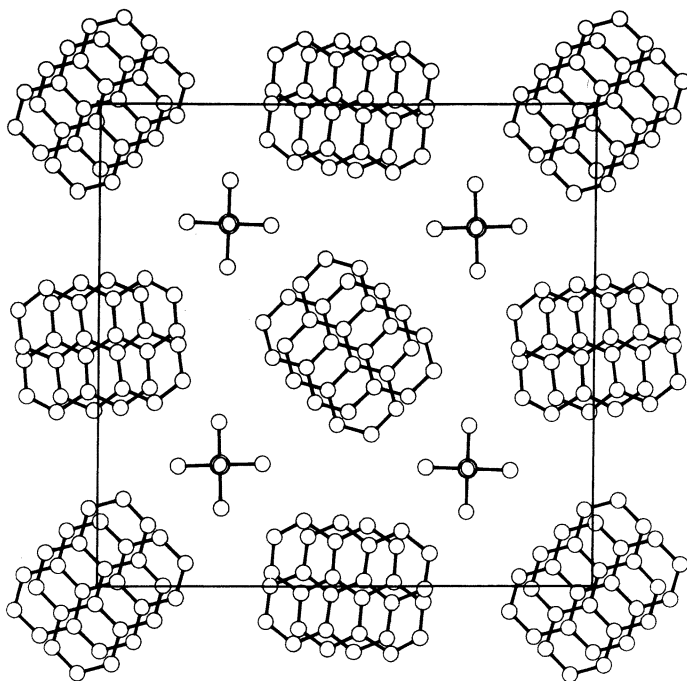


Figure 9. Crystal structure of  $\text{Py}_2\text{AsF}_6$ .

dimensional system is formed. A projection of the crystal structure is shown in Figure 10.

In contrast with all other salts for which the stacks are parallel, in this case two stacks are oriented perpendicularly to each other along the two diagonals of the  $ab$  plane of the tetragonal unit cell. Parallel columns are packed in layers so that the stacking direction alternates along the  $c$  axis. The stack consists of six rings, two of which are located on symmetry centers (i.e., DMN1 and DMN1').  $\text{SbF}_6^-$  ions and solvent molecules are placed between the stacks so that the counterions compensate for charges in both stacks. The interplanar spacings are not equal. A periodic change occurs from extremely short spacings [3.06 (3) Å between DMN2 and DMN2'] to normal spacings [3.32 (2) Å between DMN1 and DMN2]. Both overlaps connected with these are virtually identical, and  $\psi \sim 90^\circ$  (Figure 11). Preliminary experiments showed that  $\text{DMN}_3(\text{SbF}_6)_2(\text{CH}_2\text{Cl}_2)$  behaves like a two- or even three-dimensional conductor. The specific conductivity ( $\sigma \sim 10^{-1} \Omega^{-1} \text{cm}^{-1}$ ) is equal in all three crystallographic directions. This finding is somewhat surprising because it implies an effective charge transfer also in the  $c$  direction. Preliminary measurements of the ESR line width revealed a marked exchange narrowing of the line when the magnetic field was oriented along  $a$  or  $b$ , that is, along the diagonal between the two stacks. This result can be interpreted to indicate a strong interaction between the DMN

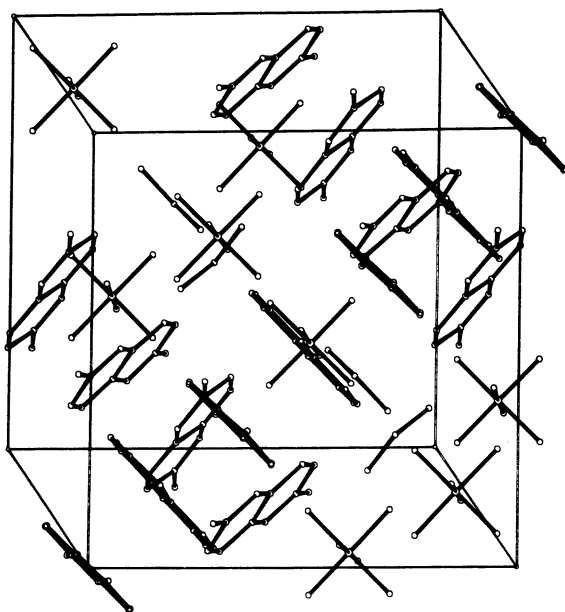


Figure 10. Crystal structure of  $\text{DMN}_3(\text{SbF}_6)_2(\text{CH}_2\text{Cl}_2)$ .

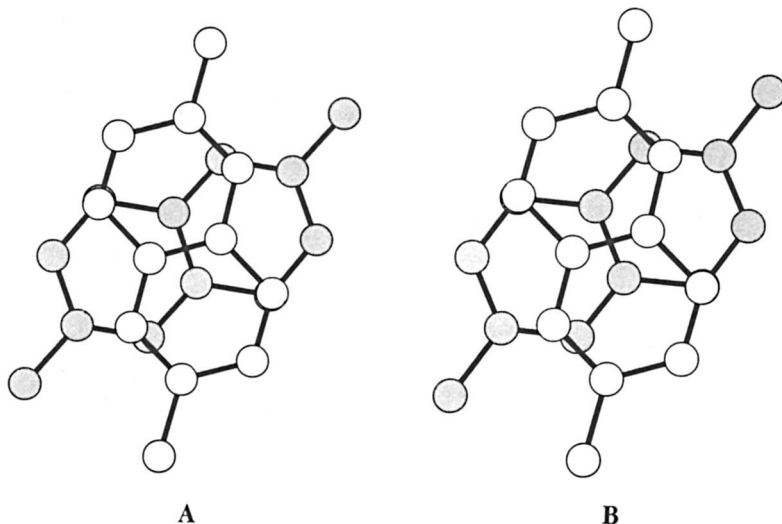


Figure 11. Molecular overlap in  $DMN_3(SbF_6)_2(CH_2Cl_2)$ . A:  $DMN1-DMN2$ , and B:  $DMN2-DMN2'$ .

rings along the stacks and also an effective charge transfer perpendicular to the stacks in the  $c$  direction (9, 16).

**Radical-Cation Salts as Organic Metals.** Structural investigations of a variety of organic complexes exhibiting high, metallike conductivities (organic metals) have established certain common structural principles. Among the most important are the following (17–19): (1) crystallization of planar, easily polarizable molecules in segregated stacks; (2) uniform interplanar spacings within the stacks; and (3) mixed valence states, that is, only partial oxidation or reduction of the stack forming molecules. All these principles are fulfilled by the structures determined for the radical-cation salts of arenes.

Specific conductivities of more than  $1000 \Omega^{-1} \text{ cm}^{-1}$  have been reported for some systems (5). In Figure 12, the temperature dependence of  $FA_2(PF_6)_{0.76}(AsF_6)_{0.24}$  is shown. In the high-temperature region, a quasi-metallic conductivity is observed. The onset of the semiconducting behavior is found at the phase-transition temperature.

The discovery of stable, quasi-metallic, radical-cation salts has stimulated many studies. A few studies concerning the metallic nature will be briefly discussed here. Most of the results were obtained with  $FA_2X$  because of its simple, well-documented structure and phase transition and its relatively high stability.

Crystals of  $FA_2X$  give an extremely narrow ESR line in the metallic region;  $\Delta H_{pp}$  (line width)  $\sim 10$  milligauss, which is the smallest line width

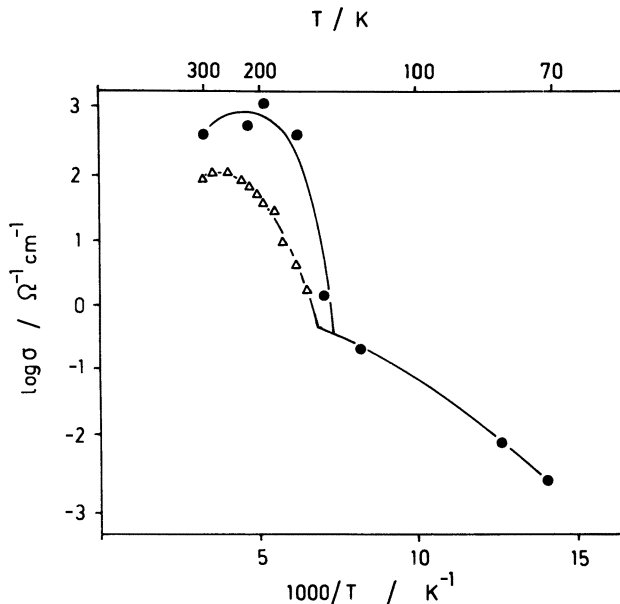


Figure 12. Temperature dependence of the specific conductivity in  $FA_2(PF_6)_{0.74}(AsF_6)_{0.26}$ . Key: ●, Δ: two different samples.

ever detected in the solid state (15, 20, 21). This line is independent of the orientation of the magnetic field and is also independent of the Larmor frequency within a wide range (15 MHz–9.4 GHz). Above the phase transition, the ESR intensity is essentially independent of temperature. Similar results are obtained with all other radical-cation salts in their metallic high-temperature states.

$^{19}F$  and  $^1H$  magnetic resonance experiments done in the same frequency range as the ESR experiments showed that the F atoms in the counterions are relaxed mainly by reorientational jumps of the octahedrons, whereas the protons on the rings are relaxed predominantly by highly mobile paramagnetic species. The Korringa relation,  $(T_{1H}T)^{-1} = \text{constant}$ , is fulfilled above the phase transition (22); thus, the assumption that  $FA_2X$  is a one-dimensional metal is vindicated by these experiments ( $T_{1H}$  is relaxation time and  $T$  is temperature). Because of their narrow ESR lines, samples of  $FA_2X$  are very useful as magnetic field probes. Because the signal is strong, small samples are sufficient to give a large signal; therefore, small and very inhomogeneous magnetic fields can be probed (15).

The metallic nature of radical-cation salts can also be shown by reflection spectroscopy. If the direction of polarization is directed parallel to the stacking direction, a steep plasma edge with a pronounced minimum is observed



(23). This observation is characteristic of the optical absorption of free carriers. In Figure 13, the reflectance spectra of some radical-cation salts are shown in comparison with those of two well-known one-dimensional metals that represent two extremes: one one-dimensional inorganic metal,  $\text{K}_2\text{Pt}(\text{CN})_4\text{Br}_{0.3} \cdot 3.2\text{H}_2\text{O}$  (KCP), and the charge-transfer complex TTF TCNQ (TTF is tetrathiafulvalene, and TCNQ is tetracyanoquinodimethane). The radical-cation salts fill the broad gap between the spectral positions of the plasma edge of these two extremes. The reflectance spectra shown are the spectra of free carriers, and an excellent fit of the experimental data can be made with this assumption (Drude model). The fit yields the optical value for the electrical conductivity,  $\sigma(\text{opt})$ , and the width of the conduction band,  $t$ . Because of the strong interactions between the rings, radical-cation salts represent a transition between the usually narrow-band organic conductors [TTF TCNQ:  $t = 0.4$  electronvolts (eV)] to the inorganic conductors. For  $\text{FA}_2\text{X}$ ,  $\delta(\text{opt}) = 1900 \Omega^{-1} \text{cm}^{-1}$  and  $t = 2.3$  eV were calculated from the fit of the reflectance spectrum.

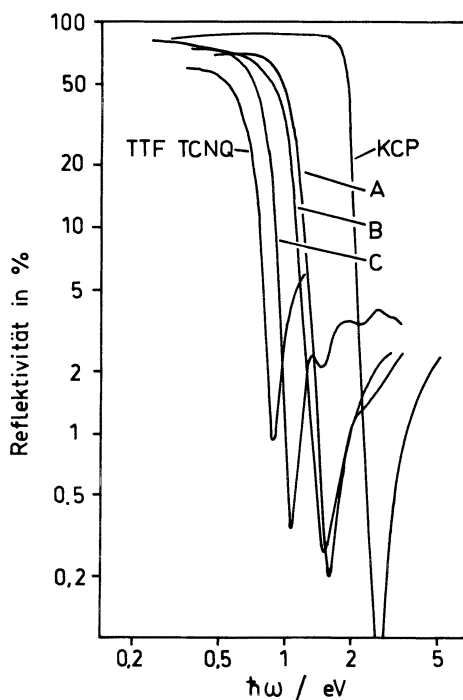


Figure 13. Reflectance spectra of radical-cation salts in comparison with the one-dimensional conductors KCP and TTF TCNQ. A:  $\text{FA}_2(\text{PF}_6)_{0.74}(\text{AsF}_6)_{0.26}$ , B:  $\text{Py}_{12}(\text{SbF}_6)_7$ , and C:  $\text{Pe}(\text{PF}_6)_{1.1}(\text{CH}_2\text{Cl}_2)_{0.8}$  (where Pe is perylene).

**Radical-Cation Salts as Models for Conducting Polymers.** Polymers that have an extended  $\pi$ -electron system in their backbones, for example, polyacetylene (PA) and poly(*p*-phenylene) (PPP), can be transformed by oxidation or reduction in the solid state (doping) to derivatives that exhibit metallike conductivity (24, 25). These materials are usually insoluble and infusible and exhibit a very complicated morphology that cannot be changed by subsequent treatment. The lack of knowledge about the structure and state of order is the cause of the current controversy about the conduction mechanism in doped polymers.

The interactions found between the aromatic rings in the radical-cation salts can be regarded as models for interchain interactions in conducting polymers. The concept that uses the structural principles found in the model compounds to construct models for the conducting polymer derivatives is illustrated in Figure 14. The radical cations created on the polymer backbone in the oxidation are thought to stabilize themselves by forming complexes with neutral chain segments in their vicinity according to reaction 2. The stack-forming elements are part of the main polymer chain. Consequently, the derived structural models can be characterized as intercalation structures in which layers of polymer chains and counterions alternate. Many of the

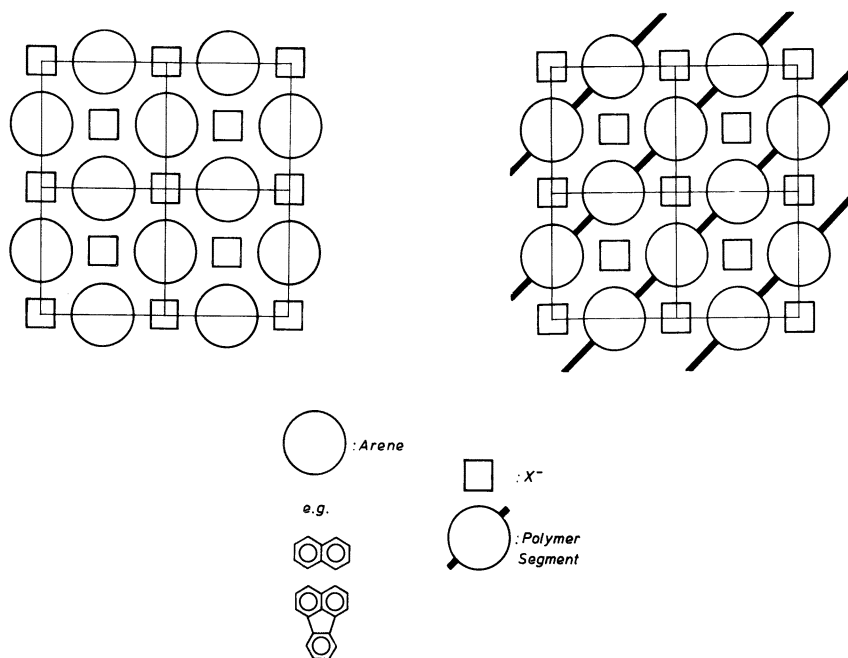


Figure 14. Analogy of the packing in radical-cation salts (left) and in conducting polymer salts (right).

structural properties of conducting polymers have been successfully explained by using this concept. Radical-cation salts of oligomers of PPP, for example, terphenyl and quaterphenyl (QP) and their substituted analogues, have been prepared in order to use the packing found in the oligomers as a model for doped PPP (8, 10).

The crystal structure of the radical-cation salt of QP,  $\text{QP}_3\text{QP}(\text{SbF}_6)_3$ , is shown in two projections in Figure 15. The structure consists of stacks of QP molecules that are separated by layers of  $\text{SbF}_6^-$  ions. All QP units are nearly aligned in one direction; thus, the packing found here could seemingly be a reasonable model for the polymer salt. The projection perpendicular to the stack reveals that an additional (neutral) QP molecule is packed in the anion layer to fill empty space. In contrast with all other salts, each QP molecule carries one positive charge. In terms of the structural principles of organic conductors given earlier, this salt should be an insulator. The relatively high conductivity observed could be explained by a hybrid of the valence bond forms shown in Chart I. This situation could be interpreted like the polymer chain; that is, more than one radical-cation site is created on one extended molecule.

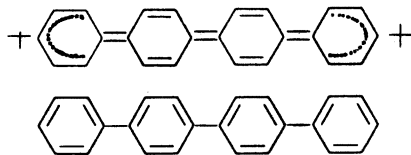
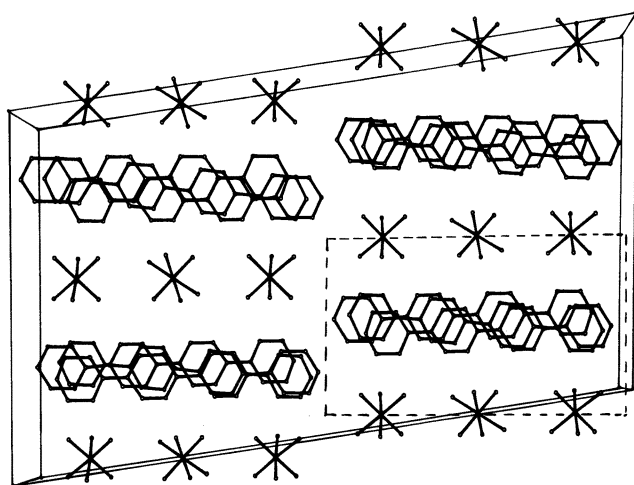


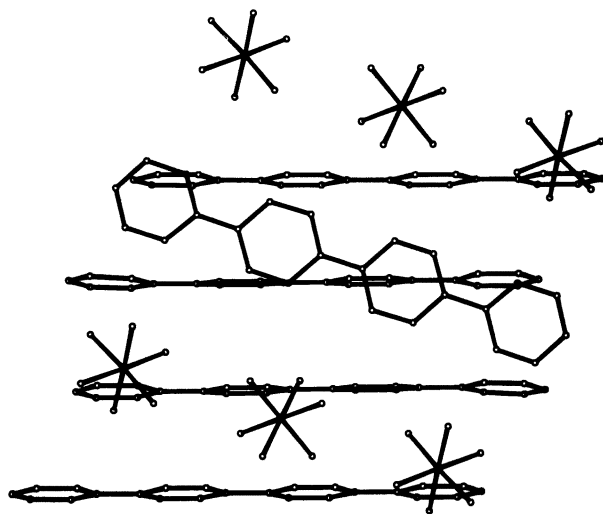
Chart I

The motif in the smaller dashed cell shown in Figure 15 was used to construct a model for the PPP salt. Both the unit cell dimensions and the composition  $(\text{C}_6\text{H}_4)_8(\text{SbF}_6)_3$  were used without further adjustment and reproduced the experimental doping level (40% per phenyl ring) and the X-ray and neutron scattering (10).

In a similar way, the packing found in the radical-cation salts could be used to solve the crystal structure of the  $\text{SbF}_6^-$  salt of PA,  $[(\text{CH})(\text{SbF}_6)_{0.06}]_x$  (26). A projection of this structure along the chain direction is shown in Figure 16. All details of the quite complicated structure will not be discussed here. The structure is incommensurate; that is, it can be described by the two sublattices also shown in Figure 16. Two types of polymer chains are found: Type 2 is located in rows of counterions filling the empty space, and type 1 (shown in black) is closely packed in a plane between these rows. The interplanar spacing (3.44 Å) allows charge transport not only along the polymer chain but also perpendicular to it by interchain charge transfer. This condition is important because the conjugation length in PA is limited



A



B

Figure 15. Crystal structure of  $QP_3QP(SbF_6)_3$ . A: Projection in the stacking direction, and B: projection perpendicular to the stacks.

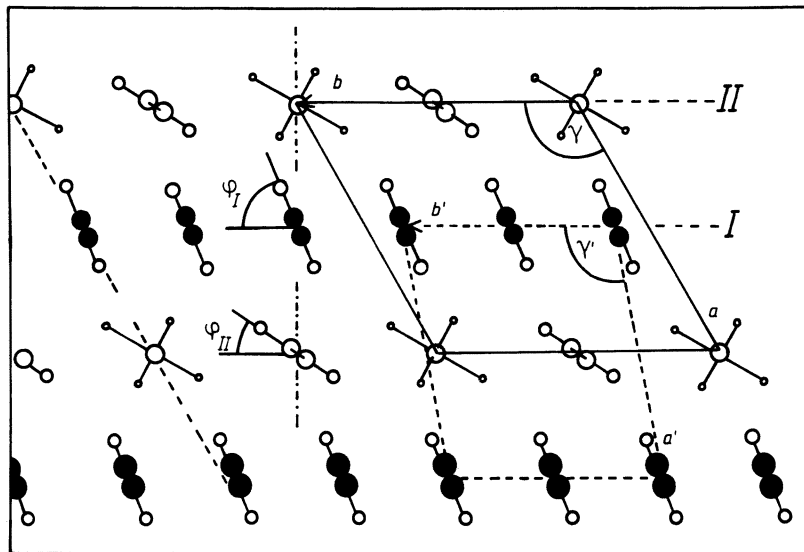


Figure 16. Crystal structure of the conducting salt of PA,  $[(CH)(SbF_6)_{0.06}]_x$ .

by a number of defects and is not sufficient to explain the macroscopically large conductivity. The conduction perpendicular to the polymer chain is assumed to be the same type as that found in the radical-cation salts of arenes.

### Acknowledgment

Petroleum Research Fund Grant No. 18537-SE covered travel expenses to the ACS National Meeting in Anaheim, CA, where this research was presented.

### References

1. Chiang, T. C.; Reddoch, A. H.; Williams, J. J. *Chem. Phys.* **1971**, *54*, 2051.
2. Fritz, H. P.; Gebauer, H.; Friedrich, P.; Ecker, P.; Artes, R.; Schubert, U. Z. *Naturforsch., B:* **1978**, *33*, 498; Fritz, H. P.; Gebauer, H.; Friedrich, P.; Schubert, U. *Angew. Chem.* **1978**, *90*, 305.
3. Kröhnke, C.; Enkelmann, V.; Wegner, G. *Angew. Chem.* **1980** *92*, 941.
4. Enkelmann, V.; Morra, B. S.; Kröhnke, C.; Wegner, G.; Heinze, J. *Chem. Phys.* **1982**, *66*, 303.
5. Keller, H. J.; Nöthe, D.; Pritzkow, H.; Wehe, D.; Werner, M.; Koch, P.; Schweitzer, D. *Mol. Cryst. Liq. Cryst.* **1981**, *62*, 181.
6. Heinze, J. *Angew. Chem.* **1984**, *96*, 823.
7. Enkelmann, V. *Habilitationschrift*, University of Freiburg, 1983.
8. Enkelmann, V.; Göckelmann, K., unpublished results.
9. Enkelmann, V.; Göckelmann, K. *Angew. Chem.* **1986**, in press.

10. Enkelmann, V.; Göckelmann, K.; Wieners, G.; Monkenbusch, M. *Mol. Cryst. Liq. Cryst.* **1985**, *120*, 195.
11. Grauf, W.; v. Schutz, J. U.; Werner, H.-P.; Wolf, H. C.; Göckelmann, K.; Enkelmann, V.; Wegner, G. *Chem. Phys.* **1986**, in press.
12. Alcacer, L.; Maki, A. H. *J. Chem. Phys.* **1974**, *78*, 215.
13. Alcacer, L.; Novais, H.; Pedroso, F.; Flandrois, S.; Coulon, C.; Chasseau, D.; Gaultier, J. *Solid-State Commun.* **1980**, *35*, 945.
14. Endres, H.; Keller, H. J.; Müller, B.; Schweitzer, D. *Acta Cryst.* **1985**, *C41*, 607.
15. Dormann, E.; Sachs, G.; Stöcklein, W.; Bail, B.; Schwoerer, M. *Appl. Phys.* **1983**, *A30*, 227.
16. v. Schütz, J. U., private communication.
17. Garito, A. F.; Heeger, A. J. *Acc. Chem. Res.* **1974**, *7*, 232.
18. Shchegolev, I. F. *Stat. Phys. Sol. (a)* **1972**, *12*, 9.
19. Zeller, H. R. *Festkörperprobleme* **1973** *13*, 31.
20. Eichele, H.; Schwoerer, M.; Kröhnke, C.; Wegner, G. *Chem. Phys. Lett.* **1981**, *77*, 31.
21. Sachs, G.; Stöcklein, W.; Bail, B.; Dormann, E.; Schwoerer, M. *Chem. Phys. Lett.* **1982**, *89*, 179.
22. Höptner, W.; Mehring, M.; v. Schütz, J. U.; Wolf, H. C.; Morra, B. S.; Enkelmann, V.; Wegner, G. *Chem. Phys.* **1982**, *73*, 253.
23. Geserich, H. P.; Koch, B.; Ruppel, W.; Wilckens, R.; Schweitzer, D.; Enkelmann, V.; Wegner, G.; Wieners, G.; Keller, H. J. *J. Phys.* **1983**, *44*, C3-1461.
24. Wegner, G. *Angew. Chem.* **1981**, *93*, 352.
25. Baeriswyl, D.; Harbeke, G.; Kiess, H.; Meyer, W.H. In *Electronic Properties of Polymers* Mort, J.; Pfister, G., Eds.; Wiley: New York, 1982.
26. Wieners, G.; Weizenhöfer, R.; Monkenbusch, M.; Stamm, M.; Lieser, G.; Enkelmann, V.; Wegner, G. *Makromol. Chem., Rapid Commun.* **1985**, *6*, 425.

RECEIVED for review September 29, 1986. ACCEPTED May 14, 1987.

# Evidence for the Types of Polynuclear Aromatic Systems in Nonvolatile Fractions of Petroleum

James G. Speight

Western Research Institute, University Station, Laramie, WY 82071

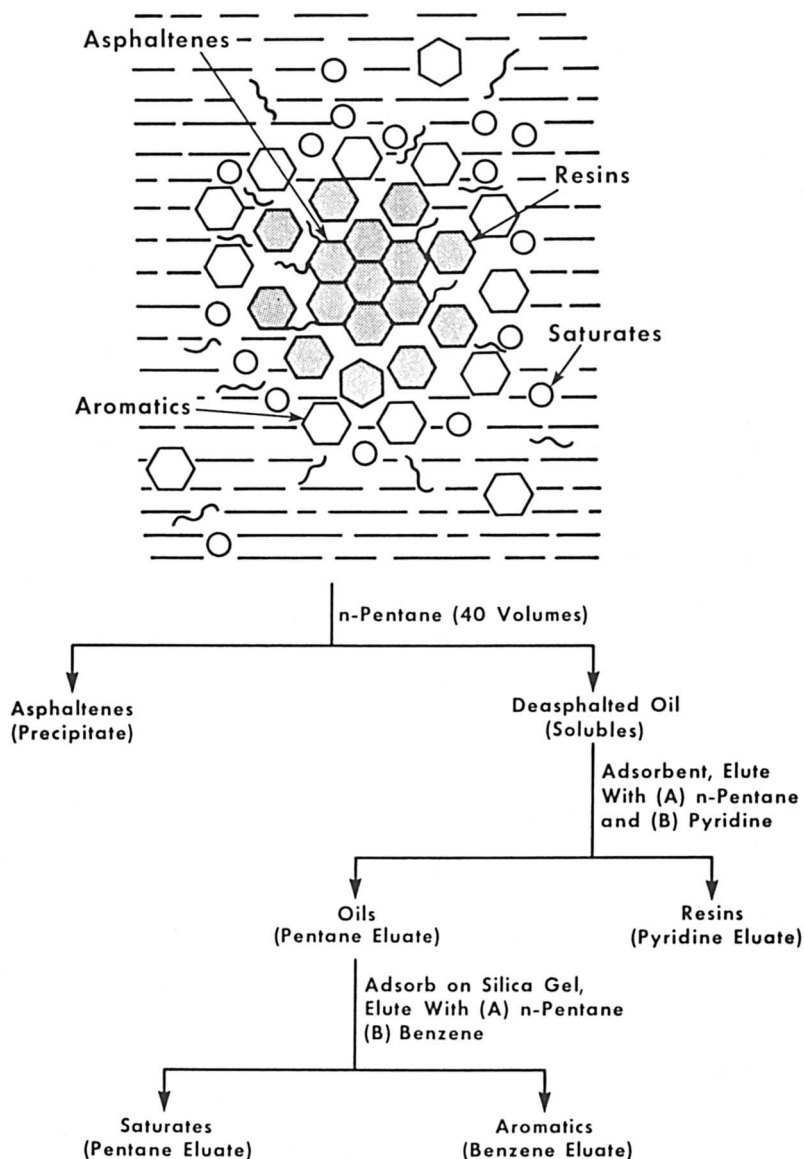
*The occurrence of aromatic systems in petroleum is well-established, and systems having one to three rings have been identified as constituents of the volatile fractions of petroleum. Previously, a concomitant increase in ring number with decrease in volatility in the higher molecular weight nonvolatile fractions of petroleum was assumed, largely on the basis of spectroscopic evidence. However, evidence produced by pyrolysis–gas chromatography–mass spectrometry and by UV spectroscopy does not support the concept of large polynuclear aromatic systems. The experimental data produced herein are more indicative of polynuclear aromatic systems having one to six rings. Such a concept is consistent with the physical and chemical behavior of petroleum asphaltenes.*

**T**HE OCCURRENCE OF MONONUCLEAR AND POLYNUCLEAR aromatic systems in nature is well documented (1–3). However, petroleum is one source of aromatic systems that is often ignored (4–7). Aromatic systems occur throughout the various boiling fractions in petroleum, and the evolution of analytical techniques such as gas chromatography (GC) and mass spectrometry (MS) has been a major asset in bringing about the identification of the volatile aromatic species. Many mononuclear, dinuclear, and even trinuclear aromatic systems have been identified in the volatile fractions of petroleum (7).

The large-ring polynuclear aromatic systems that occur in petroleum have been much more difficult to identify because they occur in the non-

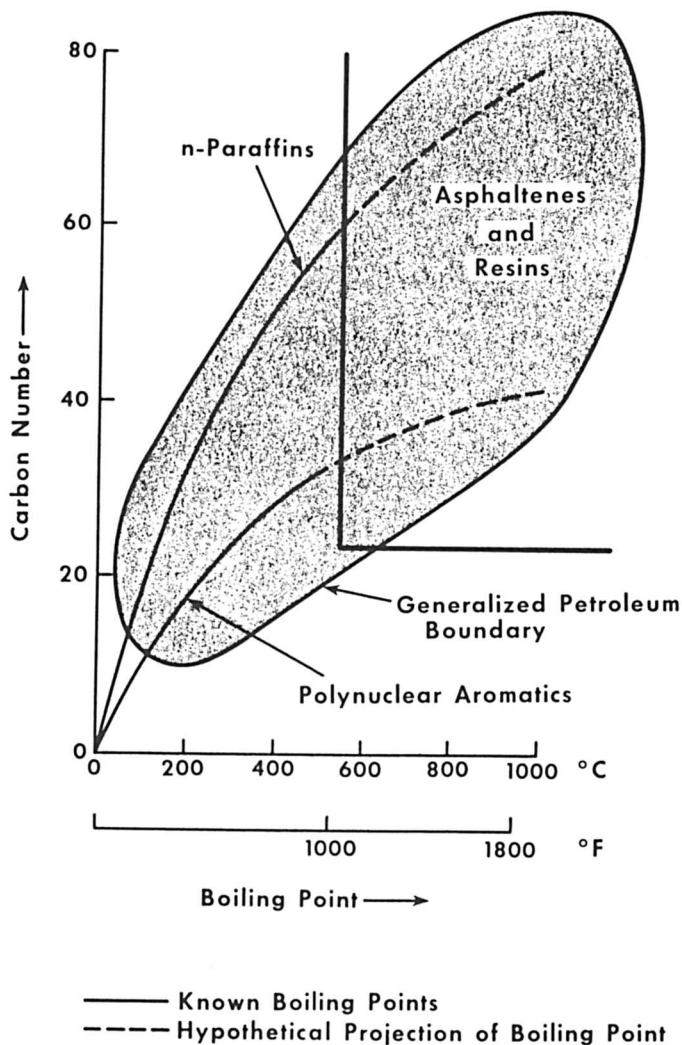
volatile fractions (e.g., resins and asphaltenes; Scheme I), particularly in the asphaltene fraction. In addition, these polynuclear aromatic systems are complex molecules that fall into molecular weight and boiling ranges for which very little is known about model compounds (Figure 1).

Researchers have attempted to identify asphaltene fractions in terms of



Scheme I. Convenient separation of petroleum into four major fractions.

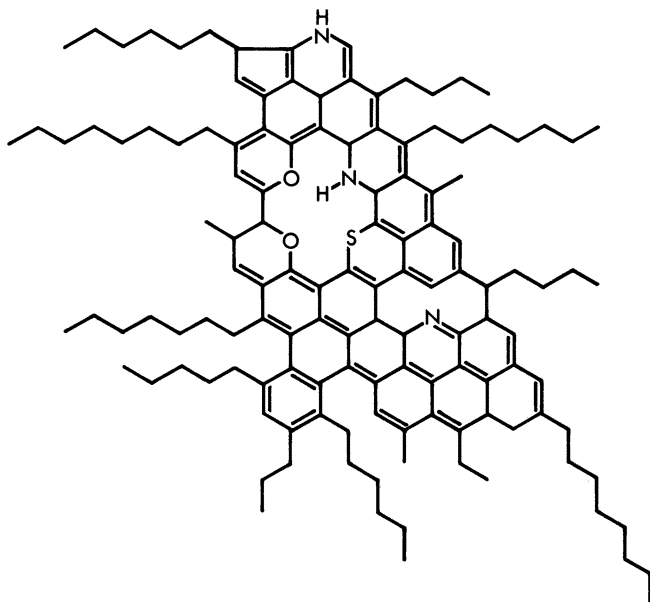




*Figure 1. Boiling point versus carbon number for the constituents of petroleum. The constituents of petroleum fall into molecular weight and boiling ranges for which the knowledge of model compounds is limited.*

an “average structure”, which has largely been derived by means of spectroscopic techniques (8, 9) and has involved the concept of a large central polynuclear aromatic system (structure 1). However, such a polynuclear aromatic system is not consistent with either the natural product history of petroleum or the behavioral characteristics of the asphaltene fraction.

A more realistic aspect of petroleum composition is based on the distribution of molecular types in petroleum and shows that petroleum is a



Structure 1. Average-structure representation of asphaltene. Asphaltenes are often represented by average structures composed of large polynuclear aromatic systems (38).

continuum of molecular types (Figure 2, ref. 10). This concept has been taken one step further and has been applied to petroleum asphaltenes (Figure 3; ref. 11). The concept promotes the rationale that petroleum asphaltenes are a solubility class and, as such, are complex mixtures in which variations of molecular weight and polarity (i.e., functionality due to the nonhydrocarbon molecules that contain nitrogen, oxygen, and sulfur) play a major role in the behavioral characteristics of the fraction.

The concept that molecular weight and polarity play a role in determining the composition of an asphaltene fraction is very realistic but does not present any indication of the nature of the polynuclear aromatic systems in the asphaltene fraction of petroleum. Thus, the purpose of this chapter is to present new data that provide indications of the ring-size distribution in petroleum asphaltenes. The evidence is accumulated by asphaltene fractionation and subsequent examination of the fractions by high-performance liquid chromatography (HPLC) using a UV detector.

### *Experimental Details*

**Asphaltene Separation.** Asphaltenes were isolated from bitumen (Athabasca) by using an excess of *n*-pentane (40 mL of  $n\text{-C}_5\text{H}_{12}$  per gram of bitumen) and following

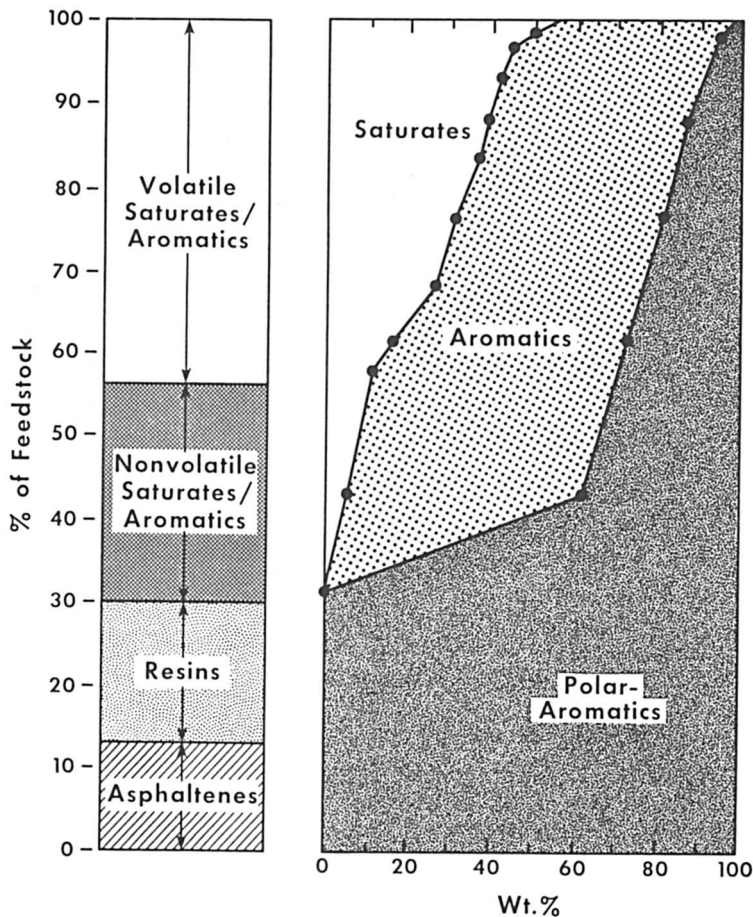


Figure 2. Representation of petroleum as a map of the various molecular types. (Reproduced with permission from reference 10. Copyright 1978.)

a recommended procedure (12) to ensure complete separation of the asphaltenes without the occlusion of nonasphaltene material.

**Asphaltene Fractionation.** Asphaltenes were separated into bases, acids, and neutral components by using a procedure described elsewhere (13). Following this initial separation, the basic fraction was then rechromatographed on a basic resin to produce a "true" basic fraction (nonadsorbed) and an amphoteric fraction (adsorbed). This procedure (Scheme II) allows asphaltenes to be separated into amphoteric species, bases, acids and neutral components. This type of separation was found to be a general feature of other asphaltenes separated from different bitumens, heavy oils, and conventional petroleum.

**Asphaltene Subfractionation.** Asphaltene subfractionation was achieved by using an adsorption method; the individual asphaltene fractions were preadsorbed onto

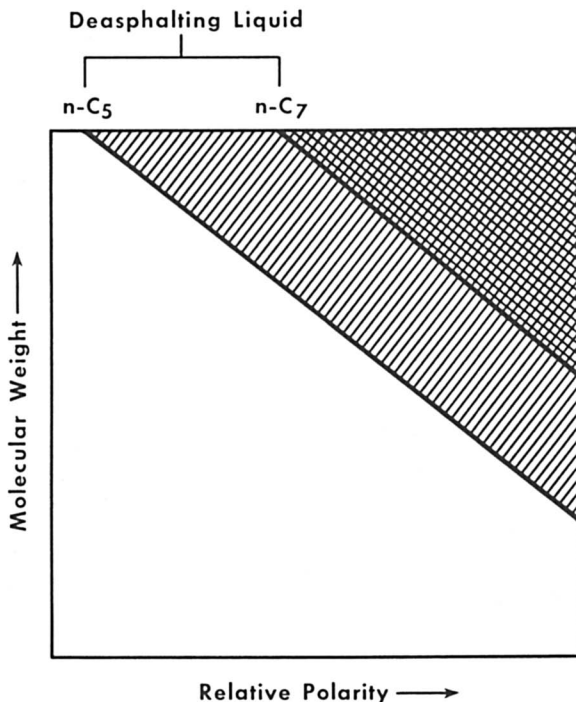


Figure 3. Representation of asphaltenes on the basis of size and polarity. (Reproduced with permission from reference 11. Copyright 1981.)

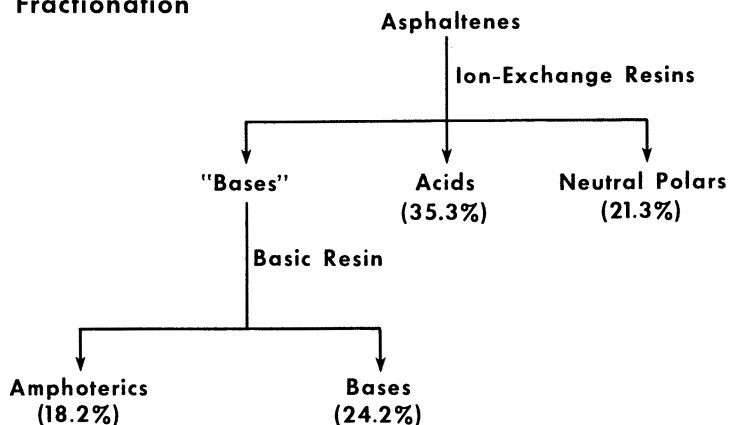
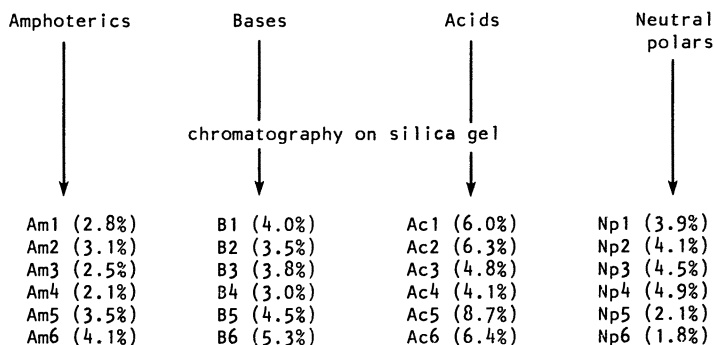
a column of silica gel and removed by sequential elution with benzene–heptane mixtures, benzene, benzene–methanol and chloroform–isopropyl alcohol (Scheme II). Elution of each fraction was terminated when the eluate was colorless, and the asphaltene fractions were recovered by solvent removal (rotary evaporation) and dried (100 °C/10 mmHg) to constant weight. Total recovery of subfractions by this method was nearly quantitative (>99%).

**Spectroscopic Techniques.** UV–visible spectra were obtained with a double-beam UV–visible spectrophotometer (Beckmann). The asphaltenes were examined as solutions in chloroform (0.005–0.1 g per mL) with chloroform in the compensating beam. IR spectra were recorded either as potassium bromide pellets (0.1 g of asphaltene per gram of potassium bromide) or as solutions in chloroform (0.1 g/mL).

<sup>13</sup>C magnetic resonance spectra were determined with a Fourier transform spectrometer (Varian XL–100–15), with deuteriochloroform as the solvent.

**Physical Properties.** Elemental analyses were determined by the Alfred Bernhard Microanalytical Laboratories. Molecular weights were determined with a vapor pressure osmometer (Mechrolab) with pyridine as the solvent.

Pyrolysis–gas chromatography–mass spectrometry (PY/GC/MS) of the asphaltenes was achieved in the manner described elsewhere (14). The amount of the asphaltene fraction volatilized was determined by weighing the pyrolysis tubes after a sequence of experiments.

**(a) Fractionation****(b) Subfractionation**

*Scheme II. Fractionation of asphaltenes (a) and subfractionation of asphaltenes on the basis of functionality (b).*

HPLC was performed with a liquid chromatograph (Waters Associates Series 6000) equipped with UV and refractive-index detectors. Asphaltene fractions were examined by using a 25- × 0.5-cm column packed with silica gel and maintained at 25 °C by an external thermostatically controlled water bath. Asphaltenes and standard polynuclear aromatic compounds were passed through the column with chloroform-isopropyl alcohol blends (90:10).

**Discussion**

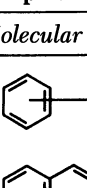



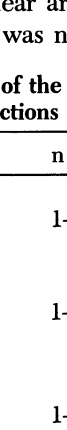

**Polynuclear Aromatic Systems in Asphaltenes.** The asphaltene fraction of petroleum is defined as the fraction that is insoluble in a low-

boiling liquid paraffin such as *n*-pentane or *n*-heptane (12). Asphaltenes are detrimental to refinery processes and are responsible for catalyst deactivation and coke deposition (15). To understand the reasons for this behavior and to assist in refinery process optimization, the molecular nature of petroleum asphaltenes has been investigated (8, 9). However, determining the actual structures of the constituents of the asphaltene fraction has proven to be difficult. Nevertheless, the various investigations have brought to light some significant facts about polynuclear aromatic systems in asphaltene structure; findings indicate that asphaltenes consist of polynuclear aromatic nuclei that carry alkyl and alicyclic systems with heteroelements (e.g., nitrogen, oxygen, and sulfur) scattered throughout in various (including heterocyclic) locations (8, 9, 16, 17).

The application of thermal techniques to study the nature of the volatile thermal fragments from petroleum asphaltenes has produced some interesting data relating to the polynuclear aromatic systems (18–22). These thermal techniques have produced strong evidence for the presence of small polynuclear aromatic systems (one to four rings) (14), and application of the techniques to the various functional fractions has confirmed the general, but unequal, distribution of these systems throughout asphaltenes.

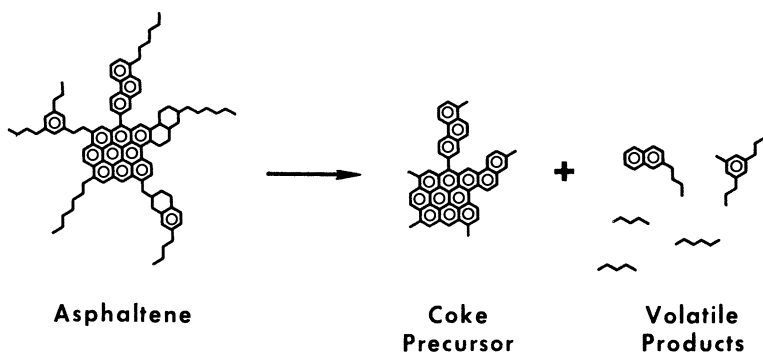
Each asphaltene fraction produced the same type of polynuclear aromatic system (Table I) in the volatile matter, but the distribution was not

**Table I. Various Aromatic Molecular Types Identified as Constituents of the Volatile Products from the Thermal Decomposition of Asphaltene Fractions**

<i>Homologous Series</i>	<i>Molecular Types</i>	<i>n</i>
Alkylbenzenes		1–7
Alkylnaphthalenes		1–4
Alkylbenzothiophenes		1–3
Alkyldibenzothiophenes		1
Alkylphenanthrenes		1
Alkylchrysenes		1

constant (Table II). The hydrocarbon distribution also was computed and indicated an overall preponderance of single-ring (cycloparaffin and alkylbenzene) species as well as the domination of saturated material over aromatic material. The preponderance of the low-molecular-weight material in the volatile products is to be anticipated on the basis that more complex systems remain as nonvolatile material and, in fact, are converted to coke. The PY/GC/MS program does not accommodate nitrogen and oxygen species. However, this matter is resolved, in part, by the concentration of nitrogen and oxygen in the nonvolatile material (coke) and the overall low proportions of these heteroatoms originally present in the asphaltenes.

The major drawback to the application of a PY/GC/MS technique to study polynuclear aromatic systems in petroleum asphaltenes is the amount of material that remains as a nonvolatile residue (Table II). The nonvolatile residue has been postulated (20) to be the result of a highly condensed polynuclear aromatic system being present in the asphaltene (Scheme III).



*Scheme III. Formation of coke precursor and volatile products from asphaltene. Coke formation has been postulated to involve large polynuclear aromatic systems. (Reproduced with permission from reference 20. Copyright 1980.)*

**Table II. Distribution of Aromatic and Nonaromatic Species Throughout Petroleum Asphaltene Fraction Determined by PY-GC-MS**

<i>Fraction</i>	<i>H/C Atomic Ratio</i>	<i>Molecular Weight<sup>a</sup></i>	<i>Volatile Aromatic (wt %)</i>	<i>Compounds Nonaromatic (wt %)</i>	<i>Residue (wt %)</i>
Amphoteric compounds	1.04	2350	51	49	63
Bases	1.06	2250	48	52	60
Acids	1.23	1910	40	60	43
Neutral polar compounds	1.29	1420	33	65	38

NOTE: Data are for Athabasca asphaltenes.

<sup>a</sup>Values were determined by vapor pressure osmometry in pyridine at 65, 75, and 85 °C and were extrapolated to room temperature.

Aside from speculation about the polynuclear aromatic systems in the residue, the majority of the nitrogen (>90%), oxygen (>50%) and sulfur (>60%) in the natural asphaltene remains in the coke (14, 18). Therefore, an alternate method of investigation was sought to determine the nature of polynuclear aromatic systems in petroleum asphaltenes.

Of all of the methods applied to determining the types of polynuclear aromatic systems in petroleum asphaltenes (8, 9, 16), one with considerable potential, but given the least attention, is UV spectroscopy (23–28). Typically, the UV spectrum of a petroleum asphaltene shows two major regions with very little fine structure, and interpretation of such a spectrum can only be made in general terms (29–31). The technique can add valuable information about the degree of condensation of polynuclear aromatic ring systems with the help of HPLC (27, 28, 32, 33).

When a high-performance liquid chromatograph is equipped with an UV detector, a benefit becomes evident. Because polynuclear aromatic hydrocarbons have different absorptivities at a given wavelength, the detector can be tuned for maximum selectivity for specific compounds, especially when the compounds have different ring numbers. Thus, an HPLC investigation of a mixture of standard polynuclear aromatic systems with the UV detector at fixed wavelengths from 240 to 360 nm confirmed the applicability of the technique (34) to determine the presence of ring-size distribution by using the different selectivities of the polynuclear aromatic systems. The one- and two-ring polynuclear aromatic systems were more prominent in the chromatogram at 240 nm but were not at all evident in the chromatogram at wavelengths >300 nm. The converse was true for the systems containing three to six rings. This situation was confirmed in the present work by examination of a standard solution of polynuclear aromatic systems (one to seven rings); systems containing one to three rings gave prominent UV detector signals at wavelengths <300 nm but gave no signals at >300 nm. On the other hand, systems containing four to seven rings gave signals at wavelengths >300 nm but gave no signals at 365 nm.

Each of the asphaltene (Athabasca) functional fractions produced a complex multicomponent chromatograph (Figure 4) but the subfractions produced a less complex and much narrower chromatograph that approximated a single peak. The subfraction peaks proved much easier to monitor with the UV detector (Table III). These data provide strong indications of the ring-size distribution of the polynuclear aromatic systems in petroleum asphaltenes. For example, amphoteric species and basic nitrogen species contain polynuclear aromatic systems having two to six rings per system. On the other hand, the acidic subfractions (phenolic–carboxylic functions) and the neutral polar subfractions (amides–imino functions) contain few if any polynuclear aromatic systems having more than three rings per system.

No case provided any strong or conclusive evidence for polynuclear aromatic ring systems containing more than six condensed rings. In all cases,



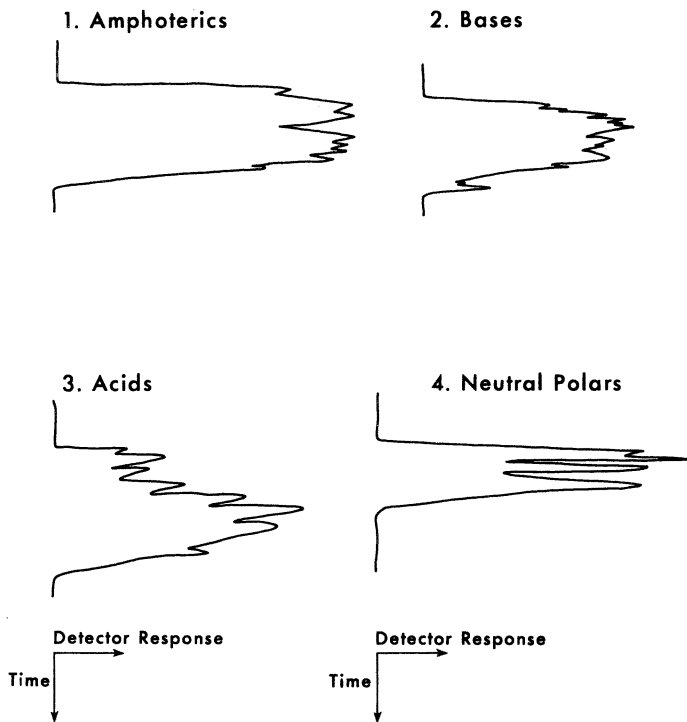


Figure 4. HPLC chromatograms of asphaltene fractions. HPLC emphasizes the complexity of the functional fractions.

the evidence favored the preponderance of the smaller systems (one to four rings).

The method is subject to the limitation of the sensitivity of polynuclear aromatic systems. Furthermore, some of the asphaltene material (<2% w/w) was irreversibly adsorbed on the adsorbent. In this case, the missing material is presumably highly polar and any deviation from the ring-size distribution outlined in the foregoing discussion is not believed to be significant enough to influence the general conclusions about the nature of the polynuclear aromatic systems in petroleum asphaltene.

**Implications for Asphaltene Structure.** These observations require some readjustment to the previous postulates of the asphaltene structure. Previously conceived hypotheses that state that the polynuclear aromatic system is large (>10 rings) are considered to be unlikely in spite of their frequent and recent occurrence in the literature. The thermolysis products are indicative of a much more open structure than previously recognized. The failure to detect (during the chromatographic examination) any strong evidence for the existence of large multiring polynuclear aromatic

**Table III. Relative Intensities of the Subfraction Peaks at Different Wavelengths**

<i>Subfraction<sup>a</sup></i>	254	280	300	320	340
<b>Amphoteric Fraction</b>					
Am1	+	+	+	+	-
Am2	+	+	+	-	-
Am3	+	+	+	+	-
Am4	+	+	+	+	+
Am5	+	+	+	-	-
Am6	+	+	+	+	-
<b>Basic Fraction</b>					
B1	+	+	+	+	-
B2	+	+	+	-	-
B3	+	+	+	-	-
B4	+	+	+	-	-
B5	+	+	+	+	+
B6	+	+	+	+	-
<b>Acidic Fraction</b>					
Ac1	+	-	-		
Ac2	+	-	-		
Ac3	+	-	-		
Ac4	+	-	-		
Ac5	+	-	-		
Ac6	+	-	-		
<b>Neutral Polar Fraction</b>					
Np1	+	-	-		
Np2	+	-	-		
Np3	+	-	-		
Np4	+	-	-		
Np5	+	-	-		
Np6	+	-	-		

NOTE: Numbers in column headings are the detector wavelengths used and are given in nanometers; + denotes an increase relative to 240 nm, and - denotes a decrease relative to 240 nm; a blank means that no bands were evident. At 365 nm, no bands were evident except for subfractions Am4, Am5, Am6, B5, and B6, for which decreases relative to 240 nm were observed.

<sup>a</sup>Am denotes amphoteric, B denotes basic, Ac denotes acidic, and Np denotes neutral polar; the numbers 1-6 are the subfraction numbers.

systems in the asphaltene fractions is evidence against structures invoking this concept.

The manner in which these moieties occur within the asphaltene fraction must, for the present, remain largely speculative. The asphaltenes are a solubility class (12, 35) and, as such, may be an accumulation of thousands of (similar/dissimilar) structural entities. Hence, caution is advised against combining a range of identified products into one (albeit hypothetical) structure. For example, it would be presumptuous (if not ludicrous) to suggest

that, on the basis of the present findings, petroleum asphaltenes are polymeric analogues of alkylbenzenes, -naphthalenes, -phenanthrenes, -benzothiophenes, and -dibenzothiophenes.

In regard to the heteroatom types in the asphaltenes, certain heteroatom types appear to be associated with certain polynuclear aromatic ring systems (Table III), although attempts have been made (8, 9) to include such functionality into average structures. In addition, the concept of large polynuclear aromatic systems ( $>10$  rings) in petroleum asphaltenes is not consistent with the natural product origins of petroleum. The presence of such systems would require conditions of temperature and pressure for their formation that are more extreme than those currently recognized as being responsible for petroleum maturation (4-7).

In terms of carbon-residue formation (Table II), heat-resistant polymers containing aromatic and heterocyclic units such as polyquinolines and polyquinoxalines have a strong tendency to form large condensed systems during pyrolysis and will finally carbonize (36). Formulas that include the occurrence of smaller polynuclear aromatic hydrocarbon systems in asphaltenes are consistent with such behavior when the majority of the nitrogen, oxygen, and sulfur species accumulate in the nonvolatile residue.

One other aspect of this chapter is the implication that high molecular weight and low polarity may not be synonymous (Table II) as defined by the relationship of molecular weight to polarity (11, 16). This concept (Figure 3) may need modification by a change in slope of the diagonal  $C_5$  or  $C_7$  line because most of the more polar species (e.g., basic nitrogen species, phenolic species, and amphoteric species) appear to occur in the higher molecular weight fractions of petroleum asphaltenes, whereas the less polar species (e.g., carbazole species and amides) appear to occur in the lower molecular weight fractions of petroleum asphaltenes.\* Nevertheless, the basic concept is sound.

The danger in all of these studies is in attempting to link together fragmented molecules produced by thermal processes into a structure that is believed to be real. Functionality and polynuclear aromatic ring systems are real, but the combination of these parameters into one or even several structures can be misleading.

Finally, preliminary data from the investigation of the resin fraction support the concept of such systems throughout the nonvolatile portion of petroleum. The data were strongly indicative of polynuclear aromatic systems similar to those found in the asphaltenes. Presumably, the major difference is in the extent to which these systems are combined to form distinct molecular species.

\*This observation is based on the molecular weights of the various fractions in pyridine (Table II), which is a solvent that promotes dissociation of associated species (37).

## Summary

Polynuclear aromatic systems occur throughout the boiling range of petroleum. Those of special interest are the systems that occur in the nonvolatile asphaltene fraction. Previous postulates invoked the concept of large polynuclear aromatic systems (10 or more rings) as the mainstay of structural types in petroleum asphaltenes. Evidence provided here favors the presence of polynuclear aromatic systems having a maximum of six aromatic rings. Indeed, the evidence favors the preponderance of smaller (one to four) ring systems in the asphaltene fraction. However, the manner in which the polynuclear aromatic systems occur within the asphaltene fraction must, for the present, remain largely speculative. Caution is advised against combining a range of identified products into one (albeit hypothetical) structure.

## References

1. *Lignins: Occurrence, Formation, Structure, and Reactions*; Sakarnen, K. V.; Ludwig, C. H., Eds.; Wiley: New York, 1971.
2. Weiss, V.; Edwards, J. M. *The Biosynthesis of Aromatic Compounds*; Wiley: New York, 1980.
3. *Kerogen: Insoluble Organic Matter from Sedimentary Rocks*; Duran, B., Ed.; Editions Technip.: Paris, 1980.
4. *Organic Geochemistry: Methods and Results*; Eglinton, G.; Murphy, B., Eds.; Springer-Verlag: New York, 1969.
5. Tissot, B. P.; Welte, D. H. *Petroleum Formation and Occurrence*; Springer-Verlag: New York, 1978.
6. *Advances in Petroleum Geochemistry*; Brooks, J.; Welte, D., Eds.; Academic: New York, 1984; Volume 1.
7. Speight, J. G. *The Chemistry and Technology of Petroleum*; Marcel Dekker: New York, 1980.
8. *The Chemistry of Asphaltenes*; Bunger, J. W.; Li, N., Eds. *Advances in Chemistry Series No. 195*, American Chemical Society: Washington, DC, 1981.
9. Tissot, B. *The Characterization of Heavy Crude Oils and Petroleum Residues*; Editions Technip: Paris, 1984.
10. Corbett, L. W.; Petrossi, U. *Ind. Eng. Chem. Prod. Res. Dev.* **1978**, *17*, 342.
11. Long, R. B. In *The Chemistry of Asphaltenes*; Bunger, J. W.; Li, N., Eds.; *Advances in Chemistry Series No. 195*, American Chemical Society; Washington, DC, 1981, p 17.
12. Speight, J. G.; Long, R. B.; Trowbridge, T. D. *Fuel* **1984**, *63*, 616.
13. Selucky, M. L.; Kim, S. S. Skinner, F.; Strausz, O. P. In *The Chemistry of Asphaltenes*; Bunger, J. W.; Li, N., Eds. *Advances in Chemistry Series No. 195*, American Chemical Society: Washington, DC, 1981, p 83.
14. Speight, J. G.; Pancirov, R. J. *Liq. Fuels Technol.* **1984**, *2*, 287.
15. Speight, J. G. In *Catalysis on the Energy Scene*; Kaliaguine, S.; Mahay, A., Eds.; Elsevier: Amsterdam, 1984, p 515.
16. Speight, J. G.; Long, R. B. In *Atomic and Nuclear Methods in Fossil Energy Research*; Filby, R. H., Ed.; Plenum: New York, 1981, p 295.
17. Girdler, R. B. *Proc. Assoc. Asphalt Paving Technol., Tech. Sess.* **1965**, *34*, 45.
18. Speight, J. G. *Prepr. Am. Chem. Soc., Div. Fuel Chem.* **1971**, *15*, 57.
19. Ritchie, R. G. S.; Roche, R. S.; Steedman, W. *Fuel* **1979**, *58*, 523.

20. Schucker, R. C.; Keweshan, C. F. *Prepr., Am. Chem. Soc., Div. Fuel Chem.* **1980**, *25*, 155.
21. Gallegos, E. J. *J. Chromatogr. Sci.* **1981**, *19*, 177.
22. Raul, P. R. *Trends Anal. Chem. (Pers. Ed.)* **1982**, *1*, 237.
23. Jaffe, H. H.; Orchin, M. *Theory and Applications of Ultraviolet Spectroscopy*; Wiley: New York, 1966.
24. *Determination of Organic Structures by Physical Methods*; Braude, E. A.; Nachod, F. C., Eds.; Academic: New York, 1955.
25. Rao, C. N. R. *Ultraviolet and Visible Spectroscopy: Chemical Applications*; Butterworths: London, 1961.
26. Friedel, R. A.; Orchin, M. *Ultraviolet Spectra of Aromatic Compounds*; Wiley: New York, 1951.
27. Lee, M. L.; Novotny, M. S.; Bartle, K. D. *Analytical Chemistry of Polycyclic Aromatic Compounds*; Academic: New York, 1981.
28. *Handbook of Polycyclic Aromatic Hydrocarbons*; Bjorseth, A. Ed.; Marcel Dekker: New York, 1983.
29. Friedel, R. A. *J. Chem. Phys.* **1959**, *31*, 280.
30. Boyd, M. L.; Montgomery, D. S. *J. Inst. Petroleum* **1963**, *49*, 345.
31. Posadov, I. A.; Pokonova, J. V.; Khusidman, M. B.; Gitlin, I. G.; Proskuryakov, V. A. *Zh. Prikl. Khim.* **1977**, *50*, 594.
32. Felix, G.; Bertrand, C.; Van Gastel, F. *Chromatographia* **1985**, *20*, 155.
33. Killops, S. D.; Readman, J. W. *Org. Geochem.* **1985**, *8*, 247.
34. Krstulovic, A. M.; Rosie, D. M.; Brown, R. P. *Anal. Chem.* **1976**, *48*, 1383.
35. Mitchell, D. L.; Speight, J. G. *Fuel* **1973**, *52*, 149.
36. Dussel, H. J.; Recca, A.; Kolb, J.; Hummel, D. O.; Stille, J. K. *J. Anal. Appl. Pyrolysis* **1982**, *3*, 307.
37. Speight, J. G.; Wernick, D. L.; Gould, K. A.; Overfield, R. E.; Rao, B. M. L.; Savage, D. W. *Rev. Inst. Francais du Petrole* **1985**, *40*, 51.
38. Svetgoff, J. *Oil and Gas J.* **1984**, *82(9)*, 79.

RECEIVED for review September 29, 1986. ACCEPTED March 2, 1987.

# Coal Aromaticity and Average Molecular Structure

N. Berkowitz

Department of Mining, Metallurgical and Petroleum Engineering, University of Alberta, Edmonton T6G 2G6, Canada

*Although the basic chemical features of coal can be qualitatively and in some instances semiquantitatively specified, "average-structure" models that purportedly reflect statistically preferred molecular structures of coal offer little that advances an understanding of coal. In part, this is due to a continuing paucity of relevant or reliable data and to the procedures used to formulate the constructs. But meaningful representations of molecular structure are currently also precluded by indications that the assumption that underlies average-structure models, namely, that there exists a more or less unique, systematic, rank-dependent, molecular chemistry of coal, is not sustained by the current evidence. Several examples, all drawn from the open literature, are presented to support the view that the chemistry of a coal is heavily influenced by its source materials and early formative history and that coals of similar rank may therefore be chemically much more diverse than is usually supposed.*

**S**INCE PUBLICATION OF THE NOW-CLASSIC STOPES-WHEELER MONOGRAPH on coal constitution in 1918 (1), the diffuse coal band that delineates itself in C versus H plots (2) or equivalent diagrams (3) has come to be regarded as implying a genetic rather than merely generic relationship among coals of different rank; and this has prompted the view that there exists a systematic, rank-dependent, molecular chemistry of coal which, if more completely understood, would allow the chemical properties and behavior of coal in specified reaction regimes to be predicted from simple rank indicators. Contemporary basic coal research is therefore heavily concentrated on structural elucidation of a (hypothesized) characteristic "average coal macromolecule"

and, in particular, centered on coal aromaticity, that is, on the fraction of carbon ( $C_{ar}/C$ ) contained in aromatic entities and on the nature of the linkages between such entities.

This focus makes it pertinent to inquire whether the assumptions from which such work proceeds are sustained by the experimental evidence at hand and to observe that there appears to be a much greater diversity of coal chemistries than is now generally envisaged.

### *Sources of Structural Information*

Credible, if perhaps not always entirely consistent, information respecting the essential features of coal structure comes from numerous, quite diverse sources. Atomic H/C ratios and heats of combustion indicate that all coals are for the greater part composed of aromatic entities and that metamorphic development operates directionally to increase the aromaticity of coal (4). X-ray diffraction data (5, 6), as well as the nature of the products of low-temperature pyrolysis (7–11) and liquefaction (12–14), allow the inference that the aromatic units are relatively small (averaging only two or three condensed rings until the anthracite stage is reached). And IR spectral analysis (15), oxidation with  $HNO_3$  or  $KMnO_4$  (16, 17), and functional group analyses (18–22) have indicated that the aromatic units are linked by hydroaromatic or short aliphatic bridge structures as well as variously substituted around their peripheries.

This picture has been broadly validated, and in some respects refined, by other work in which coal was “depolymerized” by acid-catalyzed *trans*-alkylation [as by interaction of coal with phenol and  $BF_3$  (23–27)] or by similar, less clearly defined, phenolation reactions (28–31), or selectively degraded by “specific” oxidants, such as dichromates (32–34), hypohalites (35–38), or peroxy-acids (39–43). But these studies have also revealed some previously unsuspected features. Buffer-controlled oxidation with  $Na_2Cr_2O_7$  (34) and  $KMnO_4$  (44) have indicated an occasionally significant presence of straight-chain (up to  $C_{21}$ ) and branched-chain (up to  $C_8$ ) aliphatic compounds in coal. Oxidation with performic acid (41–43) has yielded substituted compounds that are clearly related to the microbial or chemical degradation products of lignin or flavonoids. And when applied to supposedly very similar coals, virtually identical “depolymerization” or oxidation procedures often furnished distinctly different product slates (45).

However, for reasons that lie as much in the diversity of source materials and formative histories of coal as in its physical complexity and heterogeneity, few if any investigative tools will, when applied to coal, yield unequivocal qualitative, let alone quantitative, results. Most chemical procedures can and have been challenged on the grounds that they operate on coal in a much more complex and of much less certain manner than had been supposed when they were first used, and more definitive information about coal

structure has therefore been sought by recourse to spectroscopic methods of analysis, which began becoming available to coal chemists in the late 1940s.

Some of the X-ray diffraction measurements and IR spectral analyses referred to in the preceding paragraph are early examples that demonstrated the value of such approaches to coal structure. But through progressive technical refinement becoming much more powerful than these methods and therefore, since the early 1970s, commanding much greater attention than they as a route to structural data, is high-resolution NMR spectroscopy. As now applied to coal and coal derivatives, this technique typically combines cross-polarization with magic angle spinning (CP/MAS) with dipolar decoupling and can in favorable circumstances provide very good estimates of  $C_{ar}/C$  and  $H_{ar}/H$  from  $^1H$  and  $^{13}C$  NMR spectra (46–53).

Fourier transform IR (FTIR) spectroscopy (54), which offers major benefits over conventional IR spectroscopy from greater sensitivity, spectral resolution, and substantially better signal-to-noise ratios, seems capable of furnishing equally good estimates of  $C_{ar}/C$  and  $H_{ar}/H$  (55). In this case, one measures  $H_{al}$ , derives  $C_{al}$  from the stoichiometric relationship  $H_{al}/C_{al} = 1.8$ , and calculates  $C_{ar}$  by difference. However, applied to coal (as distinct from certain coal derivatives), FTIR spectroscopy has been mainly used to obtain better data for substituent functions (56, 57); and what are currently deemed to be the most authoritative data on coal aromaticity have all been recorded by  $^{13}C$  NMR spectroscopy.

It is possible that variants of this technique may eventually prove to be the best and, aside from FTIR spectroscopy, the only means for measuring carbon aromaticities without simultaneously inducing unknown or uncertain chemical changes in the coal substance. But as matters stand, the experimental limits of the technique remain to be defined (58). It has, for example, been suggested that current procedures sample only a fraction of all C atoms in coal (possibly no more than 50%) and that what is sampled may not be representative of the total (59, 60). If only for these reasons, results from NMR spectroscopy must therefore still be viewed with great caution.

However, a need for caution is also demonstrated by the wide data scatter that characterizes even the best available data sets. An illustration is provided by a recent compilation of  $C_{ar}/C$  values (61) reproduced in Figures 1 and 2 as functions of carbon contents and atomic H/C ratios, respectively. In this instance, variations that assign aromaticities ranging between 0.55 and 0.8 to a coal with, for example, 85% C, are perhaps not entirely unexpected. The data used in this compilation were not all recorded by the same NMR technique; and there are also some uncertainties respecting the origins and previous histories of the samples. (Neavel (62) has emphasized that little care tends to be exercised in ensuring proper sampling and preservation of coals studied in the laboratory.) However, pronounced anomalies,



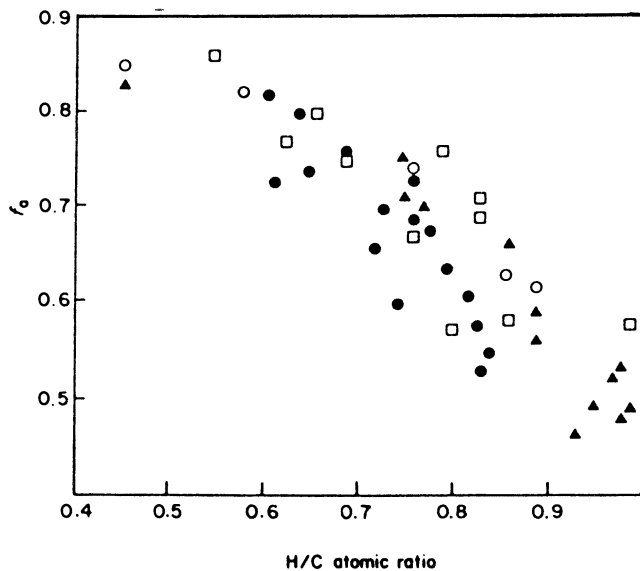


Figure 1. Variation of  $f_a (=C_{ar}/C)$  with carbon contents. (Reproduced with permission from ref. 61. Copyright 1986.)

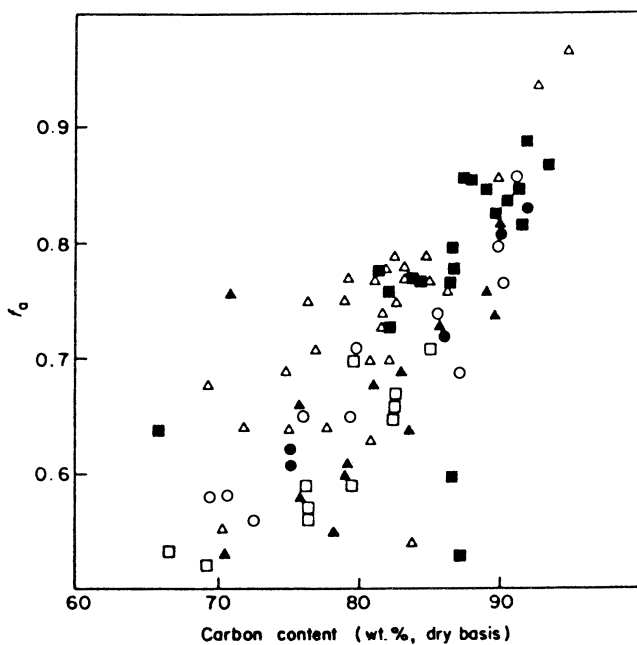


Figure 2. Variation of  $f_a$  with atomic H/C ratios. (Reproduced with permission from ref. 61. Copyright 1986.)

that is, “atypically” high or low aromaticities, are often also seen in individual data sets that correlate  $C_{ar}/C$  with coal rank, and such sets usually show only well-defined trends even when the anomalies are discounted (52, 63). Since there is, as well, no clearly discernible relationship between  $C_{ar}/C$  and  $H_{ar}/H$  (48, 49) or between  $C_{ar}/C$  and atomic  $H/C$  ratios (63), one might infer that the technical deficiencies of current NMR methods make estimates of  $C_{ar}/C$  fundamentally unreliable or, alternatively, that there is a wide inherent variation of aromaticity among seemingly similar coals.

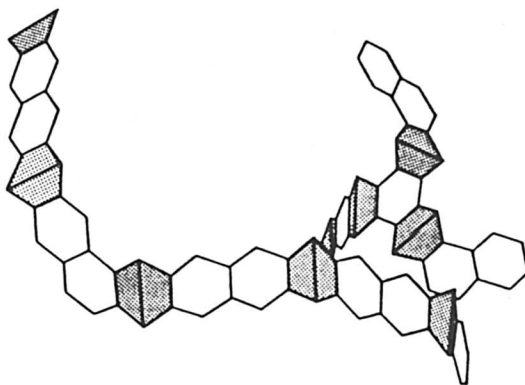
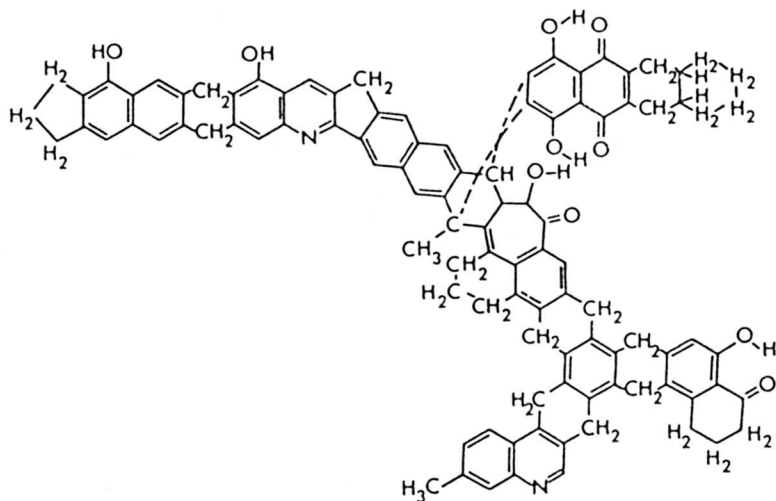
Because other means of exploring coal structure at best yield semi-quantitative data, both of these inferences bear importantly on the significance of structural models that purport to reflect the molecular structure of coal.

### *Average-Structure Models*

Historically preceded by studies of model compounds deemed to reflect one or more important coal properties (64–69), constructs designed to represent characteristic molecular configurations in coal began to be formulated in the early 1960s, and although usually tested for compliance with best extant information (and therefore presumably benefitting from the more discriminating experimental tools that have come to hand in later years) undergone relatively little change since then. Some examples (70–74) are shown in structures 1–4.

Because the models were developed from almost identical data bases, they are often similar, and differences between them tend to reflect equally possible choices rather than disagreements over substantive facts. The basic structural units are usually naphthalene-, phenanthrene-, or fluorene-like configurations that are associated with cycloparaffinic and hydroaromatic moieties, peripherally substituted by  $-OH$ ,  $-CH_3$ , or  $-O-$ , and irregularly linked together by ether- $O$  or  $-CH_2-$  bridges. Nitrogen- and sulfur-bearing heterocycles (which pyrolysis and oxidation have shown to exist in coal) are accommodated by arbitrarily replacing a C atom in a six-membered (or, less often, five-membered) ring by N or S. In some models (cf. structure 3), provision is made for occasional  $C_3$  linkages between aromatic or hydroaromatic clusters. And metamorphic development of coal is, as exemplified by structure 4, depicted by modestly enlarging the aromatic core entities at the expense of nonaromatic units and eliminating some peripheral substituents.

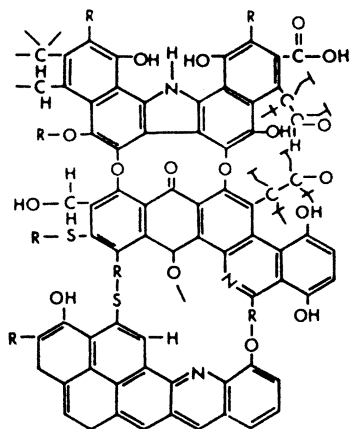
Of the most recent of these constructs (15, 74–77)], structure 5 is particularly interesting. It is intended to represent a typical “monomeric” fragment of the macromolecule of a vitrinite-rich bituminous coal with 83–84% carbon, and is the first to embody a recognition that hypothesized structural elements must be reconciled with their known or suspected antecedents in living plants as well as with observations on coal itself. Structure 5 therefore



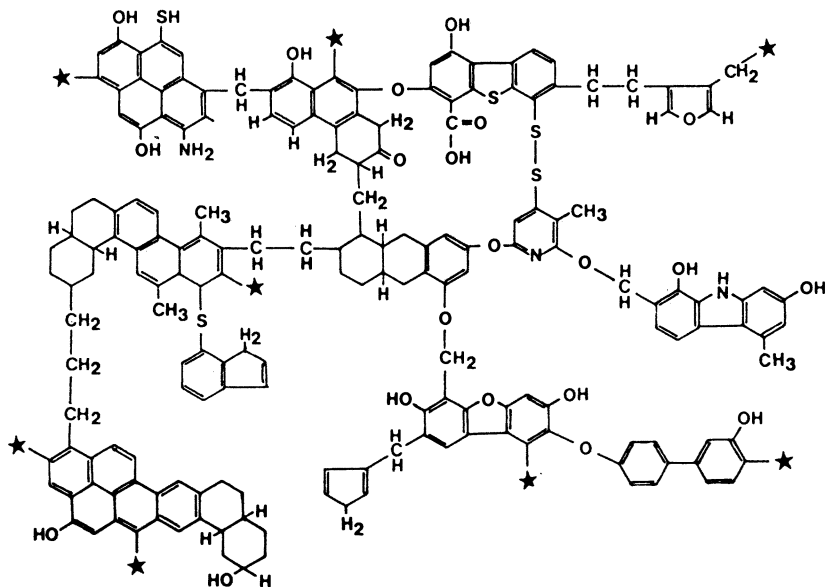
Structure 1. Hypothetical coal molecule containing ~82% carbon. The lower diagram, in which shaded areas represent alicyclic moieties, shows the spatial configuration of a simplified form of the molecule. (Adapted from references 70 and 71.)

reflects the fact that:

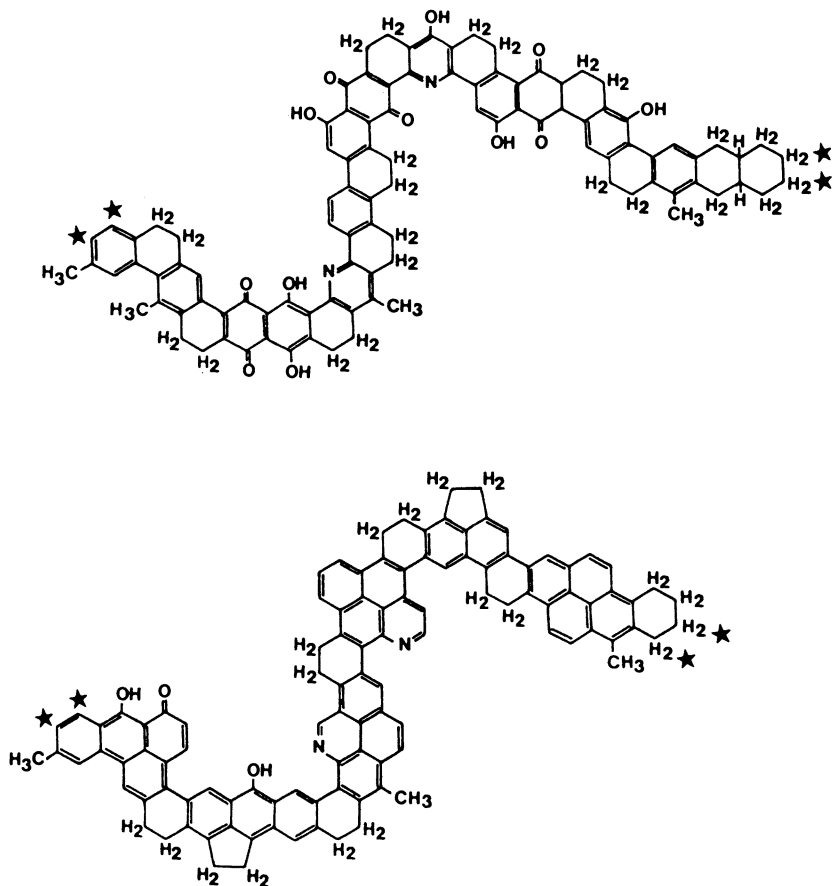
- Celluloses, hemicelluloses, and glucosides of plant matter are always more or less rapidly degraded to sugars, which can then rearrange to polyhydric phenols by replacing the oxygen in their cyclic structures with a carbon atom and then lose water, as in  $C_6H_{12}O - [3H_2O] \rightarrow C_6H_3(OH)_3$ .



Structure 2. Proposed molecular structure of bituminous coal. (Adapted from reference 72.)



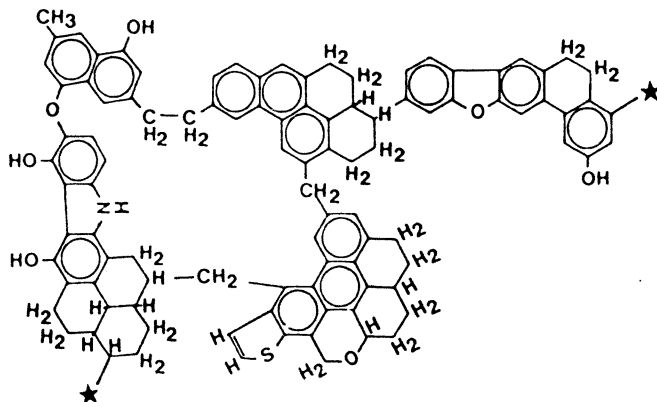
Structure 3. Proposed molecular structure of bituminous coal containing 82–83% carbon. A star (★) indicates where polymerization might occur. (Adapted from reference 73.)



Structure 4. Proposed model structures for vitrains containing ~80% carbon (top) and ~90% carbon (bottom). A star (★) indicates where polymerization might occur. (Adapted from reference 74.)

- Molecules of lignin and its primary breakdown products, which are the most important coal precursors, are now generally considered to be based on phenyl-propylene units, derivatives of which have been obtained from coal by oxidizing it with performic acid (41–43).

Significantly, all structural models were and continue to be qualified by some important, albeit not always clearly enunciated, provisos. They are never thought to depict “real” coal molecules and are merely offered as “average” molecular configurations that, even though unlikely to exist as such, could serve to describe coal by displaying all of its essential chemical characteristics. They are almost invariably envisaged as representing vitrains or, more particularly, vitrinites, which are usually the most abundant and



Structure 5. Proposed model structure of vitrinite-rich bituminous coal containing ~83–84% carbon. A star (★) indicates where polymerization might occur. (Adapted from references 75 and 76.)

homogeneous coal macerals (and therefore the only ones to have been studied in any detail). They were always, and for the most part still are, intended to illustrate the structure of relatively mature (bituminous) coal. And although frequently referred to as “molecular” models, lack of information about the size of the hypothesized macromolecules obliges one to see them only as typical “monomeric” components or unit cells of such molecules.

Viewed as no more than convenient means for summarizing and visually displaying some general features of coal structure, models are undoubtedly helpful unless, of course, they contain demonstrable flaws. For example, structure 2 shows a configuration that cannot easily be reconciled with radial distribution curves from X-ray diffraction measurements (78), which indicate an absence of significant planarity beyond 0.6 nm from any one C atom. But because development and progressive refinement of such structural models are implicitly justified by the expectation that they may eventually allow prediction of chemical behavior under specified conditions, it is important to understand their shortcomings and explore whether what is hoped to be achieved by structural modeling is a realistic objective.

An obvious weakness of “average-structure” models, no matter how carefully formulated, arises from their being averaged and from the assumption that data from diverse sources, commonly relating to different coals and obtained by different means, can be directly combined for averaging purposes. In other words, the modeling depends on judgment (or personal preference) as to which data to use and on the assumption that coals of similar rank are characterized by a similar chemistry. The model shown in structure 5 is a case in point. The carbon aromaticity (0.70) was taken as an average of four values that not only ranged from 0.65 to 0.76 but that had been determined by different methods for three different high-volatile bituminous coals and a phenol/BF<sub>3</sub>-depolymerized product. Aliphatic structures were

assessed by a matrix procedure that juxtaposed a set of  $H_{ar}$  values (equivalent to varying degrees of substitution) with different types of aliphatic substituents (such as single C atoms,  $C_n$  chains, or hydroaromatic moieties) and then selected appropriate aliphatic structures by matching the numbers of aromatic and aliphatic moieties that could accept the same number of substituents. And ether linkages (79, 80) were incorporated on the assumption of one O atom per 100 C atoms.

However, the inability of specifying the sizes, shapes, and spatial associations of the hypothesized macromolecules also detracts from any value that current structural models may possess. The question of size can be skirted by simply representing the models as "structure elements" (76, 77) (or, very loosely, "monomers" or unit cells) that are assumed to be variously polymerized in the coal. But with respect to molecular shape, which depends to some extent on how the macromolecules are thought to be associated, the models reflect little more than the preferences of their originators. Illustrations of this are the profound differences between structures 1 and 4 on the one hand and structures 2 and 3 on the other, as well as the incorporation in structure 1 of a triptycene moiety that endows the molecule with an extra spatial dimension.

The importance of this exercise of preference lies in the fact that the models can and do affect how certain aspects of coal behavior are interpreted; and this, in turn, can directly or indirectly affect technical choices in various types of coal processing. For example, the currently dominant view, which derives from the supposition that metamorphic development of coal proceeds by progressive trifunctional polycondensation (81, 82), regards the coal matrix as composed of three-dimensionally cross-linked macromolecules; and results of studies on solvent imbibition and swelling of coal (83) are considered to confirm such a structure, even though these results could be equally well interpreted on the assumption that the matrix is made up of asymmetric, physically entangled molecules (84–87). Experimental evidence for this alternative view of molecular association in coal [a view that leads to a marked preference for Given's model (70, 71) or Pitt's model (74) over those proposed by Hill and Lyon (72), Wiser (73), or Shinn (15)] is arguably no less persuasive than evidence for a three-dimensionally cross-linked matrix. For example, although a cross-linked matrix would make coal solubilization dependent on thermal rupture of C–C bonds (at or near 400 °C) and on rapid stabilization of the resultant radicals by H capping, extensive (>80%) solubilization of bituminous coals has been achieved at temperatures as low as 300 °C by reacting them with solvents such as anthracene, phenanthrene, or  $\alpha$ -naphthol (88–90), which are incapable of donating H to the coal. It has also been shown (91) that the solubility imparted to coal by alkylation (92, 93) increases with the length of the alkyl chain, even though the longer and consequently bulkier chains allow fewer alkyl groups to be introduced into the coal and alkylation then disrupts fewer C–C bonds.

In these circumstances, and noting the massive evidence from coal pyrolysis and oxidation that chemical behavior is governed by the specifics of molecular structure, averaged models can convey no more real information about coal than an equimolar mixture of, for example, benzene and cyclohexane, can provide about the properties of 1,2,3,4-tetrahydronaphthalene (Tetralin). The models obliterate the chemical reactivities of the discrete molecular species that solvent extraction has shown to exist in coal and therefore cannot accommodate interactions (such as internal H disproportionation during coal liquefaction) among such species; and they offer no information whatsoever about the probable (or statistically preferred) structures and chemical properties of exinites and inertinites, which are also likely to interact with vitrinites in some reaction regimes. (The very different H/C ratios of these maceral groups leave little doubt that their chemistries differ significantly from those of vitrinites.)

The question becomes, then, whether further refinements of models and of the methods used to formulate them are likely to provide the predictive configurations that a systematic rank-dependent molecular chemistry implies, or whether coals of similar rank and petrographic compositions can be so differentiated by their source materials and formative histories so as to make them chemically quite disparate solids.

### *Some Anomalous Rank Effects*

An extreme case of early formative history determining the chemistry and physical properties of coal, well-known for over 100 years, presents itself in the differences between humic and sapropelic coals, that is, between coals that developed in partially aerobic and wholly anaerobic stagnant environments, respectively. It is therefore quite unreasonable to assume that the components of humic coals, which developed from plant debris that decayed in environments as different as high moors and deltaic swamps, were substantially unaffected by depositional influences and are therefore unified by a rank-dependent chemistry.

In fact, although chemical research on coal has rarely focused serious attention on the possible effects of different depositional environments and has usually discounted a scatter of data in rank-based correlations as due to "normal variations" among similar coals, extant literature contains many instances of "anomalous" behavior that cannot be so easily dismissed. Some examples may serve to illustrate this:

1. In graphical-statistical constitutional analysis (94), major structural parameters for coal are derived via a "reduced molar volume",  $M_c/d$ . In this term,  $M_c$  is a reduced molecular weight per C atom calculated from elemental compositions, by means of

$$M_c = 12.01 + 1.008(\text{H/C}) + 16.00(\text{O/C}) + 14.008(\text{N/C}) + 32.06(\text{S/C})$$



where H/C, O/C, N/C, and S/C are atomic ratios, and  $d$  is the true density of the coal. However, plots of  $d$  versus the carbon contents of coals from different regions display some significant differences. For suites of western European (95) and Japanese coals (96),  $d$  falls with increasing rank from approximately 1.52 g/cm<sup>3</sup> to a well-defined minimum at approximately 85% C where  $d = 1.26\text{--}1.28$  g/cm<sup>3</sup>. However, for a series of U.S. coals (97),  $d$  passes through a shallow minimum near 80% C and among coals with less than 80% C, it assumes substantially lower values than are reported for their western European counterparts. Such relative displacement may indicate an as yet unspecifiable impact of regional geological history (98).

2. Appropriately corrected for paramagnetic contributions, the diamagnetic susceptibility ( $\chi_{\text{dia}}$ ) of a coal can reflect its average chemical structure even more directly than the density. Although relatively few measurements of this parameter have been reported,  $\chi_{\text{dia}}$  it has in most cases been found to increase rapidly with rank up to about 80% C and among coals with more than 90% C, but to change only slowly between 80% and 90% C (99). Yet, for a suite of Japanese coals,  $\chi_{\text{dia}}$  increased linearly with carbon contents and thereby suggests that these coals followed a distinctly different maturation path than most other coals.

3. In a study of Canadian Cretaceous bituminous coals from the Rocky Mountain region (100), these coals, unlike their Carboniferous counterparts, initially chemisorbed oxygen to generate carbonyl moieties rather than -OH. They also yielded much less CHCl<sub>3</sub>-soluble matter after rapid heating to and quenching from, approximately 400 °C, and because of their much higher inherent content of phenolic -OH, exhibited markedly lower Gieseler fluidities.

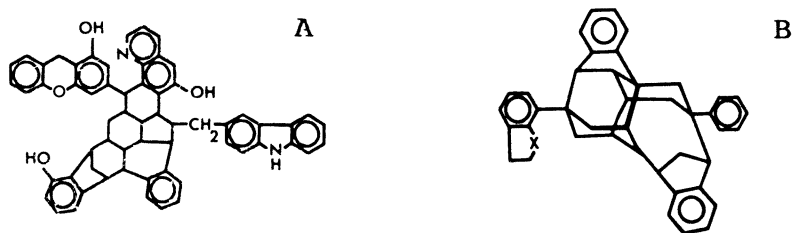
4. Although granular micrinites and semifusinites of Carboniferous coals do not soften and swell when heated, and are therefore classified as unreactive petrographic components, their equivalents in Cretaceous coals commonly display fairly pronounced plasticity (101, 102). Established standard correlations that connect coke stability with the petrographic compositions of Carboniferous coals (103) can consequently not be applied to Cretaceous coals without some modification (104).

5. In a study of coal halogenation (105), exhaustive bromination of two coals (one containing 77.7% C and the other 81.7% C) by treatment with Br-CHCl<sub>3</sub> at 0 °C, followed by hydrolysis of the brominated materials with 10% aqueous NaOH, yielded very different reaction products. In one case, hydrolysis ended after four Br atoms per 100 C atoms were replaced with -OH, while in the other it continued as an oxidation process that appeared to introduce =CO moieties and ended only after it had substituted 10 O atoms for five Br atoms per 100 C atoms.

6. In an investigation that sought to clarify the effects of coal rank on liquefaction yields (106), a computer cluster analysis of some 100 U.S. coals

in terms of 15 coal characteristics discriminated among three populations, but a useful predictive relationship between coal properties and percent conversion demanded a different set of properties for each population. Since two of the coal populations represented the U.S. Eastern (Appalachian) and Interior (Midwest) provinces, that is, Carboniferous coals with distinctly different time–temperature–pressure histories (107), while the third coal population was composed of Cretaceous coals from the Rocky Mountain region, it is difficult to avoid the conclusion that the liquefaction behavior of any particular coal is influenced by the nature of its source materials as well as by its geologic history. A similar conclusion was implicitly reached in another survey of coal liquefaction data in which grossly divergent rank variations of liquefaction yields were ascribed to different rank–reactivity relationships of coals from more or less widely separated geographic regions (108).

7. In a study of “short contact time” coal liquefaction (109), in which major product fractions were examined with respect to their structure as well as their composition, the (nominal) high-molecular-weight product fractions of two similar subbituminous coals were found to possess radically different formal structures (cf. structure 6): one showed  $C_{ar} \sim 73\%$  and  $H_{ar} \sim 60\%$ , and the other showed  $C_{ar} \sim 26\%$  and  $H_{ar} \sim 18\%$ . Significantly, both fractions were deemed to closely resemble their respective precursor coals but to be slightly more aromatized than they.



Structure 6. Proposed formal structures of high-molecular-weight fractions obtained by short-contact-time liquifaction of two subbituminous coals. A: precursor coal, western Kentucky subbituminous,  $C = 79.7\%$ ,  $H = 5.4\%$  (dry ash free),  $MW \sim 900$ ,  $C_{ar} \sim 73\%$ , and  $H_{ar} \sim 60\%$ ; and B: precursor coal, North Dakota subbituminous,  $C = 75.2\%$ ,  $H = 5.4\%$  (dry ash free),  $MW \sim 600$ ,  $C_{ar} \sim 26\%$ , and  $H_{ar} \sim 18\%$ . (Adapted from reference 109.)

## Conclusions

Observations such as those noted in the preceding section are too often simply disregarded or set aside as being “atypical”. However, taken in conjunction with observations from oxidation, solvent extraction, pyrolysis, and

the like, they point to a much greater chemical diversity of coals of similar rank than is currently assumed. The "average-structure" models so far proposed are therefore quite unlikely to offer more meaningful information about coal behavior than can be obtained from coal systematics (i. e., from empirical correlations that connect individual physical or chemical properties with rank and thereby allow a statistically probable behavioral pattern to be inferred from one or two analytical parameters.)

The cumulative evidence now at hand forces the conclusion that molecular structure and association in coal are strongly influenced, if not indeed largely determined, by the early formative history of the coal, that is, by the composition of its source materials and by the conditions that governed diagenetic change before burial. And it also suggests that subsequent metamorphic development, although progressively diminishing the distinctive chemical differences established by these factors, does not entirely obliterate them until the anthracite stage is reached. If so, chemical studies on coal directed to the formulation of predictive rank-based correlations will have to differentiate between pre- and post-Jurassic coals and to recognize the effects of the depositional environments in which they originated.

The current situation is, in a sense, not unlike an earlier one in which chemists disregarded the petrographers who emphasized the heterogeneity of coal and treated it as if it were a substantially homogeneous substance. Much might be gained by recognizing that data relating to humic coals of similar rank are not effectively equivalent. And real progress in understanding the chemistry of coal might well prove to depend on reappraisal of existing data bases with a view to separating data in light of what is known about the origins of the coals to which they relate. For practical purposes, it may also be necessary to pay much more attention to the chemistries of macerals other than vitrinites, and to possible interactions among vitrinites, exinites, and inertinites at the elevated temperatures that characterize most coal-processing regimes.

## References

1. Stopes, M. C.; Wheeler, R. V. *Dep. Sci. and Indus. Res.*, London, HMSO, 1918.
2. Seyler, C. A. *Proc. S. Wales Inst. Engrs.* **1938**, 53, 254; 396.
3. Mott, R. A. *J. Inst. Fuel* **1948**, 22, 2.
4. Berkowitz, N. *The Chemistry of Coal*; Elsevier: Amsterdam, 1985; pp 119-123.
5. Hirsch, P. B. *Proc. R. Soc. London* **1954**, A226, 14.
6. Cartz, L.; Hirsch, P. B. *Phil. Trans. R. Soc.* **1960**, A252, 557.
7. Karr, C., Jr. et al. U.S. Bureau of Mines Information Circular No. 7893, 1959.
8. Karr, C., Jr.; Comberati, J. R.; Estep, P. A. *Fuel* **1960**, 39, 475.
9. Karr, C., Jr.; Estep, P. A.; Hirst, L. L. *Anal. Chem.* **1960**, 32, 463.
10. Jäger, A.; Kattwinkel, G. *Brennst. Chem.* **1954**, 35, 353.
11. Jäger, A.; Kattwinkel, G. *Erdöl Kohle* **1955**, 8, 629.

12. *Chemistry of Coal Utilization, Suppl. Vol.* Lowry, H. H., Ed.; Wiley: New York, 1963; pp 66-78.
13. *Chemistry of Coal Utilization, 2nd Suppl. Vol.*; Elliott, M. A., Ed.; Wiley-Interscience: New York, 1981; pp 225-261.
14. Berkowitz, N. *The Chemistry of Coal*; Elsevier: Amsterdam, 1985; pp 49-55.
15. Shinn, J. H. *Fuel* 1984, 63, 1187.
16. Ruof, C. H.; Savich, T. R.; Howard, H. C. *J. Am. Chem. Soc.* 1951, 73, 3873.
17. Roy, A. N.; Howard, H. C. *J. Am. Chem. Soc.* 1952, 74, 3239.
18. Ihnatowicz, A. *Pr. Gl. Inst. Gorn.* 1952, *Komun. No.* 125.
19. Blom, L.; Edelhausen, L.; van Krevelen, D. W. *Fuel* 1957, 36, 135.
20. Kröger, C.; Darsow, G. *Erdöl Kohle* 1964, 17, 88.
21. Kröger, C.; Darsow, G.; Fuhr, K. *Erdöl Kohle* 1965, 18, 36.
22. Ignasiak, B. S.; Ignasiak, T. S.; Berkowitz, N. *Rev. Anal. Chem.* 1975, 2, 278.
23. Heredy, L. A.; Neuworth, M. B. *Fuel* 1962, 41, 221.
24. Heredy, L. A.; Kostyo, A. E.; Neuworth, M. B. *Fuel* 1963, 42.
25. *Ibid.* 1964, 43, 414.
26. *Ibid.* 1965, 44, 125.
27. Heredy, L. A.; Kostyo, A. E.; Neuworth, M. B. In *Coal Science*; Given, P. H., Ed.; ACS Advances in Chemistry 55; American Chemical Society: Washington, DC, 1966; p 493.
28. Ouchi, K.; Imuta, K.; Yamashita, Y. *Fuel* 1965, 44, 29, 205.
29. *Ibid.* 1973, 52, 156.
30. Darlage, L. J.; Weidner, J. P.; Block, S. S. *Fuel* 1974, 53, 54.
31. Darlage, L. J.; Bailey, M. E. *Fuel* 1976, 55, 205.
32. Hayatsu, R.; Scott, R. G.; Moore, L. P.; Studier, M. H. *Nature (London)* 1975, 257, 378.
33. *Ibid.* 1976, 261, 77.
34. Hayatsu, R.; Winans, R. E.; Scott, R. G.; Moore, L. P.; Studier, M. H. In *Organic Chemistry of Coal*; Larsen, J. W., Ed.; ACS Symposium Series, 71; American Chemical Society: Washington, DC, 1978, p 108.
35. Chakrabarty, S. K.; Kretschmer, H. *Fuel* 1972, 51, 160.
36. *Ibid.* 1974, 53, 132.
37. Mayo, F. R.; Kirshen, N. A. *Fuel* 1978, 57, 405.
38. *Ibid.* 1979, 58, 698.
39. Hayatsu, R.; Winans, R. E.; Scott, R. G.; Moore, L. P.; Studier, M. H. In *Organic Chemistry of Coal*; Larsen, J. W., Ed.; ACS Symposium Series, 71; American Chemical Society: Washington, DC, 1978, p 108.
40. Deno, N. C.; Greigger, B. A.; Stroud, S. G. *Fuel* 1980, 59, 694.
41. Raj, S. Ph.D. Thesis, Penn. State Univ., 1976.
42. Bimer, J.; Given, P. H.; Raj, S. *Prepr. Pap.—Am. Chem. Soc., Div. Fuel Chem.* 1977, 22(5), 169.
43. Bimer, J.; Given, P. H.; Raj, S. In *Organic Chemistry of Coal*; Larsen, J. W., Ed.; ACS Symposium Series 71; American Chemical Society: Washington, DC, 1978, p 86.
44. Hayatsu, R.; Winans, R. E.; Scott, R. G.; McBeth, R. L. *Fuel* 1981, 60, 158, 161.
45. Berkowitz, N. *The Chemistry of Coal*; Elsevier: Amsterdam, 1985; pp 155-171.
46. Pines, A.; Gibby, M. G.; Waugh, J. S. *J. Chem. Phys.* 1972, 56, 1776.
47. *Ibid.* 1973, 59, 569.
48. Bartle, K. D.; Martin, T. G.; Williams, D. F. *Fuel* 1975, 54, 226.
49. Bartle, K. D.; Jones, D. W. In *Analytical Methods for Coal and Coal Products*; Karr, J., Jr., Ed.; Academic: New York, 1978; Chapter 23.

50. Pugmire, R. J.; Grant, D. M.; Zilm, K. W.; Anderson, L. L.; Oblad, A. G.; Wood, R. E. *Fuel* **1977**, *56*, 295.
51. Zilm, K. W.; Pugmire, R. J.; Grant, D. M.; Wood, R. E.; Wisner, W. H. *Fuel* **1979**, *58*, 11.
52. Gerstein, B. C.; Murphy, P. D.; Ryan, L. M. In *Coal Structure*; Meyers, R. A., Ed.; Academic: New York, 1982; Chapter 4.
53. Retcofsky, H. L.; Link, T. A. In *Analytical Methods for Coal and Coal Products*; Karr, C., Jr., Ed.; Academic: New York, 1978; Chapter 24.
54. Griffiths, P. R. *Chemical Infrared Fourier Transform Spectroscopy*; Wiley: New York, 1975.
55. Solomon, P. R. *Prepr. Pap.—Am. Chem. Soc., Div. Fuel Chem.* **1979**, *24(2)*, 184.
56. Painter, P. C.; Coleman, M. M. *Fuel* **1979**, *58*, 301.
57. Tooke, P. B.; Grint, A. *Fuel* **1983**, *62*, 1003.
58. Davison, R. M. *Nuclear Magnetic Resonance Studies of Coal*; IEA Coal Research: London, 1986.
59. Gerstein, B. C. In *Analytical Methods for Coal and Coal Products*; Karr, C., Jr., Ed.; Academic: New York, 1978; Chapter 51.
60. Hagaman, E. W. *Anal. Chem.* **1986**, *58*, 387.
61. Sfihi, H.; Quinton, M. F.; Legard, A.; Pregermain, S.; Carson, D.; Chiche, P. *Fuel* **1986**, *65*, 1007.
62. Neavel, R. C. *Prepr. Pap.—Am. Chem. Soc., Div. Fuel Chem.* **1979**, *24*, 73.
63. Pugmire, R. J.; Wolfenden, W. R.; Mayne, C. L.; Grant, D. M. Proc. Coal Sci. Workshop, Houston, Dec. 1981, 201.
64. Entel, J.; Ruof, C. H.; Howard, H. C. *J. Am. Chem. Soc.* **1951**, *73*, 4152.
65. *Ibid.* **1952**, *74*, 441.
66. *Anal. Chem.* **1953**, *25*, 616.
67. *Fuel* **1957**, *35*, 409.
68. Huck, G.; Karweil, J. *Brennst. Chem.* **1953**, *34*, 97, 129.
69. Heredy, L. A.; Kostyo, A. E.; Neuworth, M. B. *Fuel* **1963**, *42*, 182.
70. Given, P. H. *Fuel* **1960**, *39*, 147.
71. *Ibid.* **1961**, *40*, 427.
72. Hill, G. R.; Lyon, L. B. *Ind. Eng. Chem.* **1962**, *54(6)*, 36.
73. Wisner, W. H. *Prepr. Pap.—Am. Chem. Soc., Div. Fuel Chem.* **1975**, *20(2)*, 122.
74. Pitt, J. G. In *Coal and Modern Coal Processing*; Pitt, J. G.; Millward, G. R., Eds.; Academic: London, 1979; pp 44-46.
75. Solomon, P. R. In *New Approaches in Coal Chemistry*; Blaustein, B. D.; Bockrath, B. C.; Friedman, S., Eds.; ACS Symposium Series 169; American Chemical Society: Washington, DC, 1981; p 61.
76. Heredy, L. A.; Wender, I. *Prepr. Pap.—Am. Chem. Soc., Div. Fuel Chem.* **1980**, *25(4)*, 38.
77. Wender, I.; Heredy, L.A.; Neuworth, M. B.; Dryden, I. G. C. In *Chemistry of Coal Utilization, 2nd Suppl. Vol.*; Elliott, M. A., Ed.; Wiley-Interscience: New York, 1981; pp. 503-521.
78. Nelson, J. B. *Fuel* **1954**, *32*, 153, 381.
79. Lazarov, L.; Angelova, G. *Fuel* **1968**, *47*, 333.
80. Wachowska, H.; Pawlak, W. *Fuel* **1977**, *56*, 422.
81. Dormans, H. N. M.; van Krevelen, D. W. *Fuel* **1960**, *39*, 273.
82. van Krevelen, D. W. *Fuel* **1966**, *45*, 99, 229.
83. Green, T.; Kovac, J.; Brenner, D.; Larsen, J. W. In *Coal Structure*; Meyers, R. A., Ed.; Academic: New York, 1982; Chapter 6.
84. Hombach, H. P.; Kölling, G. *Erdöl Kohle* **1972**, *25*, 644.
85. Hombach, H. P. *Erdöl Kohle* **1975**, *28*, 90.

86. Ibid. 1979, 32, 85.
87. Berkowitz, N. Proc. 11th Bienn. Lignite Symp., San Antonio, TX, 1981; U.S. Dept. Energy; GFETC/IC-82/1, vol. 1, 414.
88. Orchin, M.; Storch, H. H. *Ind. Chem.* 1948, 40, 1385.
89. Golumbic, C.; Anderson, J. R.; Orchin, M.; Storch, H. H. U.S. Bur. Mines Rep. Invest. No. 4662; U.S. Government Printing Office: Washington, DC, 1950.
90. Orchin, M.; Golumbic, C.; Anderson, J. B.; Storch, H. H. U.S. Bur. Mines, Bull. No. 505; U.S. Government Printing Office: Washington, DC, 1951.
91. Wachowska, H. *Fuel* 1979, 58, 99.
92. Sternberg, H. W.; Delle Donne, C. L.; Pantages, P.; Moroni, E. C.; Markby, R. E. *Fuel* 1971, 50, 432.
93. Sternberg, H. W.; Delle Donne, C. L. Ibid. 1974, 53, 172.
94. van Krevelen, D. W. *Coal*; Elsevier: Amsterdam, 1961.
95. Franklin, R. E. *Trans. Faraday Soc.* 1949, 45, 274.
96. Fujii, S.; Tsuboi, H. *Fuel* 1967, 46, 361.
97. Gan, H.; Nandi, S. P.; Walker, P. L., Jr. *Fuel* 1972, 51, 272.
98. Hatami, M.; Toda, Y.; Yoshida, Y. *Nenryo Kyokaiishi* 1969, 48, 235.
99. Honda, H.; Ouchi, K. *Fuel* 1957, 36, 159.
100. Berkowitz, N.; Fryer, J. F.; Ignasiak, B. S.; Szladow, A. J. *Fuel* 1974, 53, 141.
101. Nandi, B. N.; Montgomery, D. S. *Fuel* 1967, 46, 394.
102. Nandi, B. N.; Montgomery, D. S.; Proc. N. Am. Conf. on Coal Petrography, State College, Pa., 1972.
103. Shapiro, N.; Gray, R. J.; Eusner, G. R. *Proc. Blastfurn. and Raw Materials Conf.* 1961, 20, 89.
104. Ignasiak, B. S.; Berkowitz, N. *Bull. Can. Inst. Min. Metall.* 1974, July.
105. Brown, J. K.; Given, P. H.; Lupton, V.; Wyss, W. F. *J. Inst. Fuel* 1958, 31, A43.
106. Yarzab, R. F.; Given, P. H.; Davis, A.; Spackman, W. *Fuel* 1980, 59, 81.
107. Yarzab, R. F.; Baset, Z.; Given, P. H. *Geochim. Cosmochim. Acta* 1979, 43, 281.
108. Gorin, E. In *Chemistry of Coal Utilization, 2nd Suppl. Vol.*; Elliott, M. A., Ed.; Wiley-Interscience: New York, 1981; p 1845.
109. Whitehurst, D. D.; Farcasiu, M.; Mitchell, T. O.; Dickert, J. J. EPRI-AF-480, Research Project 410-1, Progr. Rept. 1976; Final Report, 1977; Electric Power Research Institute, San Francisco, CA.

RECEIVED for review November 4, 1986. ACCEPTED January 27, 1987.

# Preferred Annellated Structures of Polycyclic Aromatic Compounds in Coal-Derived Materials

Masaharu Nishioka and Milton L. Lee<sup>1</sup>

Department of Chemistry, Brigham Young University, Provo, UT 84602

*The structures and relative abundances of polycyclic aromatic compounds (both hydrocarbons and heterocycles) in a solvent-refined coal liquid and in a coal tar were compiled and compared. These structures and relative abundances were determined by detailed analyses performed in our laboratory during the past 7 years. The purpose of this comparison was to determine (1) if preferred aromatic structural features exist in the complex mixture of compounds present in a single coal-derived material and (2) to what extent these preferred structures are evident in different coal-derived materials produced from different feedstocks and under different conditions. Although different feedstocks and process conditions were associated with each of the two coal-derived products studied, remarkably similar structural trends could be seen. If one disregards the structures of the compounds produced by mild autocatalytic hydrogenation in the solvent-refined coal-liquefaction process, the structures of the remaining polycyclic aromatic compounds in both samples are similar. These results suggest that the major compounds identified are either representative of similar aromatic moieties in the original coal feedstock or are a result of processing conditions involving complex reactions that lead to similar stable final products. Because many similar aromatic moieties are found in coal in comparison with coal-derived materials, many of the same complex reactions may occur during diagenesis. Such reactions may include cyclo-coupling dehydrogenation.*

<sup>1</sup>To whom correspondence should be sent.

**C**OAL-DERIVED MATERIALS such as coal liquids and coal tars are highly aromatic, and these materials contain polycyclic aromatic compounds (PACs) as major components. Although average descriptive parameters such as molecular weight range, aromaticity, and abundances of functional groups are usually obtained to characterize such materials, detailed chemical analysis is also important for properly assessing health risks due to exposure to such materials and for understanding fundamental chemical reactions involved in upgrading technologies such as coal gasification and liquefaction (1, 2). In addition, detailed identification of constituents in coal-derived products could provide important information relevant to coal structure.

Because coal-derived liquids and tars are usually complex mixtures of organic chemicals, the separation and identification of individual PACs in these samples have been best accomplished by using open-tubular-column (capillary-column) gas chromatography (GC) (3, 4). Selective detectors for nitrogen and sulfur, as well as mass spectrometry (MS), can be easily combined with GC. Especially when authentic standard reference compounds and selective stationary phases (5–10) are used, capillary-column GC is, by far, the easiest and most reliable technique available.

During the past 7 years, we have developed and applied new methodologies using capillary-column GC for the separation and identification of PACs in coal-derived liquids. The primary samples that were used throughout these studies included a solvent-refined coal (SRC II) heavy distillate and a coal tar. Details of the isolation and identification of polynuclear aromatic hydrocarbons (PAHs) (11), sulfur heterocycles (12, 13), nitrogen heterocycles (14, 15), amino-substituted PACs (16–18), and hydroxy-substituted PACs (14, 19, 20) in an SRC II heavy distillate have already been published (11, 13, 15, 18, 21).

In the study reported here, the abundances and structural characteristics of the numerous PACs identified in the SRC II heavy distillate and the coal tar were compiled and compared. The purpose of this comparison was to determine (1) if preferred aromatic structural features exist in the complex mixture of compounds present in a single coal-derived material and (2) to what extent these preferred structures are evident in different coal-derived materials produced from different feedstocks and under different conditions. Explanations for differences in the compositions and relative abundances of PACs in these materials are proposed.

### ***Experimental Details***

The solvent-refined coal heavy distillate (SRC II HD, bp 260–450 °C) that was analyzed and used in this study was collected during the processing of a West Virginia coal from the Pittsburgh seam. Data from the analysis of a solvent-refined coal vacuum residue (SRC II VR) from the same process was also used. A coal tar was obtained from the National Bureau of Standards. This tar was a medium crude coke-oven tar



from an unknown coal feedstock. The samples were approximately 2 years old and were stored in a freezer at  $-10\text{ }^{\circ}\text{C}$ . Elemental analyses of the SRC II HD and the coal tar are given in the following table (values are weight percents):

<i>Element</i>	<i>SRC II HD</i>	<i>Coal Tar</i>
C	89.5	89.4
H	7.0	4.9
N	1.6	1.2
S	trace	0.8

Most of the compounds reported in this chapter were positively identified by comparison with standard reference compounds by using capillary GC and GC-MS. Standard compounds were obtained commercially or synthesized in one of our laboratories. The detailed identification procedures and results are reported elsewhere (11-21). The abbreviations for various PACs used in this chapter are given in the following list according to the format defined by Bartle et al. (21).

#### Abbreviations of Compound Classes Discussed in This Chapter

PAC	Polycyclic aromatic compound
PAH	Polycyclic aromatic hydrocarbon
PASH	Polycyclic aromatic sulfur heterocycle
PAOH	Polycyclic aromatic oxygen heterocycle
N-PAC	Nitrogen-containing polycyclic aromatic compound (both heterocyclic and nonheterocyclic compounds)
2°-PANH	Secondary-nitrogen polycyclic aromatic nitrogen heterocycles (nitrogen in a five-membered ring)
APAH	Amino-substituted polycyclic aromatic hydrocarbons
3°-PANH	Tertiary-nitrogen polycyclic aromatic nitrogen heterocycles (nitrogen in a six-membered ring)
HPAH	Hydroxy-substituted polycyclic aromatic hydrocarbons
APASH	Amino-substituted polycyclic aromatic sulfur heterocycles
PANSH	Polycyclic aromatic nitrogen sulfur heterocycles
HPASH	Hydroxy-substituted polycyclic aromatic sulfur heterocycles
HPANH	Hydroxy-substituted polycyclic aromatic nitrogen heterocycles

## Results and Discussion

Quantitative comparisons of the PACs in the SRC II HD and in the coal tar are given in Table I. The PACs containing two heteroatoms, such as amino-substituted polycyclic aromatic sulfur heterocycles (APASHs), polycyclic aromatic nitrogen-sulfur heterocycles (PANSHs), hydroxy-substituted polycyclic aromatic sulfur heterocycles (HPASHs), and hydroxy-substituted polycyclic aromatic nitrogen heterocycles (HPANHs), were present at 1-10 parts per million (ppm) in these samples. In comparison, the corresponding PACs containing a single heteroatom, such as the polycyclic aromatic sulfur heterocycles (PASHs), nitrogen-containing polycyclic aromatic compounds

**Table I. Quantitative Comparisons of Selected PACs in an SRC II Coal Liquid and in a Coal Tar**

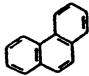
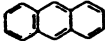
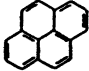
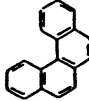
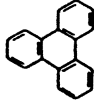
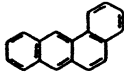
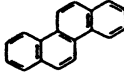
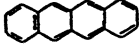
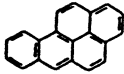
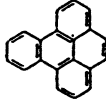

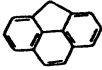
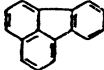
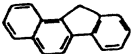
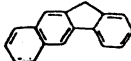
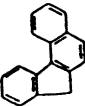
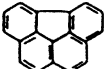
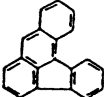
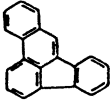
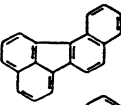
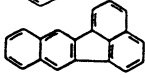
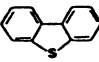
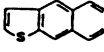
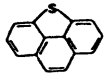
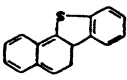
<i>Compound</i>	<i>Structure</i>	<i>Concentration<sup>a</sup></i>	
		<i>SRC II Coal liquid<sup>b</sup></i>	<i>Coal Tar</i>
PAHs			
Phenanthrene		95,000	53,000
Anthracene		3,500	12,000
Pyrene		61,000	31,000
Benzo[ <i>c</i> ]phenanthrene		— <sup>c</sup>	1,700
Triphenylene		— <sup>c</sup>	2,000
Benz[ <i>a</i> ]anthracene		2,000	8,000
Chrysene		3,600	8,600
Naphthacene		— <sup>c</sup>	— <sup>c</sup>
Benzo[ <i>a</i> ]pyrene		— <sup>c</sup>	9,700
Benzo[ <i>e</i> ]pyrene		— <sup>c</sup>	6,100
Cyclopenta-Containing PAHs			
Fluorene		13,000	13,000
4 <i>H</i> -Cyclopenta[ <i>def</i> ]phenanthrene		— <sup>c</sup>	6,300

Table I.—Continued

Compound	Structure	Concentration <sup>a</sup>	
		SRC II Coal liquid <sup>b</sup>	Coal Tar
Fluoranthene		12,000	40,000
Benzo[ <i>a</i> ]fluorene		8,900	3,700
Benzo[ <i>b</i> ]fluorene		7,700	3,600
Benzo[ <i>c</i> ]fluorene		— <sup>c</sup>	— <sup>c</sup>
Benzo[ <i>ghi</i> ]fluoranthene		— <sup>c</sup>	1,500
Benz[ <i>a</i> ]aceanthrylene		— <sup>c</sup>	400
Benz[ <i>e</i> ]acephenanthrylene		— <sup>c</sup>	7,900
Benzo[ <i>j</i> ]fluoranthene		— <sup>c</sup>	5,700
Benzo[ <i>k</i> ]fluoranthene		— <sup>c</sup>	4,900
PASHs			
Dibenzothiophene		39	1,500
Naphtho[2,3- <i>b</i> ]thiophene		— <sup>d</sup>	160
Phenanthro[4,5- <i>bcd</i> ]thiophene		140	970
Benzo[ <i>b</i> ]naphtho[2,1- <i>d</i> ]thiophene		27	53

Continued on next page.

Table I.—Continued

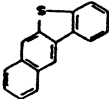
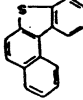
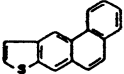
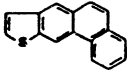
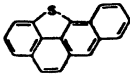
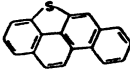
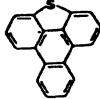
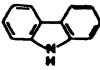
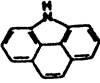
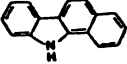
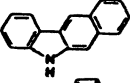
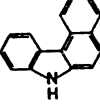
Compound	Structure	Concentration <sup>a</sup>	
		SRC II Coal liquid <sup>b</sup>	Coal Tar
Benzo[ <i>b</i> ]naphtho[2,3- <i>d</i> ]thiophene		3	6
Benzo[ <i>b</i> ]naphtho[1,2- <i>d</i> ]thiophene		2	15
Phenanthro[2,3- <i>b</i> ]thiophene		— <sup>d</sup>	4
Phenanthro[3,2- <i>b</i> ]thiophene		— <sup>d</sup>	10
Benzo[2,3]phenanthro[4,5- <i>bcd</i> ]thiophene		25	51
Chryseno[4,5- <i>bcd</i> ]thiophene		5	53
Triphenyleno[4,5- <i>bcd</i> ]thiophene		55	85
N-PACs			
Carbazole		7,400	4,400
4 <i>H</i> -Benzo[ <i>def</i> ]carbazole		— <sup>e</sup>	710
11 <i>H</i> -Benzo[ <i>a</i> ]carbazole		790	1,200
5 <i>H</i> -Benzo[ <i>b</i> ]carbazole		220	700
7 <i>H</i> -Benzo[ <i>c</i> ]carbazole		700	860

Table I.—Continued

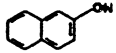
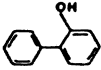
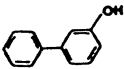
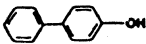
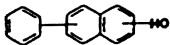
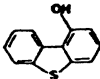
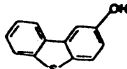
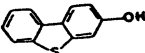
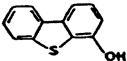
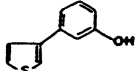
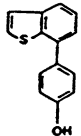
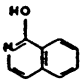
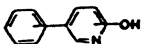
Compound	Structure	Concentration <sup>a</sup>	
		SRC II Coal liquid <sup>b</sup>	Coal Tar
1-Azadibenzothiophene		— <sup>e</sup>	1.7
2-Azadibenzothiophene		— <sup>e</sup>	— <sup>f</sup>
3-Azadibenzothiophene		— <sup>e</sup>	— <sup>f</sup>
4-Azadibenzothiophene		0.05	— <sup>f</sup>
Methylated PACs			
1-Methylphenanthrene		4,200	1,100
2-Methylphenanthrene		30,000	2,500
3-Methylphenanthrene		18,000	1,800
4-Methylphenanthrene		— <sup>c</sup>	— <sup>c</sup>
4-Methyldibenzothiophene		5	140
3-Methyldibenzothiophene		4	7
2-Methyldibenzothiophene		2	150
1-Methyldibenzothiophene		0.5	1
1-Methylcarbazole		1,700	190

Continued on next page.

Table I.—Continued

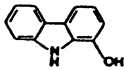
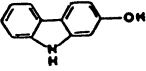
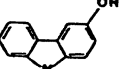
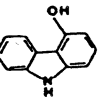
Compound	Structure	Concentration <sup>a</sup>	
		SRC II Coal liquid <sup>b</sup>	Coal Tar liquid <sup>b</sup>
2-Methylcarbazole		1,700	220
3-Methylcarbazole		3,500	160
4-Methylcarbazole		1,000	120
Amino PACs			
2-Aminobiphenyl		70	— <sup>d</sup>
3-Aminobiphenyl		50	— <sup>d</sup>
4-Aminobiphenyl		50	— <sup>d</sup>
Aminophenylnaphthalenes		— <sup>f</sup>	— <sup>d</sup>
1-Aminodibenzothiophene		0.32	— <sup>e</sup>
2-Aminodibenzothiophene		0.11	— <sup>e</sup>
3-Aminodibenzothiophene		2.5	— <sup>e</sup>
4-Aminodibenzothiophene		0.33	— <sup>e</sup>
Hydroxy PACs			
1-Hydroxynaphthalene		— <sup>d</sup>	80

Table I.—Continued

Compound	Structure	Concentration <sup>a</sup>	
		SRC II Coal liquid <sup>b</sup>	Coal Tar liquid <sup>b</sup>
2-Hydroxynaphthalene		— <sup>d</sup>	10
2-Hydroxybiphenyl		120	80
3-Hydroxybiphenyl		710	50
4-Hydroxybiphenyl		480	80
Naphthylphenols		— <sup>f</sup>	— <sup>d</sup>
1-Hydroxydibenzothiophene		3.4	1
2-Hydroxydibenzothiophene		10	1
3-Hydroxydibenzothiophene		— <sup>g</sup>	0.5
4-Hydroxydibenzothiophene		— <sup>g</sup>	0.2
3-(3-Hydroxyphenyl)thiophene		7.5	— <sup>g</sup>
7-(4-Hydroxyphenyl)benzothiophene		3	— <sup>g</sup>
1-Hydroxyisoquinoline		1.4	— <sup>g</sup>
Hydroxyphenylpyridines		— <sup>f</sup>	— <sup>g</sup>

Continued on next page.

Table I.—Continued

Compound	Structure	Concentration <sup>a</sup>	
		SRC II Coal liquid <sup>b</sup>	Coal Tar
1-Hydroxycarbazole		0.63	— <sup>g</sup>
2-Hydroxycarbazole		0.51	— <sup>g</sup>
3-Hydroxycarbazole		0.89	— <sup>g</sup>
4-Hydroxycarbazole		0.76	— <sup>g</sup>

<sup>a</sup>Approximate concentrations are given in micrograms per gram of original material.

<sup>b</sup>Concentrations of PASHs were determined for the SRC II VR, whereas concentrations of all others were determined for the SRC II HD.

<sup>c</sup>Compound was not detected at a concentration > 100 µg/g.

<sup>d</sup>Compound was not detected at a concentration > 1 µg/g.

<sup>e</sup>Compound was not detected at a concentration > 0.01 µg/g.

<sup>f</sup>Concentration of compound was not quantified because of coelution with other compounds or because several isomers were listed together.

<sup>g</sup>Compound was not detected at a concentration > 0.1 µg/g.

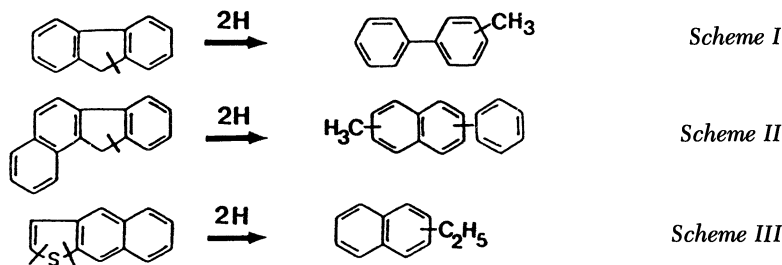
(N-PACs), and hydroxy-substituted polycyclic aromatic hydrocarbons (HPAHs) were present at 0.1–5%. In the following sections, compounds found in the two sample types are compared, and their origins are discussed. Because many details are not known concerning (1) the sources and compositions of the coal feedstocks and (2) the conditions and complexities of chemical reactions during processing, only general observations and explanations can be made. A number of exceptions to the general trends are expected in light of the complexities involved; nevertheless, noteworthy trends do exist and can be explained in a reasonable fashion.

**Mild Autocatalytic Hydrogenation.** The most significant difference between the compounds identified in the coal liquid and in the coal tar is the pronounced presence of hydrogenated compounds, tetrahydrophenanthrene, tetrahydrodibenzothiophene, and tetrahydrobenzoquinoline in the coal liquid (14). Recently, a large number of hydroaromatic compounds in the SRC II HD were identified (23, 24). Although the SRC II process is not considered to be a hydrogenation coal-liquefaction process, mild auto-

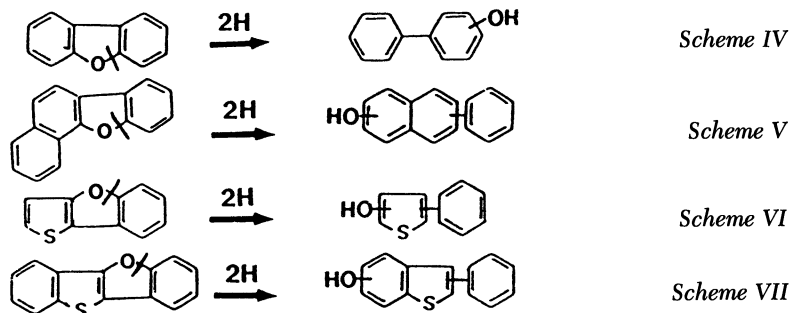


catalytic hydrogenation does take place. The 9- and 10- positions of anthracene are markedly reactive toward hydrogenation in comparison with other PAHs such as benzene, naphthalene, and phenanthrene. Similar results were reported in the correlation between the reaction constants for bromination, and reactivity values of selected PAHs (25). The abundance of anthracene relative to phenanthrene was low in the SRC II HD in comparison to that in the coal tar. This result seems to be due to the high reactivity of anthracene towards hydrogenation. Similar arguments can be applied to acridine; the abundance of acridine relative to the benzoquinolines and benzoisoquinolines in the SRC II HD was quite low (21).

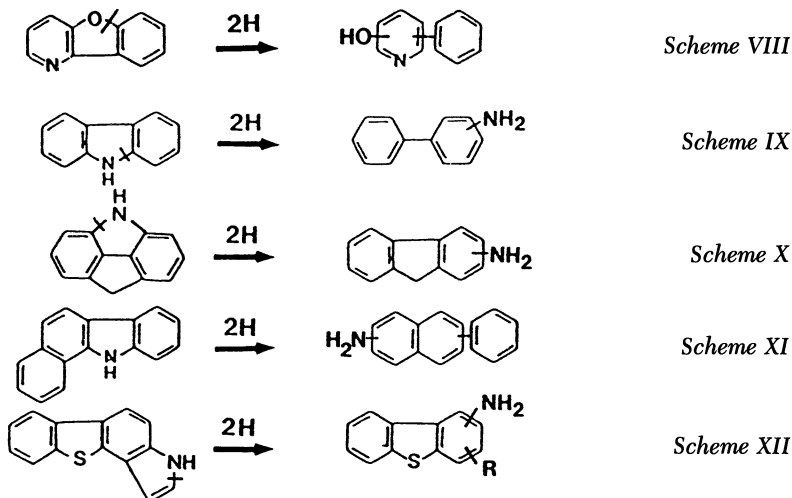
Cyclopenta-containing compounds were relatively less abundant in the SRC II HD than in the coal tar, whereas biphenyl, phenyl-naphthalene, and their alkylated isomers were found in significant concentrations in the SRC II HD (11). The cyclopenta-containing compounds such as fluorene and benzofluorene are thought to be hydrogenated as shown in Schemes I and II. The SRC II coal liquid lacked naphtho[2,3-*b*]thiophene and its benzo analogues. These compounds, with fusion on only one side of the thiophene ring, can be hydrodesulfurized more easily than thiophenic compounds with aromatic rings fused on both sides, as shown in Scheme III (26). Although the SRC II process is generally considered to be a noncatalytic thermal process in comparison with a thermal catalytic process, for example, the Exxon Donor Solvent process (27), it is assumed to be somewhat autocatalytic as discussed earlier, but only mild hydrogenation occurs. The hydrogenation reaction is important for understanding the structural characteristics of the SRC II materials.



The effects of autocatalytic hydrogenation are demonstrated by the relative abundances of PACs containing functional groups, for example, HPAHs and amino-substituted polycyclic aromatic hydrocarbons (APAHs) in the SRC II coal liquid and coal tar. The suggested reactions for HPAHs and HPASHs in the SRC II HD are shown in Schemes IV–VII. The condensed HPAHs such as the hydroxyphenanthrenes, hydroxypyrenes, and hydroxychrysenes were predominant in the coal tar, whereas the hydrogenated compounds such as the hydroxybiphenyls, naphthylphenols, hydroxyphenylthiophenes,



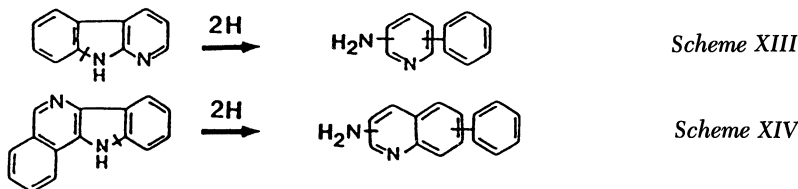
and hydroxyphenyl, benzothiophenes were major components in the SRC II HD. Similarly, the hydroxyphenylpyridines were one of the major compound types in the SRC II HD (Scheme VIII). The HPAH fraction of the SRC II HD (8.8%) was a larger percentage of the original sample than the HPAH fraction of the coal tar (2.8%). The different abundances of two- and three-ring APAHs and APASHs in the two samples can also be explained by hydrogenation (Schemes IX–XII).



Recently, quantitation of PACs in samples produced under different SRC conditions was reported (28). The concentrations of carbazole, which is thought to be the compound from which the aminobiphenyls were formed is as follows: 4500 ppm (SRC I process solvent), 2200 ppm (SRC II fuel-oil blend, which corresponds to the total process solvent fraction), and 31 ppm (high-hydrogen SRC II fuel-oil blend). The process bottoms were not re-

cycled in the SRC I process. These similar trends were also observed for fluorene and dibenzofuran. Although the compositions of the feedstocks were not known, the variation in concentration suggests the possibility of hydrogenation of carbazole, fluorene, and dibenzofuran. The most abundant aminobiphenyl isomer in the SRC II HD was 2-aminobiphenyl (15). This result also supports the suggested hydrogenation reaction. The 2-aminobiphenyl isomer may be a useful indicator of the concentration of APAHs. Similarly, 2-hydroxybiphenyl and 2-methylbiphenyl could be indicators of hydrogenation. 2-Hydroxybiphenyl, which was the most abundant hydroxybiphenyl isomer, was most highly concentrated in an SRC II middle distillate (180–392 °C) as shown by White and Li (29).

The foregoing discussion indicates that the aminophenylpyridine and aminophenylquinoline isomers would be produced by hydrogenation of heterocycles containing two nitrogen heteroatoms (Schemes XIII and XIV). These compounds were concentrated in the third fraction during adsorption chromatography on silicic acid. The major components were tentatively identified by using GC–MS as aminophenylpyridines, aminophenylquinolines, and their alkylated products (30).



**Comparative Trends in Preferred PAC Structures.** If the structures of the compounds produced by autocatalytic hydrogenation in the SRC II process as just described are disregarded, the structures of the remaining compounds in the coal liquid and coal tar are remarkably similar. Major alternate PAHs are phenanthrene, pyrene, chrysene, benz[*a*]anthracene, benzo[*a*]pyrene, benzo[*e*]pyrene, benzo[*ghi*]perylene, dibenzo[*def,mno*]chrysene, and coronene. Two major factors contributing to the existence of these major PAHs are (1) the structural composition of the coal feedstock, which is composed of crosslinked macromolecules (31–33) of biological origin, and (2) the stabilities of the aromatic components produced during processing, for which an important factor is the resonance energies for the conjugated systems.

The phenanthrene and chrysene structures could be derived from cyclic terpenoids such as abietic acid, sterols, and hopanes (34). Although triphenylene, which has the highest resonance energy among the four-ring catacondensed PAHs (35), was not present in the SRC II HD at a significant level, this compound was found in the coal tar which is a higher temperature

**American Chemical Society  
Library**

1155 16th St., N.W.  
Washington, D.C. 20036

product than the SRC II HD. The order of Hückel  $\pi$ -electron energies for the benzofluoranthene isomers is benz[*a*]aceanthrylene < benzo[*k*]fluoranthene < benzo[*j*]fluoranthene < benz[*e*]acephenanthrylene (35). The abundances of benz[*a*]aceanthrylene and benz[*e*]acephenanthrylene in the coal tar were the lowest and highest, respectively.

Although the abundances of the benzofluoranthene isomers are consistent with their resonance energies, other factors must be considered when comparing other isomer pairs. For example, in comparing benzo[*a*]pyrene with benzo[*e*]pyrene, benzo[*a*]pyrene is the less resonance-stable isomer but is the one that can be formed most easily from the biologically derived chrysene or benz[*a*]anthracene. In this case, benzo[*a*]pyrene is the most abundant isomer of the two in the coal tar. No universal rules can explain all observations; only general trends can be indicated.

Structural correlations between the PASHs and PAHs found in petroleum, coal tar, and pitch have been noted by Karcher et al. (36) and Burchill et al. (37). They found that the sulfur-containing materials contained thiophene derivatives analogous to the PAHs; the materials differed only in the replacement of one aromatic ring in the PAHs by a thiophene ring. We (13) recently reported that the structures and relative abundances of the major PASH containing three- to six rings in the SRC II VR and in the coal tar were analogous to those of the major PAHs in the same samples. By replacing one of the aromatic rings in the most abundant PAHs with a thiophene ring, the most abundant PASH could be generally derived. Similarly, this correlation holds for cyclopenta-containing PAHs and secondary-nitrogen polycyclic aromatic nitrogen heterocycles (2°C-PANH), as shown in Chart I. The most abundant cata-condensed four-ring PAHs in both samples studied here was chrysene. Benzo[*a*]fluorene benzo[*b*]naphtho[2,1-*d*]thiophene, phenanthro[3,2-*b*]thiophene, and 11*H*-benzo[*a*]carbazole, which have analogous structures to chrysene, were the most abundant among their respective isomers. Isomers such as benzo[*b*]fluorene, which also corresponds to another abundant cata-condensed four-ring PAH, namely, benz[*a*]anthracene, were also major compounds. Benzo[*a*]pyrene was more abundant than benzo[*e*]pyrene in the coal tar. The PASHs corresponding to benzo[*a*]pyrene were benzo[2,3]phenanthro[4,5-*bcd*]thiophene and chryseno[4,5-*bcd*]thiophene, whereas the only PASH corresponding to benzo[*e*]pyrene was triphenyleno[4,5-*bcd*]thiophene. The structures and relative abundances of the major PACs containing a single heteroatom are analogous to those of the major PAHs, as shown in Chart I.

Likewise, the major PACs containing two heteroatoms in both samples could be structurally derived from the major PACs containing a single heteroatom. Dibenzothiophene, phenanthro[4,5-*bcd*]thiophene, and the benzonaphthothiophenes were the major three- and four-ring PASHs in both samples; the benzoquinolines, azapyrenes, and benzophenanthridines were the major three- and four-ring N-PACs. Similarly, azadibenzothiophenes

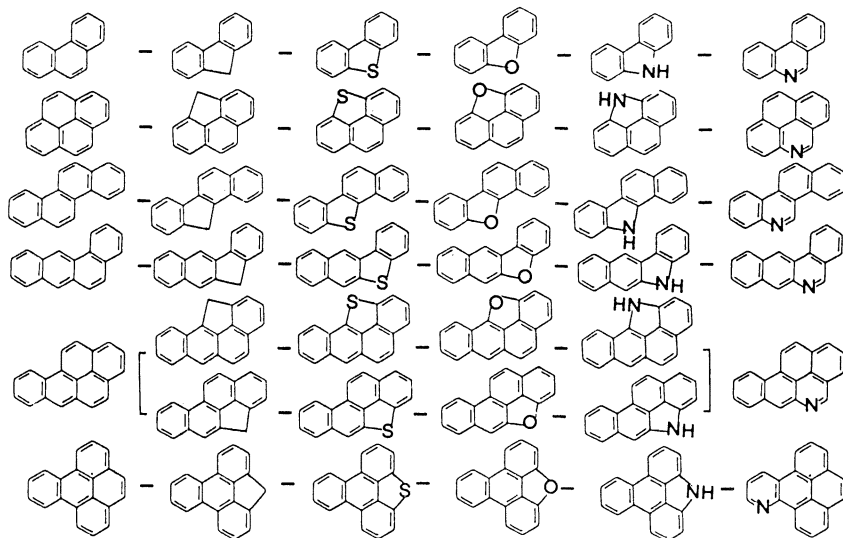


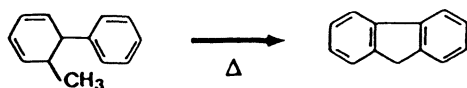
Chart I. Structural similarities of the major PACs identified in the SRC II coal liquids and in the coal tar.

and azabenzonaphthothiophenes were found in both samples. Azabenzothiophenes, aminodibenzothiophenes, and azaphenanthro[4,5-*bcd*]thiophenes were identified in one or the other of the samples at low concentrations. Similar compounds were found for the hydroxy-sulfur-containing PACs and hydroxy-nitrogen-containing PACs; that is, the structures of the major PACs containing a single heteroatom reflect those of major parent PAHs, and the structures of the major PACs containing two heteroatoms reflect those of the major PACs containing a single heteroatom.

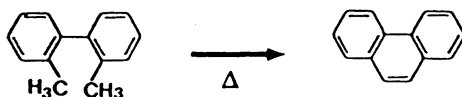
Several correlations were also found for positions of substitution on the aromatic molecules.  $\beta$  methyl-substituted isomers, such as 2- and 3-methylphenanthrene, were more abundant than  $\alpha$ -substituted isomers, such as 1- and 4-methylphenanthrene. This trend was observed for the methyl-naphthalenes, methylphenanthrenes, and methylchrysenes (11). However, the relative abundances of positions of substitution were not consistent for the methyl-dibenzothiophenes and methylcarbazoles when compared with the methylphenanthrenes; different factors are involved in their production. The methyl-substituted PACs are probably highly related to the alkyl linkages in the original coal structure. For the hydroxy- and amino-substituted PACs, hydrogenation in the SRC II process is an important factor.

**Cyclo-Coupling Dehydrogenation during Liquefaction and Coalification.** The correlations of compound structures described in the foregoing discussion suggest the possibility of similar reactions occurring

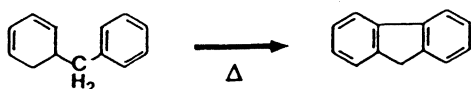
during diagenesis or coal upgrading. One important reaction is believed to be coupling dehydrogenation of aromatic moieties by heating. Model condensation reactions expected for the coupling of two aromatic moieties are shown in Schemes XV–XXII. The reactions in Schemes XV–XVII were extensively studied under heating with no catalyst by Badger (38). The PAHs, benz[*a*]anthracene and benzo[*a*]fluoranthene, can be produced according to



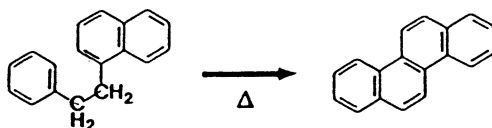
Scheme XV



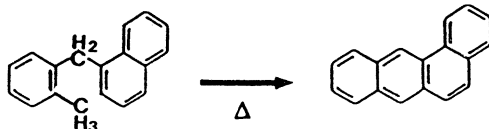
Scheme XVI



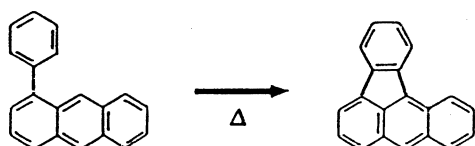
Scheme XVII



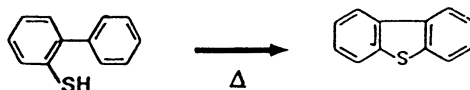
Scheme XVIII



Scheme XIX



Scheme XX

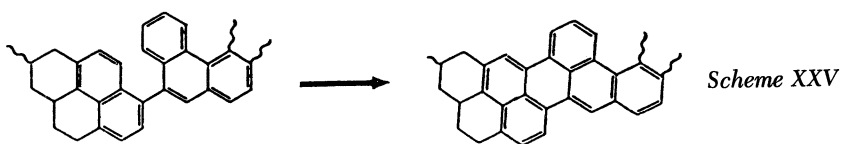
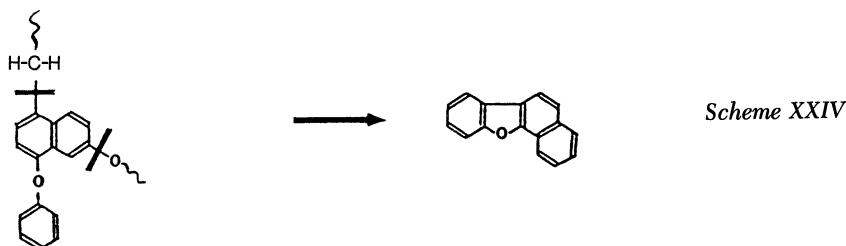
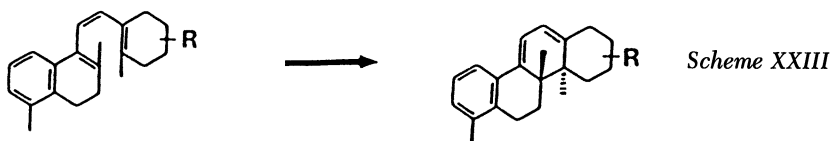


Scheme XXI



Scheme XXII

Schemes XIX and XX. Secondary cyclo-coupling dehydrogenations are apparently important for the production of highly pericondensed compounds such as dibenzo[*def,mno*]chrysene, coronene, and triphenyleno[4,5-*bcd*]thiophene (39, 40). For heteroatom-containing compounds, Schemes XXI and XXII are possible examples. Recently, many polycyclic aromatic oxygen heterocycles (PAOHs) were produced by self-coupling of hydroxy compounds by McMillen et al. (41). These types of coupling or condensation reactions may be possible for molecules such as aromatic triterpanes (Scheme XXIII) by bond breakage and ring formation of aromatic moieties linked together with alkyl or heteroatom bridges (Scheme XIV), and cyclization of aromatic moieties in a macromolecular network (Scheme XXV). Further investigation into such reactions in coal may prove to be invaluable in future studies of coal structure.



### Acknowledgment

This work was supported by the Office of Health and Environmental Research, U.S. Department of Energy, under Contract No. DE-FG02-86ER60445.

### References

1. Speight, J. G. *The Chemistry and Technology of Coal*; Marcel Dekker: New York, 1983.

2. Lee, M. L.; Novotny, M. V.; Bartle, K. D. *Analytical Chemistry of Polycyclic Aromatic Compounds*; Academic: New York, 1981.
3. *Handbook of Polycyclic Aromatic Hydrocarbons*; Bjorseth, A., Ed. Marcel Dekker: New York, 1983; pp 525–614.
4. Lee, M. L.; Yang, F. J.; Bartle, K. D. *Open Tubular Column Gas Chromatography*; Wiley: New York, 1984; pp 312–352.
5. Kuei, J. C.; Shelton, J. I.; Castle, L. W.; Kong, R. C.; Richter, B. E.; Bradshaw, J. S.; Lee, M. L. *J. High Resolu. Chromatogr. Chromatogr. Commun.* 1984, 7, 13–18.
6. Jones, B. A.; Bradshaw, J. S.; Nishioka, M.; Lee, M. L. *J. Org. Chem.* 1984, 49, 4947–4951.
7. Markides, K. E.; Nishioka, M.; Tarbet, B. J.; Bradshaw, J. S.; Lee, M. L. *Anal. Chem.* 1985, 57, 1296–1299.
8. Lee, M. L.; Kuei, J. C.; Adams, N. W.; Tarbet, B. J.; Nishioka, M.; Jones, B. A.; Bradshaw, J. S. *J. Chromatogr.* 1984, 302, 303–318.
9. Nishioka, M.; Bradshaw, J. S.; Lee, M. L.; Tominaga, Y.; Tedjamulia, M.; Castle, R. N. *Anal. Chem.* 1985, 57, 309–312.
10. Nishioka, M.; Jones, B. A.; Tarbet, B. J.; Bradshaw, J. S.; Lee, M. L. *J. Chromatogr.* 1986, 357, 79–91.
11. Nishioka, M.; Chang, H.-C.; Lee, M. L. *Environ. Sci. Technol.* 1986, 20, 1023–1027.
12. Nishioka, M.; Campbell, R. M.; Lee, M. L.; Castle, R. N. *Fuel* 1986, 65, 270–273.
13. Nishioka, M.; Lee, M. L.; Castle, R. N. *Fuel* 1986, 65, 390–396.
14. Later, D. W.; Lee, M. L.; Bartle, K. D.; Kong, R. C.; Vassilaros, D. L. *Anal. Chem.* 1981, 53, 1612–1620.
15. Nishioka, M.; Smith, P. A.; Booth, G. M.; Lee, M. L.; Kudo, H.; Muchiri, D. R.; Castle, R. N.; Klemm, L. H. *Fuel* 1986, 65, 711–714.
16. Later, D. W.; Lee, M. L.; Wilson, B. W. *Anal. Chem.* 1982, 54, 117–123.
17. Later, D. W.; Andros, T. G.; Lee, M. L. *Anal. Chem.* 1983, 55, 2126–2132.
18. Nishioka, M.; Campbell, R. M.; West, W. R.; Smith, P. A.; Booth, G. M.; Lee, M. L.; Kudo, H.; Castle, R. N. *Anal. Chem.* 1985, 57, 1868–1871.
19. Nishioka, M.; Lee, M. L.; Kudo, H.; Muchiri, D. R.; Baldwin, L. J.; Pakray, S.; Stuart, J. G.; Castle, R. N. *Anal. Chem.* 1985, 57, 1327–1330.
20. Nishioka, M.; Campbell, R. M.; Lee, M. L.; Muchiri, D. R.; Stuart, J. G.; Castle, R. N. *Anal. Chem.* 1985, 57, 2211–2215.
21. Nishioka, M. Ph.D. Thesis, The University of Hokkaido, Japan, 1986.
22. Bartle, K. D.; Lee, M. L.; Wise, S. A. *Chem. Soc. Rev.* 1981, 35, 113–158.
23. Wozniak, T. J.; Hites, R. A. *Anal. Chem.* 1985, 57, 1314–1319.
24. Wozniak, T. J.; Hites, R. A. *Anal. Chem.* 1985, 57, 1320–1327.
25. Altschuler, L.; Berliner, E. *J. Am. Chem. Soc.* 1966, 88, 5837–5845.
26. Drushel, H. V.; Sommers, A. L. *Anal. Chem.* 1967, 39, 1819–1829.
27. Furlong, L. E.; Efron, E.; Vernon, L. W.; Wilson, E. L. *Chem. Eng. Prog.* 1976, 72(8), 69–72.
28. Wilson, B. W.; Later, D. W.; Haugen, D. A. *Health Effects in Coal Conversion Processes*, DOE Report, 1985.
29. White, C. M.; Li, N. C. *Anal. Chem.* 1982, 54, 1570–1572.
30. Nishioka, M.; Booth, G. M.; Lee, M. L.; Castle, R. N. *Prepr. Pap.—Am. Chem. Soc., Div. Fuel Chem.* 1986, 31(2), 156–162.
31. Larsen, J. W.; Kovac, J.; In *Organic Chemistry of Coal*; Larsen, J. W., Ed.; ACS Symposium Series 71; American Chemical Society: Washington, DC, 1978, pp 36–49.



32. Green, T.; Kovac, J.; Brenner, D.; Larsen, J. W. In *Coal Structure*; Meyer, R. A., Ed.; Academic: New York, 1982; pp 199–282.
33. Brenner, D. *Fuel* **1985**, *64*, 167–173.
34. Given, P. H. In *Coal Science Vol. 3*; Garbaty, M. L.; Larsen, J. W.; Wender, I., Eds.; Academic: New York, 1984, pp 63–252.
35. Zahradnik, R.; Pancir, J. *HMO Energy Characteristics*; IFI/Plenum: New York, 1970.
36. Karcher, W.; Depaus, R.; van Eijk, J.; Jacob, J., In *Polynuclear Aromatic Hydrocarbons*; Jones P. W.; Leber P., Eds.; Ann Arbor Sci.: Ann Arbor, 1979; pp 341–356.
37. Burchill, P.; Herod, A. A.; Pritchard, E. *J. Chromatogr.* **1982**, *242*, 51–64.
38. Badger, G. M.; Jolad, S. D.; Spotswood, T. M. *Aust. J. Chem.* **1967**, *20*, 1439–1450.
39. Otani, S.; Sanada, Y., In *Basics of Carbonization Engineering* (Japanese); Ohmsha: Tokyo, 1980, Chapters 2, 3.
40. Otani, S. *Jpn. Pet. Inst.* **1975**, *18*, 699–704.
41. McMillen, D. F.; Chang, S.-J.; Nigenda, S. E.; Malhotra, R. *Prepr. Pap.—Am. Chem. Soc., Div. Fuel Chem.* **1985**, *30(4)*, 414–418.

RECEIVED for review September 29, 1986. ACCEPTED April 4, 1987.

# Selective Methylation of Hydroaromatic C–H Sites in Coal

## The Importance of Fluorene-Like Structural Units in Bituminous Coals

R. Rife Chambers, Jr., Edward W. Hagaman, and Madge C. Woody

Chemistry Division, Oak Ridge National Laboratory, Oak Ridge, TN 37831

*An O-methylated low-volatile bituminous coal, PSOC 1197, was treated repetitively with a series of carbanion bases and then quenched with  $^{13,14}\text{C}$  double-labeled methyl iodide. The extent of methylation depended upon the identity of the base and increased in the order 9-phenylfluorenyllithium  $\ll$  fluorenyllithium  $\sim$  trityllithium. A significant number of methyl groups (0.7 per 100 coal carbons) was introduced by using fluorenyllithium and trityllithium, but the coal was relatively unreactive toward methylation when 9-phenylfluorenyllithium was the base. Additional methyl groups could be introduced after repetitive treatments. This result and the cross-polarization/magic angle spinning  $^{13}\text{C}$  NMR spectra of the coal derivatives obtained by using fluorenyllithium as base indicate the reaction of acidic  $-\text{CH}_2-$  and  $-\text{C}(\text{H})\text{R}-$  sites. On the basis of these results, PSOC 1197 could contain a significant number (0.7–1.9 per 100 coal carbons) of fluorene-like structural units.*

**D**EFINITIVE EVIDENCE FOR THE BASIC CARBON FRAMEWORK of coal remains quite limited despite numerous investigations into coal structure. Many views of the chemical composition of coal have evolved from analyses of coal degradation products such as those obtained from oxidation, reduction, and high-temperature pyrolysis (1). Although these methods are useful for detecting compositional variations among coals of different ranks and history, attempting to relate the final products back to an original coal pre-

cursor for a given sample is virtually impossible because of the severity of the reaction conditions.

For some time, we have been interested in designing selective chemical modification reactions for coal with a particular emphasis upon characterizing the carbon skeleton of coal (2). The strategy for the approach starts with the working hypothesis that coal can be viewed as a three-dimensional macromolecule in which aromatic and hydroaromatic clusters are cross-linked to one another by various functional groups such as methylene units and polymethylene chains. In addition, the aromatic and hydroaromatic clusters, at least in bituminous coals, are assumed to be derived from polynuclear aromatic compounds (3, 4).

We recognized that the ionization constants, or  $K_a$  values, of the benzylic C–H groups in hydroaromatic compounds can vary by many orders of magnitude and that they are a sensitive indicator of structural detail. This observation suggested that these differences in acidity could be exploited as a means for selectively forming carbanions. The resulting carbanions can then serve as the focal point for preparing the coal derivatives. Furthermore, a knowledge of coal response to a series of base solutions of varying, but known, base strength is believed to be useful in assigning a structure to the reactive functional groups containing acidic C–H sites. For these reasons, we investigated the reaction of a bituminous coal with a series of carbanionic indicator base solutions followed by quenching with  $^{13,14}\text{C}$  double-labeled methyl iodide. The results from our studies of an *O*-methylated low volatile bituminous coal, PSOC 1197, indicate a significant number of acidic C–H sites with  $\text{p}K_a$  values comparable to that of fluorene. This important observation parallels our previous results with a high-volatile bituminous coal, Illinois No. 6 (2). The combined results from these two studies on coals of differing rank and history help to reinforce our previous position about coal structure, namely, that fluorene-like structural units could be an important class of polynuclear hydroaromatic clusters in bituminous coal.

### Experimental Details

**Materials.** The preparation, purification, and analyses of 9-phenylfluorene, fluorene, triphenylmethane,  $[9-^{14}\text{C}]\text{fluorene}$ , triphenyl $[^{14}\text{C}]\text{methane}$  and  $[^{13,14}\text{C}]\text{H}_3\text{I}$  have been described previously (2). Tetrabutylammonium hydroxide (Fluka, 1.5 M), *n*-Bu<sub>4</sub>NOH, was titrated against standard HCl prior to use. *n*-Butyllithium (*n*-BuLi, Aldrich, 1.6 M) was standardized periodically against diphenylacetic acid according to published procedures (5). Tetrahydrofuran (THF) was freshly distilled from LiAlH<sub>4</sub> by using triphenylmethane as an indicator.

$[^{13,14}\text{C}_2]\text{DIMETHYL SULFATE}$ . The following preparation is representative of the general methodology. To cold ( $-80\text{ }^\circ\text{C}$ )  $[^{14}\text{C}]\text{methanol}$  (124 mmol,  $719.3 \pm 2.2\text{ MBq/mol}$ ) (MBq = Mega Becquerel) (2) was carefully added freshly distilled ClSO<sub>3</sub>H (bp  $73\text{--}75\text{ }^\circ\text{C}$  at 4.0 kPa, 123 mmol). After the addition period, the cold

bath was removed, and the reaction mixture was stirred for 1 h. The mixture was then warmed to 85–90 °C and maintained in this temperature range for 3 h. The crude product was isolated by vacuum distillation (bp 88–105 °C at 3.7 kPa) and then treated with anhydrous  $K_2CO_3$ . A second distillation from BaO gave 31 mmol of [ $^{14}C_2$ ]dimethyl sulfate (bp 76–83 °C at 2.6 kPa, 50% yield) with a specific activity of  $1446 \pm 3$  MBq/mol. This product was combined with commercially available [ $^{13}C$ ]dimethyl sulfate (Merck, 99 atom %  $^{13}C$ ) to give the desired isotopic enrichments. The  $^{13}C$  assay was determined from the 1H NMR spectrum of the product, and the  $^{14}C$  radioassay was measured by combustion analysis.

**COAL SAMPLE.** The PSOC 1197 coal used in this study was a low-volatile bituminous coal from the Lower Kittanning seam in eastern Pennsylvania and was obtained through the Pennsylvania State Coal Sample Bank program. The coal was ground to particle size  $\leq 150 \mu m$  and then was stored under argon. Elemental analysis (Galbraith Labs) gave the following composition (values are weight percentages): C,  $79.31 \pm 0.09$ ; H,  $4.22 \pm 0.06$ ; N,  $1.42 \pm 0.02$ ; S,  $1.09 \pm 0.03$ ; O,  $3.61 \pm 0.26$  (by difference); ash,  $10.36 \pm 0.06$ . This analysis corresponds to the following empirical formula:  $C_{100}H_{64}N_{1.5}S_{0.5}O_3$ .

### O-Methylation and Base Hydrolysis Procedures.

**pH 12 O-METHYLATION.** A slurry of PSOC 1197 coal (0.500 g) in 1.5 mL of THF was neutralized with *n*-Bu $_4$ NOH (1.54 M, 5.39 mmol). The mixture was stirred for 16 h under argon, after which H $_2$ O (5.0 mL) was added. The pH of the sample was monitored with a double-junction, combination glass electrode (Cole–Parmer K-5998-20). The pH was adjusted to 12 by adding 0.690 M HCl. After allowing 1 h for the pH to stabilize, [ $^{13,14}C_2$ ]dimethyl sulfate (3.16 mmol,  $754.1 \pm 1.1$  MBq/mol, 51.8 atom %  $^{13}C$ ) was introduced, and the pH was maintained at 12 for 2 h by the addition of dilute *n*-Bu $_4$ NOH. After reducing the pH to 7.3 (0.1 N HCl), a second portion of [ $^{13,14}C_2$ ]dimethyl sulfate (3.16 mmol) was added, and the pH was held constant at 7 for 2 h by adding dilute *n*-Bu $_4$ NOH. Then, the sample was filtered, washed with 4 L of hot H $_2$ O, and dried under vacuum (110 °C, 6.6 Pa) overnight. The coal was assayed for its  $^{14}C$  content by combustion analysis. The number of introduced [ $^{14}C_2$ ]H $_3$  groups was calculated by using the combustion results and the elemental analysis of the coal derivative.

**pH 7 O-METHYLATION.** The procedure is analogous to that outlined for the pH 12 O-alkylation with the following exceptions: The pH was initially lowered to 7, and only one portion of [ $^{13,14}C$ ]dimethyl sulfate (3.16 mmol/0.5 g coal) was introduced during the alkylation step.

**BASE HYDROLYSIS.** To a slurry of O[ $^{13,14}C$ ]H $_3$  coal (0.25 g) in 9.7 mL of THF was introduced *n*-Bu $_4$ NOH (1.54 M, 2.45 mmol), and the resultant mixture was stirred under argon for 68 h. The sample was then transferred to a beaker, H $_2$ O (10 mL) was added, and the pH was adjusted to 2 (1 N HCl). The THF was removed under vacuum, after which the product was placed on a funnel and

washed with hot H<sub>2</sub>O (2 L). After vacuum drying (110 °C, 6.6 Pa) overnight, the coal was analyzed for the number of remaining [<sup>14</sup>C]H<sub>3</sub> groups in the manner described earlier. The number of base-labile [<sup>14</sup>C]H<sub>3</sub> groups was taken as the difference between the original number of methyl groups introduced and those remaining after hydrolysis.

**C-Methylation Procedure.** The experimental details for the C-methylation of O-methyl coal have been published elsewhere (2) and are essentially those employed here with the following modifications. First, the O-methyl PSOC 1197 coal was obtained from unlabeled dimethyl sulfate using the conditions outlined earlier for the pH 12 O-methylation. Second, the O-methyl coal was not extracted with THF prior to C-methylation because only a small fraction (ca. 1%) of the sample is soluble in hot THF. Third, benzene, not diethyl ether, was used as the organic extraction solvent for all samples prepared with 9-phenylfluorenyllithium as base because 9-phenylfluorene and its byproducts have limited diethyl ether solubility.

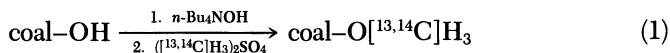
**<sup>13</sup>C NMR Measurements.** The instrumentation and complete experimental details are given in reference 19.

## Results and Discussion

**O-Methylation of PSOC 1197.** A key step in the characterization of the acidic, hydroaromatic C–H sites in coal is the initial conversion of the indigenous phenols and carboxylic acids to their methyl ether and methyl ester analogues, respectively. The success of this derivatization reaction can be evaluated on the basis of two important criteria. First, the reaction should quantitatively convert all of these structural units to their methylated derivatives. The failure to achieve this objective means that methylation will likely occur at both carbon and oxygen sites during the subsequent base-promoted alkylation reactions designed to probe the acidic C–H groups. Second, the acidic C–H sites should remain intact under the O-methylation conditions. The results from the O-methylation reaction are also important because the identity and number of O-methyl functional groups can influence the outcome of the subsequent carbon alkylation chemistry. For example, an abundance of methyl esters in the O-methylated coal could lead to covalent attachment of large amounts of base reagent, which can interfere with the interpretation of the experimental results.

Various approaches for the O-methylation of coals have appeared. These include reaction with diazomethane (7) and, more recently, base-promoted methylation in which coal is first neutralized with an aqueous tetrahydrofuran (THF) base solution followed by reaction with methyl iodide (8–10) or methyl *p*-toluenesulfonate (11). Instead, we opted to O-methylate PSOC 1197 with <sup>13,14</sup>C double-labeled dimethyl sulfate at various pH values. This approach was taken to evaluate the distribution of acidic OH sites and to determine an acceptable set of O-methylation conditions. Briefly, the coal was neu-

tralized for 16 h with a solution of *n*-Bu<sub>4</sub>NOH in aqueous THF. After lowering the pH to 12 or 7, the resulting coal anions were methylated at constant pH with [<sup>13,14</sup>C]H<sub>3</sub>)<sub>2</sub>SO<sub>4</sub> (equation 1). A full description is given in the Experimental Details section.



The <sup>14</sup>C label provides a sensitive analytical method for determining the extent of reaction and detecting subtle differences in the response of coal, and the sites of methylation can be established from the solid-state <sup>13</sup>C NMR spectra of the <sup>13</sup>C-enriched coal derivatives. To further characterize the types of reactive sites, the methylated coals were subjected to base hydrolysis with *n*-Bu<sub>4</sub>NOH in aqueous THF (12). The number of base-labile methyl groups was taken as a measure of the maximum number of methyl esters formed during the alkylation. The results from this study are presented in Table I.

Several important observations emerge from the <sup>14</sup>C combustion data. First, the methylation reaction is found to be highly pH dependent, the total number of introduced methyl groups increasing with pH. Raising the solution pH from 7 to 12 results in a net increase of 0.028 ± 0.009 methyls per 100 coal carbons, a value that is statistically significant. The dependency of this reaction on the pH indicates that methylation of PSOC 1197 requires the removal of acidic protons. Second, the base hydrolysis results indicate that a small but significant number of base-labile methyl groups, 0.028 ± 0.003 groups per 100 coal carbons, are introduced at either pH value. However, all of these base-labile methyls can be introduced at pH values ≤ 7. Thus, these reactive methyls apparently are attached to those acidic sites that form the most stable anions. From the base hydrolysis data, the maximum number of methyl esters in *O*-methylated PSOC 1197 can be set at 0.028 ± 0.003 groups per 100 coal carbons.

The pH dependency of this methylation reaction and the existence of base-labile methyl groups in the coal derivatives implicate the ionization and methylation of acidic –OH sites. However, the <sup>14</sup>C results alone do not preclude the reaction of other sites of comparable acidity. To determine if this factor is important, the pH 12 PSOC 1197 derivative was analyzed by

**Table I. *O*-Methylation of PSOC 1197 Using *n*-Bu<sub>4</sub>NOH and [<sup>13,14</sup>C]H<sub>3</sub>)<sub>2</sub>SO<sub>4</sub>**

<i>pH</i>	<i>Total</i>	<i>Base Labile</i>
12	0.096 ± 0.007	0.029 ± 0.003 <sup>a</sup>
7	0.068 ± 0.002	0.028 ± 0.003 <sup>a</sup>

NOTE: Values are the number of [<sup>14</sup>C]H<sub>3</sub> groups per 100 coal carbons. Data for ([<sup>13,14</sup>C]H<sub>3</sub>)<sub>2</sub>SO<sub>4</sub> are the following: 754.1 ± 1.1 MBq/mol <sup>14</sup>C, and 51.8 ± 1.0 atom % <sup>13</sup>C.

<sup>a</sup> Value is based on a single determination. The reported precisions are the maximum errors.

cross-polarization/magic angle spinning (CP/MAS)  $^{13}\text{C}$  NMR (13–15). The analysis was facilitated by measuring the difference spectrum, that is, pH 12  $-\text{O}[^{13,14}\text{C}]\text{H}_3$  coal minus parent coal. The subtraction criterion is the nulling of the aromatic carbon envelopes. This analytical approach assumes that the hybridization state ( $sp^3$  or  $sp^2$ ) of the coal carbons remains constant during the chemical reactions. It also assumes that tetrabutylammonium salts and THF are not retained by the coal, and thus the area change in the  $sp^3$  envelope is due to the added methyl groups. In the difference spectrum, methyl groups are observed in two distinct spectral regions, those with  $\delta > 50$  parts per million (ppm) (where  $\delta$  denotes parts per million downfield from tetramethylsilane) and those with  $\delta < 50$  ppm, in a measured ratio of 60:40.

Recent results from our laboratory (6) indicate that the  $^{13}\text{C}$  NMR response of methyl groups in chemically modified coals depends upon their local environment. Specifically, methyl groups on oxygen may be detected with a higher sensitivity than those attached to carbon atoms. In Illinois No. 6, for example, the sensitivity ratio for *O*-methyls to *C*-methyls is 1.4:1.0. Here, we will make the simplifying assumption that the  $^{13}\text{C}$  NMR response factors for the methyl groups in this *O*-methylated PSOC 1197 coal derivative are site-independent. The resonance band at 54.6 ppm (line width at half height ( $\nu_{1/2}$ ) 200 = Hz, 8 ppm), which accounts for 0.06 methyl group per 100 coal carbons, is consistent with the formation of a variety of  $-\text{OCH}_3$  functional groups. The 55-ppm resonance in the solution (9, 12) and solid-state (8, 14)  $^{13}\text{C}$  spectra of other *O*-methylated coals has frequently been assigned to nonhindered, aromatic methyl ethers that derive from methylation of phenols. However, the large chemical shift dispersion observed here does not preclude some contribution from other types of  $-\text{OCH}_3$  functional groups such as methyl esters [ $\delta(\text{CH}_3) = 49\text{--}52$  ppm (8)].

The resonance envelope with  $\delta < 50$  ppm can be explained in terms of methyl groups attached to nitrogen, sulfur, and carbon atoms. From the  $^{13}\text{C}$  NMR integration and the  $^{14}\text{C}$  values for the pH 12 sample (Table I), the maximum number of *C*-methyl groups formed under these conditions is 0.04 group per 100 coal carbons. For purposes of comparison, if the methyl groups in *O*-methyl PSOC 1197 do adopt the *O*/*C* discrimination ratio found for methylated Illinois No. 6, then the calculated maximum for *C*-methyls increases to 0.05 group per 100 coal carbons. In either case, the extent of *C*-methylation under these conditions is nominal and will have a negligible impact on the subsequent base-promoted *C*-methylation studies.

A word of caution is perhaps in order. Although *C*-methylation is nominal under these alternative *O*-methylation conditions when PSOC 1197 is the parent coal, a similar result may not be obtained for other coals that have a vastly different chemical composition. Thus, a wider range of coals must be studied before we can evaluate this reaction with regard to the criteria defined earlier.

**C-Methylation of pH 12 OCH<sub>3</sub> PSOC 1197.** We (2, 6) and others (16, 17) have demonstrated that coals will invariably retain <sup>14</sup>C-labeled reagents or their byproducts to varying degrees under a variety of reaction conditions, even after an exhaustive extraction with aqueous and organic solvents. The mechanism(s) responsible for this phenomenon are poorly understood. This phenomenon could result, for example, from specific coal-reagent interactions such as the hydrogen bonding of amines to the phenolic -OH groups, the reaction of the reagent with functional groups on the coal thus leading to covalent attachment, or physical adsorption. The important conclusion to emerge from these studies is that trace levels of organic reagents are likely to remain in the insoluble coal fraction even though the extracts test free of dissolved reagents.

For this reason, control experiments were initially run to measure the extent to which [<sup>14</sup>C]fluorene and [<sup>14</sup>C]triphenylmethane become incorporated into OCH<sub>3</sub> PSOC 1197. The pH 12 *O*-methylated coal, which was prepared by using natural abundance (CH<sub>3</sub>)<sub>2</sub>SO<sub>4</sub>, was treated with [9-<sup>14</sup>C]fluorenyllithium or [<sup>14</sup>C]trityllithium under conditions similar to those employed for the *C*-methylation study (68 h, 0 °C, THF solvent), and the reaction was quenched with water. From combustion analysis, the amounts of fluorene- and triphenylmethane-derived products that remain after the standard diethyl ether extraction are 0.23 ± 0.02 and 0.21 ± 0.02 groups per 100 coal carbons, respectively. Subsequent washing of the two samples with THF, a good swelling solvent for coal, failed to completely liberate the insoluble coal fraction of these reagents (0.17 ± 0.02 and 0.19 ± 0.02 groups per 100 coal carbons remain in the fluorene and triphenylmethane samples, respectively). Similarly, when the reaction with [9-<sup>14</sup>C]fluorenyllithium is quenched with methyl iodide instead of water, an average value of 0.18 ± 0.02 group per 100 coal carbons (three determinations) is measured for the retained fluorene.

All these results indicate a strong coal-reagent interaction, and thus suggest covalent attachment of the carbanion bases to the coal due to base-labile functional groups. Comparison of these results to the previous functional group analysis of OCH<sub>3</sub> PSOC 1197 shows that the amounts of reagent incorporation far exceed the maximum number of methyl esters (0.028 ± 0.004 group per 100 coal carbons). Consequently, nucleophilic addition of the base to the carbonyl groups of methyl esters cannot account entirely for these observations.

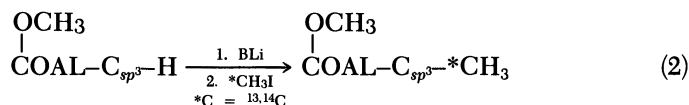
Because reagent incorporation could effect the results and conclusions of the *C*-methylation study, further examination of this phenomenon was warranted. Further study was achieved by a <sup>14</sup>C analysis of samples subjected to repetitive treatments. In the first set of experiments, a coal sample obtained from the reaction of *O*-methyl PSOC 1197 with [9-<sup>14</sup>C]-fluorenyllithium and methyl iodide was treated two additional times with [9-<sup>14</sup>C]fluorenyllithium having the same isotopic enrichment, and the re-



actions were quenched with methyl iodide. Under these serial conditions, the reagent incorporation increases from a value of  $0.15 \pm 0.02$  groups per 100 coal carbons to values of  $0.32 \pm 0.03$  and  $0.66 \pm 0.07$  groups per 100 coal carbons (single determinations) after the second and third treatments, respectively. Thus, the results obtained from a single treatment must be regarded as minimum values.

In a second set of experiments, the coal product from the initial [ $^{14}\text{C}$ ]fluorenyllithium and methyl iodide treatment was reacted with unlabeled fluorenyllithium and methyl iodide. Under this set of serial treatment conditions, run at two different isotopic enrichments, as much as 40% (w/w) of the isotopic label can be removed. The fate of the  $^{14}\text{C}$  label was established when the reaction byproducts, fluorene and 9-methylfluorene, were recovered and detected at the expected isotopic enrichment level. This important observation demonstrates that the incorporated reagent can be removed from the coal by chemical exchange and thus suggests a reversible reaction.

To examine the distribution of acidic C-H sites in PSOC 1197, derived in part from polynuclear hydroaromatic compounds, the pH 12 *O*-methyl coal was treated for 68 h at  $0^\circ\text{C}$ , in separate experiments, with an excess of the conjugate bases of 9-phenylfluorene ( $\text{p}K_a$  18.5), fluorene ( $\text{p}K_a$  22), and triphenylmethane ( $\text{p}K_a$  31) as their lithium salts (BLi); THF was used as the solvent:



In equation 2, \*C represents  $^{13,14}\text{C}$ . After 68 h, the reaction mixtures were quenched with [ $^{13,14}\text{C}$ ]H $_3$ I, and the coal derivatives were isolated by a series of diethyl ether (or benzene) and water extractions. The coal samples were then assayed for their  $^{14}\text{C}$  contents as before, and appropriate corrections were made for the amounts of reagent incorporation. The isolated derivatives were treated sequentially with base and [ $^{13,14}\text{C}$ ]H $_3$ I a total of three times.

The results from the  $^{14}\text{C}$  measurements and the  $\text{p}K_a$  values for the conjugate acids (18) of the three bases are shown in Table II. The data reveal two important trends. First, the reactivity of OCH $_3$  PSOC 1197 toward these base solutions, as measured by the numbers of introduced methyl groups, follows the order 9-phenylfluorenyllithium  $\ll$  fluorenyllithium  $\sim$  trityllithium. In other words, most of the alkylation chemistry can be accomplished by using fluorenyllithium as the base.  $^{13}\text{C}$  CP/MAS analysis of samples prepared with [9- $^{13}\text{C}$ ]fluorenyllithium has demonstrated (19) that all forms of methylated fluorene reagent, artifacts derived from reagent incorporation, make only a minor contribution ( $\leq 10\%$ ) to the total number of acidic sites measured with fluorenyllithium as base. These results suggest that the acidic

Table II. C-Methylation of OCH<sub>3</sub> PSOC 1197 Using BLi and [<sup>13,14</sup>C]H<sub>3</sub>I

Base, BLi; Treatment No.	No. of [ <sup>14</sup> C]H <sub>3</sub> per 100 Coal C <sup>a</sup>
9-Phenylfluorenyllithium (18.5)	
1	0.024 ± 0.002
2	0.042 ± 0.004
3	0.061 ± 0.006
Fluorenyllithium (22)	
1	0.71 ± 0.07
2	1.6 ± 0.2
3	1.9 ± 0.2
Trityllithium (31)	
1	0.71 ± 0.07
2	1.2 ± 0.1
3	1.7 ± 0.2

NOTE: Data for [<sup>13,14</sup>C]H<sub>3</sub>I are the following: 392.2 ± 2.2 MBq/mol <sup>14</sup>C, and 54.6 ± 1.0 atom % <sup>13</sup>C. The compounds given in the table are the bases corresponding to BLi; pK<sub>a</sub> values of BH are given in parentheses and are taken from reference 18.

<sup>a</sup> All values are single determinations. The reported precisions are the maximum errors.

C–H sites in PSOC 1197 have a narrow range of acidities; we conclude that the pK<sub>a</sub> values for these sites are comparable to that of fluorene (pK<sub>a</sub> 22).

More specifically, we can bracket the pK<sub>a</sub> values of these sites in the approximate range 19 < pK<sub>a</sub> ≤ 22 because this coal is virtually unreactive toward 9-phenylfluorenyllithium (pK<sub>a</sub> 18.5). Of particular interest, the <sup>14</sup>C data for fluorenyllithium and trityllithium are identical within experimental error. This finding establishes that only a low concentration of acidic C–H sites with 22 < pK<sub>a</sub> ≤ 31 are present in this coal.

A brief comparison of this data set with the results obtained for Illinois No. 6 is informative (2). For *O*-methyl Illinois No. 6, a high-volatile bituminous coal, values of 0.63 ± 0.03, 1.7 ± 0.1, and 2.6 ± 0.1 methyl groups per 100 coal carbons were measured after three serial alkylations using 9-phenylfluorenyllithium, fluorenyllithium, and trityllithium, respectively. Although the two data sets for these bituminous coals demonstrate a similar preference for fluorenyllithium as base, and thus a significant number of C–H sites with 19 < pK<sub>a</sub> ≤ 22, they differ in that Illinois No. 6 contains important quantities of acidic C–H groups with pK<sub>a</sub> ≤ 19 and 22 < pK<sub>a</sub> ≤ 31. Because the class of structures with 22 < pK<sub>a</sub> ≤ 31 includes 9,10-dihydroanthracene and its analogues, we conclude that this type of six-membered hydroaromatic structure is absent, or at least below the detection limit, in PSOC 1197.

The second trend revealed by the data in Table II is that, invariably, multiple treatments are required to achieve exhaustive alkylation with any of the bases, even though the coal is exposed to large excesses of base and

methylating agent in any given treatment. In fact, the data suggest that a minimum of three treatments is necessary before exhaustive alkylation can be achieved. This requirement for multiple treatments establishes that either neutralization, methylation, or both are incomplete after the first and second treatments. Because none of the samples was treated further, the number of methyls introduced after the third treatment must be regarded as the minimum number that can be added under these conditions.

Changes in the physical and/or chemical properties of coals after chemical modification can be conveniently monitored by determining the weight percent of the sample that is extractable by organic solvents. In general, large increases in extractability have been taken as an indication of a lower cross-link density in the coal product. This situation can occur through the rupture of covalent or noncovalent cross-links originally present in the parent coal. Covalent cross-links refer to those conventional covalent attachments such as C–C and C–O bonds, and noncovalent cross-links refer to those other binding forces such as hydrogen bonding and dipole–dipole interactions (20).

To determine if major physical or chemical changes accompany these base-promoted reactions, several of the  $-\text{OCH}_3$  PSOC 1197 coal derivatives, obtained by reaction with trityllithium, were exhaustively extracted with pyridine in a Soxhlet apparatus. The results, shown in Table III, do indicate that changes occur in pyridine extractability after the *O*-methyl coal is treated with trityllithium followed by protonation with water or serial alkylation with methyl iodide. The observed increases, from 2% (w/w) for the *O*-methyl coal to 28% (w/w) after the third serial alkylation, suggest a reduction in the cross-link density of the coal as a result of chemical modification. However, we cannot at present attribute this effect to a unique chemical event for at least two reasons. First, a significant extractability increase occurs even when the reaction with trityllithium is quenched with a protic source ( $\text{H}_2\text{O}$ ). This finding indicates that *C*-methylation alone is not a prerequisite for an increase in extractability. Second, the previous results from the  $^{14}\text{C}$  base incorporation

Table III. Exhaustive Pyridine Extraction of PSOC 1197 Derivatives

Coal Derivative	% Extractable (daf) <sup>a</sup>
Parent	2
pH 12 $\text{OCH}_3$	2
pH 12 $\text{OCH}_3\text{-Ph}_3\text{C}^- \text{-H}_2\text{O}$	9 <sup>b</sup>
pH 12 $\text{OCH}_3\text{-Ph}_3\text{C}^- \text{-CH}_3\text{I}$ (first treatment)	12
pH 12 $\text{OCH}_3\text{-Ph}_3\text{C}^- \text{-CH}_3\text{I}$ (second treatment)	19
pH 12 $\text{OCH}_3\text{-Ph}_3\text{C}^- \text{-CH}_3\text{I}$ (third treatment)	28

<sup>a</sup> The precision of the values is believed to be no better than +1%, absolute; daf denotes dry ash free.

<sup>b</sup> Of this value, no more than 0.23% is extracted triphenylmethane as determined by GC analysis.

studies require a second chemical process to occur under these conditions in addition to the alkylation of carbanions.

Although further study will be necessary before we can evaluate the relative importance of all the chemical events on the observed extractabilities, the cleavage of covalent cross-links probably is not a major chemical event under these base conditions. In contrast, as Stock and Mallya (21) noted, the cleavage of covalent cross-links may be important when PSOC 1197 is subjected to base-promoted alkylation using sodium amide as base.

The  $^{14}\text{C}$  data probe the number of introduced methyl groups and monitor subtle differences in the coal response toward systematic variations in the reaction conditions; however, the data do not identify all of the sites of alkylation. To obtain more definitive structural information on the sites of alkylation, the CP/MAS  $^{13}\text{C}$  NMR spectra of the three samples derived from repetitive methylation with fluorenyllithium and  $[^{13,14}\text{C}]\text{H}_3\text{I}$  were measured. Three difference spectra were obtained: 1 minus blank, 2 minus blank, and 3 minus blank, where the numbers refer to the treatment number, and the blank is the sample obtained from reaction of the *O*-methyl coal with fluorenyllithium followed by a water quench. As before, the nulling of the aromatic carbon envelopes is the subtraction criterion.

The use of the blank serves to correct for the contributions that the retained fluorene makes to the spectra. This correction is most ideal when the total amount of fluorene is identical in the two samples and when methylated fluorene reagent makes only a minor contribution to the total spectral characteristics of the methylated sample. This situation is most closely approximated for the samples labeled blank and 1. This same condition does not hold for those samples labeled 2 and 3 because fluorene retention exceeds that of the blank sample. However, this perturbation will not affect the primary conclusions derived from the spectroscopic data.

The quality of the  $^{13}\text{C}$  NMR spectra and the resulting difference spectra are illustrated in Figure 1, which shows the blank  $^{13}\text{C}$  NMR spectrum, the spectrum obtained after the third serial alkylation with  $[^{13,14}\text{C}]\text{H}_3\text{I}$ , and the corresponding difference spectrum. The three difference spectra allow us to focus on the chemical environments of the introduced methyl groups. Each spectral difference is dominated by absorptions with  $\delta < 50$  ppm, a result that suggests alkylation of carbon sites. On the other hand, the spectral characteristics change upon repetitive treatment; this finding indicates a change in the local environments of the introduced methyl groups as a function of the treatment number. Specifically, the first, second, and third difference spectra each contain a broad resonance envelope whose peak maximum occurs at 18.8 ppm ( $\nu_{1/2} = 420$  Hz, 17 ppm), 25.1 ppm ( $\nu_{1/2} = 380$  Hz, 15 ppm), and 25.7 ppm ( $\nu_{1/2} = 360$  Hz, 14 ppm), respectively. The wide distribution of chemical shifts observed for the introduced methyls, as measured by the large line widths at half height, indicates a variety of methyl-group environments. This condition occurs because of alkylation at a variety

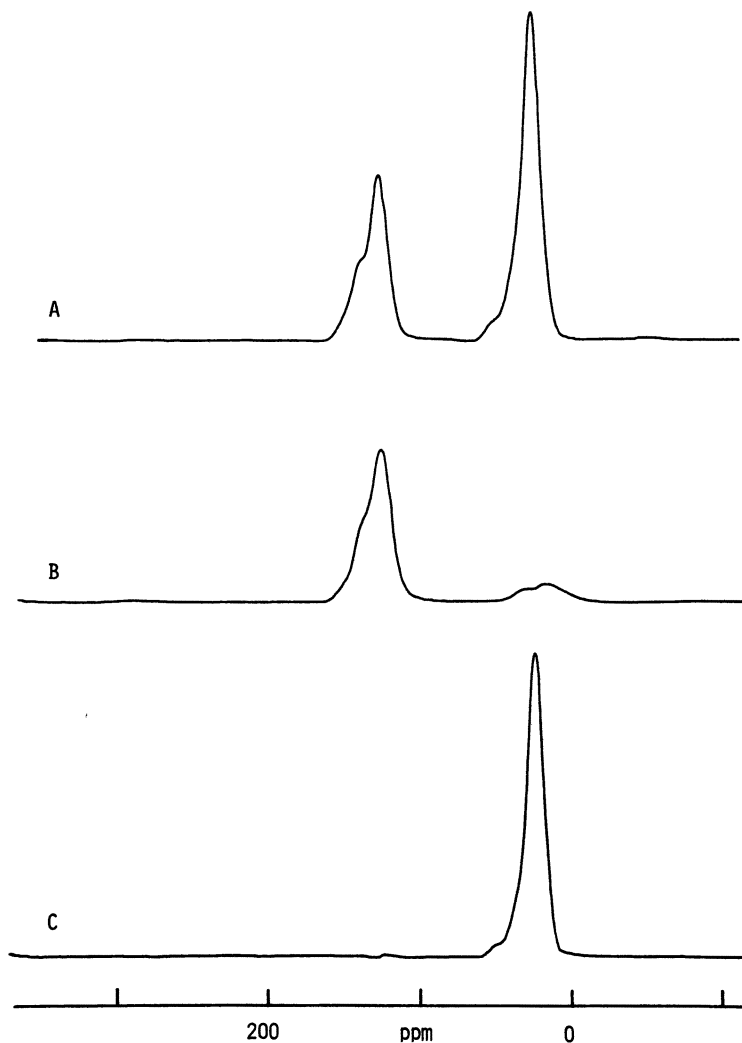


Figure 1.  $^{13}\text{C}$  CP/MAS NMR spectra of the coal product derived from treating  $\text{OCH}_3$  PSOC 1197 with fluorenyllithium. A, third serial treatment, 54.6%  $[^{13}\text{C}]\text{H}_3\text{I}$  quench; B,  $\text{H}_2\text{O}$  quench; and C, difference spectrum, A minus B.

of acidic  $-\text{CH}_2-$  and  $-\text{C}(\text{H})\text{R}-$  sites where the R group is indigenous to the coal.

The relative contributions of these two structural types cannot be accurately evaluated from these single difference spectra. As repetitive treatments are carried out, a 7-ppm downfield shift in the resonance maximum occurs; this shift is also accompanied by a gradual decrease in the peak width from 420 to 360 Hz. This downfield shift in the peak maximum and decrease

in the line width signal an accumulation of methyl-group environments with  $\delta$  ca. 26 ppm. Although a full discussion is beyond the scope of this chapter, we have independent evidence (19) based on the  $^{13}\text{C}$  NMR analysis of samples in which the isotopic enrichment of the methyl iodide is varied as a function of treatment number that this effect is due in part to the sequential conversion of a  $-\text{CH}_2-$  site to a  $-\text{C}(\text{H})\text{CH}_3-$  site and then to a  $-\text{C}(\text{CH}_3)_2-$  site. The experimental observation reported here, namely, the change in methyl-group environment as a function of treatment number, is apparently the first example demonstrating structural discrimination in the C-methyl region of a series of methylated coal derivatives as detected by solid-state  $^{13}\text{C}$  NMR.

Several structurally diverse model compounds, each containing benzylic C–H sites of varying acidity, were treated with these indicator base solutions, and the resulting carbanions were alkylated with methyl iodide (22). Those models that contained the  $-\text{CH}_2-$  functional group readily yielded the monomethyl derivative,  $-\text{C}(\text{H})\text{CH}_3-$ , as the major product, even though a large excess of base and methylating agent were present. Furthermore, the monomethyl products underwent proton abstraction and methylation to produce  $-\text{C}(\text{CH}_3)_2-$  derivatives if they were treated in a separate experiment with base and methyl iodide. The results from the study suggested that exhaustive alkylation of coal under these conditions would necessitate multiple treatments. For this reason, the  $^{14}\text{C}$  data in Table II, which demonstrate the requirement for repetitive treatments, can be cited as supporting evidence for the reaction of acidic  $-\text{CH}_2-$  sites in this coal.

### *Summary and Conclusions*

All of the experimental data indicate that the acidic C–H sites in *O*-methyl PSOC 1197 include methylene and methine structural types that are unreactive toward base-promoted methylation with 9-phenylfluorenyllithium but that are reactive when fluorenyllithium or trityllithium are the bases. In other words, the acidities for these sites are approximately represented by the range  $19 < \text{p}K_a \leq 22$ . Within the context of coal structure, this result is surprising because it implies an abundance of structural units with highly acidic C–H sites. Structural types such as fluorenes and others that form aromatic anions upon proton removal as well as structures that contain acidic C–H bonds adjacent to electron-withdrawing substituents (e.g., carbonyl groups) are implicated by our results. In a rigorous sense, our data do not allow us to attribute all of the chemistry to a unique structural type. However, from the previous  $^{14}\text{C}$  data for the initial methylation treatment, we can estimate that as much as 9% of the carbons in PSOC 1197 ( $0.71 \times 13$  carbons = 9%) could be derived from fluorene. If this estimate is accurate, then these results suggest that future pictures of coal structure need to highlight the importance of five-membered cyclopentadiene rings, a structural feature that is common to all fluorene derivatives.

## Acknowledgment

We thank the Office of Basic Energy Sciences, Division of Chemical Sciences, U.S. Department of Energy, for support of this research under Contract DE-ACO5-84OR21400 with Martin Marietta Energy Systems, Inc.

## References

1. Wender, I.; Heredy, L. A.; Neuworth, M. B.; Dryden, I. G. C. In *Chemistry of Coal Utilization*; Elliott, M. A., Ed.; Wiley: New York, 1981; Chapter 8.
2. Chambers, R. R., Jr.; Hagaman, E. W.; Woody, M. C.; Smith, K. E.; McKamey, D. R. *Fuel* **1985**, *64*, 1349-1354.
3. Hayatsu, R.; Winans, R. E.; Scott, R. G.; Moore, L. P.; Studier, M. H. *Fuel* **1978**, *57*, 541-548.
4. Hayatsu, R.; Winans, R. E.; Scott, R. G.; Moore, L. P.; Studier, M. H. In *Organic Chemistry of Coal*; Larsen, J. W., Ed.; ACS Symposium Series No. 71, American Chemical Society: Washington, DC, 1978; pp 108-125.
5. Kofron, W. G.; Baclawski, L. M. *J. Org. Chem.* **1976**, *41*, 1879-1880.
6. Hagaman, E. W.; Chambers, R. R., Jr.; Woody, M. C. *Anal. Chem.* **1986**, *58*, 387-394.
7. van Krevelen, D. W. In *Coal*; Elsevier: Amsterdam, 1961; Chapter 9.
8. Liotta, R.; Brons, G. *J. Am. Chem. Soc.* **1981**, *103*, 1735-1742.
9. Liotta, R.; Rose, K.; Hippo, E. *J. Org. Chem.* **1981**, *46*, 277-283.
10. Liotta, R. *Fuel* **1979**, *58*, 724-728.
11. Ettinger, M.; Nardin, R.; Mahasay, S. Ray; Stock, L. M. *J. Org. Chem.* **1986**, *51*, 2840-2842.
12. Stock, L. M.; Willis, R. S. *Prepr. Pap.—Am. Chem. Soc. Div. Fuel Chem.* **1985**, *30(1)*, 21-28.
13. Zilm, K. W.; Pugmire, R. J.; Larter, S. R.; Allan, J.; Grant, D. M. *Fuel* **1981**, *60*, 717-722.
14. Hagaman, E. W.; Woody, M. C. *Fuel* **1982**, *61*, 53-57.
15. Wilson, M. A.; Pugmire, R. J.; Karas, J.; Alemany, L. B.; Woolfenden, W. R.; Grant, D. M.; Given, P. H. *Anal. Chem.* **1984**, *56*, 933-943.
16. Larsen, J. W.; Urban, L. O. *J. Org. Chem.* **1979**, *44*, 3219-3222.
17. Collins, C. J.; Hagaman, E. W.; Jones, R. M.; Raaen, V. F. *Fuel* **1981**, *60*, 359-360.
18. Bors, D. A.; Kaufman, M. J.; Streitwieser, A., Jr. *J. Am. Chem. Soc.* **1985**, *107*, 6975-6982.
19. Hagaman, E. W.; Chambers, R. R., Jr.; Woody, M. C. *Ener. Fuels* **1987**, *1*, 352-360.
20. Mallya, N.; Stock, L. M. *Fuel* **1986**, *65*, 736-738.
21. Mallya, N.; Stock, L. M. *Prepr. Pap.—Am. Chem. Soc. Div. Fuel Chem.* **1984**, *30(2)*, 291-297.
22. Chambers, R. R., Jr.; Hagaman, E. W.; Woody, M. C. *Fuel* **1986**, *65*, 895-898.

RECEIVED for review December 2, 1986. ACCEPTED March 30, 1987.

# Thermal Conversion of Polynuclear Aromatic Compounds to Carbon

I. C. Lewis and L. S. Singer<sup>1</sup>

Carbon Products Division, Parma Technical Center, Union Carbide Corporation, Cleveland, OH 44101

*The pyrolysis of polynuclear aromatic compounds and their mixtures produces carbonaceous pitchlike residues and ultimately carbon and graphite. Reaction studies on model aromatic hydrocarbons can be used to illustrate the chemical changes involved in this complex process. The reactions largely involve aromatic polymerizations accompanied by bond cleavage and rearrangement. The tendency of large polynuclear aromatic compounds to associate into a liquid crystalline state plays a key role in their conversion to carbon. Studies using electron paramagnetic resonance–electron nuclear double resonance can clarify the nature of the stable free radicals that develop during carbonization. These aspects are reviewed to provide a clearer understanding of the chemistry involved in the transformation of polynuclear aromatic compounds to carbon.*

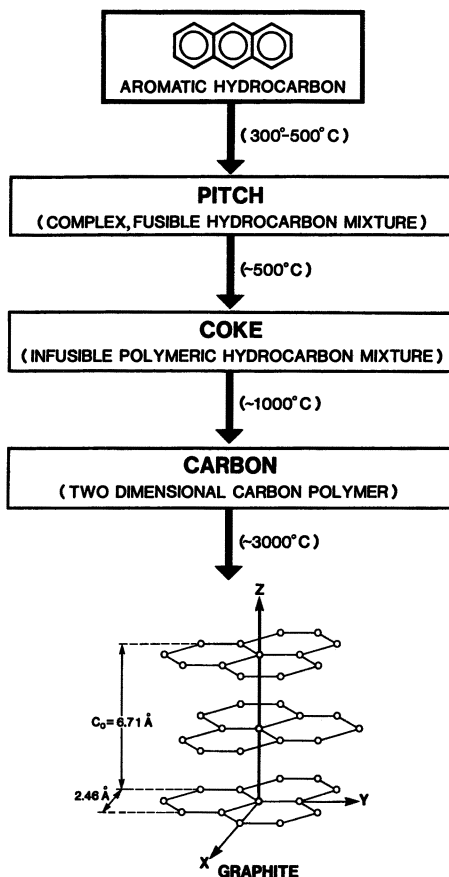
**P**OLYNUCLEAR AROMATIC COMPOUNDS can be transformed thermally into carbonaceous residues and ultimately to carbon and graphite by a process called *carbonization*. The chemistry of carbonization is exceedingly complex and encompasses a wide variety of reaction types including bond cleavage, polymerization, molecular rearrangement, and hydrogen transfer. Even with a single aromatic hydrocarbon as a starting material, pyrolysis leads initially to a diversity of products. Detailed thermal reaction studies have been carried out on a number of polynuclear aromatic compounds (1–5). Various experimental as well as theoretical techniques have been used in attempting to clarify the nature of these reactions (6–8). The literature on the thermal

<sup>1</sup>Current address: 525 Race Street, Berea, OH 44017



reactions of polynuclear aromatic mixtures as they occur naturally in petroleum and coal-derived products is extensive.

Scheme I is a generalized scheme for the transformation of a polynuclear aromatic hydrocarbon to carbon and graphite. Heat treatment at about 350–500 °C leads to a complex reaction product mixture designated as *pitch*. Further reaction at temperatures near 500 °C results in an infusible polymeric hydrocarbon mixture designated as *coke*. As the heat-treatment process continues, the remaining hydrogen is removed, and a two-dimensional carbon polymer is formed. Finally, at temperatures near 3000 °C, three-dimensionally ordered graphite is produced.



Scheme I. Transformation of a polynuclear aromatic hydrocarbon to carbon and graphite.

Providing complete reaction mechanisms for any of these stages has not been possible. However, from detailed studies of the initial thermal reactions, general concepts pertaining to the thermal conversion of polynuclear

aromatic compounds to carbon have been developed. These studies are reviewed in this chapter with the objective of clarifying the chemistry of the carbonization process.

### ***Interactions in Polynuclear Aromatic Mixtures (Nature of Pitch)***

Pitches are complex fusible aromatic mixtures generally obtained from the pyrolysis of coal- and petroleum-derived fractions. However, the pyrolysis of even a single aromatic hydrocarbon results in a product almost as complex as pitches derived from coal or petroleum.

Pitches have some unique properties that are important for the subsequent transformation to carbon. Solid pitches behave as eutectic glasses. They exhibit glass transitions and melt to a low viscosity liquid over a broad temperature range. The results of a differential scanning calorimetric (DSC) experiment for measuring the glass transition temperature of a naphthalene-derived pitch are shown in Figure 1. Pitches exhibit another significant feature, namely, a tendency to form a liquid crystalline state. The development of a mesophase stage during conversion of pitches or aromatic hydrocarbons to coke was first discovered by Brooks and Taylor (9). Depending on structure, mixtures of polynuclear aromatic compounds of a sufficiently large size form a nematic liquid crystalline phase. This phenomenon is illustrated in Figure 2, which contains polarized light photomicrographs of a petroleum pitch derived from decant oil as it is heat treated at 400 °C. This heat treatment results in volatilization of lower molecular weight components and polymerization of the more reactive species. The higher molecular

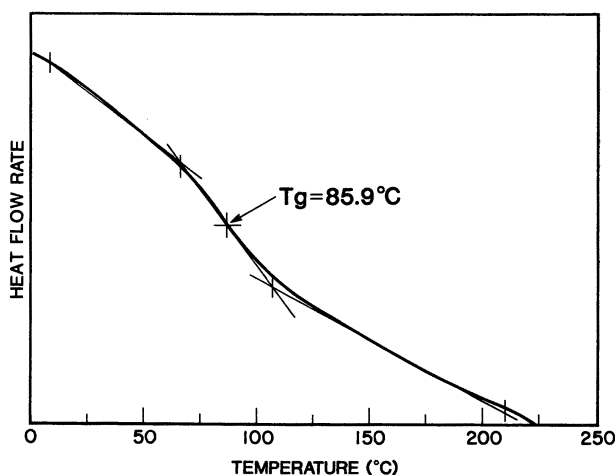
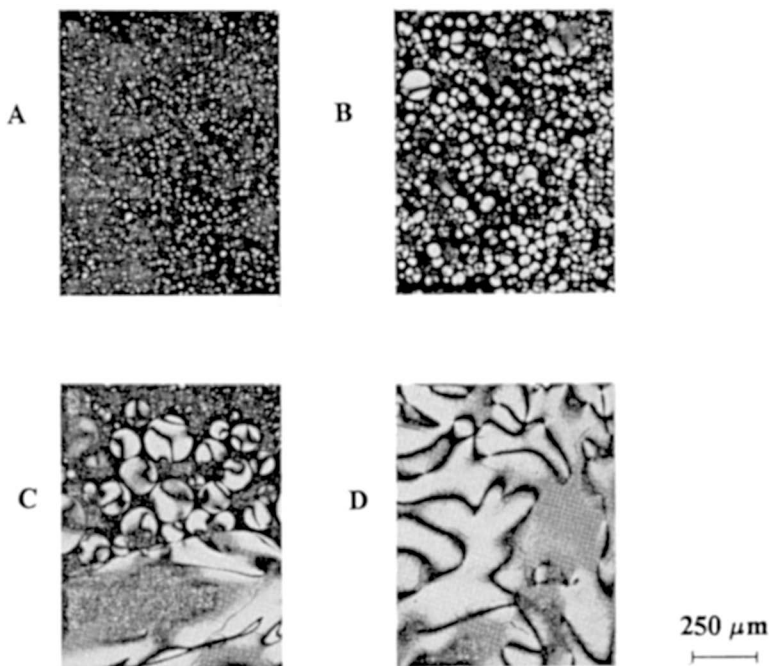


Figure 1. Determination of the glass transition temperature ( $T_g$ ) by DSC.



*Figure 2. Development of mesophase during heat treatment of petroleum pitch as observed by polarized light microscopy of polished sections at room temperature. A: 400°C, 2 h; B: 400°C, 6 h; C: 400°C, 12 h; D: 400°C, 20 h. (Reproduced with permission from reference 10. Copyright 1984.)*

weight aromatic components then tend to associate and precipitate out as anisotropic spherules from the lower molecular weight isotropic phase. As chemical reactions continue, the entire pitch is transformed to the mesophase state. Subsequent reaction leads to the formation of an anisotropic infusible solid coke. The chemical nature of mesophase pitch was recently reviewed (10). Mesophase pitches exhibit properties typical of nematic liquid crystals. However, mesophase pitches are somewhat unique in that they behave as supercooled glasses, and they exhibit nematic textures at room temperature in the solid state.

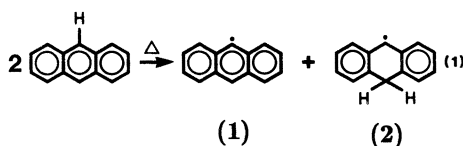
Even prior to mesophase development, polynuclear aromatic compounds in pitch have a tendency for molecular association. This phenomenon, which results primarily from van der Waals interactions, has been observed from molecular weight (11) and electron paramagnetic resonance-electron nuclear double resonance (EPR-ENDOR) experiments (12).

### ***Pyrolysis Studies of Polynuclear Aromatic Compounds***

Many studies of the pyrolysis of individual polynuclear aromatic compounds, particularly polynuclear aromatic hydrocarbons, have been published. The

pyrolysis products depend on the reaction conditions, mainly temperature, but in every instance they are complex mixtures. At very high temperatures at which reactions occur in the vapor phase, extensive molecular fragmentation occurs, and the process is exceedingly complex. Low-temperature (400–500 °C) pyrolysis in the liquid phase is more straightforward and leads to products that are amenable to analysis. Most investigations, as well as most carbon industrial processes, have emphasized thermal conversion of aromatic compounds to carbon in the liquid state. Such studies with the model compounds anthracene and naphthalene can be used to illustrate the general chemistry of the carbonization of polynuclear aromatic compounds.

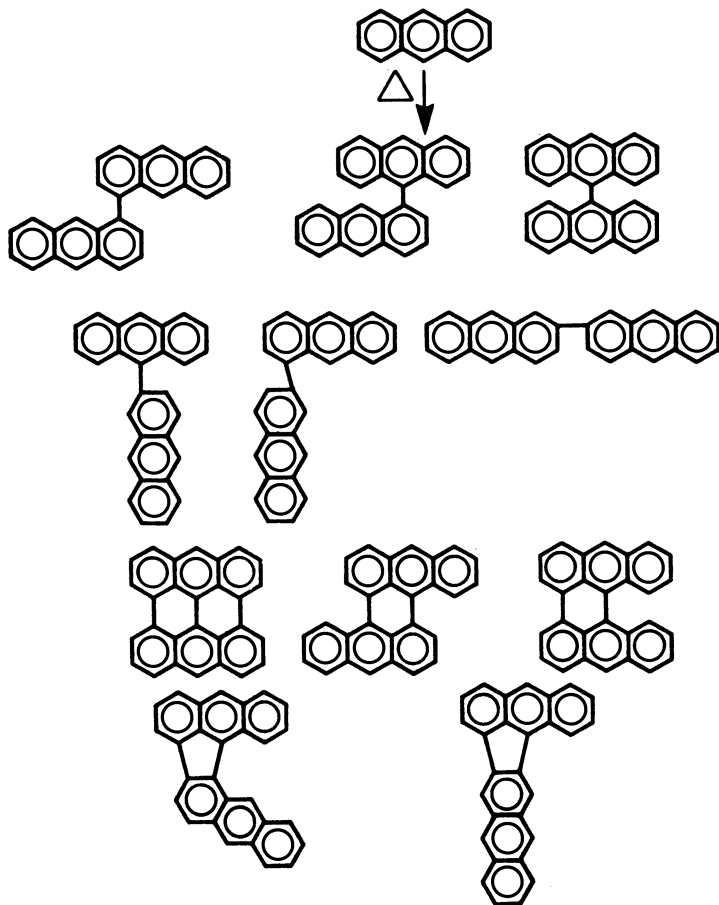
**Carbonization of Anthracene.** The pyrolysis of anthracene has been investigated extensively (13–17). The initial reaction is not well-understood, and various radical intermediates have been proposed. The thermodynamics of anthracene dissociation has been discussed by Stein (8), and the formation of the anthryl radical by a disproportionation reaction such as Scheme II is expected to be very slow because of the instability of the  $\sigma$  radical (1). A mechanism involving the direct formation of the anthryl radical by hydrogen dissociation, although not favorable, might be possible. A reaction scheme based on the formation of the radical (2) from anthracene and dihydroanthracene has also been proposed (17).



*Scheme II. Formation of the anthryl radical by a disproportionation reaction.*

Anthracene dimers as well as dihydroanthracene have been identified as initial reaction products in all pyrolysis studies of anthracene. As shown in Chart I, 11 dimers from anthracene are possible. Because the 9-position is the most reactive, one might expect a predominance of the 9,9'-dimer. However the 2,9-dimer was reported as the major product in one study (18). Many of the other possible dimers were also obtained, depending on the reaction conditions employed. Both steric effects and reactivity factors must, therefore, be taken into account for considering the possible reaction products in aromatic hydrocarbon pyrolysis. The results for anthracene show how the lack of a functional group and the nonspecificity for molecular recombination lead to complex product mixtures in aromatic pyrolysis.

The main process occurring in the pyrolysis of polynuclear aromatic compounds involves polymerization. The carbonaceous residues that form



*Chart 1. Possible dimers of anthracene. (Reproduced with permission from reference 4. Copyright 1980 Pergamon Press.)*

on heat treatment of a polynuclear aromatic hydrocarbon or heterocycle are composed largely of oligomers of the starting material. This result is apparent from the gel permeation chromatographic (GPC) curve obtained for the residue from the pyrolysis of anthracene at 440 °C; this curve is shown in Figure 3. The GPC instrument was calibrated for molecular weight by using both model polynuclear aromatic hydrocarbons and separated pitch fractions (19). The chromatogram exhibits, in addition to a peak corresponding to unreacted anthracene, peaks corresponding to dimers, trimers, and tetramers of the starting material. Additionally, the elution behavior demonstrates the presence of oligomers ranging in size up to decamers of anthracene. As stated earlier, 11 structures are possible at the dimer stage. As the degree of polymerization increases, the number of possible species becomes enor-

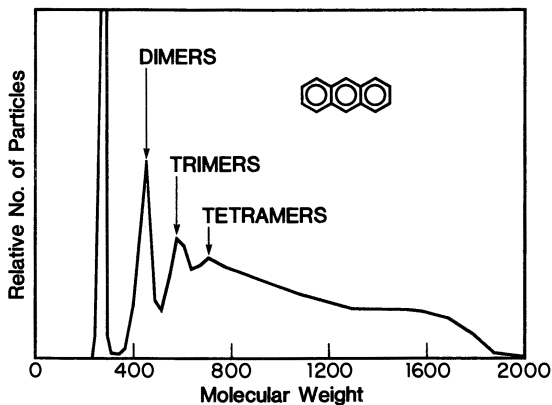


Figure 3. Molecular weight distribution of anthracene-derived pitch as measured by GPC, with quinoline as the solvent.

mous. The anthracene pyrolysis residue, therefore, exhibits all the characteristics of a pitch similar to those of very complex residues derived from petroleum or coal tar.

One can separate and identify some of the pure components in the anthracene pitch by using chromatographic and spectroscopic techniques. Dimeric species such as the various dianthryls, dibenzoperilyenes, bisanthrene, benzonaphthofluoranthenes, and tetrahydrodianthranyls, as well as monomeric species such as dihydro- and tetrahydroanthracene, have been identified in this manner. The higher molecular weight oligomers are, however, extremely difficult to separate and characterize.

We have found it useful in our studies to use field-desorption mass spectrometry (FDMS) to determine the molecular constitution of pitch materials. The mass spectrum for anthracene pitch is very complex and contains a large number of peaks in the measured mass range of 200–1350  $M/Z$  (4). Many of the major peaks correspond to oligomers of anthracene. We have identified species containing up to eight combined anthracene units. Proposed structures for some of the main oligomeric components are presented in Chart II. Although polymerization is a key reaction in the liquid-phase pyrolysis of anthracene, the presence of many species, which are not oligomers of anthracene, demonstrates that ring degradation and rearrangement are also prevalent. Proposed structures for some of these products are shown in Chart III.

With further heat treatment, the anthracene pitch is transformed to an infusible solid coke at about 500 °C and to a pregraphitic carbon at about 1000 °C. At these stages, the carbonaceous residues behave as intractable and infusible solids and can only be described in terms of average structural parameters. The conversion of anthracene to carbon involves further polymerization with continual loss of hydrogen. The rate of dehydrogenation can

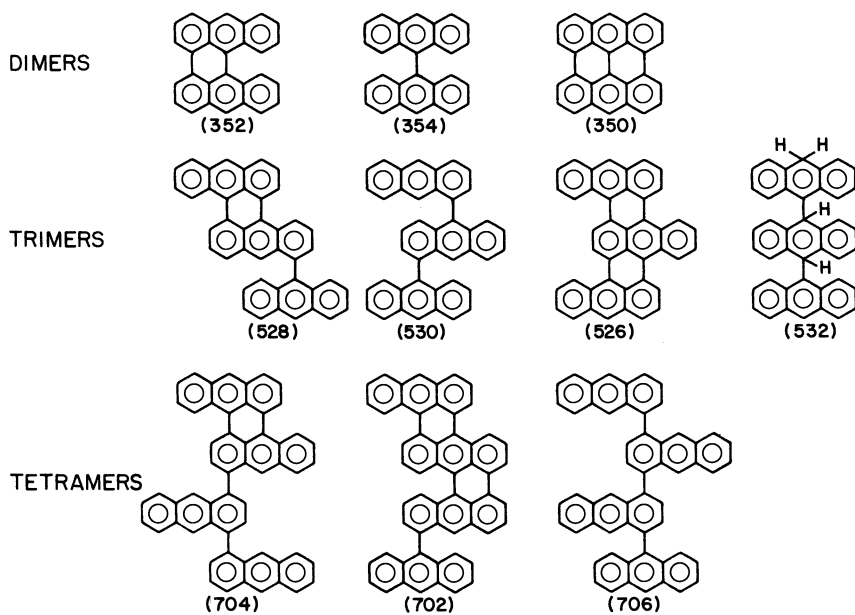


Chart II. Proposed structures for some of the oligomeric molecular species identified by FDMS in anthracene-derived pitch. (Reproduced with permission from reference 4. Copyright 1980 Pergamon Press.)

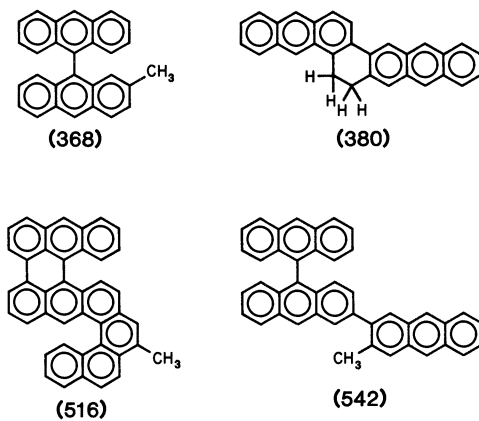


Chart III. Proposed structures for rearrangement products identified by FDMS in anthracene-derived pitch.

be followed by elemental analysis, as shown in Figure 4, which plots the hydrogen-to-carbon (H/C) ratio as a function of heat treatment temperature. The hydrogen is essentially gone at 1000 °C, and the material can be described as a disordered carbon. The polymerization sequence through the coke and carbon stages was also monitored with X-ray diffraction by Guet et al. (20). Their studies show that polymerization involves relatively small condensed ring units at the lower temperatures and the development of large condensed ring polymers at higher temperatures. A model for the average structures of anthracene-derived carbons at various stages of heat treatment is shown in Figure 5.

**Carbonization of Naphthalene.** Naphthalene is considerably more stable than anthracene and requires extended heat treatment at 500 °C or higher to effect reaction. As with anthracene, the initial reaction product is a pitchlike residue with a large number of components. The molecular weight distribution of the pitch product obtained at about 500 °C as determined by GPC is shown in Figure 6. Discrete peaks corresponding to trimers, tetramers, and pentamers can be observed. The chromatogram indicates that oligomers containing as many as 16 naphthalene units could be present. As

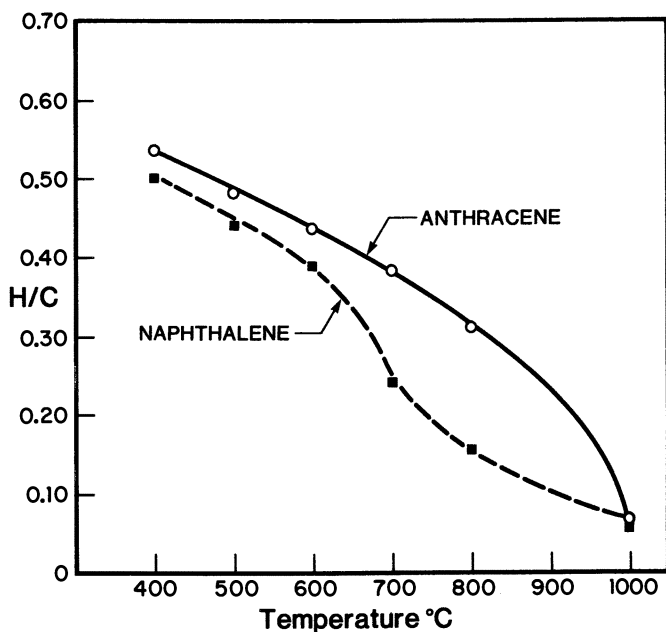


Figure 4. Plots of H/C ratio for anthracene- and naphthalene-derived pitches as a function of heat treatment temperature.



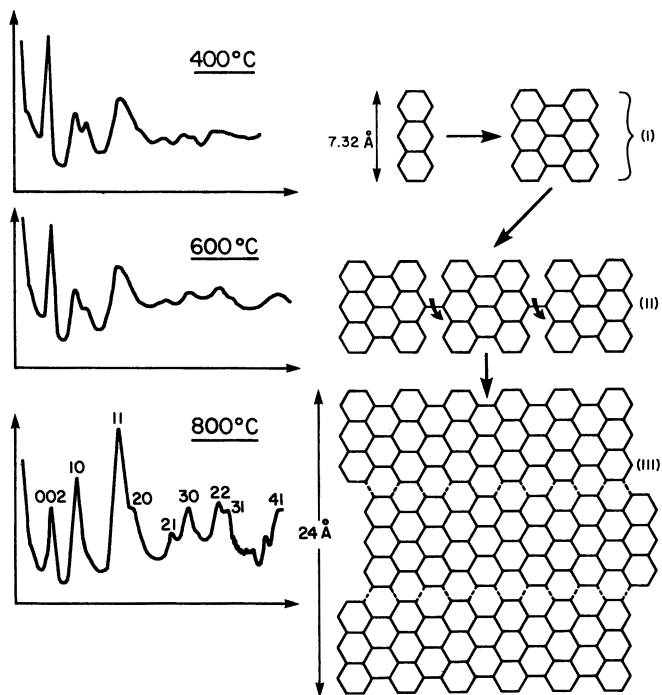


Figure 5. Average structures proposed for anthracene-derived carbons from X-ray diffraction studies. (Adapted from reference 20.)

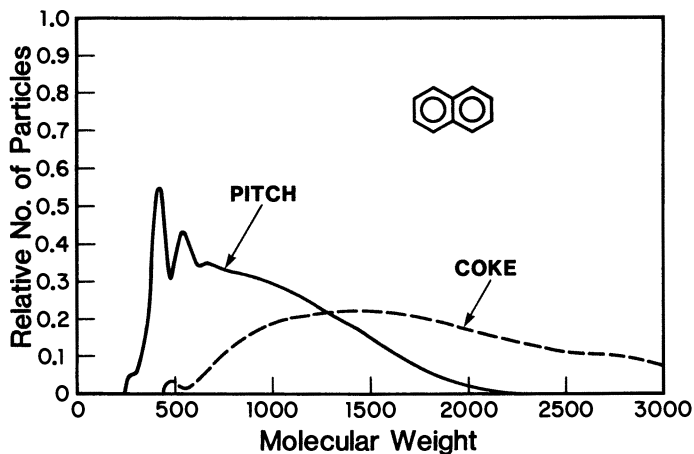


Figure 6. Molecular weight distributions of naphthalene-derived pitch and coke as measured by GPC.

the pitch is heated for a prolonged time at 500 °C, it is first transformed to a mesophase state and then to an infusible coke. The molecular weight distribution for this coke as determined by GPC is also shown in Figure 6. The GPC experiments were performed by using quinoline as the solvent. The naphthalene coke was reductively ethylated to effect its dissolution in quinoline (19). At this stage, the extent of polymerization has advanced considerably so that the product contains polymers that can contain as many as 30 or more combined naphthalene units.

The mass spectrum of naphthalene-derived pitch is shown in Figure 7. As with anthracene pitch, the spectrum is complex, but a detailed analysis shows the pitch to be largely composed of oligomeric species. Various species presumed to arise through bond cleavage and molecular rearrangement are also evident (21). Proposed structures for some major components are presented in Chart IV. Further heat treatment of the naphthalene pitch to

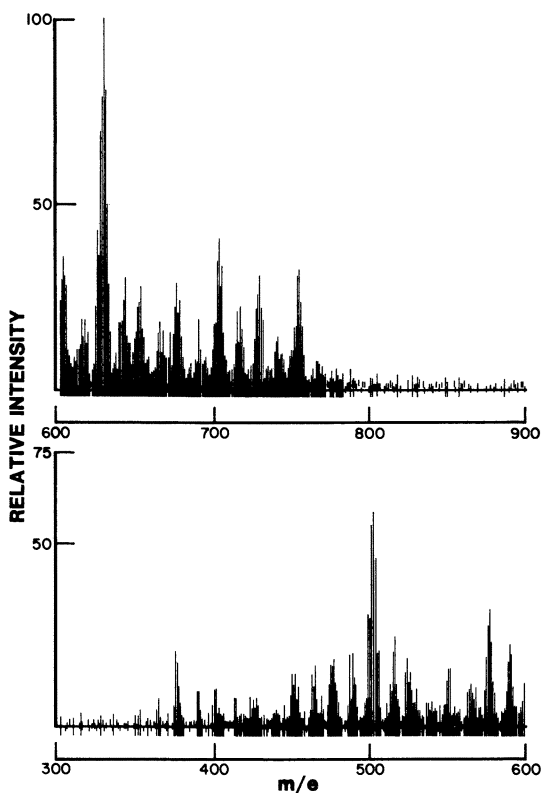


Figure 7. Mass spectrum obtained by FDMS for naphthalene-derived pitch. (Reproduced with permission from reference 21. Copyright 1984 Pergamon Press.)

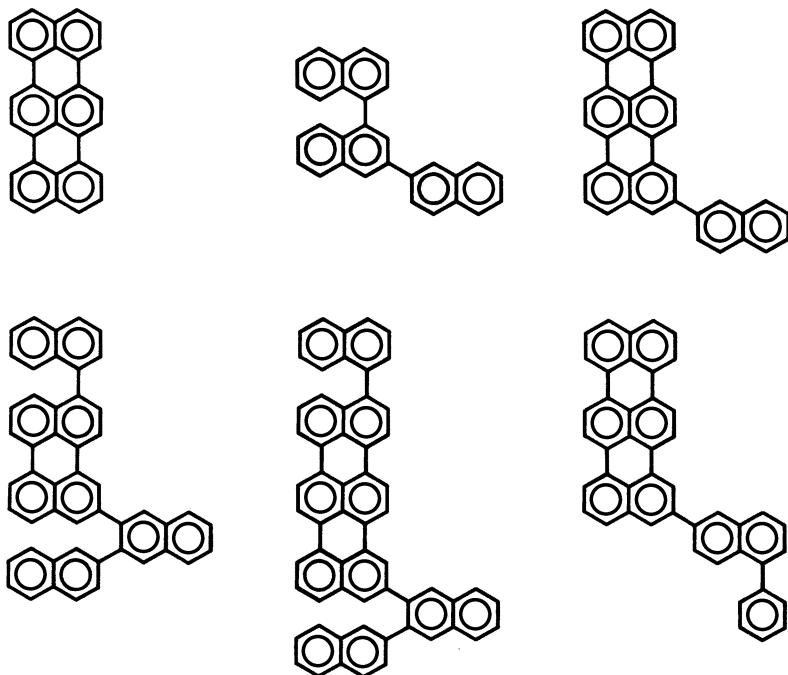


Chart IV. Proposed structures for some of the molecular species identified by FDMS in naphthalene-derived pitch.

higher temperatures results in continuing dehydrogenation and polymerization to large condensed ring structures. The rate of dehydrogenation up to 1000 °C, as monitored by elemental analysis, is shown in Figure 4. Naphthalene appears to dehydrogenate and polymerize at a faster rate than anthracene.

### ***Role of Free Radicals in Carbonization of Polynuclear Aromatic Compounds***

The thermal conversion of polynuclear aromatic compounds to carbon can be considered a free-radical process because it involves a series of bond cleavage reactions. Many of the radical intermediates are expected to be unstable and cannot be detected by conventional spectroscopic techniques. However, the carbonaceous residues from pyrolysis do contain significant amounts of stable free radicals as apparent from EPR experiments. For example, Figure 8 shows the results of EPR measurements of the free-radical content for anthracene and naphthalene pitches after heating from 400 to 700 °C. The concentration of stable free radicals increases with heat treatment temperature as the molecular size grows. The more highly condensed

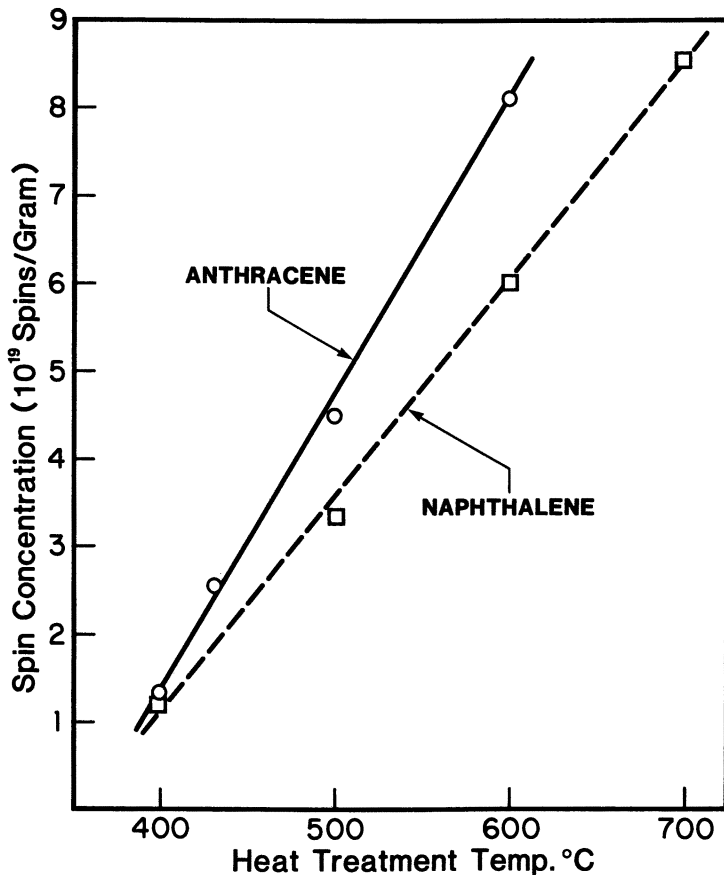
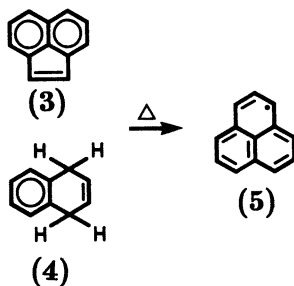


Figure 8. Spin concentrations (spins/gram) as a function of heat treatment temperature for anthracene- and naphthalene-derived pitches. Key:  $\circ$ , anthracene-derived pitch;  $\square$ , naphthalene-derived pitch.

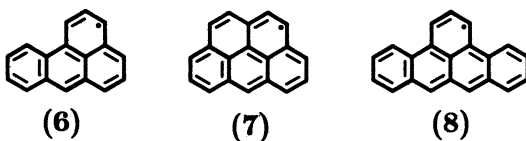
anthracene contains a higher concentration of free radicals at a given temperature than naphthalene does. The extensive literature on free-radical studies of carbonization was reviewed (22). This present discussion will be restricted to the nature of these stable radicals and their involvement in the pyrolysis of aromatic compounds.

**Odd-Alternate Polynuclear Aromatic Hydrocarbon Radicals.** Substantial evidence supports the contention that the stable free radicals formed during the pyrolysis of polynuclear aromatic compounds are odd-alternate hydrocarbon radicals. As an example, the phenalenyl radical (5) is formed during pyrolysis of a number of organic compounds including acenaphthylene (3) and dihydronaphthalene (4) (24) (see Scheme III). The



*Scheme III. Formation of the phenalenyl radical during pyrolysis of acenaphthylene and dihydronaphthalene.*

formation of phenalenyl from these compounds involves some unusual polymerization and rearrangement processes. The phenalenyl radical is extremely stable and has been observed from in situ pyrolysis of aromatic compounds at 400 °C (23). We have synthesized a number of additional odd-alternate polynuclear aromatic radicals including 3*H*-benz[*de*]anthryl (6), 2*H*-benzo[*cd*]pyrenyl (7), and 3*H*-benz[*f,g*]naphthacenyl (8) radicals. These radicals exhibit considerable stability at elevated temperatures because of the ease of delocalization of the unpaired electron. They can readily be identified and characterized through the use of EPR and ENDOR techniques (25). As an example, Figure 9 shows the ENDOR spectrum for the 2*H*-benzo[*cd*]pyrenyl radical measured at 400 K. The proton hyperfine coupling constants can be determined directly from the ENDOR spectrum and used to determine the free-electron density and the relative reactivities at the various positions in the molecule.



**Free-Radical Mechanisms of the Carbonization of Polynuclear Aromatic Compounds.** The polymerization process that transforms polynuclear aromatic compounds to carbon can occur in two distinct stages. As shown in the proposed sequence for naphthalene in Scheme IV, free-radical intermediates can be involved in both stages. The first stage of polymerization can occur through a reactive radical produced by hydrogen dissociation or by a disproportionation reaction (18). The naphthalene oligomers can then form stable odd-alternate radicals in the second-stage condensation process through the loss of a single hydrogen atom. As shown in

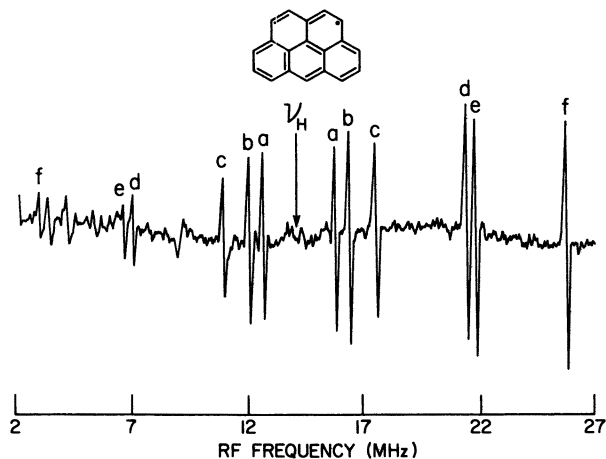
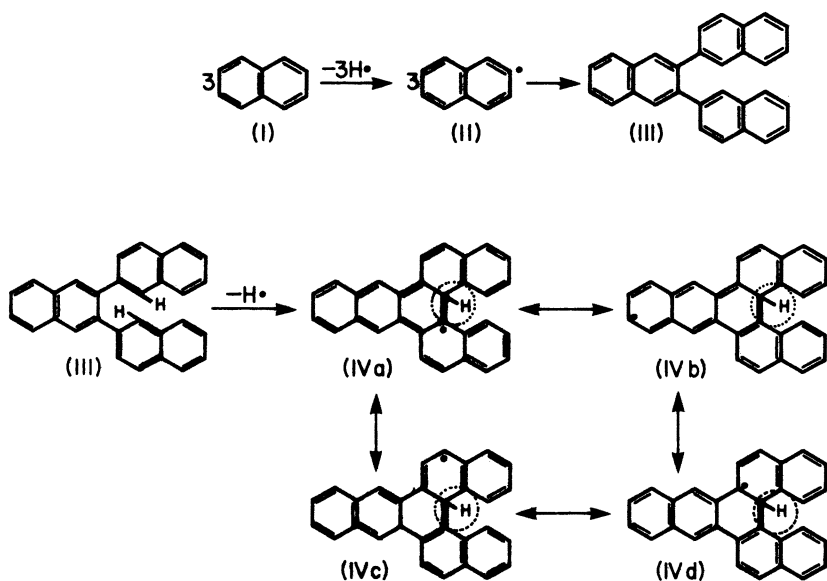


Figure 9. ENDOR spectrum of 2H-benzo[cd]pyrenyl radical measured at 400 K. (Reproduced with permission from reference 25. Copyright 1985 Wiley.)

Scheme IV, the loss of one H atom from the naphthalene trimer leads to a molecule containing a 19-carbon conjugated system and a single  $sp^3$  carbon atom. The free radical is stabilized by delocalization of the unpaired electron over the 19-carbon atom network. Loss of an additional H atom results in a fully condensed aromatic hydrocarbon containing 20 carbon atoms.



Scheme IV. Proposed mechanism for the formation of stable  $\pi$  radicals during thermal polymerization of naphthalene. (Reproduced with permission from reference 7. Copyright 1981 Pergamon Press.)

## Summary and Conclusions

The thermal conversion of polynuclear aromatic compounds to carbon is primarily a polymerization process. For aromatic hydrocarbons, this process occurs through the loss of hydrogen or substituent alkyl groups. Similar polymerization sequences are involved in thermal reactions of other aromatic components of carbonaceous materials, such as polynuclear heterocycles (26). Polymerization leads to a mixture of oligomers, and the structure depends on the site of reaction. Other reactions including hydrogen transfer and molecular rearrangement are also prevalent and contribute to the complexity of the process. The transformation of these pitch mixtures to infusible coke usually occurs through a liquid crystalline state. This development of mesophase depends on the presence of large aromatic molecules in sufficient concentration. Development of the infusible coke stage involves further polymerization and dehydrogenative condensation through  $\sigma$ -radical and odd-alternate  $\pi$ -radical intermediates. With increasing heat treatment temperatures, the carbonaceous polymers undergo continued dehydrogenation and polymerization to form the carbon precursors of three dimensionally ordered graphite.

## References

1. Badger, G. M., *Prog. Phys. Org. Chem.* **1965**, *3*, 1.
2. Lang, K. F.; Buffleb, H.; Zander, M. *Erdöl Kühle Erdgas Petrochem.* **1963**, *16*, 944.
3. Lang, K. F.; Buffleb, H.; Kalowy, J. *Chem. Ber.* **1961**, *94*, 523; *Chem. Ber.* **1960**, *93*, 303; *Chem. Ber.* **1957**, *90*, 2888.
4. Lewis, I. C. *Carbon* **1980**, *18*, 191.
5. Zander, M.; Haase, J.; Dreeskamp, H. *Erdoel Kohle Erdgas Petrochem.* **1982**, *35*, 65.
6. Fitzer, E.; Mueller, K.; Schaffer, W. In *Chemistry and Physics of Carbon*; Walker, P. L. Jr., Ed.; Marcel Dekker: New York, 1971; Vol. 7; p 237.
7. Lewis, I. C. *Carbon* **1982**, *20*, 519.
8. Stein, S. E. In *New Approaches to Coal Chemistry*; Blaustein, B. D.; Bockrath, B. C.; Freidman, S., Eds.; ACS Symposium Series 169; American Chemical Society: Washington, DC, 1981; p 97.
9. Brooks, J. D.; Taylor, G. H. *Nature* **1965**, *206*, 697.
10. Lewis, I. C. *J. de Chim. Phys.* **1984**, *81*, 751.
11. Chen, S. H.; Stevens, W. C.; Diefendorf, R. J. Abstracts of Papers, International Symposium on Carbon, Toyohashi, Japan, 1982, Abstract 1B05, pp 69-72.
12. Singer, L. S.; Lewis, I. C. *Carbon* **1984**, *22*, 487.
13. Kinney, C. R.; Nunn, R. C.; Walker, P. L. Jr. *Ind. Eng. Chem.* **1957**, *49*, 880.
14. Badger, G. M.; Donnely, J. K.; Spotswood, T. M. *Aust. J. Chem.* **1964**, *17*, 1147.
15. Lang, K. F.; Buffleb, H. *Chem. Ber.* **1961**, *94*, 1075
16. Morita, M.; Hiroshawa, K.; Takeda, S.; Ouchi, K. *Fuel* **1979**, *58*, 269.
17. Stein, S. E.; Griffith, L. L. Abstracts of Papers, 16th Biennial Carbon Conference, Philadelphia, PA, 1983, p 13.
18. Stein, S. E. *Carbon* **1981**, *19*, 421.

19. Greinke, R. A.; O'Connor, L. C. *Anal. Chem.* **1980**, *52*, 1877.
20. Guet, J. M.; Rousseaux, F.; Tchoubar, D. Proceedings of the Fifth London International Carbon and Graphite Conference, 1978, Vol. 1, p 294; *Carbon* **1977**, *15*, 211.
21. Greinke, R. A.; Lewis, I. C. *Carbon* **1984**, *22*, 305.
22. Lewis, I. C.; Singer, L. S. In *Chemistry and Physics of Carbon*; Walker, P. L., Jr.; Thrower, P. A., Eds.; Marcel Dekker: New York, 1981; Vol. 17, p 1.
23. Lewis, I. C.; Singer, L. S. *Carbon* **1964**, *2*, 115.
24. Lewis, I. C.; Singer, L. S. *Fuel* **1984**, *63*, 1478.
25. Lewis, I. C.; Singer, L. S. *Magn. Res. Chem.* **1985**, *23*, 698.
26. Greinke, R. A.; Lewis, I. C. *Carbon* **1979**, *17*, 471.

RECEIVED for review September 29, 1986. ACCEPTED March 2, 1987.



# Quantum Chemical Structure-Reactivity Relationships in Polycyclic Benzenoid Aromatic Hydrocarbons

Laszlo V. Szentpály<sup>1</sup> and William C. Herndon<sup>2</sup>

<sup>1</sup>Facultad de Química, Universidad de Guanajuato, Noria Alta, Guanajuato, GTO 36000, Mexico

<sup>2</sup>Department of Chemistry, University of Texas at El Paso, El Paso, TX 79968-0509

*Theoretical methods to predict chemical reactivity properties of polycyclic benzenoid aromatic hydrocarbons are reviewed. These methods include the usual molecular orbital (MO) quantum chemical calculations, as well as pencil-and-paper MO and valence-bond procedures to derive indexes related to the rates of chemical reactions. Justification for the pencil-and-paper procedure termed the perturbational molecular orbital-free-electron method (PMO:F) is presented, and the modifications (PMO:F $\omega$ ) of this procedure necessary to handle the differing reactivity patterns with neutral and ionic intermediates are also given. Examples of correlations of experimental results are used to illustrate these modifications.*

**T**HE QUANTUM THEORETICAL CHARACTERIZATION of the molecular structure of polycyclic benzenoid aromatic hydrocarbons (PAHs) and the relationships of structure to the physical and chemical properties of PAHs are problems that have been of concern to theoreticians (and experimentalists) for more than 50 years. In general, quantum chemical procedures can be used successfully to correlate kinetic and thermodynamic data for PAHs. These procedures are usually restricted to the  $\pi$  systems of the PAHs and normally seem to yield very good results because (1) the  $\pi$  system properties are described accurately by quantum mechanical calculations and (2) the energetics of a given type of reaction in a group of related PAHs is mainly

determined by energy differences of the respective  $\pi$  systems. In fact, the PAHs have served as the testing systems for many of the approximations used in molecular orbital (MO) and valence-bond calculations (1–5).

Quantum chemical pencil-and-paper procedures have proved to be quite useful in the PAH field (6–8). The methods that have been developed are widely applicable and easy to use, and they give good qualitative and quantitative results for correct physical reasons. We feel that reactivity indexes obtained from Hückel MO (HMO) calculations also lie in the non-computer category. Actual HMO calculations are seldom necessary because of the comprehensive tabulations of eigenvalues, eigenvectors, and derived indexes for nearly all common  $\pi$  systems with fewer than 30  $p$  orbitals (9). However, the correlative ability of HMO calculations is generally worse than results from self-consistent field- $\pi$  (SCF- $\pi$ ) or all-valence-electron SCF methods. This situation is illustrated by the work of Streitwieser et al. (10), in which rates of protodetrition of aromatic hydrocarbons are compared with several types of localization energy calculations. Correlation coefficients with the log of the rate constant are found to be 0.979, 0.970, and 0.893 for localization energies calculated by complete neglect of differential overlap (CNDO/2), SCF- $\pi$ , and HMO methods, respectively; that is, very good correlations are found for CNDO/2 and SCF- $\pi$  calculations, and a poor correlation is found for the HMO results (8).

The perturbational MO method of Longuet-Higgins (11) and Dewar (12), which was thoroughly reviewed by Dewar and Dougherty (6), has been the pencil-and-paper method of choice in numerous applications. More recently, a modified free-electron (MFE) MO approach (13–15) and a valence-bond structure-resonance theory (VBSRT) (7, 16, 17) have been applied to several PAH structure and reactivity problems. A new perturbational variant of the free-electron MO method (PMO:F) has also been derived and reported (8, 18). Both PMO:F and VBSRT qualify as simple pencil-and-paper procedures. When applied to a compilation of electrophilic substitution parameters ( $\sigma^+$ ) (19–23), the correlation coefficients of calculated reactivity indexes with  $\sigma^+$  for alternant hydrocarbons are 0.973 and 0.959, respectively (8). In this case, the performance of the PMO:F method rivals that of the best available SCF calculations for systems of this size, and that of VBSRT is sufficient for most purposes.

The purpose of this chapter is to advocate the use of PMO:F as a general tool for the consideration of PAH structure-reactivity problems, particularly in the case of large and very large PAHs. Therefore, some effort is made to delineate justifications for this method to engender its use. However, we presume that the reader is familiar with the concepts and procedures of the HMO and PMO methods (3–6). Szentpály has recently demonstrated that charge and electron-repulsion effects can be included in PMO procedures (24) and the necessary procedures to include these effects are outlined in this chapter. References and brief listings of published applications are given

where appropriate, and results from our alternate pencil-and-paper procedure, that is, VBSRT, are noted where they are available. Previously unpublished results are discussed in somewhat more detail.

### ***Free-Electron and PMO:F Methods***

The free-electron MO (FEMO) model was introduced in papers by Kuhn (25) and Bayliss (26) and explicated in a series of papers by Platt, Ruedenberg, Scherr, Ham, and Labhart principally during the 1950s. These papers have been collected in a book entitled *Free-Electron Theory of Conjugated Molecules* (27), and many of the topics covered in the papers are further discussed in a review article by Platt (28). Both works provide fascinating reading for students interested in theory and structure–reactivity relationships. Problems in the PAH area that have recently been investigated with the FEMO method include studies of ionization energies (13, 14) and reactivities in electrophilic substitution (15).

The basic differences between the FEMO and the HMO methods are (1) the FEMO method presumes the electron exists in a space (box) of continuous potential and (2) the FEMO method contains only one parameter, the neighboring distance  $D$ , rather than two parameters as in the HMO method. The meaning of the parameter  $D$  in terms of measurable quantities is defined more precisely than the integral parameters in the HMO method, and the FEMO model is closer to being an absolute theory with no adjustable parameters. When the existence of the free electron is restricted to the one-dimensional carbon-bond skeleton of the molecule, one obtains the free-electron network model. Depending upon the conditions imposed at the branch points of the C skeleton, a very close relationship between the FEMO and HMO methods and results can be demonstrated.

In developing the PMO:F method, recalling and using this FEMO and HMO isomorphism is useful. The requirements for the isomorphism are the original Kuhn branching conditions (25), as well as the requirement that the end of the free-electron path be fixed one bond length beyond terminal atoms (26, 27). Under these conditions, odd-alternant PAHs possess a non-bonding FEMO characterized by a de Broglie wavelength  $\lambda_0 = 4D$ , where  $D = 1.40 \text{ \AA}$ , the average aromatic C–C bond length. The branching conditions are equivalent to the introduction of three types of resonance integrals rather than the single exchange integral  $\beta$  of HMO theory:

$$\beta_{nn} = \gamma \text{ (between a pair of nonjoints)} \quad (1)$$

$$\beta_{jn} = (\sqrt{2/3})\gamma \text{ (between a joint and a nonjoint)} \quad (2)$$

$$\beta_{jj} = (2/3)\gamma \text{ (between a pair of joints)} \quad (3)$$

However, these are not additional parameters because the numerical multipliers are a required consequence of the appropriate branching conditions for FEMOs.

The PMO:F approach assumes that the structures of reactants and intermediates are closely related and that the relationship can be treated through the use of a perturbation MO formalism. The explicit assumptions are as follows:

1. Delocalized systems are described in terms of a FEMO model (25–28).
2. The localized bond model is adopted for  $\sigma$  bonds and isolated  $\pi$  bonds (5, 6).
3. In comparing two conjugated structures with slightly different  $\pi$  systems, the difference in energy is assumed to be that between the  $\pi$  electrons, and contributions by stretching or compression of  $\sigma$  bonds are absorbed in values of  $\pi$  energies (5, 6, 29).
4. The difference in energy between two slightly different  $\pi$  systems is obtained by first-order perturbation theory.

Concerning the third assumption, Schaad and Hess (29) demonstrated that C–C bond energy is nearly linear with  $\pi$  bond order  $p_{rs}$  within the range from 0.3 to 0.9. This condition permits the absorption of  $\sigma$  compression in values of  $\pi$  energy. The difference  $\Delta E$  in energy between two closely related systems R and R' can thus be written as follows:

$$\Delta E = \Delta E_{\sigma} + \Delta E_{\pi} \quad (4)$$

where  $\Delta E_{\sigma}$  is the difference in energy of the localized electrons in R and R', and  $\Delta E_{\pi}$  is the corresponding difference in  $\pi$  energy. Because the localized bond model is used,  $\Delta E_{\sigma}$  can be found immediately from tables of standard bond-energies (5); the problem is therefore reduced to the calculation of  $\Delta E_{\pi}$ .

The PMO:F method is implemented by calculating the energy change required to excise a reactive site (S) of the reacting molecule out of the reactant  $\pi$  system to yield the odd PAH  $\pi$  system R. This calculation is actually done by estimating the energy for the reverse process, that is, the adjoining of the excised atom to re-form the original reactant  $\pi$  system, RS. The excised site and the remaining  $\pi$  system are both odd-alternant,  $\pi$  molecular systems. Both fragment systems therefore possess a nonbonding MO (NBMO) level, and the change in  $\pi$  energy as these levels are combined can be calculated by first-order perturbation theory.

When the two formally separate fragments, R and S, are combined to

form RS, the degeneracy of the nonbonding levels of R and S leads to a first-order splitting of the degenerate levels. When two neutral  $\pi$  radicals are combined, the first-order change in energy is given by the following equation:

$$\Delta E = 2 \sum_{(rs)} \psi_0(r) \theta_0(s) \gamma = 2 \sum_{(rs)} c_{0r}^F c_{0s}^F \beta_{rs} \quad (5)$$

where  $\psi_0(r)$  and  $\theta_0(s)$  are the NBMO amplitudes on atom  $r$  of fragment R and atom  $s$  of fragment S, respectively;  $c_{0r}^F$  and  $c_{0s}^F$  are the corresponding FE–NBMO coefficients;  $\gamma$  is a constant; and  $\beta_{rs}$  is the resonance parameter across the bond linking atoms  $r$  and  $s$ . Summation goes over all bonds ( $rs$ ) connecting the fragments R and S. In the HMO model, the amplitudes are identical to the coefficients, and  $\beta_{rs} = \beta = \text{constant}$ .

Unnormalized FE–NBMO amplitudes are found by a zero-sum rule identical to that of Longuet-Higgins (11) for Hückel coefficients. Consequently, the unnormalized FEMO amplitudes precisely coincide with the unnormalized Hückel coefficients. However, to obtain correct normalization, the contributions to the density have to be integrated along the three bonds converging to a joint, whereas only two bonds converge to a nonjoint. Thus, the different  $\beta$  values are somewhat compensated by the differences in the coefficients, as shown in the following equations:

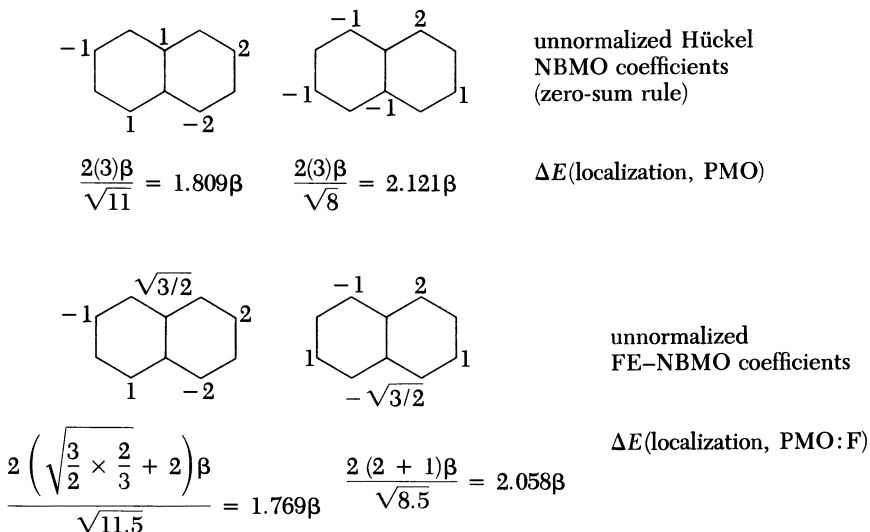
$$c_{0j}^F = \sqrt{3D/2} \psi_0(j) \quad (6)$$

$$c_{0n}^F = \sqrt{D} \psi_0(n) \quad (7)$$

Because of the different normalization, the compensation is not complete, and all FE–NBMO amplitudes and coefficients for systems containing active (starred) joints must differ from their Hückel counterparts.

The FE–NBMO and HMO–NBMO coefficients of  $\pi$  radicals corresponding to  $\alpha$ - and  $\beta$ -substitutions in naphthalene are derived in Chart I to serve as examples. In the case of  $\alpha$ -substitution, the FEMO model offers two possibilities for treating the effective potential at a bridge head atom adjacent to a substitution site, that is, either as a joint or a nonjoint atom. In the first case, an appendage of the free-electron pathway is considered to be pointing toward the  $\alpha$ -position. In this chapter, these types of atoms in PAH fragments are taken to be joint positions.

The calculations of the first-order PMO and PMO:F energies are also given, and both methods predict that the  $\alpha$ -position is more reactive (smaller localization energy) than the  $\beta$ -position, although only small differences in the numerical values of the localization energies are found. However, these small differences do prove to be significant in at least two important appli-



*Chart I. Derivation of FE-NBMO and HMO-NBMO coefficients of  $\pi$  radicals corresponding to  $\alpha$ - and  $\beta$ -substitutions in naphthalene.*

cations: (1) the correlations of  $\sigma^+$  constants for electrophilic substitutions referred to earlier and (2) gas-phase proton affinity (PA) data (30, 31) which has recently become available.

The results obtained by the four pencil-and-paper procedures are summarized in Table I. The PMO:F method shows the highest level of consistency when the nonalternant fluoranthene data is included and remains at the very good level for both applications. Partly, this situation is due to an additional modeling of the known reduced reactivity at  $\alpha$ -positions adjacent to a five-membered ring (32, 33) by treating the atom at the bridge head of the small ring as a nonjoint position (8, 34). The poor correlation of the PA data obtained with the HMO method is probably due to the PA values encompassing a wider variety of structural types than what is normally considered reasonable in HMO applications where the values of parameters are strongly dependent on structural type and application (3). Thus, the Hückel method must be interdicted for the PA application, although the correlations of the  $\sigma^+$  values are satisfactory. The significantly lower correlation coefficient with  $\sigma^+$  upon including fluoranthene values as calculated by VBSRT may be due to the problem of overcounting resonance structures in five-membered-ring  $\pi$  systems (thereby overestimating  $\pi$  resonance energies), as discussed by Stein, and co-workers (35, 36) and by Herndon (37), or a separate parametrization of VBSRT for cationic species may be mandated in analogy to the results for PMO:F $\omega$  presented later in this chapter.

Table I. Correlation Coefficients of Theory with  $\sigma^+$  and PA Values

<i>Experimental Parameter</i>	<i>PMO:F</i>	<i>PMO</i>	<i>VBSRT</i>	<i>HMO</i>	<i>SCF-<math>\pi</math></i>	<i>CNDO/2</i>
$\sigma(27)^a$	-0.973(27)	-0.960(27)	0.959(27)	-0.954(27)	0.932(22)	0.961(20)
$\sigma(32)^b$	-0.972(32)	-0.956(32)	0.918(32)	-0.940(32)		
PA(17) <sup>b</sup>	-0.958(17)	-0.930(17)	0.927(17)	-0.663(17)	0.926(10)	0.935(10)

NOTE: The number of cases in the correlation is given in parentheses.

<sup>a</sup>Cases include alternate PAH only.

<sup>b</sup>Cases include fluoranthene (five different positions for  $\sigma^+$ ).

### PMO:F $\omega$ Method

PMO:F $\omega$  stands for a paper-and-pencil procedure that allows one to differentiate between the energies of odd-alternate PAH radicals, anions, and cations (24, 38). The calculations are carried out within the free-electron perturbational MO framework. The effects of electronic charge are accounted for by a procedure that makes use of the formal principles of the HMO $\omega$  technique, a method used in HMO calculations by Wheland and Mann (39), and by Streitwieser (40). The HMO $\omega$  calculations require an iterative solution for HMO eigenvalues and eigenvectors, whereas the PMO:F $\omega$  procedure requires only a single hand calculation (to be described later).

The atoms of odd PAH radicals are electrically neutral. In these kinds of systems, simple PMO and PMO:F theories provide a reasonable description of energy differences between the ground state of  $\pi$  hydrocarbons and reactive intermediates (6, 11, 38). However, in the corresponding anions and cations, the different charges of the different atoms effectively lead to different electronegativities of the topologically distinct atoms. These differences due to the charges in ionic species can be rather important in correlating and understanding the chemistry of such species. Breakdowns of the simple HMO and PMO approximations are documented in the work of Dewar and co-workers (6, 41, 42), and Streitwieser and co-workers (43, 44) on ionic reaction intermediates. The errors found in PMO and PMO:F treatments of PAH ions are on a tolerably low level in some cases (5, 6, 8, 11); in others, they are more pronounced (24, 38). In the  $\sigma^+$  correlations summarized in Table I, large errors are not present, although an improvement in the scatter of the calculated regression (8) would be welcome.

In the HMO $\omega$  method, the carbon-atom electronegativity is assumed to depend linearly on the net atom charge  $q_r$ . A more attractive Coulombic parameter  $\alpha_r$  is attributed to a positively charged carbon atom, because of fewer electrons to screen the core. The proposed change in electronegativity is  $\omega\beta q_r$ ; the parameter  $\omega$  has an optimized value  $\omega = 1.4$ .

$$\alpha_r = \alpha_0 + \omega\beta q_r \quad (8)$$

where  $\alpha_0$  and  $\beta$  are the usual Hückel Coulombic and resonance parameters, respectively (39, 40). An iterative procedure is required because the obtained charges are derived from the eigenvector coefficients of the HMO secular matrix, which in turn depend upon the  $\alpha_r$  calculated by equation 8.

The energy of an odd PAH ionic  $\pi$  system therefore differs from that of the corresponding radical. To the first order, this extra energy (stabilizing or destabilizing) is given as follows:

$$E_{C,\omega} = \omega\beta \sum_r (1 - q_r)q_r = \omega\beta \left( \sum_r q_r - \sum_r q_r^2 \right) \quad (9)$$



where  $(1 - q_r) = Q_r$  is the total  $\pi$  charge on atom  $r$ . The notation  $E_{C,\omega}$  refers to the related charge-dispersal energy  $E_C(\text{PPP})$  (45, 46) of the Pariser–Parr–Pople model, which makes use of a similar kind of correction and whose principles can be used to justify the HMO $\omega$  method. The net charges sum to +1 and –1 for cations and anions, respectively. For odd PAH ions, we obtain the following:

$$q^2 = c_{0r}^4 = D^2\psi_0^4(r) \text{ for } r = n \quad (10)$$

$$q^2 = c_{0r}^4 = (3D/2)^2\psi_0^4(r) \text{ for } r = j \quad (11)$$

according to the PMO:F method. The combination of equations 9–11 allows the inclusion of a variable electronegativity and some electron interaction as first-order perturbations in the PMO:F method. The improved method is denoted PMO:F $\omega$  because it is the free-electron variant of the PMO– $\omega$  method of reference 24.

The discussion so far has treated only those reaction intermediates that can be formed from a parent unsubstituted PAH. We also wish to present the treatment for cases in which a delocalized  $\pi$  intermediate is formed from methyl-substituted derivatives. For example, in considering the formation of an arylmethyl cation, thermocyclic arguments (5, 6) have to be implemented to estimate the difference in  $E_{C,\omega}^+$  between the arylmethyl cation and the fragments before the union, that is, the neutral even PAH and the  $\text{CH}_2^+$  ion. The localized positive charge of the  $\text{CH}_2^+$  ion and the condition  $q_r = 0$  in the neutral even PAH leads to the following:

$$E_{C,\omega}^+(\text{reference structure}) = \omega\beta[(1 - 1) + (0 - 0)] = 0 \quad (12)$$

Thus, the PMO:F $\omega$  and PMO– $\omega$  methods correlate the formation of an arylmethyl cation with the following:

$$E_{R,\omega}^+ = E_D + E_{C,\omega}^+ = 2(1 - |c_{0b}|)\beta + (1 - \sum_r c_{0r}^4)\omega\beta \quad (13)$$

where  $c_{0b}$  is the NBMO coefficient at the methylene site. The second term may be interpreted as going beyond the usual PMO approximation of a constant ionization energy for all odd aromatic hydrocarbon radicals by introducing a specific stabilization of the cation that depends upon structural topology. The change in  $\sigma$  energy during the carbocation formation is considered to be independent of the parent molecule because such changes are well-described by the localized-bond model (5).

How are these arguments amended to deal with cases that involve anionic intermediates (42–44)? In the HMO $\omega$  method, an anionic  $\pi$  system is destabilized relative to the corresponding radical by the positive term

$$E_{C,\omega}^- = \omega\beta(-1 - \sum_r q_r^2) \quad (14)$$

because the net charges sum to  $-1$  and  $\beta < 0$  by definition. However, this situation is not at variance with Brickstock and Pople's statement (45) that ions of both signs should show the same increase of resonance stabilization in comparison with the corresponding radical. In fact, the resonance energies in reference 45 are formulated with respect to the energy of a classical ionic or radical structure. According to the HMO $\omega$  technique, any classical anion is strongly destabilized because the whole negative charge resides on a single carbon atom, as in the fragment  $\text{CH}_2^-$  which serves as the reference system before union with the neutral even PAH.

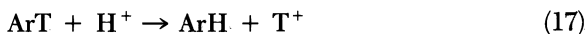
$$E_{C,\omega}^- (\text{reference}) = \omega\beta[(-1 - 1) + (0 - 0)] = -2\omega\beta \quad (15)$$

By correlating the formation of an arylmethyl anion with the difference between its  $\pi$  energy and that of the fragments, we obtain equation 16 for the anionic case: This equation is formally identical to the result given for the cationic situation in equation 13.

$$E_{R,\omega}^- = 2(1 - |c_{ob}|)\beta + (1 - \sum_r c_{0r}^4)\omega\beta \quad (16)$$

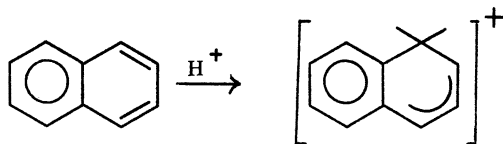
### Examples and Discussion

Electrophilic substitution is the principal chemical reaction that is presumed to characterize the concept of aromaticity (47). With this presumption, rates of protodetrutiation (equation 17) afford a prototype data set that can be used to define  $\sigma^+$  for individual sites of reaction in PAHs (19–23).



Experimental gas-phase PA values (30, 31) constitute a related set of experimental values in which the measured PA is assumed to refer to the most reactive molecular position. Comparisons of  $\sigma^+$  with various types of quantum chemical calculated parameters have been tabulated by Streitwieser et al. (10) and by us (8, 16). A summary of the results for previously used pencil-and-paper procedures and SCF methods was already presented in Table I.

The calculations presume that the rate-determining step involves protonation of the neutral PAH to yield a delocalized odd-alternate cationic species, as shown in Scheme I. The difference in energy between that of the neutral PAH and the cation is called the *localization energy*, and this localization energy is the quantity estimated by the various theoretical methods. The greater the localization energy, the less reactive the parent PAH is.



Scheme I.

PMO:F and PMO:F $\omega$  localization energies for cationic species and the experimental parameters are listed in Table II; nonbenzenoid compounds have been excluded from this table. We treat the correction term for charge interaction that characterizes the PMO:F $\omega$  procedure as a individual parameter; therefore, it is listed separately. PA values calculated by CNDO/2, an all-valence-electron SCF method (10), are also included in Table II to facilitate a comparison of PMO:F $\omega$  and a typical quantum mechanical procedure that includes the effects of electron repulsion.

In the correlation of  $\sigma^+$  using PMO:F, the results obtained parallel our previous results given in Table I. The correlation coefficient is 0.972, and the average deviation of a calculated  $\sigma^+$  from the experimental value is  $\pm 0.040$ . Proceeding to PMO:F $\omega$ , the optimized value of  $\omega$  is found to be 1.45, and in consonance with the presence of an additional parameter, the correlation coefficient rises slightly to 0.979, and the average deviation of the calculated  $\sigma^+$  falls to  $\pm 0.037$ . Calculated  $\sigma^+$  are given by the following equation:

$$-\sigma^+(\text{calculated}) = 0.727 - 0.527(\text{PMO:F}) + 0.763(1 - \Sigma q^2) \quad (18)$$

A plot of the calculated  $\sigma^+$  versus the experimental  $\sigma^+$  is shown in Figure 1.

The PMO:F result for PA values has already been given in Table I, although the correlation included the nonalternant fluoranthene and the cyclobutadienoid biphenylene. The PMO:F $\omega$  correlation equation for the PA values of the benzenoids in Table II is the following:

$$\text{PA}(\text{calculated}) = 940.4 - 86.3(\text{PMO:F}) + 69.1(1 - \Sigma q^2) \quad (19)$$

The correlation coefficient for equation 19 is 0.971, and the average deviation of a calculated PA is  $\pm 5.9$  kJ/mol. The quality of the regression analysis can be judged by examining Figure 2.

As has been found in other cases (24, 37, 38), a simple technique such as PMO:F $\omega$  gives results that are highly correlated with SCF calculations. As an example, the CNDO/2 calculated PA values (10) given in Table II are precisely correlated by the following:

$$\text{PA}(\text{calculated by CNDO/2}) = 14.32 - 1.68(\text{PMO:F}) + 2.56(1 - \Sigma q^2) \quad (20)$$

Table II. PMO:F Localization Energies,  $\sigma^+$ , and PA Values

Compound (Substitution Site)	$-\sigma^+$ <sup>a</sup>	PA <sup>b</sup> (kJ/mol)	PMO:F	PMO:F $\omega$ ( $1 - \sum q^2$ )	PA(CNDO/2) <sup>c</sup> (eV)
Benzene	0.00	786.3	2.309	0.667	12.14
Biphenyl (2)	0.22	828.2	1.940	0.754	—
Biphenyl (4)	0.25	—	1.940	0.754	—
Naphthalene (1)	0.35	821.9	1.769	0.726	13.11
Naphthalene (2)	0.25	—	2.057	0.706	12.70
Anthracene (1)	0.45	—	1.540	0.746	13.58
Anthracene (2)	0.32	—	1.835	0.711	13.10
Anthracene (9)	0.82	876.8	1.206	0.797	14.41
Phenanthrene (1)	0.34	—	1.782	0.780	13.22
Phenanthrene (2)	0.25	—	2.063	0.749	12.84
Phenanthrene (3)	0.293	—	1.943	0.781	13.00
Phenanthrene (4)	0.33	—	1.873	0.749	13.07
Phenanthrene (9)	0.37	842.0	1.728	0.708	13.32
Triphenylene (1)	0.32	836.1	1.882	0.774	13.14

Triphenylene (2)	0.24	—	1.982	0.775	13.04
Pyrene (1)	0.67	873.0	1.414	0.852	14.09
Pyrene (2)	0.22	—	2.190	0.771	12.69
Pyrene (4)	0.36	—	1.633	0.715	13.44
Naphthacene (5)	—	915.7	0.983	0.813	—
Chrysene (6)	0.47	851.2	1.569	0.790	13.71
Perylene (3)	0.74	891.8	1.244	0.853	14.49
Coronene (1)	0.44	866.7	1.667	0.824	—
Benz[ <i>a</i> ]anthracene (7)	0.64	—	1.270	0.828	—
Dibenz[ <i>a,h</i> ]anthracene(7)	0.65	—	1.393	0.836	—
Benzo[ <i>a</i> ]pyrene (6)	0.86	—	1.069	0.859	—
Dibenzo[ <i>def,mmo</i> ]chrysene (6)	0.81	—	0.962	0.861	—
Picene (5)	—	861.7	1.566	0.796	—
Benzo[ <i>ghi</i> ]perylene (4)	—	881.8	1.418	0.860	—
Styrene (β)	—	855.8	1.512	0.612	—
1,1-Diphenylethene (β)	—	897.3	1.155	0.708	—

<sup>a</sup>An increasing negative value indicates an increasing rate because  $\rho$  is negative for electrophilic substitution.

<sup>b</sup>Data are taken from references 30 and 31.

<sup>c</sup>Data are taken from reference 10.

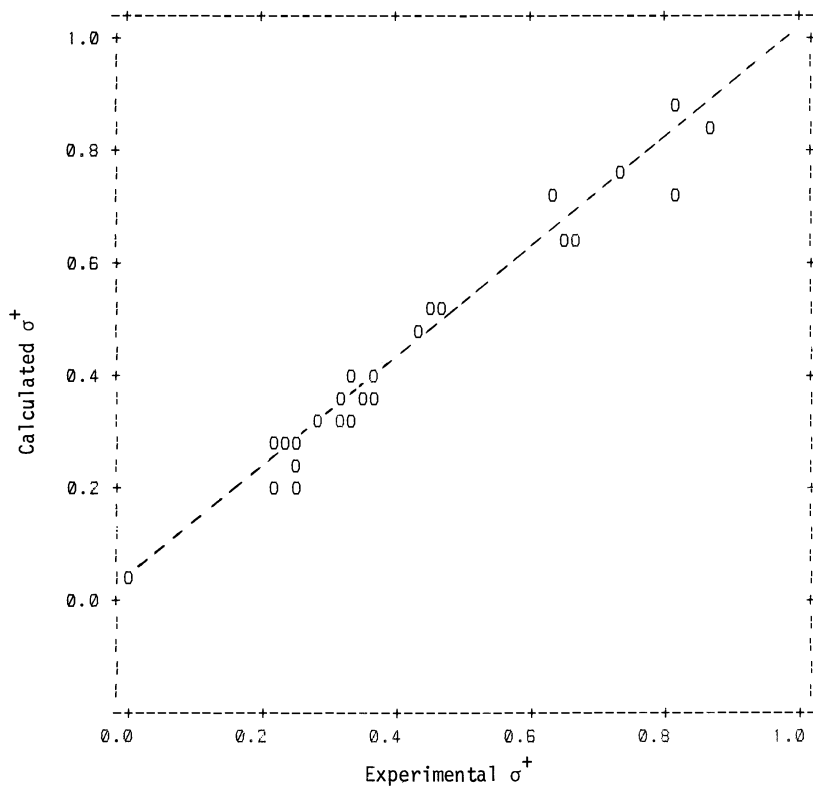


Figure 1. Calculated versus experimental  $\sigma^+$  for PAHs (see Table II).

The optimized value of  $\omega$  is 1.52, the correlation coefficient for equation 20 is 0.995, and the average deviation of a PMO:F $\omega$  PA from the corresponding CNDO/2 PA is only  $\pm 0.04$  electronvolts (eV). A plot of the results is not shown because the deviations from a straight line are too small to indicate any systematic source of the deviations. The results do indicate that the more complex CNDO/2 procedure can be accurately modeled by the PMO:F $\omega$  method, at least for this application. Whether or not one can extend this result to other types of SCF procedures is under investigation. The applications of PMO:F and PMO:F $\omega$  to other types of reactions with ionic intermediates (*see* references 37 and 38 for reviews) are also receiving consideration.

Radical abstraction and addition reactions are likely to be important components of PAH thermal chemistry (48). Paper-and-pencil procedures, particularly VBSRT, to correlate radical reactivities and the qualitative thermal behavior of PAHs and alkyl derivatives have been reviewed (35, 37, 48). Rate data were obtained by Gleicher and co-workers (49) and by Dickerman

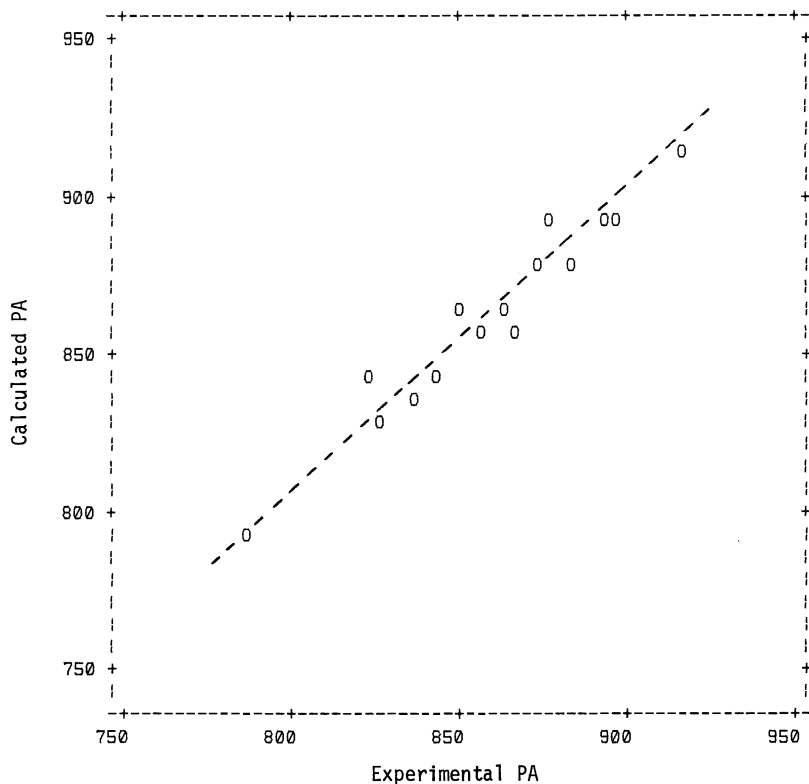
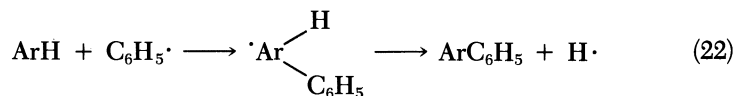
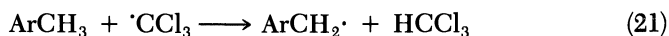


Figure 2. Calculated versus experimental PA values for PAHs (see Table II).

et al. (50) for the following reactions:



These data can be used as primary standards of comparison, and fairly good correlations with resonance energy differences calculated by VBSRT and other methods have been obtained (35, 37, 48).

This radical rate data, in the form of partial rate factors, and the relevant PMO:F calculations are summarized in Table III. The intermediate radicals, equations 21 and 22, are neutral, so PMO:F $\omega$  is not required for calculating the localization energies. The rate data have been recalculated to refer to the phenyl-substituted compound, namely, toluene or benzene, and the

Table III. Partial Rate Factors for Radical Reactions and PMO:F Calculations

Compound (Reaction Site)	Abstraction <sup>a</sup>	Stab. $\Delta E^b$	Phenylation <sup>c</sup>	Stab. $\Delta E^d$
Benzene (1)	0.00	0.000	0.00	0.000
Triphenylene (1)	0.32	0.142		
Triphenylene (2)	0.36	0.104		
Phenanthrene (2)	0.63	0.246		
Phenanthrene (3)	0.50	0.118	0.72	0.366
Phenanthrene (1)	0.52	0.182	1.13	0.527
Phenanthrene (4)	1.14	0.436		
Naphthalene (2)	0.50	0.078	0.54	0.252
Phenanthrene (9)	0.69	0.204	1.23	0.581
Naphthalene (1)	0.76	0.186	1.31	0.540
Chrysene (6)	1.10	0.278		
Anthracene (2)	1.53	0.160	1.12	0.474
Pyrene (4)	1.53	0.676		
Anthracene (1)	1.88	0.292	1.68	0.769
Pyrene (1)	2.04	0.358	1.91	0.895
Anthracene (9)	2.69 <sup>e</sup>	0.479	2.83	1.103

NOTE: All rate factors are referred to the phenyl compound.

<sup>a</sup>Values are log (relative rates) of abstraction. An arylmethyl radical intermediate is formed.

<sup>b</sup>Values are stabilization energy changes calculated by PMO:F and given in  $\beta$  units. Values are referred to benzene,  $\Delta E = 0.488\beta$ .

<sup>c</sup>Values are log (relative rates) of phenylation. Phenylation sites are on ring carbon atoms.

<sup>d</sup>Values are stabilization energy changes calculated by PMO:F and given in  $\beta$  units. Values are referred to benzene,  $2.309\beta - \Delta E$ .

<sup>e</sup>Value is corrected according to reference 49b.



localization energies are converted to stabilization energies relative to the localization energies of the same standards. The original experimental papers (49, 50) should be consulted for details regarding assumptions concerning the analysis of products.

The correlation of the arylmethyl hydrogen abstraction data with the PMO:F calculations is shown in Figure 3. The correlation coefficient is 0.911, the lowest found yet for any application of the PMO:F or PMO:F $\omega$  methods. However, this value compares favorably with the results of the VBSRT calculations (37) and the HMO calculations (49) for which the correlation coefficients are 0.933 and 0.855, respectively, for the rate data versus resonance energy differences. We also find again a very good correlation of the PMO:F localization energies with, in this case, open-shell Pariser-Parr-Pople SCF- $\pi$  calculations (49), correlation coefficient 0.963. In any event, the PMO:F calculations can be used to quantitatively correlate and predict rates of reaction in this case as well.

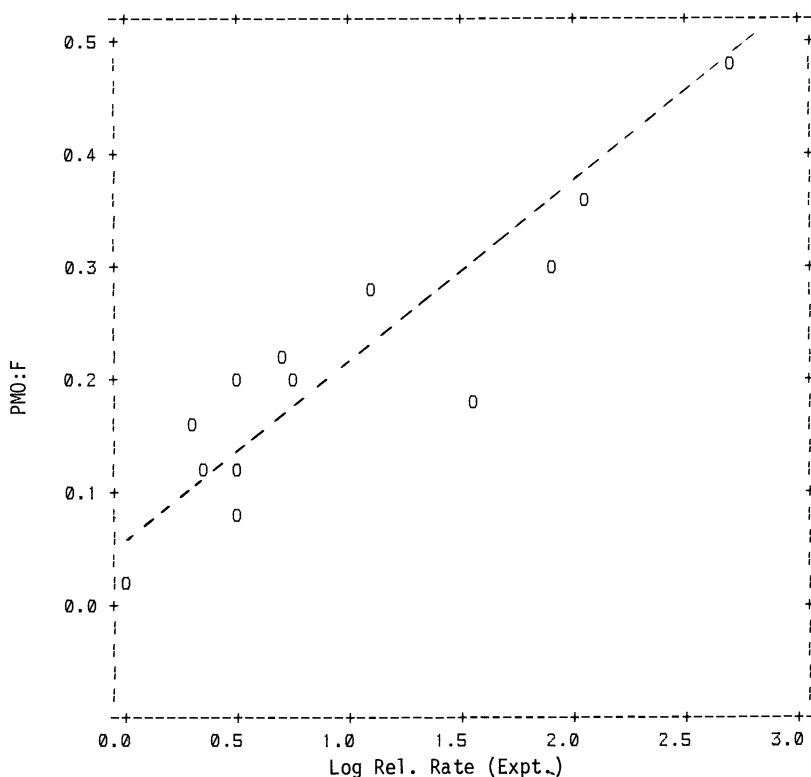


Figure 3. Calculated PMO:F energies versus experimental log (relative rates) for abstraction reactions from methyl PAHs (see Table III).

The partial rate factors for phenylation (50) are much more congruent with the PMO:F calculations, as demonstrated by the plot of the data from Table III given in Figure 4. The correlation coefficient is 0.985, and the average deviation of a partial rate factor calculated from the regression line is only  $\pm 0.10$ , which corresponds to an actual rate ratio of 1.25. The other pencil-and-paper procedures also give improved results when compared with the abstraction case. Correlation coefficients of resonance energy differences calculated by VBSRT and the HMO method with the log of the relative rate are both 0.961.

### Conclusions

In general, we find that PMO:F and PMO:F $\omega$  are useful methods to correlate and help understand PAH chemical reactivity. In every case investigated so far, the experimental data are correlated much more precisely with these methods than with the HMO method. In the majority of applications, the

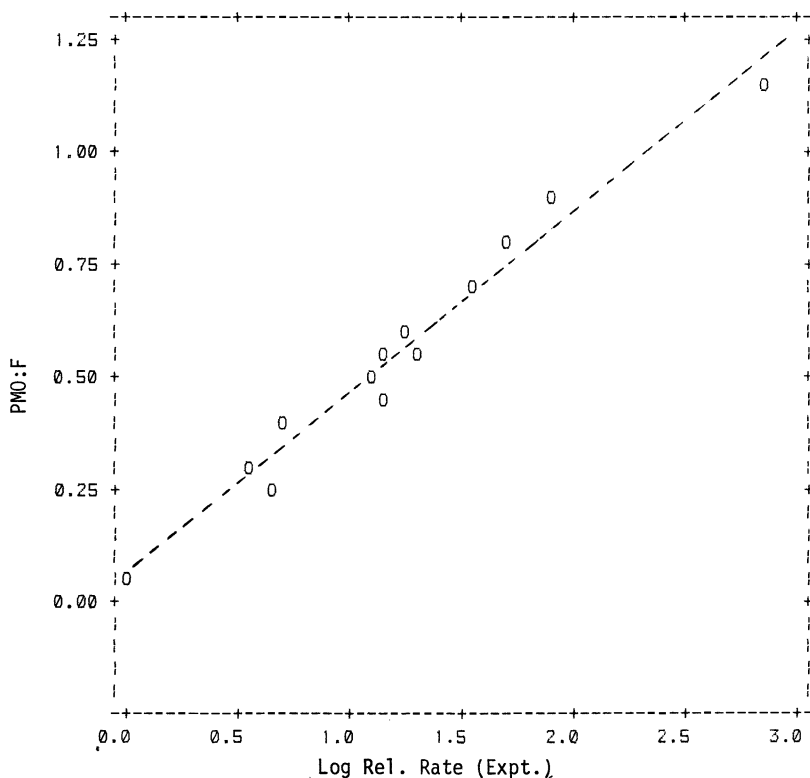


Figure 4. Calculated PMO:F energies versus experimental log (relative rates) for phenylation of PAHs (see Table III).

performance of PMO:F and PMO:F $\omega$  is as good as or is better than the performance of the best available semiempirical SCF calculations. We believe that the correlations obtained are not due to chance but result from the fact that these perturbational FEMO procedures provide an accurate modeling of electronic delocalization and charge interaction. Because the large molecular size of many PAH reactants and intermediates precludes the extensive use of ab initio calculations, we infer that these PMO procedures may be the methods of choice for the theoretical understanding of structure–reactivity relationships in large PAH systems.

The chemistry of very large PAHs has barely been explored. Large structures of this type may be involved in coal chemistry (51, 52) and in the thermal conversion of PAHs to carbon (53), as detailed elsewhere in this book. In addition, the recent postulate of a spherical C<sub>60</sub> aromatic structure for a pyrolytic graphite fragment (54) may spawn a possible new subfield of three-dimensional polycyclic aromatic chemistry. Large PAHs have also been suggested to be abundant in interstellar space surrounding carbon-rich stars (55–57), and possible candidate structures are being synthesized by Hendel et al. (58). FEMO, PMO:F, and PMO:F $\omega$  will be useful theoretical techniques to apply in these areas. However, obtaining the FEMO coefficients for large PAHs by performing hand calculations is tedious. We are developing a microcomputer program to perform the calculations, and we plan to apply PMO:F and PMO:F $\omega$  to characterizing structure–reactivity relationships in large PAHs.

### Acknowledgement

The financial support of the Robert A. Welch Foundation of Houston, TX and the Texas Advanced Technology Program is gratefully acknowledged.

### References

1. Wheland, G. W. *Resonance in Organic Chemistry*; Wiley: New York, 1955.
2. Daudel, R.; Lefebvre, R.; Moser, C. *Quantum Chemistry, Methods and Applications*; Interscience: New York, 1959.
3. Streitwieser, A., Jr. *Molecular Orbital Theory for Organic Chemists*; Wiley: New York, 1961.
4. Salem, L. *The Molecular Orbital Theory of Conjugated Systems*; Benjamin: New York, 1966.
5. Dewar, M. J. S. *The Molecular Orbital Theory of Organic Chemistry*; McGraw-Hill: New York, 1969.
6. Dewar, M. J. S.; Dougherty, R.C. *The PMO Theory of Organic Chemistry*; Plenum: New York, 1975.
7. Herndon, W. C. *Isr. J. Chem.* **1980**, *20*, 270.
8. Szentpály, L. V.; Herndon, W. C. *Croat. Chem. Acta* **1984**, *57*, 1621.
9. Streitwieser, A., Jr.; Brauman, J. I. *Supplemental Tables of Molecular Orbital Calculations*; Pergamon: New York, 1965.

10. Streitwieser, A., Jr.; Mowery, P. C.; Jesaitis, R. G.; Lewis, A. *J. Am. Chem. Soc.* **1970**, *92*, 6529.
11. Longuet-Higgins, H. C. *J. Chem. Phys.* **1950**, *18*, 265, 275, 283.
12. Dewar, M. J. S. *J. Am. Chem. Soc.* **1952**, *74*, 3341, 3345, 3350, 3353, 3355.
13. Szentpály, L. V. *Chem. Phys. Lett.* **1979**, *67*, 63.
14. Szentpály, L. V. *J. Mol. Struct.* **1980**, *60*, 391.
15. Szentpály, L. V. *Chem. Phys. Lett.* **1981**, *77*, 352.
16. Herndon, W. C. *J. Org. Chem.* **1975**, *40*, 3583.
17. Herndon, W. C. *J. Phys. Chem.* **1981**, *85*, 3040.
18. Szentpály, L. V. *J. Photochem.* **1981**, *17*, 112.
19. Streitwieser, A. Jr.; Lewis, A.; Schwager, T.; Fish, R. W.; Labana, S. *J. Am. Chem. Soc.* **1970**, *92*, 6525.
20. Baker, R.; Eaborn, C. and Taylor, R. *J. Chem. Soc., Perkin Trans.* **1972**, *2*, 97.
21. Krygowski, T. M. *Tetrahedron* **1972**, *28*, 4981.
22. Ansell, H. V.; Hirschler, M. M.; and Taylor, R. *J. Chem. Soc., Perkin Trans. 2* **1977**, 353.
23. Shafiq, Y. F. E.; Taylor, R. *J. Chem. Soc., Perkin Trans 2* **1978**, 1263.
24. Szentpály, L. V. *J. Am. Chem. Soc.* **1984**, *106*, 6021.
25. a) Kuhn, H. *Helv. Chim. Acta* **1948**, *31*, 1441. b) Kuhn, H. *Helv. Chim Acta* **1949**, *32*, 2247.
26. Bayliss, N. S. *J. Chem. Phys.* **1948**, *16*, 287.
27. *Free-Electron Theory of Conjugated Molecules: A Source Book. Papers of the Chicago Group 1949–1961*; Wiley: New York, 1964.
28. Platt, J. R. In *Handbuch der Physik/Encyclopedia of Physics*; Flugge, S., Ed.; Berlin, 1961; Vol. 37, Part 2, pp 173–281.
29. Schaad, L. J.; Hess, B. A. *J. Am. Chem. Soc.* **1972**, *94*, 3068.
30. Aue, D. H.; Bowers, M. T. In *Gas-Phase Ion Chemistry*; Bowers, M. T., Ed.; Academic: New York, 1979, Chapter 9.
31. Meot-Ner(Mautner), M. *J. Phys. Chem.* **1980**, *84*, 2716.
32. Ansell, H. V.; Taylor, R. *J. Chem. Soc., Perkin Trans 2* **1977**, 866.
33. Bancroft, K. C. C.; Howe, G. R. *J. Chem. Soc., Perkin Trans 2* **1970**, 1541.
34. Szentpály, L. V. *Int. J. Quantum Chem. Quantum Biol. Symp.* **1985**, *12*, 287.
35. Stein, S. E.; Golden, D. M. *J. Org. Chem.* **1977**, *42*, 839.
36. Robaugh D. A. Stein S. E. *J. Am. Chem. Soc.* **1986**, *108*, 3224.
37. Herndon W. C. *J. Org. Chem.* **1981**, *46*, 2119.
38. Szentpály, L. V. Thesis of Habilitation, Stuttgart, Federal Republic of Germany, 1984.
39. Wheland, G. W.; Mann, D. E. *J. Chem. Phys.* **1949**, *17*, 264.
40. Streitwieser, A., Jr. *J. Am. Chem. Soc.* **1960**, *82*, 4123.
41. Dewar, M. J. S.; Sampson, R. J. *J. Chem. Soc., Chem. Commun.* **1956**, 2789.
42. Dewar, M. J. S.; Thompson, C. C. *J. Am. Chem. Soc.* **1965**, *87*, 4414.
43. Streitwieser, A. Jr.; Langworthy, W. C.; Brauman, J. I. *J. Am. Chem. Soc.* **1963**, *85*, 1757, 1761.
44. Streitwieser, A. Jr.; Mowery, P. C.; Jesaitis, R. G.; Wright, J. R.; Owens, P. H.; Reuben, D. M. E. In *The Jerusalem Symposium on Quantum Chemistry and Biochemistry* Vol. II; Israel Acad. of Sciences and Humanities: Jerusalem, 1970; pp 160–180.
45. Brickstock, A.; Pople, J. A. *Trans. Farad. Soc.* **1954**, *50*, 901.
46. Mason, S. F. *J. Chem. Soc., Chem. Commun.* **1958**, 808.
47. Lewis, D.; Peters, D. *Facts and Theories of Aromaticity*; Macmillan: London, 1975.
48. Herndon, W. C.; *Tetrahedron* **1982**, *38*, 1389.

49. (a) Unruh, J. D.; Gleicher, G. J. *J. Am. Chem. Soc.* **1971**, *93*, 2008. (b) Arnold, J. C.; Gleicher, G. J.; Unruh, J. D. *Ibid* **1974**, *96*, 787, (c) Gleicher, G. J. In *Organic Free Radicals*; Pryor, W. A., Ed.; ACS Symposium Series 69; American Chemical Society: Washington, DC, 1978; p 227.
50. Dickerman, S. C.; Feigenbaum, W. M.; Fryd, M.; Milstein, N.; Vermont, G. B.; Zimmerman, I.; McOmie, J. F. W. *J. Am. Chem. Soc.* **1973**, *95*, 4264.
51. Lee, M. L.; Nishioka, M; Chang, H. -C. Chapter 14, in this book.
52. Speight, J. G. Chapter 12, in this book.
53. Lewis, I. C.; Singer, L. S. Chapter 16, in this book.
54. Kroto, H. W.; Heath, J. R.; O'Brien, S. C.; Curl, R. F.; Smalley, R. E. *Nature* **1985**, *318*, 162.
55. Platt, J. R. *Astrophys. J.* **1956**, *123*, 486.
56. Donn, B. *Astrophys. J.* **1968**, *152*, L129.
57. Leger, A.; Puget, J. L. *Astron. Astrophys.* **1984**, *137*, L5; Puget, J. L.; Leger, A.; Boulanger, F. *Ibid.* **1985**, *142*, L19.
58. Hendel; W.; Khan, Z. H.; Schmidt, W. *Tetrahedron* **1986**, *42*, 1127.

RECEIVED for review September 29, 1986. ACCEPTED March 30, 1987.

# Correlations Between the Spatial Configuration and Behavior of Large Polynuclear Aromatic Hydrocarbons

J. C. Fetzer

Chevron Research Company, Richmond, CA 94802-0627

*Twenty previously unreported polycyclic aromatic hydrocarbons (PAHs) were synthesized by condensing mixtures of 1-phenalenone-type ketones. These PAHs were isolated and identified by using field-ionization mass spectrometry, spectrofluorometry, and UV-visible absorbance spectrometry. The spectrometry and chromatography of these and other PAHs were compared. Correlations between the steric strain and the spectral valley depths between maximums, or chromatographic retention, were found. Steric effects were not the only factors affecting retention; resonance stability also appeared to increase retention.*

**A**NALYSES OF MATERIALS for polycyclic aromatic hydrocarbons (PAHs) have become more important in the past few years. The possible etiological effects and ubiquity of these compounds make them interesting. PAHs are found in shale oil, coal liquids, petroleum, asphalt, and many other hydrocarbon-based materials (1). When these materials are combusted, fly ash, chimney soot, and engine-derived air particulates are produced. These products have higher levels of PAHs than the original materials. Discharging of PAHs into the environment has resulted in their universal occurrence in air and water.

PAHs do not necessarily present a problem when they are found in a sample. A problem only occurs if certain PAH isomers are found. The mutagenic and carcinogenic levels of a PAH are structurally dependent. Certain isomers can be very active, whereas other similar ones are not active. For

example, of the five PAHs that contain four rings and have a molecular weight of 228, three (chrysene, benz[*a*]anthracene, and benzo[*c*]phenanthrene) are mutagenic, and two (naphthacene and triphenylene) are not (2). Analytical methods for PAH analysis must be able to differentiate specific PAH isomers to accurately assess the potential health effects.

### *Limitations in PAH Analysis*

The possible use of most techniques for PAH analysis is limited by the need to differentiate isomers. Mass spectrometry, for example, yields only PAH molecular weights because only the molecular ion gives useful information. The fragment ion spectra of most isomers are almost identical; thus, they cannot be used to identify specific isomers. PAH physical properties also limit the use of other analytical methods. Gas chromatography (GC), for example, requires volatile compounds. This limitation allows GC to be used for PAH analyses of only up to six or seven rings. The higher temperatures needed to elute larger PAHs would degrade the column stationary phases and some PAHs.

High-performance liquid chromatography (HPLC) is not limited in its application to PAH analysis. The wide variations possible in mobile and stationary phases can separate PAH mixtures with large numbers of isomers or a large number of rings. For example, several PAHs of up to 12 rings were found in a dichloromethane extract of carbon black (3). Ten compounds with a molecular weight of 424 and six compounds with a molecular weight of 448 were found by using nonaqueous reverse-phase HPLC. This analysis, however, was tedious because individual peaks had to be collected and subsequently identified by fluorescence and mass spectrometries.

The difficulties inherent in off-line analysis of HPLC peaks are becoming less of an unavoidable problem because HPLC also has another advantage over other techniques. The most commonly used HPLC detectors are ideal for PAH analysis. Fluorescence excitation–emission and UV absorbance detection are both highly sensitive and very selective for PAHs. These methods detect electronic transitions in the PAH molecules. The transition energies are determined by the PAH size and shape. Therefore, isomeric species that differ in ring configuration also differ in spectral character. The locations of absorbance maximums and the intermediate minimums, as well as the relative intensities of each, form a unique pattern characteristic of a particular PAH (4).

The development of photodiode array detectors has made it possible to acquire on-line UV–visible absorbance spectra of an HPLC eluent. In contrast with older detectors, which monitored UV absorbance at only one wavelength, the photodiode array detectors monitor all wavelengths within

a spectral range. Conventional detectors dispersed white light from a source and passed only one wavelength through the flow cell. Photodiode array detectors pass white light through the flow cell and then disperse it. The dispersed light is focused on a row of photosensitive elements (the photodiode array). These elements each measure the intensity at a particular wavelength. The total output of this array is a series of absorbance spectra of the HPLC eluent.

Another factor limiting PAH analysis has been the few compounds that are available as standards for spectral and chromatographic comparisons. A collection of commercially available standards has consisted of a few compounds having six or fewer rings (those having 24 or fewer ring carbons). The many other isomers of this size, or any larger ones, have not been easily obtained. The problem is being slowly overcome by new PAH syntheses. Even the products of these syntheses are of limited availability, and many other structures have not yet been produced. Thus, most studies have focused on the small PAHs for which standards are available; few studies have investigated the larger PAHs. Therefore, only a few PAHs have been unambiguously identified in most samples. At best, the remaining components can be tentatively identified by matching their spectra to those in the literature. This approach, however, has inherent chances of error because of different solvents and conditions. Quantitation would be impossible. Overall, analyses for PAHs have not been complete or definitive.

### ***Previous Findings***

As part of a program to analyze various materials for large PAHs, analytical standards had to be acquired. One of the ways to gain standards was through the synthesis of several large PAHs (5–7). These PAHs included five previously unreported compounds. Some were peropyrenes (dibenzo-*[cd,lm]*perylene and its benzo and dibenzo analogues). These compounds resulted by condensing a mixture of 1-phenalenone and 7*H*-benz[*de*]anthracen-7-one and isolating the resulting PAHs.

When these compounds and many other PAHs were chromatographed to see if retention time could be used as another characterizing tool, an unexpected result was found. Even though the PAH structures were ostensibly similar (if conventional graphical representations were compared), their true spatial configurations must be very different. These conformational differences resulted in vastly different spectral and chromatographic characteristics.

Some PAHs had high degrees of intramolecular steric strain because of ring locations. These PAHs assumed nonplanar configurations. Other isomers, which only differed in the location of one ring, were not significantly strained and were more planar. Their higher degree of planarity increased



interaction with the chromatographic stationary phase. Thus, the strained PAHs eluted much earlier than other, more planar, isomers. The most extreme example was the nonplanar nine-ring tetrabenz[*a,cd,j,lm*]perylene, which eluted before the planar four-ring pyrene.

The amount of elution earlier than expected could be estimated from UV-visible spectra. The earliest eluting PAHs had the shallowest minimums between absorbance maximums. As retention increased, the valley between the absorbance maximums also increased for an isomeric series. Some PAHs even showed changes in the depth of their spectral valleys as solvent composition changed. These spectral characteristics paralleled the chromatographic retention behaviors. This finding was assumed to indicate changes in a molecule's planarity with changes in solvent composition. The broadening in spectral bands can be ascribed to the greater possibility of bending and twisting motions in nonplanar structures. These effects superimpose themselves on the electronic transitions (8).

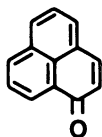
Three distinct types of PAHs were found: (1) PAHs that were planar in all of the solvents (eluting predictably and having very deep spectral valleys, (2) those that were nonplanar in all of the solvents (eluting much earlier than the planar PAHs of the same carbon number and having very shallow spectral valleys, and (3) those that had varying planarity that was dependent on solvent composition (always eluting in a varying fashion in comparison with the planar PAHs and having spectral valleys that changed depth). For example, two nine-ring isomers eluted after the seven-ring dibenz[*cd,lm*]perylene at low dichloromethane concentrations in reverse-phase HPLC. At higher concentrations, they eluted before it, and at the same time their spectra had increasingly broader absorbance bands with shallower minimums. Size-exclusion chromatography indicated a relative change in their sizes.

Although this variation in behavior was initially found for only a small set of peropyrene isomers, it has since been seen for many other PAHs of various structural types by using both normal- and reverse-phase HPLC (7, 9). The parallel trends in both the chromatographic and spectral behaviors were also seen.

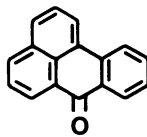
This research continues the previous work to further determine the structural features that control chromatographic retention and to see if these features can be measured by spectrometric behavior. Approximately 30 other peropyrene-type PAHs have been synthesized, isolated, and characterized. These PAHs were the products of other condensation reactions of 1-phenalenone-type ketones. 1-Phenalenone, 7*H*-benz[*de*]anthracen-7-one, and a pair of five-ring ketones were used as reactants. PAHs with 9–12 rings resulted. Their chromatography and spectrometry were studied. The new results agree with previous correlations between steric effects and chromatographic and spectral behaviors.

## Experimental Details

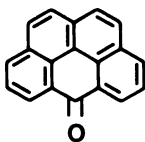
**Synthesis.** The ketones used in the syntheses were 1-phenalenone (Aldrich), 7*H*-benz[*de*]anthracen-7-one (Phaltz and Bauer), 6*H*-benzo[*de*]pyren-6-one (W. Schmidt, Biochemical Institute for Environmental Carcinogens, Ahrensburg, West Germany), and 6*H*-benzo[*fg*]naphthacen-6-one (W. Schmidt). The ketone structures are shown in Chart I.



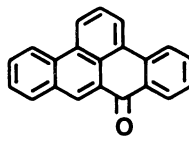
**1-phenalenone**



**7*H*-benz[*de*]anthracen-7-one**



**6*H*-benzo[*de*]pyren-6-one**



**6*H*-benzo[*fg*]naphthacen-6-one**

*Chart I. Structures of the starting ketones used.*

All solvents for extraction and chromatography were from Burdick and Jackson Laboratories (American Scientific Products), except for the solvent for spectrofluorometry, which was a purer grade of 1,2,4-trichlorobenzene that was necessary so that spectra below 400 nm could be obtained (Omnisolv from EM Scientific). All solvents were used as received.

The condensation reactions used either one ketone or a mixture of two ketones (a total of 10 separate reactions). A dry zinc dust melt caused the condensation (10). A mixture of ketone, zinc dust (J. T. Baker), sodium chloride (Leslie Salt), and zinc chloride (Mallinckrodt) (1:1:1:5 by weight, respectively) was ground, thoroughly mixed, and placed in a 50-mL flat-bottomed borosilicate glass (Pyrex) reaction vessel.

The total amount of ketone used in each reaction was 0.5–1.0 g. For the reactions that used two ketones, the ratio was generally 1:1. However, the proportion in reactions using 1-phenalenone was 1:3 (1-phenalenone to the other ketone) because 1-phenalenone was much more reactive than the other ketone. This smaller proportioning of the more reactive ketone resulted in higher yields from the cross reactions of 1-phenalenone with the other ketone rather than from the reactions of 1-phenalenone with itself.

The mixture was first heated on a high-wattage hot plate to 250–275 °C for 10

min to activate the zinc dust (ridding it of any surface zinc oxide). The temperature was raised to 330–350 °C and kept there for 30 min. The liquefied mixture was constantly stirred to make sure that the reaction was complete and that the heating was uniform. The resulting melt both condensed the ketones and reduced the resulting intermediates to the product PAHs. The melt changed from yellow to orange or red as the PAHs were made.

**Extraction and Separation.** After cooling, the product mixture was an amorphous solid. The product mixture and the reaction vessel were ground and placed in a 250-mL Soxhlet thimble. The mixture could not be easily broken up, removed from the vessel, and extracted separately; thus, a small reaction vessel was sacrificed for each reaction to ensure that all product PAHs were collected. The material was exhaustively extracted in a Soxhlet apparatus with 500 mL of dichloromethane. The solution fluoresced an intense green when UV light was shown on it with a hand-held light (Ultraviolet Products). This method was used to monitor the extent of extraction. The extraction typically lasted 75 h, and one Soxhlet cycle occurred every 10 min. After the dichloromethane extraction, the Soxhlet thimbles were immersed in 1,2,4-trichlorobenzene at 175 °C for 1 day to ensure that all the PAHs were removed. Synchronous scanning spectrofluorometry showed only traces of PAHs that were already seen in the dichloromethane extract.

Each extract was concentrated to 50 mL in a Kuderna–Danish apparatus and then diluted to 500 mL with toluene. This solution was then separated on a 75- × 1-cm i.d. glass column of basic aluminum oxide (150 g, Brockman activity grade 1, 60–100 mesh). This solution and another solution eluted from another 500 mL of toluene were combined as the first fraction. Three other fractions were collected by sequential elution with 1 L each of ethyl acetate, dichloromethane, and a 1:1 mixture of dichloromethane and methanol. The first three fractions were usually intensely fluorescent; the first fraction was blue or violet, and the other fractions were various shades of green (from aquamarine to greenish yellow, depending on the reactants). The fluorescence was used to monitor the elution of each fraction from the column. Each fraction was dried under nitrogen on a steam table and redissolved in 50 mL of dichloromethane. HPLC analyses of the fractions were then performed.

The HPLC was a Du Pont 8800 quaternary solvent system with a Hewlett–Packard (HP) 1040A photodiode array detector (5–8). Flexible disks were used for data storage, and postrun data evaluation was performed by the detector's computer (HP 85). Samples were injected with a loop injector; 10 μL was used for analytical scale, and 200 μL was used for preparative scale. Spectra were run on a spectrophotometer (Perkin–Elmer Lambda 3) for static absorbance and on a spectrofluorometer (Perkin–Elmer MPF–66) for fluorescence. Field-ionization mass spectra were obtained at a resolution of 45,000 (corresponding to a 0.01-dalton error for a mass of 450).

Normal-phase chromatography used an amino bonded-phase column (Du Pont Zorbax, 25- × 0.48-cm i.d., 5-μm spherical particle size); *n*-hexane and dichloromethane mixtures were used as the mobile phases. Reverse-phase separations used an octadecyl bonded-phase column (Vydac 201TP5, 25- × 0.46-cm i.d. for analytical scale, and 25- × 0.94-cm i.d. for preparative scale, both with 5-μm spherical particles, Separations Group); methanol and dichloromethane were the mobile phases. As in previous work (5–7, 9), the concentration of strong solvent in the mobile phase was varied from 0% to 100% for reverse-phase studies and from 0% to 30% for normal-phase studies. The peaks isolated from preparative-scale runs were further purified by separation on the analytical-scale octadecyl bonded-phase column.

During a chromatographic run, spectra were acquired manually or through a software peak-detection subroutine. The software package was an upgraded version

of the original HP software (Infometrix). It stored a spectrum when a peak maximum was detected at a preset wavelength. The second derivative of the signal was monitored for this purpose. A spectral range of 245–600 nm, with 2-nm resolution, was stored.

Retention behavior was compared with a series of planar PAHs: pyrene, benzo[*ghi*]perylene, coronene, benzo[*pqr*]naphtho[8,1,2-*bcd*]perylene, naphtho[8,1,2-*abc*]coronene, and ovalene (obtained from Aldrich or by synthesis).

## Results and Discussion

**New PAHs Found.** HPLC analyses of the fractions showed that the toluene fractions contained only the small PAHs resulting when the ketones were reduced with no condensation. The other fractions contained the desired PAHs (these fractions also had some partially reduced intermediates). The product PAHs were somewhat separated between the fractions. Thus, individual PAHs were easier to isolate by HPLC. The last fraction also contained the unreacted and intermediate ketones.

Several previously unreported PAHs were found. Chart II shows these new structures, and the box on page 317 gives their IUPAC names. Chart III shows the structures of the previously known peropyrene-type PAHs produced, and the box on page 319 also gives their names.

The structural assignments of the new PAHs are not absolute. They were based only on the known reactivities of the ketones (10–13), molecular weights from field-ionization mass spectrometry, and absorbance or fluorescence spectra. The absorbance and fluorescence spectra were used to correlate isomeric structures by applying the rules of Clar's annellation theory (4) and Aoki's resonance structure count theory (14). These two independent approaches describe how the structure of a PAH determines its absorbance-band wavelengths. Both approaches rely on spectral trends observed for numerous benzo-analogous PAH series. Important factors include the number of fully aromatic rings that can be drawn in the structure (a fully aromatic ring is defined as one with three  $\pi$  bonds) and the location and number of additional rings on various core structures.

The yields for each new PAH from the reactions varied. As mentioned earlier, 1-phenalene was the most reactive starting material, and 7*H*-benz[*de*]anthracen-7-one, 6*H*-benzo[*de*]pyren-6-one, and 6*H*-benzo[*fg*]naphthacen-6-one were progressively less reactive. Not only did the yields of individual isomers vary because of the differences in the reactivities of the ketones, but the geometry of the ketones also determined the number of possible product isomers. Thus, the reaction of two ketones, 1-phenalene and 6*H*-benzo[*fg*]naphthacen-6-one, gave two new compounds with impurities of two previously known PAHs. The yield of compound 7 was 23%, whereas that of the isomeric compound 8 was less than 1%. Each of the reacting ketones had only one reactive site, and the possible products were highly symmetrical. In contrast, the reaction using 7*H*-benz-

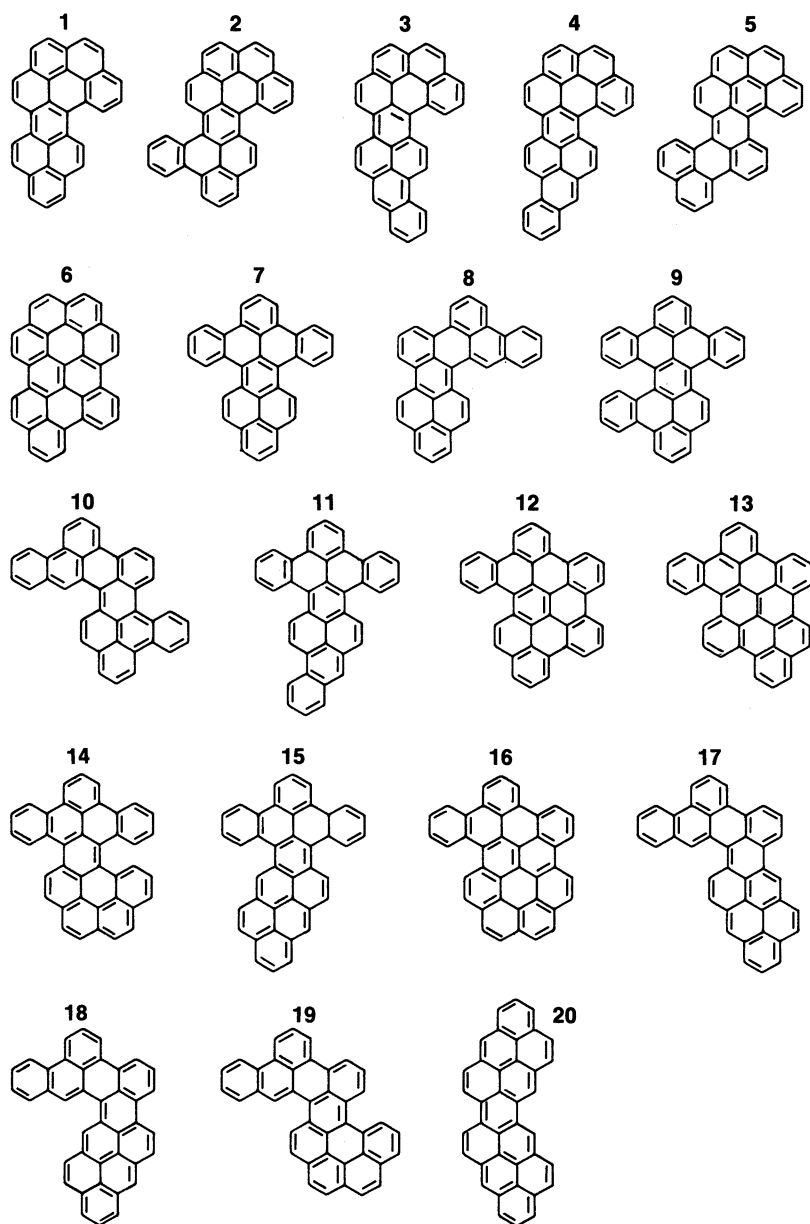


Chart II. Structures of the new PAHs produced (1–20). (The corresponding names are given in the box on page 317.)

**Names of the New Product PAHs (see Chart II)**

1. Benzo[*lm*]phenanthro[4,5,6-*abcd*]perylene
2. Dibenzo[*j,lm*]phenanthro[4,5,6-*abcd*]perylene
3. Dibenzo[*rs,vwx*]naphtho[2,1,8,7-*klmn*]hexaphene
4. Benzo[*rst*]pyreno[3,4,5-*cde*]pentaphene
5. Tribenzo[*jk,qr,uv*]naphtho[2,1,8,7-*defg*]pentacene
6. Benz[2,10]anthra[1,9,8-*abcd*]coronene
7. Tetrabenzo[*a,cd,f,lm*]perylene
8. Benzo[*lm*]phenanthro[1,10-*ab*]perylene
9. Pentabenzo[*a,cd,f,j,lm*]perylene
10. Tribenzo[*fg,ij,m*]naphtho[8,1,2-*opq*]pentaphene
11. Dibenzo[*a,rst*]phenanthro[1,10,9-*cde*]pentaphene
12. Dibenzo[*fg,ij*]benzo[5,8]phenanthro[2,1,10,9,8,7-*pqrstuv*]pentaphene
13. Benzo[*fg,ij*]benz[1,9]anthra[2,3,4,10,5-*qrst*]pentaphene
14. Tribenzo[*j,lm,o*]phenanthro[5,4,3-*abcd*]perylene
15. Benzo[*a*]naphtho[2',1',8',7',6'-*pqrst*]phenanthro[1,10,9-*cde*]pentaphene
16. Benzo[11,12]naphthaceno[4,5,6-*abcd*]coronene
17. Dibenzo[*fg,ij*]anthra[1,9,8,7-*rstu*]hexaphene
18. Benzo[*kl*]dinaphtho[1,2,3-rs:3',2',1',8',7'-*vwxyz*]hexaphene
19. Tribenzo[*fg,ij,mn*]naphtho[2,1,8,7-*rstu*]hexaphene
20. Naphth[7',8',1',2'-*vwxyz*]anthra[2,1,9,8-*klmno*]hexaphene

[*de*]anthracen-7-one and 6*H*-benzo[*de*]pyren-6-one gave five new products and 13 other known ones. The yields for the new PAHs ranged from less than 0.1% each for compounds 4 and 5 to 5% for compound 2. Most of the PAHs were the known compounds (19%). The multiple reactive sites on each ketone, as well as the possibility of asymmetrical products (for example, compounds 2 and 5 or compounds 3 and 4), made that product mixture much more complex.

Structural assignments also relied on spectral comparisons with the known peropyrene PAHs. These comparisons were used mainly to assign specific isomer structures. Structures for compounds 2–5 were assigned from the trends of compounds 22–24, 25–28, and 33–36. The last series was also compared with the previously unknown isomer, compound 20. This 11-ring PAH was also chromatographically compared with compound 36 [synthesized by Clar and Mackay (13) and obtained from W. Schmidt] to prove it was an unknown isomer. Compounds 6, 12, 13, and 16 were compared to other products of further condensation, namely, compounds 31, 32, and 37. The use of spectral comparisons with known structures for identification was possible for most of the PAHs. A small number, such as compounds 6 and 18, were the only possible products in their reactions with a particular molecular weight. Finally, a few were assigned structures by using Clar's theory (4) and Aoki's theory (14), for example, compounds 7 and 8 and compounds 12 and 13. The lower numbered compound in each pair has one

more fully aromatic ring than its isomer. These structures were assigned to the PAH with the lower wavelength absorbance because under both theories these structures have more resonance energy, and thus their electronic transitions are at a lower wavelength.

The chromatographic and spectral characters of the compounds also agreed with the structural assignments. The intramolecular steric strain pres-

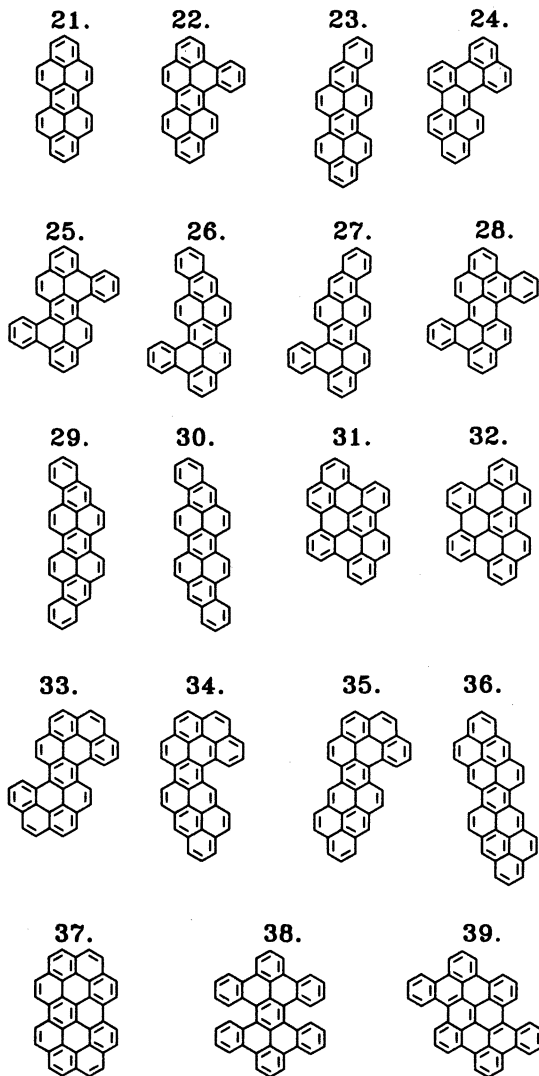


Chart III. Structures of the other (previously known) PAHs produced (21-39). (The corresponding names are given in the box on page 319.)

## Names of the Other PAHs Produced (see Chart III)

21. Dibenzo[*cd,lm*]perylene
22. Tribenzo[*a,cd,lm*]perylene
23. Benzo[*rst*]naphtho[2,1,8-*cde*]pentaphene
24. Phenaleno[1,9-*ab*]perylene
25. Tetrabenzo[*a,cd,j,lm*]perylene
26. Dibenzo[*a,rst*]naphtho[8,1,2-*cde*]pentaphene
27. Benzo[*rst*]phenanthro[1,10,9-*cde*]pentaphene
28. Dibenzo[*j,lm*]naphtho[1,8-*ab*]perylene
29. Benz[*rst*]anthra[9,1,2-*cde*]pentaphene
30. Benzo[*rst*]phenanthro[10,1,2-*cde*]pentaphene
31. Benzo[*cd*]chryseno[4,5,6,7-*ghijk*]perylene
32. Dibenzo[*fg,ij*]phenanthro[2,1,10,9,8,7-*pqrstuv*]pentaphene
33. Dibenzo[*jk,uv*]dinaphtho[2,1,8,7-*defg*:2',1',8',7'-*opqr*]pentacene
34. Benzo[*rs*]dinaphtho[2,1,8,7-*klmn*:3',2',1',8',7'-*uvwxyz*]hexaphene
35. Benzo[*de*]naphth[2,1,7,8-*stuv*]anthra[2,1,9,8-*hijkl*]pentacene
36. Dianthra[1,9,8,7-*cdefg*:1',9',8',7'-*nopqr*]pentacene
37. Naphth[2',1',8',7':4,10]anthra[1,9,8-*abcd*]coronene
38. Hexabenzo[*a,cd,f,j,lm,o*]perylene
39. Tetrabenzo[*gh,jk,tu,wx*]pyranthrene

ent in each PAH can be estimated by its structure. Many significant structural features are seen in the molecules. The most strain occurs in molecules in which a dibenzo[*c,g*]phenanthrene ([5]helicene) substructure is found (Figure 1). The presence of a benzo[*c*]phenanthrene substructure also causes strain, but not as much as the five-ring structure. Even less important are three-sided bay regions such as the one in phenanthrene.

**Chromatographic Retention and Spectral Behaviors.** The series of PAHs starting with dibenzo[*cd,lm*]perylene (compound 21) and having additional rings on the side faces (compounds 7, 9, 22, 25, and 38) have increasing steric strain and nonplanarity. Previously, a term called the *shallowness factor* was defined as the ratio of the average between the two highest absorbance maximums and the intervening minimum (7). If shallowness factors are tabulated with relative retention values and maximum absorbance wavelengths (Table I), then patterns are evident. As the number of rings increases, the shallowness factor approaches 1 (where no valley would exist), and retention decreases. However, the maximum wavelength still increases. This result shows that substantial conjugation occurs even with increased nonplanarity. The shallowness factor for compound 7 comes from its fluorescence excitation because the UV absorbance spectrum showed abnormal band shapes, possibly due to overlapping bands or a change in the conformation of the first excited state. The spectrometry of this unique compound is being further studied.



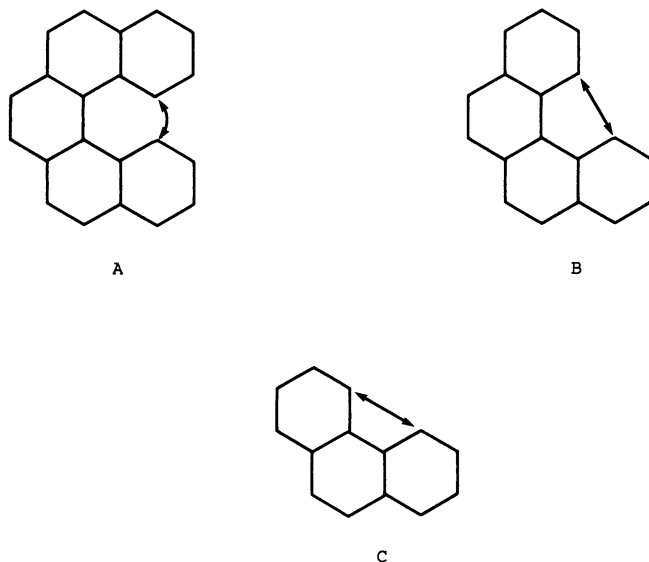


Figure 1. Significant structural features affecting the degree of PAH planarity for A, dibenzo[c,g]phenanthrene; B, benzo[c]phenanthrene; and C, phenanthrene bay regions.

Table I. Shallowness Factors, Relative Retentions, and Maximum Absorbances for Selected Compounds

Compound Number	Shallowness Factor	Relative Retention	Maximum Absorbance (nm)
21	3.92	1.51	443
22	2.17	1.13	445
25	1.35	0.98	448
7	1.31 <sup>a</sup>	0.94	446
9	1.15	0.88	451
38	1.07	0.82	466

<sup>a</sup>Value is from fluorescence excitation spectrum.

The shape and size of the aromatic halves of a peropyrene-type PAH also affect planarity. The larger peropyrenes, especially those made by using 6*H*-benzo[*de*]pyren-6-one, show more planarity than would be expected if only steric effects were considered.

Those PAHs made from 6*H*-benzo[*de*]pyren-6-one should have similar steric strain as ones resulting from 7*H*-benz[*de*]anthracen-7-one. However, they do not have the same chromatography. For example, benzo[*lm*]phenanthro[4,5,6-*abcd*]perylene (compound 1) elutes much later than the similar tribenzo[*a,cd,lm*]perylene (compound 22). Compound 1, a nine-

ring compound, is in the class of PAHs that change planarity with solvent composition. Compound **22**, an eight-ring compound, always eluted as if it were nonplanar (Figure 2). The amount of intramolecular steric strain should not be affected by where the additional ring is. Thus, the retention difference may be due to higher planarity. Possibly, the larger aromatic region resulting from 6*H*-benzo[*de*]pyren-6-one in the nine-ring PAH has more resonance than the corresponding part resulting from 7*H*-benz[*de*]anthracen-7-one in the eight-ring compound. Also, the nine-ring structure may have more rigidity and thereby prevent certain nonplanar motions.

Another indication that resonance might increase planarity is seen in Figure 3. Absorbance spectra for three similar PAHs are shown. The top spectrum is of tetrabenzo[*a,cd,j,lm*]perylene (compound **25**), which results from the condensation of 7*H*-benz[*de*]anthracen-7-one with itself. The bottom spectrum is of dibenzo[*jk,uv*]dinaphtho-2,1,8,7-*defg:2',1',8',7'-opqr*]pentacene (compound **33**), which results from 6*H*-benzo[*de*]pyren-6-one condensation. The middle spectrum is of an isomer resulting from the condensation of 7*H*-benz[*de*]anthracen-7-one with 6*H*-benzo[*de*]pyren-6-one (compound **2**). Although the three spectra are remarkably similar in band

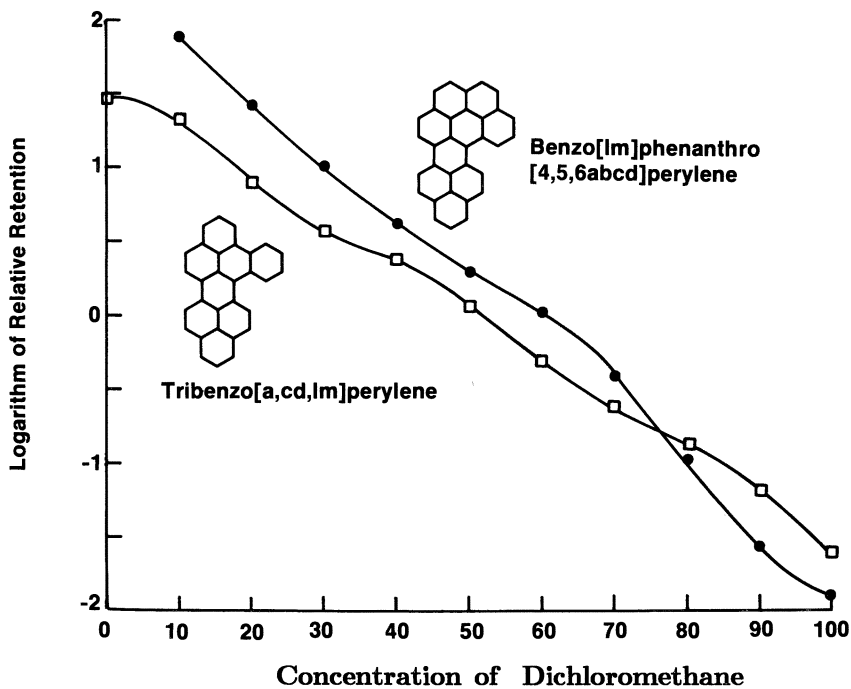


Figure 2. Elution behavior of two similar structures: benzo[*lm*]phenanthro[4,5,6-*abc*]perylene and tribenzo[*a,cd,lm*]perylene.

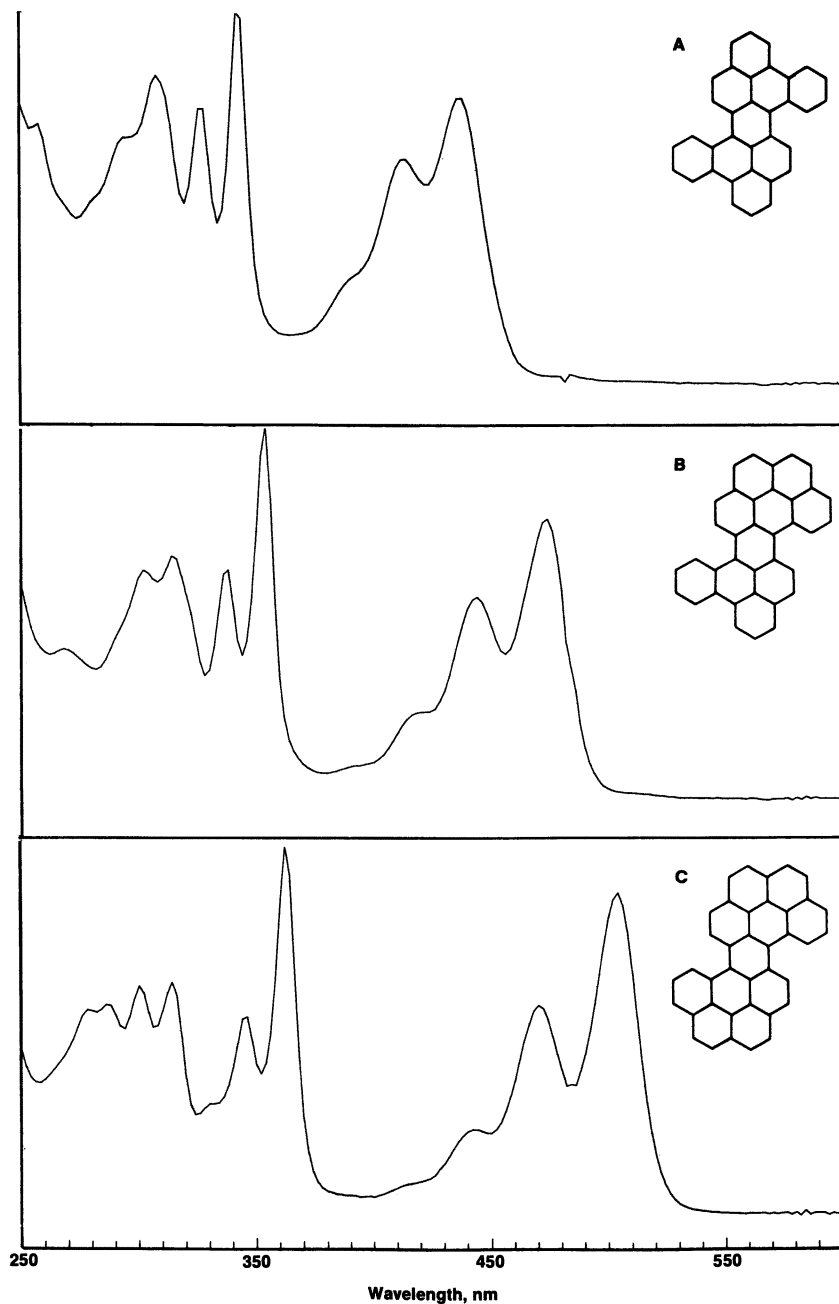


Figure 3. Absorbance spectra for the three major products of the condensation of 7H-benz[de]anthracen-7-one and 6H-benzo[de]pyren-6-one showing the increasingly deeper valleys between absorbance maximums. A: compound 25, B: compound 2, and C: compound 33.

patterns (discounting the expected bathochromic shifts from the larger ring number of compounds **2** and **33**), the shallowness of the absorbance minimums changes. The larger PAHs have deeper valleys, which indicate more planarity. Their retention also suggests they are more planar. The elution order was always the nine-ring compound first, then the 10-ring PAH, and finally the 11-ring PAH. The 10- and 11-ring compounds eluted close to the times expected of planar PAHs with the same ring numbers.

In contrast, the three predominant products in the condensation of 1-phenalenone and 6*H*-benzo[*de*]pyren-6-one are indicators of the behavior more commonly seen for the new large peropyrenes. The three products are the seven-ring compound **21**, the nine-ring compound **1**, and the 11-ring compound **33**. Figure 4 shows their reverse-phase chromatograms (with mobile phases of 40% and 85% dichloromethane in methanol). The elution order at the lower dichloromethane concentration is what would normally be expected: 7, 9, then 11 rings. An elution-order reversal occurs with more dichloromethane: The 11-ring PAH elutes first, and the seven-ring PAH elutes last. Proton and <sup>13</sup>C NMR spectra of the various compounds in weak solvents (such as *n*-hexane or methanol) and in dichloromethane show drastic differences in the carbon-hydrogen skeleton of the molecules. Hyperfine splitting indicates more interaction between protons in the dichloromethane spectra; this situation supports the postulated changes in planarity (15).

A retention-order reversal would not occur if all three molecules underwent the same interactions with the mobile and stationary phases. Different separation mechanisms must occur in each of the two chromatograms. The dichloromethane interacts differently with each PAH, as shown by different slopes in a plot of the logarithms of relative retention versus dichloromethane concentration (Figure 5). If the molecules had the same retention mechanisms, these plots would be parallel lines. The three plots are nonparallel, and only the one for dibenzo[*cd,lm*]perylene is linear. The curvature in the other two plots could indicate different interactions in each at low or high dichloromethane concentrations. This behavior could be due to the stronger solvent having increased interaction with the PAHs so that the two larger PAHs become more nonplanar.

An additional indication that planarity controls retention behavior is the behavior of the products after further condensation (compounds **8**, **31**, **32**, and **37**). These PAHs are not as sterically strained and not as likely to become nonplanar in strong solvent mixtures (because of their additional bonds) as the less condensed PAHs. Their retention times are much longer than the other reaction products. They are similar to ovalene and other large planar PAHs requiring very high dichloromethane concentrations for elution. The UV spectra of these highly condensed PAHs also did not show the shallow minimums or the changes in band shape seen for the sterically strained PAHs. Spectra for all of the new PAHs are shown in Figures 6–15.

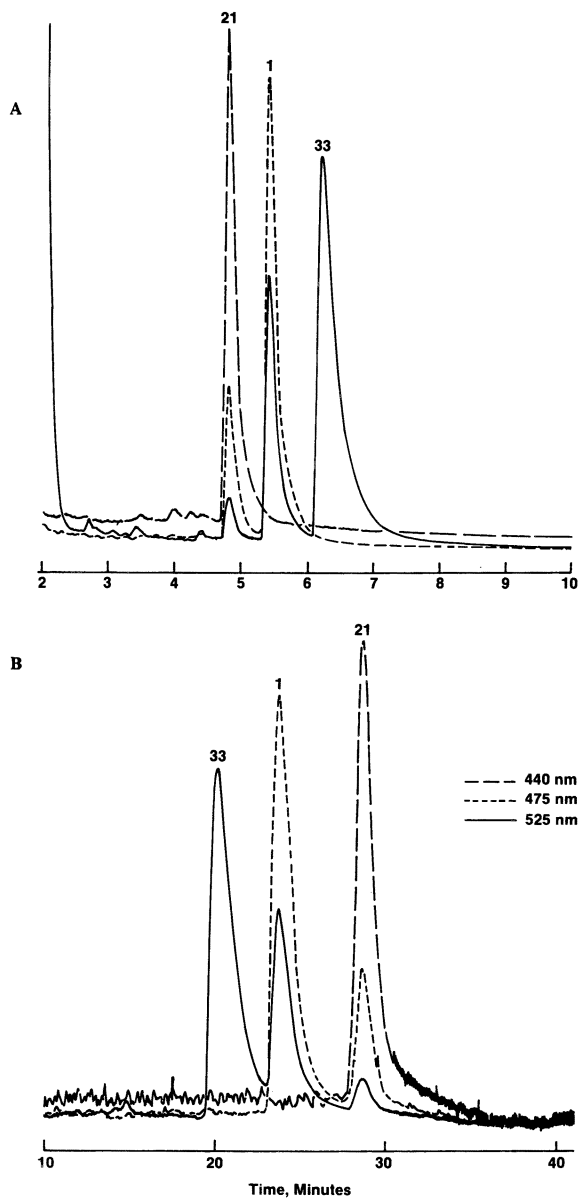


Figure 4. Reverse-phase chromatograms of the products of the condensation of 1-phenalenone and 6H-benzo[de]pyren-6-one (compounds 1, 21, and 33). A: 40% dichloromethane in methanol mobile phase, and B: 65% dichloromethane in methanol.

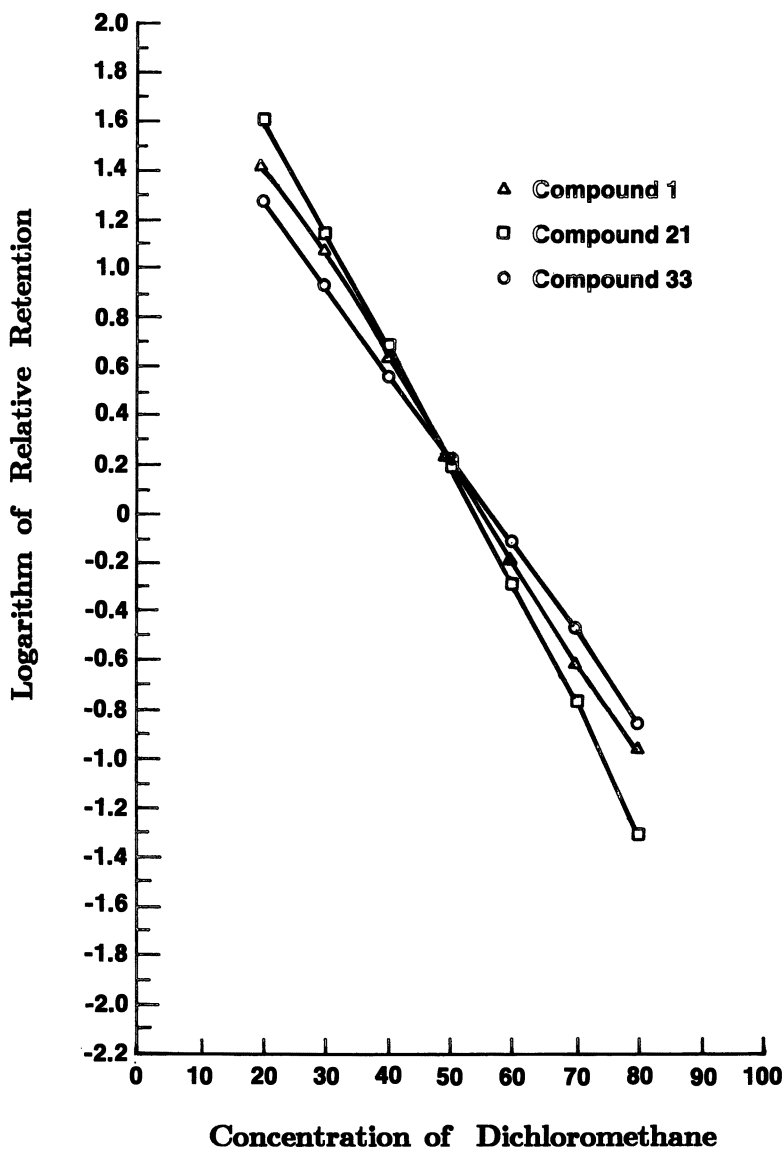


Figure 5. Plot of the logarithms of the relative retention values versus dichloromethane concentrations (%) for compounds 1, 21, and 33.

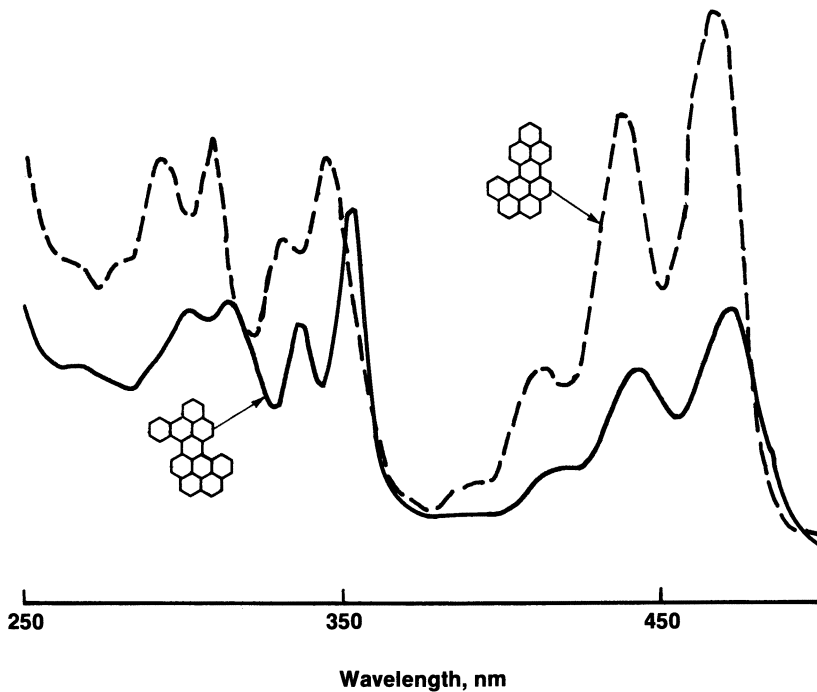


Figure 6. UV-visible absorbance spectra of compound 1 (broken line) and compound 2 (solid line).

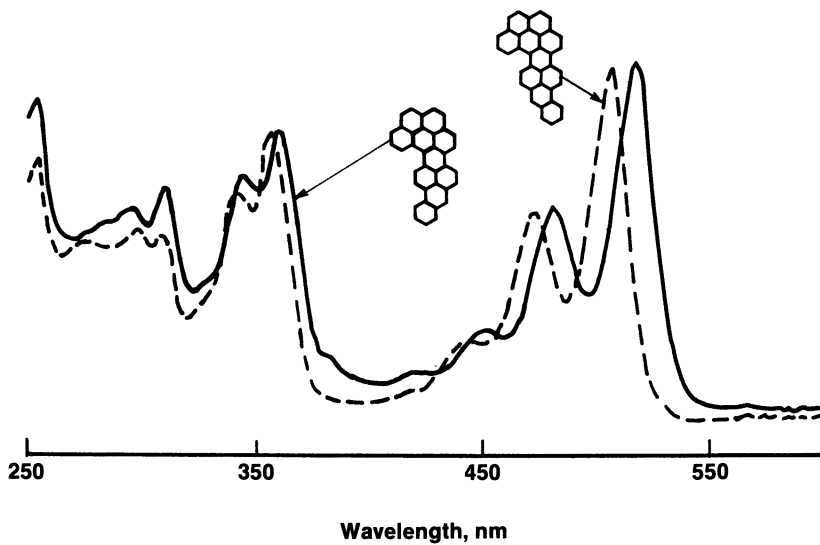


Figure 7. UV-visible absorbance spectra of compound 3 (solid line) and compound 4 (broken line).

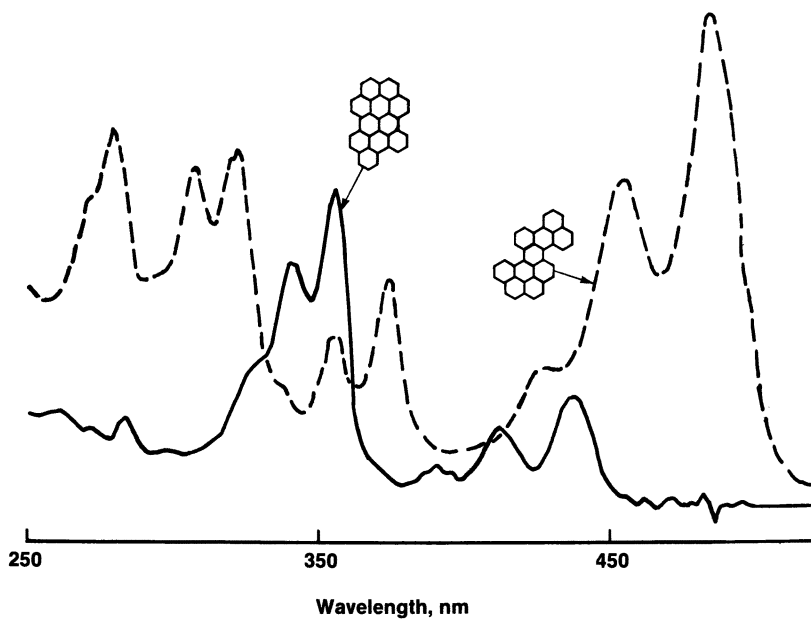


Figure 8. UV-visible absorbance spectra of compound 5 (broken line) and compound 6 (solid line).

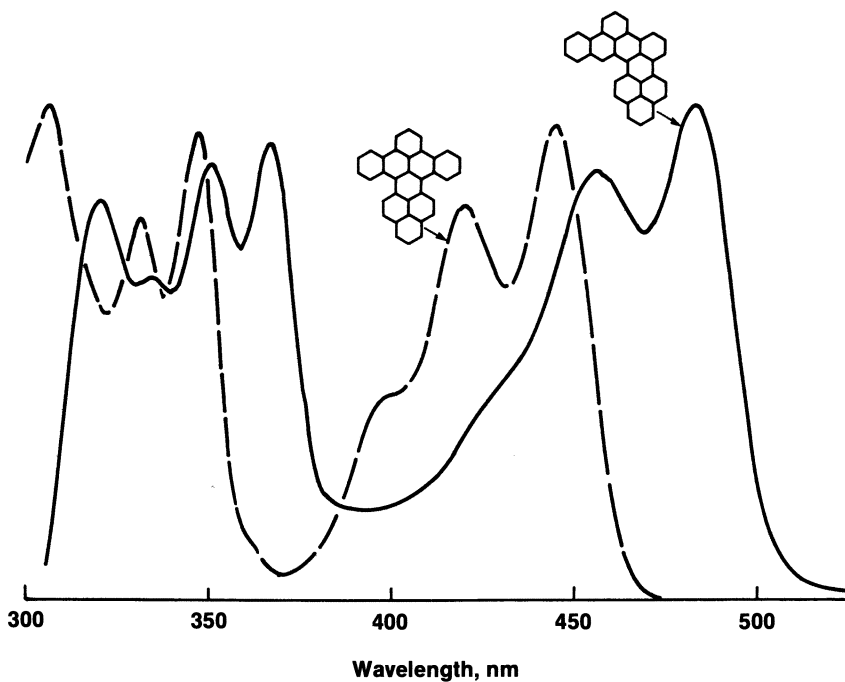


Figure 9. UV-visible absorbance spectra of compound 7 (broken line) and compound 8 (solid line).



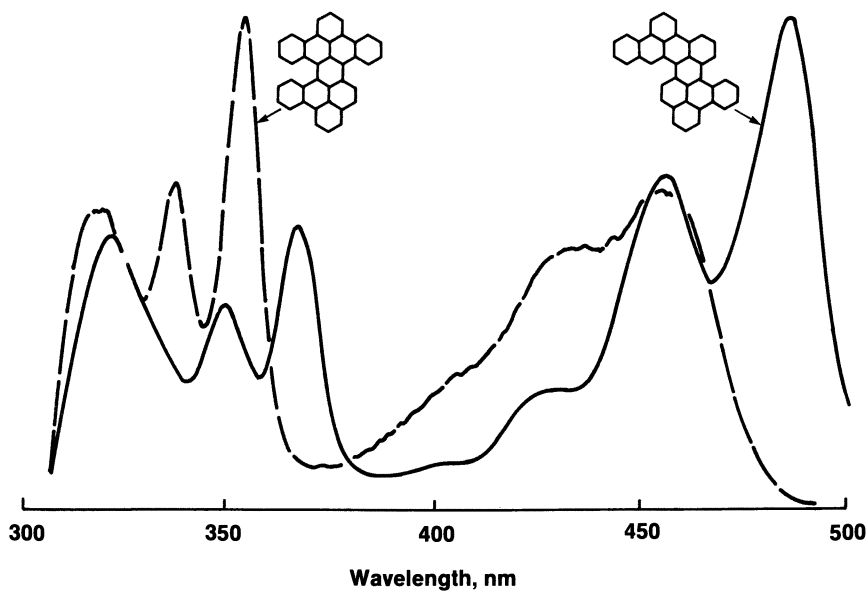


Figure 10. UV-visible absorbance spectra of compound 9 (broken line) and compound 10 (solid line).

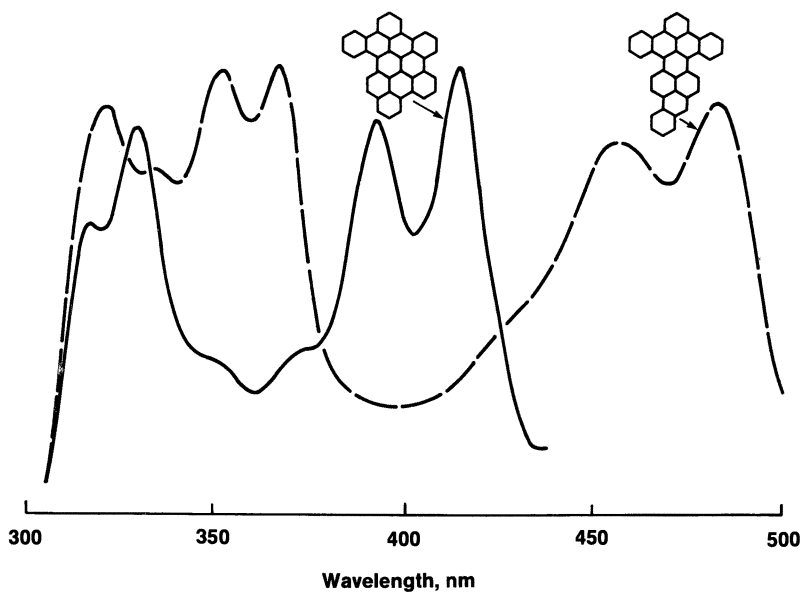


Figure 11. UV-visible absorbance spectra of compound 11 (broken line) and compound 12 (solid line).

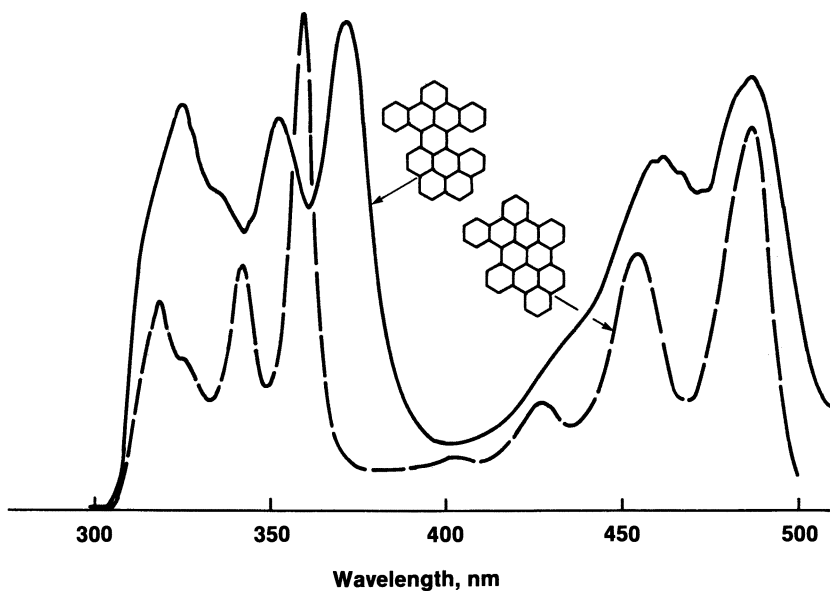


Figure 12. UV-visible absorbance spectra of compound 13 (broken line) and compound 14 (solid line).

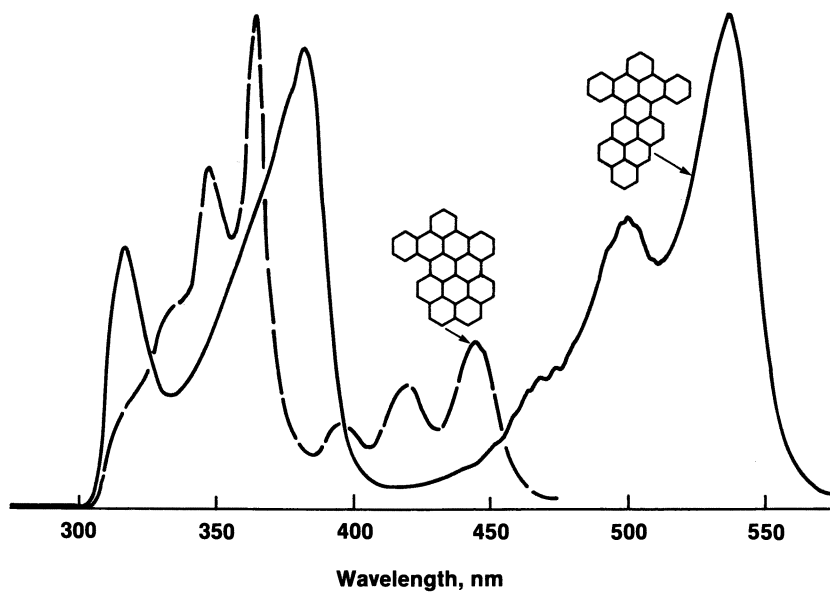


Figure 13. UV-visible absorbance spectra of compound 15 (solid line) and compound 16 (broken line).

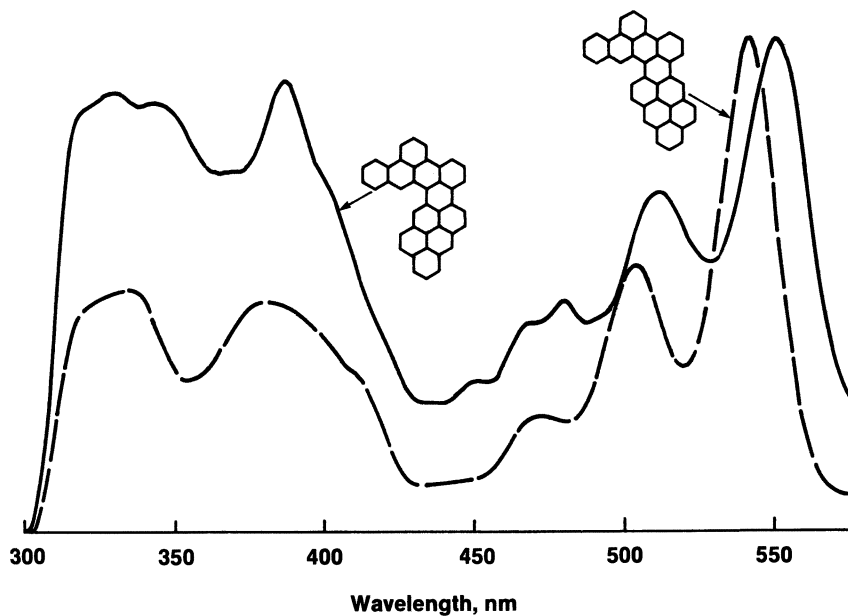


Figure 14. UV-visible absorbance spectra of compound 17 (broken line) and compound 18 (solid line).

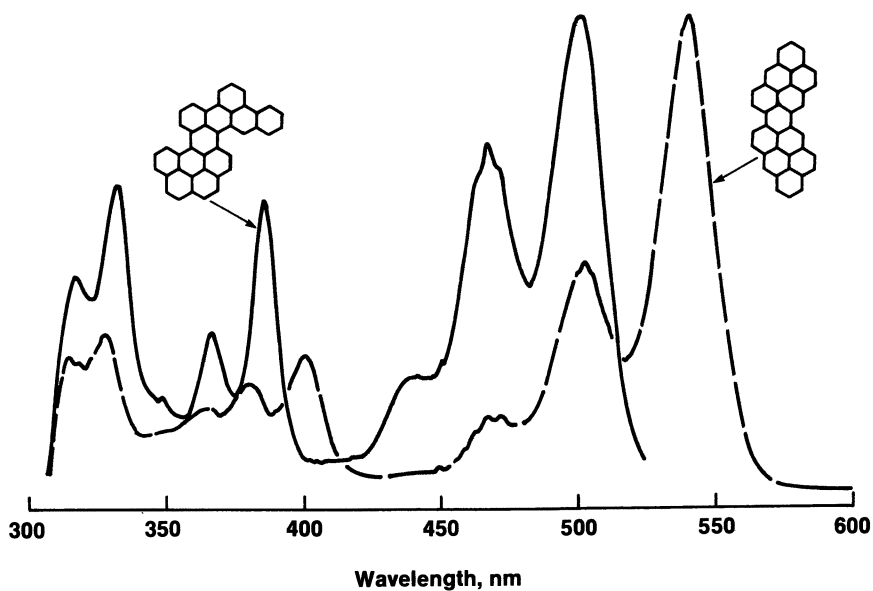


Figure 15. UV-visible absorbance spectra of compound 19 (solid line) and compound 20 (broken line).

**Separation by Shape.** Polymeric octadecyl bonded phases are able to separate PAHs because of the different three-dimensional shapes of the various isomers. Wise and Sander (16) have suggested a "slot" model in which the planar PAHs can diffuse into spaces in the octadecyl phase that similar nonplanar PAHs cannot enter. Solid-phase proton and  $^{13}\text{C}$  NMR studies of the octadecyl bonded-phase packing used in this work showed that this mechanism is likely (17). The bonded octadecyl moieties in this packing are very disordered and not very free to move when the packing is slurried with methanol. However, in dichloromethane, the bonded octadecyl moieties are in a similar environment as those seen in the spectrum of dilute octadecane in solution. The more orderly phase is able to accomplish the separation by shape because planarity affects the permeation of the bonded phase by the PAHs, and their effective areas then are able to interact with the bonded phase. The synthesis of the polymeric octadecyl coverage in the packing probably results in sheets of bonded organic material formed of methyloctadecylsiloxane chains (18, 19), that is, the slotted phase of Wise and Sander (16). Similar operations for small PAHs have been obtained by gas chromatography using liquid-crystal stationary phases.

The great power of this column to separate isomeric PAHs and the use of a photodiode array detector to gather peak spectra make it possible to find previously unseen compounds in reaction mixtures that have been thoroughly investigated by conventional methods (4). This situation has been shown in this set of new PAHs by detection of the newly found isomer (compound 20) in the product mixture from 6*H*-benzo[*de*]pyren-6-one condensation. The potential to separate and identify new PAHs could be used to identify many other new compounds in other product mixtures.

The degrees of planarity of the peropyrene-type PAHs appear to be determined by the balance between the loss in resonance energy when the molecules become nonplanar and the increases in energy due to decreased intramolecular steric strain and stronger solvation. The degree of planarity and the relative importance of these factors for each PAH structure can be estimated from the analytical behavior of that PAH. Conversely, these molecules can serve as excellent probes of the mechanisms of HPLC.

### **Acknowledgments**

I thank C. E. Rechsteiner for the field-ionization mass spectra of the new PAHs and P. Shah and L. B. Rogers (Department of Chemistry, University of Georgia, Athens, GA) for the NMR data on the octadecyl bonded-phase (Vydac) packing. I also thank Chevron Research Company for permission to publish this work.

## References

1. Lee, M. L.; Novotny, M. V.; and Bartle, K. D. *Analytical Chemistry of Polycyclic Aromatic Compounds*; Academic: New York, 1981, Chapter 2.
2. *Ibid.*, p 441.
3. Paeden, P. A.; Lee, M. L.; Hirata, Y.; and Novotny, M. *Anal. Chem.* **1980**, *52*, 2268.
4. Clar, E., *The Aromatic Sextet*; Wiley: New York, New York, 1972.
5. Fetzer, J. C.; Biggs, W. R. *J. Chromatogr.* **1984**, *295*, 161.
6. Fetzer, J. C.; Biggs, W. R. *J. Chromatogr.* **1985**, *322*, 275.
7. Fetzer, J. C.; Biggs, W. R. *J. Chromatogr.* **1985**, *348*, 81.
8. Boschi, K.; Clar, E.; Schmidt, W. *J. Chem. Phys.* **1974**, *60*, 4407
9. Fetzer, J. C.; Biggs, W. R. *J. Chromatogr.* **1987**, *388*, 87.
10. Clar, E.; Fell, G. S.; Ironside, C. T.; Balsillie, A. *Tetrahedron* **1980**, *10*, 28.
11. Halieux, A.; King, R. H.; King, G. S. D. *Helv. Chim. Acta* **1959**, *41*, 1177.
12. Fujisawa, S.; Aoki, J.; Takekawa, M.; Iwashima, S. *Bull. Chem. Soc. Jpn.* **1979**, *52*, 2159.
13. Clar, E.; Mackay, C. C. *Tetrahedron* **1972**, *28*, 8041.
14. Aoki, A. *Senyō to Yakuhia* (Dyes and Pharmaceuticals), Published by the Japanese Society for Chemical Products **1984**, *29*, 232.
15. Young, D. C.; Fetzer, J. C., unpublished results.
16. Wise, S. A.; Sander, L. C. *J. High Resolu. Chromatogr. Chromatogr. Commun.* **1985**, *8*, 248.
17. Shah, P., Rogers, L. B.; Fetzer, J. C. *J. Chromatogr.* in press; for the Experimental Procedures, see McNalley, M. E.; Rogers, L. B. *J. Chromatogr.* **1985**, *331*, 23.
18. Yates, T. Separations Group, Hesperia, California, personal communication.
19. Sander, L. C.; Wise, S. A. *Anal. Chem.* **1984**, *56*, 504.

RECEIVED for review September 29, 1986. ACCEPTED February 27, 1987.

# Electronic Interactions Between Polycyclic Arenes in Cyclophanes

Matthias W. Haenel<sup>1</sup> and Dieter Schweitzer<sup>2</sup>

<sup>1</sup>Max-Planck-Institut für Kohlenforschung, Kaiser-Wilhelm-Platz 1, D-4330 Mülheim a. d. Ruhr, Federal Republic of Germany

<sup>2</sup>Max-Planck-Institut für medizinische Forschung, Jahnstrasse 29, D-6900 Heidelberg, Federal Republic of Germany

*The  $\pi$ - $\pi$  interaction between polycyclic arenes and the effects of orientation were studied in [2.2]-, [3.3]-, and [3.2]naphthalenophanes, [2]naphthaleno[2]paracyclophanes, and syn- and anti-[2.2](2,7)fluorenophane by electron absorption and emission spectroscopy as well as by optically detected magnetic resonance (ODMR) of the excited triplet state. The  $\pi$ - $\pi$  interaction in the excited singlet and triplet state was found to be highest if a maximal number of six-membered rings of the interacting arenes in a parallel orientation are completely eclipsed. Similarly, the  $n$ - $\pi$  interaction between the nonbonding nitrogen electron pair and the aromatic  $\pi$  electrons was investigated in isomeric etheno-bridged naphthalenopyridinophanes and an anthracenopyridinophane; in these pyridinophanes, the pyridine rings are fixed perpendicularly above different sites of the naphthalene and anthracene units, respectively.*

**T**HE CHARACTERISTIC FEATURE OF BENZENE AND POLYCYCLIC ARENES is the  $\pi$ -electron system. The overlapping  $2p_z$  orbitals on each  $sp^2$ -hybridized carbon center generate an electron cloud over and under a planar hydrocarbon skeleton. This electronic structure favors intermolecular interactions between arenes in a face-to-face geometry (Figure 1). In an electronically

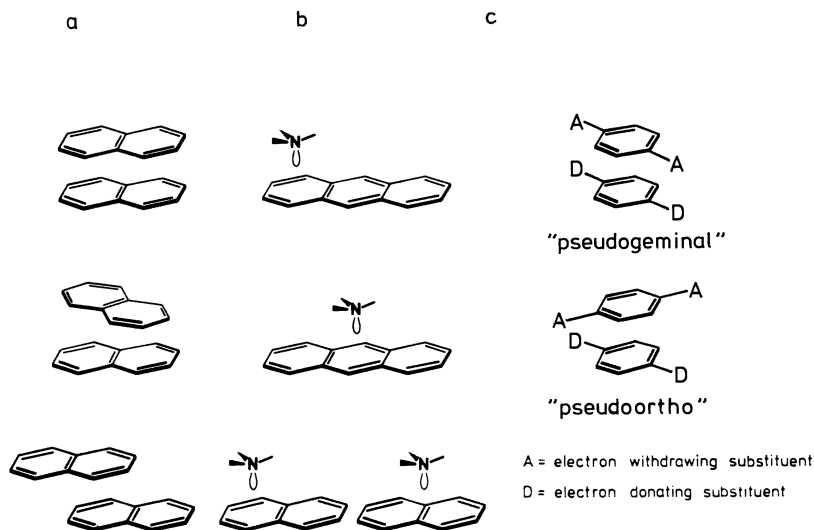


Figure 2. Effect of orientation on the electronic interactions of arene excimers (a), amine-arene exciplexes (b), and charge-transfer complexes (c).

over the central naphthalene  $\pi$  bond. Orientation is also important in charge-transfer complexes (Figure 2c). For the complex, which consists of donor and acceptor substituted benzene derivatives, the "pseudogeminal" and "pseudoortho" orientations can be distinguished (13). To investigate these orientational dependencies, we and other groups have synthesized cyclophanes (14, 15) in which two aromatic units are immovably arranged by rigid carbon skeletons in different face-to-face orientations. In this chapter, the  $\pi$ - $\pi$  electron interaction between polycyclic arenes and the effects of orientation are discussed for [2.2]-, [3.3]-, and [3.2]naphthalenophanes (1-12), isomeric [2]naphthaleno[2]paracyclophanes (13-15), and *syn*- and *anti*-[2.2](2,7)fluorenophane (17 and 18) (see Chart I).

Similar model compounds of amine-arene exciplexes require rigid skeletons linking an amine nitrogen and a polycyclic arene in such a manner that the nonbonding nitrogen electron pair is pointing toward the opposite aromatic  $\pi$ -electron system (Figures 1 and 2). However, the nitrogen inversion makes it difficult to locate the electron pair of aliphatic amines. An alternative is the perpendicular orientation of an aromatic nitrogen heterocycle, such as pyridine, which can interact with an opposite polycyclic arene only through its nitrogen electron pair and not through its  $\pi$  electrons. These geometric requirements are fulfilled by [2](2,6)pyridino[2]paracyclophan-1,9-diene (19), which together with the saturated compound (20) has been described by Boekelheide and co-workers (16-18). According to dynamic  $^1\text{H}$  NMR spectroscopy, the pyridine ring in 20 is flipping between the two

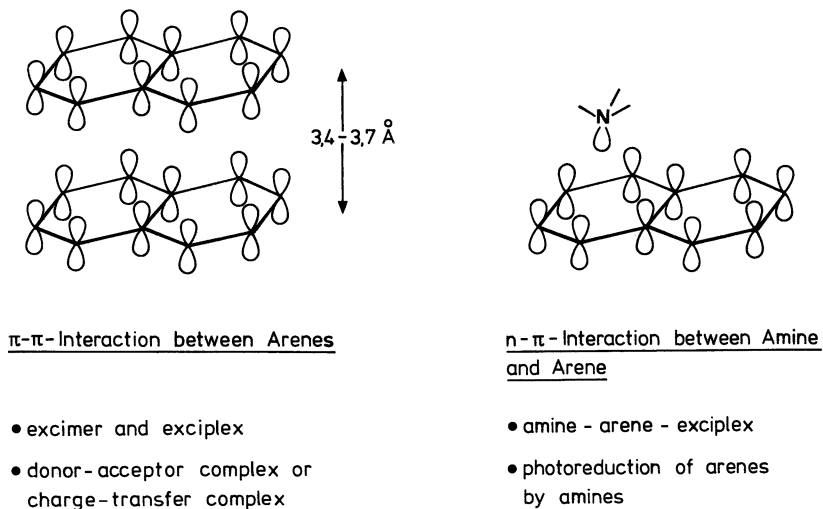


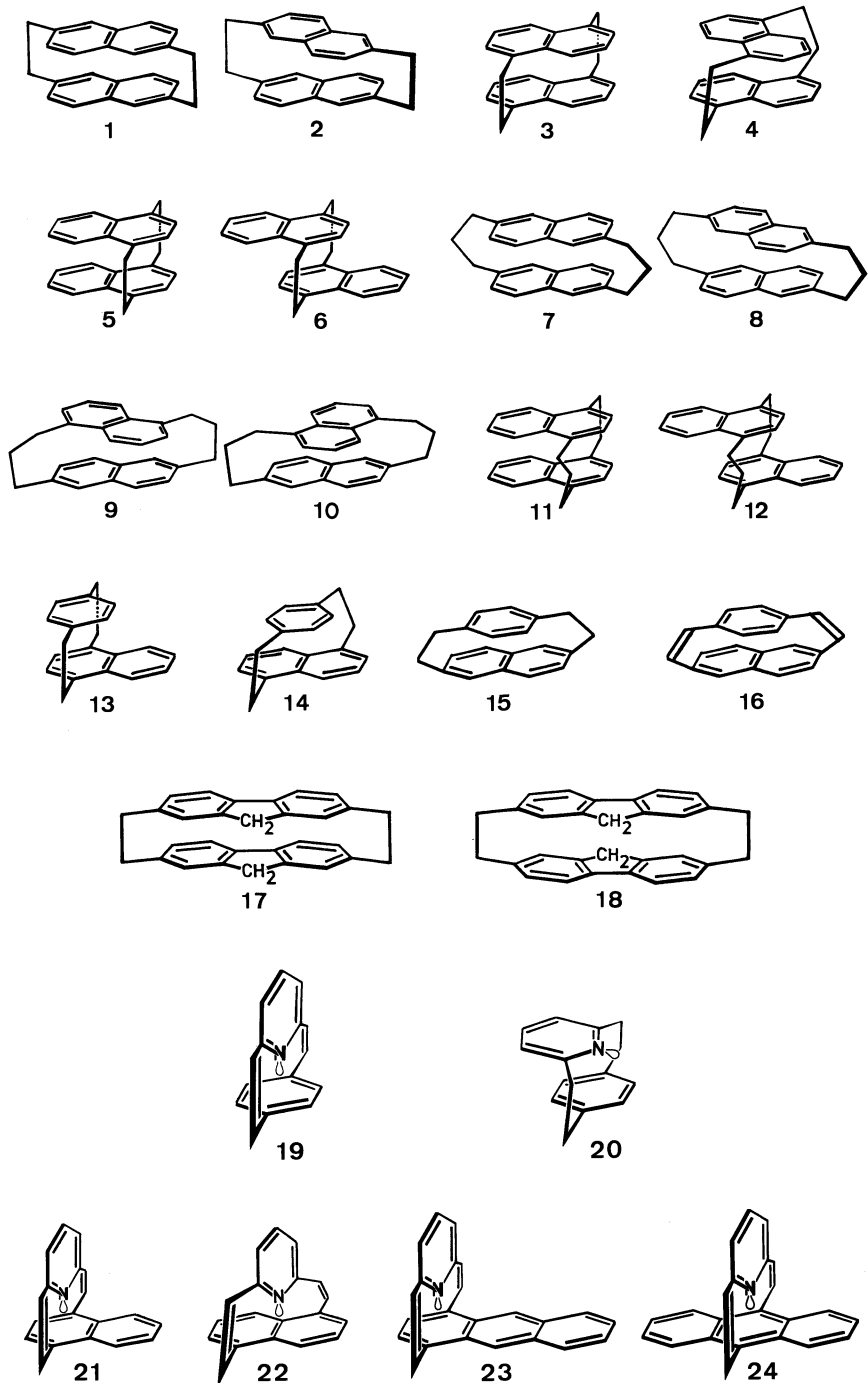
Figure 1. Electronic interactions of arenes.

excited state, the binding  $\pi$ - $\pi$  interaction leads to the formation of excited dimers or complexes, which are called excimers or exciplexes, respectively (1-4). The electronic ground state usually is attractive only if some charge transfer is induced between electron-donor and electron-acceptor systems (5). A similar  $n$ - $\pi$  interaction between a nonbonding nitrogen electron pair and aromatic  $\pi$  electrons is involved in the formation of amine-arene exciplexes (6-8) and in the photoreduction of arenes by amines (9, 10).

The classic example for the  $\pi$ - $\pi$  electron interaction between polycyclic arenes is the pyrene excimer (11). Upon UV excitation of a  $10^{-5}$  M pyrene solution, the structured fluorescence of monomeric pyrene molecules is mainly observed. The increase of the concentration to  $10^{-3}$  M diminishes the monomeric fluorescence, and a new broad and completely structureless excimer band appears, which is red-shifted by  $5000-6000 \text{ cm}^{-1}$ . This phenomenon can be explained through potential curves of the electronic ground state and the excited singlet state (1, 12). The spectroscopic shift between the fluorescence of the excimer and the monomer depends on the depth of the potential well in the excited state; that is, the red shift is proportional to the binding energy of the excimer.

Figure 2 raises the question of how the electronic interaction depends on the orientation. For instance, three different orientations are shown for the naphthalene excimer (Figure 2a). In the amine-anthracene exciplex (Figure 2b), the nitrogen can be located over one of the outer six-membered rings or over the inner six-membered ring of anthracene. At the bottom of Figure 2b, an orientation is shown in which the nitrogen is located directly



*Chart I. Cyclophanes*

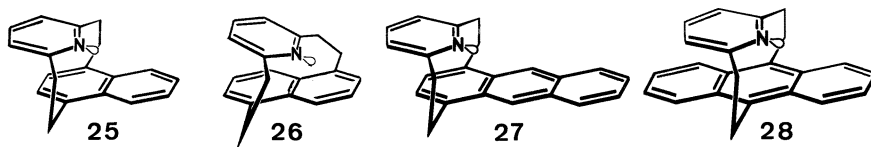
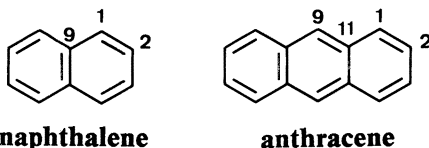


Chart I. Continued.

identical conformations in which the aromatic units have more or less parallel orientations (16, 18). However, for the diene (19), the rectangular geometry between pyridine and benzene was found in the crystalline state (17), which apparently is also the conformation present in solution (16, 18). Therefore, the etheno-bridged naphthaleno- and anthracenopyridinophane systems (21–24) were selected as model compounds of amine–arene exciplexes. The pairs of isomers 21 and 22 and 23 and 24 differ in that the nitrogen lone pair is interacting with different sites of the naphthalene or anthracene  $\pi$ -electron system. Orientational effects should be detectable in their spectroscopic properties. The corresponding ethano-bridged cyclophanes (25–28) are expected to have more parallel aromatic units. If both series of cyclophanes are compared spectroscopically,  $n$ - $\pi$  and  $\pi$ - $\pi$  electron interactions might become distinguishable.



### Experimental Details

The following cyclophanes were synthesized as described in the literature: achiral and chiral [2.2](2,6)naphthalenophane (1 and 2, respectively; 19, 20); achiral and chiral [2.2](1,5)naphthalenophane (3 and 4, respectively; 21); *syn*- and *anti*-[2.2](1,4)naphthalenophane (5 and 6, respectively; 22, 23); achiral and chiral [3.3](2,6)naphthalenophane (7 and 8, respectively; 24); [3.3](1,5)(2,6)naphthalenophanes (9 and 10, respectively; 24); *syn*- and *anti*-[3.2](1,4)naphthalenophane (11 and 12, respectively; 25); isomeric [2](1,4)-, [2](1,5)-, and [2](2,6)naphthaleno[2]paracyclophane (13, 14, and 15, respectively; 26); *syn*- and *anti*-[2.2](2,7)fluorenophane (17 and 18, respectively; 27); isomeric [2](1,4)- and [2](1,5)naphthaleno[2](2,6)pyridinophane-1,11-diene (21 and 22, respectively; 28, 29); isomeric [2](1,4)- and [2](1,5)naphthaleno[2](2,6)pyridinophane (25 and 26, respectively; 28, 29); [2](1,4)anthraceno[2](2,6)pyridinophane-1,13-diene (23; 30); and [2](1,4)anthraceno[2](2,6)pyridinophane (27; 30).

UV spectra were obtained with a Varian spectrometer (Cary 15 and 17). Fluorescence, phosphorescence spectra, and the zero-field splitting parameters  $D$  and  $E$  of the triplet state were determined at 1.3K with an apparatus (31) for optical detection of magnetic resonance (ODMR) which was similar to the one described by Zuclich et al. (32).

## Results and Discussion

**[2.2]-, [3.3]-, and [3.2]Naphthalenophanes.** In the series of the [2.2]-, [3.3]-, and [3.2]naphthalenophanes (1–12), each structure type formed a pair of two stereoisomers (*syn*- and *anti*-isomers or diastereomers): The naphthalenophanes, linked at the naphthalene 1,4-positions by two ethano bridges or one ethano and one propano bridge, were obtained as *syn*-isomers 5 and 11 and *anti*-isomers 6 and 12 (23, 25). The naphthalene units overlap in 5 and 11 with both six-membered rings and in 6 and 12 with only one six-membered ring. Two ethano or two propano bridges at the naphthalene 2,6- or 1,5-positions generated the achiral isomers 1, 3, and 7, in which the naphthalene units are completely eclipsed, and the chiral isomers 2, 4, and 8, in which the naphthalene units are crossed by about 40° (19–21, 24). Especially interesting are the [3.3](1,5)(2,6)naphthalenophanes (9 and 10), which contain one 1,5- and one 2,6-bridged naphthalene unit: Two diastereomers are formed (24) in which the naphthalene units are slightly and strongly crossed (crossing angles are about 40° in 9 and about 80° in 10). In *syn*- and *anti*-[3.2](1,4)naphthalenophane (11 and 12), the planes of the naphthalene units are inclined to each other by about 15° because the two bridges have different lengths.

Figure 3 shows the result of the X-ray structural analysis (33) of the

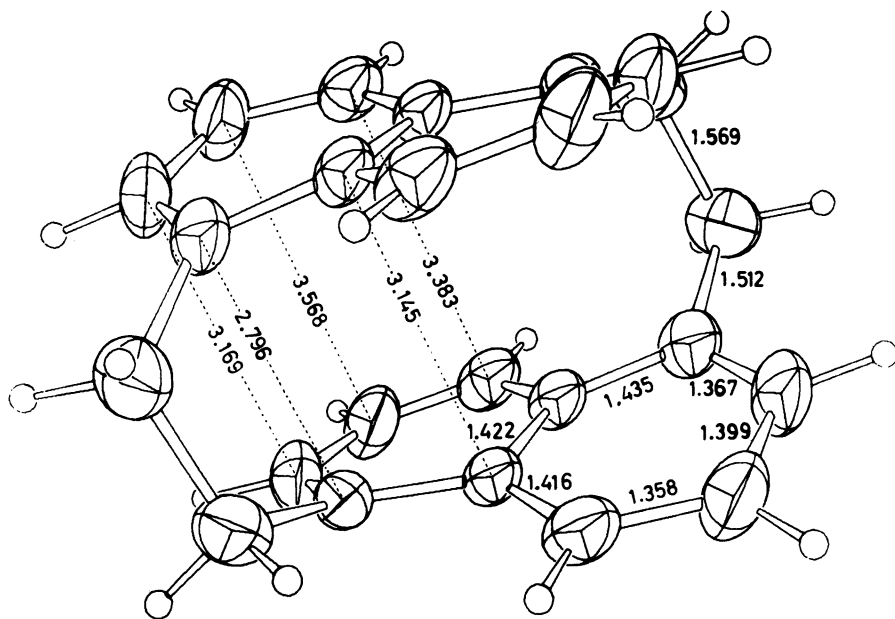


Figure 3. Molecular structure (33) of the achiral [2.2](1,5)naphthalenophane (3).

achiral [2.2](1,5)naphthalenophane (**3**). The naphthalene units are considerably deformed. The transannular distance varies from 2.8 Å between the bridged naphthalene carbons in the 1,5-positions up to 3.6 Å between the naphthalene carbons in the 3,7-positions. Certainly some contribution of the deformation on the electronic absorption and emission spectra have to be considered which cannot be separated easily from the pure electronic effects. In this regard, the less strained [3.3]naphthalenophanes are presumably the better models.

Compared with the monomeric dimethylnaphthalenes, the electronic absorption spectra of the naphthalenophanes exhibit bathochromic shifts together with the appearance of new bands and the loss of vibronic structure (19–25). As an example, Figure 4 shows the UV absorption spectra of **1**, **2**,

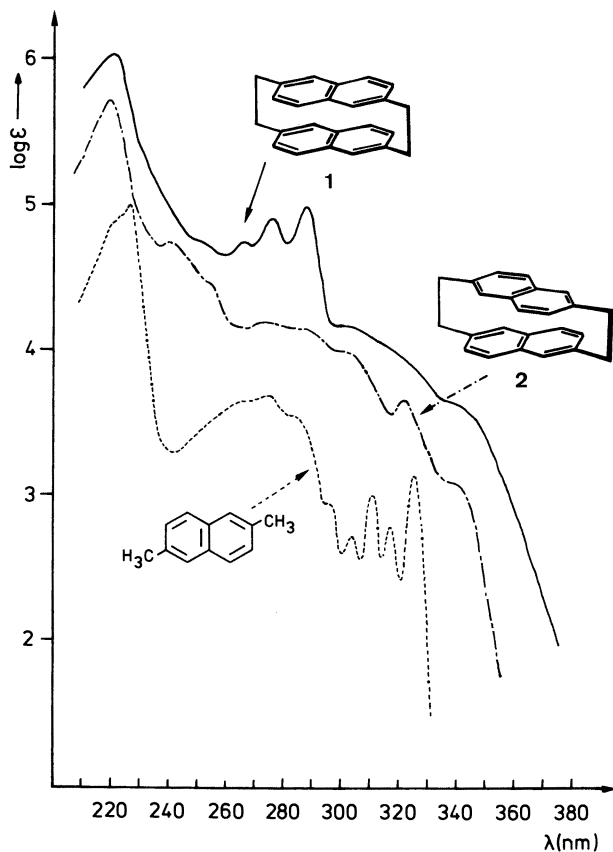


Figure 4a. UV absorption spectra of **1**, **2**, and 2,6-dimethylnaphthalene in cyclohexane. The spectrum of **1** is shifted by 0.5 ordinate unit, and that of **2** is shifted by 1 ordinate unit. (Reproduced with permission from reference 20. Copyright 1983 VCH Verlagsgesellschaft)

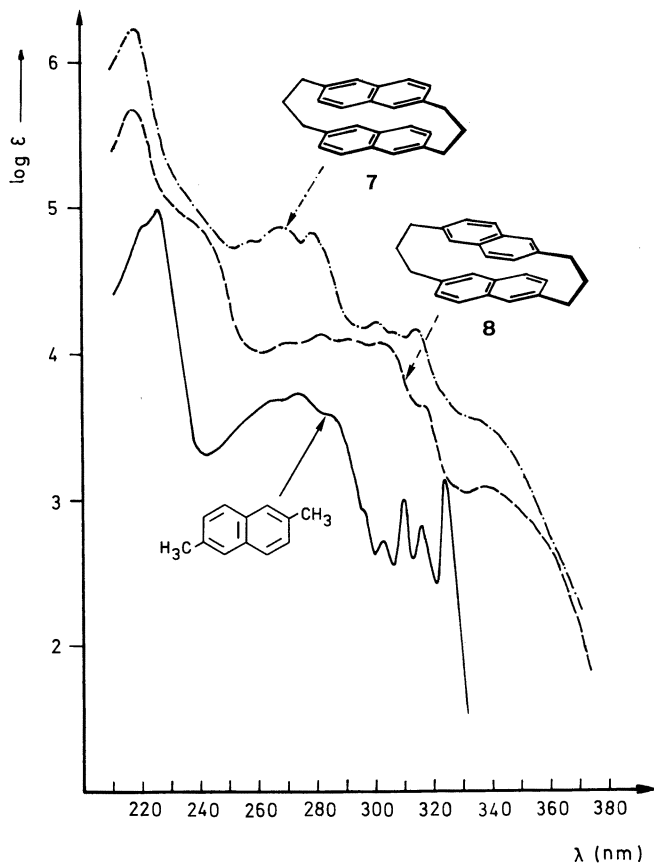


Figure 4b. UV absorption spectra of 7, 8, and 2,6-dimethylnaphthalene in cyclohexane. The spectrum of 7 is shifted by 0.5 ordinate unit, and that of 8 is shifted by 1 ordinate unit. (Reproduced with permission from reference 24. Copyright 1981 VCH Verlagsgesellschaft)

7, 8, and 2,6-dimethylnaphthalene (19, 20, 24). In the case of the [2.2](2,6)naphthalenophanes, the achiral isomer 1 exhibits a stronger bathochromic shift and hence a stronger  $\pi$ - $\pi$  electronic interaction than the chiral isomer 2, which has crossed naphthalene units. However, in the case of the [3.3](2,6)naphthalenophanes, this differentiation is not so clear, even though the spectra of 7 and 8 resemble those of 1 and 2.

In the emission spectra (31, 34, 35), the orientational effects are differentiated much more clearly (Figure 5). At 1.3 K, monomeric 2,6-dimethylnaphthalene emits a sharply structured fluorescence from the excited singlet state  $S_1$ ; however, only structureless red-shifted bands, typical of excimers and dimers, appear in the case of naphthalenophanes 1, 2, 7, and 8. The fluorescence red shift of excimers relative to the monomer, as mentioned

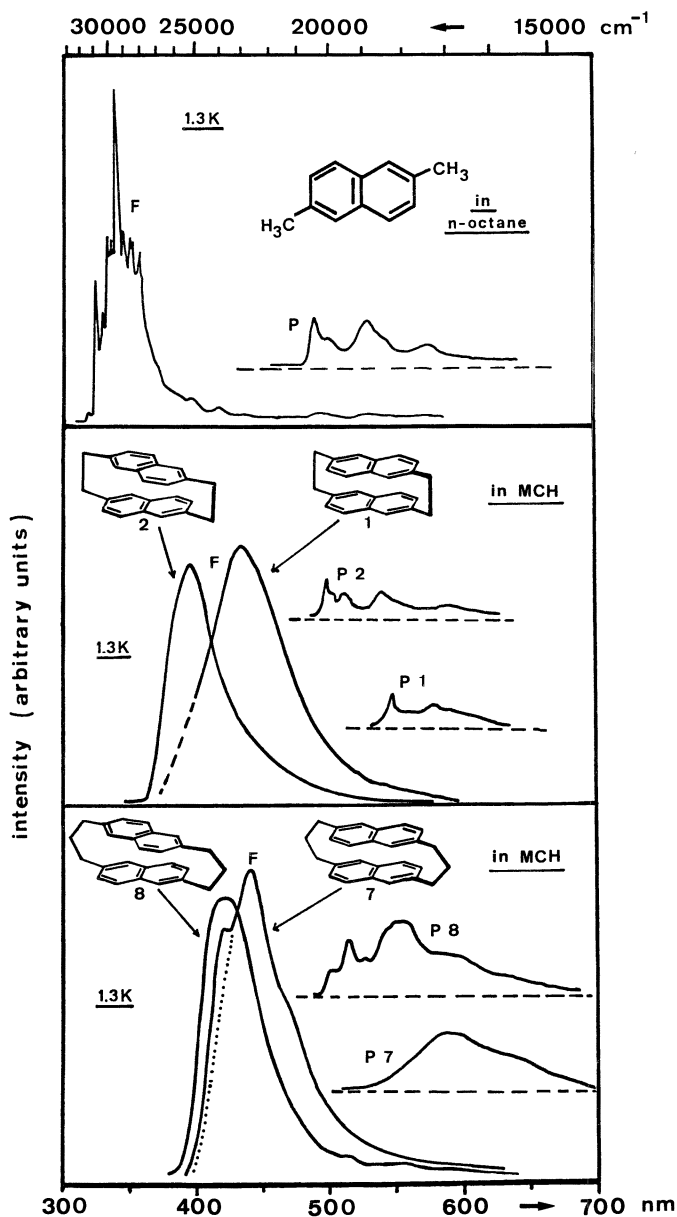


Figure 5. Fluorescence (F) and phosphorescence (P) of 2,6-dimethylnaphthalene and naphthalenophanes 1, 2, 7, and 8 in octane or methylcyclohexane (MCH  $c < 10^{-3}$  mol/L) at 1.3 K. In the fluorescence of 7, contamination by 8 apparently causes the shoulder at  $23,700\text{ cm}^{-1}$ , which is not observed in the emission of crystals of 7 (31).

earlier, is proportional to the excimer binding energy in the excited singlet state (1, 12). In both pairs of naphthalenophanes (1, 2 and 7, 8), the fluorescence red shift is found to be stronger for the achiral isomers 1 and 7, which have eclipsed naphthalene units. Phosphorescence, the emission from the excited triplet state  $T_1$ , is also observed. The vibronic structure is partly retained, and the phosphorescence red shifts are much smaller than those found in the fluorescence (36–38). However, the same gradation between isomers 1, and 7, 8 is observed as in the fluorescence.

The excited triplet state  $T_1$  is characterized by two unpaired electrons and is accessible to further experimental investigations because of its longer lifetime and magnetic property. As a consequence of the dipole–dipole interaction between the two unpaired electrons, the excited triplet state  $T_1$  is split into three sublevels,  $T_x$ ,  $T_y$ ,  $T_z$ , even in the absence of an external magnetic field. This zero-field splitting is described by two parameters,  $D$  and  $E$  (39).  $D$  is inversely proportional to the cube of the average distance between the two triplet electrons and is a sensitive measure for their average distance. As shown by the  $D$  values for benzene ( $0.16 \text{ cm}^{-1}$ ), naphthalene ( $0.10 \text{ cm}^{-1}$ ), and anthracene ( $0.07 \text{ cm}^{-1}$ ), the  $D$  parameter decreases with increasing size of the  $\pi$ -electron system. This relationship is found because the dipole–dipole and Coulombic repulsion causes the triplet electrons to separate as far as possible.  $E$  depends on the symmetry of the electron-spin distribution in the triplet state, but it is not considered in this context. In the case of the cyclophanes, the reduction of the  $D$  parameter relative to the monomeric aromatic unit can be used as an additional measure for the electronic interaction in the excited triplet state (31, 34–38). For molecules that emit phosphorescence, the zero-field splitting parameters  $D$  and  $E$  of the excited triplet state can be determined by ODMR. In principle, ODMR is a double-resonance experiment between UV light and microwaves (31, 40).

The fluorescence and phosphorescence red shifts and the reduction of the  $D$  parameters of naphthalenophanes 1–12 relative to the corresponding dimethylnaphthalenes are summarized in Table I. If the pairs of stereoisomers are compared (and only these should be compared), the isomer with completely eclipsed naphthalene units always has the strongest fluorescence red shift and hence the strongest bonding  $\pi$ – $\pi$  interaction in the excited singlet state. A small rotation by about  $40^\circ$  to crossed orientations of the naphthalene units decreases the red shifts from 5500 to  $3450 \text{ cm}^{-1}$ , from 7000 to  $6300 \text{ cm}^{-1}$ , and from 6200 to  $5200 \text{ cm}^{-1}$  for the diastereomeric [2.2](2,6)naphthalenophanes (1 and 2), [2.2](1,5)naphthalenophanes (3 and 4), and [3.3](2,6)naphthalenophanes (7 and 8), respectively. However, in the case of the [3.3](1,5)(2,6)naphthalenophanes (9 and 10), the fluorescence red shift increases from  $3500 \text{ cm}^{-1}$  (in 9) to  $3900 \text{ cm}^{-1}$  (in 10) if the crossing angle between the naphthalene units is increased from about  $40^\circ$  to about  $80^\circ$ . Apparently, the potential surface of the excited singlet state possesses a second minimum for a geometry in which the naphthalene units are strongly

**Table I. Fluorescence and Phosphorescence Red Shifts and Reductions of the Zero-Field Splitting Parameter  $|D|$  of Cyclophanes in Dilute Vitreous Solutions at 1.3 K**

Structure Number	Matrix <sup>a</sup>	Red Shift <sup>b</sup> (cm <sup>-1</sup> )		Reduction <sup>c</sup> (0/0)
		Fluorescence	Phosphorescence	
1	MCH	5500 ± 200	2100 ± 100	29
2	MCH	3450 ± 200	300 ± 100	8
3 <sup>d</sup>	PMMA <sup>e</sup>	7000 ± 200	2800 ± 100	24
4 <sup>d</sup>	PMMA <sup>e</sup>	6300 ± 200	1750 ± 100	11
7	MCH	6200 ± 200	2450 ± 300	33
8	MCH	5200 ± 200	400 ± 100	12
9	MCH	3500 ± 200	400 ± 100	9
10	MCH	3900 ± 200	1150 ± 100	15
5	MCH	7250 ± 200	3000 ± 200	43
6	MCH	5600 ± 200	1400 ± 100	10
11	MCH	7400 ± 200	2100 ± 100	36
12	MCH	5900 ± 200	1300 ± 100	10
13	MTHF	2500 ± 200	1900 ± 100	21
14	MTHF	1800 ± 200	1450 ± 100	6
15	MTHF	1200 ± 200	800 ± 100	9
18	MTHF	2600 ± 300	700 ± 200	7.8
17	MTHF	3900 ± 300	1100 ± 200	13.8

NOTE: Data for 1–12 are relative to the corresponding monomeric dimethylnaphthalenes; data for 13, 14, and 15 are relative to 1,4-, 1,5-, and 2,6-dimethylnaphthalene, respectively; and data for 17 and 18 are relative to 2,7-dimethylfluorene.

<sup>a</sup>MCH is methylcyclohexane, PMMA is poly(methyl methacrylate), and MTHF is 2-methyl-tetrahydrofuran. Concentrations of the compounds in these matrices were  $<10^{-3}$  mol/L.

<sup>b</sup>The red shifts are given between fluorescence maxima and phosphorescence 0→0 transitions.

<sup>c</sup>Reductions of  $|D|$  are given as  $[(|D|_{\text{mon}} - |D|)/|D|_{\text{mon}}] \times 100$ .

<sup>d</sup>The structural assignments of 3 and 4 are reversed in reference 35, because of the X-ray structure of 3 (Figure 3) and <sup>1</sup>H NMR spectroscopy at 360 MHz, the original wrong assignments were revised (21).

<sup>e</sup>The fluorescence red shifts of 3 and 4 in MCH are  $7700 \pm 200$  cm<sup>-1</sup> and  $5500 \pm 200$  cm<sup>-1</sup>, respectively.

SOURCE: Data are taken from references 31 and 34–38.

crossed. However, this second minimum is higher in energy than the potential well in which the two naphthalene units are fully eclipsed. Theoretical investigations of the naphthalene excimer have predicted exactly such a potential surface with a second minimum of higher energy in which the naphthalenes are crossed by about 70° (41–43).

As shown by the fluorescence red shifts of the *syn*- and *anti*-isomers of [2.2]- and [3.2](1,4)naphthalenophane (5, 6 and 11, 12, respectively), the  $\pi$ - $\pi$  electronic interaction in the excited singlet state is also diminished by a translation so that the overlap of the naphthalenes is reduced from two to only one six-membered ring. The small angle, by which the naphthalene planes in 11 and 12 are inclined to each other because of the different lengths of the two bridges, apparently has only a minor effect on the excited singlet state.



For the excited triplet state, the phosphorescence red shifts and the reductions of the  $D$  parameter show a similar orientational dependence. As in the excited singlet state, the  $\pi$ - $\pi$  electronic interaction decreases if the naphthalenes are rotated from fully eclipsed to slightly crossed orientations, and it increases again to about one-half of the original amount if the rotation proceeds to strongly crossed orientations. However, this behavior is in sharp contrast with calculations. According to calculations, the naphthalene triplet excimer should be stabilized by the rotation discussed and by an inclination so that the naphthalenes in the direction of their short axes are no longer coplanar (41). The stabilization due to inclination seems to be disproved by **11** and **12**, in which the angle of inclination is estimated to be  $15^\circ$ .

**[2]Naphthaleno[2]paracyclophanes.** In the naphthalenophanes discussed so far, two arenes of the same kind were interacting. To investigate the electronic  $\pi$ - $\pi$  interaction between arenes that differ in their electronic excitation energies, the structurally isomeric [2]naphthaleno[2]paracyclophanes (**13**–**15**) were selected as exciplex models. The *para*-disubstituted benzene ring is oriented differently over the naphthalene unit linked by the ethano bridges at the 1,4-, 1,5-, and 2,6-positions for **13**, **14**, and **15**, respectively. The spectroscopic comparison of **13** and **14** seemed to be especially interesting in respect to orientational effects: In **13**, formally only one six-membered ring of the naphthalene is overlapping with the opposite benzene, whereas in **14** (and also in **15**), the entire naphthalene unit is involved in the interaction. On the other hand, in **13**, the  $2p_z$  orbitals of the benzene carbon atoms are located directly opposite to the corresponding naphthalene carbon orbitals; therefore, the transannular overlap between these pairs of opposite  $2p_z$  orbitals is maximal. However, as shown by the molecular structure (33) in Figure 6, the carbon atoms of benzene and naphthalene are staggered in **14** (and also in **15**). Consequently, the transannular overlap of the single carbon  $2p_z$  orbitals between benzene and naphthalene is expected to decrease.

In **15**, the orbital overlap between benzene and naphthalene is restricted additionally by steric constraints: Because **15** formally is generated by connecting both ends of the shorter *p*-xylene and the longer 2,6-dimethylnaphthalene, a “bow” and a “bowstring” must be formed. The X-ray structures of **15** and its corresponding diene (**16**) confirm this expectation; the structures show almost planar benzene rings and extremely bent naphthalene units (44). Thus, relative to **13** and **14**, the electronic interaction in **15** is expected to be smaller, whereas the extreme deformation might cause further significant spectroscopic effects. Especially because the diene (**16**) now can be prepared in reasonable yields, the properties of these highly strained compounds are being studied in more detail (44).

The results of emission spectroscopy and the ODMR measurements of **13**–**15** are summarized in Table I (31). Relative to the corresponding 1,4-, 1,5-, and 2,6-dimethylnaphthalenes, the fluorescence and phosphorescence

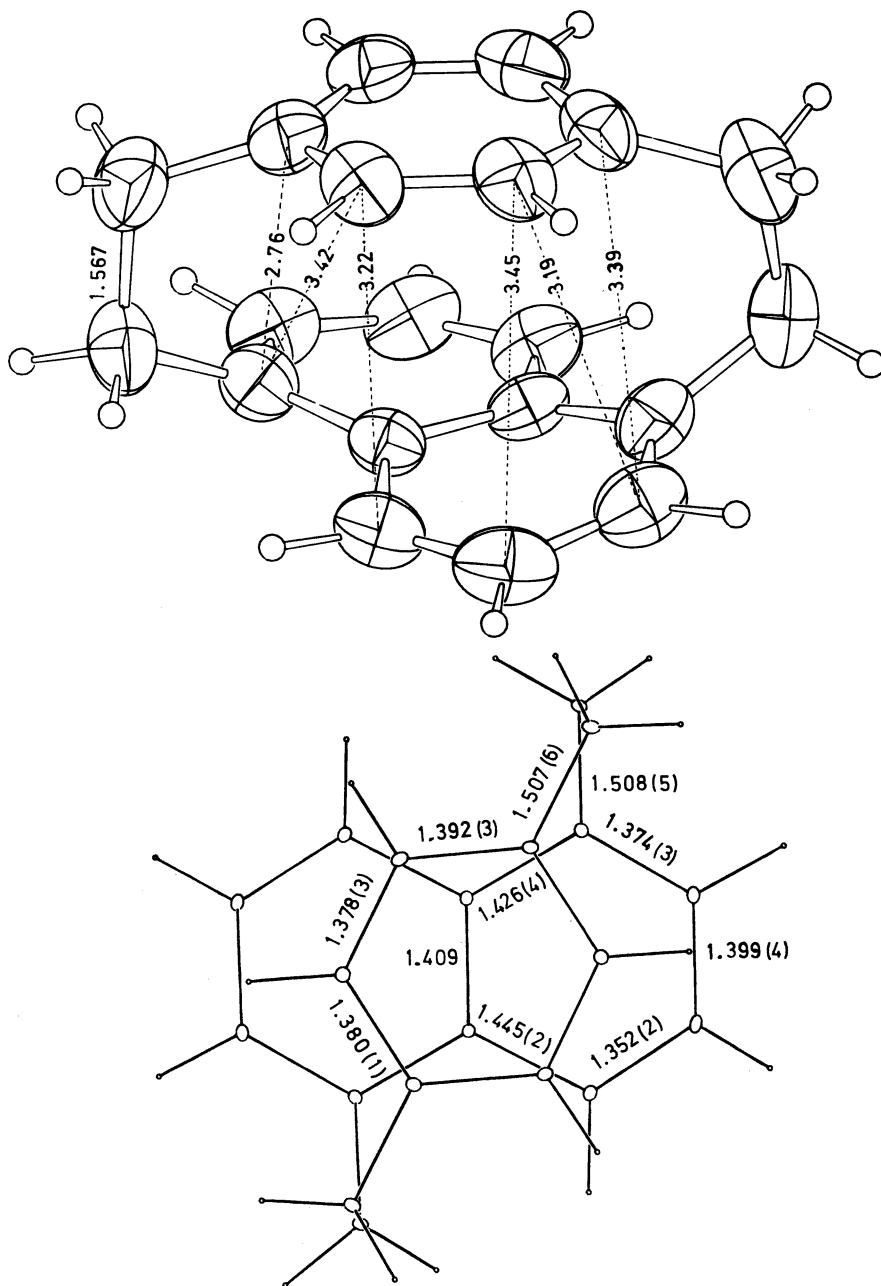


Figure 6. Molecular structure (33) of [2](1,5)naphthalen[2]paracyclophane (14).

red shifts of **13**–**15** decrease in the order  $13 > 14 > 15$ . This sequence means that both in the excited singlet and triplet states, the electronic  $\pi$ – $\pi$  interaction between benzene and naphthalene is highest if, as in **13**, the carbon atoms of benzene and naphthalene are eclipsed to enable maximal overlap between each pair of opposite carbon  $2p_z$  orbitals (36). In contrast with the order of the phosphorescence red shifts, **15** exhibits a stronger reduction of the  $D$  parameter than **14**. The extreme deformation of the naphthalene unit in **15** might be responsible for an additional reduction of the  $D$  parameter (45).

Compared with the [2.2]naphthalenophanes (**1**–**6**), the fluorescence red shifts of the naphthalenoparacyclophanes **13**–**15** are much smaller, whereas the phosphorescence red shifts are about the same magnitude (Table I). Especially interesting is the comparison between **13** and **6**, which have comparable structures with 1,4-disubstituted benzene and naphthalene units, respectively. Whereas the fluorescence red shift of naphthalenoparacyclophane **13** is less than one-half of that for naphthalenophane **6**, the phosphorescence of **13** has a  $500\text{-cm}^{-1}$  larger red shift. Apparently, in **13**, the excited triplet state is additionally lowered in energy by contributions of configuration interaction with higher excited states and/or by charge-transfer terms (31). In agreement with an additional energy decrease through charge-transfer terms, the reduction of the  $D$  parameter in **13** relative to 1,4-dimethylnaphthalene is 21%, which is more than twice as large as the 10% reduction for **6** (31, 46).

***syn*- and *anti*-[2.2](2,7)Fluorenophane.** As a further example to study the orientational dependence of the  $\pi$ – $\pi$  interaction between polycyclic arenes, *syn*- and *anti*-[2.2](2,7)fluorenophane (**17** and **18**) were synthesized (27). Because of the five-membered ring, the 2,7-substituents of fluorene form an angle of  $155^\circ$ . This geometry causes the fluorene units to be eclipsed in the *syn*-isomer (**17**) and staggered in the *anti*-isomer (**18**). As shown by the molecular structure of **18** (Figure 7), the fluorene units are considerably bent outward. Therefore, the transannular distances in the central region of the molecule are unusually large ( $3.63 \text{ \AA}$  between the planes of the five-membered rings). The transannular overlap between the carbon  $2p_z$  orbitals should be significant mainly in the neighborhood of the bridges. From the projection at the bottom of Figure 7, the staggered arrangement of the fluorene carbon atoms is evident. Because the carbon atoms and their  $2p_z$  orbitals must be eclipsed in the *syn*-isomer (**17**), a larger  $\pi$ – $\pi$  interaction is expected for the *syn*-isomer (**17**) than for the *anti*-isomer (**18**).

The emission spectroscopy and ODMR measurements summarized in Table I for **17** and **18** confirm these expectations (the spectra are shown in references 37 and 38). According to the fluorescence red shifts of  $3900$  and  $2600 \text{ cm}^{-1}$ , the electronic interaction in the excited singlet state is larger in the *syn*-isomer (**17**) than in the *anti*-isomer (**18**). As was already observed in

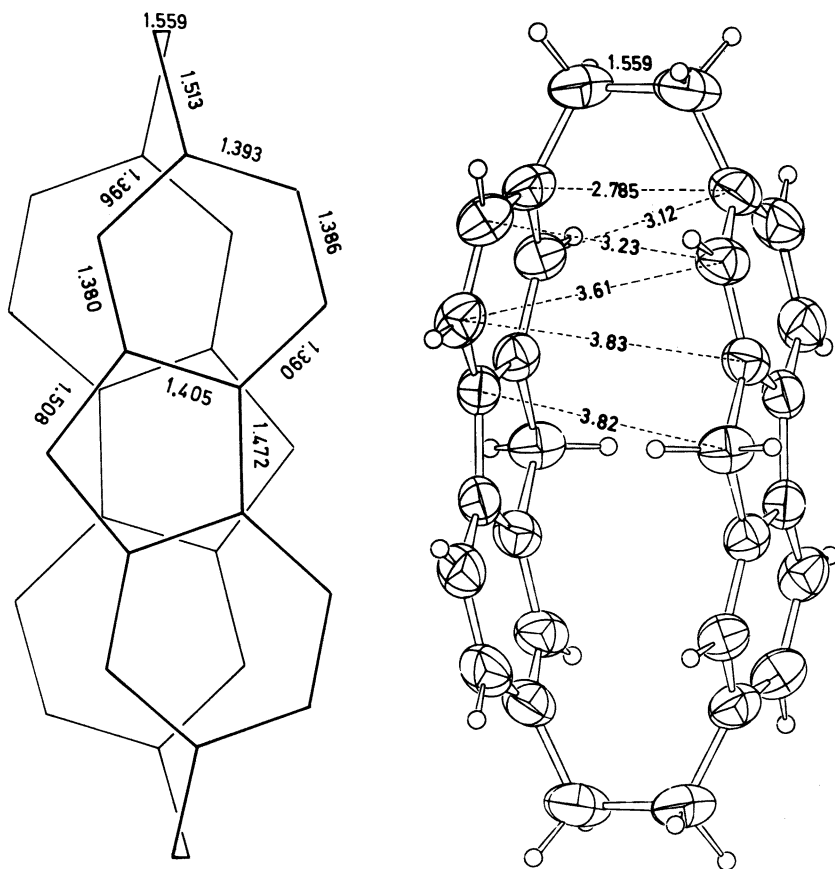


Figure 7. Molecular structure of anti-[2.2](2,7)fluoreno-phane (18). (Reproduced with permission from reference 27. Copyright 1985 VCH Verlagsgesellschaft)

the case of the naphthalenophanes, the  $\pi$ - $\pi$  interaction in the excited triplet state  $T_1$  is considerably smaller than in the excited singlet state  $S_1$  (36-38); however, the orientational dependence of the electronic interaction is similar in both excited states.

By reaction with *n*-butyllithium, 17 and 18 can be converted into the red *syn*- and *anti*-[2.2](2,7)fluoreno-phane dianions in which the electron-rich 9-fluorenyl anions are the interacting arenes (27). A second example of such double-layered dianions, the [2.2](4,7)indenophane dianion, has been described recently (47).

**Naphthalenopyridinophanes and Anthracenopyridinophanes.** As model compounds for amine-arene exciplexes, isomeric [2](1,4)- and [2](1,5)naphthaleno[2](2,6)pyridinophane-1,11-diene (21 and

**American Chemical Society  
Library**

1155 16th St., N.W.  
Washington, D.C. 20036

**22**), and for comparison the corresponding saturated naphthalenopyridinophanes (**25** and **26**) were synthesized (28, 29).  $^1\text{H}$  NMR and X-ray structural analysis indicated that the etheno bridges in **21** and **22** indeed enforce the required rectangular geometry between naphthalene and pyridine (28). According to the X-ray structural analysis (Figure 8, middle), **22** exhibits rectangular geometry; it has an interplanar angle of  $87^\circ$  for one of the two independent molecules in the unit cell. Because of packing, this angle is  $65^\circ$  for the second molecule (Figure 8, right). On the other hand, for the corresponding cyclophane (**26**) linked by ethano bridges, interplanar angles of  $24^\circ$  and  $29^\circ$  are observed in the two independent molecules of the unit cell (Figure 8, left). Because of these different conformations,  $n-\pi$  interaction is expected to exist exclusively in the etheno-bridged naphthalenopyridinophanes (**21** and **22**), whereas  $\pi-\pi$  interaction should be dominant in the ethano-bridged compounds (**25** and **26**).

This difference in the electronic interaction and strong orientational effects are indicated by the electronic absorption and emission spectra of the two pairs of isomers (**21**, **22** and **25**, **26**). In the UV spectra (Figure 9), the two dienes (**21** and **22**) exhibit enormous bathochromic shifts relative to the monomeric dimethylnaphthalenes and 2,6-dimethylpyridine. The absorption edge for the yellow **22** is shifted 50 nm to longer wavelengths than for the colorless **21**. This difference is due only to the different location of the nitrogen electron pair: In the first case it is directly over the central naphthalene  $\pi$  bond, and in the second case it is over the electronic hole in the center of a naphthalene six-membered ring. The ethano-bridged cyclophanes (**25** and **26**) also show absorptions shifted to longer wavelengths, but on the whole the bathochromic shifts observed for the  $\pi-\pi$  interaction are much smaller than for the  $n-\pi$  interaction.

In the fluorescence emission at 1.3 K (Figure 10), these differences are

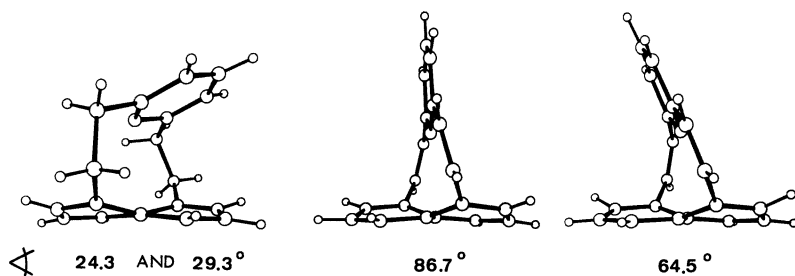


Figure 8. Molecular structures of [2](1,5)naphthaleno[2](2,6)pyridinophane-1,11-diene (**22**, two independent molecules, middle and right) and [2](1,5)naphthaleno[2](2,6)pyridinophane (**26**, left). The interplanar angles between naphthalene and pyridine are given for each pair of the two independent molecules **22** and **26** in the unit cells. (Reproduced with permission from reference 28. Copyright 1985 VCH Verlagsgesellschaft)

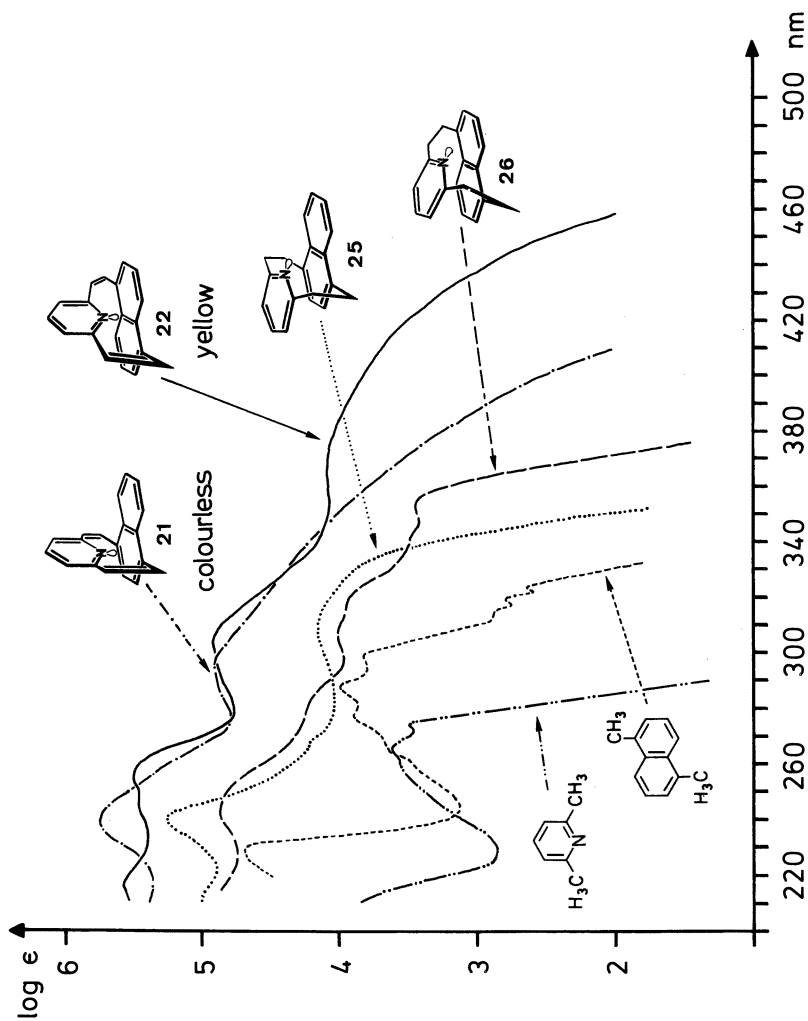


Figure 9. UV absorption spectra of **21**, **22**, **25**, **26**, 1,5-dimethylnaphthalene, and 2,6-dimethylpyridine in cyclohexane. The spectra of **25** and **26** are shifted by 0.5 ordinate unit, and those of **21** and **22** are shifted by 1 ordinate unit. (Reproduced with permission from reference 28. Copyright 1985 VCH Verlagsgesellschaft)

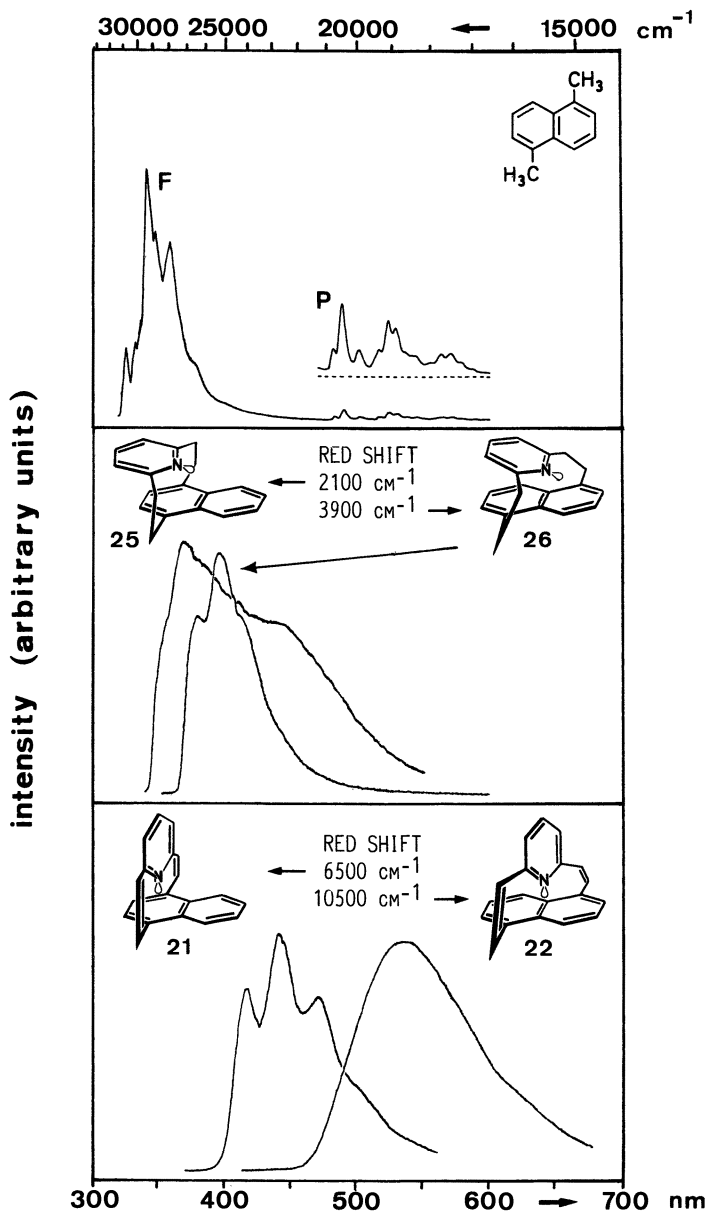


Figure 10. Emission spectra of 1,5-dimethylnaphthalene, 21, 22, 25, and 26 in *n*-octane ( $c < 10^{-3}$  mol/L) at 1.3 K. (Reproduced with permission from reference 28. Copyright 1985 VCH Verlagsgesellschaft)

even more pronounced. Compared with the structured fluorescence of the corresponding dimethylnaphthalenes, the ethano-bridged cyclophanes (**25** and **26**) possess fluorescence red shifts of 2100 and 3900  $\text{cm}^{-1}$ , respectively. Compared with the naphthalenophanes (**1–12**), these values correspond to  $\pi$ – $\pi$  interactions of moderate size.

The red shifts observed for the etheno-bridged cyclophanes (**21** and **22**) are much stronger; they reach 6500  $\text{cm}^{-1}$  in **21** and the enormous value of 10,500  $\text{cm}^{-1}$  in **22**. Fluorescence red shifts of this magnitude usually are observed only in charge-transfer complexes between donor- and acceptor-substituted arenes (**46**). The spectroscopic difference of 4000  $\text{cm}^{-1}$  between the isomers **21** and **22** corresponds to about 11 kcal/mol (47 kJ/mol). Because no phosphorescence could be detected for all the naphthalenopyridinophanes, the excited triplet states could not be investigated by ODMR techniques (**48**).

In the case of the anthracene compounds, so far we could synthesize only [2](1,4)anthraceno[2](2,6)pyridinophane-1,13-diene (**23**) and the corresponding ethano-bridged compound (**27**); in both of these compounds, pyridine is arranged over an outer anthracene ring (**30**). Therefore, a comparison of nitrogen over an outer anthracene ring, as in **23**, with nitrogen over the inner anthracene ring, as in **24**, is not yet possible. However, anthracenopyridinophane **23** can be compared with naphthalenopyridinophane **21**, both of which have the same geometric arrangement of the nitrogen lone pair over the center of an aromatic six-membered ring. Relative to 1,4-dimethylnaphthalene, the fluorescence of **23** is red-shifted by  $4500 \pm 500 \text{ cm}^{-1}$  (the spectra are shown in reference **30**). This red shift is considerably less than the red shift of  $6500 \pm 300 \text{ cm}^{-1}$  for the fluorescence of **21** relative to 1,4-dimethylnaphthalene (**28**). Actually, a priori, one could have expected the reverse order for **21** and **23** because anthracene is a much better electron acceptor than naphthalene; thus, a charge transfer from the occupied non-bonding nitrogen orbital to the lowest unoccupied molecular orbital of anthracene should be preferred.

An explanation of the experimental result is attempted by adapting a bonding model that previously has been used by Colpa et al. (**36**) to describe the excimer-type  $\pi$ – $\pi$  bonding in cyclophanes. According to this model, the bonding in the excited singlet state between naphthalene (**29**) or anthracene (**30**) and an amine nitrogen, which is located over the center of an aromatic six-membered ring, can be described by  $\sigma$ -type bonds between the nitrogen orbital and the six carbon  $2p_z$  orbitals (Figure 11). Then, the total bond density ( $d_i^{nn}$ ) is the sum of these six contributions, which again are described by a product of two quantities,  $P_{ij}$  and  $F_{ij}$ . The quantity  $P_{ij}$  is essentially geometric quantity (**36**) and therefore should be identical or very similar in the naphthalene and anthracene exciplex models (**21** and **23**, respectively). The quantity  $F_{ij}$  is the charge or electron density, that is, the probability of finding an electron on each single center. As an approximation (**36**), the spin



densities of the naphthalene and anthracene radical anions are used; these can be calculated (49, 50) or determined experimentally (51–53). As shown in Table II, the spin density in the 1-position of naphthalene is twice as large as that of anthracene; in addition, the spin density in the 2-position of naphthalene is also larger than that of anthracene. Therefore, in comparison with **21**, a smaller total bond density  $d_t^{n\pi}$  in the excited singlet state and hence a smaller fluorescence red shift are predicted for the anthracenopyridinophane (**23**); these predictions are in accordance with the experimental results. On the other hand, the very high spin density in the anthracene 9,10-positions should cause a strong exciplex bond if the nitrogen electron pair is located over the inner anthracene ring. For [2](9,10)anthraceno[2](2,6)pyridinophane-1,13-diene (**24**), which is the isomer of **23** and could not yet be synthesized, a fluorescence red shift that is larger than that for **23** and presumably exceeding that for **21** is predicted.

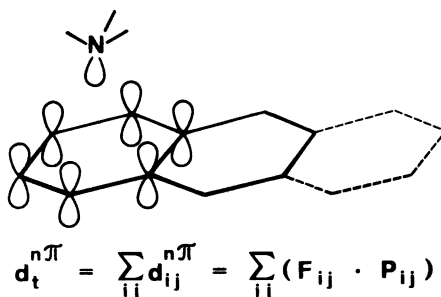


Figure 11. Bonding model for amine-arene exciplexes.

Table II. Calculated Spin Densities for the Radical Anions (Cations) of Naphthalene and Anthracene

n	$c_{in}^2$	$\rho_n$
Naphthalene		
1	0.181	0.222
2	0.069	0.047
9	0	-0.037
Anthracene		
1	0.097	0.118
2	0.048	0.032
9	0.193	0.256
11	0.008	-0.028

NOTE:  $n$  is the position of the carbon in naphthalene or anthracene (see structure **29** or **30**, respectively);  $c_{in}^2$  is the HMO (Hückel molecular orbital) spin density, which is the square of the LCAO (linear combination of atomic orbitals) coefficient of the single-occupied HMO  $\psi_i$  at the center  $n$  (49); and  $\rho_n$  is the McLachlan spin density (50).

SOURCE: Reproduced with permission from reference 30. Copyright 1986 Verlag der Zeitschrift für Naturforschung.

## Conclusions

The orientation of interacting aromatic  $\pi$ -electron systems strongly influences the extent of the electronic interaction. The investigations of naphthalenophanes (1–12), naphthalenoparacyclophanes (13–15), and fluorenophanes (17–18) indicate that in the excited singlet state, as well as in the excited triplet state, the  $\pi$ – $\pi$  interactions between two arenes are the highest if their planes are parallel and the maximal number of their six-membered rings are completely eclipsed. This geometry enables maximal overlap between the single pairs of carbon  $2p_z$  orbitals located directly opposite each other. Similarly, the  $n$ – $\pi$  interaction in the amine–arene exciplex models (21–23), in which the nitrogen electron pair is pointing toward aromatic  $\pi$ -electron systems, is determined by the overlap between the lone-pair orbital and each of the carbon  $2p_z$  orbitals involved. A simple model using the spin densities of aromatic radical anions is useful to predict the  $n$ – $\pi$  interactions in the amine–arene exciplexes.

## Acknowledgment

The investigations described were started within the group of H. A. Staab at the University of Heidelberg and at the Max-Planck-Institut für medizinische Forschung, Heidelberg; they were continued at the Max-Planck-Institut für Kohlenforschung, Mülheim/Ruhr. We thank H. A. Staab and K. H. Hausser, Max-Planck-Institut für medizinische Forschung, Heidelberg, for generous support and detailed discussions. The excellent contributions of our co-workers and colleagues (their names are listed in our cited papers) are gratefully acknowledged. The work was supported by Fonds der Chemischen Industrie, Frankfurt am Main, and Deutsche Forschungsgemeinschaft, Bad Godesberg. Petroleum Research Fund Grant No. 18537–SE covered travel expenses to the ACS National Meeting in Anaheim, CA, where this research was presented.

## References

1. Förster, Th. *Angew. Chem.* **1969**, *81*, 364; *Angew. Chem. Int. Ed. Engl.* **1969**, *8*, 333.
2. Stevens, B. *Adv. Photochem.* **1971**, *8*, 161.
3. *Organic Molecular Photophysics*; Birks, J. B., Ed.; Wiley: New York, 1973, 1975; Vols. 1, 2.
4. *The Exciplex*; Gordon, M.; Ware, W. R., Eds.; Academic: New York, 1975.
5. *Molecular Association*; Foster, R., Ed.; Academic: New York, 1975, 1979; Vols. 1, 2.
6. Kuzmin, M. G.; Guseva, L. N. *Chem. Phys. Lett.* **1969**, *3*, 71.
7. Nakashima, N.; Mataga, N.; Ushio, F.; Yamanaka, C. *Z. Phys. Chem. (Frankfurt—Main)* **1972**, *79*, 150.
8. Chandross, A.; Thomas, H. T. *Chem. Phys. Lett.* **1971**, *9*, 393.
9. Davidson, R. S. *J. Chem. Soc., Chem. Commun.* **1969**, 1450.

10. Baltrop, J. A.; Owers, R. J. *J. Chem. Soc., Chem. Commun.* **1970**, 1462.
11. Förster, Th.; Kasper, K. *Z. Phys. Chem. (Frankfurt—Main)* **1964**, *1*, 275.
12. Stevens, B.; Ban, M. I. *Trans. Faraday Soc.* **1964**, *60*, 1515.
13. Rebafka, W.; Staab, H. A. *Angew. Chem.* **1974**, *86*, 234; *Angew. Chem. Int. Ed. Engl.* **1974**, *13*, 203.
14. *Cyclophanes I and II*; Keehn, P. M.; Rosenfeld, S. M., Eds.; Academic: New York, 1983; Vols. 1, 2.
15. Vögtle, F., Ed. *Top. Curr. Chem.* **1983**, *113*, 115.
16. Boekelheide, V.; Galuszko, K.; Szeto, K. S. *J. Am. Chem. Soc.* **1974**, *96*, 1578.
17. Weaver, L. H.; Matthews, B. W. *J. Am. Chem. Soc.* **1974**, *96*, 1581.
18. Reingold, I. D.; Schmidt, W.; Boekelheide, V. *J. Am. Chem. Soc.* **1979**, *101*, 2121.
19. Haenel, M. W.; Staab, H. A. *Chem. Ber.* **1973**, *106*, 2203.
20. Blank, N. E.; Haenel, M. W. *Chem. Ber.* **1983**, *116*, 827.
21. Haenel, M. W. *Chem. Ber.* **1978**, *111*, 1789.
22. Cram, D. J.; Dalton, C. K.; Knox, G. R. *J. Am. Chem. Soc.* **1963**, *85*, 1088.
23. Wasserman, H. H.; Keehn, P. M. *J. Am. Chem. Soc.* **1969**, *91*, 2374.
24. Blank, N. E.; Haenel, M. W. *Chem. Ber.* **1981**, *114*, 1520.
25. Blank, N. E.; Haenel, M. W. *Chem. Ber.* **1981**, *114*, 1531.
26. Haenel, M. W. *Chem. Ber.* **1982**, *115*, 1425.
27. Haenel, M. W.; Irngartinger, H.; Krieger, C. *Chem. Ber.* **1985**, *118*, 144.
28. Haenel, M. W.; Lintner, B.; Benn, R.; Ruffńska, A.; Schroth, G.; Krüger, C.; Hirsch, S.; Irngartinger, H.; Schweitzer, D. *Chem. Ber.* **1985**, *118*, 4884.
29. Haenel, M. W.; Lintner, B.; Benn, R.; Ruffńska, A.; Schroth, G. *Chem. Ber.* **1985**, *118*, 4922.
30. Haenel, M. W.; Lintner, B.; Schweitzer, D. *Z. Naturforsch.* **1986**, *31b*, 223.
31. Schweitzer, D. Habilitationsschrift, University of Heidelberg, 1980.
32. Zuchich, J.; Schweitzer, D.; Maki, A. H. *Photochem. Photobiol.* **1973**, *18*, 161.
33. Irngartinger, H.; University of Heidelberg, in preparation.
34. Schweitzer, D.; Colpa, J. P.; Behnke, J.; Hausser, K. H.; Haenel, M. W.; Staab, H. A. *Chem. Phys.* **1975**, *11*, 373.
35. Schweitzer, D.; Colpa, J. P.; Hausser, K. H.; Haenel, M. W.; Staab, H. A. *J. Lumin.* **1976**, *12/13*, 363.
36. Colpa, J. P.; Hausser, K. H.; Schweitzer, D. *Chem. Phys.* **1978**, *29*, 187.
37. Schweitzer, D.; Hausser, K. H.; Haenel, M. W. *Chem. Phys.* **1978**, *29*, 181.
38. Schweitzer, D.; Haenel, M. W. *Chem. Ber.* **1985**, *118*, 163.
39. McGlynn, S. P.; Azumi, T.; Kinoshita, M. *Molecular Spectroscopy of the Triplet State*; Prentice Hall: Englewood Cliffs, N.J., 1969.
40. Hausser, K. H.; Wolf, H. C. *Adv. Magn. Reson.* **1976**, *8*, 85.
41. Chandra, A. K.; Lim, E. C. *Chem. Phys. Lett.* **1977**, *45*, 79.
42. Chandra, A. K.; Sudhindra, B. S. *Mol. Phys.* **1974**, *28*, 695.
43. Azumi, T.; Azumi, H. *Bull. Chem. Soc. Jpn.* **1966**, *39*, 1829, 2317.
44. Haenel, M. W.; Blank, N. E.; Wientges, H.; Krüger, C.; in preparation.
45. Wasserman, E.; Hutton, R. S.; Bramwell, F. B. *J. Am. Chem. Soc.* **1976**, *98*, 7529.
46. Schweitzer, D.; Hausser, K. H.; Taglieber, V.; Staab, H. A. *Chem. Phys.* **1976**, *14*, 183.
47. Frim, R.; Raulfs, F.-W.; Hopf, H.; Rabinovitz, M. *Angew. Chem.* **1986**, *98*, 160; *Angew. Chem. Int. Ed. Engl.* **1986**, *25*, 174.
48. Lintner, B.; Schweitzer, D.; Benn, R.; Ruffńska, A.; Haenel, M. W. *Chem. Ber.* **1985**, *118*, 4907.
49. Heilbronner, E.; Bock, H. *Das HMO-Modell und seine Anwendung*; Grundlagen und Handhabung; 2nd ed.; Verlag Chemie: Weinheim, 1978; Vol. 1, p 267.

50. McLachlan, A. D. *Mol. Phys.* **1960**, *3*, 233.

51. Bolton, J. R.; Fraenkel, G. K. *J. Chem. Phys.* **1964**, *40*, 3307.

52. Snyder, L. C.; Amos, T. J. *Chem. Phys.* **1965**, *42*, 3670.

53. Gerson, F.; Weidmann, B.; Heilbronner, E. *Helv. Chim. Acta* **1964**, *47*, 1951.

RECEIVED for review November 11, 1986. ACCEPTED January 27, 1987.

# Desulfurization of Benzonaphthothiophenes and Dibenzothiophene with a Raney Nickel Catalyst Its Relationship to $\pi$ -Electron Density

Masatoshi Nagai<sup>1,4</sup>, Hideo Urimoto<sup>2,5</sup>, Kazuya Uetake<sup>2</sup>,  
Noriyuki Sakikawa<sup>2</sup>, and Richard D. Gonzalez<sup>3</sup>

<sup>1</sup>Department of Chemical Engineering, Tokyo University of Agriculture and Technology, Koganei, Tokyo 184 Japan

<sup>2</sup>Department of Industrial Chemistry, Nihon University, Chiyodaku, Tokyo 101 Japan

<sup>3</sup>Department of Chemical Engineering, University of Illinois at Chicago, Chicago, IL 60680

*Desulfurization of polynuclear thiophenes was performed by continuous stirring with a Raney nickel catalyst in ethanol at 0–78.8 °C. The major products were biphenyl in the desulfurization of dibenzothiophene,  $\alpha$ -phenylnaphthalene in the desulfurization of benzo[b]naphtho[1,2-d]thiophene, and  $\beta$ -phenylnaphthalene in the desulfurization of benzo[b]naphtho[2,3-d]thiophene and benzo[b]naphtho[2,1-d]thiophene. Observation of these products shows that the main reaction pathway is the extrusion of a sulfur atom to give the corresponding hydrocarbon. The  $\pi$ -electron densities of the sulfur atoms, which were calculated by using simple Hückel molecular orbital theory, are considered to be related to the adsorption of the sulfur compounds to the surface and consequently to the C–S bond-breaking rate.*

<sup>4</sup>Author to whom correspondence should be directed

<sup>5</sup>Current address: Houkuba Chemical Company, O'Hatano, Kanagawa 257 Japan

**H**YDRODESULFURIZATION OF HEAVY PETROLEUM FEEDSTOCKS and coal-derived liquids requires the conversion of high-molecular-weight compounds such as dibenzothiophene and the benzonaphthothiophenes (1–3). Several studies have investigated the mechanism of hydrodesulfurization of polynuclear thiophenes on cobalt or nickel molybdenum catalysts at high pressures (4–6). However, only a few investigations have related the chemical reactivity of these compounds to their electronic structure (7–9). The adsorption and hydrodesulfurization of the simple sulfur compound, thiophene, were studied recently by using quantum chemistry (10–12); however, thiophene can easily be decomposed even when it is not adsorbed at high temperatures and pressures. Nag et al. (7) noted that the reactivity of a polynuclear sulfur-containing compound is not determined solely by the size of the molecule. In addition, Geneste and co-workers (8, 9) reported that the first step in the hydrotreating reaction of benzonaphthothiophene was related to the Coulombic interaction term in the complete neglect of differential overlap (CNDO) calculations. Because competition occurs between the different processes (hydrogenation and desulfurization) during reaction, the relationship between desulfurization and the electronic properties of the compounds under reaction conditions is difficult to understand. Furthermore, because the calculation of electronic structures necessarily involves many  $\sigma$  bonds of partially saturated rings (8, 9), as well as contributions from the  $d$  electrons of the sulfur atom and many  $\pi$  electrons of high-molecular-weight compounds, the electronic structure of hydrogenated polynuclear thiophenes is difficult to estimate. Therefore, a catalyst and reaction conditions under which desulfurization takes place without hydrogenation should be selected.

Thiophenes are easily desulfurized to form hydrocarbons without hydrogenation on a Raney nickel catalyst by constant stirring in a solvent (13, 14). Because a Raney nickel catalyst has a strong affinity for electronegative atoms such as oxygen and sulfur (15), the  $\pi$ -electron density on a sulfur atom during desulfurization is possibly related to the adsorption of a sulfur atom to the catalyst surface during reaction. Simple Hückel theory can be used to calculate the  $\pi$ -electron density of a sulfur atom and other reaction indexes such as  $\pi$ -bond order and the highest occupied molecular orbital (HOMO) and lowest unoccupied molecular orbital (LUMO) coefficients. In this study, such calculations are used because all four compounds considered have similar  $\pi$ -electron configurations and the same number of  $\pi$  bonds being formed or broken: dibenzothiophene, benzo[*b*]naphtho[1,2-*d*]thiophene, benzo[*b*]naphtho[2,3-*d*]thiophene, and benzo[*b*]naphtho[2,1-*d*]thiophene. In addition, thiophene and benzo[*b*]thiophene were studied to compare their behavior with that of the four compounds just listed.

The desulfurization studies were performed in a batch reactor over a Raney nickel catalyst, and ethanol was used as the solvent. To avoid hydrogenation, the catalytic studies were performed at low temperature with continuous stirring. The dependence of the rate of desulfurization on the

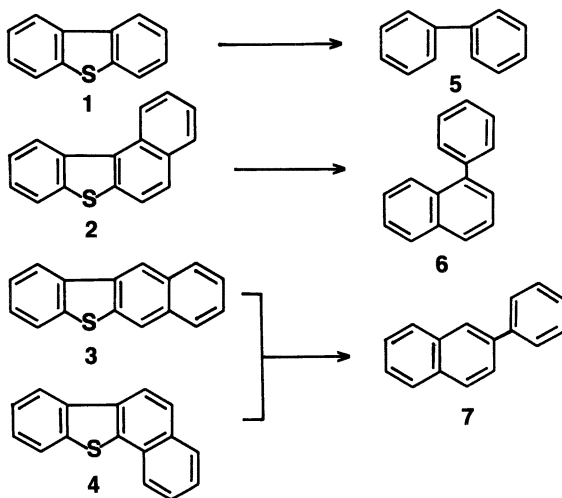
electronic structure of the compounds was considered by using simple Hückel molecular orbital calculations. The mechanism of the adsorption and desulfurization of dibenzothiophene and the benzonaphthothiophenes is also discussed.

### Experimental Details

The Raney nickel catalyst was prepared according to the procedure described by Adkins and Billia (16) for W-7 Raney nickel. Following preparation, the catalyst was stored under ethyl ether and an inert atmosphere for about 1 month at 0 °C. Dibenzothiophene (1), benzo[*b*]naphtho[1,2-*d*]thiophene (2), benzo[*b*]naphtho[2,3-*d*]thiophene (3), and benzo[*b*]naphtho[2,1-*d*]thiophene (4) (see Scheme I) were synthesized according to procedures described elsewhere (17–20).

Ten milliliters of absolute ethanol was placed in a pear-shaped flask equipped with a thermometer, a Dimroth condenser, and an electronic stirrer. By using filter paper, 0.2 g of catalyst was carefully dried. An accurate weight was obtained by weighing before and after the catalyst was added to the flask. The sample (0.2–1.47 mmol) was added to the ethanol solution with the Raney nickel catalyst. The flask was immediately placed in a glycerol bath at room temperature. After the solution temperature was quickly raised to the desired value, the stirrer was started and the initiation time was recorded. After the reaction, the flask was removed from the glycerol bath and cooled to room temperature.

The reaction products were analyzed by conventional gas chromatography using 20% Apiezon grease or 5% Silicone OV-17 packings (Kogyo Inc.), and acenaphthene was used as an internal standard. The reaction products were identified by comparing their retention times with those obtained for known samples. The simple Hückel calculations were performed on a microcomputer (NEC Corporation model PC-9801VM2).



Scheme I. Desulfurization of dibenzothiophene (1) and the benzonaphthothiophenes (2–4).

## Results and Discussion

**Desulfurization of Dibenzothiophene.** Changes in the desulfurization of dibenzothiophene as a function of reaction time are shown in Figure 1. Biphenyl (5) was the principal product, and only small amounts of unidentified high-molecular-weight compounds were formed. Initially, the rate of desulfurization was rapid, and desulfurization occurred to some extent before the reaction temperature was reached. Equilibrium was reached in each case after a reaction time of about 30 min. This result indicates that the reaction is a reversible process.

The effect of the catalyst-to-dibenzothiophene ratio on the rate of the desulfurization at 78.8 °C for 60 min is shown in Table I. This table shows that the rate of desulfurization does not depend on the amount of dibenzothiophene because the extent to which desulfurization occurred was proportional to the weight of the catalyst. This result suggests that the reaction between dibenzothiophene and the Raney nickel catalyst is stoichiometric.

**Desulfurization of the Benzonaphthothiophenes.** Desulfurization of the benzonaphthothiophenes over a Raney nickel catalyst was performed at 78.8 °C for 60 min. In each case, the initial amount of sample was 0.2 mmol, and the weight of the catalyst was 0.2 g. The major products were  $\alpha$ -phenylnaphthalene (6) in the desulfurization of 2 and  $\beta$ -phenylnaphthalene (7) in the desulfurization of 3 and 4. Observation of these products shows that the reaction occurs through the extrusion of a sulfur atom to give

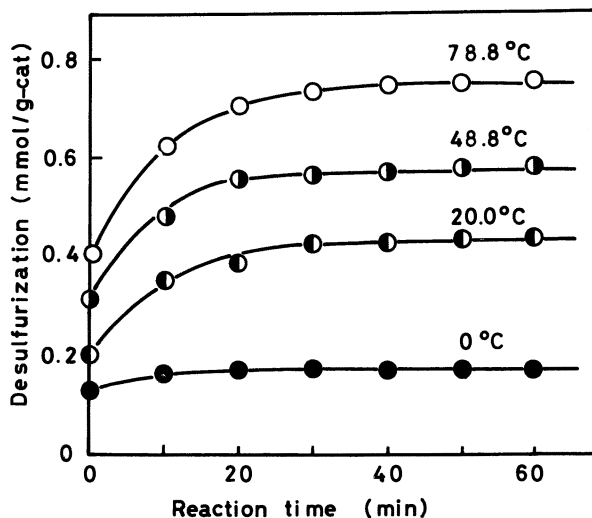


Figure 1. Changes in the desulfurization of dibenzothiophene as a function of reaction temperature. The initial amount of sample was 0.294 mmol, and the catalyst weight was 0.2 g. ○: 78.8; ◐: 48.8; ◑: 20.0; ●: 0°



**Table I. Effect of the Catalyst-to-Dibenzothiophene Ratio on the Desulfurization Rate at 78.8 °C for 60 min**

<i>Catalyst-to-Dibenzothiophene Ratio<sup>a</sup></i>	<i>Extent of Desulfurization (%)</i>	<i>Desulfurization<sup>b</sup></i>
0.2:1.13	13.4	0.757
0.4:1.13	25.9	0.732
0.76:1.13	50.0	0.743
1.13:1.13	76.0	0.760

<sup>a</sup>Catalyst values are given in grams, and dibenzothiophene values are given in millimoles.

<sup>b</sup>Desulfurization values are reported as millimoles of product per gram of catalyst per hour.

the corresponding hydrocarbon without any hydrogenation of the aromatic ring occurring either prior to or following the removal of the sulfur. The desulfurization rates, reported as millimoles of product per gram of catalyst per hour, were as follows for 1–4: 0.777, 0.626, 0.857, and 0.581, respectively. Thus, the desulfurization rates for the four compounds decreased in the following order: **3** > **1** > **2** > **4**. This result shows that the three-ring thiophene is not always more reactive than the four-ring compounds because the reactivity of dibenzothiophene is lower than that of **3**. This result is consistent with the study done by Sapre et al. (6) in which **3** was found to be more reactive than **1** on a sulfided CoMo–Al<sub>2</sub>O<sub>3</sub> catalyst. Thus, the reactivity of polynuclear thiophenes is not governed solely by the size of the molecule but by other elements that are related to the molecular structure.

**Electronic Structure Calculations.** Parameters appropriate for the thiophene molecule are given in review articles by Zahradník and co-workers (21, 22) and Zdražil and Sedláček (23). The following values were adopted for the Coulomb ( $\alpha$ ) and resonance ( $\beta$ ) integrals:  $\alpha_s = \alpha_c + \beta_{CC}$ ;  $\alpha_{C(S)} = \alpha_c + 0.1\beta_{CC}$ ; and  $\beta_{CS} = 0.8\beta_{CC}$ . By using these parameters, the Hückel molecular orbitals of free polynuclear thiophenes prior to adsorption were calculated. The frontier electron densities [Fr(E), Fr(N), and Fr(R)] of the sulfur atoms of the polynuclear thiophenes are shown in Table II. The indexes of Fr(E), Fr(N), and Fr(R) represent the ease of electrophilic, nucleophilic, and radical reactions, respectively, at the sulfur atoms of the compounds. The  $\pi$ -electron densities of the polynuclear thiophenes are shown in Chart I and Table III. The  $\pi$ -electron densities of the sulfur atoms of the four compounds studied decreased in the following order: **3** > **1** > **2** > **4**. In contrast, the  $\pi$ -electron densities of the sulfur atoms of thiophene (**8**) and benzothiophene (**9**) were much lower than those of the polynuclear thiophenes, even though **8** and **9** were more readily desulfurized.

**Relation Between Desulfurization and  $\pi$ -Electron Density.** The desulfurization of the polynuclear thiophenes over the Raney nickel catalyst was the primary reaction in that sulfur was removed to give

**Table II. Frontier Electron Densities of Sulfur Atoms of Polynuclear Thiophenes**

Density Designation	1	2	3	4
Fr(E)	0.372	0.660	0.110	0.315
Fr(N)	0	0.047	0.068	0.083
Fr(R)	0.186	0.354	0.089	0.199

NOTE: Values are the frontier electron densities of the sulfur atoms of the corresponding compounds.

**Table III.  $\pi$ -Electron Densities of Thiophenes Determined by Using Simple Hückel Molecular Orbital Theory**

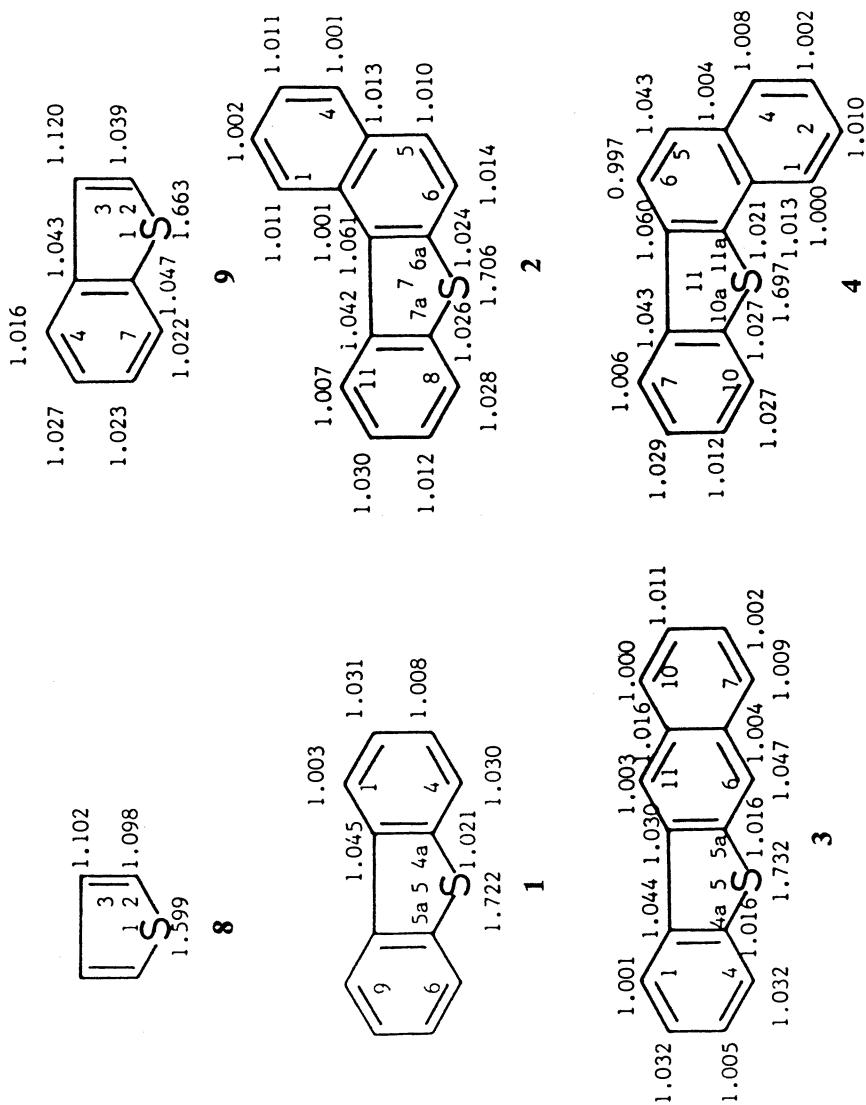
Density Designation	1	2	3	4	8	9
$q_s^a$	1.722	1.706	1.732	1.697	1.599	1.663
$q_s - q_c^b$	0.677	0.645	0.685	0.637	0.501	0.543

<sup>a</sup>Values in this row are the  $\pi$ -electron densities of the sulfur atoms of the corresponding compounds.

<sup>b</sup>Values in this row are the differences between the  $\pi$ -electron densities of the sulfur atoms and the highest  $\pi$ -electron densities of the carbon atoms in the corresponding compounds.

the corresponding hydrocarbons without ring saturation. This result suggests that the perpendicular adsorption of the sulfur atoms of these compounds to the nickel atoms is preferred during the reaction. Zdražil and Sedláček (23) reported that one-point adsorption occurred at the sulfur atom, although adsorption horizontal to the surface is energetically preferred. Furthermore, **4** might be expected to have a steric hindrance for the desulfurization because the benzene ring is on the side of the sulfur atom. However, the  $\pi$ -bond order between C-10a and S-11 of **4** (0.401) is similar to the  $\pi$ -bond order between C-7a and S-7 of **2** (0.402). Thus, **4** is more easily desulfurized than expected, even though it has a steric hindrance. Therefore, the preferential fission of a C–S bond can offset the effect of steric hindrance, and thus, the interaction of the  $\pi$ -electrons of the sulfur atom with the catalyst surface is more important than the molecular size.

Eisch et al. (24) performed a mechanistic study of the desulfurization of dibenzothiophene by a nickel(0)–bipyridyl complex and reported that a radical anion of the thiophene nucleus was formed and underwent C–S bond cleavage into S<sup>-</sup> and an aromatic radical. In addition, they suggested that the oxidative reaction of the nickel(0)–bipyridyl complex toward dibenzothiophene had the characteristics of stepwise electron transfer rather than nucleophilic attack. However, no correlations occurred between the desulfurization rate and the reaction indexes of Fr(E), Fr(N), and Fr(R), as shown in Table II. The results suggested no evidence for either electron transfer or nucleophilic attack in this study. Moreover, the radical reaction was not

Chart I.  $\pi$  - Electron densities of polynuclear thiophenes.

the determining step in the desulfurization of the thiophenes on the catalyst, although the mechanism of desulfurization over a Raney nickel catalyst most generally is a free-radical mechanism (14, 25–27).

However, Figure 2 shows a suitable correlation between the  $\pi$ -electron densities of the sulfur atoms of the polynuclear thiophenes and the rates of the desulfurization reactions. These reactions are stoichiometric reactions between the Raney nickel catalyst and the polynuclear thiophenes. For example,



where DBT is dibenzothiophene and BP is biphenyl. Therefore, the  $\pi$ -electron density of the sulfur atom is related to the strength of adsorption of the sulfur atom to a surface nickel atom of the Raney nickel catalyst. Hauptmann and Wladislaw (25) also reported that desulfurization was responsible for the first step of the reaction, that is, the adsorption of the organic compound on the metallic surface.

In the first step, the unshared electron pair of the sulfur is attracted to a low-valent nickel atom of the Raney nickel catalyst surface. The compound is adsorbed on the surface through the unshared electron pair of sulfur, which acts as an electron donor. Therefore, the carbon–sulfur bond is weak-

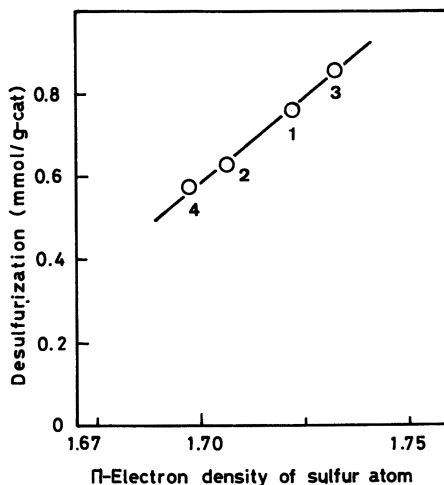


Figure 2. Relationship between the desulfurization of polynuclear sulfur compounds and the  $\pi$ -electron densities of their sulfur atoms. The initial amount of sample in each case was 0.2 mmol, the weight of the catalyst was 0.2 g, and the reaction time was 60 min.

ened, and a free radical is formed. The hydrogen present on the catalyst surface then reduces the radical to the corresponding hydrocarbon.

On the other hand, for **8** and **9**, the difference ( $q_s - q_c$ ) between the  $\pi$ -electron density of the sulfur atom and that of the carbon atom with the highest  $\pi$ -electron density (C-3) is small. Furthermore, the bond between C-2 and C-3 of these compounds is adsorbed competitively with the C-S bond. If this situation were not the case, these two molecules would chemisorb by a multistep mechanism (28). According to the multistep mechanism, thiophene molecules are chemisorbed in such a way that the bond between C-2 and C-3 is coordinated to an anion vacancy at the surface, and the adjacent sulfur center interacts with a contiguous sulfur atom on the surface. Therefore, the mechanism by which the three- and four-ring compounds are desulfurized is quite different from that of the one- and two-ring compounds, namely, **8** and **9**, respectively.

## References

1. Poirier, M.; Das, B. S. *Fuel* **1984**, *63*, 361.
2. Lucke, R. B.; Later, D. W.; Wright, C. W.; Chess, E. K.; Weimer, W. C. *Anal. Chem.* **1985**, *57*, 633.
3. Kong, R. C.; Lee, M. L.; Iwao, M.; Tominaga, Y.; Pratap, R.; Thompson, R. D.; Castle, R. N. *Fuel* **1984**, *63*, 702.
4. Welson, M. F.; Fisher, I. P.; Kring, J. F. *J. Catal.* **1985**, *95*, 155.
5. O'Brien, W. S.; Chen, J. W.; Nayak, R. V.; Carr, G. S. *Ind. Eng. Chem. Process Des. Dev.* **1986**, *25*, 221.
6. Sapre, A. V.; Broderick, D. H.; Fraenkel, D.; Gates, B. C.; Nag, N. K. *AIChE J.* **1980**, *26*, 690.
7. Nag, N. K.; Sapre, A. V.; Broderick, D. H.; Gates, B. C. *J. Catal.* **1979**, *57*, 509.
8. Guida, A.; Levache, D.; Geneste, P. *Bull. Soc. Chim. Fr.* **1983**, II-170.
9. Geneste, P.; Guida, A.; Jevache, D. *Bull. Soc. Chim. Fr.* **1983**, II-136.
10. Ruetter, F.; Ludena, E. V. *J. Catal.* **1981**, *67*, 266.
11. Harris, S.; Chianelli, R. R. *J. Catal.* **1984**, *86*, 400.
12. Joffre, J.; Geneste, P.; Lerner, D. A. *J. Catal.* **1986**, *97*, 543.
13. Pettit, G. R.; Van Tamelen, E. E. In *Organic Reactions*; Academic: New York, 1962; Vol. 12, p 356.
14. Mckinley, J. B. In *Catalysis*; Enmett, P. H., Ed.; Reinhold: New York, 1957; Vol. V, Chapter 6.
15. Mitsui, K. In *Catalytic Reduction*; Tokyo Kagaku Dojin.: Tokyo, 1970; p 62 (in Japanese).
16. Adkins, H.; Billia, H. R. *J. Am. Chem. Soc.* **1948**, *70*, 695.
17. Gilman, H.; Jacoby, A. L. *J. Org. Chem.* **1938**, *3*, 108.
18. Campaigne, E.; Osborn, S. W. *J. Heterocycl. Chem.* **1968**, *5*, 655.
19. Klemm, L. H.; Karckesy, J. J.; Lawrence, R. F. *J. Heterocycl. Chem.* **1978**, *15*, 773.
20. Rabindran, K.; Tilak, B. D. *Proc. Indian Acad. Sci.* **1953**, *37A*, 564.
21. Zahradník, R.; Párkányi, C.; Horák, V.; Kovtecký, *Collect. Czech. Chem. Commun.* **1963**, *28*, 776.

22. Zahradník, R.; Párkányi, C. *Collect. Czech. Chem. Commun.* **1965**, *30*, 195.
23. Zdražil, M.; Sedláček, J. *Collect. Czech. Chem. Commun.* **1977**, *42*, 3133.
24. Eisch, J. J.; Hawrence, L. E.; Han, K. I. *J. Org. Chem.* **1983**, *48*, 2963.
25. Hauptmann, H.; Wladislaw, B. *J. Am. Chem. Soc.* **1950**, *72*, 707, 710.
26. Hauptmann, H.; Walter, W. F.; Marino, C. *J. Am. Chem. Soc.* **1958**, *80*, 5832.
27. Badger, G. M.; Sasse, W. H. F. *J. Chem. Soc.* **1957**, 3862.
28. Kwart, H.; Schuit, G. C. A.; Gates, B. C. *J. Catal.* **1980**, *61*, 128.

RECEIVED for review September 29, 1986. ACCEPTED May 29, 1987.

# Interrelation of Polynuclear Aromatic Hydrocarbons and Carbonaceous Materials

Lawrence B. Ebert and Joseph C. Scanlon

Corporate Research Laboratories, Exxon Research and Engineering Company,  
Annandale, NJ 08801

*Themes linking polynuclear aromatic hydrocarbons to solid carbonaceous materials, including fossil fuels and graphite, are explored. X-ray diffraction proves that one may intercalate metaanthracite coal and calcined petroleum coke in the same sense that graphite may be intercalated. The chemistry of reductive protonation of large aromatic crystallites is investigated.*

**T**HE TERM "AROMATIC" HYDROCARBON originates from the existence of many pleasant-smelling, naturally occurring oils, such as those from cinnamon, vanilla, and cloves, which contain molecules related to benzene. Polynuclear aromatic hydrocarbons are also found in nature, most frequently in coal and petroleum. A book on the chemistry of polynuclear aromatic hydrocarbons thus can generate themes relevant to the chemistry of fossil fuels, and this idea is developed in several chapters in this book (1-4). In this final chapter, we shall discuss issues linking the chemistry of polynuclear aromatic hydrocarbons, fossil fuels, and the ultimate aromatic compound, graphite. In studying this interface, one sees the relevance of the organic chemistry of pure compounds and the possible utility of the materials science of carbonaceous solids in learning more of the chemistry of fossil fuels.

The relation between polynuclear aromatic hydrocarbons and fossil fuels is discussed in introductory organic chemistry textbooks, which mention that coal and petroleum are the commercial sources of many aromatic hydrocarbons (5, 6). The chemistry discussed in these basic texts is generally limited

to substitution reactions (electrophilic and nucleophilic, with no change in hybridization of carbon atoms) and addition reactions (such as the oxidative addition of bromine or the reductive addition of hydrogen to yield some carbon atoms that are  $sp^3$  hybridized). These texts point out that polynuclear aromatic hydrocarbons are more reactive than benzene (5, 6). The concept of reactivity of the  $\pi$  electrons can be quantified by measurement of ionization potential (IP) and electron affinity (EA), which also allows comparison of molecular species with graphite.

### *Graphite as a Polynuclear Aromatic “Hydrocarbon”*

As the size of polynuclear aromatic hydrocarbons increases, a gradual decline in IP and an increase in EA occur; these changes culminate in graphite, for which  $IP = EA = 4.39$  electronvolts (eV) (7). This trend suggests that larger fused-ring aromatic hydrocarbons will be more reactive than smaller ones in reactions involving electron transfer, whether the reactions involve electron addition (reduction) to form aromatic anions or electron removal (oxidation) to form aromatic cations. This concept of a hierarchy in electron-transfer reactivity has been appreciated in work on both model compounds (8) and on coals (9). Additionally, one sees that graphite, far from being inert, is actually more reactive to both reduction and oxidation than most aromatic hydrocarbons; in fact, ions of polynuclear aromatic hydrocarbons will react with graphite via electron transfer to form intercalation compounds (10).

The increasing importance of electron-transfer reactions with increasing aromatic hydrocarbon size is illustrated in the reaction of bromine with various aromatic compounds. With benzene (with a Lewis acid) and with naphthalene, electrophilic substitution occurs, and with anthracene, oxidative addition occurs (6); however, with graphite, only oxidation to the exclusion of carbon–bromine bond formation occurs, even at a stoichiometry of  $C_8Br$  (11, 12).

Graphite translational symmetry elements can be related to reactivity classes of aromatic hydrocarbon molecules. As illustrated in Figure 1, the acene class of aromatic hydrocarbons (e.g., anthracene, naphthacene, and pentacene) can be defined in terms of growth along the graphite [110] direction of translational periodicity. The phenacene class of aromatic hydrocarbons (e.g., phenanthrene, chrysene, and picene) can be defined in terms of growth along the graphite [100] direction of translational periodicity, although detailed X-ray diffraction studies show that phenacenes, in contrast with graphite, are slightly nonplanar (13). The reactivity of acenes to either reduction or oxidation increases rapidly with molecular size, whereas the reactivity of phenacenes changes rather slowly (7). For a given molecular size, an acene is more reactive than a phenacene, and, in this book, Nishioka and Lee (4) discuss differences in reactivity between phenanthrene and anthracene in the hydrogenation of a coal liquid.



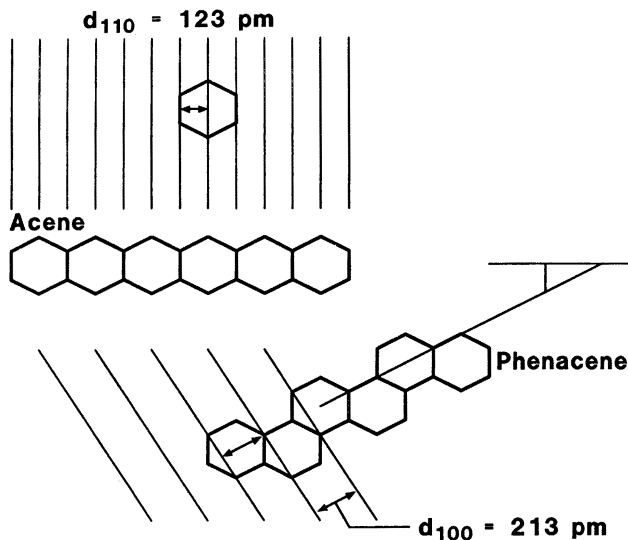


Figure 1. Illustration of the acene and phenacene molecular classes defined in terms of graphite translational periodicity axes. In terms of the phenacenes, by starting at the lower left, one may generate phenanthrene (three rings), chrysene (four rings), and picene (five rings).

The interrelation between molecular reactivity and translational periodicity can have experimental implications. In benzenoid solids, one observes X-ray diffraction peaks arising from periodicity along the (110) direction at distance  $d = 1.23 \text{ \AA}$  (123 pm) and from periodicity along the (100) direction at  $d = 2.13 \text{ \AA}$  (213 pm). For a material with no preferred growth direction, such as graphite, the crystallite size predicted by using the Scherrer equation evaluation of diffraction line width (14), will be comparable for both peaks. However, if a direction of growth is preferred, caused perhaps by preferred sites of molecular reactivity, unequal crystallite sizes from the (110) and (100) line widths will be seen (7, 15). Such an analysis should be relevant to various ladder polymers (16–19) and to the proposal of chiral graphite (20). Ruland and Plaetschke (21) have outlined a diffraction method to determine preferred (100) and (110) orientation in carbon fibers arising from the pyrolysis of different benzenoid materials (21). Significantly, fibers derived from polyacrylonitrile ladder polymer, which is an acene, had the opposite preferred orientation to fibers derived from petroleum mesophase pitch, which presumably is composed primarily of phenacenes (2, 4).

The interrelation of initial molecular symmetry and reactivity with final structure is an important issue in fossil fuels, as in the pyrolysis of coal or petroleum to make coke. In the general area of pyrolysis of aromatic hydrocarbons, several reviews have been published (22–24), and in this book, Lewis and Singer discuss recent advances in this field (25).

Coal and petroleum are more complex than simple pure polynuclear aromatic hydrocarbons or graphite because the fossil fuels contain not only aliphatic groups, but also elements other than carbon and hydrogen. Unlike many of the polynuclear aromatic compounds discussed in this book, coal and petroleum are not fully soluble in common organic solvents partly because of cross-linking through aliphatic groups and partly because of the effect of the other elements, such as sulfur, nitrogen, and oxygen. Thus, a chemical reaction that is predicated on the solvation of the converted aromatic hydrocarbon, such as many of the reductive chemistries discussed in this book, may not be completely effective in reacting with the fossil fuels.

An alternative starting point in chemically reacting fossil fuels is to treat them as if they were graphite. As noted earlier, graphite and larger polynuclear aromatic hydrocarbons are far from inert with respect to electron-transfer reactions, and thus the use of chemistry known to work for graphite may be of possible use in the investigation of coal, petroleum, and their derivatives. In the next two sections, we will discuss aspects of reduction and oxidation of carbonaceous solids and thereby parallel the chapters in this book on the reduction and oxidation of polynuclear aromatic hydrocarbon molecules.

## ***Reduction of Carbonaceous Solids***

**Formation of the Graphite Intercalation Compound  $C_8K$ .** Graphite will react directly with potassium metal at 110 °C under inert gas to form a bronze-colored intercalation compound of stoichiometry  $C_8K$  (26). This compound is first-stage, meaning that every interlayer void in the graphite is filled with potassium. (*Stage* is defined as the ratio of graphite layers to guest layers.) This condition is demonstrated by X-ray diffraction. A sketch of a Debye–Scherrer photograph of a polycrystalline graphite  $C_8K$  compound is shown in Figure 2; the lines readily index to an orthohexagonal Bravais lattice of  $a_0 = 4.961 \text{ \AA}$ ,  $b_0 = 8.592 \text{ \AA} = \sqrt{3}a_0$ , and  $c_0 = 21.76 \text{ \AA}$ , or to the equivalent hexagonal lattice of  $a_0 = 4.961 \text{ \AA}$  and  $c_0 = 21.76 \text{ \AA}$  (10, 11). Figure 3 presents variable-temperature Guinier–Simon X-ray diffraction data that show that the  $C_8K$  intercalation compound is destroyed by heating under a nitrogen flow at 500 °C.

**Formation of  $C_8K$  from Metaanthracite Coal.** This relatively simple chemistry can also cause intercalation of nongraphitic, but benzenoid, carbonaceous solids. Figure 4 presents a Debye–Scherrer X-ray diffraction photograph of a polycrystalline  $C_8K$  compound formed by the insertion of potassium metal at 110 °C into a metaanthracite from Newport County, RI (27). A sketch of this photograph is also shown in Figure 4. The initial crystallite size along the  $c$  axis, the direction of stacking, was 124 Å, as measured from the line width of the (002) line at  $d = 3.36 \text{ \AA}$ . The most

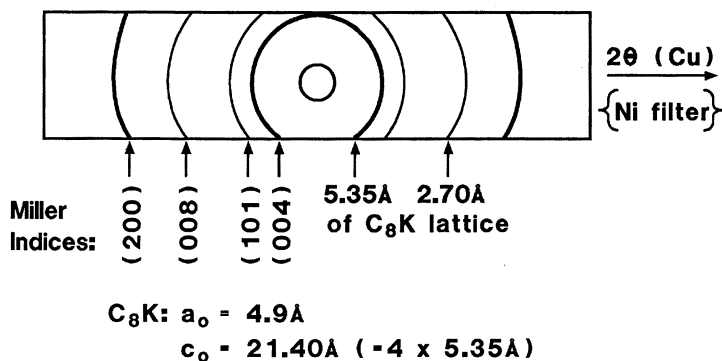


Figure 2. A sketch of Debye-Scherrer X-ray diffraction photograph of  $C_8K$  made from polycrystalline graphite and potassium metal. The indexing is done with respect to the hexagonal Bravais lattice of  $C_8K$ , which is degenerate with the orthohexagonal lattice. In the figure, the peak labelled (101) is at 4.2 Å; this index is equivalent to the (111) peak of the orthohexagonal system. It is likely that the broad 4.2-Å peak also represents the (100) of the hexagonal lattice (equal to the (110) of the orthohexagonal system). The peak labelled (200) in the figure is at 2.1 Å this index is equivalent to both the (200) and (040) peaks of the orthohexagonal system.

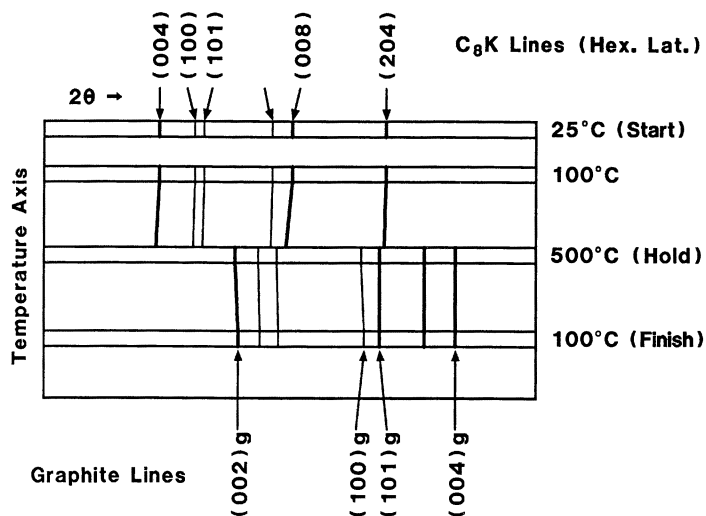


Figure 3. Variable-temperature X-ray diffraction of  $C_8K$  in flowing nitrogen. The temperature increases from 100 to 500 °C and then decreases back to 100 °C.

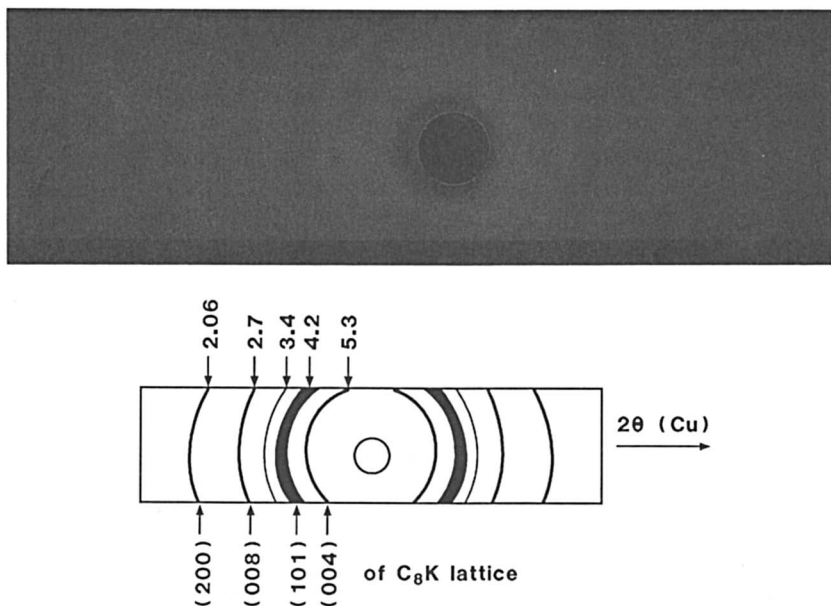


Figure 4. Debye-Scherrer X-ray diffraction photograph of  $C_8K$  made from metaanthracite coal and potassium metal (top), and sketch of this photograph (bottom).

intense lines of the product of the reaction with potassium are at 5.3, 4.2, 2.7, and 2.2 Å, which index as the (004), (111) [and possibly (110)], (008), and (220) lines of the orthohexagonal  $C_8K$  Bravais lattice. Diffraction peaks still occur at  $d = 3.36$  Å and  $d = 1.68$  Å, which could be the (002) and (004) lines of the initial coal; however, the intensity ratio of the peak at  $d = 5.3$  Å [the (004) line of the  $C_8K$ ] to the peak at 1.68 Å [maybe the (004) line of the initial coal] is 10.8; this ratio suggests that the intercalated product is the principal product. For an equal weight mixture of graphite  $C_8K$  and graphite, this intensity ratio is 1.6.

An additional argument in favor of the presence of intercalation is the temperature dependence of the line width of the electron spin resonance signal. Although the starting metaanthracite shows a derivative extremum line width of  $12.5 \pm 1.0$  gauss (G) that is independent of temperature, the  $C_8K$  product shows a line width that depends upon temperature:

$$\Delta H \text{ (gauss)} = 0.0354T + 14.28 R^2 = 0.9500 \quad (1)$$

where  $T$  is the temperature in kelvin. This linear dependence is similar to that reported for the graphite  $C_8K$  compound (28) and is the behavior expected for metallic conductors.

The ability of metaanthracite coal to intercalate potassium metal is presumably related, in part, to its large crystallite size and to its low H/C ratio (H/C = 0.036; 93.29% C, 0.28% H; dry basis). For an anthracite coal (Wilkes-Barre, PA) with a crystallite size of 15 Å and an H/C ratio of 0.30 (83.31% C, 2.11% H), as well as for a low-volatile bituminous coal (Ireland mine, WV) with no measurable stacking and an H/C ratio of 0.83 (69.10% C, 4.83% H), the reaction with potassium at 110 °C gave no evidence for the formation of an intercalation compound.

**Formation of  $C_8K$  from Calcined Petroleum Coke.** Materials that are less crystalline than metaanthracite do form intercalation compounds. Calcined petroleum cokes are formed by thermolysis at approximately 1400 °C of “green” petroleum cokes, which in turn are made by thermolysis of aromatic petroleum streams in delayed cokers operating in the range of 400–500 °C (29–32). (Immature cokes of higher H/C ratio are termed “green”; they are not green in color.) The crystallite size, measured both in the direction of aromatic stacking (*c* axis) and in the in-plane direction (*a* axis) is of the order 50–60 Å, which is less than half the crystallite size of the metaanthracite. However, literature reports indicate that such materials do form intercalation compounds with potassium metal (33, 34).

By reacting a commercially available calcined coke with potassium metal at 110 °C, we confirmed the ability of such cokes to intercalate potassium (35). Figure 5 presents a Debye–Scherrer X-ray diffraction photograph of a  $C_8K$  product formed from a calcined coke from a different manufacturer. A sketch of this photograph is also shown in Figure 5. This second coke had

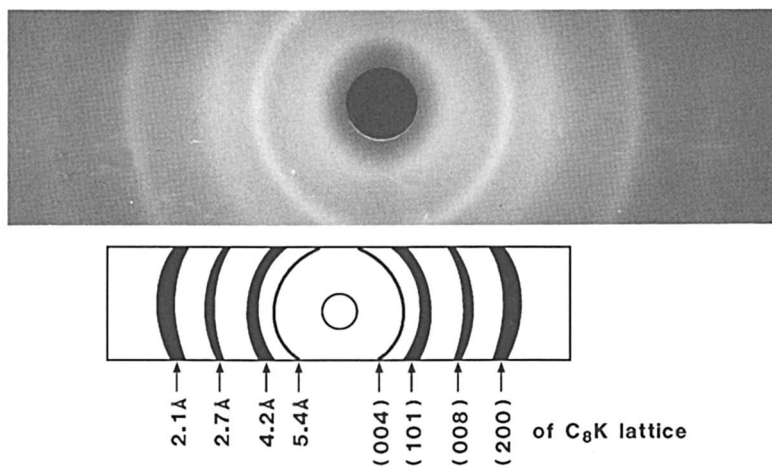


Figure 5. Debye–Scherrer X-ray diffraction photograph of  $C_8K$  made from calcined petroleum coke and potassium metal (top), and sketch of this photograph (bottom).

crystallite sizes similar to the first coke and a comparable low H/C ratio of 0.013 (98.95% C, 0.11% H); the sulfur level was 0.45%.

**Protonation and Rehybridization of Aromatic Anions.** These intercalation compounds of benzenoid, but nongraphitic, materials can be of relevance to themes in fossil-fuel chemistry. One challenging proposal is that chemistries of reduction, followed by protonation, can cause hydrogen uptake and rehybridization of  $sp^2$  carbon both in coals and in graphite. Specifically, X-ray scattering studies of seven vitrains and a graphite suggested "that conversion of planar aromatic layers to buckled hydrogenated rings had taken place", following treatment with lithium in ethylenediamine (36). The studies also reported that, "even with graphite of different origins, hydrogen increases of up to about 30 hydrogens per 100 carbon atoms were obtained", following reduction with alkali metal in glycol ethers and a quench with protonating reagents (36). Such reports are related to work in graphite science in which the protonation of the graphite intercalation compound  $C_8K$  with water was stated to lead to the new intercalation compound  $C_8H$  (37, 38). We shall discuss the plausibility of the two reductions of graphite by solution-state approaches and then give new data pertinent to the  $C_8K-H_2O$  reaction.

The claims for the rehybridization of graphite in the solution-state approaches were based on the following: (1) major changes in the X-ray diffraction at low scattering angles, and (2) the increase in hydrogen content of the reduced product.

The reaction of graphite with alkali metal in amine solvents to yield intercalation compounds is known in the literature (10). In such reactions, which are unaccompanied by carbon rehybridization, intercalation causes major changes in X-ray diffraction at low scattering angles, and for concentrated compounds, the most intense peak will be at angles lower than the initial graphite (002) line (10). Solvents typically cointercalate with the alkali metal, and in the specific case of graphite reacting with lithium and ethylenediamine, 1 mol of ethylenediamine intercalates per mole of intercalated lithium (10). The behavior of graphite with alkali metals and various ethers is similar (39).

Thus, one sees that the changes observed in graphite upon reduction in the liquid phase can be accounted for on the basis of intercalation without invoking any rehybridization of graphitic  $sp^2$  carbon atoms to  $sp^3$  carbons. Furthermore, if a two-dimensional polymeric (C-H) network of naphthenic carbon were generated, one could predict that the principal basal-plane diffraction peak would occur at 5.2 Å on the basis of the known structure of the two-dimensional fluoronaphthene, namely poly(carbon monofluoride) (15, 40).

**Reaction of  $C_8K$  Made from Graphite with Water.** For the reaction of graphite  $C_8K$  with water, three different models are proposed for the product:

1. The  $C_8H$  proposal of Bergbreiter and Killough (37, 38) in which  $C_8K$  is assumed to react much like an anion of a polynuclear aromatic hydrocarbon.
2. The  $C_{16}^{-}K^+(H_2O)_{2.5}$  proposal of Ebert and co-workers (41–43) in which a fraction of the intercalated potassium in  $C_8K$  behaves as potassium metal and in which the graphitic macrocarbanion is resistant to protonation. The product is considered to be a poorly crystalline intercalation compound containing  $K^+$  and water. This model serves as a counterpoint to a model assuming rehybridization of carbon, as discussed in the preceding section.
3. The graphite and KOH model of Schlogl and Boehm (44) in which poorly crystalline graphite encapsulates potassium hydroxide. The graphite is uncharged, and the KOH (or perhaps KOH monohydrate) exists in crystallites observable (at least in part) by X-ray diffraction. Although Schlogl and Boehm (44) refer to their product as a residue compound, it is not a residue compound in the commonly accepted sense because it contains the elements H and O, which do not occur in the initial parent intercalation compound.

Although proposal 1 is most closely related to the liquid-state reductions discussed earlier, the current debate in the graphite community is between proposals 2 and 3; proposal 1 is currently discounted. However, although proposal 1 may be of marginal significance for the large crystallites characteristic of graphite, the situation with intercalated carbonaceous material of smaller crystallite size is unclear. For this reason, we discuss the reaction of water with  $C_8K$  made from petroleum cokes at 1400 °C.

**Reaction of  $C_8K$  Made from Petroleum Coke with Water.** The coke discussed in reference 35 contained 99.40% C, 0.17% H, and 0.31% S. In the presence of a stoichiometric amount of potassium at 110 °C, 5.693 g of the coke (471 mmol of C) reacted with 2.342 g (59.9 mmol) of potassium to form bronze-colored  $C_8K$ . Under helium, 3.048 g of this product was reacted with excess  $H_2O$ , thoroughly rinsed, and dried to constant mass at 110 °C under a 50- $\mu$ mHg vacuum. Hydrogen gas was evolved on contacting this  $C_8K$  with water. The yield of solid was 2.392 g solid of analysis 89.66% C, 5.94% K, 0.96% H, 0.22% S, and 3.26% O. The empirical formula of the product is thus  $C_{49}KH_{6.3}O_{1.3}S_{0.045}$ .

To get a true picture of the final H/O atomic ratio, we must correct for the hydrogen initially in the coke (the initial amount of oxygen is more than an order of magnitude smaller than the final amount, so we will ignore it). The 3.048 g of the C<sub>8</sub>K contained 2.161 g of coke, which contained 2.148 g of C, 3.67 mg of H, and 6.70 mg of S. The 2.392 g of recovered product contained 2.145 g of C (99.3% recovery of carbon!), 0.142 g of K, 0.02296 g of H, 0.00526 g of S, and 0.07798 g of O. The H/O ratio of added material is [(0.02296 - 0.00367)/1.008]/(0.07798/15.9994) = 3.93.

If the only reaction of this coke were the intercalation of water, the H/O ratio should be 2, as it is in the case of the product of the reaction of graphite C<sub>8</sub>K with water. If we were dealing with the encapsulation of KOH monohydrate, the H/O ratio should be <2. The high H/O ratio is consistent with some reductive protonation of the crystallites of the calcined coke to generate new C–H bonds. However, in terms of the foregoing discussion about changes in the X-ray diffraction pattern of reductively protonated vitrains and graphite, we note that the *d* value of the (002) band of the water-treated coke C<sub>8</sub>K was at 3.49 Å. This value is essentially the same as the starting coke value of 3.46 Å and is in no way suggestive of a total rehybridization of all carbons in a given microcrystallite. This inference is consistent with the stoichiometry because the amount of hydrogen that could have been added to carbon (19.14 mmol – 9.75 mmol as water) amounts to only one hydrogen for every 19 carbon atoms (179 mmol of C per 9.39 mmol of H).

In terms of sulfur removal by potassium, we have (0.00670 – 0.00526)/0.00670 = 21% removal. This amount of sulfur (1.44 mg, 44.9 μmol) would require the consumption of 89.8 μmol of potassium, which is 0.4% of the 22.68 mmol of K in the 3.048 g of C<sub>8</sub>K. The overwhelming majority of the potassium went to the intercalation reaction rather than to sulfur removal; however, with other substrates such as coals, this balance could well be different.

We found that this calcined coke also forms an intercalation compound with cesium metal in which the (008) line at 2.98 Å of the C<sub>8</sub>Cs lattice (10) is observable. In this synthesis, 0.844 g of coke (0.839 g (69.8 mmol) of C was reacted with 1.563 g (11.76 mmol) of Cs at 110 °C for 1 h. (Excess Cs was used as an internal standard for <sup>133</sup>Cs-NMR experiments to be reported elsewhere.) A portion of this sample was quenched with water, rinsed, and dried, and the product was found to have the following empirical formula: C<sub>72</sub>CsH<sub>10.5</sub>O<sub>3.8</sub>S<sub>0.033</sub>. As in the case of the coke C<sub>8</sub>K–water products, cesium is observed in this product (12.52 wt %), and the H/O atomic ratio is >2.

**Frontier between Polynuclear Aromatic Compounds and Graphite.** The calcined petroleum coke shows chemistry that contains components of both graphite and polynuclear aromatic hydrocarbons. Like graphite, the calcined petroleum coke forms first-stage intercalation compounds with both potassium and cesium metals. These compounds are iden-



tified by the presence of the correct Bravais lattice, as shown by X-ray diffraction, and by the absence of the initial Bravais lattice. Also, upon reaction with water followed by rinsing, not all of the initial alkali metal can be removed from the calcined petroleum coke. Furthermore, there is evidence for the incorporation of water in the final solid-phase product. On the other hand, like polynuclear aromatic hydrocarbons, the anions from the coke react with water to (possibly) generate C–H bonds.

Where does the frontier between large polynuclear aromatic hydrocarbons and graphite lie? The answer is difficult to determine. Coronene,  $C_{24}H_{12}$ , reacts with potassium at 110 °C to form a solid black product with an electron spin resonance signal whose line width depends linearly on temperature but whose area follows the Curie law (7). Neither X-ray diffraction nor intuition suggests that this product be called an intercalation compound, yet the electron spin resonance indicates that potassium metal can react with larger polynuclear aromatic compounds in the absence of a solvent (7, 45, 46). Thus, a gradual transition in chemistry may occur from solvated aromatic anions (such as the naphthalene radical anion in tetrahydrofuran) to nonsolvated localized aromatic anions [such as coronene with  $K(0)$ ] to nonsolvated delocalized anions [such as graphite with  $K(0)$ ].

In general, the intercalation of benzenoid, but nongraphitic, solids with chemical reductants has been studied more than the intercalation of these solids with chemical oxidants. Herold (47) suggested that soft carbons, such as those obtained from petroleum, have acceptor defects, which favor the addition of electrons (reduction) to the benzenoid structure. Hooley (48) discussed the divergences in terms of threshold pressure effects. Nevertheless, the oxidation of carbonaceous solids has been studied, and these studies are discussed in the next section.

### *Oxidation of Carbonaceous Solids*

Early approaches to the oxidation of carbonaceous solids were destructive in nature and led to  $CO_2$  and possibly to organic acids (49–52). More recently, the oxidative intercalation of nongraphitic materials was reported (53–55).

Lazarov et al. (54) reacted a bituminous coal from Bulgaria (87.2% C, dry ash free) with several metal chlorides in carbon tetrachloride. The conditions used were those known to make intercalation compounds of graphite, and the authors reported that rather concentrated adducts formed with  $SbCl_5$ ,  $AlCl_3$ ,  $FeCl_3$ , and  $MoCl_5$ . No (002) band of the initial coal was observed in the adducts; this finding is consistent with the presence of intercalation. Coals of bituminous ranks show only a short-range order of aromatic stacking; the typical arrangement is only two to three layers (7–10.5 Å), and a liquidlike structure is considered to be optimum at 89% C (dry ash free) (56). Thus, in contrast with the petroleum cokes, the diffraction pattern of the final intercalation compound could be difficult to see. Furthermore, other

complexities are possible in the diffraction, including the presence of other peaks (57) and distributions of dihedral angles between aromatic planes (58).

In general, aromatic hydrocarbons and presumably fossil fuels containing aromatic molecules do not form extended "stacks" of molecules as embodied by a column of poker chips. H–H and H–C interactions are significant structural determinants for hydrocarbon molecules (59–60) and can lead to arrangements other than the graphitelike stack. To see a diffraction peak in the range of 3.3–3.8 Å and infer a graphite structure is potentially naive.

For petroleum cokes formed in the temperature range of 1600–2800 °C, X-ray diffraction was useful in monitoring the oxidative intercalation by  $\text{SbCl}_5$ ,  $\text{Br}_2$ , and  $\text{CrO}_3$ -acetic acid (55). With crystallite sizes in the direction of stacking between 300 and 600 Å, these cokes behave much as graphite with respect to oxidative intercalation; they even show such subtle behavior as stage disorder (analogous to graphite) in the case of the  $\text{SbCl}_5$  product. Furthermore, electron microprobe data on the  $\text{CrO}_3$  adduct showed an irregular Cr concentration profile, which suggested that intercalation occurred only at the edges of crystallites and did not proceed to the interior. This new result on an intercalation compound of coke is quite relevant to understanding the analogous graphite compound. For the graphite compound, diffraction results suggested the presence of both intercalated and nonintercalated phases, and magnetic resonance suggested that the intercalated chromium species, in contrast with most intercalated species, was immobile (61). Combining the information from both coke and graphite, we see that this intercalation system is rather special; the inability of the inserted species to be translationally free precludes the complete intercalation of the interlamellar voids.

In several studies, researchers attempted both the reduction and oxidation of carbonaceous solids (48, 54, 62, 63). One group claimed that graphite, oxidatively intercalated by  $\text{CdCl}_2$ , can be later reductively intercalated by sodium (64). In any event, various chemistries will attack both graphite and carbonaceous solids, and various physical techniques can prove this attack.

### *The Future*

In studying both polynuclear aromatic hydrocarbons and carbonaceous solids, X-ray diffraction has proved to be a valuable tool; this book contains elegant structural studies on both aromatic anions (65) and aromatic cations (66). NMR, including both  $^{13}\text{C}$  NMR in the solid state (67–72) and various two-dimensional spectroscopies (73–75), will have a dramatic impact in the future on both polynuclear aromatic hydrocarbons and carbonaceous solids.

The materials to be studied promise to be ever more challenging, ranging from soots and combustion exhausts (76–78), to mesophase materials from petroleum (79), through the graphite–diamond interface (80–81), antiaromatic compounds (82), carbon clusters (83, 84), and interstellar materials

(85–89). Furthermore, work on aromatic hydrocarbons should prove of relevance in other areas such as electrochemistry (90), gasification (91), and carbon reactivity in general (92–95). Finally, aromatic hydrocarbons themselves continue to provide exciting chemistry (96–98).

### Note Added in Proof

We were unable to cover some areas related to polynuclear aromatic molecules that are currently attracting attention.

Discotic liquids crystals (also termed columnar) are frequently composed of a central core composed of a polynuclear aromatic molecule substituted with pendant paraffin chains. Although liquids, they have crystalline order in certain directions, as shown by narrow X-ray diffraction peaks. Brown and Crooker wrote a basic discussion (99) and Hinov compiled a literature review for the period 1977–1984 (100). Other papers show the relation to polynuclear aromatics (101–110).

One usually does not relate polynuclear aromatic compounds to diamonds, yet recent work on dense, “diamondlike” films shows the presence of  $sp^2$ -hybridized carbons (111–113). Thus, the chemistry of polynuclear aromatic compounds may be of relevance to this exciting new materials area.

Finally, much more needs to be done in interrelating the chemistry of aromatic molecules to the chemistry of carbonaceous solids. A comparison of the chemistry of dibenzothiophene to the chemistry of sulfur functionality in petroleum residues recently was published (114) as well as a comparison of soot to polynuclear aromatics (115).

### References

1. Chambers, R. R.; Hagaman, E. W.; Woody, M. C., Chapter 15 in this book.
2. Speight, J. G., Chapter 12 in this book.
3. Berkowitz, N., Chapter 13 in this book.
4. Nishioka, M.; Lee, M. L., Chapter 14 in this book.
5. Roberts, J. D.; Caserio, M. C. *Basic Principles of Organic Chemistry*; Benjamin: New York, 1964 (third printing); pp 770–771; pp 810–825.
6. Morrison, R. T.; Boyd, R. N. *Organic Chemistry*; Allyn and Bacon: Boston, 1966 (second edition, fifth printing); pp 1038–1072.
7. Ebert, L. B. in *Chemistry of Engine Combustion Deposits*; Plenum: New York, 1985; pp 303–376.
8. Paul, D. E.; Lipkin, D.; Weissman, S. I. *J. Am. Chem. Soc.* **1956**, *78*, 116.
9. Sternberg, H. W.; Delle Donne, C. L.; Pantages, E. C.; Markby, R. E. *Fuel* **1971**, *50*, 432.
10. Novikov, Yu. N.; Vol'pin, M. E. *Russ. Chem. Rev. (Engl. Transl.)* **1971**, *40*, 733.
11. Ebert, L. B. *Annu. Rev. Mater. Sci.* **1976**, *6*, 181.
12. Ebert, L. B.; DeLuca, J. P.; Thompson, A. H.; Scanlon, J. C. *Mater. Res. Bull.* **1977**, *12*, 1135.
13. De, A.; Ghosh, R.; Roychowdhury, S.; Roychowdhury, P. *Acta Crystallogr. Sect. C: Cryst. Struct. Commun.* **1985**, *41*, 907.

14. Azaroff, L. V. *Elements of X-ray Crystallography*; McGraw-Hill: New York, 1968; pp 551–552.
15. Ebert, L. B.; Scanlon, J. C.; Mills, D. R. *Liq. Fuels Technol.* **1984**, *2*, 257.
16. Kaplan, M. L. UK Patent Application GB 2 065 652, filed Dec. 16, 1980.
17. Tanaka, K.; Ueda, K.; Koike, T.; Yamambe, T. *Solid State Commun.* **1984**, *51*, 943.
18. Murakami, M.; Yoshimura, S. *Mol. Cryst. Liq. Cryst.* **1985**, *118*, 95.
19. Satoh, M.; Uesugi, F.; Tabata, M.; Kaneto, K.; Yoshino, K. *Chem. Commun.* **1986**, 979.
20. Sokolov, V. I. *J. Struct. Chem. (Engl. Transl.)* **1985**, *25*, 331.
21. Ruland, W.; Plaetschke, R. Abstracts of Papers, 17th Biennial Conference on Carbon; Lexington, KY; 1985; pp 356–357.
22. Fitzer, E.; Mueller, K.; Schaefer, W. *Chem. Phys. Carbon* **1971**, *7*, 237.
23. White, J. L. *Prog. Solid State Chem.* **1974**, *9*, 59.
24. Lewis, I. C.; Singer, L. S. *Chem. Phys. Carbon* **1981**, *17*, 1.
25. Lewis, I. C.; Singer, L. S., Chapter 16 in this book.
26. Lalancette, J. M.; Rollin, G.; Dumas, P. *Can. J. Chem.* **1972**, *50*, 3058.
27. Ergun, S.; Mentser, M.; O'Donnell, H. J. *Science* **1960**, *132*, 1314.
28. Ebert, L. B.; Mills, D. R.; Scanlon, J. C. *Mater. Res. Bull.* **1982**, *17*, 1319.
29. Scott, C. B. *Chem. Ind.* **1967**, *1*, 1124.
30. Scott, C. B.; Folkins, H. O. *J. Met.* **1972**, *24*, 25.
31. Kurami, H. *J. Jpn. Petrol. Inst.* **1973**, *16*, 366.
32. Kakuta, M.; Tanaka, H.; Sato, J.; Noguchi, K. *Carbon* **1981**, *19*, 347.
33. Berger, D.; Carton, B.; Metrot, A.; Herold, A.; *Chem. Phys. Carbon* **1975**, *12*, 1.
34. Terai, T.; Takahashi, Y. *Carbon* **1984**, *22*, 91.
35. Ebert, L. B.; Mills, D. R.; Scanlon, J. C.; Garcia, A. R. *Carbon* **1987**, *25*, 313.
36. Wender, I.; Heredy, L. A.; Neuworth, M. B.; Dryden, I. G. C. In *Chemistry of Coal Utilization*; Elliot, M. A., Ed.; Wiley: New York, 1981; Second Supplementary Volume; pp 425–479. See especially pp 433, 446.
37. Bergbreiter, D. E.; Killough, J. M. *Chem. Commun.* **1976**, p. 913.
38. Bergbreiter, D. E.; Killough, J. M. *J. Am. Chem. Soc.* **1978**, *100*, 2126.
39. Herold, A. In *Intercalated Layered Materials*; D. Reidel: Dordrecht, 1979; pp 323–421.
40. Ebert, L. B.; Brauman, J. I.; Huggins, R. A. *J. Am. Chem. Soc.* **1974**, *96*, 7841.
41. Ebert, L. B.; Matty, L.; Mills, D. R.; Scanlon, J. C. *Mater. Res. Bull.* **1980**, *15*, 251.
42. Ebert, L. B. *Carbon* **1985**, *23*, 585.
43. Ebert, L. B.; Mills, D. R.; Garcia, A. R.; Scanlon, J. C. *Mater. Res. Bull.* **1985**, *20*, 1453.
44. Schlogl, R.; Boehm, H. P. *Carbon* **1984**, *22*, 351.
45. Berthelot, M. *Ann. Chim. (Paris)* **1967**, *12*, 155.
46. Beguin, F.; Setton, R. *Carbon* **1972**, *10*, 539.
47. Herold, A., op. cit. pp 332–333.
48. Hooley, J. G. In *Preparation and Growth of Materials with Layered Structures*; D. Reidel: Dordrecht, 1977; pp 1–33.
49. Bone, W. A.; Quarendon, R. *Proc. Roy. Soc. London, A* **1926**, *110*, 537.
50. Blayden, H. E.; Riley, H. L. *J. Soc. Chem. Ind., London Trans. Commun.* **1935**, p 159T.
51. Van Krevelen, D. W. *Fuel* **1950**, *29*, 282.
52. Hayatsu, R.; Winans, R. E.; Scott, R. G.; Moore, L. P.; Studier, M. H. In *Organic Chemistry of Coal*; Larsen, J. W., Ed.; ACS Symposium Series 71;

- American Chemical Society: Washington, D. C., 1978; pp 108–125. See especially p 108.
53. Besenhard, J. O.; Fritz, H. P. *Angew. Chem. Int. Ed. Engl.* **1983**, *22*, 950.
  54. Lazarov, L.; Nietfeld, G.; Puschmann, K.; Angelov, S.; Stumpp, E. *Fuel* **1984**, *63*, 952.
  55. Preiss, H.; Lunkenheimer, C.; Nissel, U. *Cryst. Res. Technol.* **1986**, *21*, 1199.
  56. Hirsch, P. B. *Proc. Roy. Soc. London, A* **1954**, *226*, 143. See especially pp 155–156.
  57. Blayden, H. E.; Gibson, J.; Riley, H. L. *Proceedings of the Conference on the Ultra-fine Structure of Coals and Cokes*, 1944; pp 176–231.
  58. Blundell, T.; Singh, J.; Thornton, J.; Burley, S. K.; Petsko, G. A. *Science* **1986**, *234*, 1005.
  59. Kitaigorodsky, A. I. *Molecular Crystals and Molecules*; Academic: New York, 1973.
  60. Burley, S. K.; Petsko, G. A. *J. Am. Chem. Soc.* **1986**, *108*, 7995.
  61. Ebert, L. B.; Matty, L. *Synth. Met.* **1982**, *4*, 345.
  62. Lazarov, L.; Stefanova, M.; Petrov, K. *Fuel* **1982**, *61*, 58.
  63. Brooks, J. D.; Spotswood, T. M. In *Proceedings of the Fifth Conference on Carbon*; Pergamon: New York, 1962; pp 416–pl421.
  64. Furdin, G.; Hachim, L.; Guerard, D.; Herold, A. C. R. *Acad. Sci. Ser. C* **1985**, *301*, 579.
  65. De Boer, E.; Gribnau, M. C. M., Chapter 3 in this book.
  66. Enkelmann, V., Chapter 11 in this book.
  67. Clague, A. D. H. *Helv. Phys. Acta* **1985**, *58*, 121.
  68. Estrade-Szwarczopf, H. *Helv. Phys. Acta* **1985**, *58*, 139.
  69. Klinowski, J.; Thomas, J. M. *Endeavour* **1986**, *10*, 2.
  70. Wang, P. K.; Ansermet, J. P.; Rudaz, S. L.; Wang, Z.; Shore, S.; Slichter, C. P.; Sinfelt, J. H. *Science* **1986**, *234*, 35.
  71. Hagaman, E. W.; Chambers, R. R.; Woody, M. C. *Anal. Chem.* **1986**, *58*, 387.
  72. Erbatur, G.; Erbatur, O.; Coban, A.; Davis, M. F.; Maciel, G. E. *Fuel* **1986**, *65*, 1273.
  73. Bax, A. *Two-Dimensional Nuclear Magnetic Resonance in Liquids*; D. Reidel: Dordrecht, 1982.
  74. Bax, A. *J. Mag. Res.* **1984**, *57*, 314.
  75. Menger, E. M.; Vega, S.; Griffen, R. G. *J. Am. Chem. Soc.* **1986**, *108*, 2215.
  76. Ramdahl, T.; Zielinska, B.; Arey, J.; Atkinson, R.; Winner, A. M.; Pitts, J. N. *Nature* **1986**, *321*, 425.
  77. Fetzner, J. C.; Biggs, W. R.; Jinno, K. *Chromatographia* **1986**, *21*, 439.
  78. Williams, P. T.; Bartle, K. D.; Andrews, G. E. *Fuel* **1986**, *65*, 1150.
  79. *Petroleum-Derived Carbons*; Bacha, J. D.; Newman, J. W.; White, J. L., Eds.; ACS Symposium Series 303; American Chemical Society: Washington, D.C., 1986.
  80. Hiraki, A.; Kawakami, Y.; Kawano, T.; Hayashi, M.; Tokumura, M.; Miyasato, T. *Nucl. Instrum. Methods Phys. Res. Sect. B* **1985**, *7/8*, 479.
  81. Tsuda, M.; Nakajima, M.; Oikawa, S. *J. Am. Chem. Soc.* **1986**, *108*, 5780.
  82. Glukhovtsev, M. N.; Simkin, B. Y.; Minkin, V. I. *Russ. Chem. Rev. (Engl. Transl.)* **1985**, *54*, 54.
  83. Rohlfling, E. A.; Cox, D. M.; Kaldor, A. *J. Chem. Phys.* **1984**, *81*, 3322.
  84. Cox, D. M.; Trevor, D. J.; Reichmann, K. C.; Kaldor, A. *J. Am. Chem. Soc.* **1986**, *108*, 2457.
  85. Sivaram, C.; Shah, G. A. *Astrophys. Space Sci.* **1985**, *117*, 199.
  86. Smith, P. P. K.; Buseck, P. R. *Science* **1982**, *216*, 984.
  87. Whittaker, A. G. *Science* **1985**, *229*, 485.

88. Smith, P. P. K.; Buseck, P. R. *Science* **1985**, *229*, 486.
89. Ogilvie, K. W.; Coplan, M. A.; Bochslev, P.; Geiss, J. *Science* **1986**, *232*, 374.
90. Ebert, L. B. In *Proc. Workshop on Electrochemistry of Carbon*; ECS Proc.; Electrochemical Society: Pennington, NJ, 1984; Vol. 84-5, pp 595-607.
91. Wood, B. J.; Sancier, K. M. *Catal. Rev.-Sci. Eng.* **1984**, *26*, 233.
92. Donnet, J. B. *Carbon* **1982**, *20*, 267.
93. Rozploch, F. *High Temp.-High Pressures* **1985**, *17*, 523.
94. Gutsze, A.; Orzesko, S. *Adv. Colloid Interface Sci.* **1985**, *23*, 215.
95. Zander, M. *Fuel* **1986**, *65*, 1019.
96. Fiedler, J.; Huber, W.; Mullen, K. *Angew. Chem. Int. Ed.* **1986**, *25*, 443.
97. Neumann, G.; Mullen, K. *J. Am. Chem. Soc.* **1986**, *108*, 4105.
98. Mullen, K. *Angew. Chem. Int. Ed.* **1987**, *26*, 204.
99. Brown, G. H.; Crooker, P. P. *Chem. Eng. News* **1983**, *61*, 24.
100. Hinov, H. P. *Mol. Cryst. Liq. Cryst.* **1986**, *136*, 221.
101. Levelut, A. M. *J. Phys. Lett.* **1979**, *40*, L-81.
102. Mamlok, L.; Malthete, J.; Tinh, N. H.; Destrade, C.; Levelut, A. M. *J. Phys. Lett.* **1982**, *43*, L-641.
103. Saeva, F. D.; Reyonlds, G. A.; Kaszczuk, L. *J. Am. Chem. Soc.* **1982**, *104*, 3524.
104. Piechocki, C.; Simon, J.; Skoulios, A.; Guillon, D.; Weber, P. *J. Am. Chem. Soc.* **1982**, *104*, 5245.
105. Minas, H.; Murawski, H.-R.; Stegemeyer, H.; Sucrow, W. *J. Chem. Soc., Chem. Commun.* **1982**, 308.
106. Frenkel, D.; Eppenga, R. *Phys. Rev. Lett.* **1982**, *49*, 1089.
107. Safinya, C. R.; Liang, K. S.; Varady, W. A. *Phys. Rev. Lett.* **1984**, *53*, 1172.
108. Safinya, C. R.; Clark, N. A.; Liang, K. S.; Varady, W. A.; Chiang, L. Y. *Mol. Cryst. Liq. Cryst.* **1985**, *123*, 205.
109. Ohta, K.; Takagi, A.; Muroki, H.; Yamamoto, I.; Matsuzaki, K.; Inabe, T.; Maruyama, Y. *J. Chem. Soc., Chem. Commun.* **1986**, 883.
110. Andre, J.-J.; Bernard, M.; Piechocki, C.; Simon, J. *J. Phys. Chem.* **1986**, *90*, 1327.
111. Robertson, J.; O'Reilly, E. P. *Phys. Rev. Lett. B* **1987**, *35*, 2946.
112. Angus, J. C. *Thin Solid Films* **1986**, *142*, 145.
113. Angus, J. C.; Mirtich, M. J.; Wintucky, E. G. In *Metastable Materials Formation by Ion Implantation*; Elsevier: New York, 1982; pp 433-440.
114. Ebert, L. B.; Mills, D. R.; Scanlon, J. C. *Prep. Pap.—Am. Chem. Soc., Div of Petrol. Chem.* **1987**, *32*, 419.
115. Ebert, L. B.; Scanlon, J. C.; Clausen, C. A. *Prep. Pap.—Am. Chem. Soc., Div of Petrol. Chem.* **1987**, *32(3)*, 440.

RECEIVED for review January 19, 1987. ACCEPTED March 11, 1987.

# AUTHOR INDEX

- Bartlett, Neil, 169  
Berkowitz, N., 217  
Chambers, R. Rife, Jr., 255  
Cohen, Yoram, 53  
de Boer, E., 39  
Ebert, Lawrence B., 109,367  
Eisch, John J., 89  
Enkelmann, V., 177  
Fetzer, J. C., 309  
Gonzalez, Richard D., 357  
Gribnau, M. C. M., 39  
Haenel, Matthias, 333  
Hagaman, Edward W., 255  
Herndon, William C., 1,287  
Hum, Georgina P., 155  
Lee, Milton L., 235  
Lewis, I. C., 269  
Milliman, George E., 109  
Mills, Daniel R., 109  
Nagai, Masatoshi, 357  
Nishoika, Masaharu, 235  
Rabideau, Peter W., 73  
Rabinovitz, Mordecai, 53  
Richardson, Thomas J., 169  
Ross, David S., 155  
Sakikawa, Noriyuki, 357  
Scanlon, Joseph C., 109,367  
Schmitt, Robert J., 155  
Schweitzer, Dieter, 333  
Shine, Henry J., 127  
Singer, L. S., 269  
Sorok, Miroslaw, 127  
Speight, James G., 201  
Szentpály, Laszlo v., 287  
Szwarc, Michael, 13  
Tanzella, Francis L., 169  
Uetake, Kazuya, 357  
Urimoto, Hideo, 357  
Woody, Madge C., 255

# AFFILIATION INDEX

- Brigham Young University, 235  
Chevron Research Company, 309  
Exxon Research and Engineering Company,  
109,367  
Indiana University–Purdue University at  
Indianapolis, 73  
Max-Planck-Institut für Kohlenforschung,  
333  
Max-Planck-Institut für Polymerforschung,  
177  
Max-Planck-Institut für medizinische  
Forschung, 333  
Nihon University, 357  
Oak Ridge National Laboratory, 255  
SRI International, 155  
State University of New York at  
Binghamton, 89  
Technical University, 127  
Texas Tech University, 127  
The Hebrew University of Jerusalem, 53  
Tokyo University of Agriculture and  
Technology, 357  
Union Carbide Corporation, 269  
Universidad de Guanajuato, 287  
University of Alberta, 217  
University of California at Berkeley, 169  
University of California at San Diego, 13  
University of Nijmegen, 39  
University of Texas at El Paso, 1,287  
Western Research Institute, 201

# SUBJECT INDEX

## A

Abstraction reactions, energies vs.  
experimental log (relative rates),  
301,303f

Acenes, definition in terms of graphite  
translational periodicity axes, 369  
Aggregation, effect on redox potentials, 16–  
21  
Alkali aromatic pairs, single crystals, 39–51  
Alkali cations, solvation, 23

# AUTHOR INDEX

- Bartlett, Neil, 169  
Berkowitz, N., 217  
Chambers, R. Rife, Jr., 255  
Cohen, Yoram, 53  
de Boer, E., 39  
Ebert, Lawrence B., 109,367  
Eisch, John J., 89  
Enkelmann, V., 177  
Fetzer, J. C., 309  
Gonzalez, Richard D., 357  
Gribnau, M. C. M., 39  
Haenel, Matthias, 333  
Hagaman, Edward W., 255  
Herndon, William C., 1,287  
Hum, Georgina P., 155  
Lee, Milton L., 235  
Lewis, I. C., 269  
Milliman, George E., 109  
Mills, Daniel R., 109  
Nagai, Masatoshi, 357  
Nishoika, Masaharu, 235  
Rabideau, Peter W., 73  
Rabinovitz, Mordecai, 53  
Richardson, Thomas J., 169  
Ross, David S., 155  
Sakikawa, Noriyuki, 357  
Scanlon, Joseph C., 109,367  
Schmitt, Robert J., 155  
Schweitzer, Dieter, 333  
Shine, Henry J., 127  
Singer, L. S., 269  
Sorok, Miroslaw, 127  
Speight, James G., 201  
Szentpály, Laszlo v., 287  
Szwarc, Michael, 13  
Tanzella, Francis L., 169  
Uetake, Kazuya, 357  
Urimoto, Hideo, 357  
Woody, Madge C., 255

# AFFILIATION INDEX

- Brigham Young University, 235  
Chevron Research Company, 309  
Exxon Research and Engineering Company,  
109,367  
Indiana University–Purdue University at  
Indianapolis, 73  
Max-Planck-Institut für Kohlenforschung,  
333  
Max-Planck-Institut für Polymerforschung,  
177  
Max-Planck-Institut für medizinische  
Forschung, 333  
Nihon University, 357  
Oak Ridge National Laboratory, 255  
SRI International, 155  
State University of New York at  
Binghamton, 89  
Technical University, 127  
Texas Tech University, 127  
The Hebrew University of Jerusalem, 53  
Tokyo University of Agriculture and  
Technology, 357  
Union Carbide Corporation, 269  
Universidad de Guanajuato, 287  
University of Alberta, 217  
University of California at Berkeley, 169  
University of California at San Diego, 13  
University of Nijmegen, 39  
University of Texas at El Paso, 1,287  
Western Research Institute, 201

# SUBJECT INDEX

## A

Abstraction reactions, energies vs.  
experimental log (relative rates),  
301,303f

Acenes, definition in terms of graphite  
translational periodicity axes, 369  
Aggregation, effect on redox potentials, 16–  
21  
Alkali aromatic pairs, single crystals, 39–51  
Alkali cations, solvation, 23



- Alkali metal–biphenyl complexes  
 alkali ionic radii, 43,44*t*  
 bond lengths, 43,44*t*  
 characteristics, 40  
 crystallographic data, 41*t*  
 geometry 42,43*t*  
 physical properties, 44,45  
 preparation, 40  
 stereoscopic views of unit cells, 41,42*f*
- Alkyl radicals, H-atom abstraction from the solvent, disproportionation, and recombination, 144,145
- 9-Alkylanthracenes, reduction at the site of substitution, 82,83
- Alkynes  
 mechanistic pathways for oligomerization, 106  
 reaction and oligomerization, 90,99–103  
 trimerization, 89,90
- Amine–arene exciplexes  
 bonding model, 351,352*f*  
 effect of orientation on the electronic interactions, 334,335*f*  
 example compounds, 335,337
- Amino-substituted polycyclic aromatic hydrocarbon, reactions, 245,246
- 2-Aminobiphenyl, identification in solvent-refined coal-heavy distillate, 247
- Aminophenylpyridine, preparation by hydrogenation, 247
- Aminophenylquinoline, preparation by hydrogenation, 247
- Anionic  $\pi$  system, destabilization, 295,296
- Anodic oxidation, aromatic compounds, 138
- Anthracene  
 carbonization, 273–277  
 dimers, 273,274  
 metal–ammonia reduction, 78  
 reaction with sodium and ammonia, 74–75  
 reductive alkylation, 76*t*
- Anthracene dianion,  $^1\text{H}$  NMR spectrum 55,60*f*
- Anthracene-derived carbons, average structures, 277,278*f*
- Anthracene-derived pitch  
 carbonization, 275,277*f*  
 components, 275  
 H–C ratio vs. heat-treatment temperature, 277*f*  
 mass spectrum, 275  
 molecular weight distribution, 274,275*f*  
 possible species, 274,275  
 proposed structures for oligomeric molecular species, 275,276  
 proposed structures for rearrangement products, 275,276  
 spin concentrations vs. heat-treatment temperature, 280,281*f*
- Anthracenopyridinophanes  
 bonding model, 351,352*f*  
 calculated spin densities, 351,352*t*  
 fluorescence, 351
- Anthryl radical, formation by disproportionation reaction, 273
- Antiaromatic species, definition, 55
- Antiaromaticity, definition, 53,54
- Arene excimers, effect of orientation on the electronic interactions, 334,335*f*
- Arene radical cation, intermediate in N(IV) nitration of pyrene, 162
- Arene-to-counterion ratio, for electrocrystallization, 178,179
- Arenes, electronic interactions, 333,334*f*
- Aromatic anions, protonation and rehybridization, 374
- Aromatic carbon–carbon ratio  
 data scatter problems, 219,221  
 vs. atomic H–C ratios, 219,220*f*  
 vs. carbon contents, 219,220*f*
- Aromatic cation radical, coupling with neutral radicals, 127
- Aromatic compounds  
 anodic oxidation, 138  
 elimination of  $\text{F}^+$ , 175,176  
 nitration, 155
- Aromatic hydrocarbons  
 electron affinities, 13–16  
 electron capture reduction, 13  
 origination of term, 367  
 relationship to carbonaceous materials, 367–379
- Aromatic nitration  
 coupling reaction, 135  
 in gas phase, 137,138  
 in solution, 132–137  
 role of charge-transfer complexes, 132
- Aromatic rings  
 bond cleavage, 85  
 coupling with lithium reagents, 103,104  
 coupling with nickel(0) reagents, 104,105  
 dimerization, 83,84
- Aromatic substitution reactions, role of charge-transfer complexes, 132
- Aromatic systems, occurrence in petroleum, 201
- Aromatic triterpanes, condensation reactions, 251
- Aromaticity  
 calculated vs. experimental plot, 297,301*f*  
 characterization by electrophilic substitution, 296  
 definition, 53,54  
 values, 296–299*t*
- Aromatics, component of petroleum, 202,203*f*
- Aryl–aryl bonds, cleavage, 85
- Aryl–benzyl bonds, cleavage, 85
- Aryl-substituted cyclobutadienes, dimerization, 105
- Asphaltenes, 211  
 aromatic molecular types of products from thermal decomposition, 208*t*  
 average-structure, 203,204  
 component of petroleum, 202,203*f*  
 definition, 207,208  
 distribution of aromatic and nonaromatic species, 209*t*  
 formation of coke precursor and volatile products, 209,210  
 fractionation, 205,207

- Asphaltenes—*Continued*  
 heteroatom types, 213  
 high-performance liquid chromatograms, 210,211f  
 hypothetical structure, 211–213  
 physical properties, 206,207  
 relative intensities of the subfraction peaks, 211,212t  
 representation on the basis of size and polarity, 204,206f  
 separation, 204,205  
 spectroscopic techniques, 206  
 subfractionation, 205–207  
 UV spectrum, 210
- Autocatalytic hydrogenation, mild, of coal-derived materials, 245
- Average coal macromolecule, structural elucidation, 217
- Average-structure models of coal  
 advantages, 224,225  
 bituminous coal, 221,223  
 characteristics, 224,225  
 development, 221  
 disadvantages, 225–227  
 effect of coal processing, 226  
 hypothetical molecule containing 82% C, 221,222  
 vitrains, 221–225

## B

- Base hydrolysis, procedure, 257,258
- 7*H*-Benz[*de*]anthracen-7-one, structures, 313
- 3*H*-Benz[*de*]anthryl radical, structure, 282
- Benzene  
 reaction with C<sub>6</sub>F<sub>6</sub>AsF<sub>6</sub>, 170,171  
 reaction with O<sub>2</sub>AsF<sub>6</sub>, 170
- Benzenoid compounds, examples of nonplanarities, 5,6
- 3*H*-Benz[*f,g*]naphthacenyl radical, structure, 282
- Benzofluoranthene isomers  
 abundancies in coal tar, 248  
 order of Hückel π-electron energies, 248
- 6*H*-Benzofgnaphthacen-6-one, structures, 313
- Benzonaphthothiophenes  
 desulfurization products, 360  
 desulfurization rates, 361
- Benzo[*b*]naphtho[1,2-*d*]thiophene,  
 desulfurization, 359
- Benzo[*b*]naphtho[2-*d*]thiophene,  
 desulfurization, 359
- Benzo[*c*]phenanthrene, structure, 4
- 6*H*-Benzo[*de*]pyren-6-one, structures, 313
- 2*H*-Benzo[*cd*]pyrenyl radical  
 ENDOR spectrum, 282,283f  
 structure, 282
- Benzyl-benzyl bonds, cleavage, 85
- 1,1'-Binaphthyl, cyclization, 96
- Biphenyl, reductive alkylation, 75,76t
- 4-Biphenylcarboxylic acid, reduction, 80,81
- Biphenylene, dimerization, 105

- 2-(2-Biphenyl)-1,1-diphenylethene,  
 cyclization, 97
- Birch reduction  
 description, 73  
 pathway, 77
- Bis(5-hexenyl)mercury  
 preparation, 130,131  
 reaction with sulfonium ion perchlorate, 131,132
- Bis(naphthalene) salts, preparation, 169,170
- Bituminous coal  
 average-structure models, 221,223  
 reaction with metal chlorides, 377
- Bond cleavage of aromatic rings, pathway, 85
- Born-Haber cycle for the formation of the carbon-metal bond, schematic, 91f
- Buckminsterfullerene  
 electronic properties, 9  
 formation mechanism, 9,10  
 Hückel calculations, 9  
 structure, 8
- tert*-Butyllithium, catalyst for reductive dimerization, 92
- tert*-Butylmagnesium chloride, reaction with sulfonium ion perchlorate, 142t,144
- tert*-Butylphenylacetylene  
 metal reaction products, 100–102  
 reductive dimerization, 94

## C

- C<sub>8</sub>K  
 Debye-Scherrer X-ray diffraction photography, 373f  
 formation from calcined petroleum coke, 373,374  
 formation from metaanthracite coal, 370,372,373  
 made from graphite, reaction with water, 375  
 made from petroleum coke, reaction with water, 375,376
- C<sub>60</sub> cluster, structure, 7
- Calcined petroleum coke, components, 376,377
- Carbocyclic dianions, HOMO-LUMO energy gap vs. <sup>1</sup>H NMR line shape, 61–65
- Carbon-atom clusters  
 formation, 7,9,10  
 properties, 7,8
- Carbon-carbon bond  
 formation mediated by lithium metal, 103,104  
 organolithium compounds as electron-transfer agents in formation, 104
- Carbon-metal bond, Born-Haber cycle for the single-electron transfer response, 93f
- Carbonaceous materials  
 future research, 378,379  
 oxidation, 377,378

- Carbonaceous materials—*Continued*  
 reduction, 370–377  
 relationship to polynuclear aromatic hydrocarbons, 367–379
- Carbonization  
 anthracene, 273–277  
 chemistry, 269  
 naphthalene, 277–280
- Carbonization of polynuclear aromatic compounds, role of free radicals, 280–283
- Catalytic trimerization, diphenylacetylene, 98
- Cation radicals coupled with neutral radicals, isomer distribution vs. products, 136,137
- Charge-transfer complexes  
 effect of orientation on the electronic interactions, 334,335f  
 role in electrophilic aromatic substitution, 132  
 role in nitration, 132,133
- Chrysene, preparation, 247
- Coal  
 anomalous rank effects, 227–229  
 average-structure models, 221–227  
 bromination, 228  
 carbon skeleton, 256  
 description of low-volatile bituminous sample, 257  
 diamagnetic susceptibility, 228  
 effects of coal rank on liquefaction yields, 228,229  
 evidence for basic carbon framework, 255  
 reduced molar volume, 227,228  
 sources of structural information, 218
- Coal aromaticity, definition, 218
- Coal tar  
 elemental analysis, 236,237  
 quantitative comparisons of polycyclic aromatic compounds, 237–244t  
 reactions of polycyclic aromatic compounds containing functional groups, 245,246  
 structural similarities of polycyclic aromatic compounds, 248,249
- Coal-derived materials  
 characterization, 236  
 identification of polycyclic aromatic compounds, 236
- Coke, definition, 270
- Complete neglect of differential overlap method  
 correlation coefficients, 291–293t  
 quantum chemical measurements, 288
- Compounds, proposed sequence, 282,283
- Concentration factors, determination, 130
- Condensed polycyclic benzenoid aromatic hydrocarbons, description, 3
- Conducting polymers  
 analogy of the packing, 196f,197  
 radical-cation salts as models, 196–199
- Connectivity, determination, 111,112
- Contact ion pairs  
 definition, 15
- Contact ion pairs—*Continued*  
 discussion, 39  
 example, 50f,51
- Corannulene, description, 7
- Coronene  
 chemistry, 377  
 H<sup>+</sup> elimination, 176  
 IR spectra, 171,172f  
 oxidation, 170,175,176  
 oxidation with AsF<sub>6</sub>, 172  
 oxidation with excess C<sub>6</sub>F<sub>6</sub>AsF<sub>6</sub>, 171,172  
 oxidation with O<sub>2</sub>AsF<sub>6</sub>, 171
- Coronene salts, X-ray powder diffraction data, 172,173
- Coulombic energy, gain, 25
- Coulombic parameter, calculation, 294
- CrO<sub>3</sub> adduct, oxidative intercalation, 378
- Crystal structures  
 molecular overlap, 183,186f  
 projections, 183–185f
- Cyanide ion  
 low oxidation potential, 138  
 reaction, 138
- Cyclization, 1,1'-binaphthyl, 96  
 2-(2-biphenyl)-1,1-diphenylethene, 97  
*o*-diphenylbenzene, 96
- Cyclocoupling dehydrogenation, model reactions, 250
- Cyclooctatetraene, preparation of single crystals, 41
- Cyclopenta-containing compounds  
 hydrogenation, 245  
 identification in solvent-refined coal heavy distillate, 245
- Cyclopentylmethylsulfonium salt, preparation and characterization, 143
- Cyclophanes  
 structures, 335–337  
 synthesis, 337
- Cyclopropyltriphenylsilane, reductive dimerization, 96,97

## D

- Decacycene  
 reductive methylation, 118,119  
 structures of products, 119
- Desulfurization  
 benzonaphthothiophenes, 360,361  
 dibenzothiophene, 360f  
 experimental procedures, 358,359  
 thiophene, 358  
 vs.  $\pi$ -electron density of sulfur atoms, 361,362,364f,365
- Diagenesis, definition, 250
- 9,10-Dialkylanthracenes, reduction, 80
- Diamagnetic susceptibility, description, 228
- Dianions  
 equilibrium with neutral precursors, 74–76t  
 irreversible protonation, 75,76
- Dianions from nonplanar aromatic compounds, properties, 7

- Diazine  $4n$   $\pi$  dianions, paratropicity, 66
- Dibenzocyclooctatetraene, equilibrium with neutral precursors, 75
- Dibenzodioxin, reaction with nitrating agents, 136,137
- Dibenzonickelole-bis(triethylphosphine), isolation, 98
- Dibenzothiophene  
changes in desulfurization vs. time, 360f  
desulfurization, 359  
effect of catalyst-dibenzothiophene ratio on rate of desulfurization, 360,361t
- Dibenzothiophene chemistry, reductive alkylation, 120,121
- Dibenzoa,cnaphthacene dianion,  $^1\text{H}$  NMR spectrum, 68f,69
- Dibenzoc,dphenanthrene, structure, 4,5
- Dibutylmercury, reaction with sulfonium ion perchlorate, 145-149
- Dimerization, of unstable radical anions, 34-36f
- Dimerization of aromatic rings, pathway, 83,84
- 1,2-Dimethoxyethane, effect of aggregation on redox potentials, 17,18f
- Dimethylmercury, reaction with perylene cation radical, 149,150
- 1,4-Dimethylnaphthalene, predominant isomer, 134
- 2,6-Dimethylnaphthalene, crystal structure of radical-cation salt, 191-193
- $^{13,14}\text{C}_2$ Dimethyl sulfate, preparation, 256-257
- Diphenylacetylene  
catalytic trimerization, 98  
competitive cyclizing and noncyclizing dimerizations, 96  
cyclizing dimerization, 95  
long-term interaction with lithium, 96  
metal reaction products, 100-102  
noncyclizing dimerization, 95,96  
reductive dimerization, 92
- o*-Diphenylbenzene, cyclization, 96
- 1,1-Diphenylethene, relative electron affinity, 34-36f
- 1,4-Diphenylphthalazine dianion,  $^1\text{H}$  NMR spectrum 55,59f
- 2,3-Diphenylquinoxaline dianion,  $^1\text{H}$  NMR spectrum 55,59f
- Discotic liquids crystals, description, 379
- Disproportionation  
endothermicity, 19,20  
equilibrium reactions, 18  
equilibrium constants, 19,20f  
kinetics, 27-32  
mechanism, 28-32  
temperature dependence, 19,21f  
thermodynamics, 21-26
- Disproportionation constant  
relationship to size of aromatic hydrocarbon, 25,26f  
techniques for determination, 25,26
- 2,3-Di-*p*-tolylbenzogquinoxaline dianion,  $^1\text{H}$  NMR spectrum, 69,70f
- Double-labeled dimethyl sulfate, *o*-methylation of bituminous coal, 258,259
- Doubly charged carbocyclic systems as disodium salts, spectral patterns and HOMO-LUMO energy gaps, 55,56t
- Doubly charged heterocyclic systems as disodium salts, spectral patterns and HOMO-LUMO energy gaps, 55,57t
- Drude model, metallic nature of radical-cation salts, 195
- Durene, nitration, 135

## E

- Electrocrystallization of radical-cation salts  
crystal formation, 177,178f  
effect of experimental conditions, 178-181t
- Electron affinity  
aromatic hydrocarbons, determination, 13  
1,1-diphenylethene, 35
- Electron capture  
aromatic hydrocarbons, 13  
plasma studies, 31  
primary products, 31
- Electron spin resonance spectrum of phenanthrene dianion, 55,56,62f
- Electron spin resonance techniques, disproportionation constant determination, 26
- Electron transfer between an organic substrate and a metal  
effect of ionization potential, 92  
influencing factors, 90,91  
state of metal, 91,92
- Electron transfer of cation radicals with neutral radicals  
free energies, 150,151t  
reorganization energies, 150
- Electronic absorption spectra,  
naphthalenophanes, 339,340f
- Electronic interactions, effect of orientation, 334,335f
- Electronic structure calculations, thiophene, 361,362t,363
- Electrophilic aromatic substitution  
reactions, 127-128  
role of charge-transfer complexes, 132
- Electrophilic attack of polynuclear aromatic hydrocarbons by nitrosated nitrogen tetroxide, reaction, 156
- Electrophilic displacement, pathway, 148,149
- Electrophilic substitution  
characterization of aromaticity, 296  
rate-determining step, 296
- Ethyl 9-anthrate, sodium-ammonia reduction, 84
- Ethyl radicals, scavenging, 139
- Excimers, definitions, 334
- Exciplexes, definition, 334
- Extraction, polycyclic aromatic hydrocarbons, 314,315

## F

- Flash photolysis  
description for disproportionation kinetics, 27  
of barium ion–naphthacene ion, 31  
of *trans*- and *cis*-stilbene, 32–34f  
study of electron capture, 31,32
- Fluoranthene, electrocrystallization, 178
- Fluoranthene salts  
crystal structure, 179,182f,183  
electrocrystallization, 179  
structural phase transitions, 183–186f
- [2.2](2,7)Fluorenophane  
fluorescence, 346–347  
molecular structure, 346,347f  
phosphorescence, 346–347
- Fluorenyllithium, use in *C*-methylation of coal, 262–264
- Fluorescence  
naphthalenophanes, 340–344  
[2.2](2,7)fluorenophane, 346  
[2]naphthaleno[2]paracyclophanes, 344,346
- Fluorescence excitation–emission, use in PAH analysis, 310,311
- Fossil-fuel structures, chemistry, 124
- Fourier transform–IR spectroscopy, analysis of coal structure, 219
- Free energies of electron transfer, calculations, 150,151t
- Free radicals, role in carbonization of polynuclear aromatic compounds, 280–283
- Free-electron molecular orbital model, description, 289
- Free-electron–nonbonding molecular orbital coefficients of  $\pi$  radicals, 291,292  
unnormalized amplitudes, 291
- Free-energy compensation, for metal–hydrocarbon adduct, 91
- Free-radical mechanisms of the carbonization of polynuclear aromatic compounds, stages, 282
- Frontier electron densities, polynuclear thiophenes, 361,362t

## G

- Gas-phase coupling of cation radicals with neutral radicals, reactions, 137,138
- Graphite  
chemistry, 123,124  
formation, 270  
rehybridization, 374
- Graphite as a polynuclear aromatic hydrocarbon  
electron-transfer reactivity, 368  
interrelation between molecular reactivity and translational periodicity, 368  
translational symmetry elements, 368,369f
- Graphite intercalation compound  $C_8K$   
formation, 370  
sketch of Debye–Scherrer X-ray diffraction photograph, 370–372f

- Graphite intercalation compound  $C_8K$ —*Continued*  
variable-temperature X-ray diffraction data, 371f
- Grignard reagents, reaction with sulfonium ion perchlorate, 140–145

## H

- $H^+$  elimination, coronene, 176
- Helicenes, description, 7
- Heteroatom-containing compounds, cyclocoupling dehydrogenations, 251
- Heterocyclic dianions, HOMO–LUMO energy gaps vs.  $^1H$  NMR line shape, 65,66f
- Hexafluorobenzenehexafluoroarsenate, oxidizing power, 169
- Hexafluorobenzenehexafluoroarsenate(V), oxidizing agent, 173,174
- High-performance liquid chromatography, limitations in PAH analysis, 310
- High-resolution NMR spectroscopy, analysis of coal structure, 219
- HOMO–LUMO energy gaps  
relationships to line shapes for  $4n$   $\pi$ -conjugated polycyclic anions, 55–57t  
vs.  $^1H$  NMR line shape for carbocyclic dianions, 61–65  
vs.  $^1H$  NMR line shape for heterocyclic dianions, 65,66f  
vs. paratropic shifts, 56–71
- Hückel molecular orbital calculations  
correlation coefficients, 291–293t  
description, 298  
quantum chemical measurements, 288
- Hückel's rule, definition of aromaticity, 54
- Humic coals, difference from sapropelic coals, 227
- Hydrocarbon products, formation, 143,144
- Hydrodesulfurization, thiophenes, 358
- Hydroxy-substituted polycyclic aromatic hydrocarbons, reactions, 245,246
- Hydroxy-substituted polycyclic aromatic sulfur heterocycles, reactions, 245,246

## I

- Ion pair solution, forms, 39
- Ion pairs, definition, 15
- IR spectral analysis of coal structure, 219
- Isolation, organonickel intermediates, 98,99
- Isomerization  
methylphenylacetylene, 95  
unstable radical anions, 32,34f

## K

- $K_{\pm}$ , determination for ion pairs, 17
- Ketones, reduction via electron transfer, 92,93

- Kinetics of disproportionation  
 difference spectrum of flash photolysis,  
 27,28*f*  
 rate constants, 27,29*t*  
 reactions, 27  
 Korringa relation, definition, 194

## L

- Liquefaction yields, effects of coal rank,  
 228,229  
 Lithium ion, solvation, 23  
 Lithium metal  
 carbon-carbon bond formation, 103,104  
 examples of reactions, 94-97  
 reaction products and organometallic  
 intermediates, 99  
 Lithium reagents, coupling of aromatic  
 rings, 103  
 Localization energy  
 calculated vs. experimental plot, 297,300*f*  
 definition, 296  
 values, 296-299*t*  
 Loose ion pairs, *See* Solvent-separated ion  
 pairs, 17  
 Low-valent transition metals  
 disruption of aromatic systems, 89,90  
 formation of aromatic systems, 89,90  
 reaction with aromatic nuclei, 89  
 Low-volatile bituminous coal  
 C-methylation, 261-267  
 O-methylation, 258,259*t*,261  
 pyridine extraction, 264*t*,265  
 sites of alkylation, 265,266

## M

- Mass spectrometry, limitations in PAH  
 analysis, 310  
 Measurement methods, 288,289  
 Mechanism of disproportionation  
 flash photolysis of barium ion-  
 naphthacene ion, 31  
 reaction of sodium salt of naphthacene  
 dianions with naphthacene, 28-30*f*  
 Mesitylene, nitration, 135  
 Mesophase pitch, development, 271,272*f*  
 Metal-ammonia reduction  
 conditions, 78  
 effect of reaction conditions, 81,82  
 effect of substituents, 80,81  
 pathway, 77  
 prediction of products, 78-80  
 reduction at the substitution site, 82,83  
 C-Methylation, procedure, 258  
 C-Methylation of bituminous coal  
<sup>13</sup>C CP/MAS NMR spectrum,  
 265,266*f*,267  
 covalent attachment of the carbonion  
 bases, 261-262  
 distribution of acidic C-H sites,  
 262,263*t*,264  
 extent of <sup>14</sup>C incorporation, 261

- C-Methylation of bituminous coal—  
*Continued*  
 mechanism, 261  
 number of treatments, 263,264  
 physical and chemical changes, 264,265  
 sites of methylation, 265,266  
 O-Methylation, procedure, 257  
 O-Methylation of bituminous coal  
 approaches, 258,259  
<sup>14</sup>C combustion data, 259*t*  
 criteria, 258  
 pH dependency, 259,260  
 resonance envelope, 260  
 3-Methylbiphenyl, reduction, 81  
 Methyl groups in chemically modified coals  
 effect of local environment on <sup>13</sup>C NMR  
 response, 260  
 resonance envelope, 260  
 Methylnaphthalene cation radicals  
 nitration, 133*t*,134  
 predominant isomer, 134*t*,135  
 Methylphenylacetylene  
 metal reaction products, 100-102  
 reductive dimerization and isomerization,  
 95  
 Micrinites, plasticity, 228  
 Modified free-electron molecular orbital  
 method, quantum chemical  
 measurements, 288  
 Molecular overlap pattern, pyrene radical-  
 cation salts, 188,190*f*,191  
 Molecular symmetry and reactivity with  
 final structure, 369

## N

- N(IV) nitration of pyrene  
 cell effect, 160,161  
 effect of NO, 161*t*,162  
 effect of oxygen, 161*t*,162*f*  
 effect of headspace on nitropyrene yields,  
 163  
 evidence, 163,164  
 kinetic runs, 158  
 rate algebra, 164,165*f*  
 reaction mechanisms, 164,165  
 reaction order determination, 158,160*f*  
 reaction rate, 162,163  
 reaction scheme, 64  
 stoichiometry, 163  
 N(V) nitration, role, 158,159*f*  
 Naphthacene dianion, <sup>1</sup>H NMR spectrum  
 55,58*f*  
 Naphthalene  
 alkali-metal reduction, 84  
 carbonization, 277-280  
 effect of reaction conditions on reduction,  
 81,82  
 effect of substituents on reduction, 80,81  
 nitration, 133*t*,134  
 perylene reduction, 117,118  
 proposed mechanism for the formation of  
 stable  $\pi$  radicals, 282,283  
 reaction with excess AsF<sub>6</sub>, 171  
 reductive alkylation, 76*t*

- Naphthalene cation radicals, predominant isomer, 134*t*,135
- Naphthalene dianion, HOMO–LUMO energy gap, vs.  $^1\text{H}$  NMR line shape, 65,66
- Naphthalene-derived pitch  
 H–C ratio vs. heat-treatment temperature, 277*f*  
 mass spectrum, 279*f*  
 molecular weight distribution, 277–279  
 proposed structures for molecular species, 279,280  
 spin concentrations vs. heat-treatment temperature, 280,281*f*
- [2]Naphthaleno[2]paracyclophanes  
 fluorescence, 344,346  
 molecular structure, 344,345*f*  
 phosphorescence, 344,346
- Naphthalenophanes  
 electronic absorption spectra, 339,340*f*  
 emission spectra, 340–344  
 excited triplet state, 342  
 molecular structures, 338*f*,339  
 stereoisomers, 338
- Naphthalenopyridinophanes  
 calculated spin densities, 351,352*t*  
 fluorescence, 348,350*f*,351  
 molecular structures, 347,348*f*  
 UV spectra, 348,349*f*
- New polycyclic aromatic hydrocarbons  
 absorbance spectra, 321,322*f*,324  
 elution behavior, 321*f*  
 IUPAC names, 315,317  
 maximum absorbances, 319,320*t*  
 relative retention vs. dichloromethane concentration, 324*f*,326  
 relative retentions, 319,320*t*  
 reverse-phase chromatograms, 323*f*,325  
 separation by shape, 326,331  
 shallowness factors, 319,320*t*  
 structural assignments, 315  
 structures, 315,316  
 UV–visible spectra, 326–330*f*  
 yields, 315,317
- Nickel(0) complexes  
 coupling of aromatic rings, 104–106  
 examples of reactions, 97–99
- Nitration, naphthalenes, 133*t*,134
- Nitration of polynuclear aromatic hydrocarbons, electron transfer, 155,156
- Nitration of pyrene by N(IV)  
 degrees of N(IV) dissociation, 157  
 dissociation constant for N(IV), 157,158
- Nitration of pyrene in methylene chloride, comparison of N(IV) and N(V), 158, 159*f*
- Nitric acid, role in nitration, 158,159*f*
- Nitrogen(IV), reaction with polynuclear aromatic hydrocarbons, 156
- $^{13}\text{C}$  NMR spectroscopy, measurements, 258
- $^1\text{H}$  NMR line shape  
 vs. HOMO–LUMO energy gaps for carbocyclic dianions, 61–65  
 vs.  $^1\text{H}$  NMR line shape for heterocyclic dianions, 65,66*f*
- $^1\text{H}$  NMR line shapes, of  $4n$   $\pi$  carbocyclic and heterocyclic dianions, 55–62
- $^1\text{H}$  NMR paratropic shifts  
 calculation, 58–60  
 vs. HOMO–LUMO energy gap, 56,58,63*t*,64*f*
- Nuclear Overhauser effect  
 measurement, 111  
 for proton connectivity  
 irradiation of methine C–H, 114  
 irradiation of methyl singlet at  $\delta$  1.42, 114  
 irradiation of the methyl doublet at  $\delta$  0.79, 115,116  
 irradiation of the  $\delta$  6.52 olefinic resonance, 114
- ## O
- Octafluoronaphthalenehexafluoroarsenate  
 preparation, 174  
 reactions, 174,175
- Odd–alternate polynuclear aromatic hydrocarbon radicals, formation of phenalenyl radical, 281,282
- Olefinic cation radicals, reaction with triplet oxygen, 139
- Oligomerization of alkynes, mechanistic pathways, 105,106
- Organic metals, crystal structures of radical–cation salts, 193
- Organolithium compounds, electron-transfer agents in carbon–carbon bond formation, 104
- Organometallic processes, electron transfers, 93
- Organonickel intermediates, isolation, 98
- Oxidation of carbonaceous solids  
 bituminous coal, 377  
 stacking, 377,378
- Oxidized poly(*p*-phenylene), IR spectrum, 170,171
- ## P
- Paraquat cation radical, scavenging of alkoxy radicals, 138
- Paratropic shift, HOMO–LUMO energy gap, 70,71
- Paratropicity  
 influencing factors, 54  
 vs. structure, 68–70  
 vs. topology, 67*f*–69
- Peropyrenes, synthesis, 311
- Perturbational molecular orbital method  
 correlation coefficients, 291–293*t*  
 quantum chemical measurements, 288
- Perturbational variant of the free-electron molecular orbital model  
 assumptions, 290  
 correlation coefficients, 291–293*t*  
 development, 289

- Perturbational variant of the free-electron molecular orbital model—*Continued*  
 energy of odd PAH ionic  $\pi$  system, 294,295  
 formation of arylmethyl cation, 295  
 HMO $\omega$  calculations, 292,294  
 implementation, 290,291  
 localization energies, 296–299*t*  
 $\pi$  energy calculation, 290  
 resonance integrals, 289
- Perylene, structures of products, 119,120*f*
- Perylene cation radical, reaction with dimethylmercury, 149,150
- Perylene chemistry, <sup>1</sup>H-NMR product of reductive methylation, 112,113*f*  
 conventional numbering scheme for the protons, 112,114*f*  
 formation of C-1/C-q isomer of dimethyldihydroperylene, 113  
 formation of C-3/C-q isomer of dimethyldihydroperylene, 112,113  
 liquid-state <sup>13</sup>C NMR of enriched materials, 116  
 liquid-state <sup>13</sup>C NMR of other materials, 117  
 NOE approach, 113–116  
 reduction in the presence of naphthalene, 117,118  
 regioisomers, 112,113  
 second-moment NMR analysis, 116
- Petroleum  
 boiling point vs. carbon number for constituents, 202,203*f*  
 representation as a map of the various molecular types, 203–205*f*  
 separation into four fractions, 202
- pH 12 *o*-methylation, procedure, 257  
 pH 7 *o*-methylation, procedure, 257
- 1-Phenalenone, structures, 313
- Phenalenyl radical  
 formation, 281,282  
 stability, 282
- Phenancenes, definition in terms of graphite translational periodicity axes, 369
- Phenanthrazine dianion  
 effect of temperature on <sup>1</sup>H NMR spectra, 66*f*  
 vs. <sup>1</sup>H NMR line shape, 66*f*,67
- Phenanthrene, preparation, 247
- Phenanthrene dianion  
<sup>1</sup>H NMR spectrum 55,61*f*  
 ESR spectrum, 55,56,62*f*
- Phenothiazine  
 nitration, 136  
 oxidation, 136  
 ring contraction, 98
- Phenoxathiin, ring contraction, 98
- Phenyl radicals, trapping, 140
- Phenylation, energies vs. experimental log (relative rates), 303,304*f*
- 9-Phenylfluorenyllithium, use in C-methylation of coal, 262–264
- Phosphorescence  
 [2.2](2,7)fluorenohane, 346  
 naphthalenophanes, 340–344  
 [2]naphthaleno[2]paracyclophanes, 344,346
- Photodiode array detectors, use in PAH analysis, 310,311
- $\pi$  energy  
 calculation, 290  
 first-order change, 290,291
- $\pi$ -electron densities, thiophenes, 361–363
- $\pi$ -electron density of sulfur atoms vs. desulfurization, 361,362,364*f*,365
- Picene, structure, 6
- Pitches  
 definition, 270,271  
 glass transition temperature determination, 271*f*  
 unique properties, 271
- Planar, fused-ring systems, coplanar stacking, 175
- Planarity  
 effect of shape and size of aromatic halves, 320  
 effect of solvent composition, 320,321*f*
- Platt's peripheral model, definition of aromaticity, 54
- Poly(*p*-phenylene)  
 crystal model for radical-cation salt, 197,199*f*  
 preparation, 175
- Polybenzenoid dianions  
 HOMO–LUMO energy gaps, 56,58,63*t*  
 structures, 58
- Polybenzenoid systems, representatives of antiaromatic systems, 55
- Polycyclic aromatic carbons, comparative trends in preferred structures
- Polycyclic aromatic compounds  
 abbreviations of compounds, 237  
 identification in coal-derived materials, 236  
 nonplanarity, 4–6  
 quantitative comparisons in coal-derived materials, 237–244*t*  
 structural similarities in coal-derived materials, 248,249
- Polycyclic aromatic hydrocarbon analysis  
 elution, 312  
 limitations, 310,311  
 previous findings, 311,312  
 retention time, 311  
 steric strain, 311,312
- Polycyclic aromatic hydrocarbons, 246, 247  
 absorbance spectra, 321,322*f*,324  
 characteristics, 309  
 chromatographic behaviors, 312  
 elution behavior, 321*f*  
 extraction and separation, 314,315  
 influencing factors, 247  
 isolation of new compounds, 315–319  
 IUPAC names, 315–319  
 maximum absorbance, 319,320*t*  
 partial rate data, 301,302*t*  
 radical abstraction and addition reactions, 300,301  
 relative retention vs. dichloromethane concentration, 324*f*,326  
 relative retentions, 319,320*t*  
 reverse-phase chromatograms, 323*f*,325



## Polycyclic aromatic hydrocarbons—

*Continued*

- separation by shape, 326,331  
 shallowness factors, 319,320*t*  
 spectral behaviors, 312  
 structural dependence of mutagenicity  
 and carcinogenicity, 309,310  
 structures, 315,318  
 synthesis, 313,314  
 types, 312
- Polycyclic aromatic oxygen heterocycles,  
 cyclocoupling dehydrogenations,  
 251
- Polycyclic benzenoid aromatic hydrocarbons,  
 quantum chemical structure–reactivity,  
 287–304
- Polycyclic benzenoid ribbons, structure,  
 4
- Polyhedral three-dimensional aromatic  
 hydrocarbons  
 formation, 7,9,10  
 properties, 7,8
- Polymorphism, pyrene radical–cation salts,  
 183,186–191
- Polynuclear aromatic compound–alkali metal  
 solutions, preparation, 73,74
- Polynuclear aromatic compounds  
 chemistry, 1,2  
 effect of substituents, 80  
 prototype substructure, 1  
 pyrolysis studies, 272–280  
 thermal reaction studies, 269,270
- Polynuclear aromatic hydrocarbon radical  
 cations  
 electrophilic attack, 156–167  
 reaction with N(IV), 156
- Polynuclear aromatic hydrocarbons  
 nitration, 155  
 transformation to graphite and carbon,  
 270
- Polynuclear aromatic mixtures, interactions,  
 271,272
- Polynuclear aromatic systems in asphaltenes  
 distribution of species, 209*t*  
 formation of coke precursor and volatile  
 products, 209,210  
 high-performance liquid chromatograms,  
 210,211*f*  
 hypothetical structure, 211,213  
 molecular types, 208*t*,209  
 relative intensities of subfractionation  
 peaks, 210,212*t*  
 UV spectrum, 210
- Potassium–biphenyl–tetraglyme  
 alkali ionic radii, 43,44*t*  
 bond lengths, 43,44*t*  
 crystallographic data, 41*t*  
 formation, 40  
 geometry, 42,43*t*  
 physical properties, 44,45  
 stereoscopic view of unit cell, 41,42*f*
- Potassium–cyclooctatetraene–diglyme  
 crystal structure, 45,46*f*  
 crystallographic data, 45,46*t*  
 ESR spectrum, 45,47–49*f*  
 spin-density distribution and molecular  
 orientation, 45
- Potentiometric determination of electron  
 affinity  
 apparatus, 14,15*f*  
 determination of equilibrium constant,  
 17  
 titration curve, 14,16*f*
- Potentiometric or polarographic techniques,  
 disproportionation constant  
 determination, 25,26
- Pyrene  
 formation of polynitropyrenes, 166  
 N(IV) nitration, 158,160*f*,161  
 nitration, 135,157–167
- Pyrene excimer,  $\pi$ – $\pi$  interaction, 334
- Pyrene radical–cation salts  
 crystal structure, 186,188,189*f*  
 crystallographic data, 186,188*t*  
 molecular overlaps, 188,190*f*,191  
 polymorphism, 183,186–191  
 projection for  $\text{Py}_2\text{AsF}_6$ , 191*f*  
 rotation photographs, 186,188*f*
- Pyrene– $\text{N}_2\text{O}_4$  donor–accepted complex  
 formation, 164  
 observed rate constant, 164  
 rate constant vs. concentration of N(IV),  
 164,165*f*
- Pyridine cation radical, reactions, 139
- Pyridine extraction, low-volatile bituminous  
 coal, 264*t*,265
- Pyrolysis, polynuclear aromatic compounds  
 272–280

## Q

- Quantum theoretical characterization,  
 applications, 287,288
- Quarterary carbon, site of reductive  
 alkylation, 121–124
- Quaterphenyl  
 crystal structure of radical–cation salt,  
 197,198*f*  
 valence bond forms, 197

## R

- Radical abstraction and addition reactions  
 energies vs. rates, 301,303,304*f*  
 partial rate data, 301,302*t*  
 reactions, 300
- Radical anions  
 equilibrium with neutral precursors, 74  
 metal–ammonia reduction, 77  
 unstable, *See* Unstable radical anions
- Radical displacement, pathway, 149
- Radical–cation salt of 2-dimethylnaphthalene  
 crystal structure, 191,192*f*  
 molecular overlap, 192,193*f*
- Radical–cation salts  
 analogy of the packing, 196*f*,197  
 chemical syntheses by electron oxidation  
 of neutral aromatic precursors, 173–  
 176

- Radical-cation salts—*Continued*  
 crystal structure of poly(*p*-phenylene),  
 197,199f  
 crystal structure of quaterphenyl, 197,198f  
 models for conducting polymers, 196–199  
 preparation via single-boundary three-  
 dimensional aromatic hydrocarbons, 7  
 reaction chemistry, 169  
 structural principles, 179–199
- Radical-cation salts as organic metals  
<sup>19</sup>F magnetic resonance, 194  
 electron spin resonance, 193,194  
 reflectance spectra, 194,195f  
 structural principles, 193  
 temperature dependence of specific  
 conductivity, 193,194f
- Radical-cation salts of arenes,  
 electrocrystallization, 177–181
- Randić conjugated circuits, definition of  
 aromaticity, 54
- Raney nickel catalyst, use in desulfurization  
 of thiophane, 358,359
- Reaction mechanism, N(IV) nitration of  
 pyrene, 164–167
- Reactions of cation radicals with  
 nucleophiles, 127,128
- Redox potentials  
 effect of aggregation, 16–21  
 effect of ion-pair structure, 17,18f  
 effect of solvent, 17,18f
- Reduced molar volume, definition, 227,228
- Reductive alkylation  
 of anthracene, naphthalene, and biphenyl,  
 75,76t  
 affected carbons, 121–124  
 application, 109  
 dibenzothiophene, 120,121  
 mechanism, 75  
 regiochemistry, 122,123  
 sulfur functionality, 123
- Reductive dimerization  
*tert*-butylphenylacetylene, 94,95  
 cyclopropyltriphenylsilane, 96,97  
 diphenylacetylene, 95,96  
 methylphenylacetylene, 95
- Reductive methylation  
 controversial aspects, 110,111  
 decacyclene, 110,118,119  
 dibenzothiophene, 110  
 perylene, 110
- Reductive protonation, dianion of perylene,  
 123,124
- Reductive ring opening,  
 tetraphenylcyclobutadienenickel(II)  
 bromide dimer, 99
- Resins, component of petroleum, 202,203f
- Ring contraction, sulfur heterocycles, 98
- Rotation photographs, pyrene radical-cation  
 salts, 186,188f
- Rubidium-biphenyl-tetraglyme  
 alkali ionic radii, 43,44t  
 bond lengths, 43,44t  
 crystallographic data, 41t  
 formation, 40  
 geometry, 42,43t  
 physical properties, 44,45  
 stereoscopic view of unit cell, 41,42f
- Rubidium-cyclooctatetraene-diglyme  
 crystal structure, 45,46f  
 crystallographic data, 45,46t  
 ESR spectrum, 45–47f

## S

- Salts of aromatic systems, stability, 178,179
- Sapropelic coals, difference from humic  
 coals, 227
- Saturates, component of petroleum,  
 202,203f
- Second-moment NMR analysis of  
 dimethyldihydroperylene, 116
- Self-consistent field methods, correlation  
 coefficients, 291–293t
- Semifusinites, plasticity, 228
- Separation, polycyclic aromatic  
 hydrocarbons, 314,315
- Shallowness factor  
 definition, 319  
 values, 319,320t
- Single crystals of alkali aromatic ion pairs,  
 preparation, 40
- Single-boundary polynuclear aromatic  
 compounds, description, 3
- Single-boundary three-dimensional aromatic  
 hydrocarbons  
 examples, 3–6  
 photoconductivities, 6  
 preparation of radical-cation salts, 7  
 properties of dianions, 7  
 relationship between molecular structure  
 and photoconductivity, 6,7
- Single-electron transfer, Born-Haber cycle  
 for response of carbon-metal bond, 93f
- Sodium salt of naphthalene dianions with  
 naphthalene, mechanism of reaction,  
 28–30f
- Sodium-biphenyl-triglyme  
 alkali ionic radii, 43,44t  
 bond lengths, 43,44t  
 crystallographic data, 41t  
 formation, 40  
 geometry, 42,43t  
 physical properties, 44,45  
 stereoscopic view, 41,42f
- Sodium-terphenyl-tetrahydrofuran  
 crystallographic data, 50  
 stereoscopic view, 50f,51
- Solvent-refined coal heavy distillate  
 elemental analysis, 236–237  
 identification of cyclopenta-containing  
 compounds, 244  
 identification of hydroaromatic  
 compounds, 244,245  
 mild autocatalytic hydrogenation, 244–  
 247  
 quantitative comparisons of polycyclic  
 aromatic compounds, 237–244t  
 reactions of polycyclic aromatic  
 compounds containing functional  
 groups, 245,246  
 structural similarities of polycyclic  
 aromatic compounds, 248,249

- Solvent-separated ion pairs  
 definition, 15  
 discussion, 39
- Spectrophotometric determination of  
 electron affinity  
 determination of equilibrium constant, 17  
 reactions, 14
- Spectrophotometric methods,  
 disproportionation constant  
 determination, 26
- Stable dianions, metal–ammonia reduction,  
 78
- Stable monoanions, metal–ammonia  
 reduction, 77
- Stage, definition, 370
- cis*-Stilbene, flash photolysis, 32–34*f*  
*cis*-Stilbene precursor, trapping, 97  
*trans*-Stilbene, flash photolysis, 32–34*f*
- Stoichiometry of pyrene nitration by N(IV),  
 effects of mass balances and yield ratios,  
 163
- Structural assignments of polycyclic aromatic  
 hydrocarbons  
 features vs. planarity, 319,320*f*  
 influencing factors, 315,317  
 spectral comparisons, 317–319
- Structure vs. paratropicity of  $4n$   $\pi$  electron  
 dianions, 68–70
- Subbituminous coals, high-molecular-weight  
 product fractions, 229
- 2-Substituted naphthalenes, reduction,  
 80,81
- Sulfonium ion perchlorate  
 reaction with bis(5-hexenyl)mercury,  
 131,132  
 reaction with dibutylmercury, 129,130  
 reaction with di-5-hexenylmercury, 146–  
 149  
 reaction with dibutylmercury, 145,146*t*  
 reaction with RMgCl, 140–145
- Sulfur heterocycles, ring contraction, 98

## T

- Terphenyl, preparation of single crystal, 41
- Tetrabenzo-1,2-dinickelcin-1,2-  
 bis(triethylphosphine), isolation, 99
- Tetrahydropyran, effect of aggregation on  
 redox potentials, 17,18*f*
- (*E,E*)-1,2,3,4-Tetraphenyl-1,3-butadiene,  
 interception, 97,98
- Tetraphenylcyclobutadienenickel(II) bromide  
 dimer, reductive ring opening, 99
- Tetraphenylethene  
 apparent equilibrium constants, 19,20*f*  
 equilibrium constants, 19,20*f*  
 shape of dianion, 20,21  
 temperature dependence of  
 disproportionation, 19,21*f*
- Thermal reactions of polynuclear aromatic  
 compounds, techniques for studying,  
 260–270

- Thermodynamics of disproportionation  
 apparatus, 21,22*f*  
 disproportionation constant vs. reciprocal  
 temperature, 22–24*f*  
 effect of cations and solvents on  
 disproportionation constant, 24,25*t*  
 effect of Coulombic forces, 24,25  
 enthalpy, 22  
 entropy, 22  
 factors favoring disproportionation, 25  
 potential vs. temperature, 22–24*f*  
 solvation of alkali cations, 23
- Thianthrene, ring contraction, 98
- Thianthrene 5-oxide, structure, 129
- Thianthrene cation radical, structure,  
 128,129
- 5-Thianthrenium perchlorates, preparation,  
 139
- Thiophene  
 desulfurization, 358  
 frontier electron densities, 361,362*t*  
 hydrodesulfurization, 358  
 $\pi$ -electron densities, 361,362*t*,363
- Three-dimensional polynuclear aromatic  
 compounds, structure, 3
- Tight ion pairs, *See* Contact ion pairs, 17
- Topology vs. paratropicity of  $4n$   $\pi$  electron  
 dianions, 67*f*–69
- Tribenzo $a,c$ ,*i*phenazine dianion, <sup>1</sup>H NMR  
 spectrum, 68,69*f*
- Triphenylene, preparation, 247
- Trityllithium, use in C-methylation of coal,  
 262–264
- Truncated icosahedral carbon cluster,  
 Hückel calculations, 9

## U

- Unstable monoanions, metal–ammonia  
 reduction, 77,78
- Unstable radical anions  
 dimerization, 34–36*f*  
 isomerization, 32–34*f*
- UV absorbance, use in PAH analysis,  
 310,311

## V

- Valence-bond structure–resonance theory,  
 quantum chemical measurements, 288
- Vitrains, average-structure models,  
 221,222,224,225

## X

- X-ray diffraction measurements, analysis of  
 coal structure, 219